

Julius-Maximilians-Universität Würzburg



Copper(I) catalyzed borylation and cross-coupling reactions

vorgelegt von

Antonius Eichhorn

aus Bamberg

Würzburg 2018



Eingereicht am:

an der Fakultät für Chemie und Pharmazie der Julius-Maximilians-Universität Würzburg.

1. *Gutachter: Prof. Dr. Todd Marder*
2. *Gutachter: Prof. Dr. Udo Radius*

der Dissertation.

1. *Prüfer: Prof. Dr. Todd Marder*
2. *Prüfer: Prof. Dr. Udo Radius*
3. *Prüfer:*

des öffentlichen Promotionskolloquiums.

Datum des öffentlichen Promotionskolloquiums:

Die Experimente zur vorliegenden Arbeit wurden in der Zeit von Oktober 2012 bis März 2017 am Institut für Anorganische Chemie der Julius-Maximilians-Universität Würzburg in Betreuung von Prof. Dr. Udo Radius and Prof. Dr. Todd B. Marder durchgeführt.

Table of contents

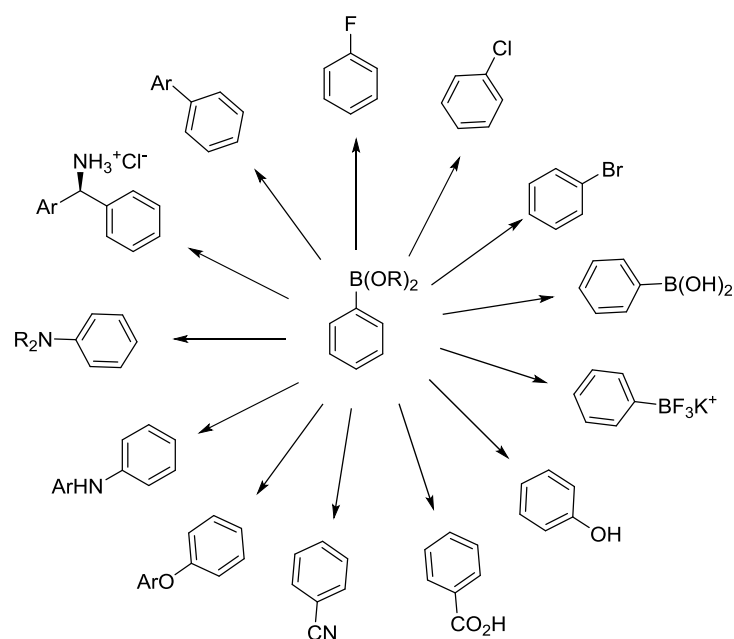
1	Introduction	1
1.1	Organoboronic esters in organic synthesis.....	1
1.2	History of organoboronic esters	2
1.3	Recent developments	6
1.4	Cross-coupling reactions using copper as catalyst	9
1.5	Substrate-ligand interactions.....	13
2	Motivation	14
3	Results and Discussion.....	15
3.1	Synthesis of NHC-stabilized copper(I) complexes	15
3.1.1	NHC-stabilized copper(I)-halide complexes.....	15
3.1.2	CaaC ^{Me} -stabilized copper(I)-chloride complex	24
3.1.3	Synthesis of NHC-stabilized copper(I)-base complexes.....	26
3.1.4	Synthesis of NHC-stabilized copper(I)-aryl complexes	32
3.2	Reactivity of NHC-stabilized copper(I) complexes.....	41
3.2.1	Reactivity of NHC-stabilized copper(I)-fluoride with boron compounds ..	41
3.2.2	Reactivity of NHC-stabilized copper(I)-base complexes with diboron(4) compounds	46
3.2.3	Reactivity of [Cu(Dipp ₂ Im)(O ^t Bu)] with aryl boronic esters.....	67
3.2.4	Reactivity of NHC-stabilized copper(I)-aryl complexes in stoichiometric cross-coupling reactions	76
3.3	Reactivity of copper(I) complexes in catalytic cross-coupling reactions.....	79
3.3.1	Copper(I) catalyzed cross-coupling of aryl iodides with PN donor ligands	79
3.3.2	Copper(I) catalyzed cross-coupling of aryl iodides with Xantphos as ligand	81
3.4	Reactivity of carbon-based Lewis bases with aryl boronic esters and diboron(4) compounds ^[300-301]	88
3.4.1	B-B bond oxidative addition	89

3.4.2	NHC adducts of aryl boronic esters	95
3.4.3	Reversible B-C bond oxidative addition.....	101
3.4.4	Ring expansion reaction at CaaC ^{Me}	112
4	Summary.....	115
4.1	Synthesis and stoichiometric model reactions of copper(I) complexes.....	115
4.2	Interactions of carbenes with arylboronic esters and diboron(4) compounds..	118
5	Zusammenfassung	120
5.1	Synthese und stöchiometrische Modell-Reaktionen von NHC-stabilisierten Kupfer(I)-Komplexen.....	120
5.2	Wechselwirkungen von Carbenen mit Arylboronsäureestern und Diboran(4)-Verbindungen	123
6	Experimental Section	126
6.1	General procedures	126
6.2	Synthesis of known compounds	137
6.3	Synthesis of new compounds	171
7	Crystallographic data	234
8	Appendix.....	302
8.1	Abbreviations.....	302
8.2	List of compounds.....	306
8.3	Additional NMR data and crystal structures.....	310
8.3.1	Additional NMR data	310
8.3.2	NHC adducts of organoboronic ester	388
8.3.3	Aryl boronic esters	393
9	Bibliography.....	395
10	Eidesstattliche Erklärung	411
11	Affidavit.....	411
12	List of publications	413
13	Acknowledgment/Danksagung.....	415

1 Introduction

1.1 Organoboronic esters in organic synthesis

Organoboronic acids and their derivatives represent an interesting and versatile class of compounds. Over the past few decades, they have become very important due to their stability, ease of use in synthesis, availability, tolerance to a variety of functional groups (in their cross-coupling and other reactions) and mild environmental impact.^[1-4] Besides using aryl boronic esters, for example, in cancer therapy,^[5-6] the main field of application is undoubtedly in organic synthesis, where they have become one of the most versatile classes of reagents for the synthesis of many organic compounds.^[3, 7-10] Most prominent, besides C-heteroatom cross-coupling^[11-12] and conjugate addition,^[13] is the Suzuki-Miyaura cross-coupling reaction.^[7] This palladium-catalyzed C-C bond-forming reaction is essential for organic synthesis. The importance of this field was recognized when Suzuki, Heck and Negishi were awarded the Nobel prize for Chemistry in 2010.^[7, 14] Another huge potential of this class of compounds is the large number of possible functionalizations, some of which are shown in Scheme 1.^[8]

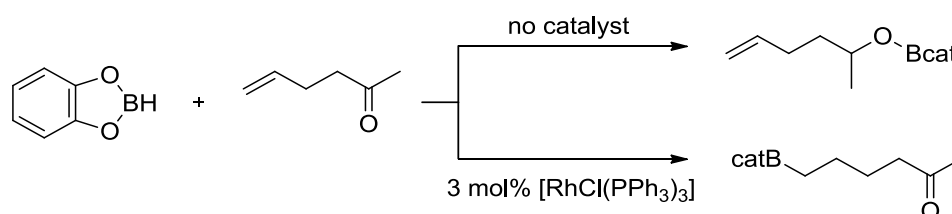


Scheme 1: Some possible functionalizations of aryl boronic esters.

The versatility of organoboronic esters has led to an increase in interest, with demand multiplying. Therefore, it is necessary to discover better and cheaper synthetic routes to these valuable reagents.

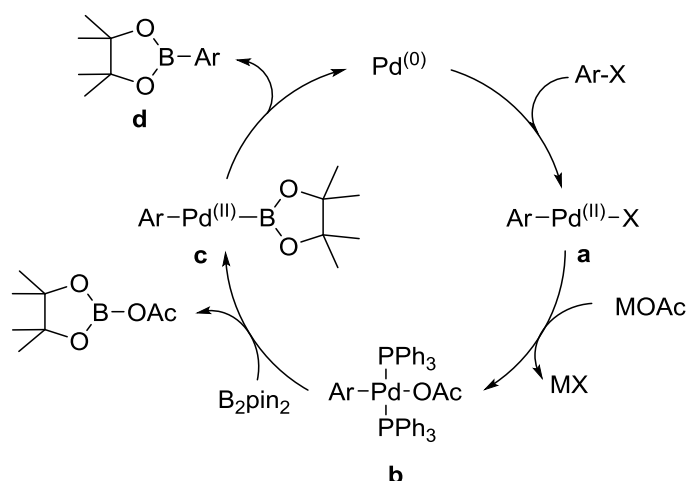
1.2 History of organoboronic esters

In the 1950s, organoboronic acids were prepared by the treatment of trialkyl borates with magnesium or lithium alkyl reagents.^[15-22] To obtain the free boronate, a further hydrolysis step is required which is often then subjected to transesterification with an alcohol.^[23] This methodology is, due to the use of strong reagents, restricted to simple substrates free of most functional groups. This drawback, and the growing interest in this compound class, led to the development of alternative synthetic routes. The hydroboration reaction, which is the addition of a hydrogen-boron bond to C=C, C=N, and C=O double bonds, as well as carbon-carbon triple bonds, has been studied extensively by Nobel prize winner H. C. Brown. This reaction opened new routes for the formation of alkyl and vinyl boronates from alkenes and alkynes,^[24-54] which were promoted in the mid-1980s by the use of transition metal catalysts containing rhodium. Among the first examples was the use of $[\text{RhCl}(\text{PPh}_3)_3]$ by Nöth and co-workers (Scheme 2).^[55-58]



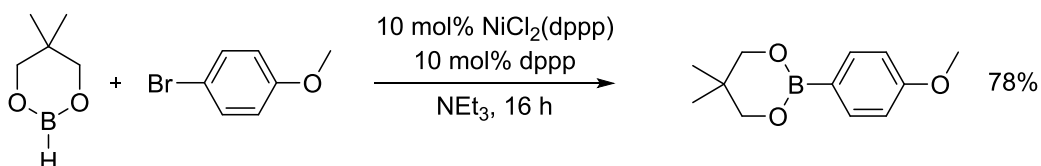
Scheme 2: Example of the influence of a rhodium catalyst on the hydroboration of an enone with catecholborane from Nöth *et al.*

Starting from alkenes^[59-77] and alkynes^[78-89], transition metal-catalyzed diboration is another well-established synthetic route to different boronates (Scheme 3).^[90-91]



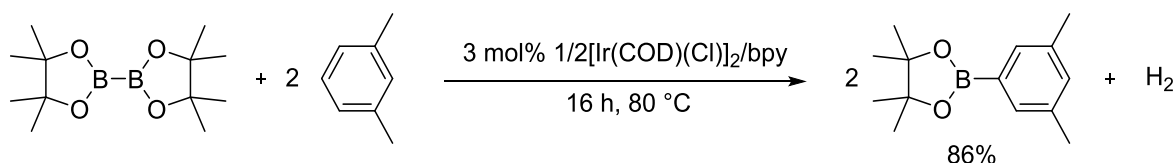
Scheme 5: Proposed catalytic cycle for the palladium-catalyzed borylation of aryl halides with alkoxy diboron reagents.

Subsequently, the nickel-catalyzed borylation of aryl halides emerged as an alternative synthetic route. Apart from using a cheaper transition metal, it was also reported that *in situ* generated neopentyl glycol borane could be used as a boron source in place of B_2pin_2 for the borylation of different aryl iodides and bromides (Scheme 6).^[108-110]



Scheme 6: Nickel-catalyzed borylation using neopentyl glycol borane as the boron source.

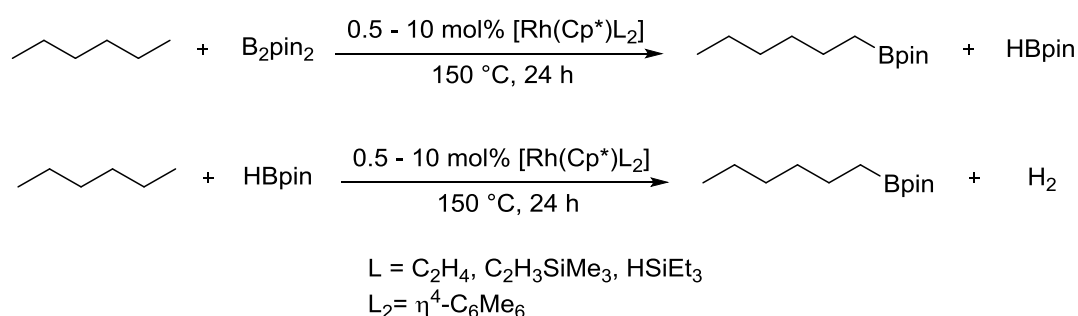
Borylation is not limited to Ar-X bonds, as the iridium-catalyzed C-H-borylation developed by Hartwig, Miyaura, Ishiyama, Smith and Marder shows.^[111-112] This reaction is controlled predominantly by steric effects of the aromatic starting compound, which means that borylation does not occur *ortho* to a substituent if there are less sterically demanding positions. It works with catalyst loadings as low as 0.02 mol% and, in some cases, it can utilize both boron units of the bis(pinacolato)diboron with hydrogen elimination (Scheme 7).^[113-114]



Scheme 7: An example reaction of iridium-catalyzed C-H borylation of arenes.

Our group was able to expand this iridium-catalyzed C-H borylation to N-containing heterocycles in 2006.^[115] Via a fruitful cooperation with Professor Steel and co-workers, we discovered that it was possible to accelerate the reaction by using microwave-assisted conditions. Furthermore, a one-pot, single-solvent process for tandem C-H borylation-Suzuki-Miyaura cross-coupling was established.^[116-118]

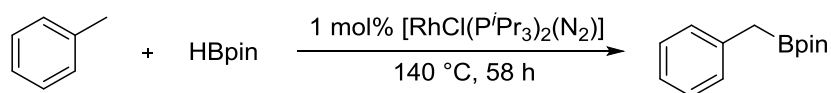
Another potentially versatile reaction is aliphatic C-H borylation using a rhodium catalyst under thermal conditions (Scheme 8).^[119-121]



Scheme 8: Example for the C-H borylation of alkanes using a rhodium catalyst.

Borylation takes place exclusively at the least hindered and most electron poor primary C-H bond, but no reaction is observed in the absence of primary C-H bonds. This selectivity can be used to functionalize polyolefins through borylation, which could, for example, undergo oxidation to form hydroxyl-capped polymers.^[122]

Under similar conditions, Marder *et al.* observed benzylic C-H borylation at toluene, *p*-xylene and mesitylene (Scheme 9).^[123] The products formed represent an important class of synthetic intermediates, and thus various synthetic routes were developed since then.^[124-128]



Scheme 9: Rhodium-catalyzed benzylic C-H borylation reported by Marder *et al.* in 2001.

Yu *et al.* were the first to C-H borylate enantioselectively. They used a Pd(II) moiety and a chiral, bidentate ligand.^[129] The group of Mankad was able to use a bimetallic system of either Cu/Fe or Zn/Fe under photochemical conditions to show that C-H borylation is not limited to noble metals.^[130-131]

1.3 Recent developments

Transition metal-catalyzed borylations reactions are, because of good atom efficiency, very important for larger scale synthesis and industrial relevant preparation. However, the well-established catalysts also have two major drawbacks, firstly, the cost of the metal and secondly, its toxicity, which makes the removal of metal residues from the products (especially for pharmaceutical and agrochemical purposes) necessary.^[132-134] Consequently, this has led to a search for other metals that can perform new or complementary reactions successfully,^[135] but are less expensive, Earth abundant and non-toxic such as copper. Since copper is an essential trace element, that is vital to the health of prokaryotes and eukaryotes alike,^[136-137] its environmental impact is relatively mild. Biocompatible copper catalysts for *in vivo* imaging were synthesized^[138] and several copper transporters have been identified that can transport Cu(I) as well as Cu(II) through the membranes of mammalian cells.^[139-143] In humans, for example, copper is essential to the brain development, the proper functioning of organs and metabolic processes.^[137, 143-144] The huge number of publications over the past few years concerning catalytically-active copper systems shows the potential of this metal and the interest of the chemical community in this area (see Diagram 1).^[145-147]

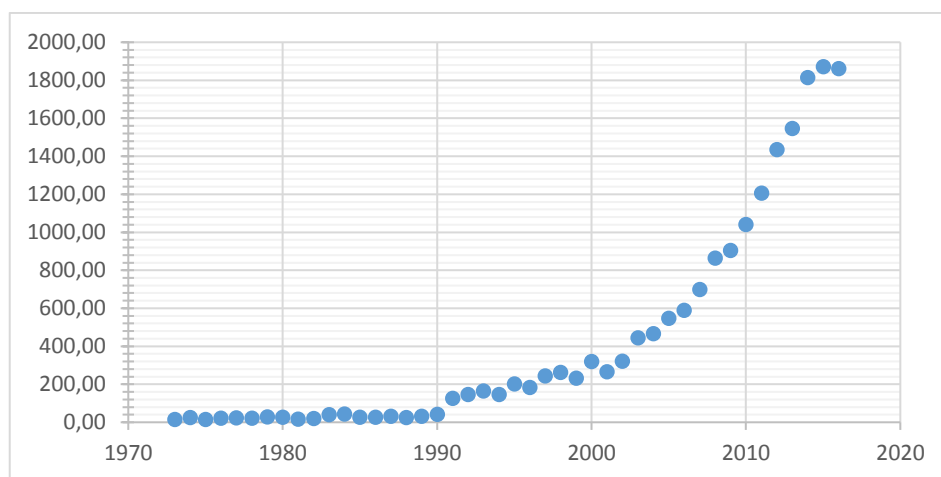
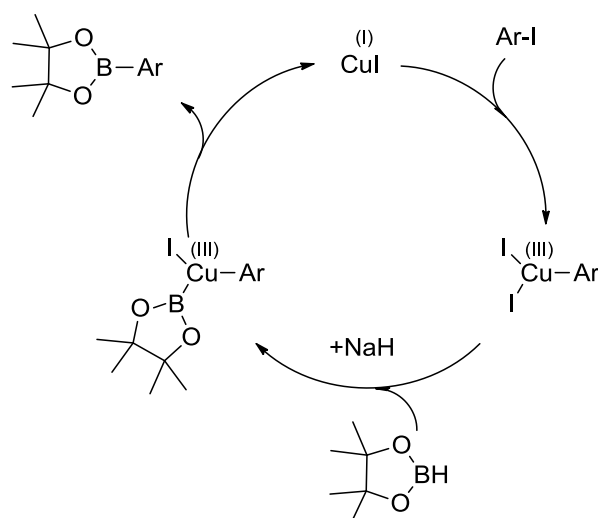


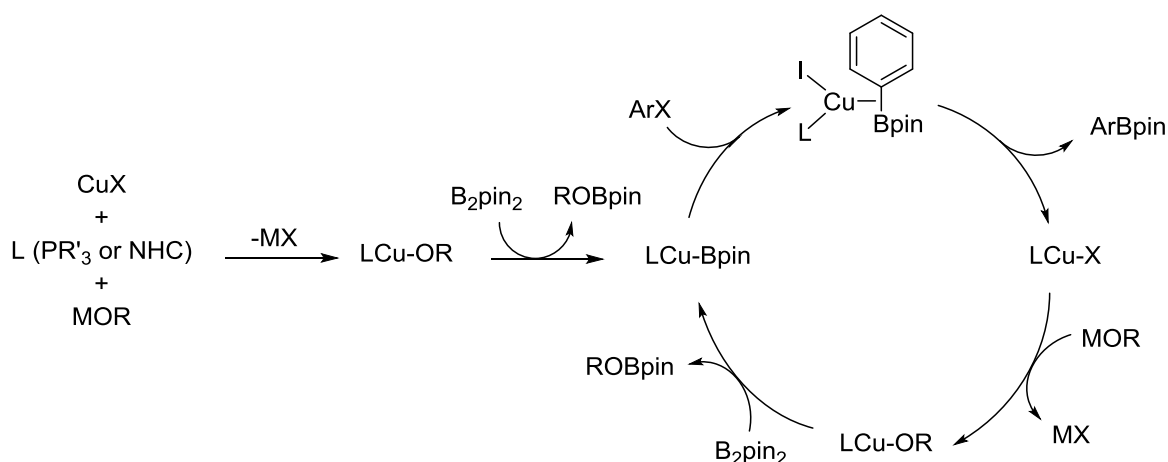
Diagram 1: Number of publications on "copper catalyzed" since 1970.

The first examples of copper-promoted or catalyzed β -boration reactions of α,β -unsaturated substrates were published in the year 2000 by Hosomi *et al.* and Miyaura *et al.*, respectively.^[148-149] The use of copper in aryl halide borylation reactions was first reported by Ma and co-workers in 2006, when they discovered the use of copper(I)iodide and sodium hydride in the borylation reaction of aryl iodides with pinacolborane. Attempts to use aryl bromides under the same reaction conditions gave much lower conversions. A catalytic cycle was proposed, which involves copper(III) species (Scheme 10).^[150] However, no further evidence was presented.



Scheme 10: Proposed catalytic cycle for the copper(I)-catalyzed borylation of aryl iodides from Ma *et al.*

In 2009, Marder *et al.* published a facile route to aryl boronates using copper(I) and diboron reagents. The borylation system consists of 1.5 equivalents of B_2pin_2 and potassium *tert*-butoxide, the substrate (aryl iodides or bromides), 10 mol% of copper(I) iodide, and 13 mol% of *tributylphosphine*. The reaction was carried out over 17 hours at room temperature to obtain isolated yields that were good to almost quantitative for a wide variety of substrates. At a temperature of 60 °C, the system gave 100 percent conversion within 2.5 hours with catalyst loadings as low as 3 mol%. It was also possible to use bis(neopentylglycolato)diboron as a reagent to form the corresponding boronates. Based on the stoichiometric reaction of a structurally characterized NHC-copper(I) boryl complex with an aryl iodide, and other stoichiometric and well-known/studied copper(I) reactions, a catalytic cycle was proposed (Scheme 11). Mechanistic investigations were undertaken with the corresponding NHC complexes, which were less reactive than the phosphine analogs, and were supported by DFT calculations.^[151]



Scheme 11: Plausible catalytic cycle for the copper(I)-catalyzed borylation using phosphine or NHC, respectively, as ligands and diboron reagents as the boron source.

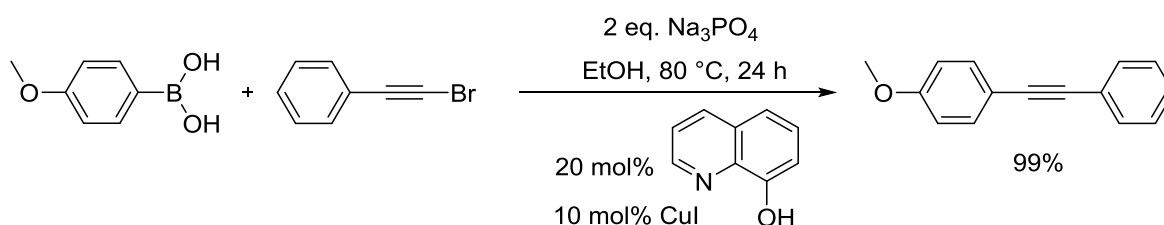
The potential of this system was revealed when its ability to borylate primary and secondary alkyl halides (iodides, bromides and chlorides) and pseudohalides was discovered together with the groups of P.G. Steel and L. Liu.^[4] Many synthetically important functional groups including alcohol, ester, cyano, ketone, ether, olefin, amide, ketal, and silyl ether groups were well tolerated with moderate to very good yields. Furthermore, good reactivity was shown when arene- and heterocycle-containing compounds were used

as substrates.^[4] This methodology made it possible to obtain many desired organoboronates in a robust synthesis with high functional group tolerance and without production of any toxic metal residues.

1.4 Cross-coupling reactions using copper as catalyst

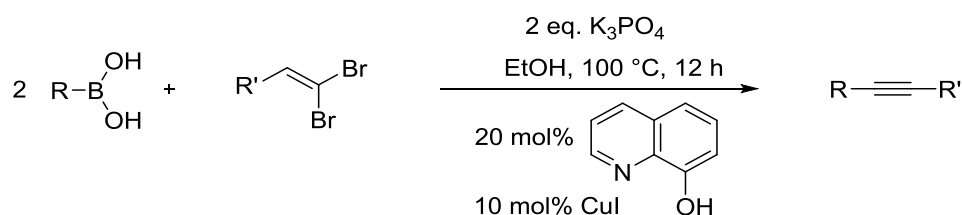
The carbon-carbon bond forming cross-coupling reactions of organocopper reagents with alkyl halides are, next to Grignard or organolithium reagents, among the most important in organic synthesis.^[152-154] However, the major drawback of the compounds is the low atom efficiency (for example, only one alkyl group could be transferred from a cuprate), which led to the development of copper-catalyzed alkylation reactions of Grignard reagents.^[155-161] These catalytic reactions are much easier to carry out and are significantly less expensive. Recent research has focused on replacing the Grignard reagents with organoboron reagents, which have a higher functional group tolerance, are commercially available and easier to store and purify.^[162-163]

The copper(I)-catalyzed formation of 1,2-disubstituted acetylenes was achieved by J. Yang and co-workers using copper(I) iodide and 8-hydroxyquinoline as catalyst and organoboronic acids and 1-bromo-2-substituted acetylenes as substrates (Scheme 12). The cross-coupling products were obtained in good to excellent yields.^[164]



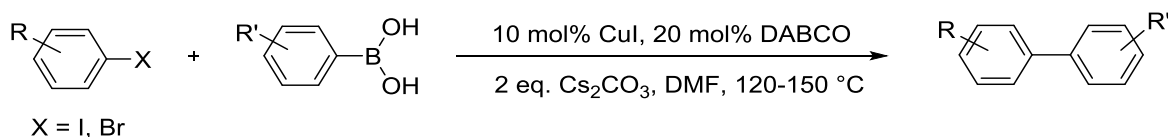
Scheme 12: Copper(I) iodide-catalyzed Suzuki coupling reaction of organoboronic acids with alkynyl bromides.

This system was optimized for 1,1-dibromo-1-alkenes as substrates by Tan *et al.*, using K₃PO₄ at slightly elevated temperatures (Scheme 13).^[165]



Scheme 13: Cross-coupling reaction of organoboronic acids with 1,1-dibromo-1-alkenes.

The first example of a copper(I) catalyzed cross-coupling which uses aryl halides was published by Wang and Li.^[166] They showed CuI/DABCO to be an inexpensive and efficient catalytic system for the cross-coupling of aryl iodides with organoboronic acids (Scheme 14).

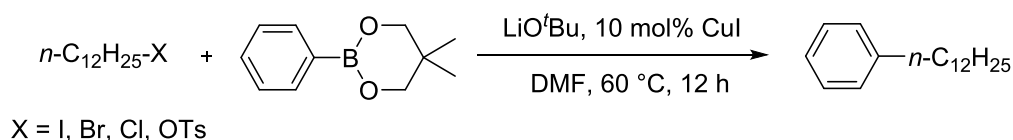


Scheme 14: Suzuki-Miyaura type cross-coupling using CuI/DABCO as catalyst.

The system was less efficient for aryl bromides, and higher temperatures were necessary to obtain satisfactory yields. For less activated aryl bromides, stoichiometric amounts of copper were required.

Besides copper(II) oxide, the group of Ye also found copper(I) compounds such as Cu₂O, CuBr and CuI to be active in Suzuki-Miyaura type cross-couplings using 2,2'-diamino-6,6'-dimethylbiphenyl as ligand.^[167]

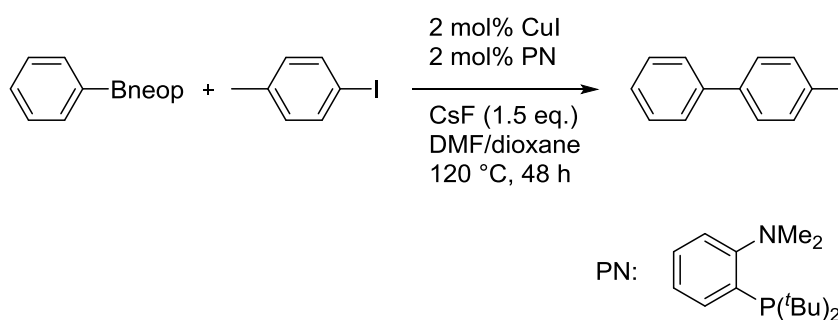
An impressive example is the 'copper-catalyzed cross-coupling reaction of organoboron compounds with primary alkyl halides and pseudohalides' from Liu and co-workers.^[168] This system uses 10 mol% copper(I) iodide, lithium *tert*-butoxide, aryl boronates (neopentyl glycol boronic esters, aryl boronic acid, aryl boroxine and pinacol boronic esters), DMF as solvent and alkyl halides such as iodides, bromides, chlorides, and tosylates as a pseudohalide, at 60 °C (Scheme 15).



Scheme 15: Copper(I) catalyzed cross-coupling of aryl boronates with alkyl halides and pseudohalides.

The reaction is again very tolerant towards functional groups (ether, ester, cyano, amide) and, as the reaction is tolerant towards aryl halide bonds, additional cross-coupling reactions are possible. Under these conditions, alkyl boronates are not suitable substrates, but alkyl 9-BBN reagents could be used to form $\text{sp}^3\text{-sp}^3$ bonds. When radical scavengers were used, there was no effect on the reaction yield, and a transmetalation step between the copper(I) and the boronate ester to form an organocopper intermediate is involved in the reaction mechanism.

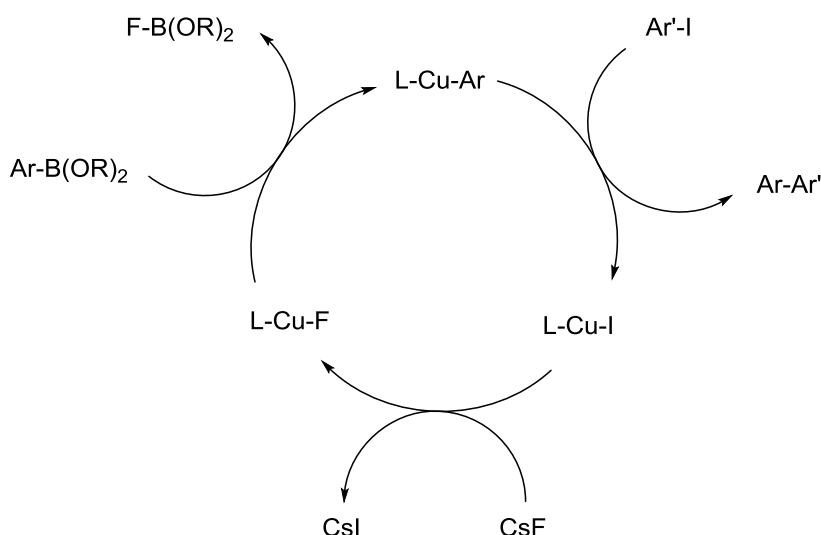
In 2014, Giri *et al.* published a catalytic system which consists of copper(I) iodide and a phosphorus-nitrogen ligand.^[169] It is the first system capable of cross-coupling aryl neopentyl glycol esters with aryl substrates, in this case aryl iodides. Reaction conditions are harsh with a temperature of 120 °C and a reaction time of two days (Scheme 16). Yields up to 95% were obtained. For aryl-heteroaryl and heteroaryl-heteroaryl couplings, the reaction also proceeds under ligand-free conditions.



Scheme 16: Copper(I)-catalyzed cross-coupling of a neopentyl glycol ester with aryl iodides.

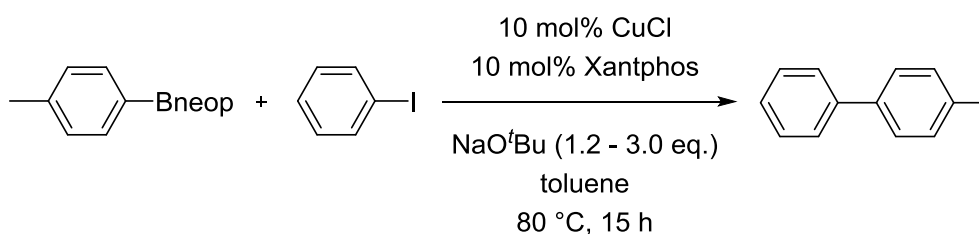
They proposed a catalytic mechanism for which they could provide X-ray structures for every intermediate complex as well as a NMR proof for the formed fluoroboron byproduct (Scheme 17). In a stepwise stoichiometric NMR-monitored reaction, Giri *et al.* were able to carry out the individual reactions in the proposed catalytic cycle, and observe the predicted signals for the products of each step *in situ*. Also noteworthy is that this system tolerates

other boron containing substrates. With *p*-iodotoluene, they were able to use nine different phenylboron reagents to obtain the desired product in fair to very good yields. Thus, 2-phenyl-6-methyl-1,3,6,2-dioxazaborocane-4,8-dione, phenylboronic acid pinacol glycol ester, phenylboronic acid ethylene glycol ester, phenylboronic acid 1,3-propanediol ester, triphenylboroxine, phenylboronic acid, cesium tetraphenylborate and potassium phenyltrifluoroborate were used.



Scheme 17: Proposed catalytic cycle for the copper(I)-catalyzed cross-coupling.

Another copper(I)-catalyzed cross-couplings reaction was published by Brown *et al.* a few month later. Albeit that only aryl boronic esters of neopentyl glycol were suitable substrates, the reaction conditions are a lot milder (80 °C in toluene for 15 hours) compared with those the previous system required (Scheme 18).^[170]



Scheme 18: Mild copper(I)-catalyzed cross-coupling reaction.

The copper-catalyzed borylation and the cross-coupling of the produced organoboronic esters to form new C-C bonds is an excellent system, which has many capabilities. This new chemical route with all its benefits and advantages still needs to be improved.

1.5 Substrate-ligand interactions

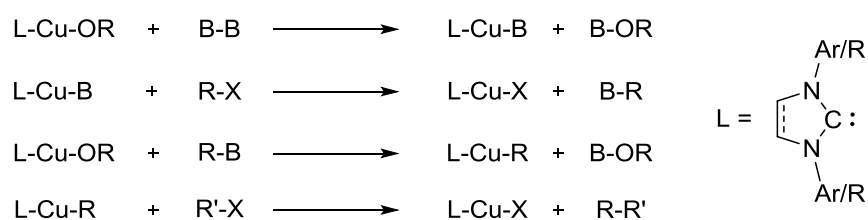
In a catalytic reaction, many different and reactive compounds coexist in the reaction mixture. The larger the scale and the more expensive the starting materials and accordingly the final products are, the more important high yields and selectivities are. Reaction optimization is done by screening of numerous reaction parameters and compounds as well as by fundamentally understanding the reaction parameters as well as the reactivity of each component with all others. While both methods are successful and benefit from each other, the later one is more scientific due to knowledge gained, which could help us to understand the specific process and can be used to predict other, related reactions.

N-Heterocyclic carbenes, for example, are intensively used as ligands in transition-metal chemistry^[171-173] and to stabilize low-valent main group elements^[174-181] as well as transition metals.^[182-183] They have widely been regarded as spectator ligands, although decomposition of the NHC via reactions with substrates showed their non-innocence in theory as ^[184-190] as well as in practice.^[191-198] Detailed investigations of the reactivity of NHCs with diboron compounds, for example, showed that ring expansion of the NHC can occur at temperatures as low as -40 °C.^[199-200] Very recently, new applications for NHCs and other Lewis bases as catalysts have emerged in metal-free transformations.^[201-222] Thus, organocatalysis is a fast growing research field with great potential for a more sustainable chemistry as it is conform to the twelve principles of green chemistry.^[223-224]

Hence, the interactions of all involved reactions partners and relevant parameters are of great interest for improvement of the reaction itself and development of related reactions, but also for a deeper understanding of the chemistry and possible new reactions pathways.

2 Motivation

The system for copper(I)-catalyzed borylation of aryl halides with phosphines as ligands, which was reported in 2009 by Lin and Marder *et al.*, works well.^[151] For better insight into the reaction mechanism, the isolation of postulated intermediates would allow us to conduct stoichiometric model reactions using NHCs as ligands (Scheme 19).



Scheme 19: Stoichiometric model reactions to obtain a better insight into catalytic reaction mechanisms.

A wide variety of NHC-stabilized copper(I) complexes, namely chlorides, alkoxides, alkyls, aryls and boryls were prepared in order to begin screening of the stoichiometric model reactions with well-defined species.

In addition, the potential of NHC-stabilized copper(I) complexes with respect to cross-coupling reactions is of great interest. Therefore, the transmetalations of different copper alkoxide complexes with different organoboronic esters and different diboron reagents were to be monitored as a first step towards understanding the kinetics of the entire cross-coupling process.

Finally, the reactivity of the substrates directly with the ligands employed, as well as the properties of the formed products was to be investigated, to help understand the specific processes going on in catalytic reactions.

3 Results and Discussion

3.1 Synthesis of NHC-stabilized copper(I) complexes

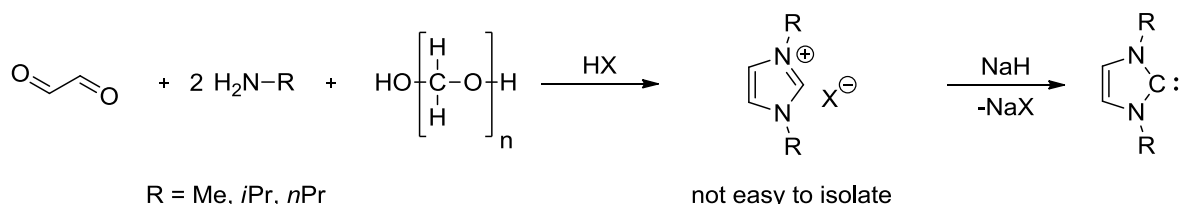
In the following chapter the synthesis and important spectroscopic data for complexes of the type [Cu(L)X], [Cu(L)OR] and [Cu(L)(aryl)] are given.

3.1.1 NHC-stabilized copper(I)-halide complexes

This type of complex is one of the best starting points for NHC copper(I) chemistry, due to the ease of synthesis using various routes and the stability of (some of) the complexes to air, water and light.^[225]

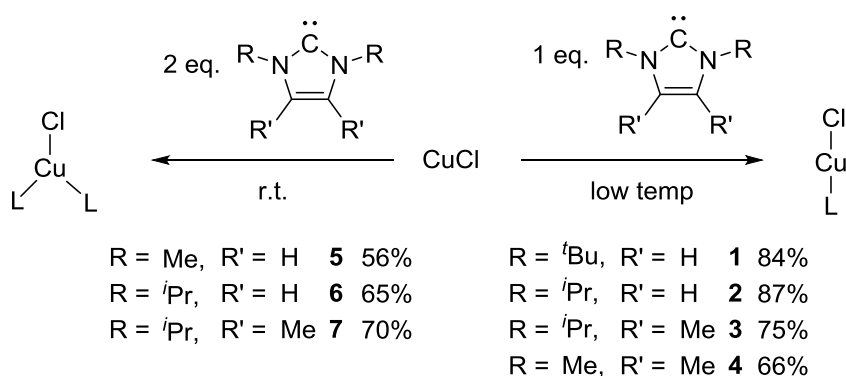
3.1.1.1 Synthesis of NHC-stabilized copper(I)-chloride complexes

The broad scope and effectiveness of *N*-heterocyclic carbene (NHC) copper(I) complexes of the type [Cu(NHC)(halide)] in catalytic transformations has been demonstrated in several publications.^[226-234] One of the most common routes to the copper(I) chloride complex is the reaction of CuX with *in situ* formed NHC.^[225] However, there are several disadvantages to this route, for example, including the use of strong bases *in situ* and the need for exact stoichiometry to prevent the formation of undesired side products such as [Cu(I)(base)] or [Cu(NHC)(base)]. A more convenient way to synthesize [Cu(NHC)(halide)] complexes is from copper(I) oxide with the corresponding halide salt of the imidazolium precursor.^[235] This route is effective for most NHCs giving good to excellent yields, and it can be performed in technical grade solvents such as CH₂Cl₂, toluene and even water. The only drawback is the need for the imidazolium salt that is not easily available for all carbenes, for example, for small alkyl NHCs. These are synthesized in a two-step reaction with the halide salt not being isolated (Scheme 20). Another route to prepare the halide salt is by reacting the NHC with the acid of the desired halogen. However, this requires the isolation of the free carbene, which makes the copper(I) oxide route less attractive for small alkyl NHCs.



Scheme 20: Standard two-step synthesis for symmetric and small alkyl NHCs.

The syntheses of [Cu(NHC)(X)] complexes were investigated with compounds starting from small alkyl NHCs and copper(I) chloride. The equimolar reaction, at low temperature, of free carbenes with copper(I) chloride yielded solids which are sensitive to both light and air (Scheme 21).



Scheme 21: Synthetic route for the formation of [Cu(NHC)(Cl)] and [Cu(NHC)₂(Cl)].

The reaction of copper(I) chloride with 1,3-di-*tert*-butylimidazolin-2-ylidene, 1,3-di-*iso*-propylimidazolin-2-ylidene, 1,3-di-*iso*-propyl-4,5-dimethylimidazolin-2-ylidene and 1,3,4,5-tetramethylimidazolin-2-ylidene provided the mono NHC-stabilized [Cu(NHC)(Cl)] complex in 66% to 87% yield at low temperature. The NMR data match those reported in the literature^[236] and is in the expected range, respectively. Complexes **1**, **2**, **3** and **4** were fully characterized and the molecular structures are shown in Figure 1.

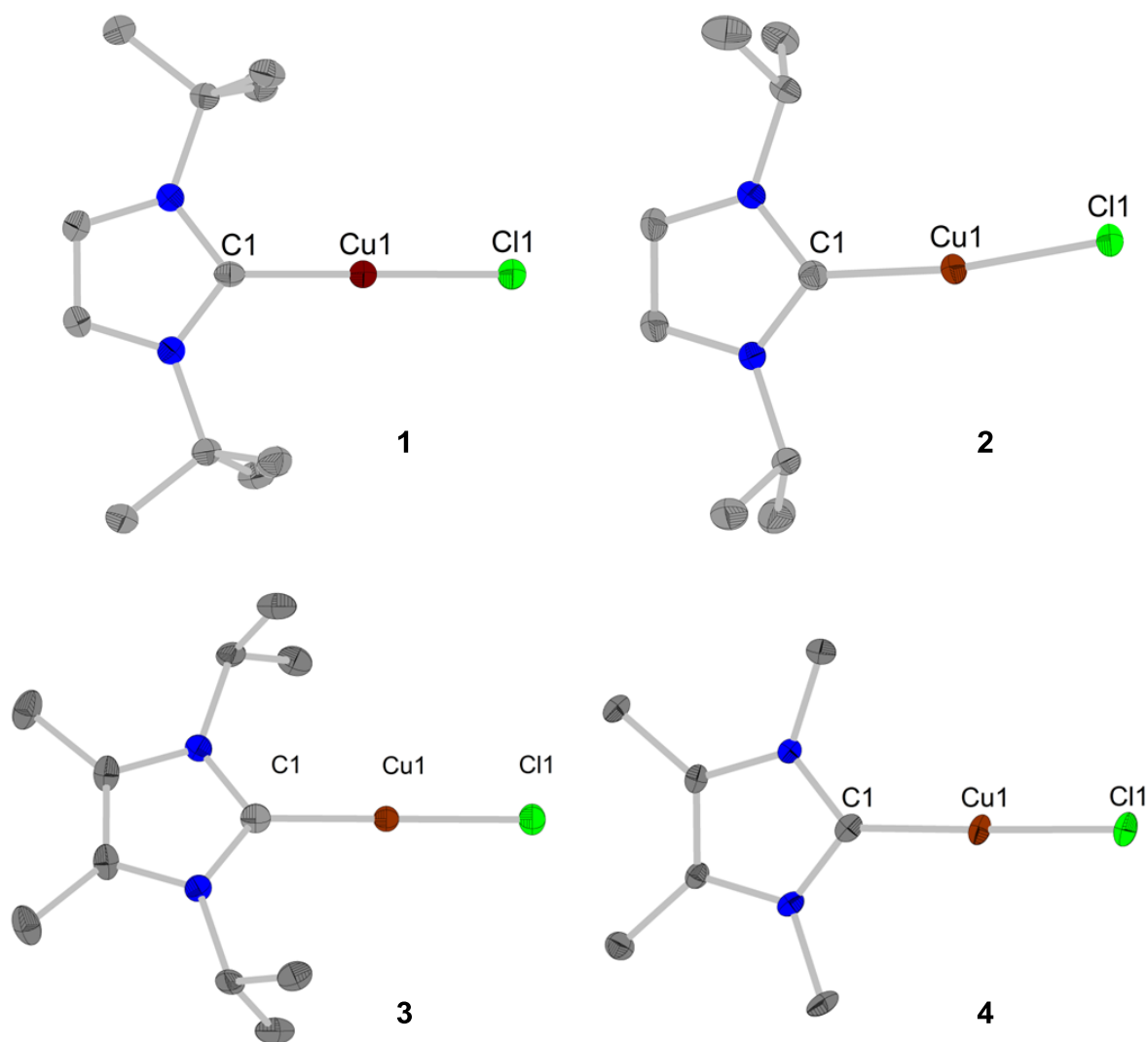


Figure 1: Element (color): carbon (grey), nitrogen (blue), copper (maroon), chlorine (green). Hydrogen atoms are omitted for clarity and the thermal ellipsoids are drawn at 50% probability. Top left: Molecular structure of $[\text{Cu}(\text{Bu}_2\text{Im})(\text{Cl})]$ **1**. Selected bond lengths (\AA) and angles (deg): Cu–C1 1.879(2), Cu–Cl 2.0937(7), C1–Cu–Cl 180.00(0) $^\circ$. Top right: Molecular structure of $[\text{Cu}(\text{Pr}_2\text{Im})(\text{Cl})]$ **2**. Selected bond lengths (\AA) and angles (deg): Cu–C1 1.8781(14), Cu–Cl 2.1055(4), C1–Cu–Cl 170.95(5) $^\circ$. Bottom left: Molecular structure of $[\text{Cu}(\text{Pr}_2\text{ImMe}_2)(\text{Cl})]$ **3**. Selected bond lengths (\AA) and angles (deg): Cu1–C1 1.886(3), Cu1–Cl1 2.1056(9), C1–Cu1–Cl1 180.00(0) $^\circ$. Bottom right: Molecular structure of $[\text{Cu}(\text{Me}_4\text{Im})(\text{Cl})]$ **4**. Selected bond lengths (\AA) and angles (deg): Cu1–C1 1.878(2), Cu1–Cl1 2.1081(5), C1–Cu1–Cl1 177.93(7) $^\circ$.

From the reaction of copper(I) chloride with two equivalents of 1,3-di-methylimidazolin-2-ylidene, 1,3-di-*iso*-propylimidazolin-2-ylidene and 1,3-di-*iso*-propyl-4,5-dimethylimidazolin-2-ylidene at room temperature the bis NHC-stabilized $[\text{Cu}(\text{NHC})_2(\text{Cl})]$ were obtained in 56% to 70% yield. In addition to NMR spectroscopy and HRMS it was possible to characterize complexes **6** and **7** by X-ray diffraction (Figure 2).

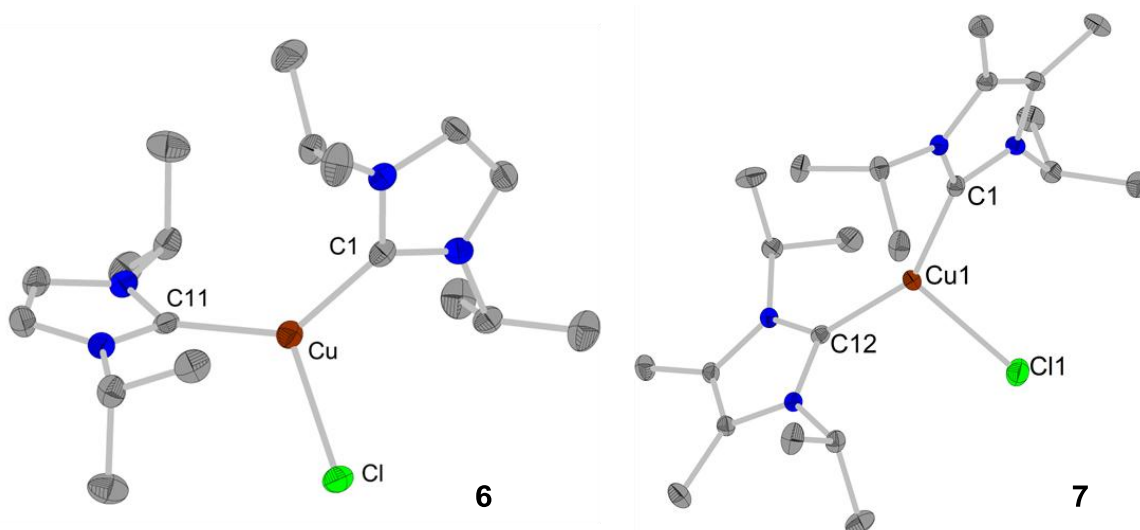


Figure 2: Element (color): carbon (grey), nitrogen (blue), copper (maroon), chlorine (green). Hydrogen atoms are omitted for clarity and the thermal ellipsoids are drawn at 50% probability. Left: Molecular structure of $[\text{Cu}(\text{iPr}_2\text{Im})(\text{Cl})]$ **6**. Selected bond lengths (Å) and angles (deg): Cu–C1 1.921(4), Cu–C11 1.938(4), Cu–Cl 2.3668(11), C1–Cu–Cl 112.6(1), C11–Cu–Cl 113.9(1), C1–Cu–C11 133.5(2). Right: Molecular structure of $[\text{Cu}(\text{iPr}_2\text{ImMe}_2)(\text{Cl})]$ **7**. Selected bond lengths (Å) and angles (deg): Cu1–C1 1.886(3), Cu1–Cl1 2.1056(9), C1–Cu1–Cl1 180.00(0)°.

The 1:1 reaction of 1,3-di-methylimidazolin-2-ylidene with copper(I) chloride yielded a grey powder (85% yield). The ^1H NMR spectrum displays one singlet for six protons with a chemical shift of 2.70 ppm and one singlet for two protons with a shift of 5.52 ppm. The $^{13}\text{C}\{^1\text{H}\}$ NMR spectrum shows three signals at 38.5 ppm, 123.1 ppm and 177.8 ppm. Layering a saturated THF solution of compound **8** with hexane at 6 °C yielded crystals suitable for X-ray diffraction. The structure is shown in Figure 3.

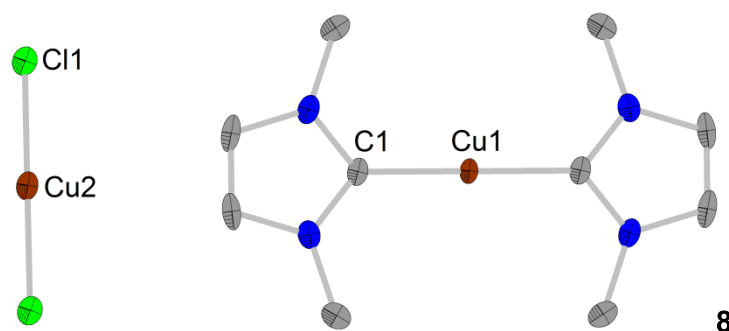


Figure 3: Molecular structure of $[\text{Cu}(\text{Me}_2\text{Im})_2]^+[\text{Cu}(\text{Cl})_2]^-$ **8**. Element (color): carbon (grey), nitrogen (blue), copper (maroon), chlorine (green). Hydrogen atoms are omitted for clarity and the thermal ellipsoids are drawn at 50% probability. Selected bond lengths (Å) and angles (deg): Cu–C1 1.889(8), Cu2–Cl 1.1150(8), C1–Cu–C 180.00(0)°.

The structure obtained shows that **8** is ionic, composed of a $[\text{Cu}(\text{Pr}_2\text{Im})_2]^+$ cation and a $[\text{CuCl}_2]^-$ anion. In addition to Cu1 and Cu2 sitting on two crystallographic inversion centers, both are lying together with C1 and Cl1, respectively, on a crystallographic twofold axis and on a mirror plane.

For further characterization of compound **8**, an X-ray powder pattern was recorded and also simulated from the X-ray crystal structure. The results are shown in Figure 4.

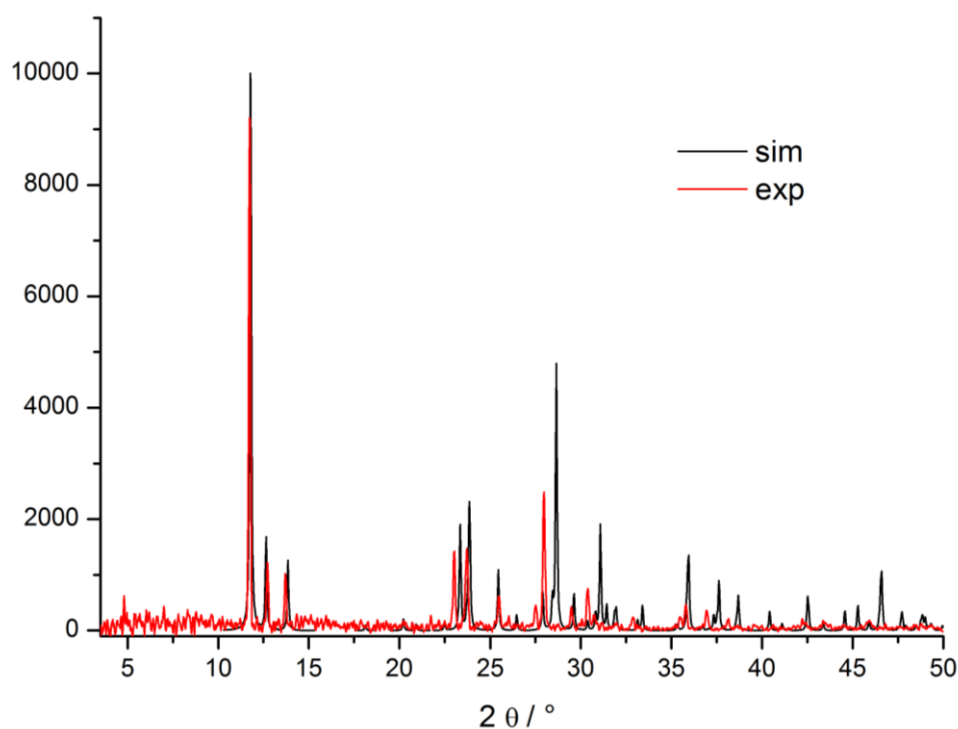


Figure 4: Powder pattern of **8**, simulated from the single crystal structure (black) and recorded (red).

The powder pattern shows that most reflections of the simulation and the measurement are in good agreement, apart from the temperature dependent (-173 °C crystal structure and 20 °C powder pattern) shifts to lower theta in the single-crystal measurement. This proves that compound **8** exists as an ionic species in the bulk material, as was found in the single-crystal X-ray structure.

Table 1 gives a comparison of the $^{13}\text{C}\{^1\text{H}\}$ NMR chemical shifts of the carbene-carbons and key bond distances and angles found in the crystal structures of the mono- and bis-NHC copper(I) chloride complexes.

Table 1: Comparison of mono- and bis-NHC copper(I) chloride complexes.

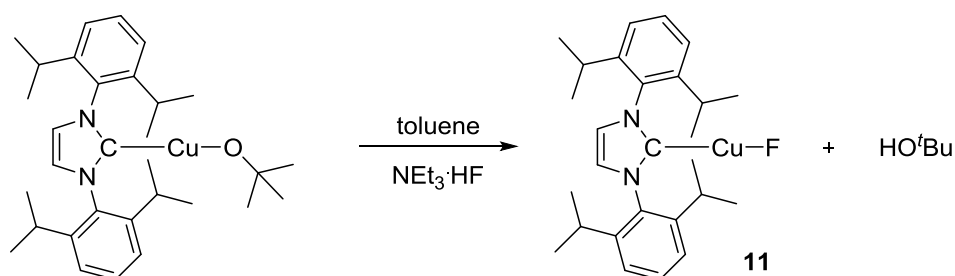
	$^{13}\text{C}\{^1\text{H}\}$ – NMR: C _q [ppm]	Distance: C _(NHC) -Cu [Å]	Distance: Cl-Cu [Å]	Angle: C _(NHC) -Cu-Cl [°]	Angle: C _(NHC) -Cu- C _(NHC) [°]
[Cu(^t Bu ₂ Im)(Cl)] 1	174.1	1.879(2)	2.0937(7)	180(0)	
[Cu(ⁱ Pr ₂ Im)(Cl)] 2	174.5	1.8781(14)	2.1055(4)	170.95(5)	
[Cu(ⁱ Pr ₂ ImMe ₂)(Cl)] 3	169.7	1.886(3)	2.1056(9)	180(0)	
[Cu(Me ₄ Im)(Cl)] 4	175.2	1.878(2)	2.1081(5)	177.93(7)	
[Cu(Me ₂ Im) ₂ (Cl)] 5	183.8				
[Cu(ⁱ Pr ₂ Im) ₂ (Cl)] 6	184.7	1.921(4) 1.938(4)	2.3668(11)	113.9(1) 133.5(2)	133.5(2)
[Cu(ⁱ Pr ₂ ImMe ₂) ₂ (Cl)] 7	183.9	1.939(2) 1.942(3)	2.4381(11)	106.69(8) 105.91(8)	147.37(11)
[Cu(Me ₂ Im) ₂] ⁺ [Cu(Cl) ₂] ⁻ 8	177.8	1.889(8)	1.1150(8)		

The bis-NHC complexes have somewhat longer C1-Cu1 as well as much longer Cl1-Cu1 bond lengths than the analogous mono-NHC complexes, which is in good agreement with the known [CuCl(ⁱPr₂bimy)₂] complex.^[237] In both cases, the resonance of the carbene-carbon atom in the $^{13}\text{C}\{^1\text{H}\}$ NMR spectrum is shifted downfield by 10 to 14 ppm when compared with the mono-substituted analogs. Compared with [Cu(NHC)(Cl)] complexes with sterically more demanding NHCs ([Cu(Cy₂Im)(Cl)] C1-Cu 2.114(11), Cu-Cl 2.136(4); [Cu(Mes₂Im)(Cl)] C1-Cu 1.956(10), Cu-Cl 2.091(2); [Cu(Dipp₂Im)(Cl)] C1-Cu 1.953(8), Cu-Cl 2.089(3)),^[231, 236, 238-239] complexes **1** - **4** show smaller C1-Cu distances while the Cu-Cl distances are in the same range (mean C1-Cu 1.880 Å, Cu-Cl 2.1032 Å). The NHC with the methylated backbones shows the biggest influence in the structures of complex **4**. While complex **8**, with the

stabilizing the copper(I) moiety. Complex **10** was isolated in 78% yield and fully characterized.

3.1.1.2 Synthesis of NHC-stabilized copper(I)-fluoride complex

In 2008, Ball and co-workers published the synthesis of the NHC-stabilized copper(I) fluoride complex, $[\text{Cu}(\text{Dipp}_2\text{Im})(\text{F})]$.^[244] This versatile complex which is used in hydrocarboxylation,^[245] asymmetric trifluoromethylation^[246] and asymmetric hydrosilylation of ketones^[247-248] could potentially be used in reactions with diboron reagents. The formation of a boron-fluorine bond (bond energy of 646 kJ/mol at 298 K),^[249] could be the driving force for the reaction and could provide a route to form a copper(I) boryl complex.^[169] To follow this pathway, the monomeric complex $[\text{Cu}(\text{Dipp}_2\text{Im})(\text{F})]$ **11** was synthesized by the reaction of $[\text{Cu}(\text{Dipp}_2\text{Im})(\text{O}^t\text{Bu})]$ with $\text{NEt}_3 \cdot \text{HF}$ (Scheme 23).



Scheme 23: Synthesis of $[\text{Cu}(\text{Dipp}_2\text{Im})(\text{F})]$ **11** from $[\text{Cu}(\text{Dipp}_2\text{Im})(\text{O}^t\text{Bu})]$ and $\text{NEt}_3 \cdot \text{HF}$.

The ^1H , $^{13}\text{C}\{^1\text{H}\}$ and ^{19}F NMR data recorded for this complex match those reported in the literature.^[244] In addition, it was possible to grow single crystals of **11** suitable for X-ray diffraction for the first time (Figure 5).

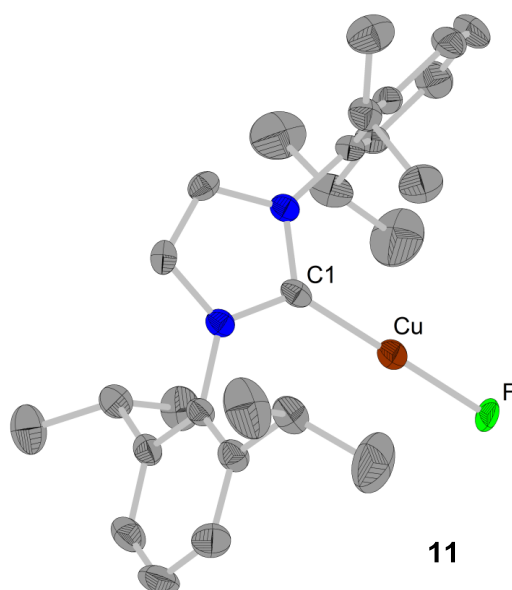


Figure 5: X-ray crystal structure of $[\text{Cu}(\text{Dipp}_2\text{Im})(\text{F})]$ **11**. Element (color): carbon (grey), nitrogen (blue), copper (maroon), fluorine (green). Hydrogen atoms are omitted for clarity and the thermal ellipsoids are drawn at 50% probability. Selected bond lengths (Å) and angles (deg): Cu–C1 1.852(3), Cu–F 1.8306(17), C1–Cu–F 180.00(0).

Complex **11** crystallizes in the monoclinic space group $C2/c$. The coordination around the metal center is ideally linear with C1–Cu–F lying on a crystallographic twofold axis and therefore having a bond angle of 180° . The bond length of C1–Cu is 1.852(3) Å and Cu–F is 1.8306(17) Å. In Table 2, a comparison of **11** with halide complexes of the type $[\text{Cu}(\text{Dipp}_2\text{Im})(\text{halide})]$ is given.

Table 2: Comparison of $[\text{Cu}(\text{Dipp}_2\text{Im})(\text{F})]$ **11** with other halide complexes of the same NHC ligand.

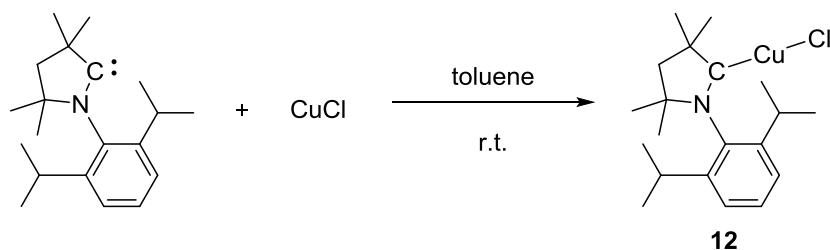
	Distance: $C_{(\text{NHC})}\text{-Cu}$ [Å]	Distance: Cl-Cu [Å]	Angle: $C_{(\text{NHC})}\text{-Cu-Cl}$ [°]
$[\text{Cu}(\text{Dipp}_2\text{Im})(\text{F})]$ 11	1.852(3)	2.0937(7)	180(0)
$[\text{Cu}(\text{Dipp}_2\text{Im})(\text{Cl})]$ ^[239]	1.953(8)	2.089(3)	180(0)
$[\text{Cu}(\text{Dipp}_2\text{Im})(\text{Br})]$ ^[236]	1.884(2)	2.2090(4)	180(0)
$[\text{Cu}(\text{Dipp}_2\text{Im})(\text{I})]$ ^[236]	1.870(8)	2.3804(9)	180(0)

All Dipp_2Im -stabilized copper(I) halide complexes exhibit a $C_{(\text{NHC})}\text{-Cu-Cl}$ angle of 180° . Complex **11** shows the smallest C1–Cu distance of all $[\text{Cu}(\text{Dipp}_2\text{Im})(\text{X})]$ complexes. Albeit

that there is a trend to larger Cu-X distance with larger atomic numbers is observed, [Cu(Dipp₂Im)(Cl)] has a slightly shorter Cu-X bond distance than **11**.^[236, 239]

3.1.2 CaaC^{Me}-stabilized copper(I)-chloride complex

Due to their significantly greater π -backbonding capabilities, cyclic allylic amino carbenes (CaaC) are an interesting alternative to NHC ligands.^[250-251] The π -back donation to a suitable ligand could lower the energy of certain transition states involving bending of a d^{10} -ML₂ (LCu(X)) fragment and thus accelerate catalytic reactions.^[151, 182] In a similar manner to the NHCs, the CaaC^{Me}-stabilized copper(I) chloride complex was synthesized (Scheme 24).



Scheme 24: Synthesis of [Cu(CaaC^{Me})(Cl)] **12**.

All NMR signals were in the expected range with the carbene-carbon atom having a chemical shift in the ¹³C{¹H} NMR spectrum of 249.6 ppm, which is shifted significantly downfield compared to NHC-stabilized copper(I) complexes (see 4.1.1). It was also possible to grow single crystals suitable for X-ray diffraction from a saturated benzene solution at room temperature (Figure 6).

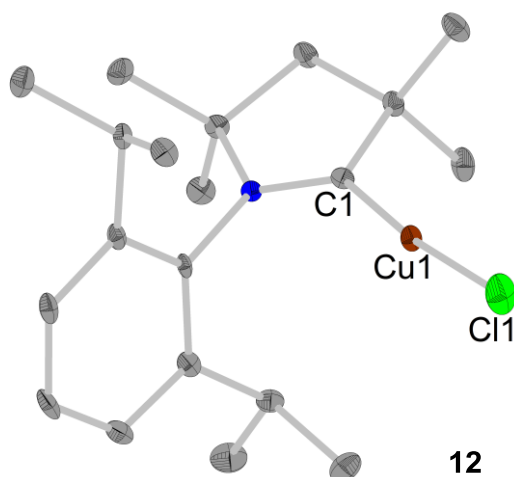


Figure 6: X-ray crystal structure of $[\text{Cu}(\text{CaaC}^{\text{Me}})(\text{Cl})]$ **12**. Element (color): carbon (grey), nitrogen (blue), copper (maroon), chlorine (green). Hydrogen atoms are omitted for clarity and the thermal ellipsoids are drawn at 50% probability. Selected bond lengths (Å) and angles (deg): Cu1–C1 1.879(3), Cu1–Cl1 2.1084(8), C1–Cu1–Cl1 173.96(10).

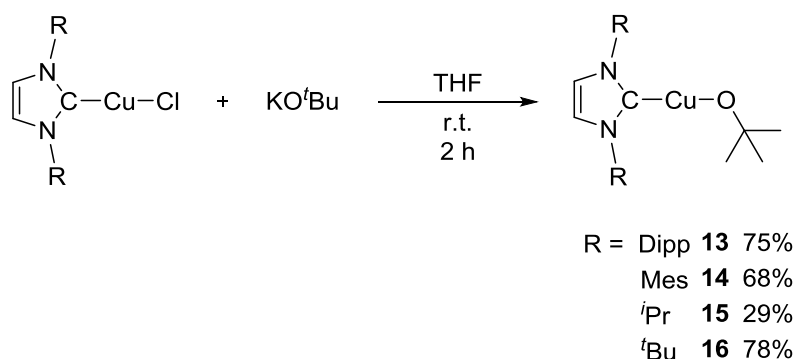
Complex **12** crystallizes in the monoclinic space group $P2_1/n$. The coordination around the metal center is slightly bent with a C1–Cu1–Cl1 angle of $173.96(10)^\circ$. C1–Cu1 and Cu1–Cl1 bond length are 1.879(3) Å and 2.1084(8) Å, respectively. Similar angles ($170.95(5)^\circ$ - $180(0)^\circ$) and bond length (1.8781(14) – 1.886(3), 2.0937(7) – 2.1081(5)) were observed for mono-NHC copper chloride complexes indicating that the greater π -backbonding of the CaaC ligand does not have an influence on that parameter in the ground state.

3.1.3 Synthesis of NHC-stabilized copper(I)-base complexes

Copper(I) alkoxide complexes are very important intermediates in catalytic borylations as well as in cross-coupling reactions, making them an important starting material for stoichiometric model reactions.

3.1.3.1 Synthesis of NHC-stabilized copper(I)-alkoxide complexes

The complexes $[\text{Cu}(\text{Dipp}_2\text{Im})(\text{O}^t\text{Bu})]$ **13** and $[\text{Cu}(\text{Mes}_2\text{Im})(\text{O}^t\text{Bu})]$ **14** are already known and can be prepared by adding one equivalent of KO^tBu to $[\text{Cu}(\text{NHC})(\text{Cl})]$ (NHC = Dipp_2Im , Mes_2Im) in THF (Scheme 25).^[245, 252] The ^1H and $^{13}\text{C}\{^1\text{H}\}$ NMR spectroscopic data are in accordance with those reported in the literature.^[245, 252]



Scheme 25: Synthesis of the NHC-stabilized copper(I) *tert*-butoxide complexes **13**, **14**, **15** and **16**.

By analogy with literature reports, the equimolar reactions of $[\text{Cu}(i\text{Pr}_2\text{Im})\text{Cl}]$ and $[\text{Cu}(t\text{Bu}_2\text{Im})\text{Cl}]$ with freshly sublimed KO^tBu afforded $[\text{Cu}(i\text{Pr}_2\text{Im})(\text{O}^t\text{Bu})]$ **15** and $[\text{Cu}(t\text{Bu}_2\text{Im})(\text{O}^t\text{Bu})]$ **16** in 29% and 78% yield, respectively (Scheme 25).^[253] Compound **15** was fully characterized. For compound **16** the molecular structure was investigated by X-ray diffraction (Figure 7).

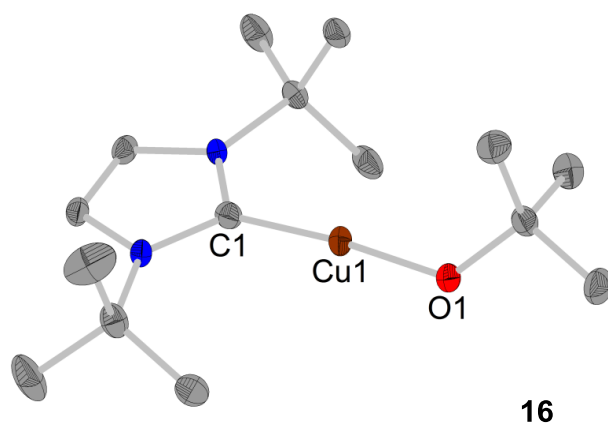


Figure 7: Molecular structure of $[\text{Cu}(\text{tBu}_2\text{Im})(\text{O}^t\text{Bu})]$ **16**. Element (color): carbon (grey), nitrogen (blue), copper (maroon), oxygen (red). Hydrogen atoms are omitted for clarity and the thermal ellipsoids are drawn at 50% probability. Only one of the two molecules in the asymmetric unit is shown. Selected bond lengths (Å) and angles (deg): C1–Cu 1.880(3) [1.874(3)], Cu–O1 1.816(2) [1.810(2)], C1–Cu–O1 174.53(11) [173.94(11)], Cu1–O1–C 127.64(19) [125.89(7)].

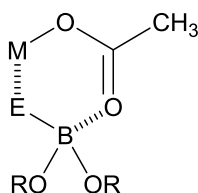
Compound **16** crystallizes in the monoclinic space group $P2_1/c$ with two independent molecules in the asymmetric unit. The Cu–C1 bond length is 1.880(3) [1.874(3)] Å and that of Cu1–O1 is 1.816(2) Å [1.810(2)]. The angle around the copper center is 174.53(11)° [173.94(11)]. This central angle deviates by 4.5° from the angle found in the literature known and structurally characterized $[\text{Cu}(\text{Dipp}_2\text{Im})(\text{O}^t\text{Bu})]$ complex **13** (179.05(7)) (Table 3).^[252]

Table 3: Comparison of the bond lengths and angles found in both structurally characterized, NHC-stabilized copper(I) *tert*-butoxide complexes.

	Distance: Cu1–C1 [Å]	Distance: Cu1–O1 [Å]	Angle: C1–Cu1–O1 [°]	Angle: Cu1–O1–C _{tBu} [°]
$[\text{Cu}(\text{tBu}_2\text{Im})(\text{O}^t\text{Bu})]$ 16	1.880(3) [1.874(3)]	1.816(2) [1.810(2)]	174.53(11) [173.94(11)]	127.64(19) [125.89(7)]
$[\text{Cu}(\text{Dipp}_2\text{Im})(\text{O}^t\text{Bu})]$ 13	1.8641(18)	1.8104(13)	179.05(7)	122.85(12)

3.1.3.2 Synthesis of NHC-stabilized copper(I)-acetato complexes

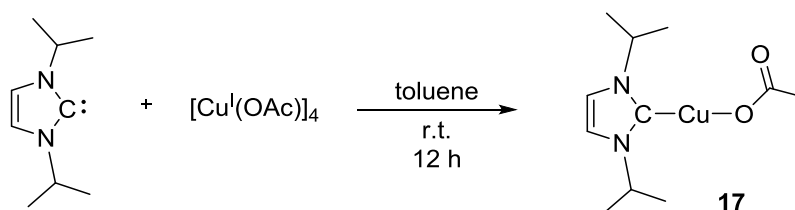
Metal acetates can be effective in transmetalation reactions involving C-B(OR)₂ and (RO)₂B-B(OR)₂ systems due to the formation of a six-membered ring transition state (Scheme 26). As such, and given the lower basicity of acetate compared with alkoxides, these may prove useful in both stoichiometric model reactions as well as catalytic processes.



E = C or B unit

Scheme 26: Six-membered transition state of metal acetates and C-B(OR)₂ or (RO)₂B-B(OR)₂ transmetalations.

The compounds [Cu(Dipp₂Im)(OAc)]^[254] and [Cu(Mes₂Im)(OAc)]^[255] are known. However, it was possible to synthesize and fully characterize the novel complex **17** with a small alkyl NHC as ligand (Scheme 27).



Scheme 27: Synthesis of [Cu(*i*Pr₂Im)(OAc)] **17**.

The reaction of 1,3-di-*iso*-propylimidazolin-2-ylidene with copper(I) acetate afforded an off-white powder **17** in 32% yield. The ¹H NMR spectrum shows, besides sharp signals for protons attached to the NHC ligand, a broadened signal for the acetate protons, indicative of a dynamic process within the acetate moiety. The ¹³C{¹H} NMR spectrum shows the signals for the NHC ligand as well as a broadened signal at 176.1 ppm for the carbonyl carbon atom. The methyl carbon atoms of the acetate group might not have been detected because of dynamic binding in solution. In 2D-NMR spectra a peak for the methyl protons was found at 23.1 ppm. In ¹H VT-NMR spectra recorded in toluene-*d*₈ the dynamics were

still observed at -39 °C. At an elevated temperature of 70 °C, the signals were also broadened. Besides elemental analysis and HRMS compound **17** was also characterized by X-ray diffraction (Figure 8).

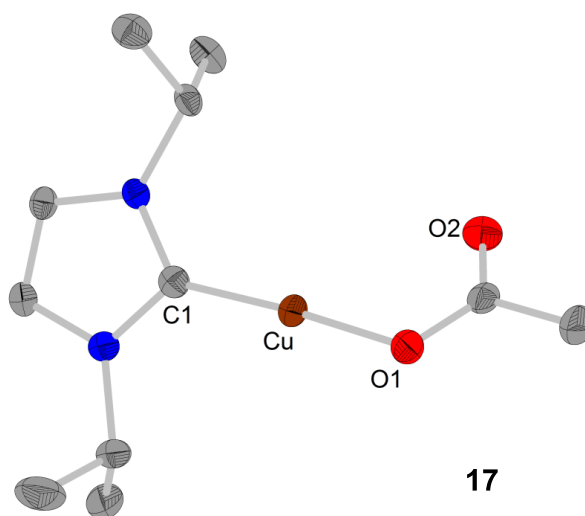


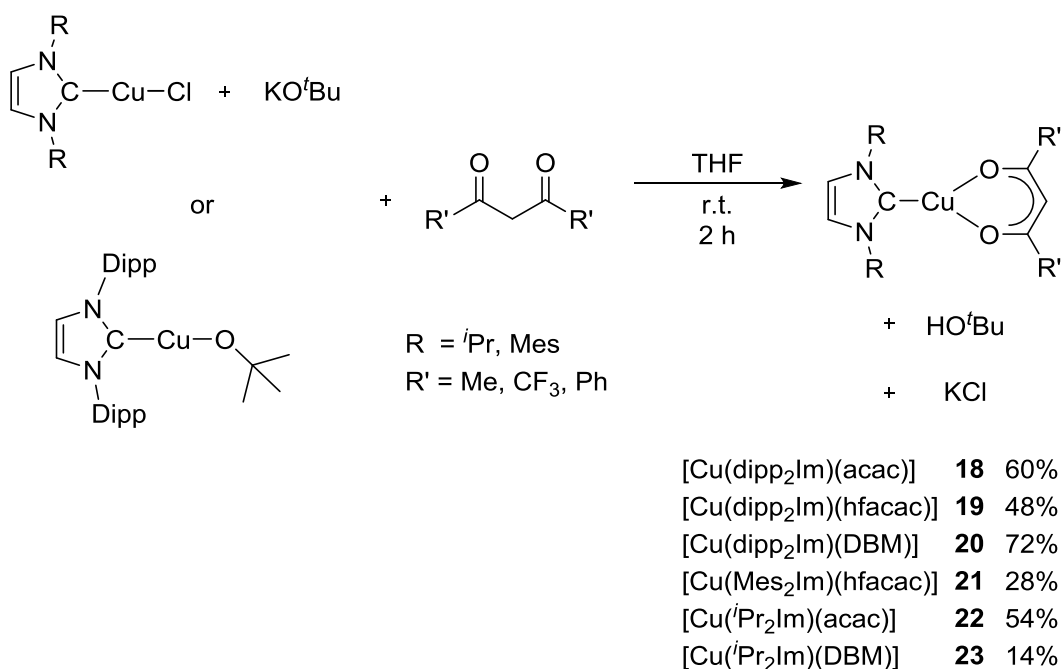
Figure 8: X-ray crystal structure of $[\text{Cu}(\text{Pr}_2\text{Im})(\text{OAc})]$ **17**. Element (color): carbon (grey), nitrogen (blue), oxygen (red), copper (maroon). Hydrogen atoms are omitted for clarity and the thermal ellipsoids are drawn at 50% probability. Only one of the two molecules in the asymmetric unit is shown. Selected bond lengths (Å) and angles (deg): C1–Cu 1.8700(18) [1.8731(18)], Cu–O1 1.8683(13) [1.8713(14)], C1–Cu–O1 177.30(8)° [176.02(7)°].

Compound **17** crystallizes in the monoclinic space group $P2_1/c$ with two molecules in the asymmetric unit with slightly different bond lengths and angles. The distance from the carbonyl oxygen O2 to the copper atom is 2.7628(15) Å [2.8243(16)] with a carbon-oxygen distance of 1.236(3) Å [1.236(3)]. The coordination around the copper atom is close to linear with a C1–Cu–O1 angle of 177.30(8)° [176.02(7)°]. The bond lengths are 1.8700(18) Å [1.8731(18)] for C1–Cu and 1.8683(13) Å [1.8713(14)] for the Cu–O1 bond. The crystal structure reveals a monodentate acetate ligand. A literature search showed that in crystal structures of phosphine-stabilized copper(I) acetate complexes the bidentate binding mode is predominant, but in NHC-stabilized analogs only the monodentate binding mode is found.^[254-255] DFT calculations on a very similar complex ($[\text{Cu}(\text{Me}_2\text{Im})(\text{OAc})]$) performed by Sadighi *et al.* showed that the bidentate binding mode is more stable by just 1.1 kcal/mol with an uncertainty of ± 5 kcal/mol. With both binding modes at almost the same energy and both optimized structures not fitting the bond lengths and angles found in the crystal structure of $[\text{Cu}(\text{Dipp}_2\text{Im})(\text{OAc})]$, they suggest attractive intermolecular interactions between the carbonyl oxygen atom and the backbone proton of a second NHC (2.238 and

2.347 Å for [Cu(Dipp₂Im)(OAc)].^[254] With an intermolecular O-H bond length of 2.2931(14) and 2.2433(13) Å complex **17** shows also short distances, possibly explaining the monodentate binding mode.

3.1.3.3 Synthesis of NHC-stabilized copper(I)-acetylacetonate complexes

Alternative chelating ligands would be acetylacetonate (acac), hexafluoroacetylacetonate (hfacac) or dibenzoylmethane (DBM). These have a low basicity due to delocalization of the negative charge, and the bidentate coordination mode could be useful in chelating boron as well as copper. The synthesis was either done by a literature^[226] approach, starting from [Cu(NHC)(Cl)], KO^tBu and the diones, or by reaction of the isolated alkoxide complex [Cu(Dipp₂Im)(O^tBu)] with the diones (Scheme 28).



Scheme 28: The two applied synthetic pathways to NHC-stabilized copper(I) complexes bearing acetylacetonate derivatives.

Besides NMR spectroscopy and HRMS, the complexes **18-21** and **23** were characterized by X-ray diffraction (Figure 9).

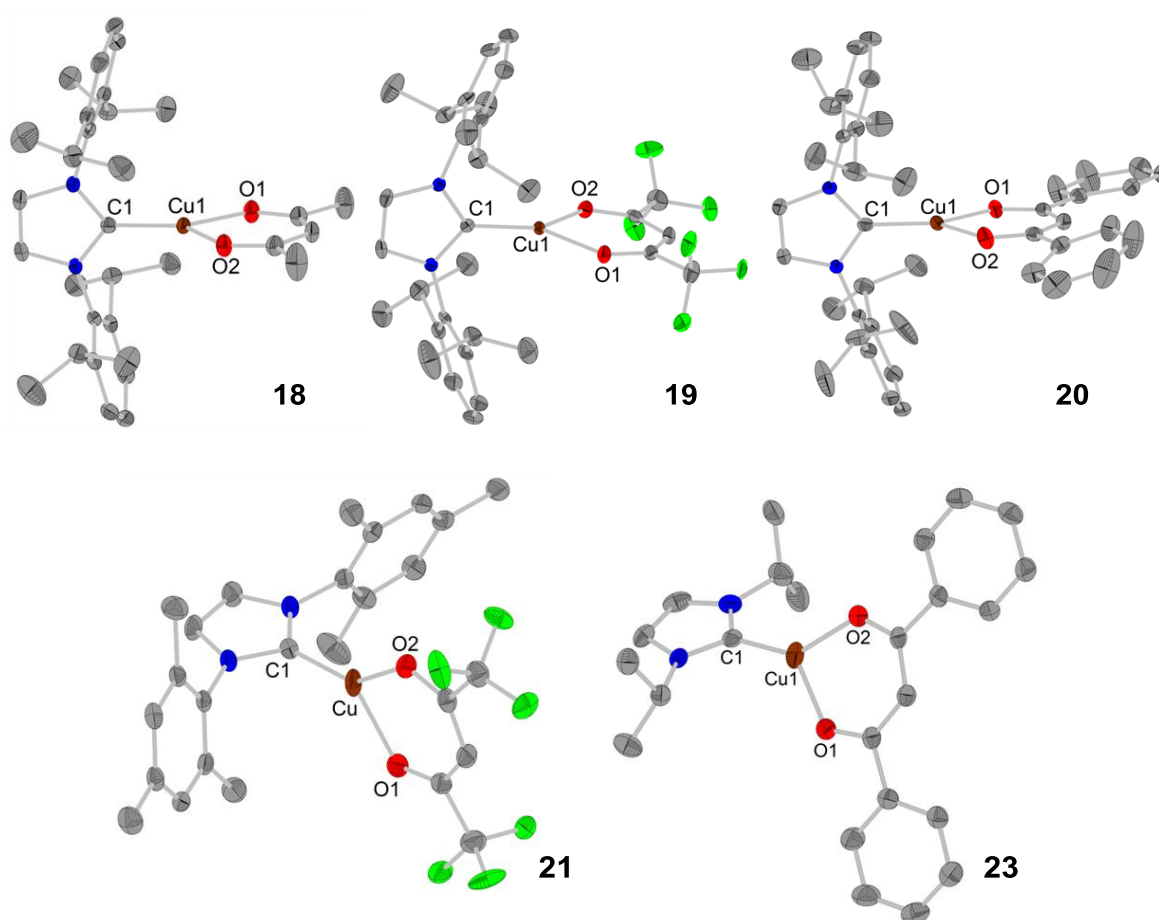


Figure 9: Element (color): carbon (grey), nitrogen (blue), copper (maroon), oxygen (red), fluorine (green). Hydrogen atoms are omitted for clarity and the thermal ellipsoids are drawn at 50% probability. Top right: Molecular structure of $[\text{Cu}(\text{Dipp}_2\text{Im})(\text{acac})]$ **18**. Only one of the two molecules in the asymmetric unit is shown. Selected bond lengths (\AA) and angles (deg): C1-Cu1 1.867(2), Cu1-O1 2.2017(18), Cu1-O2 1.9728(18), C1-Cu1-O1 125.86(8), C1-Cu1-O2 142.40(9), O1-Cu1-O2 91.71(7), NC1N-O1Cu1O2 Top middle: Molecular structure of $[\text{Cu}(\text{Dipp}_2\text{Im})(\text{DBM})]$ **20**. Selected bond lengths (\AA) and angles (deg): C1-Cu1 1.8555(17), Cu1-O1 1.9566(12), Cu1-O2 1.9897(14), C1-Cu1-O1 138.74(7), C1-Cu1-O2 130.74(7), O1-Cu1-O2 90.50(5), NC1N-O1Cu1O2 Top right: Molecular structure of $[\text{Cu}(\text{Dipp}_2\text{Im})(\text{hfacac})]$ **19**. Selected bond lengths (\AA) and angles (deg): C1-Cu1 1.868(3), 1.873(3), Cu1-O1 2.019(3), 2.132(3), Cu1-O2 1.993(3), 1.941(3), C1-Cu1-O1 132.61(13), 152.18(13), C1-Cu1-O2 138.27(13), 118.10(13), O1-Cu1-O2 89.11(10), 87.87(12), NC1N-O1Cu1O2 Bottom left: Molecular structure of $[\text{Cu}(\text{Mes}_2\text{Im})(\text{hfacac})]$ **21**. Selected bond lengths (\AA) and angles (deg): C1-Cu1 1.862(2), Cu1-O1 1.9765(18), Cu1-O2 2.0783(18), C1-Cu1-O1 140.96(9), C1-Cu1-O2 129.54(9), O1-Cu1-O2 89.49(7), NC1N-O1Cu1O2 83.29(8) Bottom right: Molecular structure of $[\text{Cu}(\text{Pr}_2\text{Im})(\text{DBM})]$ **23**. Only one of the three molecules in the asymmetric unit is shown. Selected bond lengths (\AA) and angles (deg): C1-Cu1 1.862(2), 1.875(2), 1.862(3), Cu1-O1 1.9945(19), 1.9774(17), 1.9968(19), Cu1-O2 1.9706(18), 2.0064(18), 2.0121(19), C1-Cu1-O1 130.33(9), 128.60(9), 131.39(10), C1-Cu1-O2 139.15(9), 140.16(9), 138.37(11), O1-Cu1-O2 90.43(7), 90.93(7), 90.17(8), NC1N-O1Cu1O2 47.96(14), 73.34(16), 36.51(15).

A comparison of selected bond lengths and angles is given in Table 4.

Table 4: Comparison of the bond lengths and angles found in NHC-stabilized copper(I) acetylacetonate complexes 18-21 and 23.

	Distance: C1-Cu1 [Å]	Distance: Cu1-O1 [Å]	Distance: Cu1-O2 [Å]	Interplanar-Angle: NC1N-O1Cu1O2 [°]
[Cu(Dipp ₂ Im)(hfacac)] 19	1.868(3) [1.873(3)]	2.019(3) [2.132(3)]	1.993(3) [1.941(3)]	83.27(12) [54.54(16)]
[Cu(Dipp ₂ Im)(DBM)] 20	1.8555(17)	1.9566(12)	1.9897(14)	89.32(6)
[Cu(Dipp ₂ Im)(acac)] 18	1.867(2)	2.0217(18)	1.9728(18)	90.00(6)
[Cu(Mes ₂ Im)(hfacac)] 21	1.862(2)	1.9765(18)	2.0783(18)	83.29(8)
[Cu(ⁱ Pr ₂ Im)(DBM)] 23	1.865(2) [1.875(2)] [1.862(3)]	1.9945(19) [1.9774(17)] [1.9968(19)]	1.9706(18) [2.0064(18)] [2.0121(19)]	47.96(14) [73.34(16)] [36.51(15)]

In all cases the typical bidentate binding mode of the acac ligands is observed, with the sum of the angles around the trigonal planar metal center being 358.15° to 360°. The Dipp₂Im ligated complex **20** bearing the larger DBM ligand shows the shortest C1-Cu (1.8555 Å) as well as (mean) Cu-O distance (1.9732 Å). Compared to the monodentate [Cu(ⁱPr₂Im)(OAc)] **17** (1.8698 Å) and [Cu(^tBu₂Im)(O^tBu)] **16** (1.813 Å) copper(I) base complexes, the Cu-O bond lengths found in copper(I) acac type complexes **18** - **21** and **23** are significantly longer (average: 2.0025 Å).

3.1.4 Synthesis of NHC-stabilized copper(I)-aryl complexes

For insights into the mechanism of copper(I) catalyzed cross-coupling reactions of aryl boronates with aryl or alkyl halides it is important to determine and understand the individual steps of the catalytic cycle. As mentioned earlier, stoichiometric model reactions could help to identify intermediates especially with a (related) system that forms more

stable intermediates. The reaction of an L-copper(I) aryl complex with an aryl halide seems to be essential for the cross-coupling reaction. The barrier to this step was calculated (DFT) to be higher in energy than the reaction of the L-Cu-OR with an organoboronate,^[256] which makes this reaction the rate determining step of the process. For this reason, it was necessary to synthesize and characterize different complexes of the type [Cu(NHC)(Ar)], which could then be used for determining the rate of the reaction with a range of aryl or alkyl halides. The fact that examples of these compounds are rare means that their synthesis has to be studied, and reliable, repeatable routes have to be developed.

Three different syntheses of the NHC-stabilized copper(I) aryl complexes were investigated. The first one was the addition of a free carbene to a copper(I) aryl compound (Figure 10). The second was a transmetalation reaction, between a [Cu(NHC)(O^tBu)] complex and an organo boronic ester reagent. Finally, the synthesis of an aryl complex was attempted by adding an aryl Grignard reagent to an NHC-stabilized copper(I) halide complex under salt elimination conditions.

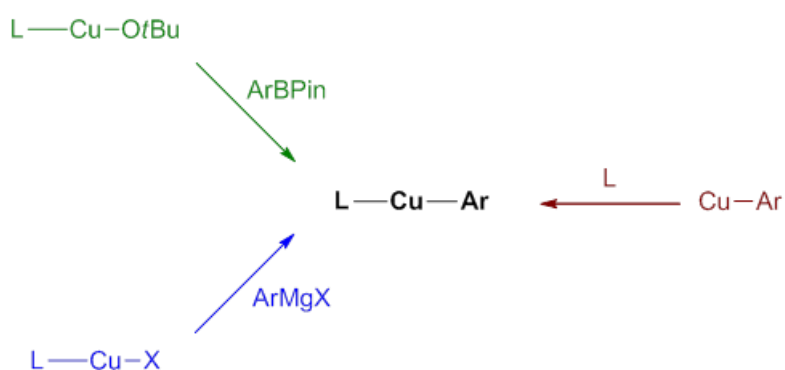
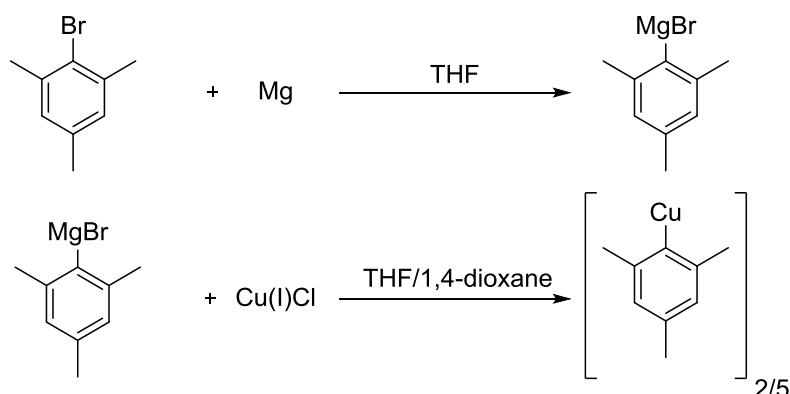


Figure 10: The three plausible routes to NHC-stabilized copper(I) aryl complexes.

3.1.4.1 Synthesis of [Cu(NHC)(Ar)] via reaction of a free carbene and a copper aryl compound

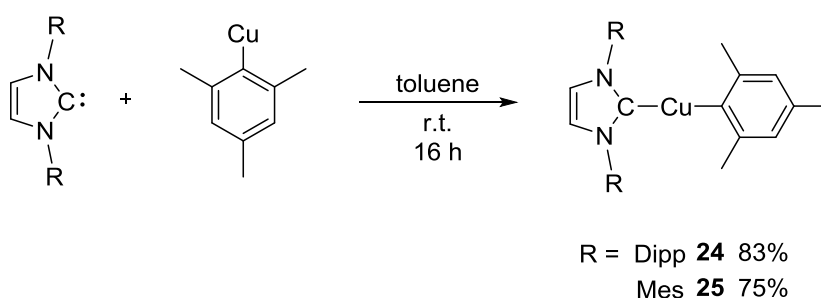
Mesityl copper(I) was synthesized from copper(I) chloride and the mesityl Grignard reagent (Scheme 29).^[257] The product was obtained as light yellow crystals, which were characterized by ¹H and ¹³C{¹H} NMR spectroscopy. The literature known modes of

aggregation (pentameric and dimeric) of mesitylcopper(I) in solution were observed in the ^1H NMR spectrum in C_6D_6 .^[258]



Scheme 29: Synthesis of mesitylcopper(I) via a Grignard reagent.

In analogy with literature reports, one equivalent of Dipp_2Im and Mes_2Im , respectively, in toluene was added to a solution of one equivalent of mesitylcopper(I) in toluene, to afford $[\text{Cu}(\text{Dipp}_2\text{Im})(\text{Mes})]$ **24** and $[\text{Cu}(\text{Mes}_2\text{Im})(\text{Mes})]$ **25**, respectively, as white solids.^[259]



Scheme 30: Synthesis of $[\text{Cu}(\text{Dipp}_2\text{Im})(\text{Mes})]$ **24 and $[\text{Cu}(\text{Mes}_2\text{Im})(\text{Mes})]$ **25**.**

The compounds were characterized by HRMS and NMR spectroscopy. It was also possible to obtain single crystals of **24** and **25** suitable for X-ray diffraction. The molecular structures of these complexes are shown in Figure 11.

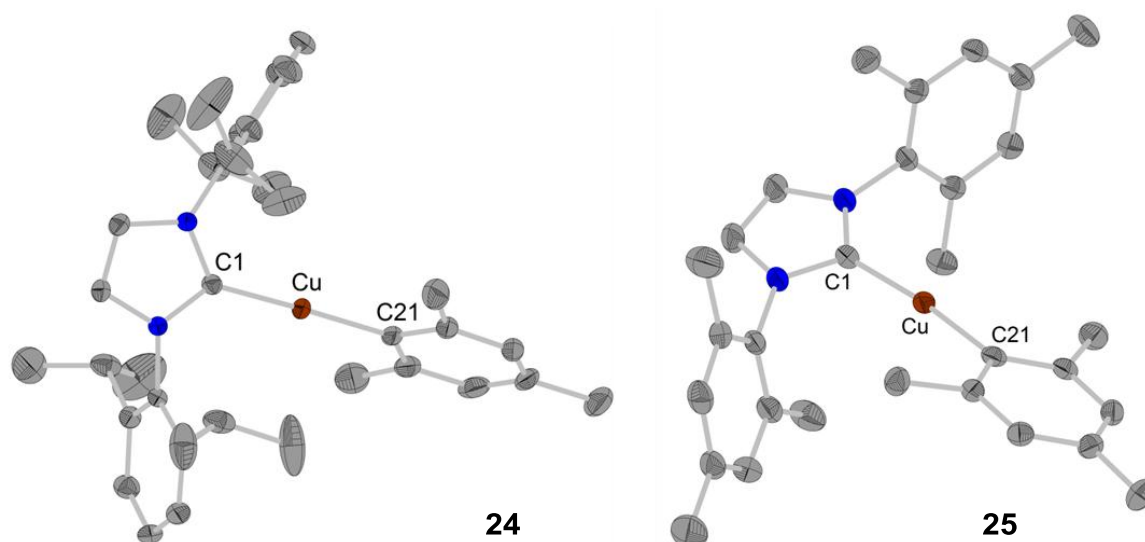
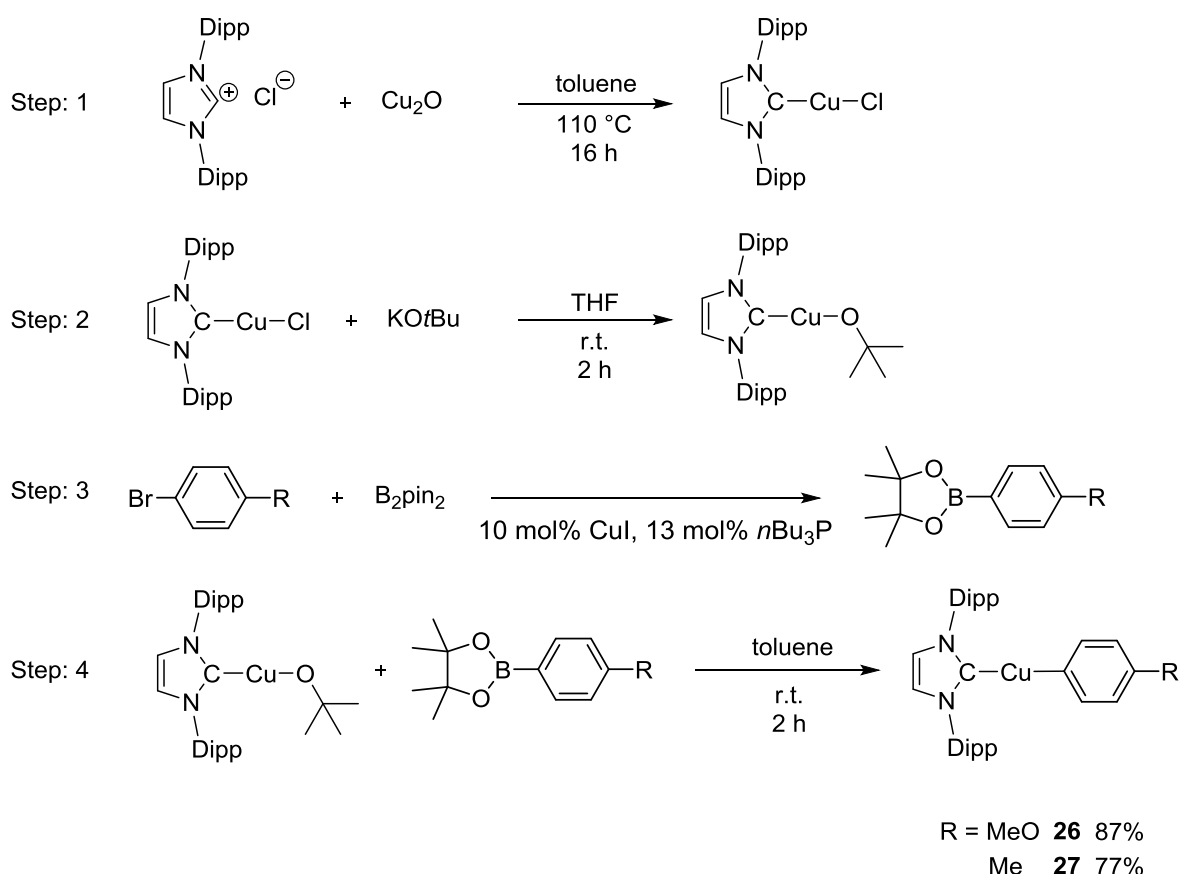


Figure 11: Element (color): carbon (grey), nitrogen (blue), copper (maroon). Hydrogen atoms are omitted for clarity and the thermal ellipsoids are drawn at 50% probability. Left: Molecular structure of $[\text{Cu}(\text{Dipp}_2\text{Im})(\text{Mes})]$ **24**. Selected bond lengths (\AA) and angles (deg): Cu–C1 1.9008(18), Cu–C21 1.9188(18), C1–Cu–C21 177.60(7). Right: Molecular structure of $[\text{Cu}(\text{Mes}_2\text{Im})(\text{Mes})]$ **25**. Only one of the two molecules in the asymmetric unit is shown. Selected bond lengths (\AA) and angles (deg): Cu–C1 1.895(2) [1.898(2)], Cu–C21 1.919(2) [1.916(2)], C1–Cu–C21 173.58(10) [176.64(10) $^\circ$].

3.1.4.2 Synthesis of $[\text{Cu}(\text{NHC})(\text{Ar})]$ via reaction of copper(I)-alkoxides with organoboron reagents

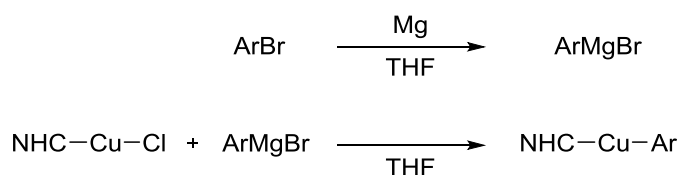
According to a literature procedure, $[\text{Cu}(\text{Dipp}_2\text{Im})(4\text{-MeO-C}_6\text{H}_4)]$ **26** was synthesized in four steps (Scheme 31).^[260] Firstly, the reaction of the NHC hydrochloride salt with copper(I) oxide in hot toluene was carried out to form the NHC-stabilized copper(I)-chloride.^[235] Secondly, the alkoxide complex was then synthesized by addition of potassium *tert*-butoxide in THF. Thirdly, the copper-catalyzed borylation of 1-bromo-4-methoxybenzene with bis(pinacolato)diboron was conducted, which had been established earlier by Marder *et al.*^[151] Finally, **26** was obtained in 87% yield from the reaction of the copper(I) alkoxide complex with 4-MeO-C₆H₄Bpin in toluene at room temperature.^[260] In a similar manner $[\text{Cu}(\text{Dipp}_2\text{Im})(4\text{-Me-C}_6\text{H}_4)]$ **27** was synthesized. The products were characterized by NMR spectroscopy and HRMS.



Scheme 31: Four step synthesis of $[\text{Cu}(\text{Dipp}_2\text{Im})(4\text{-R-C}_6\text{H}_4)]$ **26** and **27** (R = MeO, Me) using organoboron reagents.

3.1.4.3 Synthesis of $[\text{Cu}(\text{NHC})(\text{Ar})]$ via copper(I)-halides and Grignard reagents

All NHC-stabilized copper(I) aryl complexes in this section were synthesized from the NHC-copper chloride and the corresponding Grignard reagents, which were obtained from magnesium and the aryl bromide in THF (Scheme 32). The Grignard reagent was prepared immediately before use and the concentration was determined by hydrolysis of a defined volume of the reagent followed by titration with 0.1 M hydrochloric acid using phenolphthalein as the indicator.



Scheme 32: General synthetic route to $[\text{Cu}(\text{NHC})(\text{Ar})]$ complexes using Grignard reagents.

With this route it was possible to synthesize [Cu(Dipp₂Im)(*p*-tolyl)] **27**, [Cu(Mes₂Im)(*p*-tolyl)] **28**, [Cu(Dipp₂Im)(C₆F₅)] **29**, [Cu(Mes₂Im)(C₆F₅)] **30**, [Cu(Dipp₂Im)(4-CF₃-C₆H₄)] **31**, [Cu(Mes₂Im)(4-CF₃-C₆H₄)] **32**, [Cu(Dipp₂Im)(3,5-(CF₃)₂-C₆H₃)] **33**, [Cu(Mes₂Im)(3,5-(CF₃)₂-C₆H₃)] **34**, [Cu(Dipp₂Im)(Dipp)] **35**, [Cu(Mes₂Im)(Dipp)] **36**, [Cu(^{*t*}Bu₂Im)(Dipp)] **37**, [Cu(Dipp₂Im)(duryl)] **38**, [Cu(Mes₂Im)(duryl)] **39**, [Cu(^{*i*}Pr₂Im)(duryl)] **40**, [Cu(Dipp₂Im)(C₆Me₅)] **41**, [Cu(Mes₂Im)(C₆Me₅)] **42**, [Cu(^{*t*}Bu₂Im)(C₆Me₅)] **43**, and [Cu(^{*i*}Pr₂Im)(C₆Me₅)] **44**. For complexes **29**, **30**, **33**, **37**, **40** and **42** it was possible to grow single crystals suitable for X-ray diffraction. The structures are shown in Figures 12 and 13.

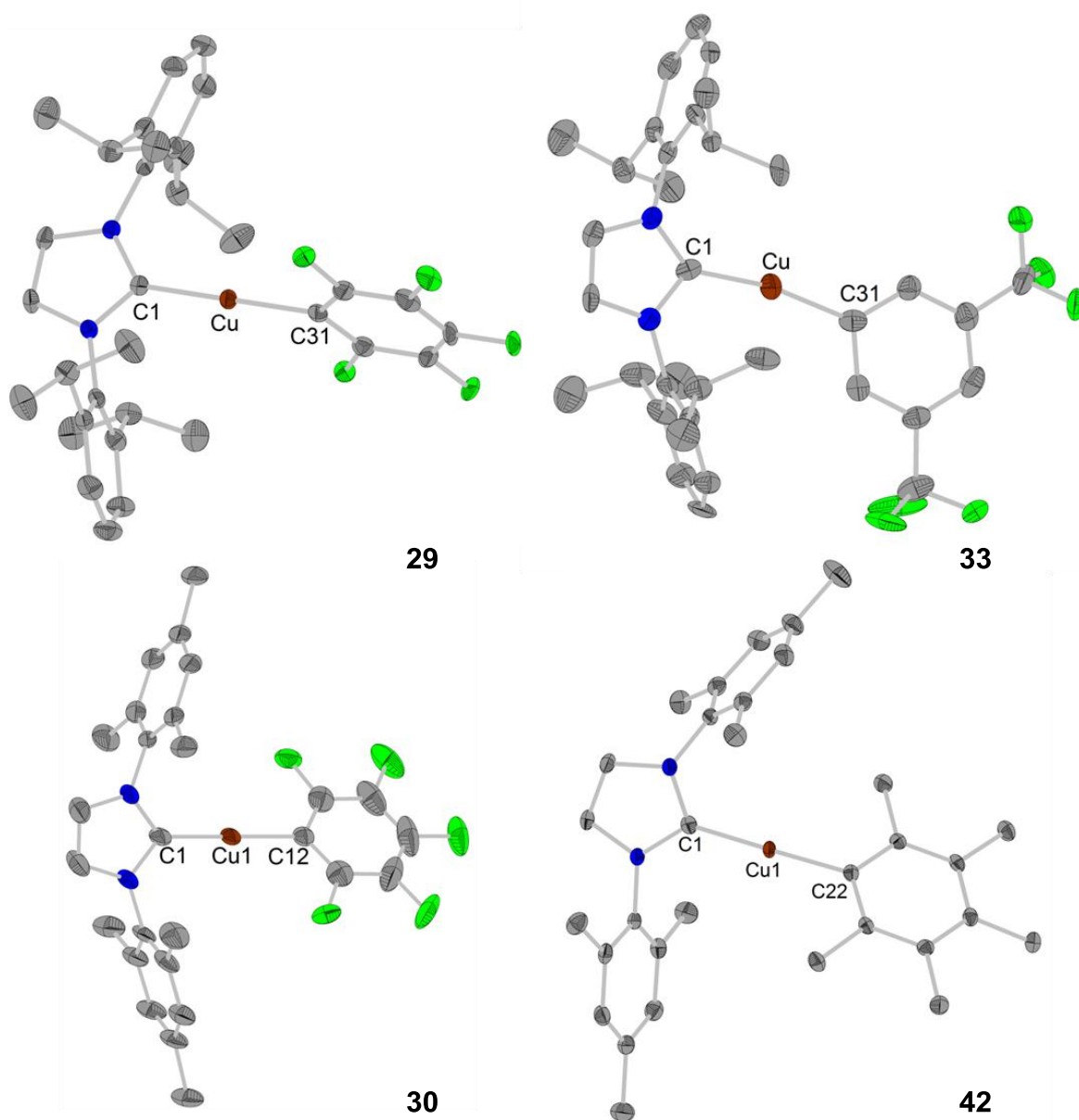


Figure 12: Element (color): carbon (grey), nitrogen (blue), copper (maroon), fluorine (green). Hydrogen atoms are omitted for clarity and the thermal ellipsoids are drawn at 50% probability. Top left: Molecular structure of [Cu(Dipp₂Im)(C₆F₅)] **29**. Selected bond lengths (Å) and angles (deg): C1–Cu 1.906(3), Cu–C31 1.915(3), C1–Cu–C31 180.00°. Top right: Molecular structure of [Cu(Dipp₂Im)(3,5-(CF₃)₂-C₆H₄)] **33**. Only one of the two molecules in the asymmetric unit is shown. Selected bond lengths (Å) and angles (deg): C1–Cu

1.876(12) Å [1.844(12)], Cu–C31 1.936(13) Å [1.912(13)], 168.6(5)° [166.2(6)°]. Bottom left: Molecular structure of [Cu(Mes₂Im)((C₆F₅)] 30. Selected bond lengths (Å) and angles (deg): C1–Cu1 1.888(5) Å, Cu–C12 1.952(5) Å, C1–Cu1–C12 180.00(0). Bottom right: Molecular structure of [Cu(Mes₂Im)(C₆Me₅)] 43. Selected bond lengths (Å) and angles (deg): Cu–C1 1.8961(16), Cu–C22 1.9182(15), C1–Cu–C22 179.14(7), NC1N–CC22C 37.40(7).

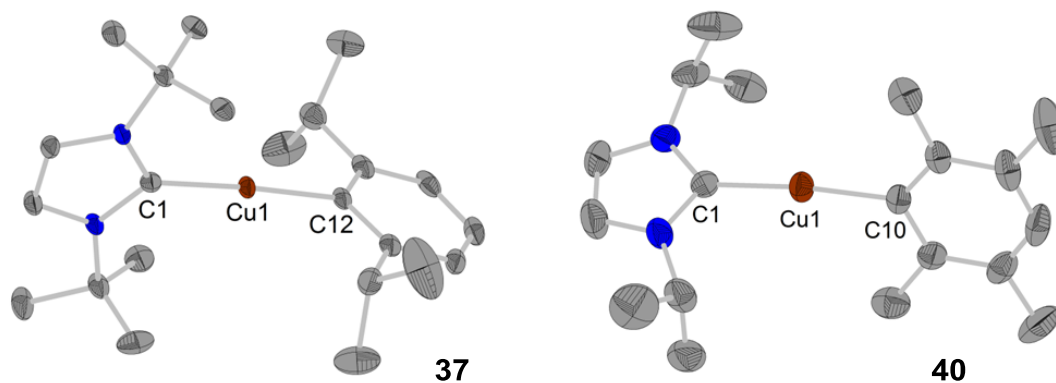


Figure 13: Element (color): carbon (grey), nitrogen (blue), copper (maroon), fluorine (green). Hydrogen atoms are omitted for clarity and the thermal ellipsoids are drawn at 50% probability. Left: Molecular structure of [Cu(^tBu₂Im)(Dipp)] 37. A minor disordered part is omitted for clarity. Selected bond lengths (Å) and angles (deg): Cu–C1 1.905(4), Cu–C12 1.930(4), C1–Cu–C12 175.62(15), NC1N–CC12C 90.00(10). Right: Molecular structure of [Cu(ⁱPr₂Im)(duryl)] 40. A minor disordered part is omitted for clarity. Selected bond lengths (Å) and angles (deg): Cu–C1 1.906(4), Cu–C10 1.919(3), C1–Cu–C10 174.53(14), NC1N–CC10C 65.9(2).

A comparison of selected bond lengths and angles as well as NMR spectroscopic data of the synthesized [Cu(NHC)(Ar)] complexes is given in Table 5.

3 Results and Discussion

Table 5: Comparison of NMR spectroscopic data and of the bond lengths and angles of NHC-stabilized copper(I) aryl complexes.

	$^{13}\text{C}\{^1\text{H}\} -$ NMR: C_{NHC}	Distance: C1-Cu [Å]	Distance: Cu- $C_{(\text{Ar})}$ [Å]	Angle: C1-Cu- $C_{(\text{Ar})}$ [°]	Interplanar Angle: NC1N- $\text{CC}_{(\text{Ar})}\text{C}$ [°]
[Cu(Dipp ₂ Im)(Mes)] 24	186.4	1.9008(18)	1.9188(18)	177.60(17)	64.56(7)
[Cu(Mes ₂ Im)(Mes)] 25	184.7	1.895(2) 1.898(2)	1.919(2) 1.916(2)	173.58(10) 176.64(10)	32.93(8) 28.40(8)
[Cu(Dipp ₂ Im)(4-MeO-C ₆ H ₄)] 26 ^[260]	186.2	1.903(4)	1.913(4)	177.27(16)	
[Cu(Dipp ₂ Im)(<i>p</i> -tolyl)] 27	186.0				
[Cu(Mes ₂ Im)(<i>p</i> -tolyl)] 28 ^[261]	184.3				
[Cu(Dipp ₂ Im)(C ₆ F ₅)] 29	183.1	1.906(4)	1.915(4)	180	75.90(8)
[Cu(Mes ₂ Im)(C ₆ F ₅)] 30	181.5	1.888(5)	1.953(5)	180	38.58(11)
[Cu(Dipp ₂ Im)(4-CF ₃ -C ₆ H ₄)] 31	185.0				
[Cu(Mes ₂ Im)(4-CF ₃ -C ₆ H ₄)] 32	183.3				
[Cu(Dipp ₂ Im)(3,5-(CF ₃) ₂ -C ₆ H ₃)] 33	186.4	1.904(3)	1.918(3)	166.50(11)	7.1(2)
[Cu(Mes ₂ Im)(3,5-(CF ₃) ₂ -C ₆ H ₃)] 34	183.0				
[Cu(Dipp ₂ Im)(Dipp)] 35	185.8				
[Cu(Mes ₂ Im)(Dipp)] 36	183.8				
[Cu(^t Bu ₂ Im)(Dipp)] 37	180.1	1.905(4)	1.930(4)	175.62(15)	90.00(10)
[Cu(Dipp ₂ Im)(duryl)] 38	186.4				
[Cu(Mes ₂ Im)(duryl)] 39	184.7				
[Cu(ⁱ Pr ₂ Im)(duryl)] 40	179.4	1.906(4)	1.919(3)	174.53(14)	65.9(2)
[Cu(Dipp ₂ Im)(C ₆ Me ₅)] 41	186.6				
[Cu(Mes ₂ Im)(C ₆ Me ₅)] 42	184.9	1.8961(16)	1.9182(15)	179.14(7)	37.40(7)
[Cu(^t Bu ₂ Im)(C ₆ Me ₅)] 43	180.5				
[Cu(ⁱ Pr ₂ Im)(C ₆ Me ₅)] 44	179.7				

In the $^{13}\text{C}\{^1\text{H}\}$ NMR spectra the carbene-carbon atoms were detected within a range of 7 ppm. The $^i\text{Pr}_2\text{Im}$ ligand shows the lowest chemical shift (178.4 – 179.7 ppm), followed by $^t\text{Bu}_2\text{Im}$ (180.1 – 180.5 ppm). The larger Mes_2Im and Dipp_2Im NHCs showed resonances for their carbene-carbon atoms at higher chemical shifts (181.5 – 186.6 ppm).

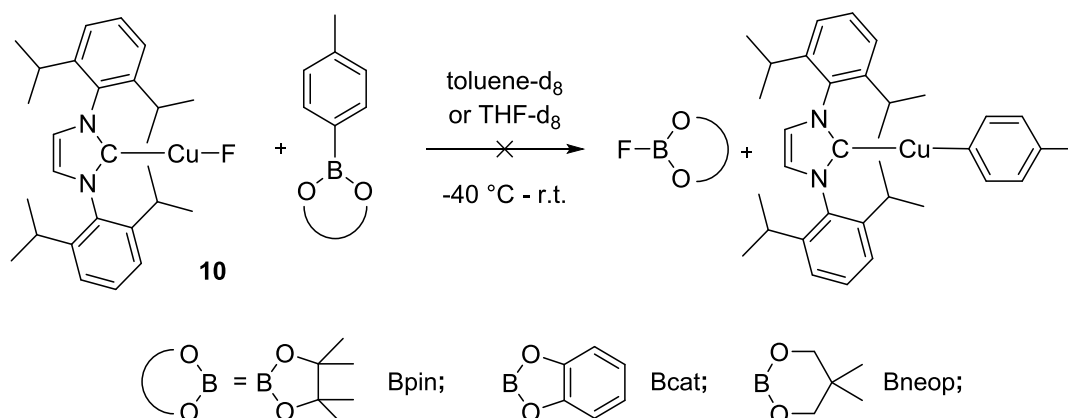
In complex $[\text{Cu}(\text{Dipp}_2\text{Im})(\text{Mes})]$ **24** and $[\text{Cu}(\text{Mes}_2\text{Im})(\text{Mes})]$ **25**, wherein the aryl ligand is mesityl, a correlation of the steric demand of the NHC and the interplanar angle is observed. In complex **24**, with the *ortho-iso*-propyl groups of the Dipp_2Im ligand pointing towards the central atom, the interplanar angle is 64.56° , while in **25**, with *ortho*-methyl groups an angle of 32.93 and 28.40° , respectively, was observed. In complex **24** (1.9188 \AA) as well as in **25** (average: 1.9175 \AA) the Cu-C_{Ar} distances are, compared to the ones found in tetrameric CuMes_4 (in average: 1.9925 \AA), shortened by 0.074 and 0.075 pm , respectively.^[257] For comparison the only structurally characterized phosphine copper aryl complex $[\text{Cu}(\text{PPh}_3)(\text{Dmp})]$ ($\text{Dmp} = 2,6\text{-Mes}_2\text{C}_6\text{H}_3$) has a Cu-C_{Ar} distance of $1.922(3) \text{ \AA}$ and is slightly bent at the copper center $168.82(8)^\circ$.^[259] In complex $[\text{Cu}(^t\text{Bu}_2\text{Im})(\text{Dipp})]$ **37** the sterically demanding Dipp moiety has the largest interplanar angle of 90° . In complex $[\text{Cu}(\text{Dipp}_2\text{Im})(3,5\text{-(CF}_3)_2\text{-C}_6\text{H}_3)]$ **33**, wherein the aryl moiety is *ortho* H-substituted, this angle is only 7.1° . Complex **33** also shows the smallest angle around the copper atom of 166.5° .

3.2 Reactivity of NHC-stabilized copper(I) complexes

In stoichiometric model reactions well-defined copper(I) complexes were tested against various substrates to help understand their basic reactivity as well as possible interactions in catalytic reactions.

3.2.1 Reactivity of NHC-stabilized copper(I)-fluoride with boron compounds

Giri *et al.* demonstrated that the complex [Cu(PN)F]-complex (PN = *o*-di-*iso*-propylphosphino-*N,N*-dimethylbenzamine) reacts with aryl-Bneop to form [Cu(PN)(Ar)] quantitatively.^[169] In order to understand the reactivity of the [Cu(Dipp₂Im)(F)] with organoboronic esters, stoichiometric reactions with *p*-tolylBpin, *p*-tolylBcat and *p*-tolylBneop were carried out (Scheme 33). After the precooled solvent was added to the precooled reaction mixture, ¹H, ¹⁹F and ¹¹B VT-NMR spectra were recorded immediately. The samples were checked for any precipitate before the measurement at low temperature (-78°C) and at the end of the measurement (room temperature) to keep the temperature during the measurement as constant as possible. Thereby it was not possible to determine what the state of aggregation was while the measurement took place, something which has to be taken into account when interpreting the data. Unless stated otherwise, the depicted state of aggregation refers to observations from both before and after the measurement.



Scheme 33: *In situ* VT-NMR monitored reactions of complex 10 with different organoboronic esters.

The *in situ* VT-NMR monitored reactions of complex **10** with *p*-tolylBpin, *p*-tolylBcat and *p*-tolylBneop showed different reactivity in toluene- d_8 than in THF- d_8 (see Appendix Figures 60 to 84 for detailed spectra). In toluene- d_8 poor solubility of the intermediates was observed as white precipitates formed for *p*-tolylBcat and *p*-tolylBneop and gel formation was observed in the case of *p*-tolylBpin. In THF- d_8 clear solutions were obtained for *p*-tolylBcat and *p*-tolylBneop, while for *p*-tolylBpin a white precipitate was observed. In all cases the Cu-F signal (-240 ppm) in the ^{19}F NMR spectra was absent from the start at low temperature, indicative of a fast reaction of the two components. In none of the reactions in toluene- d_8 was the desired reactivity forming the copper aryl complex and the corresponding F-B(OR) $_2$ moiety observed, but either broad signals or signals which could not be assigned to specific compounds were detected (see Appendix Figures 60 to 70). In the reaction of **10** with *p*-tolylBcat the signals in the ^{19}F NMR spectra showed proton coupling (see Appendix Figure 66), while the signals in the ^{19}F NMR spectra of the reaction with *p*-tolylBneop boron coupling (see Appendix Figure 70) was observed. The coupling to different nuclei in similar reactions indicate that various reactions pathways do occur. This plus the fact that poor solubility was observed make it difficult to draw conclusions from that data for the reactions in toluene- d_8 .

In the reaction of complex **10** with *p*-tolylBpin and *p*-tolylBneop in THF- d_8 the formation of the desired complex $[\text{Cu}(\text{Dipp}_2\text{Im})(p\text{-tolyl})]$ was detected (Figure 14).



Figure 14: Comparison of the ^1H NMR spectrum of complex $[\text{Cu}(\text{Dipp}_2\text{Im})(p\text{-tolyl})]$ **27** (middle) with *in situ* ^1H VT-NMR spectrum of the reaction of $[\text{Cu}(\text{Dipp}_2\text{Im})\text{F}]$ with *p*-tolylBneop (top) and *in situ* ^1H VT-NMR spectrum of the reaction of $[\text{Cu}(\text{Dipp}_2\text{Im})\text{F}]$ with *p*-tolylBpin (bottom) in THF- d_8 at room temperature.

In both cases product formation was observed once the samples were heated to room temperature. However, the reactions did not show full conversion 24 h later and no further increase of product formation was observed. The ratio of the septet of the aryl complex and another septet, which could not be assigned to a specific compound, is 1:2.4 for the reaction with *p*-tolylBpin and 1:1.7 for the reaction with *p*-tolylBneop. Two days later no considerable changes in the ratios were observed. The ^{11}B NMR spectra showed three peaks at 3.4, 21.6 and 32.0 ppm in the reaction with *p*-tolylBpin and among other four peaks at -0.8, -0.3, 16.9 and 26.7 ppm in the case of *p*-tolylBneop. These signals as well as the signals in the ^{19}F NMR spectra (at -123.8, -140.6 and -145.4 ppm for the reaction with *p*-tolylBpin and among other at -144.0, -146.1, -147.7 and -154.6 ppm for the reaction with *p*-tolylBneop) and the additional set of signal in the ^1H NMR spectra could not be assigned to specific compounds. No signals for the expected byproducts FBpin (^{11}B : 22.3 ppm; ^{19}F : -150.9 ppm in THF- d_8) and FBneop (^{11}B : 19.1 ppm; ^{19}F : -150.6 ppm in DMF- d_7) were

detected.^[169, 192, 262-263] Although the desired products were observed and identified via comparison with the complex of interest the reactivity goes beyond the equation in Scheme 33. That clearly shows that both substances show high reactivity and that the reaction pathways (the desired as well as unexpected ones) are similar in activation energies as they do occur under identical reaction conditions.

The solutions of the fluorine complex $[\text{Cu}(\text{Dipp}_2\text{Im})(\text{F})]$ with *p*-tolylBcat showed one signal at -138.7 ppm (plus a shoulder at 0.07 ppm downfield) in the ^{19}F NMR spectra and two broad signals in the ^{11}B NMR spectra at 32.1 and 9.8 ppm throughout the entire temperature range. The signal at -138.7 ppm in the ^{19}F NMR spectrum and the singlet in the ^{11}B NMR spectrum at 9.8 ppm might arise from a fluorine adduct of *p*-tolylBcat, since $\text{Cs}[(p\text{-tolylBpin})(\text{F})]$ was observed at -133.0 and 7.0 ppm, respectively (in DMSO).^[264] In the ^1H NMR spectra sharp signals (from -50 to -10 °C) for one Dipp_2Im moiety, two catecholate moieties and two *p*-tolyl moieties were detected in a 1.6:1.5:1.2:1.5:1 ratio. Three more signals in the aromatic region were detected which could not be assigned to specific moieties (Figure 15).

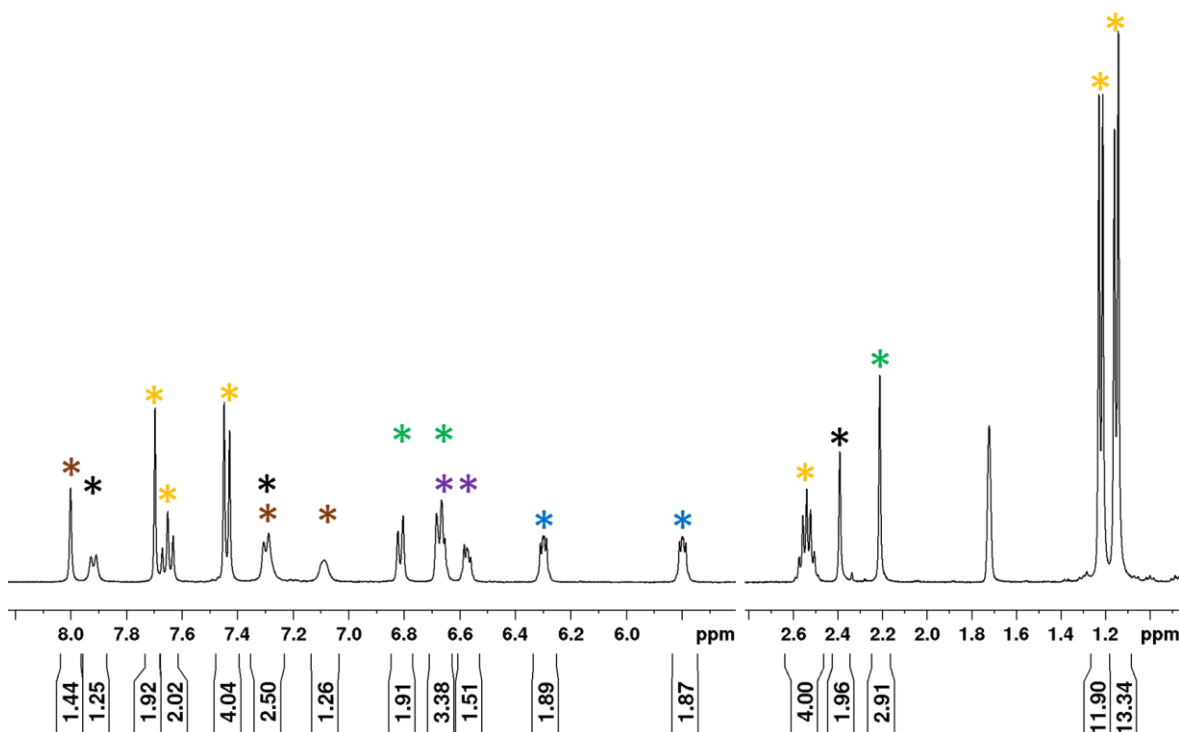
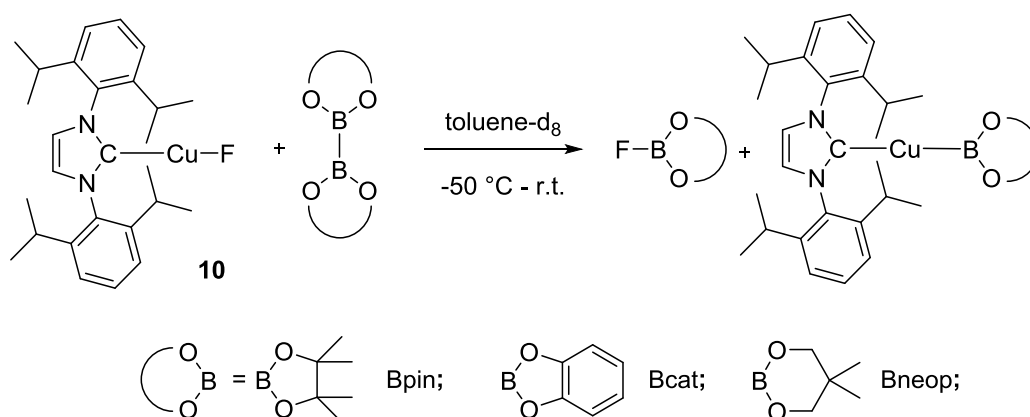


Figure 15: *In situ* ^1H NMR spectrum of the reaction of $[\text{Cu}(\text{Dipp}_2\text{Im})\text{F}]$ with *p*-tolylBcat in THF-d_8 at -10 °C. orange asterisk for the Dipp moiety; blue and purple asterisk for the catecholate moieties; green and black asterisk for the *p*-tolyl moieties, brown asterisk for signals not assigned.

From room temperature on signals in the ^1H NMR spectra were broadened and new sharp signals with catecholate coupling pattern were detected within the next 24 h next to the mentioned resonances. In the ^{11}B and ^{19}F NMR spectra multiple new signals were detected after 24 h at room temperature. This reactions shows interesting and relative selective reactivity (until the sample was heated to room temperature), albeit the formation of a copper(I) aryl complex was not observed and the reaction pathway remains unclear.

In several *in situ* VT-NMR monitored reactions in toluene- d_8 , complex **10** was tested for reactivity with diboron compounds from $-50\text{ }^\circ\text{C}$ to room temperature (Scheme 34).



Scheme 34: *In situ* VT-NMR monitored reactions of complex **10** with different diboron compounds.

The reactions showed that complex **10** is highly reactive towards diboron compounds, as the signal for the Cu-F moiety was not observed, but multiple signals between -118.1 and -140.9 ppm were detected at $-50\text{ }^\circ\text{C}$ in the ^{19}F NMR spectra. In the ^{11}B NMR spectra at $-50\text{ }^\circ\text{C}$ peaks were detected between 32.3 ppm and 0.0 ppm. However at higher temperatures multiple signals in the ^{11}B as well as in the ^{19}F NMR spectra were observed for all reactions, which could not be assigned to specific compounds (see Appendix Figures 85 to 93). In the case of B_2pin_2 , besides peaks in the ^{11}B NMR spectra at 4.2 , 21.1 , 21.7 and 31.3 ppm a broad resonance at 41.8 ppm was detected at room temperature. This is indicative for a copper boryl complex. The literature known boryl complex $[\text{Cu}(\text{Dipp}_2\text{Im})(\text{Bpin})]$ shows resonance in the ^{11}B NMR spectrum in C_6D_6 at 41.7 ppm.^[265] The high number of signals in all spectra showed that multiple reaction pathways were observed and that the formed products are not stable in solution. The instability of *in situ*

formed fluoro-boronic ester moieties was observed previously in borylation reactions of diazonium salts with the fluoride adduct of B₂pin₂.^[192] Herein, the Lewis acidic FBpin species abstracts another fluoride to give F₂Bpin⁻. However, the reaction pathways in this reactions remains unclear. The lability of similar NHC stabilized copper(I) boryl species in solution at room temperature is documented as well.^[238, 265-266]

The stoichiometric *in situ* VT-NMR monitored reactions of [Cu(Dipp₂Im)F] **10** with aryl boronic esters and diboron compounds showed high reactivity even below -50 °C. Furthermore, the solvent not only has an impact on the solubility of the starting materials and intermediates but also on the reaction and with that on its outcome. The high number of intermediates and reaction products showed that multiple reaction pathways are present, which apparently are similar in activation energies. The reactions with aryl boronic ester showed that transmetalation does occur as an NHC stabilized copper(I) aryl complex was formed. In the stoichiometric reaction of **10** with diboron compounds most reaction pathways remain unclear, but it shows that at least in the case of B₂pin₂ boryl formation does occur. Both observations could show application in NHC-stabilized copper(I) catalytic reactions.

3.2.2 Reactivity of NHC-stabilized copper(I)-base complexes with diboron(4) compounds

In model stoichiometric reactions it was observed that copper(I) boryl species play a crucial role in the catalytic cycle.^[151] As of yet there are only a few NHC stabilized copper(I)-boryl complexes that have been isolated and characterized in detail.^[238, 265-272] The molecular structure of the NHC-stabilized copper(I) boryl complexes [Cu(Dipp₂Im)(Bpin)], [Cu(Dipp₂ImCl₂)(Bpin)] and [Cu(Dipp₂Im)(Bneop)] derived from B₂pin₂ and B₂neop₂, respectively, have been studied by X-ray diffraction.^[238, 265, 271] From unsymmetric diboron compounds Kleeberg *et al.* was able to synthesize the diamino-boryl complexes [Cu(Dipp₂Im)(dmab)], [Cu(Dipp₂Im)(dbab)], [Cu(Dipp₂Im){B(NCH₃CH₂)₂}], [Cu(^tBu₂Im)(dmab)] and [Cu(^s/Pr₂Im){B(NCH₃CH₂)₂}].^[269, 271] The copper(I) complexes [Cu(^sDipp₂Im)₂(μ-Bcat)][BF₄], [Cu(ⁱPr₂ImMe₂)₂(μ-dmab)₂], [Cu(ⁱPr₂ImMe₂)₂(μ-Bpin)₂] and

[Cu(^tBu₂Im)₂(μ-Bpin)₂], where the boryl moiety shows a bridging coordination, were investigated by Sadighi *et al.* as well as Kleeberg and coworkers.^[266, 271] From lithium boryl compounds the NHC-stabilized boryl complexes [Cu(Mes₂Im){B(NDippCH)₂}] and [Cu(Mes₂Im){B(NDippCH₂)₂}] were synthesized and, interestingly, the bromo and cyano stabilized complexes [Li(THF)₃][Cu{B(NDippCH₂)₂}(Br)] and [Li(THF)₃][Cu{B(NDippCH)₂}(CN)] were also obtained via this route.^[267-268, 270, 272] In Table 6 an overview of literature known NHC-stabilized copper(I) boryl complexes is given.

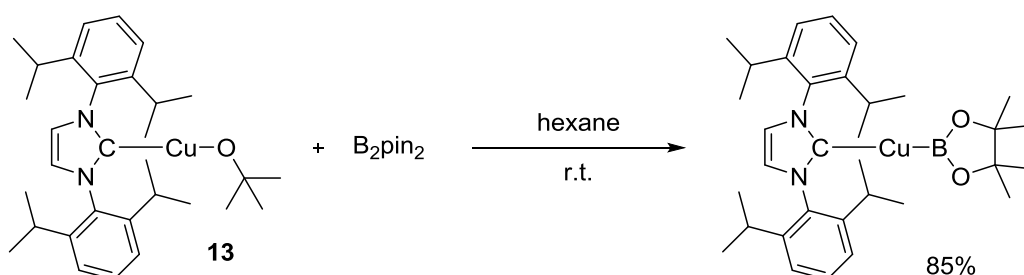
3 Results and Discussion

Table 6: Overview of known copper(I) boryl complexes. *fast decomposition in solution was observed, therefore only characterized by ¹H NMR (no ¹³C or ¹¹B NMR spectra).^[238] **no analytical data published.^[265]

	¹¹ B NMR:	Distance: Cu-B [Å]	Distance: Cu-C _{NHC} [Å]	Angle: C _{NHC} -Cu-B [°]
[Cu(Dipp ₂ Im)(Bpin)]	41.7 (C ₆ D ₆)	2.002(3)	1.937(2)	168.07(10)
[Cu(Dipp ₂ ImCl ₂)(Bpin)]	-	2.001(3)	1.923(4)	165.51(15)
[Cu(Dipp ₂ Im)(Bneop)]	42.3 (C ₆ D ₆)	2.007(6)/ 2.000(5)	1.932(4)/ 1.928(5)	174.8(2)/ 174.6(2)
[Cu(sDipp ₂ Im) ₂ (μ-Bcat)][BF ₄]	-	2.051(6) 2.041(6)	1.941(5) 1.923(5)	72.1(2) (Cu-B-Cu)
[Cu(^t Bu ₂ Im) ₂ (μ-Bpin) ₂]		2.188(2)/ 2.236(2)	1.935(2) 2.2338(5)	115.50(7) 125.07(8)
[Cu(ⁱ Pr ₂ ImMe ₂) ₂ (μ-Bdmab) ₂]		2.178(3)/ 2.240(3)	1.939(3) 2.2592(7)	123.62(11) 117.81(11)
[Cu(ⁱ Pr ₂ ImMe ₂) ₂ (μ-Bpin) ₂]		2.176(1)/ 2.237(1)	1.912(1) 2.2243(3)	125.16(5) 115.33(5)
[Cu(Dipp ₂ Im)(Bdmab)]	44.1 (THF-d ₈)	1.995(4)	1.930(4)	174.8(2)
[Cu(Dipp ₂ Im)(Bdbab)]	47.0 (C ₆ D ₆)	1.994(4)/ 1.986(4)	1.932(3)/ 1.926(3)	172.1(1)/ 178.9(1)
[Cu(Dipp ₂ Im{B(NCH ₃ CH ₂) ₂ })]	45.4	2.008(3)/ 2.009(3)	1.934(3)/ 1.935(3)	172.1(29)/ 178.9(1)
[Cu(^t Bu ₂ Im)(Bdmab)]		1.993(4)/ 1.997(4)	1.953(4)/ 1.948(4)	175.5(2)/ 175.6(2)
[Cu(s ⁱ Pr ₂ Im){B(NCH ₃ CH ₂) ₂ }]		2.002(2)	1.944(2)	180(0)
[Cu(Mes ₂ Im){B(NDippCH) ₂ }]	38.9 (C ₆ D ₆)	1.980(2)	1.918(2)	179.43(9)
[Cu(Mes ₂ Im){B(NDippCH ₂) ₂ }]	44.7 (C ₆ D ₆)	1.983(3)	1.915(3)	179.41(15)
[Li(THF) ₃][Cu{B(NDippCH ₂) ₂ }(Br)]	45.4 (THF-d ₈)	1.983(4)	2.32(3) (Cu-Br)	172.0(1)
[Li(THF) ₃][Cu{B(NDippCH) ₂ }(CN)]	38.6 (C ₆ D ₆)	1.973(6)	1.906(7) Cu-C _{CN}	176.9(2)
[Cu(Mes ₂ ImMe ₂)(Bpin)]*	-	-	-	-
[Cu(Cy ₂ Im)(Bpin)]**	-	-	-	-

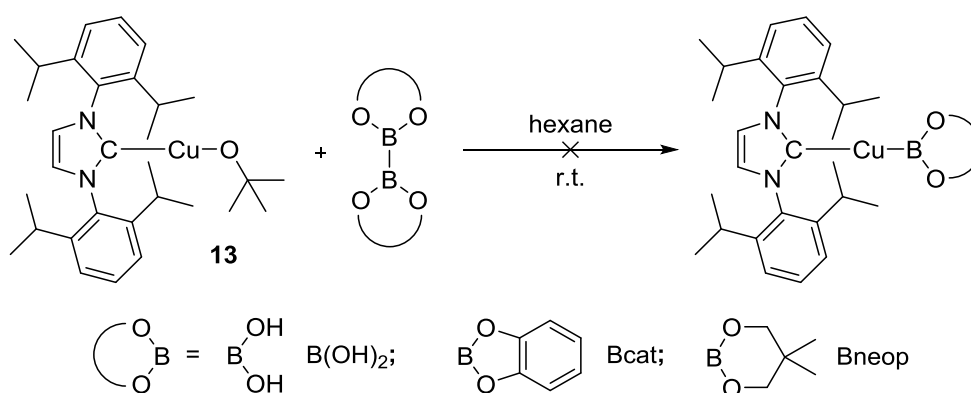
3.2.2.1 Reactivity of NHC-stabilized copper(I)-alkoxide complexes with diboron(4) compounds

The known complex $[\text{Cu}(\text{Dipp}_2\text{Im})(\text{Bpin})]$ was synthesized in accordance with the literature^[265] by reaction of $[\text{Cu}(\text{Dipp}_2\text{Im})(\text{O}^t\text{Bu})]$ **13** with B_2pin_2 in *n*-hexane at room temperature (Scheme 35).



Scheme 35: Synthesis of $[\text{Cu}(\text{Dipp}_2\text{Im})(\text{Bpin})]$ from $[\text{Cu}(\text{Dipp}_2\text{Im})(\text{O}^t\text{Bu})]$ **13** and B_2pin_2 .

In a similar manner, the synthesis of the boryl compounds from the diboron compounds B_2neop_2 , B_2cat_2 and $\text{B}_2(\text{OH})_4$ were also investigated (Scheme 36).



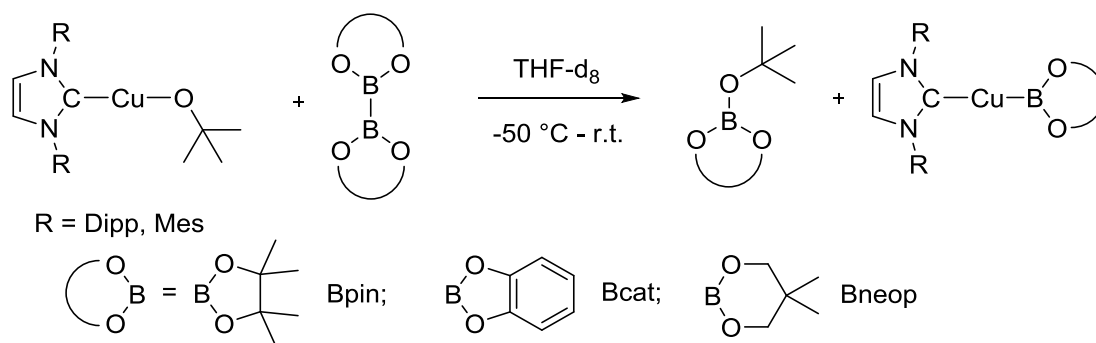
Scheme 36: Attempts to synthesize new copper(I) boryl complexes.

The reaction **13** with B_2neop_2 turned into a black suspension and a copper mirror within 5 minutes. The ^{11}B NMR spectrum of the reaction mixture in C_6D_6 showed a resonance at 27 ppm and a signal at 17.8 ppm along with peaks with low intensities at about 1.0 ppm. In THF-d_8 the resonance of $^t\text{BuOBneop}$ is observed at 15.3 ppm, so the signal at 17.8 ppm might be indicative for the formation of the expected byproduct.^[273]

The reaction of B_2cat_2 with **13** yielded a light orange powder, which showed poor solubility in C_6D_6 . The 1H NMR spectrum indicated the formation of a new compound, but no signals could be detected in the ^{11}B NMR spectrum. It should be noted that $tBuOBcat$ could have been lost in the work-up. Resonances in the 1H NMR spectrum using CD_3CN as solvent were different compared to the sample run in C_6D_6 , and three signals in the ^{11}B NMR spectrum with chemical shifts of 7.9, 11.1 and 14.3 ppm were observed. The compound could not be characterized, but decomposition in CD_3CN seems to take place.

The reaction of $B_2(OH)_4$ with complex **13** gave a white solid and forms a yellow solution in C_6D_6 . This solution turns dark brown within minutes. The 1H NMR spectrum in C_6D_6 showed more than one set of resonances which is likely could due to decomposition. No signal was detected in the ^{11}B NMR spectrum.

These experiments showed clearly that the reactivity of complex **13** with other diboron compound than B_2pin_2 is not straight forward and that multiple other reaction pathways are present. For further investigation on the copper(I) boryl complex formation *in situ* VT NMR spectroscopy studies were carried out between -40 °C and -50 °C, respectively, and room temperature in deuterated toluene- d_8 and THF- d_8 (Scheme 37).



Scheme 37: *In situ* VT-NMR monitored reactions of copper(I) alkoxide complexes with diboron compounds.

The *in situ* monitored reaction of **13** and B_2pin_2 in THF- d_8 showed the clean formation of the desired boryl complex and the byproduct $tBuOBpin$ (see Appendix Figures 95 to 98). The reaction was completed when -10 °C was reached, albeit some B_2pin_2 starting material was left (Figures 16 and 17). The excess of B_2pin_2 might arise from weighing errors. From room temperature on, slow decomposition was observed.

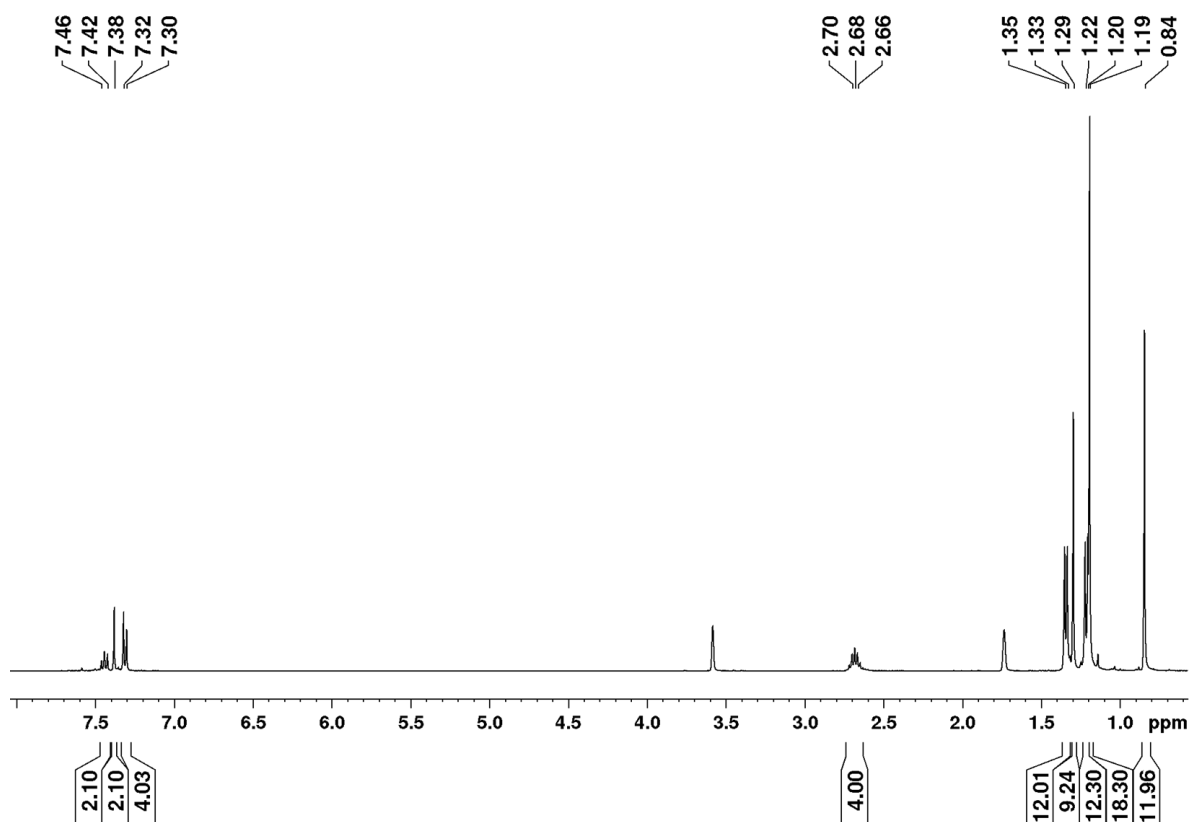


Figure 16: *In situ* ^1H VT-NMR spectrum of the reaction of $[\text{Cu}(\text{Dipp}_2\text{Im})(\text{O}^t\text{Bu})]$ with B_2pin_2 in THF-d_8 at $-10\text{ }^\circ\text{C}$ showing complete formation of the complex $[\text{Cu}(\text{Dipp}_2\text{Im})(\text{Bpin})]$ and $^t\text{BuOBpin}$ as well as an excess of B_2pin_2 at 1.19 ppm.

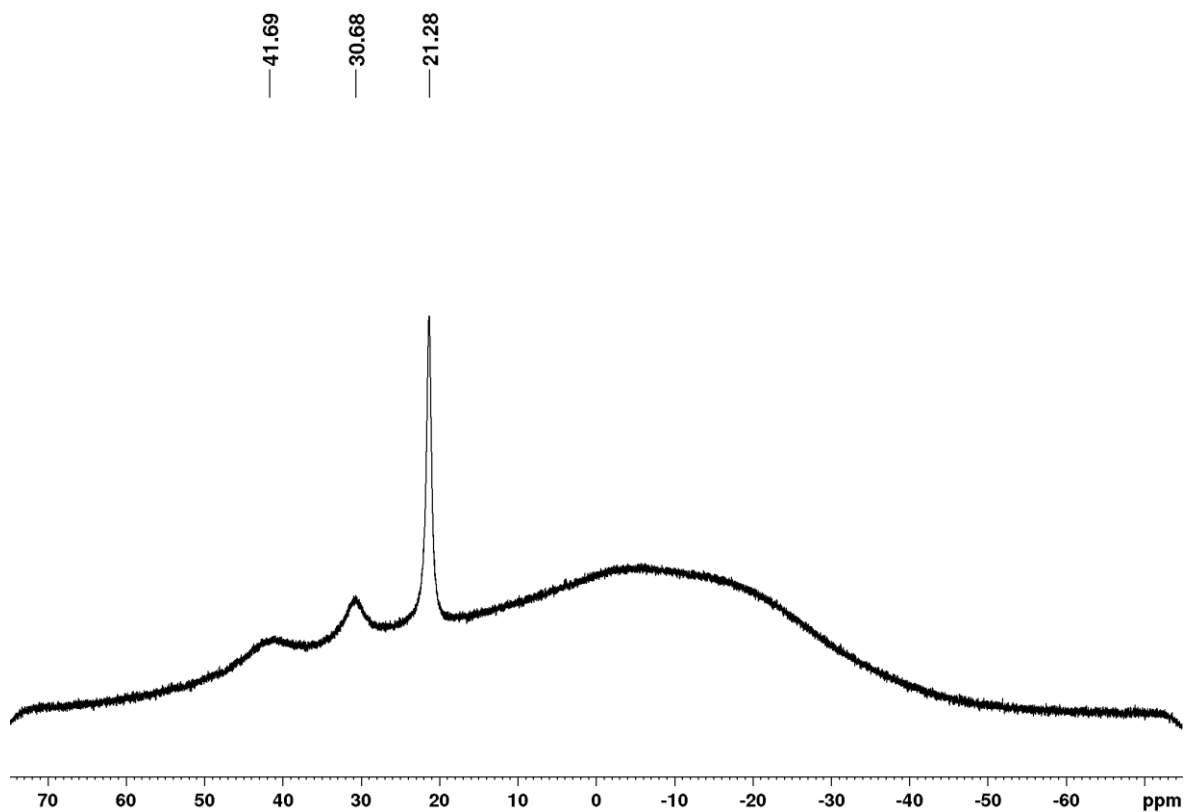


Figure 17: *In situ* ^{11}B VT-NMR spectrum of the reaction of $[\text{Cu}(\text{Dipp}_2\text{Im})(\text{O}^t\text{Bu})]$ with B_2pin_2 in THF-d_8 at $-10\text{ }^\circ\text{C}$ showing the boryl complex $[\text{Cu}(\text{Dipp}_2\text{Im})(\text{Bpin})]$ (41.7 ppm), the byproduct $^t\text{BuOBpin}$ (21.3 ppm) and remaining starting material B_2pin_2 (30.7 ppm).

One signal at 0.64 ppm was detected in the ^1H NMR spectra at $-50\text{ }^\circ\text{C}$ and $-30\text{ }^\circ\text{C}$. It might correspond to an intermediate between the alkoxide complex and the boryl complex where both starting materials are linked via the oxygen of the alkoxide group (Scheme 38).^[151] The signal was only observed in the spectra recorded at $-50\text{ }^\circ\text{C}$ and $-30\text{ }^\circ\text{C}$, when the conversion was not complete but ongoing (Figure 18). The remaining signals of the intermediate might either be broad due to dynamics and with that hard to track or overlaid by the signals of the other complexes having similar chemical shifts.

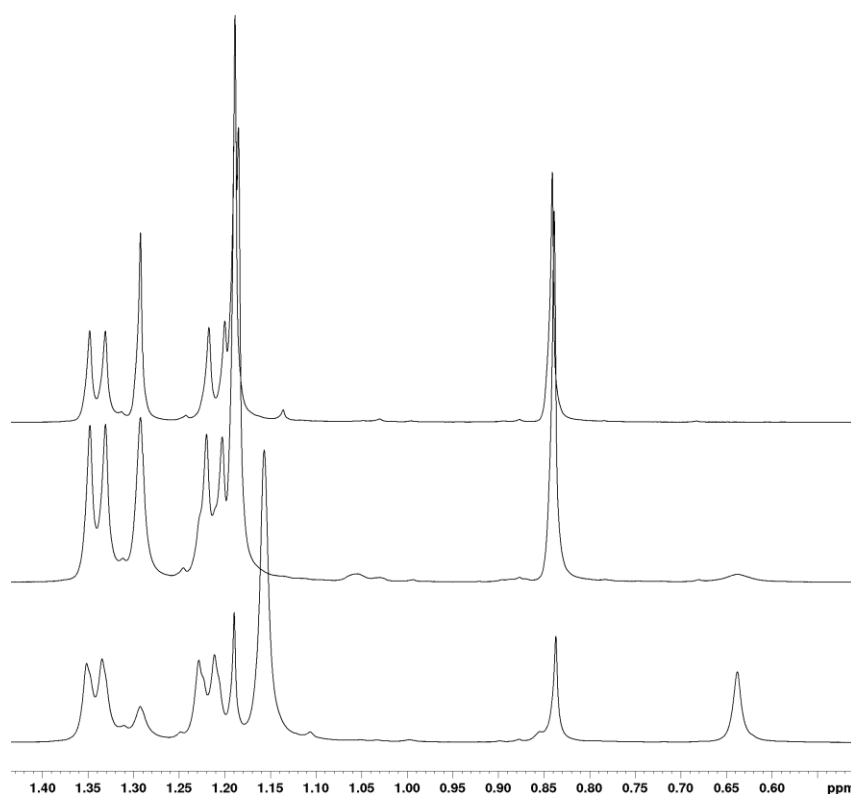
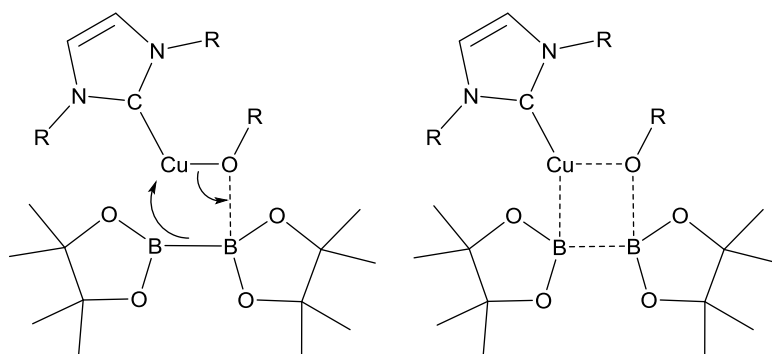


Figure 18: *In situ* ^1H VT-NMR spectra of the reaction of $[\text{Cu}(\text{Dipp}_2\text{Im})(\text{O}'\text{Bu})]$ and B_2pin_2 in THF-d_8 showing the signal of a possible intermediate at 0.64 ppm at low temperature when the conversion was not complete. Bottom: ^1H NMR spectrum recorded at $-50\text{ }^\circ\text{C}$. Middle: ^1H NMR spectrum recorded at $-30\text{ }^\circ\text{C}$. Top: ^1H NMR spectrum recorded at $-10\text{ }^\circ\text{C}$.



Scheme 38: Possible intermediate (left) and a transition state (right) towards boryl formation from a diboron compound and an alkoxide copper(I) complex.^[151]

The fast reaction of the intermediate towards the boryl complex is indicative for a low energy barrier and with that in good agreement with DFT-calculations from Marder *et al.* Theoretical studies with simplified reactants (B_2eg_2 as diboron reagent and Me_2Im as ligand) calculated an energy barrier of 3.9 kcal/mol for this step.^[151]

Complex **13** showed a different reactivity towards B_2cat_2 than to B_2pin_2 (see Appendix Figures 101 and 102). In the 1H NMR spectrum recorded at $-50\text{ }^\circ C$ two sets of signals for the $Dipp_2Im$ ligand and four singlets in the region of the *tert*-butoxide group (1.25 to 0.38 ppm) were detected. The ^{11}B NMR spectrum showed one signal of low intensity in the region of tetracoordinate boron moieties at 8.1 ppm. Upon warming, the peak reached its maximum at a temperature of $-10\text{ }^\circ C$ when new peaks at 43.0, 22.0 and 14.5 ppm in way lower intensities started to appear. The peak at 43.0 ppm is indicative of boryl formation, while the peak at 22.0 ppm is in the range of the expected byproduct tBuOBcat . $MeOBcat$ and $EtOBcat$ show resonance in the ^{11}B NMR spectrum at 23.5 (in C_6D_6) and 22.6 ppm (in $CDCl_3$), respectively.^[274-276] About one hour after the sample was heated to room temperature the 1H and the ^{11}B NMR spectra showed signals for the boryl complex and the tBuOBcat byproduct almost exclusively (Figures 19 and 20). Within the next 24 hours decomposition of the $[Cu(Dipp_2Im)(Bcat)]$ complex by decreasing signal intensities and the formation of four new septets (and the corresponding set of signals) as well as signals with coupling patterns typical for catecholate protons was observed.

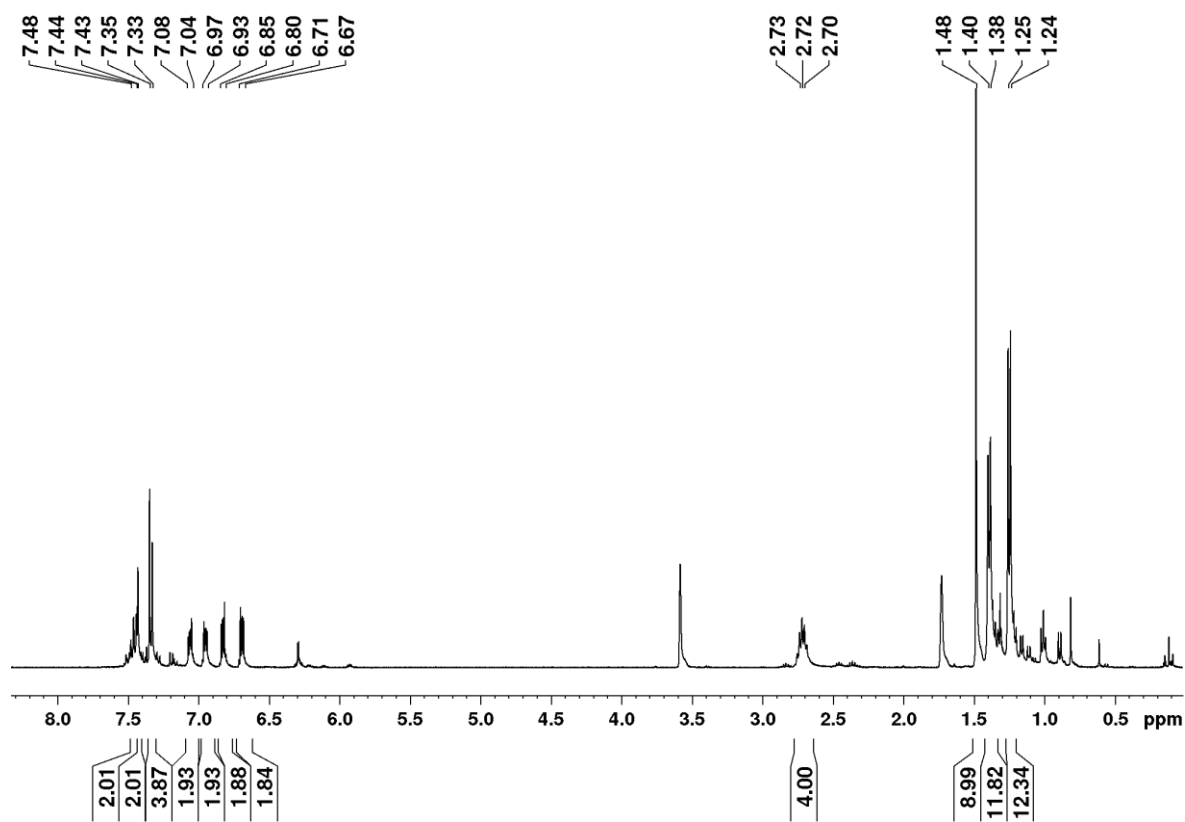


Figure 19: *In situ* ^1H NMR spectrum of the reaction of $[\text{Cu}(\text{Dipp}_2\text{Im})(\text{O}^t\text{Bu})]$ with B_2cat_2 in THF-d_8 , 44 min after warming to room temperature.

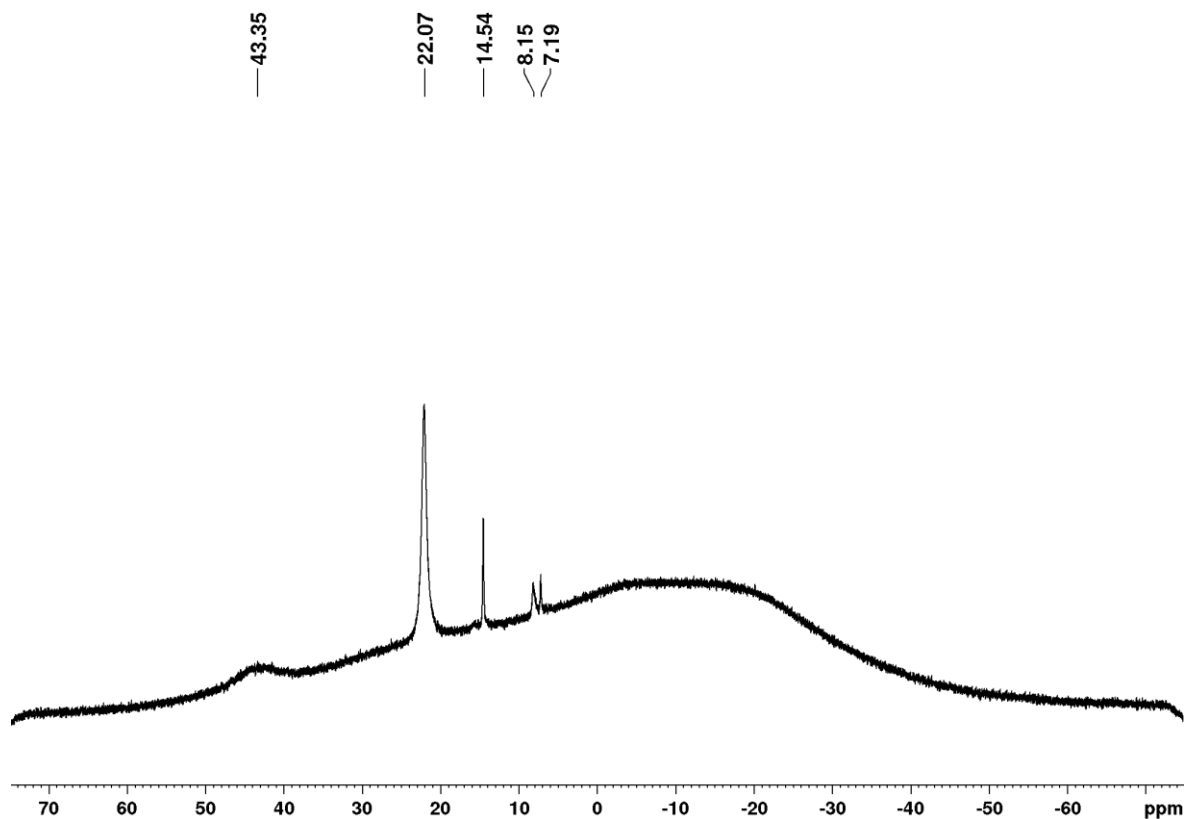
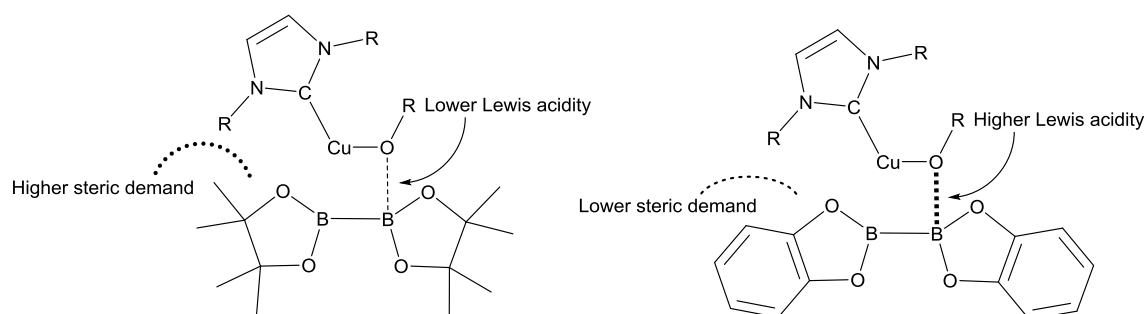


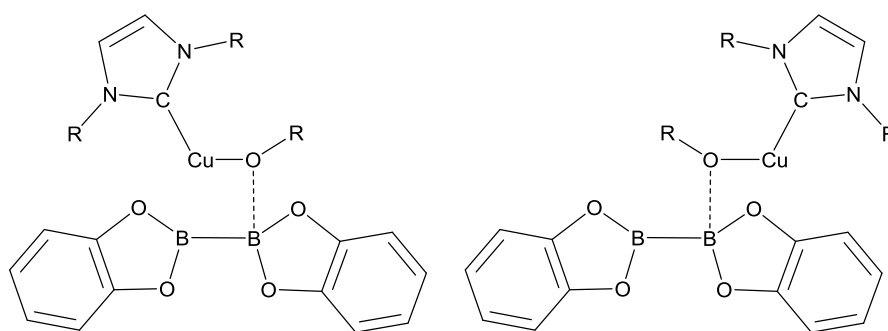
Figure 20: *In situ* ^{11}B NMR spectrum of the reaction of $[\text{Cu}(\text{Dipp}_2\text{Im})(\text{O}^t\text{Bu})]$ with B_2cat_2 in THF-d_8 , 44 min after warming to room temperature.

In contrast to the formation of $[\text{Cu}(\text{Dipp}_2\text{Im})(\text{Bpin})]$ the reaction pathway towards the boryl formation of $[\text{Cu}(\text{Dipp}_2\text{Im})(\text{Bcat})]$ is slightly different from the NMR spectroscopic point of view. Firstly the low intensities of the signal in the ^{11}B NMR spectra at low temperature and secondly the chemical shifts, which is indicative for a tetracoordinate boron moiety, and secondly, the fact that the reaction of $[\text{Cu}(\text{Dipp}_2\text{Im})(\text{O}^t\text{Bu})]$ with B_2pin_2 was complete as soon as a temperature of $-10\text{ }^\circ\text{C}$ was reached, while in the case of B_2cat_2 one hour at room temperature was needed to complete boryl formation. Albeit being the more reactive of the two in for example alkene diboration reactions, B_2cat_2 seems to form more stable, longer-lived intermediates than B_2pin_2 in alkoxide mediated metathesis reactions (Scheme 39).^[277]



Scheme 39: Differences in steric demand and Lewis acidity of B_2pin_2 versus B_2cat_2 in the Lewis acid-base adduct like intermediate towards boryl formation.

That might arise from its higher Lewis acidity and lower steric demand compared to its pinacolate counterpart. These characteristics of B_2cat_2 versus B_2pin_2 also have a distinct influence on adduct formation with NHCs (see Chapter 3.4.2). In the case of boryl formation it might even lead to a slightly different reaction pathway where, for example, a stable adduct with the alkoxide complex, having a different orientation towards the B-B bond, is formed (Scheme 40). This intermediate is likely to have a higher activation energy towards boryl formation since the second boron moiety and the copper atom are not aligned for interaction.



Scheme 40: Structures of possible Lewis acid-base adducts prior to copper boryl formation. Left: Intermediate with the copper atom aligned for further interaction. Right: Intermediate with the copper atom not aligned for further interaction.

In the synthesis of mononuclear nickel boryl complexes, Mindiola *et al.* found evidence for a Lewis acid-base adduct intermediate in their NMR spectroscopic data.^[278] In subsequent DFT calculations they proposed two intermediates similar in energy (relative difference in electronic energy = 5.17 kcal/mol). While the ‘aligned intermediate’ is moderately lower in energy, their calculations showed that both adducts are reasonable from an energetic point of view. Thus, the adduct of B_2cat_2 with complex $[Cu(Dipp_2Im)(O^tBu)]$ might be lower in energy and, in addition, in an orientation without Cu-B interactions for directly forming the four-membered transition state on the path to the boryl complex. This might explain the observed higher activation energy in the reaction of complex **13** and B_2cat_2 .

In the case of B_2neop_2 and $[Cu(Dipp_2Im)(O^tBu)]$ **13** one peak at 16.3 ppm was detected in the ^{11}B NMR spectra at $-50\text{ }^\circ C$ (see Appendix Figure 100). This signal likely arises from the expected byproduct tBuOBneop as it was observed at 15.3 ppm in THF- d_8 by Ogoshi *et al.* and similar moieties such as EtOBneop resonate at 18.7 ppm (in $CDCl_3$).^[273, 276] In the 1H NMR spectra a set of singlets at 3.57, 1.28 and 0.92 ppm with a ratio of 4:9:6 match those found for the tBuOBneop byproduct.^[273] When a temperature of $10\text{ }^\circ C$ was reached an additional signal in the ^{11}B NMR spectra at 39.5 ppm was detected which is indicative of boryl formation (42.3 ppm in C_6D_6),^[271] but rapid decomposition was observed in the following spectra (Figure 21). Interestingly, in a rate similar to the decomposition of the signal at 39.5 ppm the growth of a peak at 27.8 ppm was observed. This peak at 27.8 ppm might correspond to B_2neop_2 formed by reductive elimination. Kleeberg *et al.* observed reductive elimination of B_2pin_2 from the dimeric complex $[Cu(^tBu_2Im)_2(\mu-Bpin)_2]$ as well as B_2dmab_2 from the dimeric complex $[Cu(^iPr_2ImMe)_2(\mu-Bdmab)_2]$.^[271] Signals in the 1H NMR

spectra recorded at room temperature at 3.45 and 0.88 ppm with an integral ratio of 4:6 were detected, which matches those found for free B_2neop_2 in THF- d_8 (Figure 22). This possible decomposition route is in agreement with the observation at the end of the investigation when a black suspension and a copper mirror were witnessed, as it requires the formation of copper(0). The 1H NMR spectrum recorded 24 h after warming to room temperature shows the set of signals for B_2neop_2 , the byproduct tBuOBneop and the free $Dipp_2Im$ ligand in a ratio close to 1:1:1 (Figure 22).^[279] The occurrence of the signal of the byproduct without any detectable signs of the boryl product at the beginning of the investigation leads to the possibility that the complex $[Cu(Dipp_2Im)(Bneop)]$ is not formed directly but forms a dynamic intermediate, which is not detected due to broadened signals.

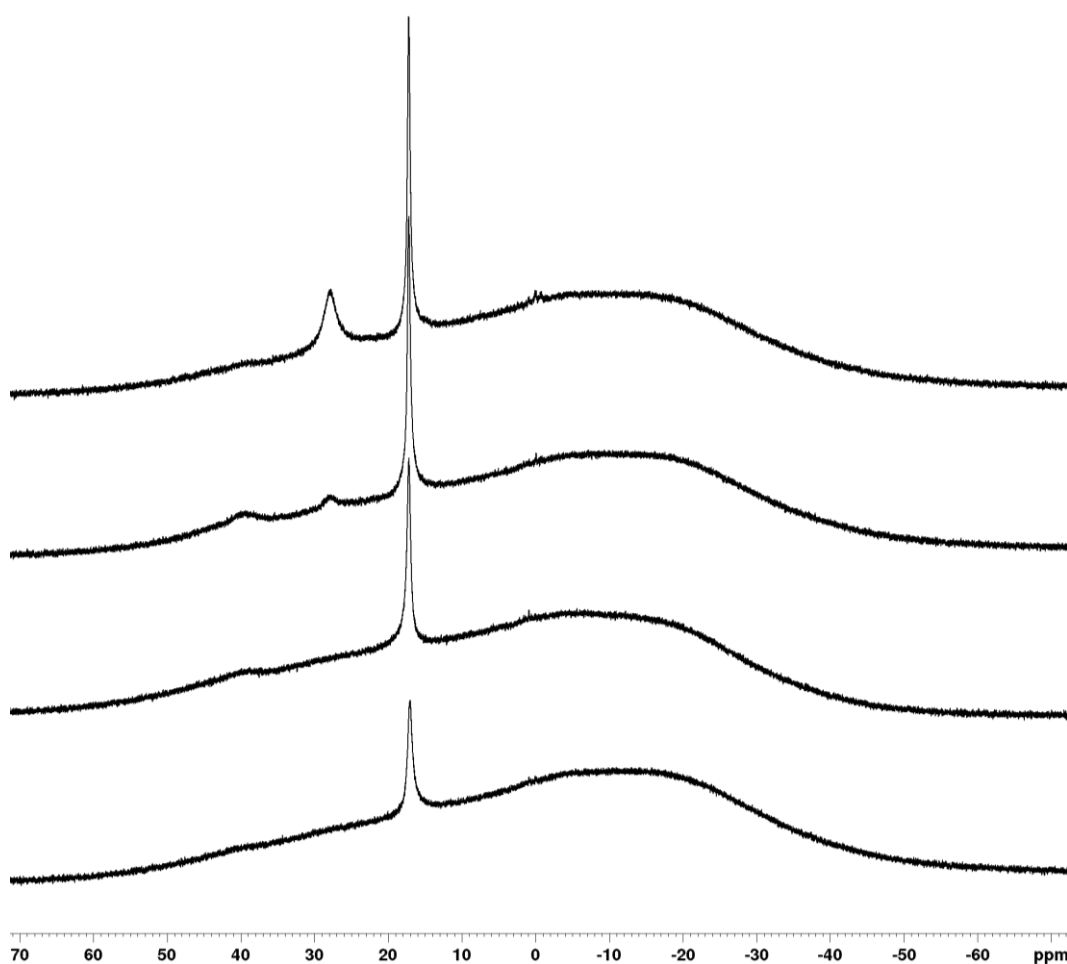


Figure 21: *In situ* ^{11}B VT-NMR spectra of the reaction of $[Cu(Dipp_2Im)(O^tBu)]$ 13 and B_2neop_2 in THF- d_8 . From Bottom to Top: ^{11}B NMR spectrum recorded at -10 °C; ^{11}B NMR spectrum recorded at 10 °C; ^{11}B NMR spectrum recorded at room temperature; ^{11}B NMR spectrum recorded 1 h after warming to room temperature.

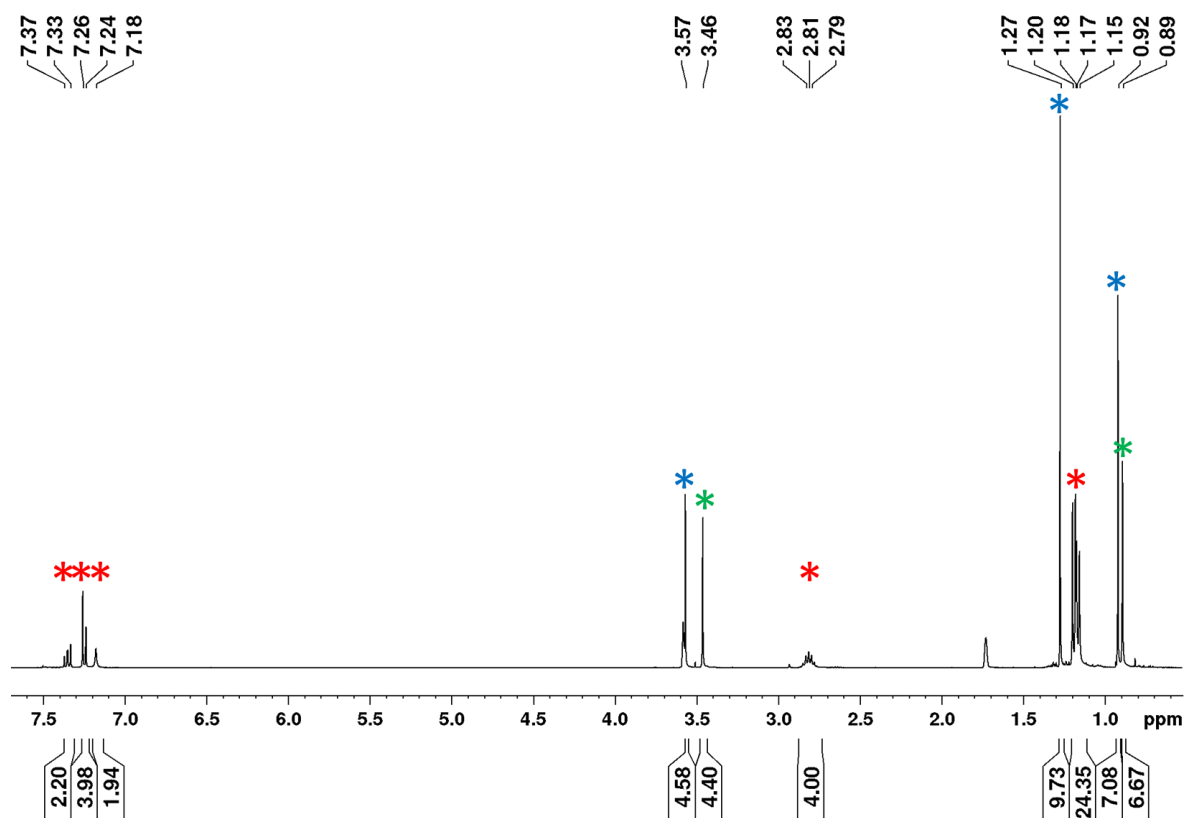
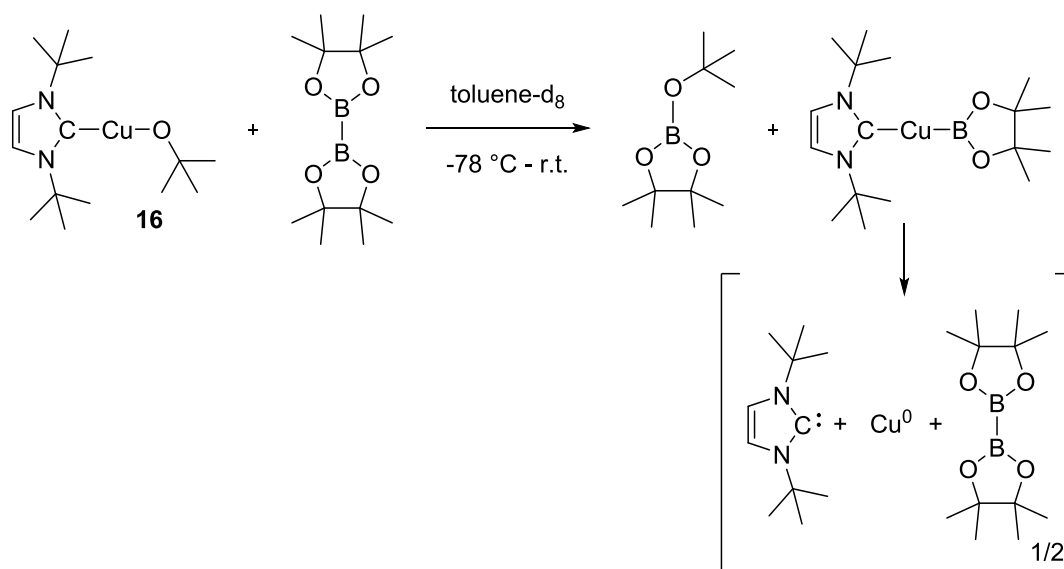


Figure 22: *In situ* ^1H NMR spectrum of the reaction of $[\text{Cu}(\text{Dipp}_2\text{Im})(\text{O}^t\text{Bu})]$ **13** and B_2neop_2 in THF-d_8 recorded 24 h after warming to room temperature. Green asterisk: Signals for B_2neop_2 . Blue asterisk: Signals for $^t\text{BuOBneop}$. Red asterisk: Signals for the free Dipp_2Im ligand.

When $[\text{Cu}(^t\text{Bu}_2\text{Im})(\text{O}^t\text{Bu})]$ **16** was reacted with B_2pin_2 in toluene- d_8 at -78 $^\circ\text{C}$, a yellow solution was obtained, which became a red solution at -50 $^\circ\text{C}$ and a dark suspension upon warming to -10 $^\circ\text{C}$ and higher (Scheme 41). In the ^1H NMR spectra broad signals which could not be assigned to a specific compound were detected (see Appendix Figure 103). No significant changes upon warming the sample from -50 $^\circ\text{C}$ to -20 $^\circ\text{C}$ in 10 $^\circ\text{C}$ increments were observed in the ^1H NMR spectra.



Scheme 41: Low temperature reaction of $[\text{Cu}(\text{tBu}_2\text{Im})(\text{O}^t\text{Bu})]$ **15** with B_2pin_2 .

At $-50\text{ }^\circ\text{C}$ the ^{11}B NMR spectra showed a peak at 21.6 ppm. Upon warming the sample to $-20\text{ }^\circ\text{C}$ a new, broad peak at 32.3 ppm started to appear and grow (Figure 23). The signal at 21.6 ppm might belong to $^t\text{BuOBpin}$ as it was observed at 21.5 ppm in C_6D_6 , and similar RO-Bpin moieties, like MeOBpin and EtOBpin, show resonances at almost the same chemical shift.^[192, 276, 280-282] The broad peak at 32.2 ppm might arise from B_2pin_2 which is generated in a fast decomposition of a possibly formed copper(I) boryl complex. Kleeberg *et al.* observed the formation of the dimeric boryl complex $[\text{Cu}(\text{tBu}_2\text{Im})_2(\mu\text{-Bpin})_2]$ under similar conditions in THF-d_8 as well as the decomposition via reductive elimination of B_2pin_2 , the formation of $\text{Cu}(0)$ and free $^t\text{Bu}_2\text{Im}$ NHC.^[271] This is in good agreement with the observation of a black suspension and a copper mirror at the end of the investigation.

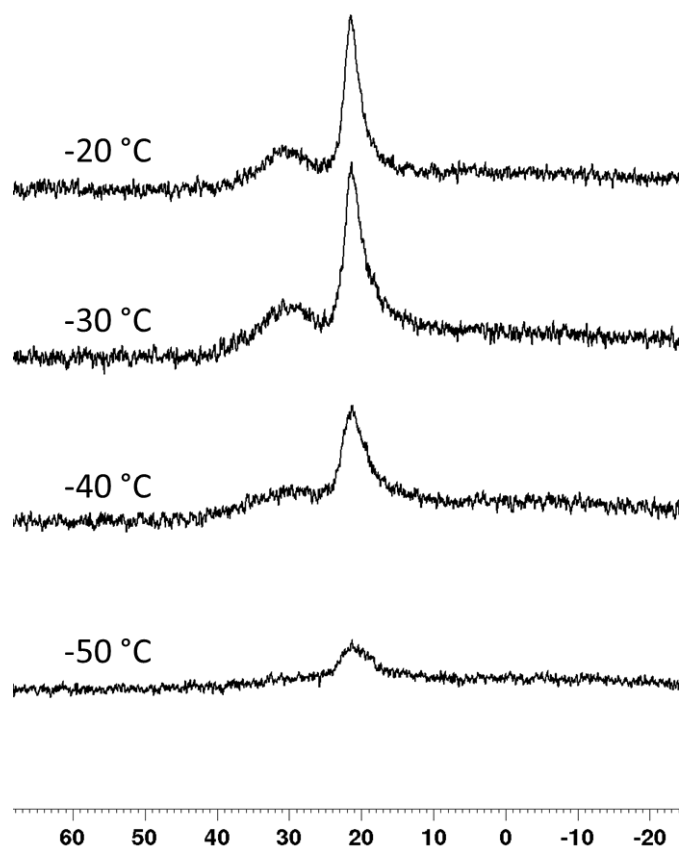
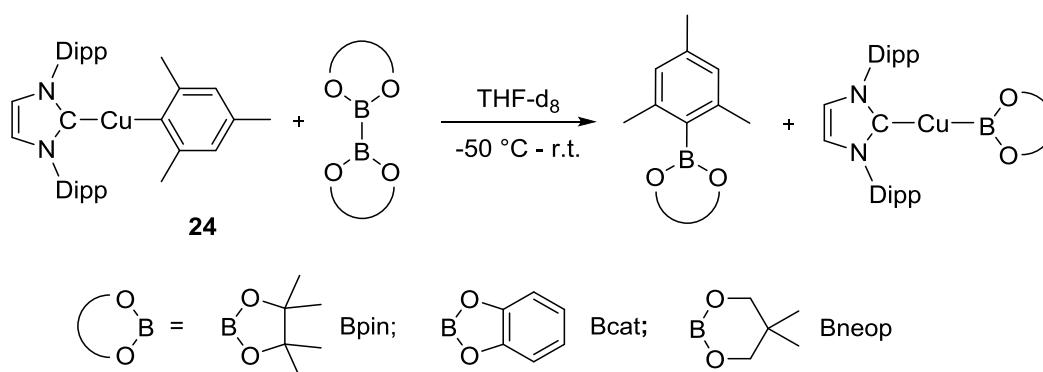


Figure 23: *In situ* ^{11}B VT-NMR spectra of the reaction of **16** with B_2pin_2 in toluene- d_8 .

The reactions of Dipp_2Im stabilized copper(I) alkoxide complexes with diboron compounds generally led to the formation of the corresponding copper(I) boryl complex. In the case of B_2pin_2 , the NMR spectroscopic data are unambiguous and isolation of the boryl complex in stoichiometric reactions is feasible. In the reaction of $[\text{Cu}(\text{Dipp}_2\text{Im})(\text{O}^t\text{Bu})]$ **13** and B_2cat_2 , boryl formation was observed as a broad signal at 43.0 ppm in the ^{11}B NMR spectra, but fast decomposition was observed. One signal for the intermediate in the ^{11}B NMR at 8.1 ppm, indicating tetracoordinate boron, was observed. This, plus the fact that the signal for the boryl complex was not witnessed until higher temperatures than with B_2pin_2 , showed once more the difference in reactivity of the two diboron compounds. These studies also showed that the boryl complexes formed are highly unstable in these reaction mixtures as in all cases decomposition in solution was observed. In the cases of $[\text{Cu}(\text{Dipp}_2\text{Im})(\text{O}^t\text{Bu})]$ with B_2neop_2 and $[\text{Cu}(^t\text{Bu}_2\text{Im})(\text{O}^t\text{Bu})]$ with B_2pin_2 the formation of signals for the diboron starting material were observed after it was completely consumed. These likely arise from reductive elimination from formed boryl complexes leaving copper(0) and the ligand.

3.2.2.2 Reactivity of NHC-stabilized copper(I)-aryl complexes with diboron(4) compounds

As a milder base with more sterical hinderance complex $[\text{Cu}(\text{Dipp}_2\text{Im})(\text{Mes})]$ **24** was reacted with the diboron compounds B_2pin_2 , B_2cat_2 and B_2neop_2 in THF-d_8 in *in situ* NMR monitored reactions (see Appendix Figures 105 to 110 for detailed spectra).



Scheme 42: *In situ* VT-NMR monitored reactions of $[\text{Cu}(\text{Dipp}_2\text{Im})(\text{Mes})]$ **24** with diboron compounds.

The reactions of **24** with the diboron compound B_2neop_2 showed no reactivity until room temperature was reached (see Appendix Figures 109 and 110). In the ^{11}B NMR spectrum, a signal at 17.6 ppm of low intensity was detected; 24 hours later only minor changes in the intensities were observed. A reaction with slightly modified reaction conditions, for example, higher concentration or at moderately elevated temperature seems appropriate.

In the reaction of **24** with B_2pin_2 the starting materials were detected in the ^1H as well as ^{11}B NMR spectra until room temperature was reached (see Appendix Figures 105 and 106). From room temperature on, at least three new set of signals appeared in the ^1H NMR spectra, which could not be assigned to specific compounds. In the ^{11}B NMR spectra one new peak at 42.0 ppm, indicative of boryl formation, in very low intensity and another new peak at 21.3 ppm were detected. It should be noted that the expected byproduct MesBpin (32.2 ppm in CDCl_3) resonates at almost the same frequency as the starting material B_2pin_2 and thus could not be detected by ^{11}B NMR spectroscopy. Over the next 24 h, decomposition of the boryl species via a decrease in signal intensity of the peak at 42.0 ppm in the ^{11}B NMR spectra was observed. Another set of signals in the ^1H NMR spectra was observed likewise.

Compared to the reactions with B_2neop_2 and B_2pin_2 complex **24** showed a higher and simultaneously cleaner reactivity towards B_2cat_2 (see Appendix Figures 107 and 108). From $-30\text{ }^\circ\text{C}$ on the growth of signals indicative for the boryl complex (43.3 ppm) and the MesBcat (33.1 ppm) byproduct^[283] were observed in both the ^1H and the ^{11}B NMR spectra. Only one peak in the ^{11}B NMR spectra of low intensity at 14.5 ppm indicates a side reaction. Conversion was complete, when room temperature was reached (Figures 24 and 25). Even 24 h later, the lack of significant changes in the NMR spectra indicates the stability of the products formed.

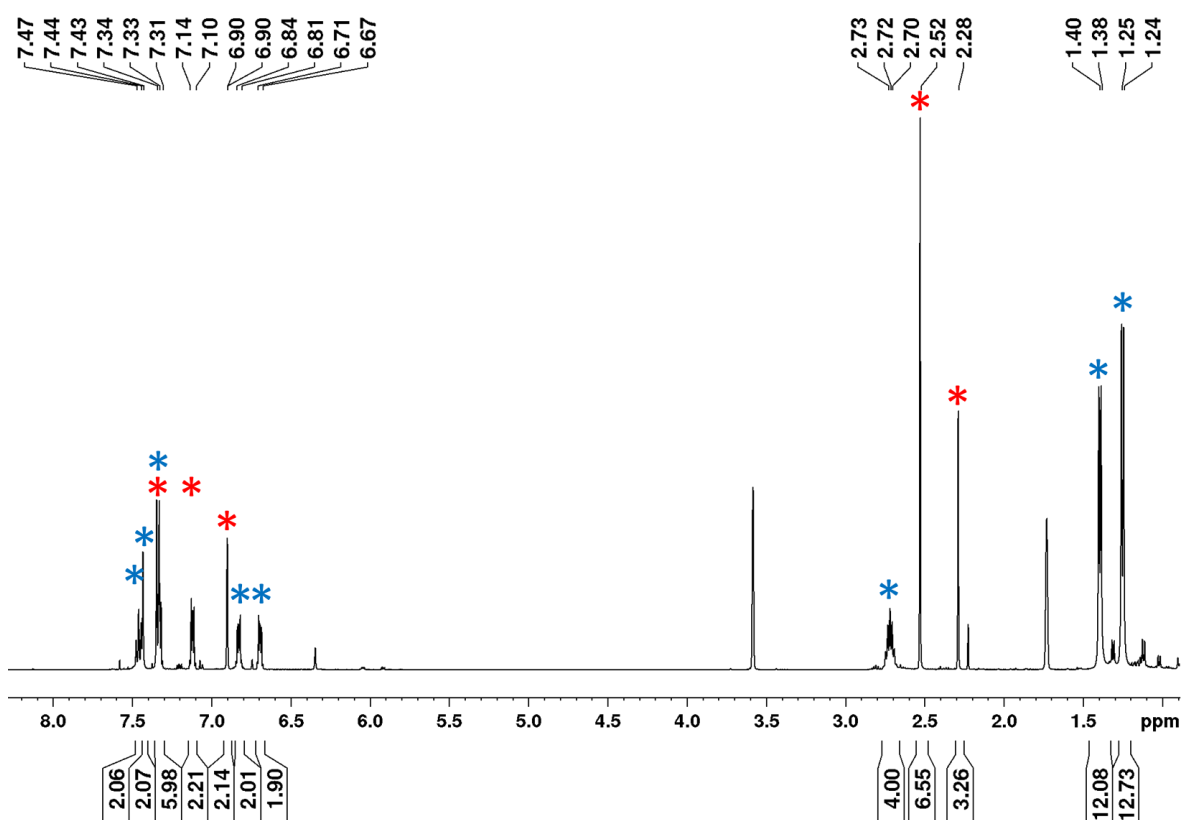


Figure 24: *In situ* ^1H VT-NMR spectrum of the reaction of $[\text{Cu}(\text{Dipp}_2\text{Im})(\text{Mes})]$ with B_2cat_2 in THF-d_8 after more than 24 h at room temperature. Blue asterisk: $[\text{Cu}(\text{Dipp}_2\text{Im})(\text{Bcat})]$. Red asterisk: MesBcat.

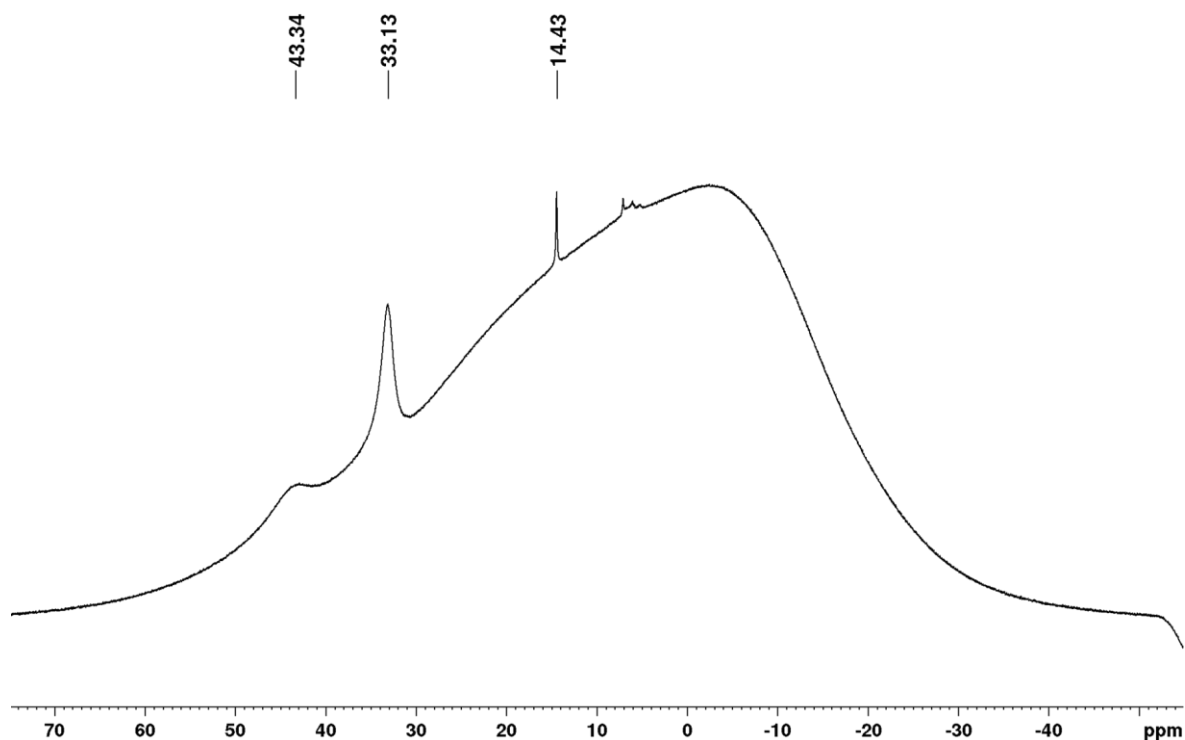


Figure 25: *In situ* ^{11}B VT-NMR spectrum of the reaction of $[\text{Cu}(\text{Dipp}_2\text{Im})(\text{Mes})]$ with B_2cat_2 in THF-d_8 after more than 24 h at room temperature.

A comparison of the ^1H NMR spectrum of the reaction of $[\text{Cu}(\text{Dipp}_2\text{Im})(\text{Mes})]$ with B_2cat_2 and the ^1H NMR spectrum of the reaction of $[\text{Cu}(\text{Dipp}_2\text{Im})(\text{O}^t\text{Bu})]$ with B_2cat_2 shows that in both cases the same complex is formed. The signals as well as the integral ratios are superimposable (Figure 26). However, the byproducts are different and were marked with red (MesBcat) and green asterisk ($^t\text{BuOBcat}$) in the Figure.

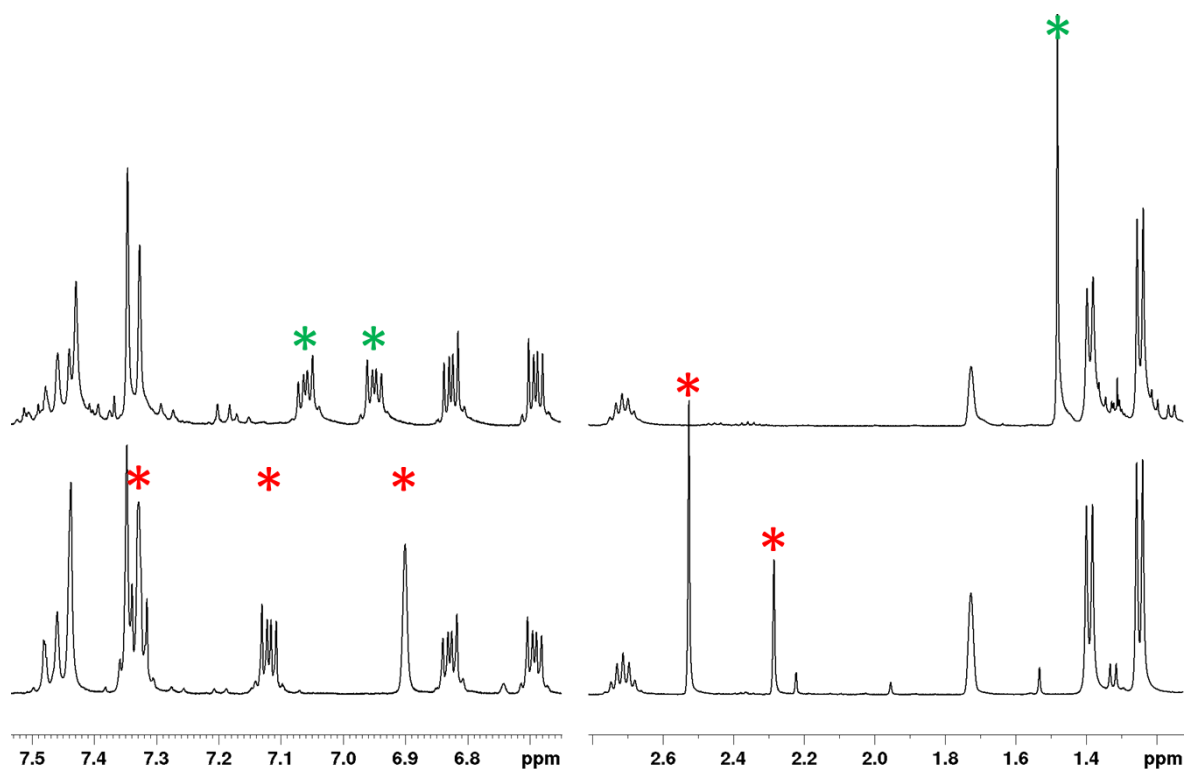


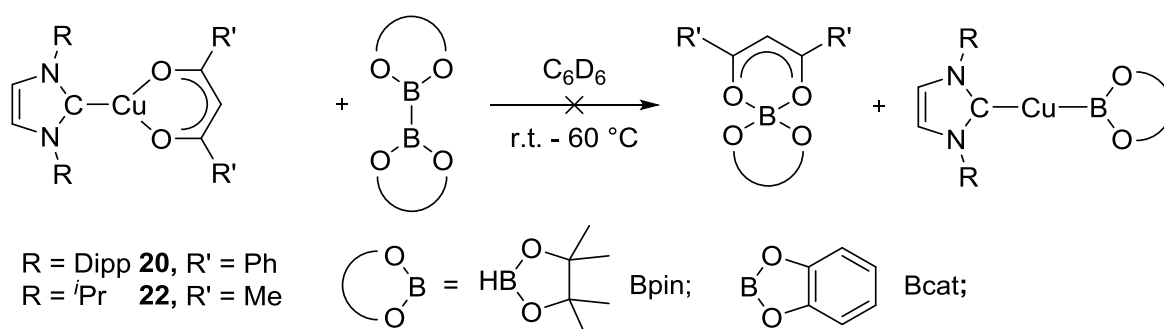
Figure 26: Comparison of the *in situ* ^1H NMR spectrum of the reaction of $[\text{Cu}(\text{Dipp}_2\text{Im})(\text{Mes})]$ with B_2cat_2 recorded at room temperature in THF-d_8 (bottom) and the *in situ* ^1H NMR spectrum of the reaction of $[\text{Cu}(\text{Dipp}_2\text{Im})(\text{O}^t\text{Bu})]$ with B_2cat_2 recorded after 45 min after warming to room temperature in THF-d_8 (Top). Red asterisk for the MesBcat byproduct and green asterisk for the $^t\text{BuOBcat}$ byproduct. The signal of the ^tBuO moiety is cut off for space reasons.

After the NMR experiments each reaction mixture of $[\text{Cu}(\text{Dipp}_2\text{Im})(\text{Mes})]$ with the diboron compounds B_2pin_2 , B_2cat_2 and B_2neop_2 was checked for reactivity towards iodobenzene and analyzed by GCMS. To one part of the reaction mixture ethyl acetate was added and to the second part iodobenzene was added before ethyl acetate was added. The mixtures with iodobenzene changed color from reddish to brown solutions to black suspensions. Subsequent GCMS analysis showed the formation of the respective boronic ester of 2,4,6-trimethylbenzene for all three reactions. In the mixture with iodobenzene a signal for borylated benzene was detected in the case of B_2pin_2 and B_2cat_2 besides other signals, which could not be assigned to specific compounds. The phenylboronate species detected in the GCMS provides additional evidence for the formation of the copper boryl complexes.

In the *in situ* VT NMR monitored reaction of $[\text{Cu}(\text{Dipp}_2\text{Im})(\text{Mes})]$ with B_2cat_2 and B_2pin_2 no intermediates prior to boryl formation were observed. This could either be because no intermediate were formed or more likely due to fast reaction of the formed intermediate towards the boryl complex. However, it is remarkable that the complex $[\text{Cu}(\text{Dipp}_2\text{Im})(\text{Bcat})]$ is stable in solution for an extended period of time. While boryl formation was also observed in the reaction of B_2cat_2 with the alkoxide complex $[\text{Cu}(\text{Dipp}_2\text{Im})(\text{O}^t\text{Bu})]$ decomposition of the formed species was observed under, apart from the byproduct, the same reaction conditions. The difference in lifetime of the boryl complex in the two reaction mixtures suggests that the side products formed are crucial for determining the stability of the boryl species in solution and not the complex itself. Separation of $[\text{Cu}(\text{Dipp}_2\text{Im})(\text{Bcat})]$ from such a reaction mixture seems viable.

3.2.2.3 Reactivity of NHC-stabilized copper(I) acetylacetonate complexes with diboron(4) compounds

The Cu(II) bis-acetylacetonate complex $[\text{Cu}(\text{Mes}_2\text{Im})(\text{acac})_2]$ is an effective catalyst precursor for the borylation of primary alkyl bromides, wherein the diboron(4) moiety is activated and a boron moiety chelated by an acetylacetonate group generated.^[284] As a mild alternative to alkoxide complexes in attempts to synthesize copper(I) boryl complexes from $[\text{Cu}(\text{NHC})\text{base}]$ and a diboron(4) compound the low basicity, bidentate acetylacetonate type moiety might be useful. It could chelate the boron atom forming $(\text{acac})\text{B}(\text{OR})_2$ and thus, lowering its reactivity and leave a possibly boryl complex unharmed. Therefore, the reactivity of complex $[\text{Cu}(\text{Dipp}_2\text{Im})(\text{DBM})]$ **20** and $[\text{Cu}(\text{'}\text{Pr}_2\text{Im})(\text{acac})]$ **22** with the diboron compounds B_2pin_2 and B_2cat_2 was investigated (Scheme 43).



Scheme 43: Reaction of complex $[\text{Cu}(\text{Dipp}_2\text{Im})(\text{DBM})]$ **20** and $[\text{Cu}(\text{'Pr}_2\text{Im})(\text{acac})]$ **22** with the diboron(4) compounds B_2pin_2 and B_2cat_2 .

The acetylacetonate complex **20** showed no reactivity towards B_2pin_2 at room temperature. Even after several hours, only the starting materials were detected in the 1H and ^{11}B NMR spectra (see Appendix Figure 111 and Figure 112). Heating the sample to 60 °C for 4 h afforded a new peak in the ^{11}B NMR spectra at 21.8 ppm. In the 1H NMR spectra the ratio from the complex to the diboron compound increased but no other changes were detected. The next 20 h at 60 °C turned the reddish solution into a green suspension with black precipitates and a copper mirror. No starting material in the ^{11}B NMR was detected but the intensity of peak at 21.8 ppm increased. It is very likely that a possibly formed copper boryl complex would not withstand a temperature of 60 °C in solution.

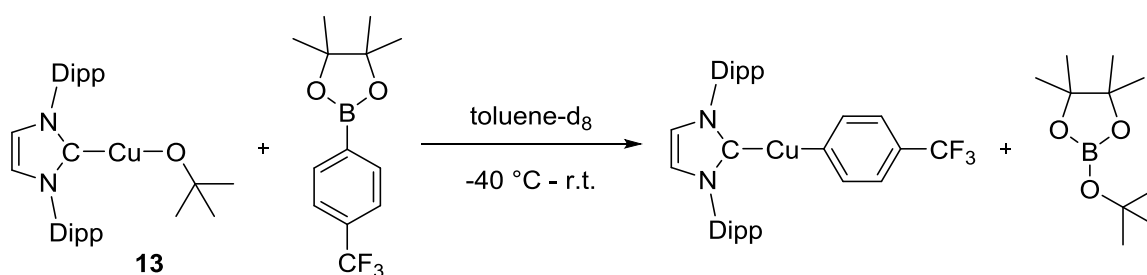
When complex **20** was reacted with B_2cat_2 two peaks in the ^{11}B NMR spectra were observed at 14.7 and 10.7 ppm (see Appendix Figure 114). The 1H NMR spectrum showed the starting complex and a new one in a 1:2.9 ratio (see Appendix Figures 113 and 115). Heating the sample to 60 °C for 4 h and 24 h did not change the spectra substantially.

In the 1H NMR spectrum of $[Cu(iPr_2Im)(acac)]$ **22** and B_2pin_2 after 5 minutes at room temperature, broadened signals with chemical shifts identical with those of the starting complex next to a singlet for B_2pin_2 (see Appendix Figures 116 and 118) were observed. In the ^{11}B NMR spectrum a signal for B_2pin_2 at 31.6 ppm was detected next to a peak at 21.8 and a sharp peak 3.6 ppm (see Appendix Figure 117). Six hours later only the peak 21.8 ppm prevails and a new peak at 10.2 ppm was detected. The 1H NMR spectra showed a new peak at 1.50 ppm.

The fate of the reactions of $[Cu(Dipp_2Im)(DBM)]$ **20** and $[Cu(iPr_2Im)(acac)]$ **22** with diboron compounds is unclear. In none of the reaction was substantial copper boryl formation observed, albeit that boryl complexes are very likely not stable at elevated temperatures. In the case of boryl formation and temperature dependent decomposition, at least complete conversion should have been observed, which was not the case. It rather seemed, especially in the reaction of **20** and B_2pin_2 , that catalytic decomposition of the diboron compound occurred, while most of the metal complex remained intact.

3.2.3 Reactivity of [Cu(Dipp₂Im)(O^tBu)] with aryl boronic esters

A crucial step in cross-coupling reactions, besides the C-C bond-forming step itself, is the transmetalation step of [Cu(NHC)(O^tBu)] complexes with organoboronic esters. The reaction of [Cu(Dipp₂Im)(O^tBu)] with *para*-trifluoromethyl-phenylBpin was monitored by ¹⁹F NMR spectroscopy at low temperature in order to follow the reaction and detect possible intermediates (Scheme 44).



Scheme 44: Low temperature reaction of [Cu(Dipp₂Im)(O^tBu)] 13 with 4-CF₃-C₆H₄Bpin.

A Young's NMR tube was charged with the complex as well as the substrate and cooled to -100 °C before precooled toluene-d₈ was added. The sample was shaken and the first spectrum was recorded at -40 °C. In the ¹⁹F NMR spectrum, a very small peak due to starting material (4-CF₃-C₆H₄Bpin: ¹¹B NMR (-38 °C) = 31.3 ppm, ¹⁹F NMR (-38 °C) = -62.3 ppm) at -62.2 ppm and a new, predominant signal at -60.4 ppm were detected (Figure 27). The following ¹⁹F NMR spectra at -40 °C showed the new peak at -60.4 ppm, but no peak for the product ([Cu(Dipp₂Im)(4-CF₃-C₆H₄)]): ¹⁹F NMR (-38 °C) = -61.0 ppm).

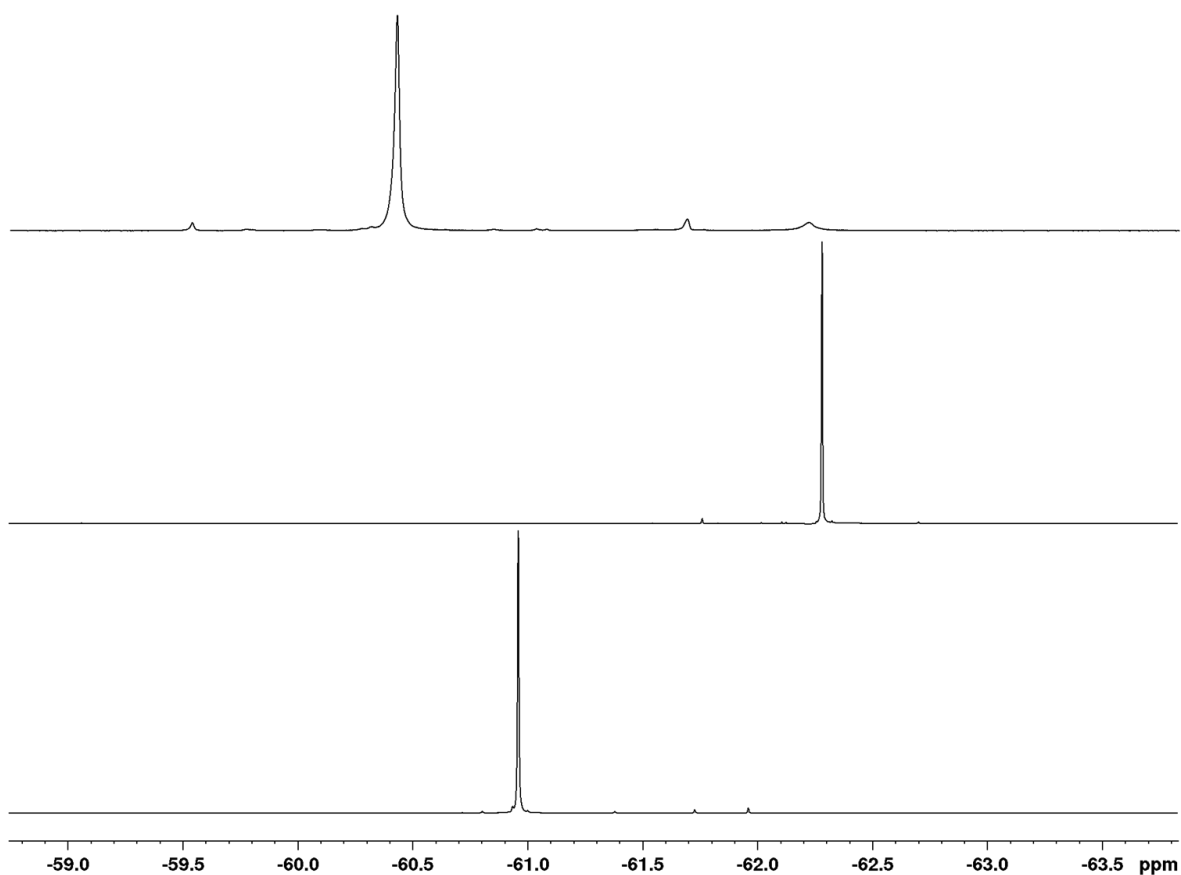


Figure 27: *In situ* ^{19}F VT-NMR spectra of the reaction of $[\text{Cu}(\text{Dipp}_2\text{Im})(\text{O}^t\text{Bu})]$ **13** with $4\text{-CF}_3\text{-C}_6\text{H}_4\text{Bpin}$ at -40 °C. Top: Reaction mixture at -40 °C, $T_0 + 2$ min. Middle: Starting material, $4\text{-CF}_3\text{-C}_6\text{H}_4\text{Bpin}$ at -38 °C. Bottom: Product $[\text{Cu}(\text{Dipp}_2\text{Im})(4\text{-CF}_3\text{-C}_6\text{H}_4)]$ at -38 °C.

In the ^{11}B NMR spectra at -40 °C no signals of the starting materials or the byproduct $^t\text{BuOBpin}$ (^{11}B NMR 21.2 ppm (in CDCl_3)^[285] and 21.5 ppm (in C_6D_6)^[192]) were detected; instead, a new peak at 7.7 ppm was observed (Figure 28).

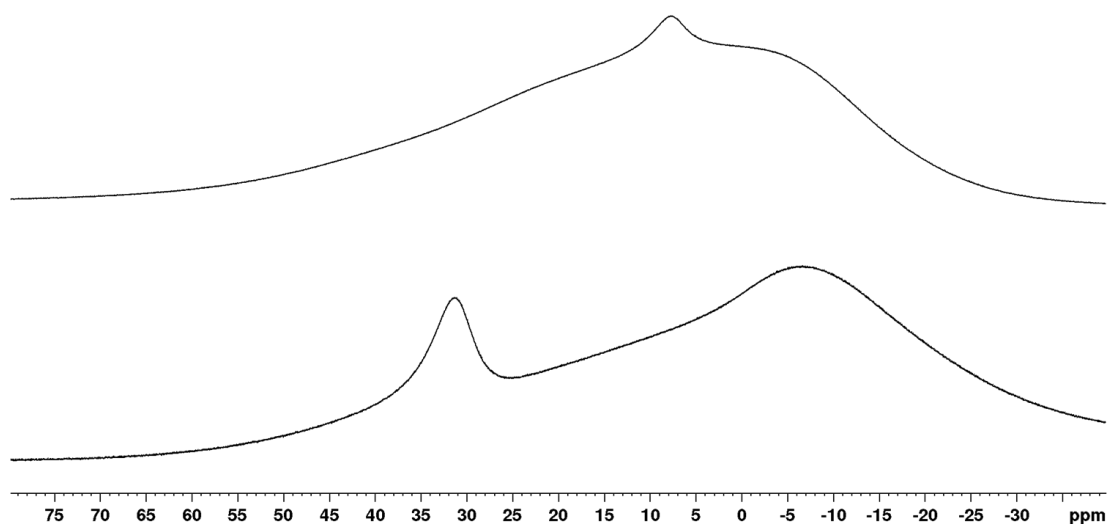


Figure 28: *In situ* ^{11}B VT-NMR spectra of the reaction of $[\text{Cu}(\text{Dipp}_2\text{Im})(\text{O}^t\text{Bu})]$ **13** with $4\text{-CF}_3\text{-C}_6\text{H}_4\text{Bpin}$ at -40 °C. Top: Reaction mixture at -40 °C, $T_0 + 32$ min. Bottom: Starting material, $4\text{-CF}_3\text{-C}_6\text{H}_4\text{Bpin}$, at -38 °C.

The signals in the ^1H NMR spectra at -40 °C were broadened and showed splitting of, for example, the methine protons of the Dipp moiety, possibly due to the temperature dependent diminished rotation of the Dipp ligand (Figure 29).

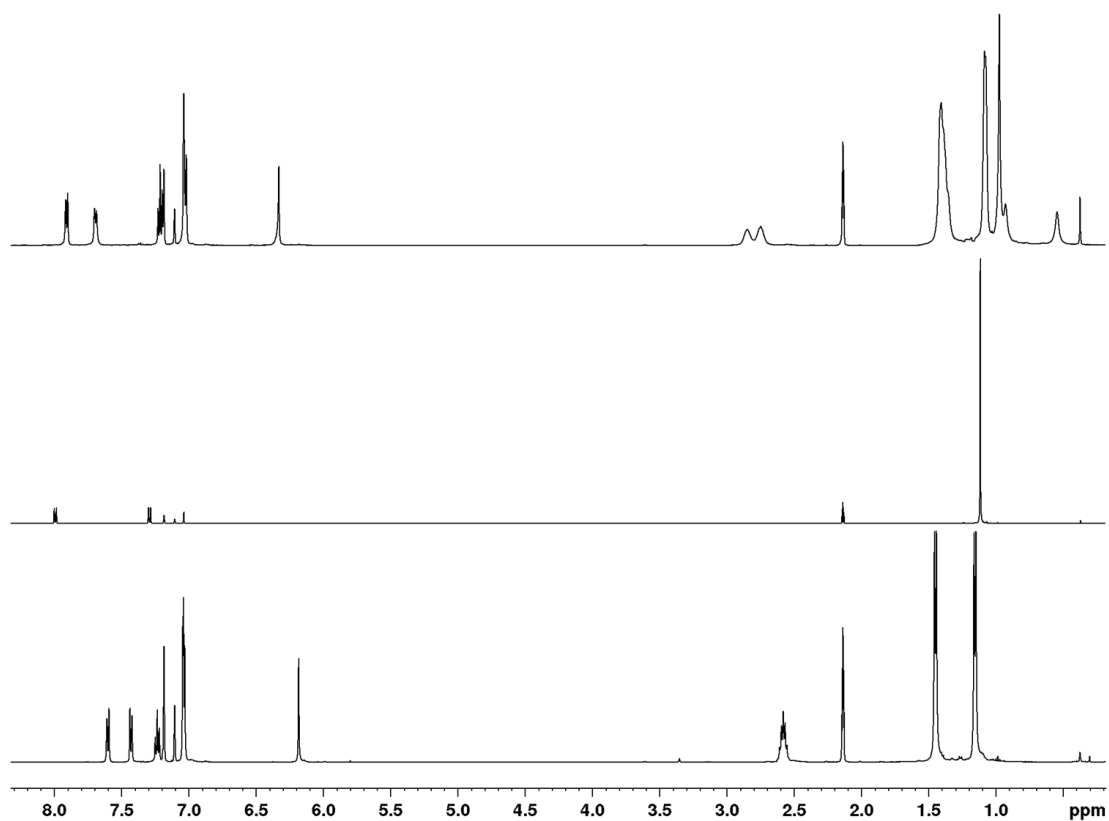


Figure 29: *In situ* ^1H VT-NMR spectra of the reaction of $[\text{Cu}(\text{Dipp}_2\text{Im})(\text{O}^t\text{Bu})]$ **13** with $4\text{-CF}_3\text{-C}_6\text{H}_4\text{Bpin}$ at -40 °C. Top: Reaction mixture at -40 °C, $T_0 + 6$ min. Middle: Starting material, $4\text{-CF}_3\text{-C}_6\text{H}_4\text{Bpin}$ at -38 °C. Bottom: Product $[\text{Cu}(\text{Dipp}_2\text{Im})(4\text{-CF}_3\text{-C}_6\text{H}_4)]$ at -38 °C.

The sample was kept at $-40\text{ }^{\circ}\text{C}$ for 2 h, but no progression of the reaction was observed. The reaction mixture was heated stepwise ($-30\text{ }^{\circ}\text{C}$ for 1.5 h; $-20\text{ }^{\circ}\text{C}$ for 1 h, $-10\text{ }^{\circ}\text{C}$ for 1 h) and spectra recorded. At higher temperatures, the signals in the ^1H NMR spectrum sharpened and the signals for the methine protons of the *iso*-propyl moieties coalesced, while in the ^{19}F NMR spectra broadening of the signal and a temperature dependent shift (at $-40\text{ }^{\circ}\text{C}$ -60.4 ppm ; at $-10\text{ }^{\circ}\text{C}$ -60.9 ppm ; at $20\text{ }^{\circ}\text{C}$ -62.1 ppm) was observed. At a sample temperature of $-5\text{ }^{\circ}\text{C}$ the growth of new peaks and decline of the mentioned ones in the ^1H , ^{19}F and ^{11}B NMR spectra was observed. The mixture was monitored for 3 days at $-5\text{ }^{\circ}\text{C}$, before the temperature was stepwise raised to $20\text{ }^{\circ}\text{C}$ ($0\text{ }^{\circ}\text{C}$ for 1 h, $10\text{ }^{\circ}\text{C}$ for 1 h) (Figures 30 to 32).

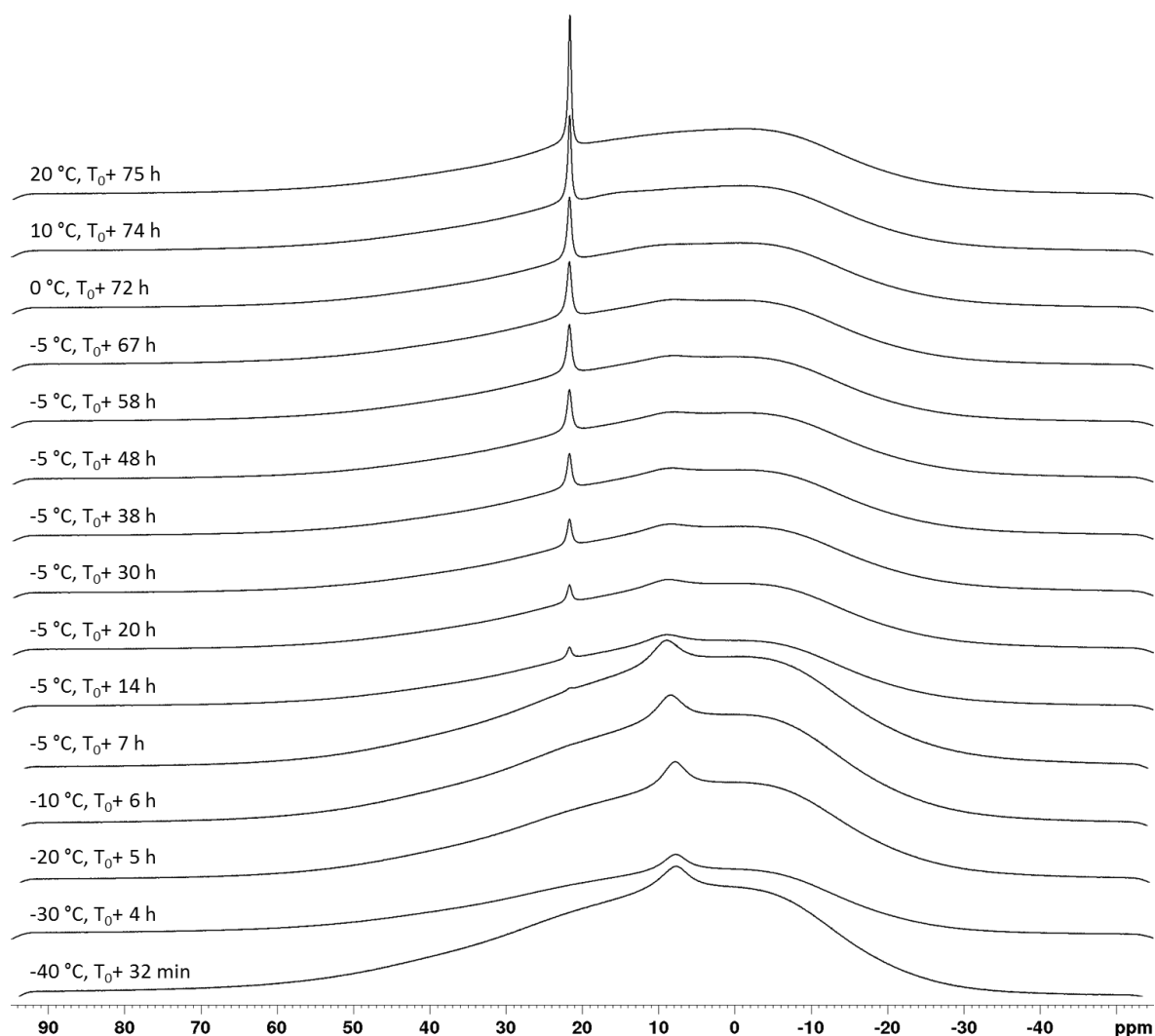


Figure 30: *In situ* ^{11}B VT-NMR spectra of the reaction of $[\text{Cu}(\text{Dipp}_2\text{Im})(\text{O}^t\text{Bu})]$ 13 with $4\text{-CF}_3\text{-C}_6\text{H}_4\text{Bpin}$.

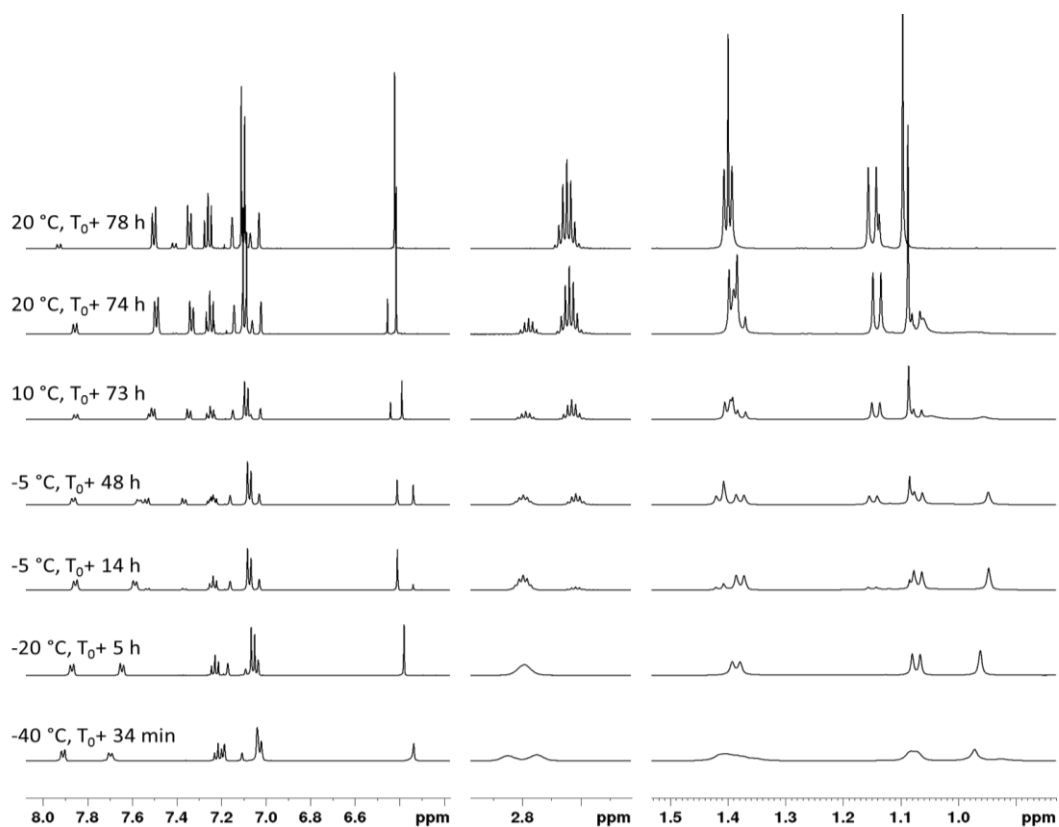


Figure 31: *In situ* ^1H VT-NMR spectra of the reaction of $[\text{Cu}(\text{Dipp}_2\text{Im})(\text{O}^t\text{Bu})]$ 13 with $4\text{-CF}_3\text{-C}_6\text{H}_4\text{Bpin}$.

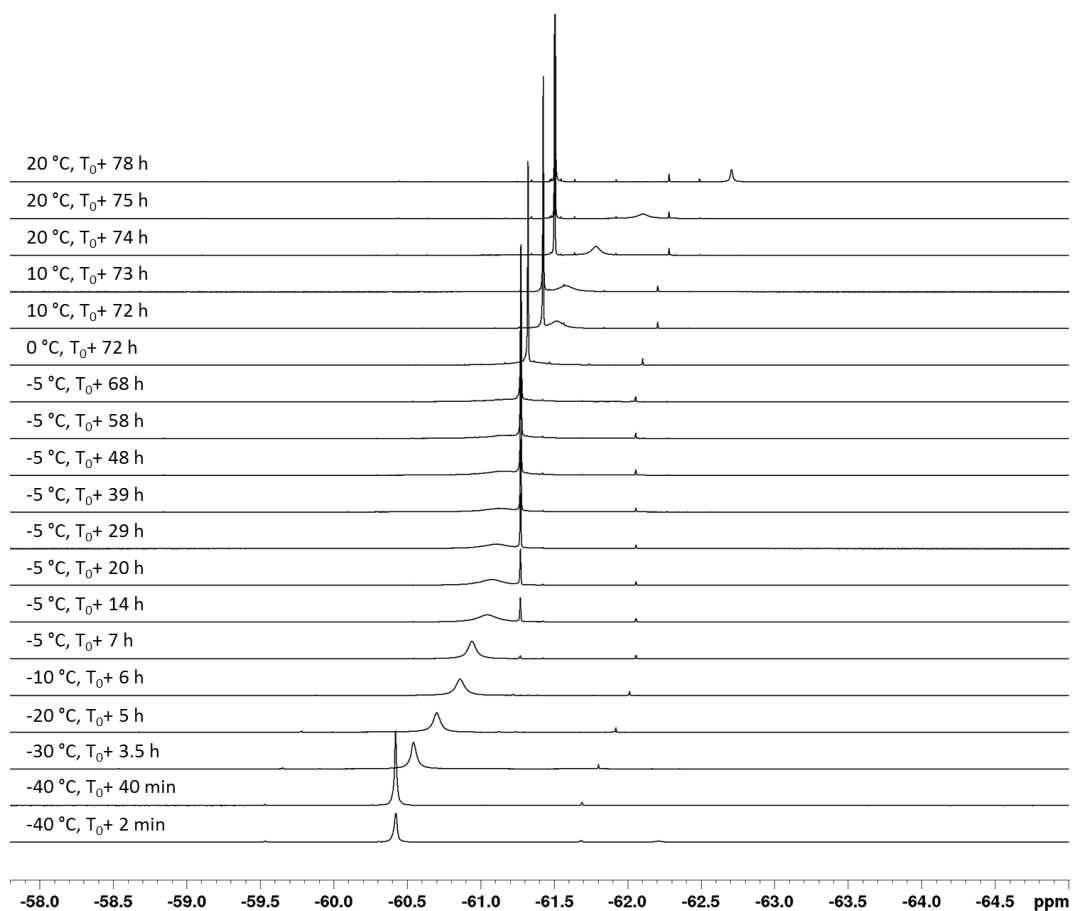


Figure 32: *In situ* ^{19}F VT-NMR spectra of the reaction of $[\text{Cu}(\text{Dipp}_2\text{Im})(\text{O}^t\text{Bu})]$ 13 with $4\text{-CF}_3\text{-C}_6\text{H}_4\text{Bpin}$. The signal of the spectrum at $T_0 + 78$ h is cut off because of space reasons.

The new peaks observed in the ^1H and ^{19}F NMR spectra from the reaction mixture fit well the resonance found for the isolated complex $[\text{Cu}(\text{Dipp}_2\text{Im})(4\text{-CF}_3\text{-C}_6\text{H}_4)]$ measured in C_6D_6 at room temperature (Figures 33 and 34) as well as the signals expected for the $^t\text{BuOBpin}$ byproduct (Figure 35).

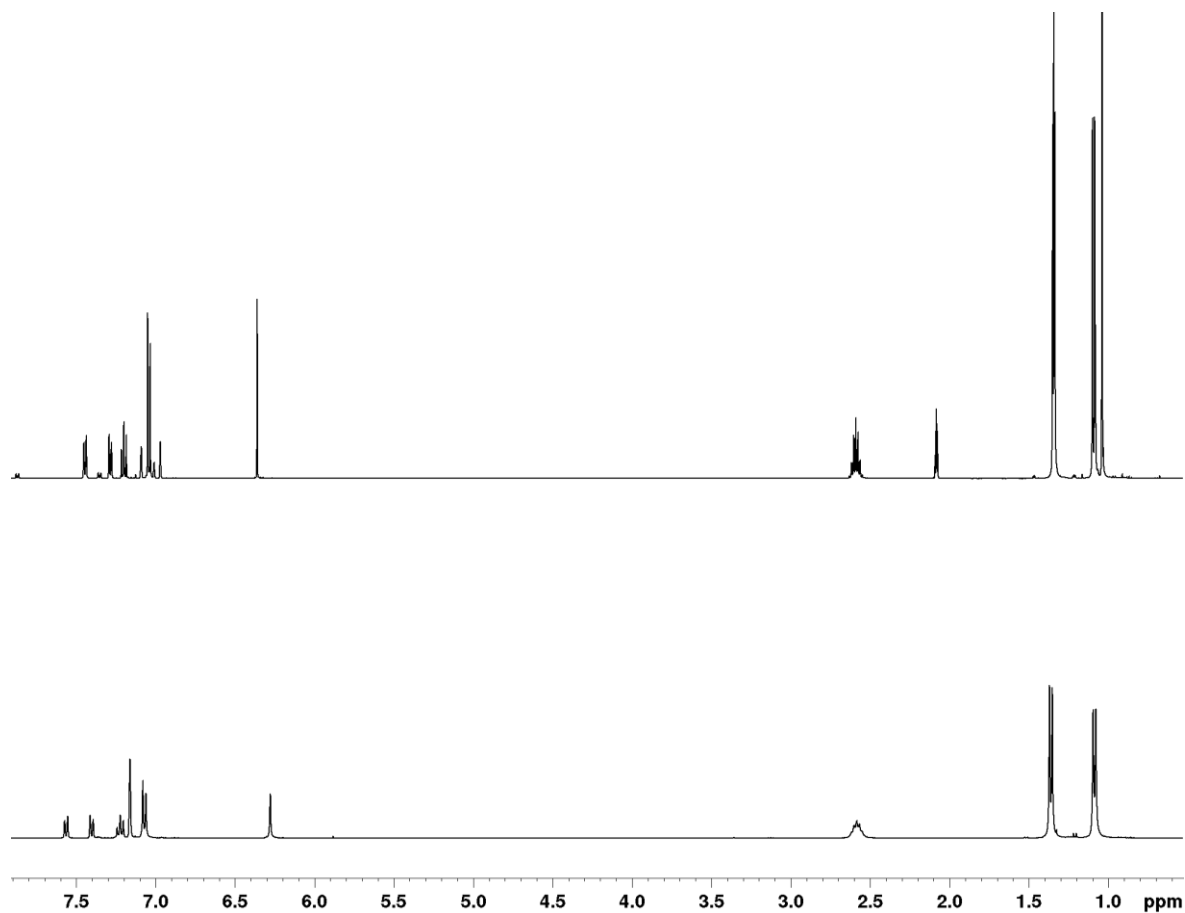


Figure 33: Comparison of the ^1H NMR spectrum of the reaction mixture of $[\text{Cu}(\text{Dipp}_2\text{Im})(\text{O}^t\text{Bu})]$ **13** with 4- $\text{CF}_3\text{-C}_6\text{H}_4\text{Bpin}$ in toluene-d_8 after 78 h (Top) with the ^1H NMR spectrum of the isolated complex $[\text{Cu}(\text{Dipp}_2\text{Im})(4\text{-CF}_3\text{-C}_6\text{H}_4)]$ in C_6D_6 (Bottom).

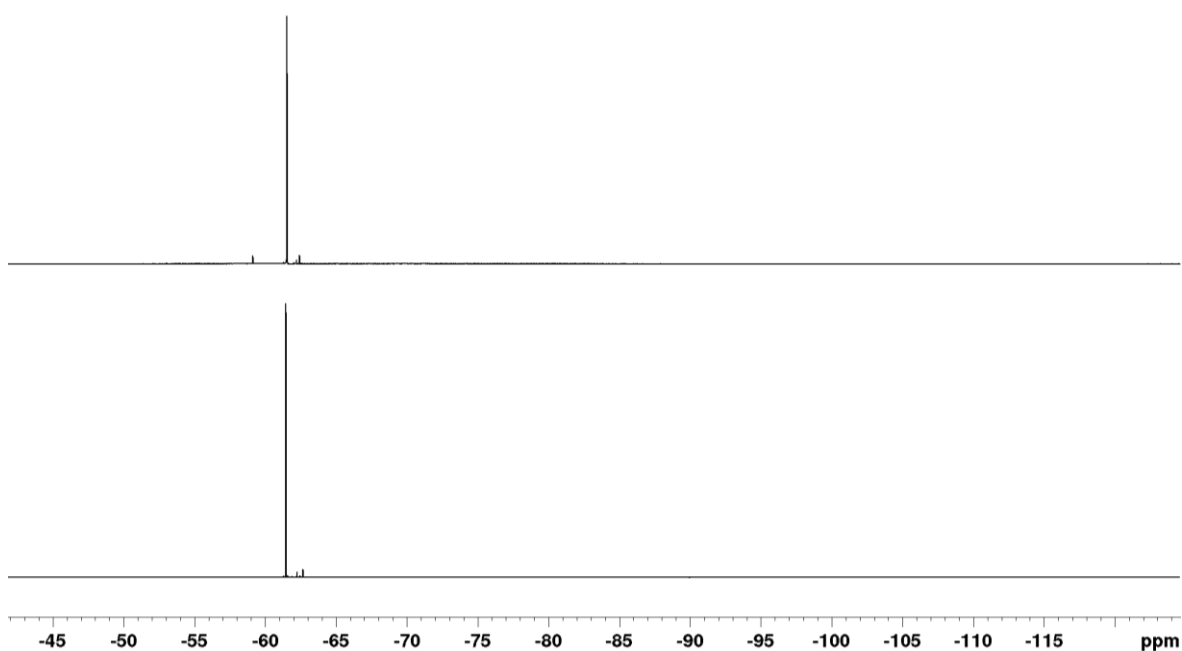


Figure 34: Comparison of the ^{19}F NMR spectrum of the reaction mixture of $[\text{Cu}(\text{Dipp}_2\text{Im})(\text{O}^t\text{Bu})]$ 13 with 4- $\text{CF}_3\text{-C}_6\text{H}_4\text{Bpin}$ in toluene-d_8 after 78 h (Top) with the ^{19}F NMR spectrum of the isolated complex $[\text{Cu}(\text{Dipp}_2\text{Im})(4\text{-CF}_3\text{-C}_6\text{H}_4)]$ in C_6D_6 (Bottom).

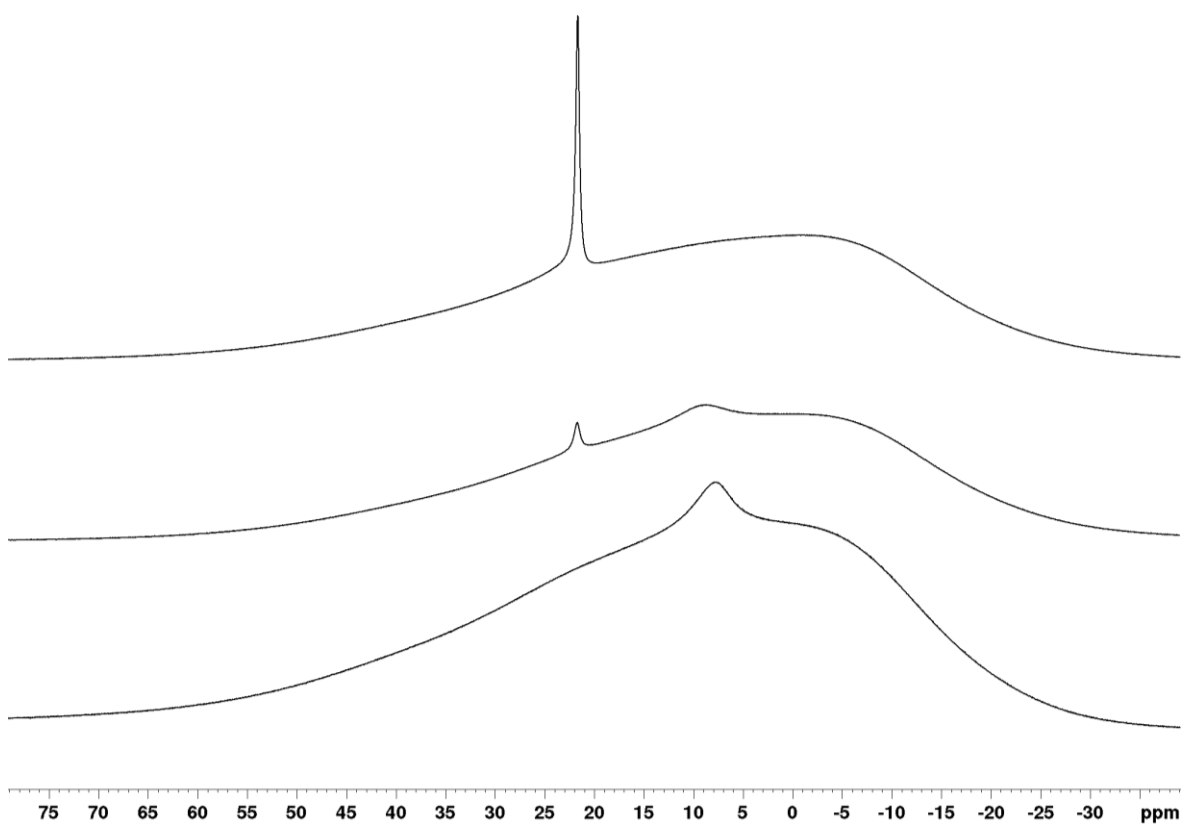


Figure 35: *In situ* ^{11}B VT-NMR spectra of the reaction of $[\text{Cu}(\text{Dipp}_2\text{Im})(\text{O}^t\text{Bu})]$ 13 with 4- $\text{CF}_3\text{-C}_6\text{H}_4\text{Bpin}$. Bottom: At $T_0 = +4$ min and -40 °C. Middle: At $T_0 = +18$ h and -5 °C. Top: At $T_0 = +78$ h and r.t.

The reaction showed complete conversion of the starting materials to one product (plus the expected byproduct ^tBuOBpin) in the ¹H, ¹¹B and ¹⁹F NMR spectra. Only trace amounts of other resonances were found in the ¹H and ¹⁹F NMR spectra (Figure 36).

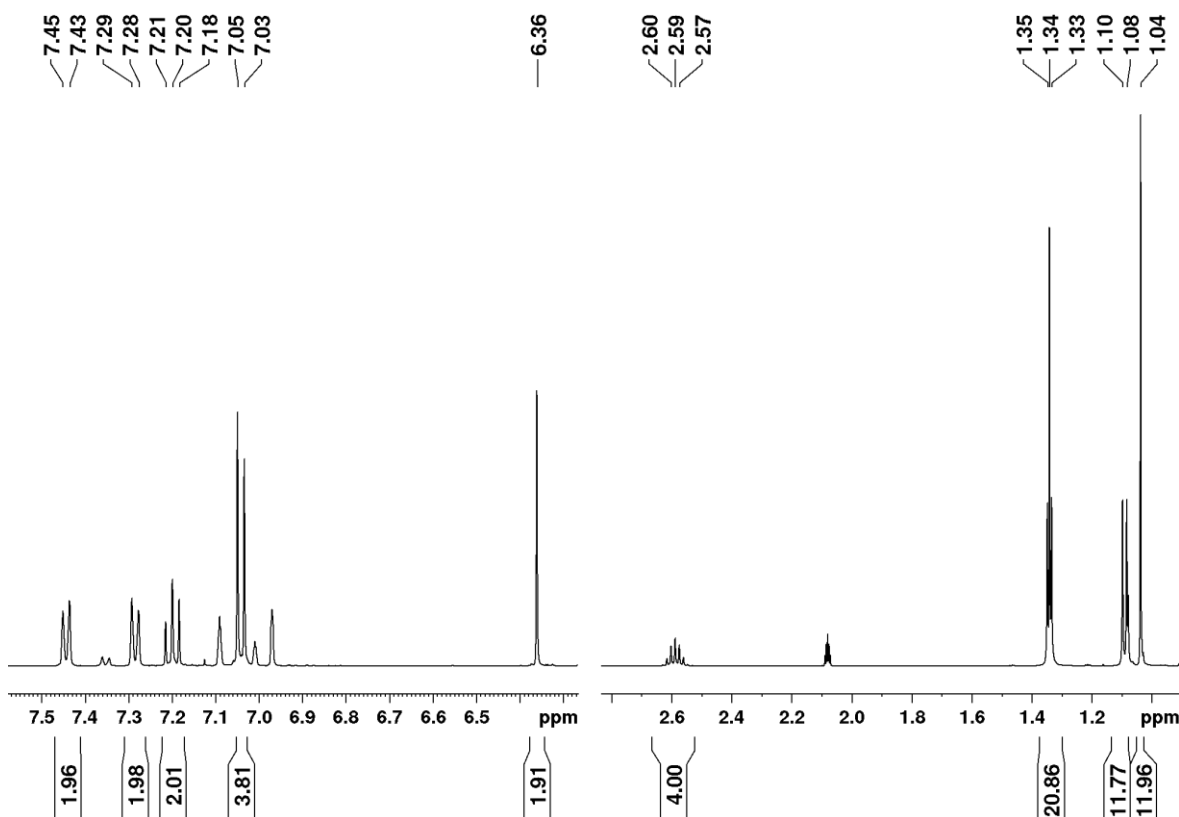
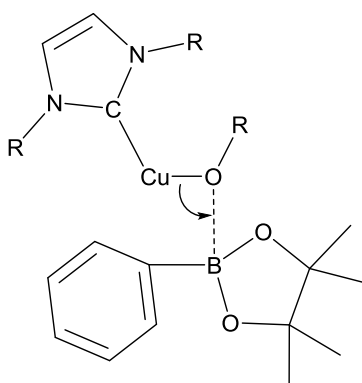


Figure 36: *In situ* ¹H VT-NMR spectrum of the reaction of [Cu(Dipp₂Im)(O^tBu)] **13** with 4-CF₃-C₆H₄Bpin in toluene-*d*₈ after 78 h.

One intermediate was observed, which was stable up to a temperature of -5 °C. The upfield shift in the ¹¹B NMR spectra of the intermediate signal (7.7 ppm) compared to the resonance of the starting material (31.3 ppm) and the byproduct ^tBuOBpin (21.6 ppm) shows that the new species has higher electron density and likely arise from an intermediate in which the boron is quarternized. A possible structure could be an adduct wherein the ^tBuO oxygen atom coordinates the boron atom (Scheme 45).



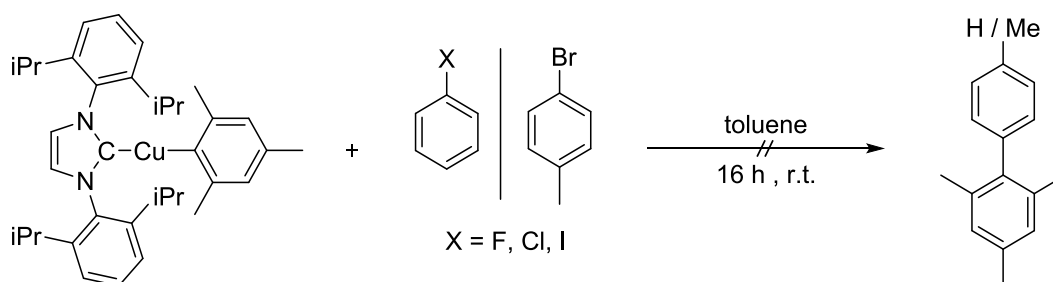
Scheme 45: Possible intermediate in the copper(I) catalyzed cross-coupling reaction.

This interpretation of the spectra recorded is supported by Hou *et al.*, who found a similar adduct intermediate of the alkoxide complex $[\text{Cu}(\text{Dipp}_2\text{Im})(\text{OMe})]$ and an alkyl 9-BBN reagent towards the formation of the copper(I) alkyl complex.^[260, 286] In X-ray diffraction investigations of the intermediate they determined a Cu-O distance of 1.859(2) Å. The Cu-O bond length in the alkoxide complexes $[\text{Cu}(\text{Dipp}_2\text{Im})(\text{O}^t\text{Bu})]$ and $[\text{Cu}(\text{Dipp}_2\text{Im})(\text{OEt})]$ is 1.8104(13) and 1.799(3) Å, respectively.^[252, 287] The elongated Cu-O bond length in the intermediate (compared to the alkoxide complexes) is indicative for a lowered bond order as in the intermediate there is less electron density between the copper atom and the oxygen atom. The B-C_{alkyl} distance in the intermediate is 1.631(4) Å. In compounds in which 9-BBN is exclusively bond to an alkyl moiety and thus having a sp²-hybridized boron atom the B-C_{alkyl} bond length is much shorter with values between 1.555(6) and 1.572(2).^[288-289] Since both the Cu-O and the B-C_{alkyl} bond are elongated in the intermediate facile formation of the copper(I) alkyl complex can easily occur. Although the copper alkyl complex was not observed by Hou *et al.* in the reaction with alkyl 9-BBN reagents, the formation of the corresponding complexes with aryl and alkenyl boronic neopentyl glycolate esters is documented.^[260, 286] However, in the reaction of $[\text{Cu}(\text{Dipp}_2\text{Im})(\text{O}^t\text{Bu})]$ **13** and with 4-CF₃-C₆H₄Bpin clean formation of the complex $[\text{Cu}(\text{Dipp}_2\text{Im})(4\text{-CF}_3\text{-C}_6\text{H}_4)]$ and the corresponding intermediate adduct were witnessed in our *in situ* ¹H, ¹¹B and ¹⁹F VT-NMR experiments.

3.2.4 Reactivity of NHC-stabilized copper(I)-aryl complexes in stoichiometric cross-coupling reactions

As the reaction of a phosphine-stabilized copper(I) aryl complex with an aryl halide was calculated to have the highest energy barrier for cross-coupling reactions,^[256] we wanted to address this point with our related, NHC-stabilized, system. Therefore, stoichiometric reactions of NHC-stabilized copper(I) aryl complexes with aryl halides were carried out to determine the reactivity of the more stable analogs.

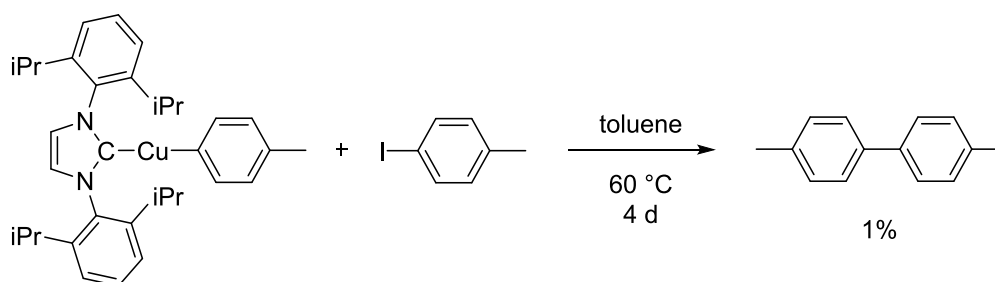
The complex $[\text{Cu}(\text{Dipp}_2\text{Im})(\text{Mes})]$ **24** was reacted with different aryl halides. One equivalent of **24** and one equivalent of the aryl halide was stirred for 16 hours at room temperature in toluene (Scheme 46).



Scheme 46: Screening of $[\text{Cu}(\text{Dipp}_2\text{Im})(\text{Mes})]$ **24** against different aryl halides.

In situ ^1H NMR spectra of the reactions of **24** with fluorobenzene, chlorobenzene, iodobenzene and *p*-bromotoluene showed only signals for the starting materials.

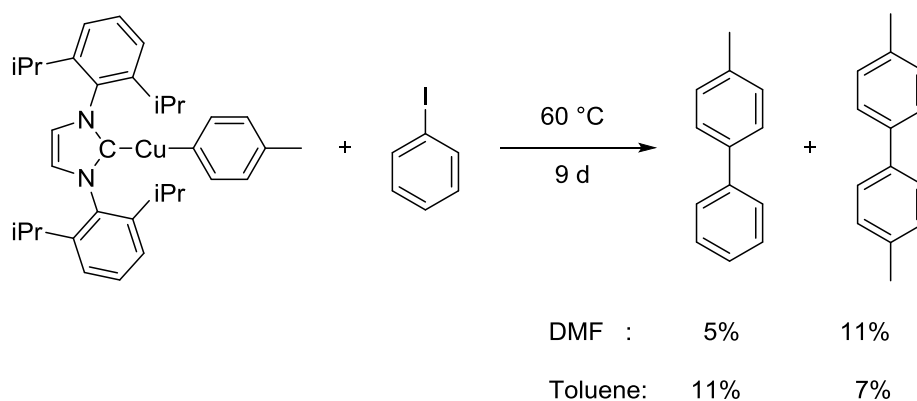
The screening was repeated at higher temperatures and also with a complex bearing less demanding substituents (Scheme 47). The yields were determined using GCMS and a multiple point internal standard method.



Scheme 47: Stoichiometric reaction of $[\text{Cu}(\text{Dipp}_2\text{Im})(p\text{-tolyl})]$ **27** with 4-iodotoluene at 60 °C.

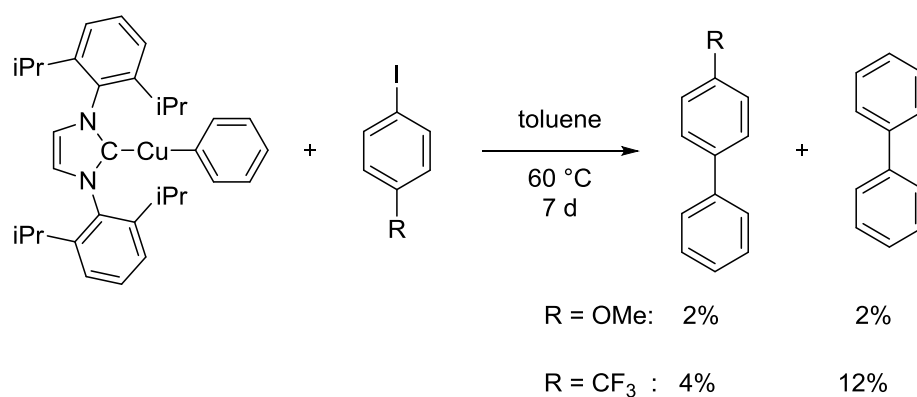
After four days at 60 °C only 1 percent of the product was formed indicating the reaction to be very slow.

The reaction of $[\text{Cu}(\text{Dipp}_2\text{Im})(p\text{-tolyl})]$ with iodobenzene at 60 °C in toluene afforded 11% product and 7% homo-coupled side product within 9 days. In DMF, the reaction products are 5% for the cross-coupled product and 11% for the side product (Scheme 48).



Scheme 48: Stoichiometric reactions of $[\text{Cu}(\text{Dipp}_2\text{Im})(p\text{-tolyl})]$ 27 with iodobenzene in DMF and toluene at 60 °C.

To investigate the influence of the electronic densities of the substrate on the reaction $[\text{Cu}(\text{Dipp}_2\text{Im})(\text{C}_6\text{H}_5)]$ was reacted with 1-iodo-anisole as well as 1-iodo-4-trifluoromethylbenzene in toluene at 60 °C for seven days.



Scheme 49: Investigation of the influence of electronics on the cross-coupling.

The yields were 2 and 4%, respectively, while the formation of the side product was 2 and 11%, respectively. As substrates, the corresponding aryl bromides were investigated as well, but the yields were lower than those found for the iodides.

Furthermore, it was not possible to observe a reaction of **22** with the partially fluorinated 1,2,3-trifluorobenzene after 16 hours at room temperature. The reactions of **22** with perfluorinated benzene and toluene, respectively, at 70 °C showed the formation of [Cu(Dipp₂Im)(F)] and another species in the ¹⁹F NMR spectrum. The complexes [Cu(Dipp₂Im)(*p*-tolyl)] **14** and [Cu(Dipp₂Im)(4-CF₃-C₆H₄)] **18** showed similar reactivity with C₆F₆. However, attempts to characterize this species failed.

The low yields, side product formation and long reactions times observed in the stoichiometric cross-coupling reactions of NHC-stabilized copper(I) aryl complexes showed that NHC-stabilized copper(I) might be too stable to undergo this decisive step efficiently.

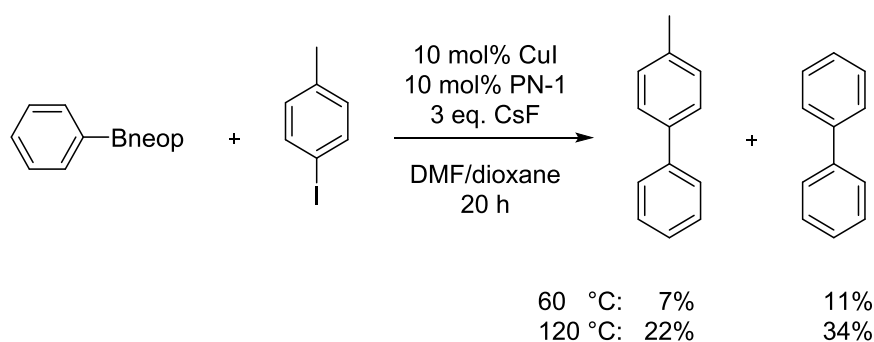
3.3 Reactivity of copper(I) complexes in catalytic cross-coupling reactions

As NHC-stabilized copper(I) complexes showed insufficient reactivity in stoichiometric cross-coupling reactions, catalytic cross-coupling systems with bidentate, hemi-labile ligands were investigated.

3.3.1 Copper(I) catalyzed cross-coupling of aryl iodides with PN donor ligands

The copper(I) catalyzed cross-coupling system published by Giri *et al.* is capable of cross-coupling aryl- and heteroaryl iodides with a variety of aryl boron reagents giving good to very good yields.^[169] One down side of this system are the harsh reaction condition of 120 °C and 48 h reaction time. To obtain a more capable catalytic system, based on the findings of Giri *et al.*, the steric demand of the ligand (ⁱPr₂ instead of ^tBu₂) was reduced as well as more flexible phosphorus-nitrogen ligands such as Davephos and ^tBuDavePhos were tested in catalytic cross-coupling reactions.

The first catalytic reactions were performed under the following conditions: CuI (10 mol%), PN-1 (10 mol%), CsF (3 eq.), phenylboronic acid neopentyl glycol ester (1 eq.) and 4-iodotoluene (1 eq.) in a 1:1 mixture of DMF and dioxane at 60 °C for 20 hours. The screening showed that the PN-1 ligand is capable of cross-coupling the applied substrates to the desired biaryl compound (7%), but homo-coupling of the aryl borononic ester predominated (11%) and the yields were very low. At a temperature of 120 °C the yields were higher (22%) with the same the product/homo-coupling ratio (1:1.5) (Scheme 50).



Scheme 50: Screening of a slightly modified routine for the copper(I) catalyzed cross-coupling of aryl iodides with PN-1 as ligand.

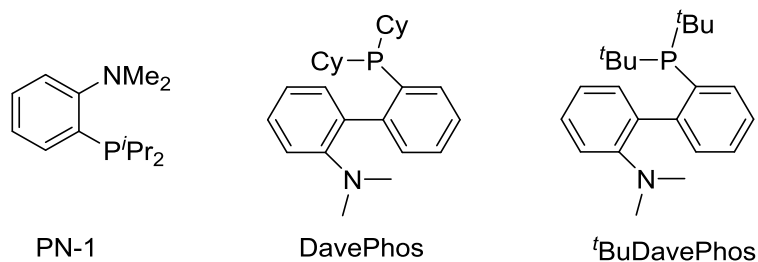
Optimization of the reaction conditions were investigated at a reaction temperature of 80 °C for 20 hours. At first the influence of the solvent was investigated. In all solvents applied cross-coupling was observed, but at very low yields (Table 7, section one). However, homo-coupling was significantly present especially in the reaction with THF as solvent (56%). Reactions in DMF showed the best yield (28%) and the best product/homo-coupling ratio (1.2:1). All other attempts for reaction optimizations, namely base screening (Table 7, section two) and ligand screening (Table 7, section three), did not provide better results than those obtained from: CuI (10 mol%), PN-1 (10 mol%), CsF (3 eq.) in DMF for 20 hours at 80 °C.

Table 7: Optimization of the copper(I) catalyzed cross-coupling reaction of aryl boronic neopentyl glycol esters with aryl iodides.* = 20mol% were used for monodentate ligands.

ligand (10 mol%)	base (3 eq.)	solvent	X coupling in %	homo-coupling in %
PN1	CsF	DMF	28	23
PN1	CsF	DMF/dioxane	22	34
PN1	CsF	THF	4	56
PN1	CsF	MTBE	4	22
PN1	CsF	Dioxane	3	10
PN1	CsF	toluene	1	24
PN1	KF	DMF	6	1
PN1	NMe ₂ F	DMF	2	65
PN1	KO ^t Bu	DMF	-	10
PN1	LiO ^t Bu	DMF	1	54
PN1	KOMe	DMF	-	-
PN1	NaOMe	DMF	-	30
Xantphos	CsF	DMF	4	8
Davephos	CsF	DMF	-	-
^t BuDavephos	CsF	DMF	3	3
ⁱ Pr ₂ Im	CsF	DMF	2	5
Dipp ₂ Im	CsF	DMF	3	8
Mes ₂ Im	CsF	DMF	2	8

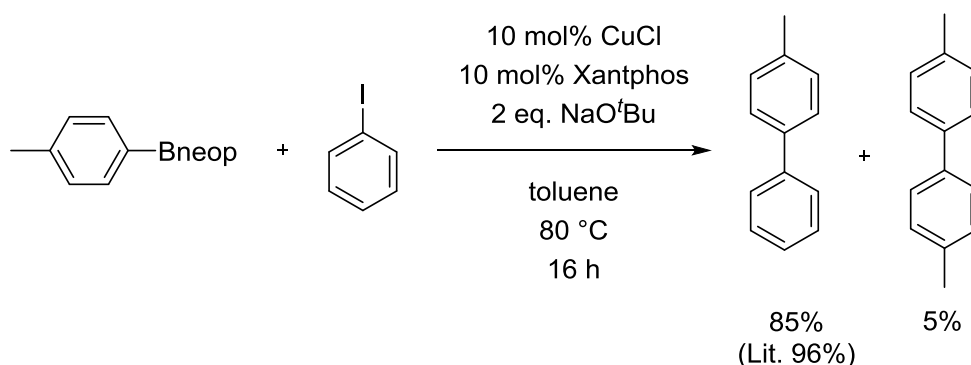
3 Results and Discussion

NEt ₃	CsF	DMF	-	-
bpy	CsF	DMF	-	-
dtbpy	CsF	DMF	-	-
PPh ₃ *	CsF	DMF	2	8
P(<i>n</i> Bu) ₃ *	CsF	DMF	2	54



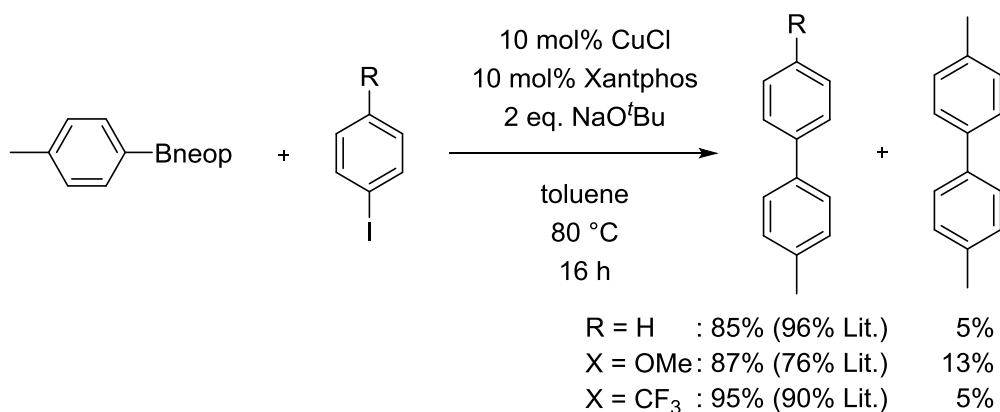
3.3.2 Copper(I) catalyzed cross-coupling of aryl iodides with Xantphos as ligand

The milder copper(I) catalyzed system published by Brown *et al.* was investigated for optimization.^[170] In attempts to reproduce the catalysis of *p*-tolyl boronic acid neopentyl glycol ester and iodobenzene, with the method reported, 87% yield were observed instead of the reported 99% (3 eq. base). In addition, 5% homo-coupling of the aryl boronic substrate was observed, a side reaction which was not addressed in the publication. In a slightly modified protocol, using only two equivalents base instead of three and copper(I) chloride and Xantphos instead of the isolated complex, the yields were almost identical to what was found for the reported routine (Scheme 51).



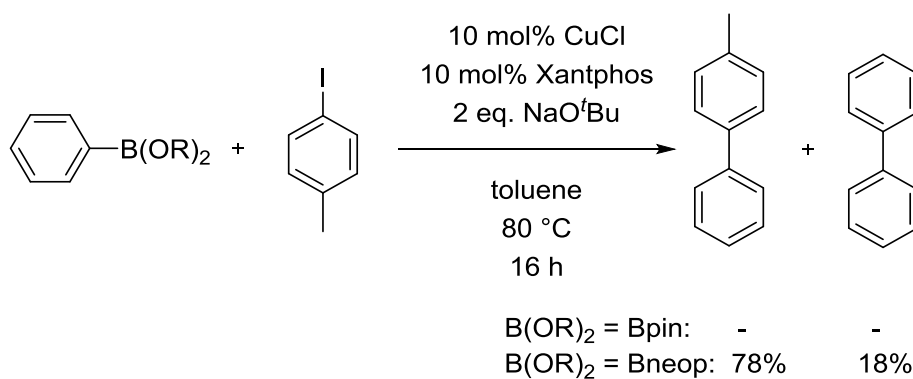
Scheme 51: Screening of a slightly modified routine for the copper(I) catalyzed cross-coupling of aryl iodides with Xantphos as ligand.

Aryl iodides with neutral, electron withdrawing and electron donating groups were tested as substrates (Scheme 52). Electron withdrawing groups seem to promote the catalysis (95% yield, only 5% homo-coupling), while electron donating groups showed a higher percentage of homo-coupling (87% yield, 13% homo-coupling) compared to the other substrates. The trend observed in yields fits with the published data.^[170]



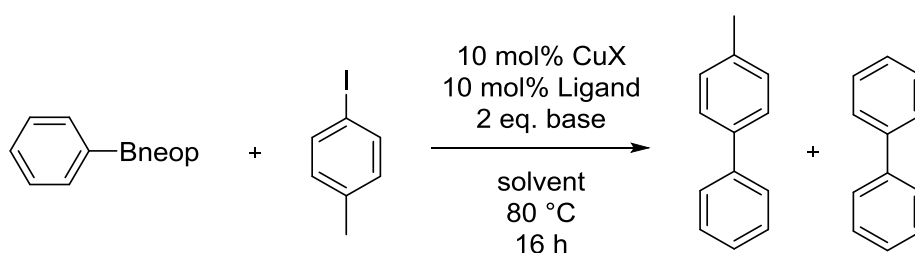
Scheme 52: Substrate screening for the copper(I) catalyzed cross-coupling of aryl iodides with Xantphos as ligand.

When phenyl boronic acid pinacol ester and 4-iodotoluene were applied as substrates no cross-coupling nor homo-coupling was observed (Scheme 53). Literature reported 44% isolated yield for the cross-coupling of phenyl boronic acid pinacol ester with 4-iodochlorobenzene.^[170] Maybe the electron withdrawing effect is essential for the less reactive pinacolate esters. With phenyl boronic acid neopentyl glycol ester and 4-iodotoluene, a 78% yield and 18% homo-coupling was observed.



Scheme 53: Screening for different aryl boronic esters as substrates for the copper(I) catalyzed cross-coupling of aryl iodides with Xantphos as ligand.

For optimization of the reaction conditions the influence of the metal halide (Table 8, first section), the solvent (Table 8, second section), the base (Table 8, third section) and the ligand (Table 8, fourth section) on this (unpublished) reaction were tested (Scheme 54).



Scheme 54: Cross-coupling reaction of phenyl boronic acid neopentyl glycol ester with 4-iodotoluene.

When copper(I) bromide was used as the metal salt the cross-coupling was diminished while the homo-coupling was enhanced. With copper(I) iodide no reactions were observed, while Brown *et al.* reported almost the same yields for copper(I) bromide and iodide than for copper(I) chloride for the cross-coupling of *p*-tolyl boronic acid neopentyl glycol ester with iodobenzene. The absence of a copper salt shut the reaction down, which is in accordance with literature. The solvent had a large impact on the reaction as well. While no solvent showed nearly as high yields as toluene, the reaction with THF as solvent showed almost quantitative homo-coupling. Reaction with sodium methoxide as base showed 100% conversion, but more homo-coupling was observed than with sodium *tert*-butoxide. The lithium and potassium salts of *tert*-butoxide showed to be much less effective than the sodium analog. For monodentate ligands 20 mol% were used, but homo-coupling predominated. No other ligand was nearly as effective in this cross-coupling reaction as Xantphos.

3 Results and Discussion

Table 8: Optimization of the copper(I) catalyzed cross-coupling reaction of aryl boronic neopentyl glycol esters with aryl iodides * = 20 mol% was used for monodentate ligands.

Metal salt	Ligand (10 mol%)	Base (2 eq.)	solvent	cross-coupling in %	homo-coupling in %
CuCl	Xantphos	NaO ^t Bu	toluene	78	18
CuBr	Xantphos	NaO ^t Bu	toluene	29	34
CuI	Xantphos	NaO ^t Bu	toluene	-	-
none	Xantphos	NaO ^t Bu	toluene	-	1
CuCl	Xantphos	NaO ^t Bu	EtOH	2	2
CuCl	Xantphos	NaO ^t Bu	water	5	2
CuCl	Xantphos	NaO ^t Bu	THF	13	86
CuCl	Xantphos	NaO ^t Bu	DMF	13	58
CuCl	Xantphos	NaO ^t Bu	dioxane	32	40
CuCl	Xantphos	NaO ^t Bu	MTBE	28	47
CuCl	Xantphos	LiO ^t Bu	toluene	30	35
CuCl	Xantphos	KO ^t Bu	toluene	-	26
CuCl	Xantphos	NaOMe	toluene	60	40
CuCl	Xantphos	KOMe	toluene	34	66
CuCl	Xantphos	NMe ₄ F	toluene	-	-
CuCl	Xantphos	CsF	toluene	1	-
CuCl	Xantphos	KF	toluene	3	14
CuCl	Xantphos	none	toluene	-	-
CuCl	dppe	NaO ^t Bu	toluene	40	28
CuCl	PPh ₃ *	NaO ^t Bu	toluene	4	69
CuCl	P(<i>n</i> Bu) ₃ *	NaO ^t Bu	toluene	26	62
CuCl	Mes ₂ Im	NaO ^t Bu	toluene	17	31
CuCl	Dipp ₂ Im	NaO ^t Bu	toluene	-	22
CuCl	dtbpy	NaO ^t Bu	toluene	23	71
CuCl	NEt ₃ *	NaO ^t Bu	toluene	8	11
CuCl	DavePhos	NaO ^t Bu	toluene	-	1
CuCl	^t BuDavePhos	NaO ^t Bu	toluene	-	-

3 Results and Discussion

CuCl	PN-1	NaO ^t Bu	toluene	-	-
CuCl	none	none	toluene	- (<2)	13

Attempts to synthesize the corresponding Xantphos-stabilized copper(I) chloride and iodide, respectively, complex for the use as precoordinated catalysts in cross-coupling reactions, yielded the corresponding tetracoordinate acetonitrile complexes **45** and **46** (Figure 37).

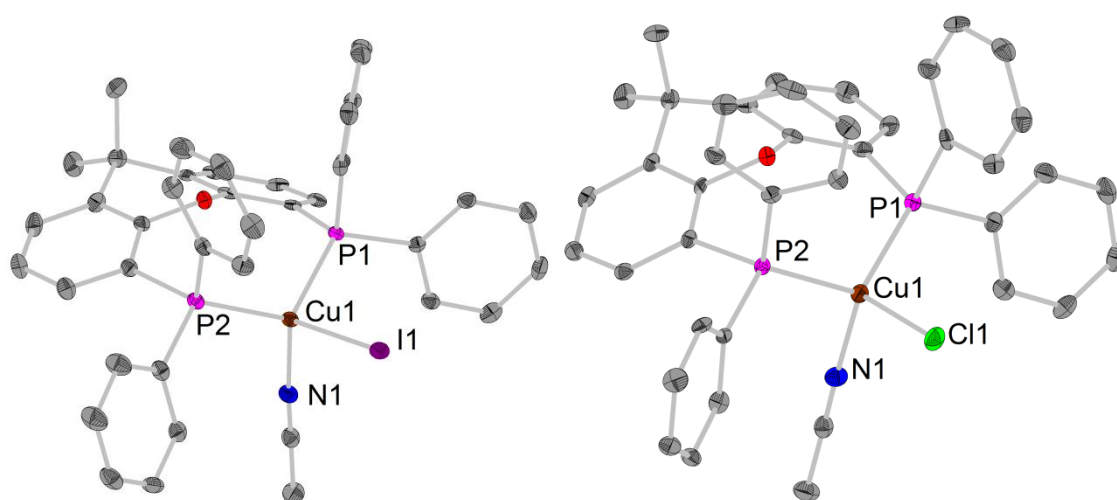


Figure 37: Element (color): carbon (grey), nitrogen (blue), copper (maroon), chlorine (green), phosphorus (pink), iodide (purple). Hydrogen atoms and solvent molecules are omitted for clarity and the thermal ellipsoids are drawn at 50% probability. Left: Molecular structure of [Cu(Xantphos)(I)(MeCN)] **45**. Selected bond lengths (Å) and angles (deg): Cu1–P1 2.2744(10), Cu1–P2 2.2788(12), Cu1–I1 2.6471(6), Cu1–N1 2.014(4), P1–Cu1–P2 115.98(4)°, P1–Cu1–I1 100.81(3)°, P1–Cu1–N1 110.14(11)°, P2–Cu1–I1 110.15(3)°, P2–Cu1–N1 114.24(10)°, N1–Cu1–I1 104.00(10)°. Right: Molecular structure of [Cu(Xantphos)(Cl)(MeCN)] **46**. Selected bond lengths (Å) and angles (deg): Cu1–P1 2.2759(6), Cu1–P2 2.2789(6), Cu1–Cl1 2.3424(10), Cu1–N1 2.018(2), P1–Cu1–P2 115.32(2)°, P1–Cu1–Cl1 109.14(2)°, P1–Cu1–N1 116.44(6)°, P2–Cu1–Cl1 103.08(2)°, P2–Cu1–N1 107.26(6)°, N1–Cu1–Cl1 104.22(6)°.

The Cu1–N1 bond lengths ([Cu(Xantphos)(I)(MeCN)] **45** 2.014(4) and [Cu(Xantphos)(Cl)(MeCN)] **46** 2.018(2) Å) are slightly longer than the one found in [Cu(Xantphos)(MeCN)][PF₆] (1.941(2) Å) where the weakly coordinating PF₆ anion is not bonded to the metal center.^[290] This complex also shows an angle of 164.8(2)° around the acetonitrile nitrogen atom, while the four coordinate complexes **46** (174.1(3)°) and **45** (175.6(4)°) have closer to linear coordination.^[290] Compared to the three coordinate complexes [Cu(Xantphos)(I)] (2.5041(10) Å) and [Cu(Xantphos)(Cl)] (2.1955(9) Å) the Cu–X

bond lengths are elongated by 14.3 and 8.0 pm or 5.7% and 3.6%, respectively.^[291-292] The same is found for the Cu-O distance, while in complex **45** and **46** the distance is 3.240(2) and 3.2694(19) Å, respectively, in the three coordinate complexes they are 2.829(5) and 2.976(2) Å, respectively.^[291-292] In other Xantphos-stabilized copper(I) halide complexes wherein the metal center is quarternized by, for example, nitrogen or sulfur donors, the trends in the molecular structures described above are identical.^[291, 293]

From the synthesis of a Xantphos-stabilized copper(I) *tert*-butoxide complex from [Cu(Xantphos)(Cl)] and KO^tBu in acetonitrile an acetonitrile-oligomerization product was obtained at room temperature (Figure 38).

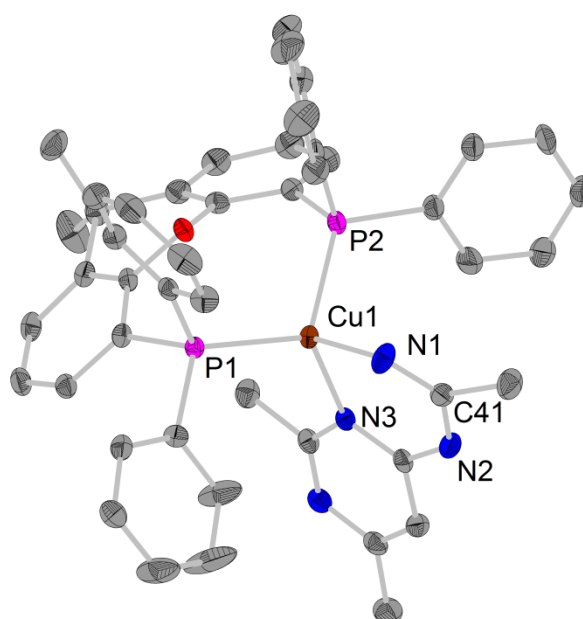


Figure 38: Molecular structure of [Cu(Xantphos)(MeCN)₄] **47**. Element (color): carbon (grey), nitrogen (blue), copper (maroon). Hydrogen atoms and solvent molecules are omitted for clarity and the thermal ellipsoids are drawn at 50% probability. Selected bond lengths (Å) and angles (deg): Cu1–P1 2.2621(15), Cu1–P2 2.2779(12), Cu1–N1 1.989(2), Cu1–N3 2.057(2), N1–C41 1.298(3), C41–N2 1.341(3), P1–Cu1–P2 113.13(4)°, P1–Cu1–N1 104.05(7)°, P1–Cu1–N3 115.34(7)°, P2–Cu1–N1 112.50(7)°, P2–Cu1–N3 116.54(6)°, N1–Cu1–N3 92.66(8)°.

In copper(I) complex **47** the central metal is coordinate by Xantphos as well as a tetramer of acetonitrile. The oligomeric binds in a bidentate fashion through two nitrogen atoms N1 and N3 with fairly similar Cu–N bond lengths (1.989(2) and 2.057(2) Å).

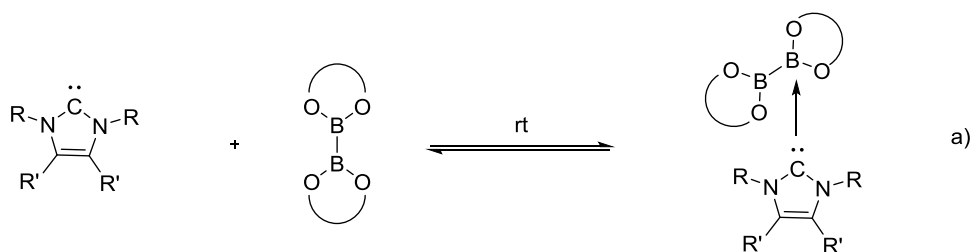
The oligomerization of α -hydrogen containing nitriles is known for sodium,^[294] Grignard reagents^[295] as well as sodium and potassium methoxide^[296-297] at elevated temperatures. Catalytic oligomerization was found using $[\text{IrH}(\text{CO})(\text{PPh}_3)_3]$ ^[298] as well as sodium hydride.^[299] Albeit the reaction pathway not being entirely new it is still worth mentioning for similar reactions and the choice of solvent.

The investigations on catalytic copper(I) cross-coupling systems showed that a certain steric demand seems necessary for a efficient catalysis. In the case of the PN donor ligand system the steric demand of the ligand was reduced compared to the ligand use in the publication, in order to obtain a more capable system being efficient at lower temperature. But the system proved to be less effective than the original, at lower as well as at the same reaction conditions. In addition a significant amount of homo-coupling was observed, a side reaction which was also observed in the copper(I)-catalyzed cross-couplings with Xantphos, although this was not mentioned in the publication.^[170] In both reactions setups the use of THF as solvent showed a distinct increase in homo-coupling. In the catalysis with Xantphos as ligand 86% homo-coupling was observed.

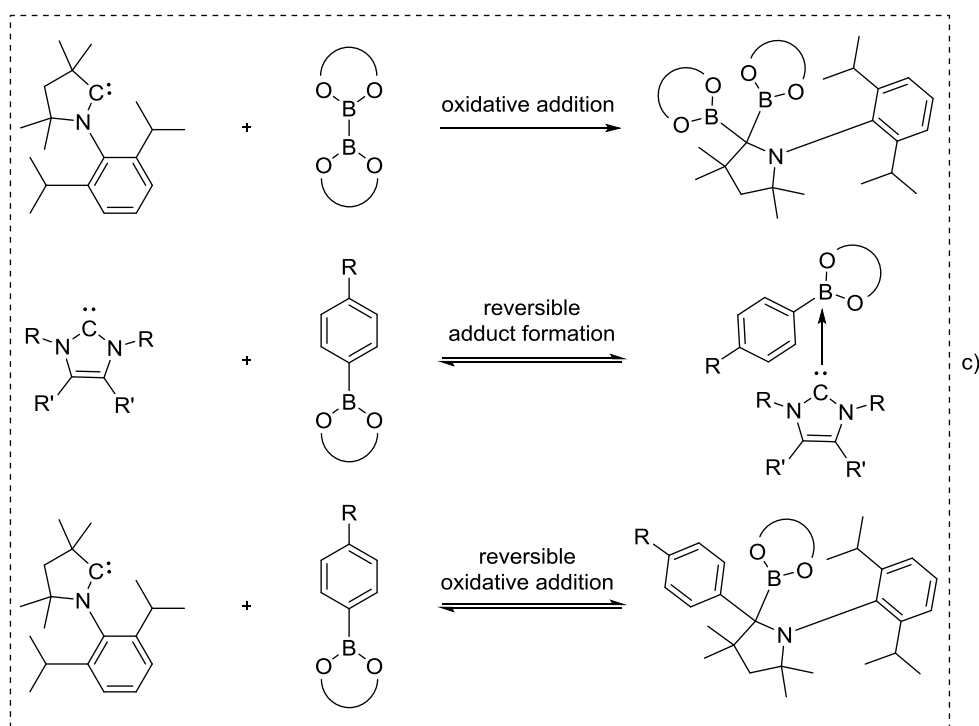
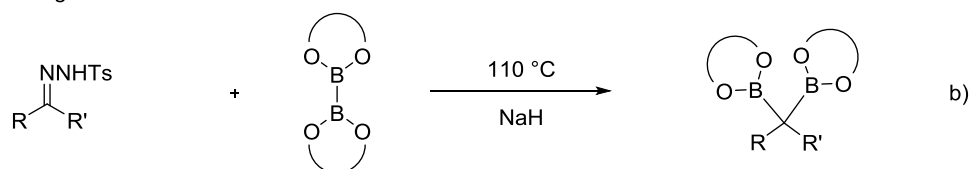
3.4 Reactivity of carbon-based Lewis bases with aryl boronic esters and diboron(4) compounds^[300-301]

The quest for a more sustainable chemistry has led to the development of metal-free catalytic processes.^[223] Lewis bases, and especially *N*-heterocyclic carbenes (NHCs) have recently emerged as organocatalysts in C-C, B-C, N-C, O-C and Si-C bond forming processes.^[192, 201-222] In 2012, the first β -borylation reaction of α,β -unsaturated compounds, promoted by NHCs was reported.^[203-204] In such cases, the NHCs form an sp^2 - sp^3 adduct^[302] with the diboron(4) compound,^[303] which weakens the B-B bond and thus facilitates the B-C bond formation (Scheme 55a).^[304] A variety of NHC ring expansion reactions were also observed as a result of rearrangement processes of similar mono- and bis-NHC adducts of diboron(4) compounds^[199] as well as other substrates.^[191, 193-198] Computational investigations based on a four step reaction mechanism calculated the ring opening process to be thermally feasible for NHC adducts after E-H bond activation, but too high in energy for adducts of cyclic alkyl amino carbenes (CaaC).^[305] Compared to NHCs, CaaCs have greater electrophilicity and a smaller HOMO-LUMO gap.^[250-251] These characteristics enable CaaCs to activate small molecules such as CO,^[306-307] H₂,^[308] P₄^[309-310] and other enthalpically strong single bonds, such as B-H, Si-H, P-H and N-H.^[311] *In situ* formed diazo compounds, which might function as precursors for dialkyl carbenes, showed insertion into B-B as well as B-Si bonds, forming *gem*-diboryl and *gem*-silylboryl compounds at elevated temperatures (Scheme 55b).^[312] Herein, we report the oxidative addition of B-B bonds at a carbene-carbon atom at room temperature, the reversible binding of NHCs to organoboronate esters as well as the first reversible oxidative addition at a carbon center at room temperature (Scheme 55c).

Marder 2012; Marder, Radius 2015, 2016



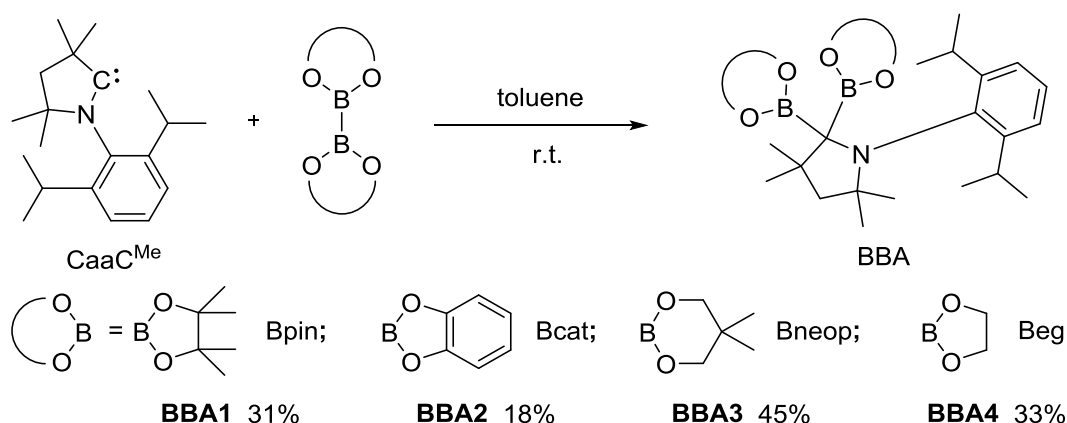
Wang: 2014



Scheme 55: Reactivity of carbenes with diboron(4) compounds as well as organoboronic esters.

3.4.1 B-B bond oxidative addition

The cyclic alkyl amino carbene CaaC^{Me} was reacted with the diboron(4) compounds B_2eg_2 , B_2pin_2 , B_2neop_2 and B_2cat_2 at room temperature (Scheme 56). *In situ* NMR experiments recorded at room temperature showed the immediate insertion of the carbene carbon atom into the B-B bond and complete conversion without any detectable adduct or intermediate.



Scheme 56: Reaction scheme of CaaC^{Me} with the diboron compounds B_2pin_2 , B_2cat_2 , B_2neop_2 and B_2eg_2 .

In all cases, the B-B bond activation products (BBA) were characterized by ^1H , ^{11}B , $^{13}\text{C}\{^1\text{H}\}$ NMR, HRMS and X-ray crystallography (Figure 42). The ^{11}B NMR spectra showed only a slight downfield shift compared to the starting materials (Table 9). This is consistent with that expected for a boryl group bound to a carbon atom rather than another boryl group.

Table 9: ^{11}B NMR shift of the starting compound and the BBA products.

^{11}B NMR	B_2eg_2	B_2pin_2	B_2neop_2	B_2cat_2
Starting material	31.7 ppm	30.6 ppm	28.4 ppm	30.6 ppm
BBA Product	32.9 ppm	31.6 ppm	29.4 ppm	34.5 ppm

However, in the ^1H NMR spectrum of the BBA product of the reaction of B_2pin_2 with CaaC^{Me} a doubling of all signals was observed. While the other, sterically less demanding diols are equivalent due to rotation around the B-C bonds, the Bpin moieties do not rotate rapidly due to their greater steric demand (Figure 39). Thus, two different orientations of the Bpin groups must be present as observed previously for *gem*-bis Bpin compounds.^[313]

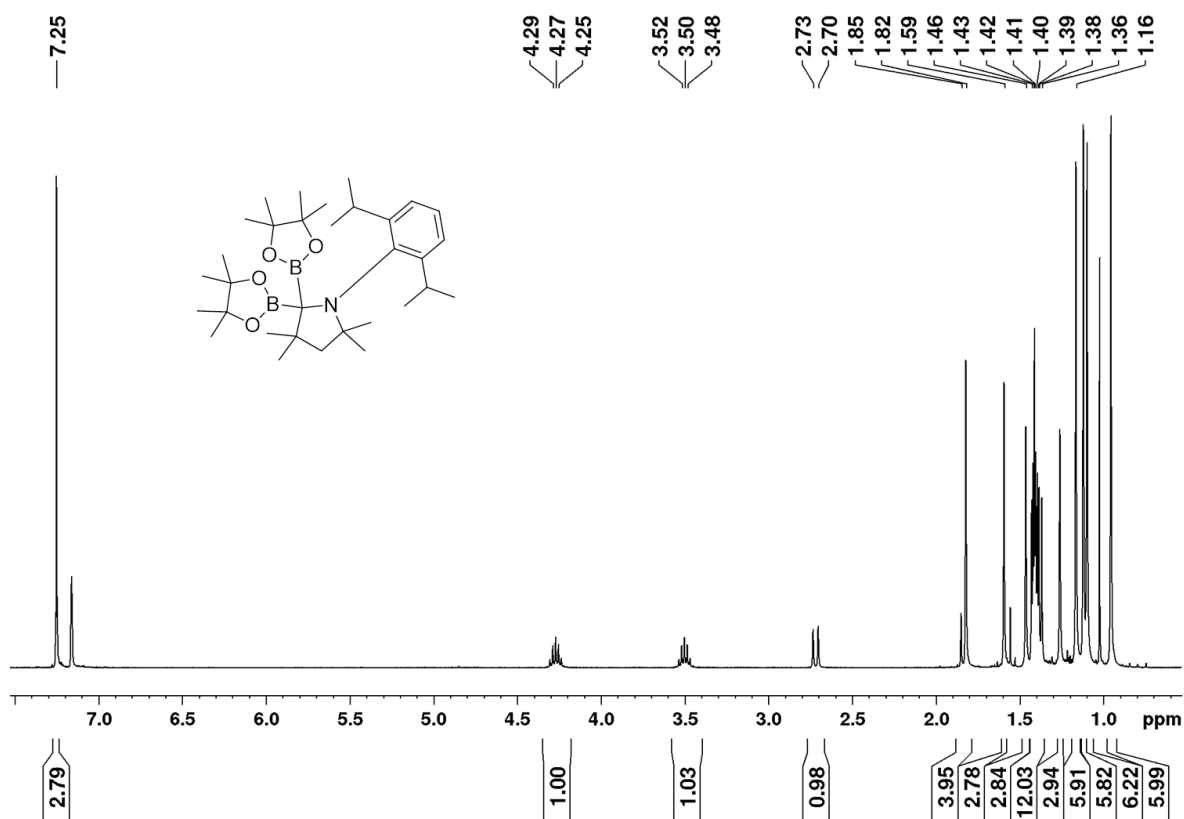


Figure 39: ¹H NMR spectrum of the BBA product of the reaction of B₂pin₂ with CaaC^{Me}.

Another feature was observed in the case of the ¹H NMR spectrum of the BBA product of the reaction of B₂neop₂ with CaaC^{Me}, in which two doublets of doublets with a ‘roofing’ effect were observed for the neopentyl glycol methylene protons. This is because these protons are diastereotopic even without the presence of a chiral center; the ‘roofing’ effect is dependent on the field strength, as shown in Figure 41.

3 Results and Discussion

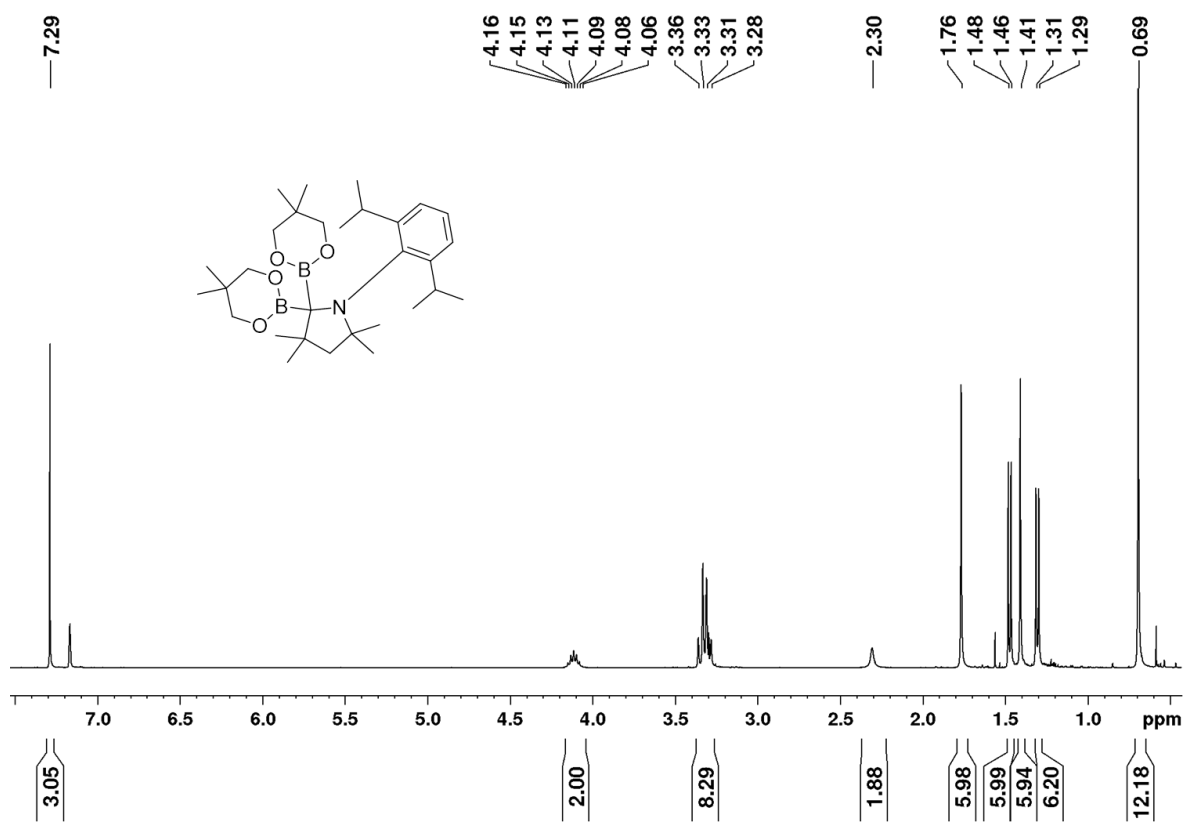


Figure 40: ^1H NMR spectrum of the BBA product of the reaction of B_2neop_2 with CaaC^{Me} .

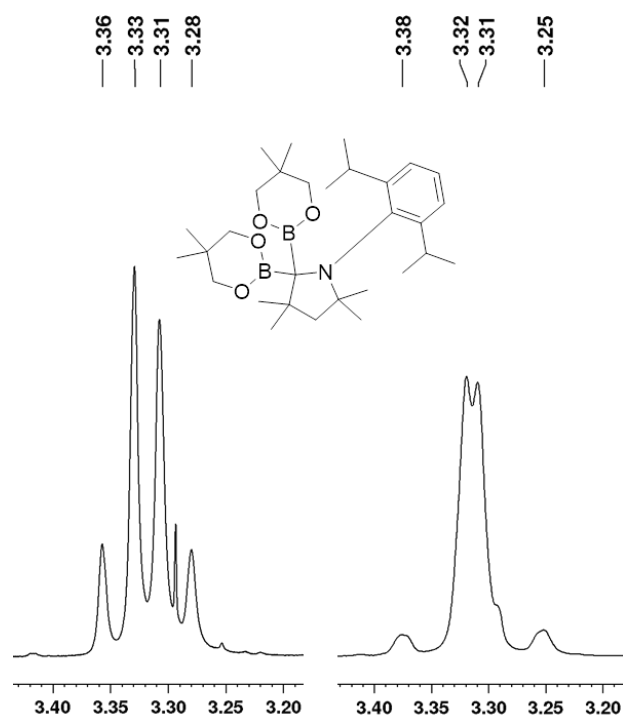


Figure 41: Expansion of the ^1H NMR spectrum in the region of the AB-spin system of the BBA $\text{B}_2\text{neop}_2 \cdot \text{CaaC}^{\text{Me}}$ measured at 400 MHz (left) and at 200 MHz (right).

The products derived from B_2eg_2 and B_2pin_2 crystallize in the triclinic space group $P-1$, while the products of B_2cat_2 and B_2neop_2 crystallize in the monoclinic space group $P2_1/n$ and the orthorhombic spacegroup $Pna2_1$, respectively (Figure 42).

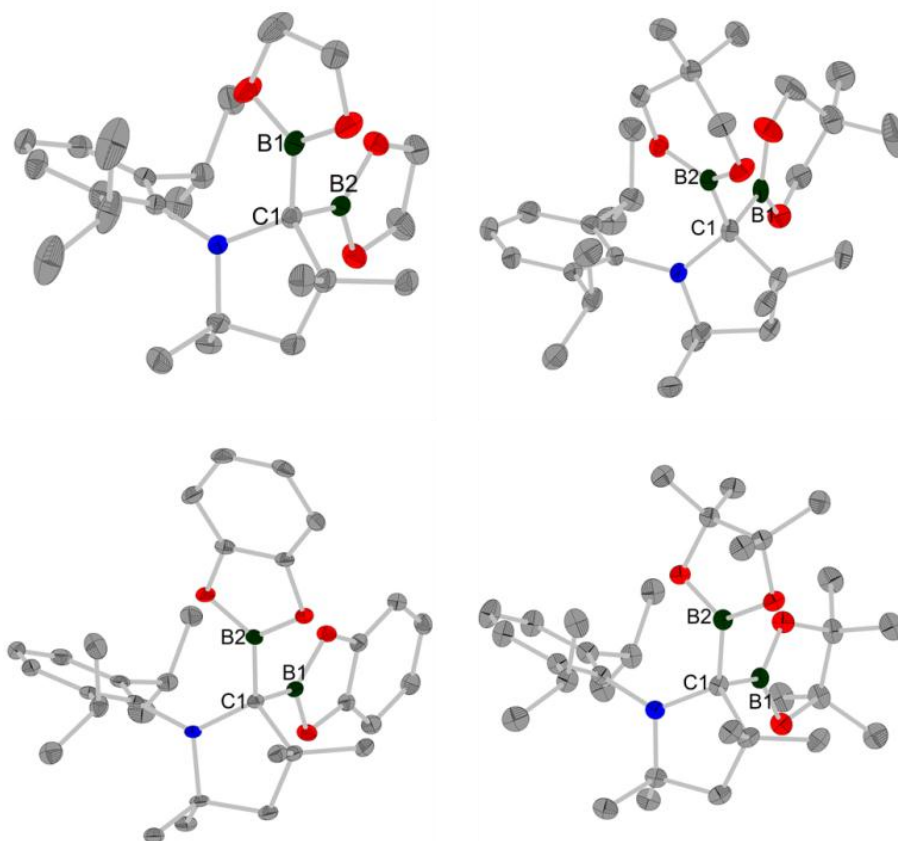


Figure 42: Hydrogen atoms are omitted for clarity and the thermal ellipsoids are drawn at 50% probability. Element (color): carbon (grey), nitrogen (blue), boron (dark green). Top, left: Molecular structure of BBA $B_2eg_2 \cdot CaaC^{Me}$ (BBA4). Selected bond lengths (Å) and angles (deg): C1-B1 1.581(2), C1-B2 1.605(2), O1-B1 1.366(2), O2-B1 1.371(2), O3-B2 1.372(2), O4-B2 1.373(2), B1-B2 2.519(3), B1-C1-B2 104.42(13), N-C1-Cx 100.65(12), OB1O-OB2O 83.40(13). Top, right: Molecular structure of BBA $B_2neop_2 \cdot CaaC^{Me}$ (BBA3). Selected bond lengths (Å) and angles (deg): C1-B1 1.624(3), C1-B2 1.600(3), O1-B1 1.358(3), O2-B1 1.359(2), O3-B2 1.366(2), O4-B2 1.359(2), B1-B2 2.534(3), B1-C1-B2 103.63(17), N-C1-Cx 100.36(16), OB1O-OB2O: 78.5(2). Bottom, left: Molecular structure of BBA $B_2cat_2 \cdot CaaC^{Me}$ (BBA2). Selected bond lengths (Å) and angles (deg): C1-B1 1.5963(19), C1-B2 1.5780(19), O1-B1 1.3867(18), O2-B1 1.3907(17), O3-B2 1.3923(17), O4-B2 1.3840(17), B1-B2 2.544(2), B1-C1-B2 106.54(10), N-C1-Cx 100.81(10), OB1O-OB2O 73.91(15). Bottom, right: Molecular structure of BBA $B_2pin_2 \cdot CaaC^{Me}$ (BBA1). Selected bond lengths (Å) and angles (deg): C1-B1 1.626(2), C1-B2 1.584(3), O1-B1 1.371(2), O2-B1 1.373(2), O3-B2 1.370(2), O4-B2 1.368(2), B1-B2 2.510(2), B1-C1-B2 102.88(13), N-C1-Cx 100.10(12), OB1O-OB2O 75.34(18).

The former carbene carbon atom is tetrahedral, with the two boryl moieties oxidatively added to it. On average, the B-B separation is elongated from ca. 1.699 Å in the starting materials to ca. 2.530 Å in the products (Table 10).

Table 10: Important bond length and angles of boron-boron bond activation products of CaaC^{Me}. *SM = starting material. ** = mean value of the two conformers found in the asymmetric unit.

BBA of CaaC ^{Me} and	C1-B1 [Å]	C1-B2 [Å]	B1-B2 [Å] SM*	B1-B2 [Å]	B1-C1-B2 [°]	OB1O- OB2O[°]
B ₂ pin ₂ BBA1	1.626(2)	1.584(3)	1.702(5)** ^[200]	2.510(2)	102.88(13)	75.34(18)
B ₂ cat ₂ BBA2	1.5963(19)	1.5780(19)	1.678(3) ^[314]	2.544(2)	106.54(10)	73.91(15)
B ₂ neop ₂ BBA3	1.624(3)	1.600(3)	1.710(3)** ^[200]	2.534(3)	103.63(17)	78.5(2)
B ₂ eg ₂ BBA4	1.581(2)	1.584(3)	1.704(3) ^[200]	2.519(3)	104.42(13)	83.40(13)

To test whether the BBA products are prone to CaaC ring expansion reactions or if they are at equilibrium with the starting compounds (i.e. B-B oxidative addition is reversible), VT-NMR experiments were performed. The product of B₂neop₂ and CaaC^{Me} was dissolved in C₆D₆ and ¹H NMR spectra were recorded at 25 °C, 50 °C and 80 °C. None of the recorded spectra showed the formation of a new species nor did the product show any signs of decomposition (Figure 43).

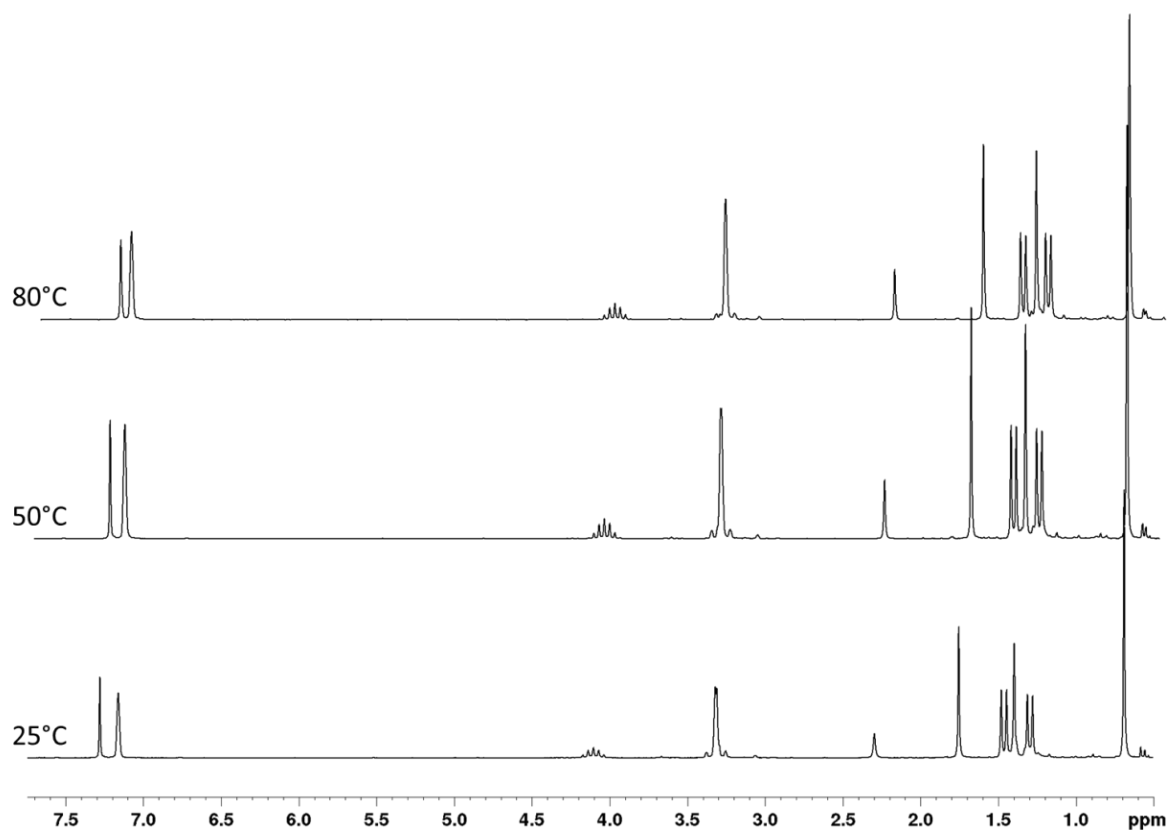
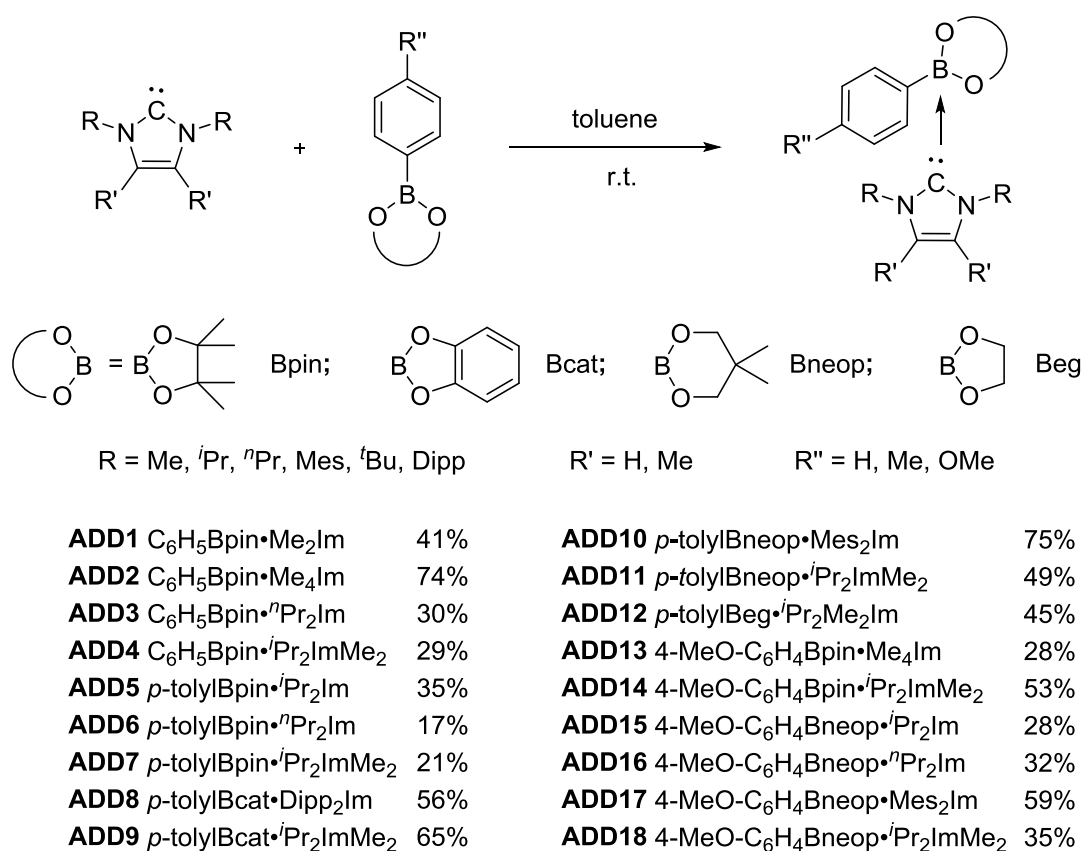


Figure 43: ^1H VT-NMR spectra of the BBA product of CaaC^{Me} and B_2neop_2 BBA3.

3.4.2 NHC adducts of aryl boronic esters

Preliminary studies have been reported on the synthesis and characterization of neutral NHC adducts of diboron compounds. The B-B bond in these $\text{sp}^2\text{-sp}^3$ adducts is elongated, and calculations showed that the bond strength is lessened, compared to the one found in the $\text{sp}^2\text{-sp}^2$ diboron(4) compound.^[304] This activated bond facilitates the transfer of one of the boron moieties to a substrate. As the Suzuki-Miyaura cross-coupling is one of the most widely used transition metal-catalyzed C-C bond forming reactions, organoboronate substrates, have recently received great attention.^[315] Nevertheless, the reactivity of aryl boronates with NHCs has not been reported. The same principle of B-E bond activation observed for adducts of diboron compounds could apply to aryl boronates and NHCs. In aryl boronates, an sp^2 hybridized boron atom is linked to an sp^2 hybridized carbon atom. An NHC could quarternize the boron atom and thus weaken the B-C bond, potentially

providing an organocatalyzed system for C-C bond forming processes. Therefore, the reactivity of NHCs with aryl boronic esters was examined (Scheme 57).



Scheme 57: Reaction of NHCs with aryl boronate esters.

The reaction of sterically less demanding NHCs such as Me₂Im, Me₄Im, ⁱPr₂Im, ⁿPr₂Im, ⁱPr₂ImMe₂ with aryl boronic esters showed adduct formation. Sterically more demanding NHCs such as Mes₂Im showed adduct formation with neopentyl glycol boronic esters, but did not bind to pinacol esters. Hence, no shifts in the ¹¹B NMR spectra were observed and the starting materials were isolated. The bulky Dipp₂Im and ^tBu₂Im only formed adducts with aryl boronic esters of catechol. These differences in reactivity are a result of steric effects and Lewis acidity. Pinacolate esters have the greatest steric demand, while neopentyl glycol esters are able to flip the six membered ring to minimize steric interactions (Figure 44; see Figures 164 to 169 and Table 91 for additional crystal structures and comparison). Catecholate esters are the most Lewis acidic of the three.^[316]

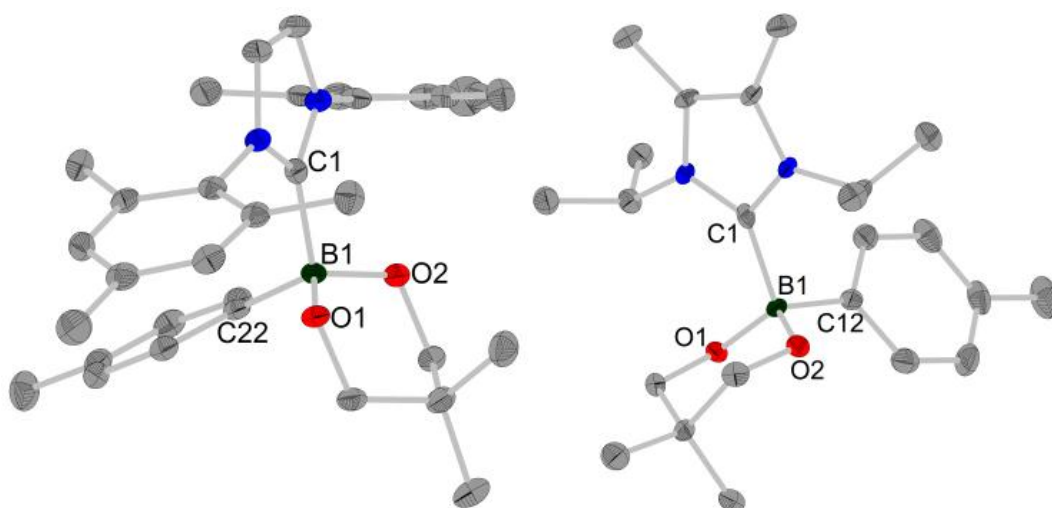
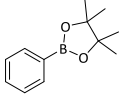
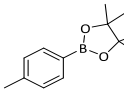
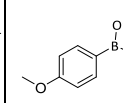
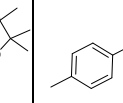
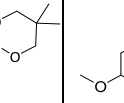
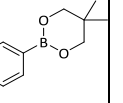
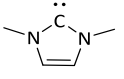
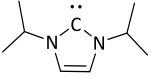
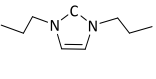
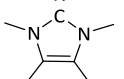
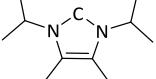
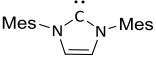
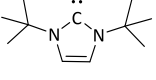
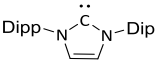


Figure 44: Crystal structures of the adducts of Mes_2Im and ${}^i\text{Pr}_2\text{ImMe}_2$ with p -tolylBneop, where the neopentyl glycolate moiety minimizes the steric interaction with the sterically demanding Mes_2Im NHC by flipping the ring away from the ligand.

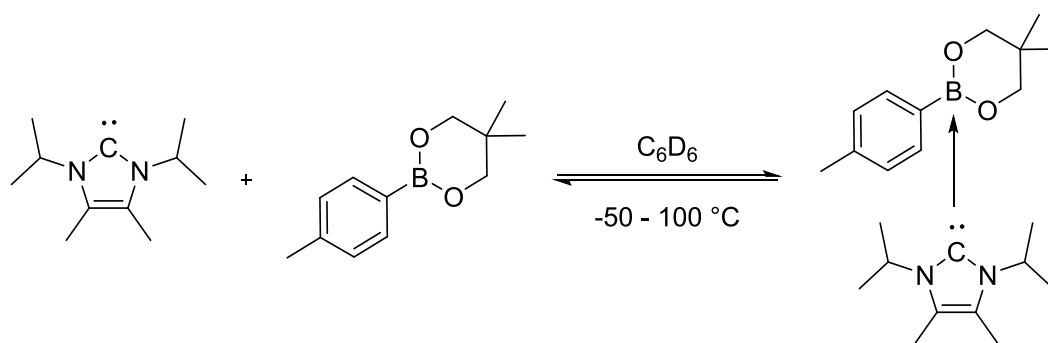
In the case of adduct formation, an upfield shift of the boron resonance in the ${}^{11}\text{B}$ NMR spectrum was observed, due to the quaternization of the boron atom. Whilst the starting compounds resonate at ca. 30 ppm, the adducts were observed between 10.6 and 2.5 ppm. Table 11 shows the ${}^{11}\text{B}$ NMR shifts observed from the reaction mixture of various NHCs with various aryl boronic esters in C_6D_6 for comparison.

3 Results and Discussion

Table 11: ^{11}B NMR shifts of NHC adducts of aryl boronic esters. Green: adducts formation was observed. Red: no adducts formation; only the starting material was observed. Values in brackets correspond to *in situ* experiments, in which the adduct was not isolated.

^{11}B NMR (in ppm)						
Free boronic ester	31.4	31.5	31.3	27.3	27.2	32.7
	4.5	(4.8)	(4.5)	(5.3)	(3.9)	(9.8)
	(4.9)	5.4	(4.7)	(2.9)	3.3	(9.8)
	4.8	5.4	(4.9)	(3.0)	2.5	(9.6)
	4.6	(4.6)	4.6	(2.1)	(2.2)	(9.6)
	5.0	6.1	6.0	10.6	4.2	10.3
	X	X	X	10.2	9.1	(10.4)
	X	X	X	X	X	(9.9)
	X	X	X	X	X	8.8

In the ^1H NMR spectra recorded at room temperature, reversible binding of the NHC to the organoboronate ester was observed as broadened signals. In particular, the methine protons of *iso*-propyl groups and the methyl protons of pinacolate and methylene protons of neopentyl glycolate groups, respectively, were prone to broadening. VT-NMR experiments were employed to examine the temperature dependence of this reversible adduct forming process (Scheme 58 and Figure 45).



Scheme 58: Reversible formation of $i\text{Pr}_2\text{ImMe}_2 \cdot p\text{-tolylBneop}$.

At higher temperatures, the signal for the methine protons of the *iso*-propyl moiety is shifted upfield and appears as a septet. At lower temperatures, the septet is broadened and shifted downfield, while the signals of the methylene protons show coupling as they form an AB-spin system when the adduct form is predominant. The ^{11}B VT-NMR spectra showed a downfield shift of the boron resonance at higher temperature. At $-40\text{ }^\circ\text{C}$, the resonance was detected at 5.5 ppm, while at $100\text{ }^\circ\text{C}$, it was observed at 13.3 ppm.

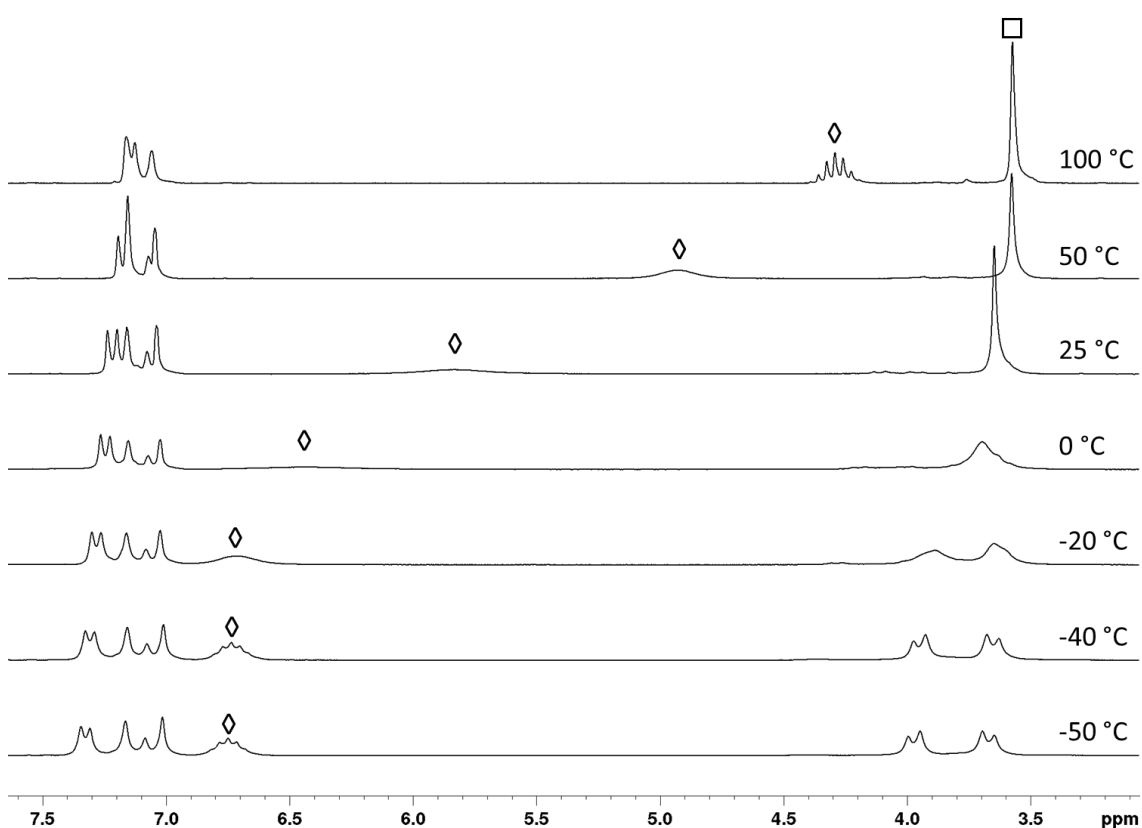


Figure 45: ^1H VT-NMR spectra of $p\text{-tolylBneop} \cdot i\text{Pr}_2\text{ImMe}_2$. Square: Methylene protons of the neopentyl glycol ester. Diamond: Septet of the CH protons of the *iso*-propyl groups.

For all substrates examined, adducts with the NHC $i\text{Pr}_2\text{ImMe}_2$ were characterized by X-ray diffraction (Table 12).

Table 12: Important bond length and angles of adducts of $i\text{Pr}_2\text{ImMe}_2$.

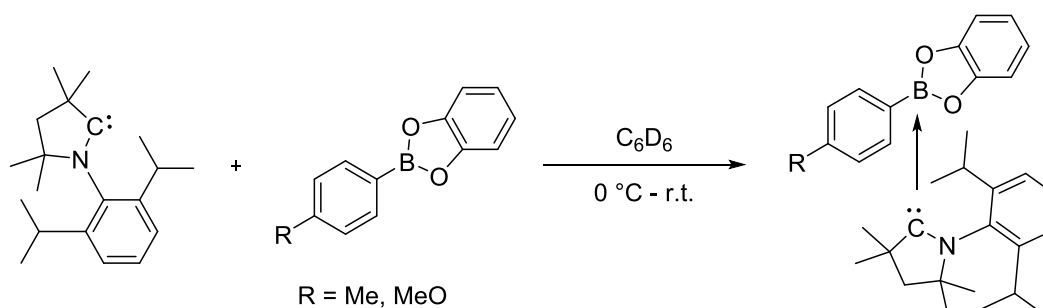
Adduct of $i\text{Pr}_2\text{ImMe}_2$ with	$i\text{C-B1}$ [Å]	C1-B1 [Å]	$i\text{CB1C1}$ [°]	$\text{OB1O-}i\text{CBC1}$ [°]
$\text{C}_6\text{H}_4\text{Bpin}$	1.632(2)	1.689(2)	107.41(12)	89.39(11)
p -tolylBpin	1.633(2)	1.694(2)	103.46(11)	87.67(10)
4-MeO- $\text{C}_6\text{H}_4\text{Bpin}$	1.629(2)	1.691(3)	106.02(15)	87.65(11)
p -tolylBneop	1.620(2)	1.697(2)	107.47(11)	87.78(8)
4-MeO- $\text{C}_6\text{H}_4\text{Bneop}$	1.6191(17)	1.7194(19)	110.37(10)	89.30(16)
p -tolylBcat	1.610(3)	1.661(3)	109.15(15)	87.60(12)

The longest carbene carbon atom-boron atom bond length in this adduct series is found for $i\text{Pr}_2\text{ImMe}_2 \bullet 4\text{-MeO-C}_6\text{H}_4\text{Bneop}$; it is 1.7194(19) Å. For the p -tolyl boronic esters it is shortest in the case of p -tolylBcat, which is in agreement with theory as the Bcat moiety is more Lewis acidic than Bpin and Bneop and thus forms stronger donor-acceptor bonds. The *ipso* carbon-boron bond length of 1.610(3) Å is also the shortest. Compared to the starting material p -tolylBcat (1.533(2) Å) it is elongated by 5%.^[317] In the $i\text{Pr}_2\text{ImMe}_2$ adducts of p -tolylBneop (1.620(2) versus 1.565(2) Å) and p -tolylBpin (1.633(2) versus 1.550(4) Å) it is elongated by 4% and 5%, respectively.^[151] A trend is found in the angle formed by the *ipso* carbon atom and the carbene carbon atom around boron atom. It is widest in the adduct with p -tolylBcat (109.15(15)°), second in the case of p -tolylBneop (107.47(11)°) and narrowest for p -tolylBpin (103.46(11)°). Since this angle is opposite to the ester moiety it shows indirect correlation with the steric demand of the ester group (with pinacolate being the most and catecholate the least demanding). No trend was observed for the interplanar angle found between the OB1O plane and the *ipso* carbon-boron-carbene carbon plane.

Compared with NHC adducts of diboron compounds,^[199, 302] no decomposition or ring expansion reaction was observed for the NHC adducts of aryl boronate esters at higher temperatures. The addition of a second equivalent of NHC, and subsequent heating to 80 °C, showed no effect either.

3.4.3 Reversible B-C bond oxidative addition

In contrast, reaction of CaaC^{Me} with organoboronate esters usually leads to insertion of the CaaC^{Me} into the B-C bond (*vide infra*). The better σ -donating and π -accepting properties of cyclic alkyl amino carbenes (CaaCs) compared to NHCs thus have a significant impact on reactivity of these compounds. However, for the reaction of CaaC^{Me} with *p*-tolylBcat and 4-MeO-C₆H₄Bcat adduct formation was observed (Scheme 59).



Scheme 59: Reaction of CaaC^{Me} with *p*-tolylBcat (ADD19) and 4-MeO-C₆H₄Bcat (ADD20), respectively.

Besides elemental analysis, NMR spectroscopy and HRMS, the adduct of CaaC^{Me} and *p*-tolylBcat **ADD19** was also characterized by X-ray diffraction (Figure 46).

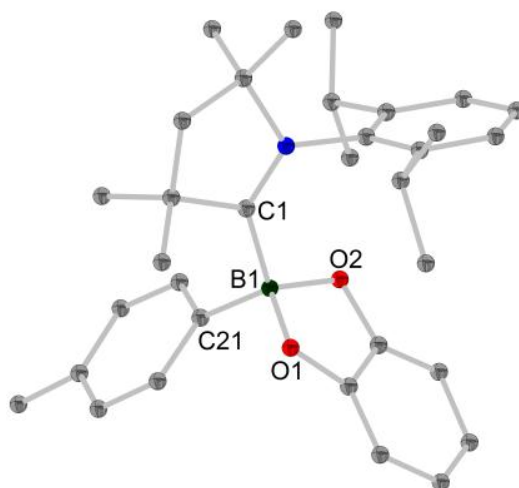
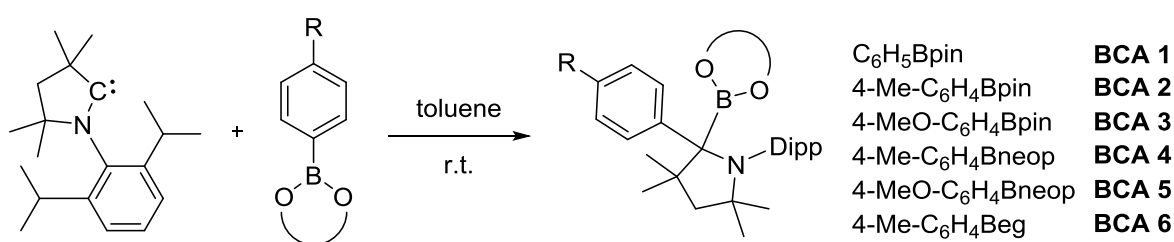


Figure 46: Molecular structure of the adduct *p*-tolylBcat•CaaC^{Me} ADD19. Element (color): carbon (grey), nitrogen (blue), boron (dark green), oxygen (red). Only one of the three molecules in the asymmetric unit is displayed. Hydrogen atoms as well as the minor part of the disorder are omitted for clarity and the thermal ellipsoids are drawn at 50% probability. C21-B1 1.598(4) (1.578(3)[1.416(15)])(1.615(3)), C1-B1 1.677(4) (1.670(3)) (1.648(4)), C1-B1-C21 118.5(2) (106.66(18)[134.5(6)]) (110.14(17)), NC1C-C21B1 45.1(2) (30.44(14)[55.1(5)]) (45.36(15)), O1B1O2-C1B1C21 87.8(1) (89.85(16)) (89.14(16)).

Yet the reactions of *p*-tolylBpin, *p*-tolylBneop, *p*-tolylBeg, C₆H₅Bpin, 4-MeO-C₆H₄Bpin and 4-MeO-C₆H₄Bneop with CaaC^{Me} showed different reactivity and yielded B-C bond activation products, which were characterized by ¹H, ¹¹B, ¹³C{¹H} NMR spectroscopy, HRMS and X-ray crystallography (Scheme 60, Figure 47 and Figure 48).



Scheme 60: Reaction of CaaC^{Me} with *p*-tolylBpin, *p*-tolylBeg, C₆H₅Bpin, 4-MeO-C₆H₄Bpin and 4-MeO-C₆H₄Bneop to boron carbon bond activation products.

In Table 13 important bond length and angles of the crystal structures of the BCA products **BCA1-6** are displayed for comparison.

Table 13: Important bond length and angles of boron-carbon bond activation products of CaaC^{Me}.

BCA of CaaC ^{Me}	C1-B1 [Å]	C1-C21 [Å]	C21-B1 [Å]	C21-C1-B1 [°]	NC1C21-B1C1C _{Caac} [°]	OB1O-C _{Ar} C21C _{Ar} [°]
<i>p</i> -tolylBpin	1.6218(18)	1.5389(17)	2.5434(17)	107.14(10)	80.35(5)	78.50(10)
<i>p</i> -tolylBneop	1.6310(16)	1.5364(15)	2.5355(16)	106.32(9)	85.54(6)	72.23(10)
<i>p</i> -tolylBeg	1.591(2)	1.567(2)	2.492(2)	104.18(11)	83.86(12)	84.69(13)
4-MeO-C ₆ H ₄ Bpin	1.620(2)	1.5379(19)	2.543(2)	107.27(11)	84.15(8)	79.49(12)
4-MeO-C ₆ H ₄ Bneop	1.627(2)	1.5404(19)	2.543(2)	107.84(11)	86.69(7)	67.77(12)
C ₆ H ₅ Bpin	1.621(2)	1.536(2)	2.523(2)	106.10(13)	84.94(10)	82.65(16)

In all BCAs the distance between the *ipso* carbon atom and the boron atom is ca. 2.5 Å. With a typical boron carbon single B-C_{Ar} bond length being 1.56 Å, this clearly shows that the bond is activated.^[318] The bond length of *ipso* carbon atom to the former carbene carbon atom in contrast perfectly matches the values for carbon-carbon single bonds of 1.54 Å.^[318-319] The bond length of the former carbene carbon atom to the boron atom is ca. 1.62 Å. The BCA of the sterically less demanding *p*-tolylBeg showed the shortest C1-B1 bond length of 1.591(2) indicating the steric influence around the central carbon atom on that value. This influence is also observed in the angle spanned by the *ipso* carbon atom and the boron atom around the former carbene carbon atom. Hence, the narrowest angle was observed in the BCA of *p*-tolylBeg (104.18(11)°), while the BCAs of the aryl boronic esters of pinacol and neopentyl glycol showed angles between 106.10(13) and 107.84(11)°.

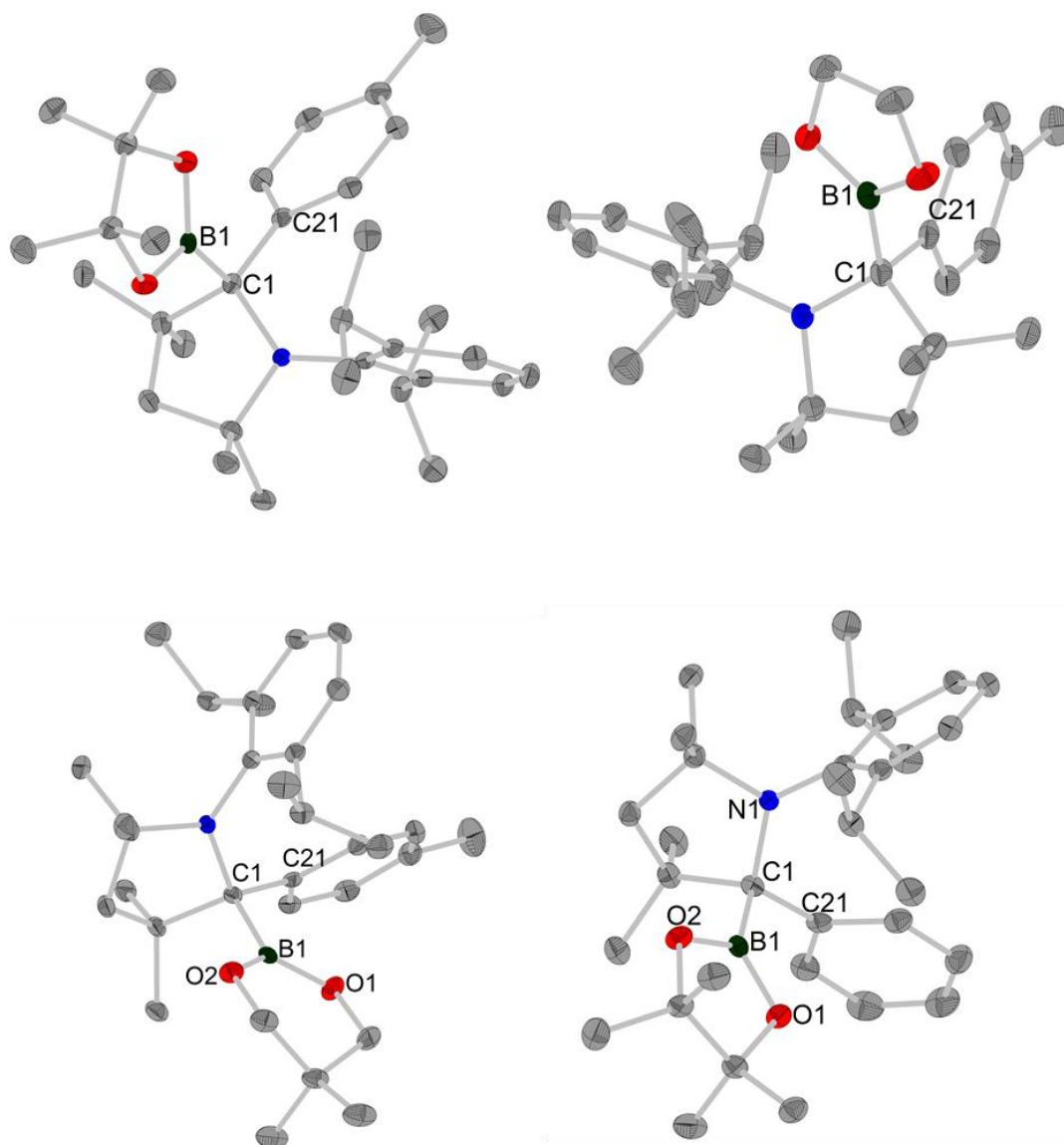


Figure 47: Element (color): carbon (grey), nitrogen (blue), boron (dark green). Hydrogen atoms are omitted for clarity and the thermal ellipsoids are drawn at 50% probability. Top, left: Molecular structure of *p*-tolylBpin•CaaC^{Me} BCA2. Selected bond lengths (Å) and angles (deg): C1-B1 1.6218(18), O1-B1 1.3622(17), O2-B1 1.3711(17), C1-C21 1.5389(17), B1-C21 2.5434(17), B1-C1-C21 107.14(10), N-C1-Cx 99.77(9), OB1O-C_{Ar}C21C_{Ar} 78.50(10), NC1C21-B1C1C_{CaaC} 80.35(5). Top, right: Molecular structure of *p*-tolylBeg•CaaC^{Me} BCA6. Selected bond lengths (Å) and angles (deg): C1-B1 1.591(2), O1-B1 1.361(2), O2-B1 1.3678(16), C1-C21 1.567(2), B1-C21 2.492(2), B1-C1-C21 104.18(11), N-C1-Cx 101.16(14), OB1O-C_{Ar}C21C_{Ar} 84.69(13), NC1C21-B1C1C_{CaaC} 83.86(12). Bottom, left: Molecular structure of *p*-tolylBneop•CaaC^{Me} BCA4. Selected bond lengths (Å) and angles (deg): C21-B1 2.5355(16), C1-B1 1.6310(16), O1-B1 1.3599(13), O2-B1 1.3629(14), C21-C1 1.5364(15), OB1O-C_{Ar}C21C_{Ar} 72.23(10), NC1C21-B1C1C_{CaaC} 85.54(6). Bottom, right: Molecular structure of C₆H₅BPIn•CaaC^{Me} BCA1. Selected bond lengths (Å) and angles (deg): C21-B1 2.523(2), C1-B1 1.621(2), B1-O1 1.367(2), B1-O2 1.368(2), C21-C1 1.536(2), OB1O-C_{Ar}C21C_{Ar} 82.65(16), NC1C21-B1C1C_{CaaC} 84.94(10).

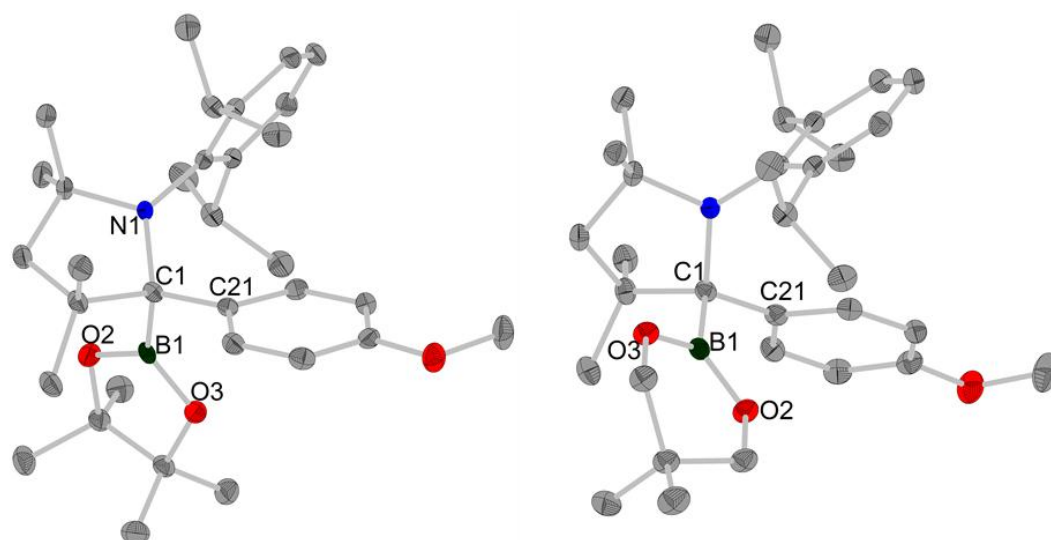
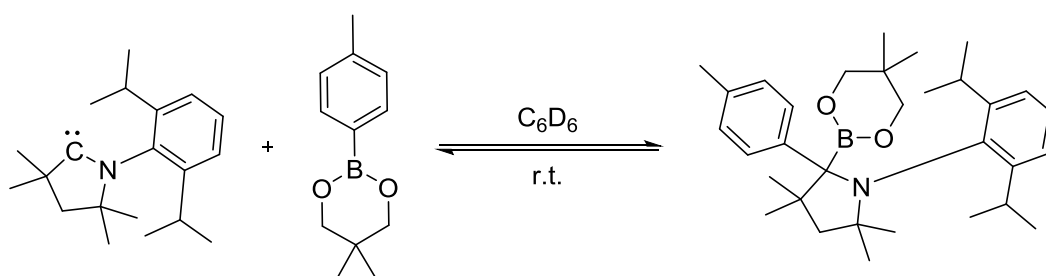


Figure 48: Element (color): carbon (grey), nitrogen (blue), boron (dark green). Hydrogen atoms are omitted for clarity and the thermal ellipsoids are drawn at 50% probability. Left: Molecular structure of 4-MeO-C₆H₄BPin•CaaC^{Me} BCA3. Selected bond lengths (Å) and angles (deg): C21-B1 2.543(2), C1-B1 1.620(2), B1-O1 1.3703(18), B1O2 1.3607(19), C21-C1 1.5379(19), OB1O-C_{Ar}C21C_{Ar} 79.49(12), NC1C21-B1C1C_{Caac} 84.15(8). Right: Molecular structure of 4-MeO-C₆H₄Bneop•CaaC^{Me} BCA5. Selected bond lengths (Å) and angles (deg): C21-B1 2.561(2), C1-B1 1.627(2), B1-O1 1.3690(18), B1-O2 1.358(2), C21-C1 1.5404(19), OB1O-C_{Ar}C21C_{Ar} 67.77(12), NC1C21-B1C1C_{Caac} 86.69(7).

In contrast to the reaction of CaaC^{Me} with aryl-Bcat esters, the reaction of CaaC^{Me} with *p*-tolylBneop, monitored by NMR spectroscopy (Scheme 61), showed no adduct formation nor were any intermediates observed in the ¹H and ¹¹B NMR spectra. Only the growth of the BCA product was observed (Figure 49).



Scheme 61: Reversible reaction of CaaC^{Me} with *p*-tolylBneop, as demonstrated by *in situ* NMR spectroscopy.

The reaction stopped after about 16 h, although starting material remained. Based on the ratio of the signals at 3.42 ppm and 3.76 ppm, the ratio of product to starting material was 1:0.44 at the end of the reaction at room temperature.

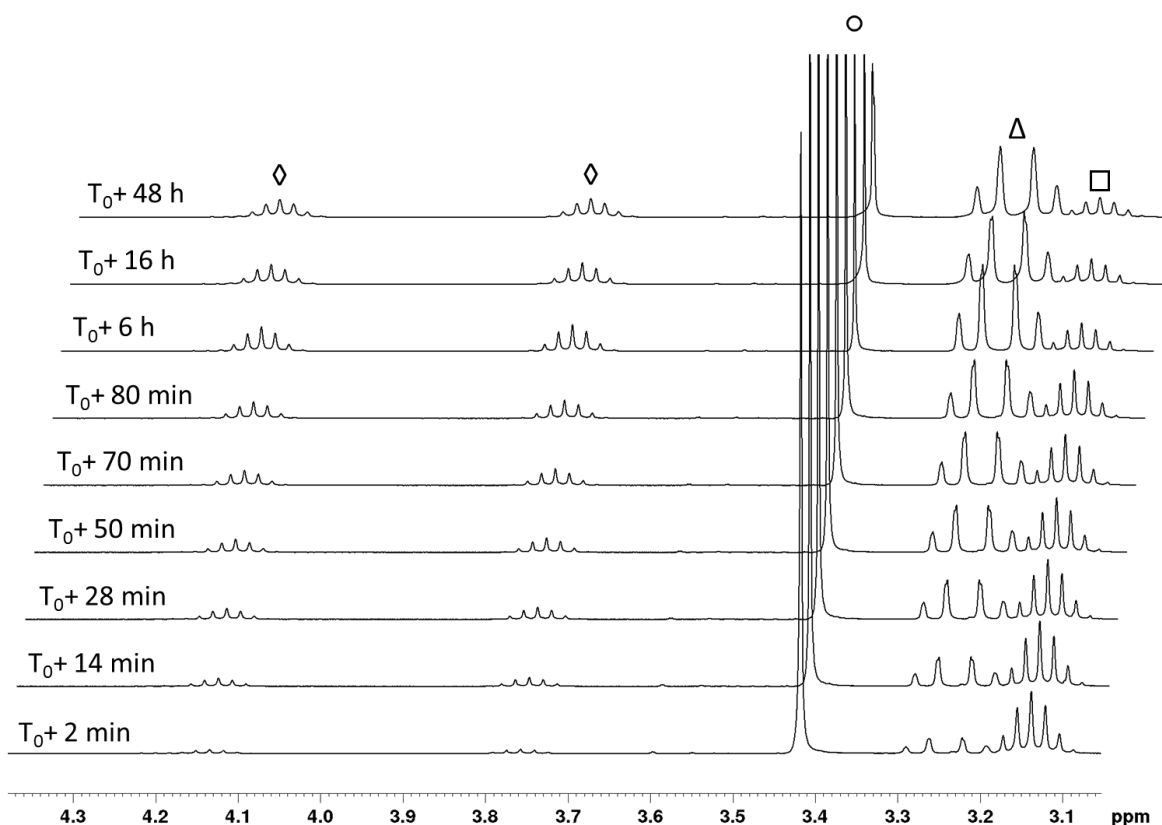


Figure 49: Consecutive ^1H NMR spectra of the reversible reaction of *p*-tolylBneop with CaaC^{Me} . Square: septet corresponding to the Dipp moiety of the free CaaC^{Me} . Triangle: AB-spin system corresponding to the methylene protons in the BCA product. Circle: singlet corresponding to the methylene protons of free *p*-tolylBneop. Diamond: septets corresponding to the Dipp moiety in the BCA product.

Heating the sample from 25 °C to 30 °C showed that the ratio of product to starting material dropped to 1:0.62. At 40 °C, the ratio is 1:1.01. At 80 °C, 15% product and 85% starting material were observed. Cooling the sample again to 25 °C shifted the equilibrium back towards the oxidative addition product (Figure 50). Multiple cooling/heating cycles were applied to demonstrate the reversibility of the reaction.

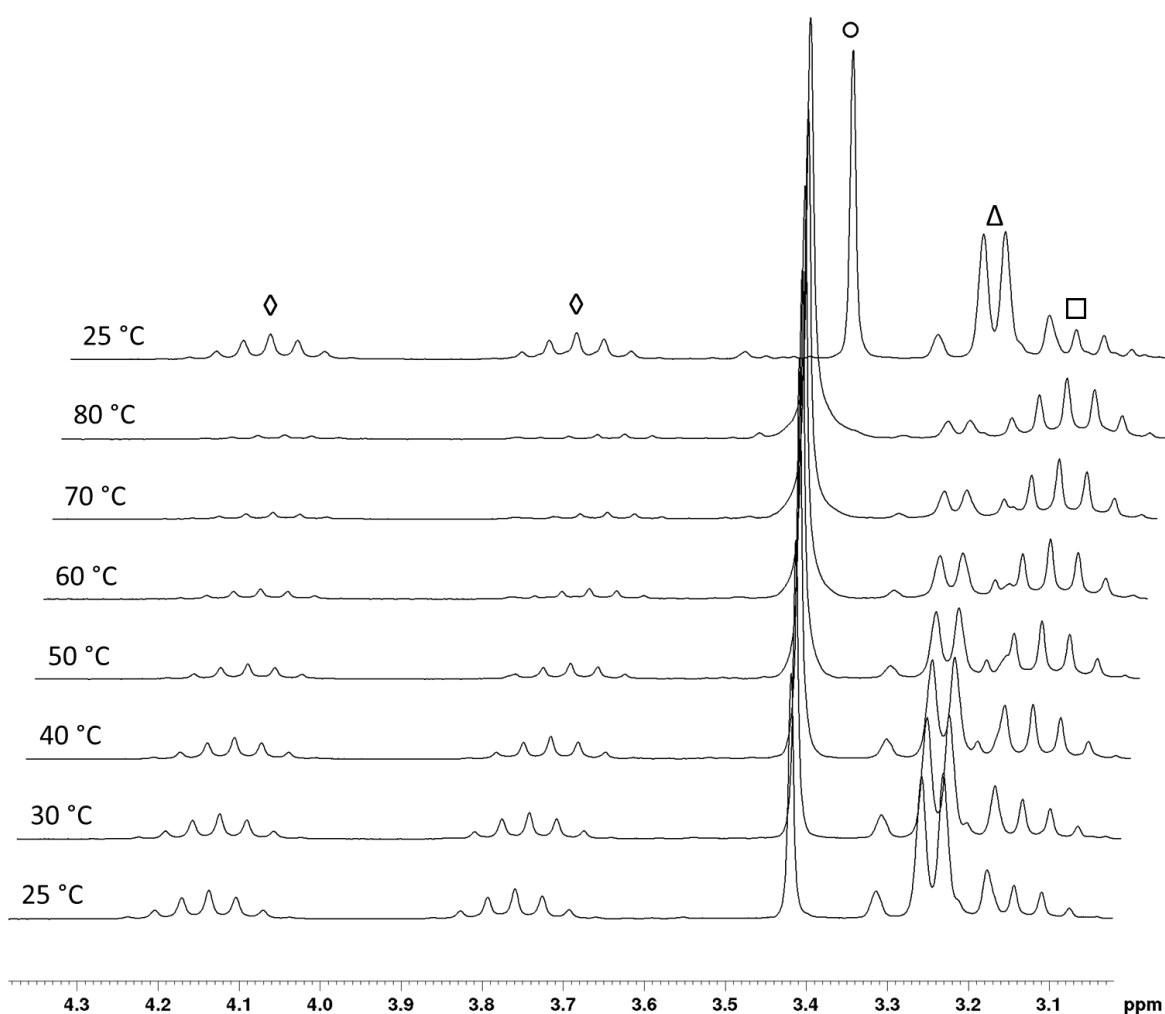


Figure 50: ^1H VT-NMR spectra of the reversible reaction of *p*-tolylBneop with CaaC^{Me} . Square: septet corresponding to the Dipp moiety of free CaaC^{Me} . Triangle: AB-spin system corresponding to the methylene protons in the BCA product. Circle: singlet corresponding to the methylene protons of the free *p*-tolylBneop. Diamond: septets corresponding to the Dipp moiety in the BCA product.

The same dynamic equilibrium behavior was found for the other BCA products. The isolated products were stable in the solid state, as NMR spectra of these compounds recorded one month after isolation demonstrate. When one of these compounds, i.e. BCA *p*-tolylBpin• CaaC^{Me} , was dissolved in C_6D_6 and spectroscopically analyzed immediately, a clean spectrum of the product was observed (Figure 51).

3 Results and Discussion

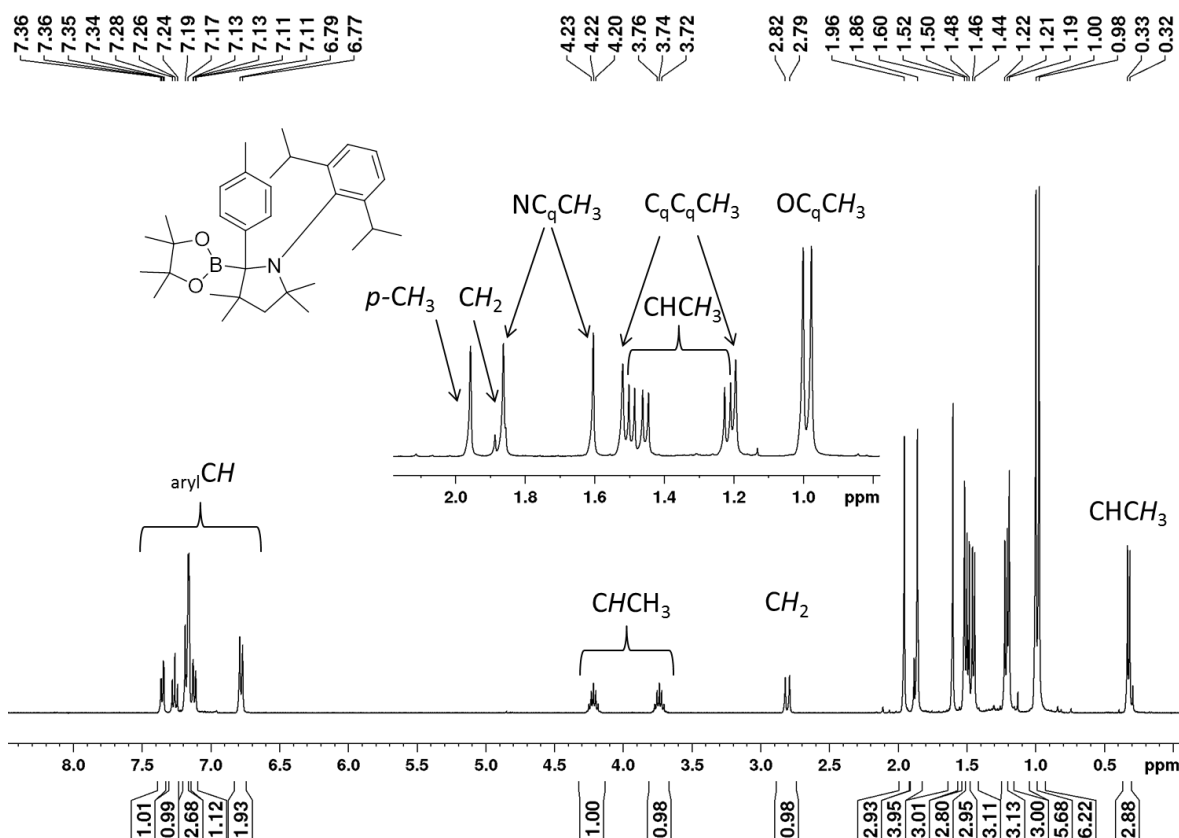


Figure 51: ^1H NMR spectrum of BCA2 directly after dissolving (C_6D_6 at 25 °C).

However, NMR spectra recorded a few hours later showed signals corresponding to free CaaC^{Me} and $p\text{-tolylBpin}$ (Figure 52). The two septets with a chemical shift at 4.22 and 3.74 ppm result from the product, while the septet at 3.14 ppm matches the septet of the free CaaC^{Me} in C_6D_6 . Other peaks also correspond to those of the free CaaC^{Me} , including the singlets at 1.13 and 2.07 ppm. In addition, there are multiplets in the aromatic region which correspond to those of free $p\text{-tolylBpin}$ in C_6D_6 . In the ^{11}B NMR spectrum no significant shift was observed, due to the fact that the starting material as well as the product resonate at almost the same frequency.

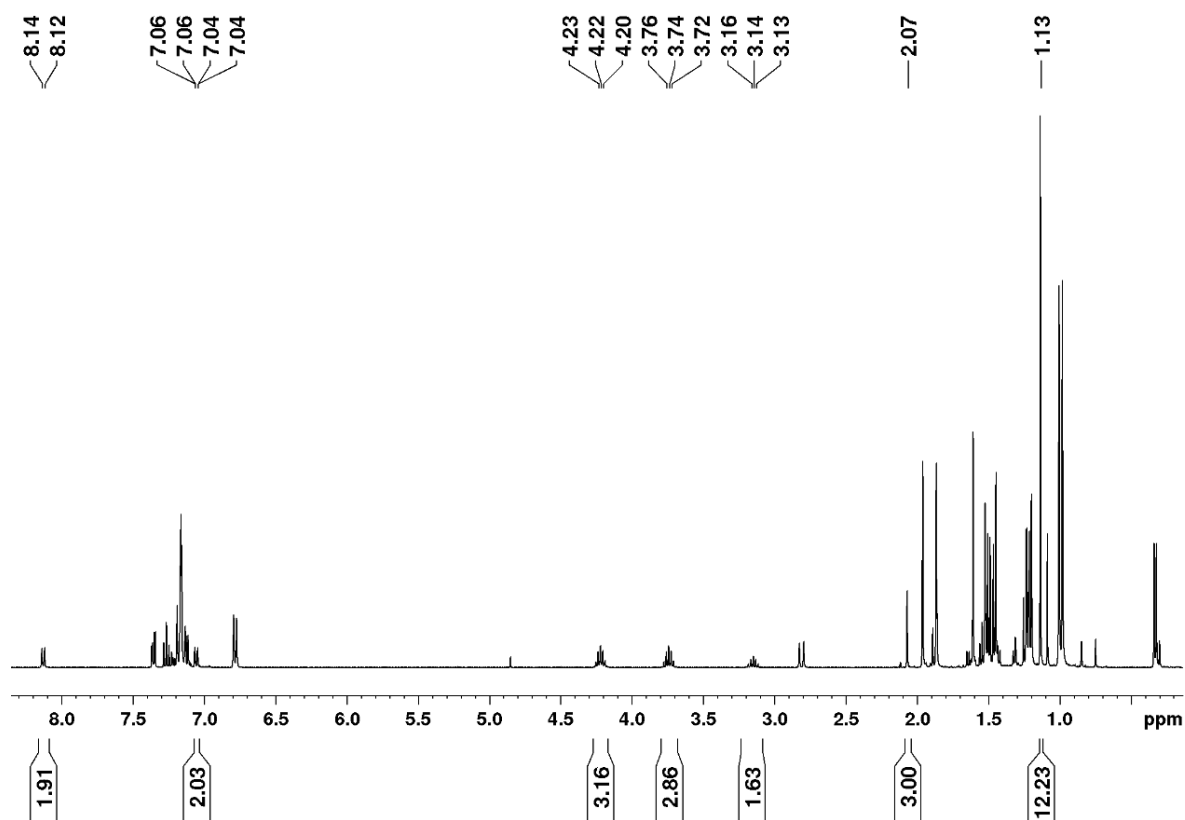


Figure 52: ^1H NMR spectrum of BCA2 recorded 24 h after dissolving (C_6D_6 at $25\text{ }^\circ\text{C}$).

When this sample was heated to $80\text{ }^\circ\text{C}$ for 1 h, and the NMR spectrum was then recorded at $25\text{ }^\circ\text{C}$ a complete shift of the equilibrium to the reactants was observed (Figure 53). For comparison, selected regions of the ^1H NMR spectra of *p*-tolylBpin, CaaC^{Me} and the reactions mixture of *p*-tolylBpin• CaaC^{Me} are displayed in Figure 54. All signals found in the spectrum of the reaction mixture (bottom) can be found in either the spectrum of the CaaC^{Me} (middle) or that of the organoboronic ester (top). Product formation was observed again when this sample was kept at room temperature. The cycle, heating to $80\text{ }^\circ\text{C}$ and cooling to room temperature, was repeated multiple times, showing the same reactivity pattern (Figure 55).

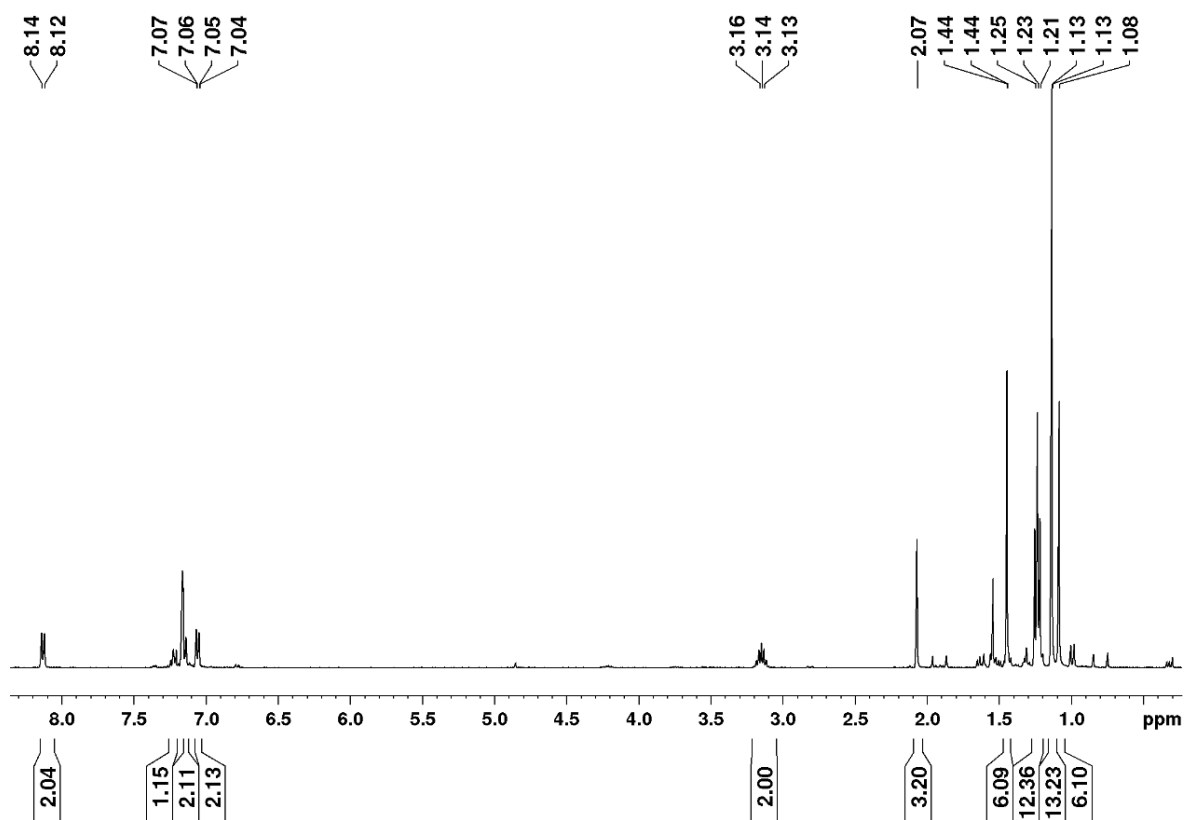


Figure 53: ^1H NMR spectrum of BAC2 recorded at 25 °C after heating to 80 °C for 1 h (C_6D_6 at 25 °C).

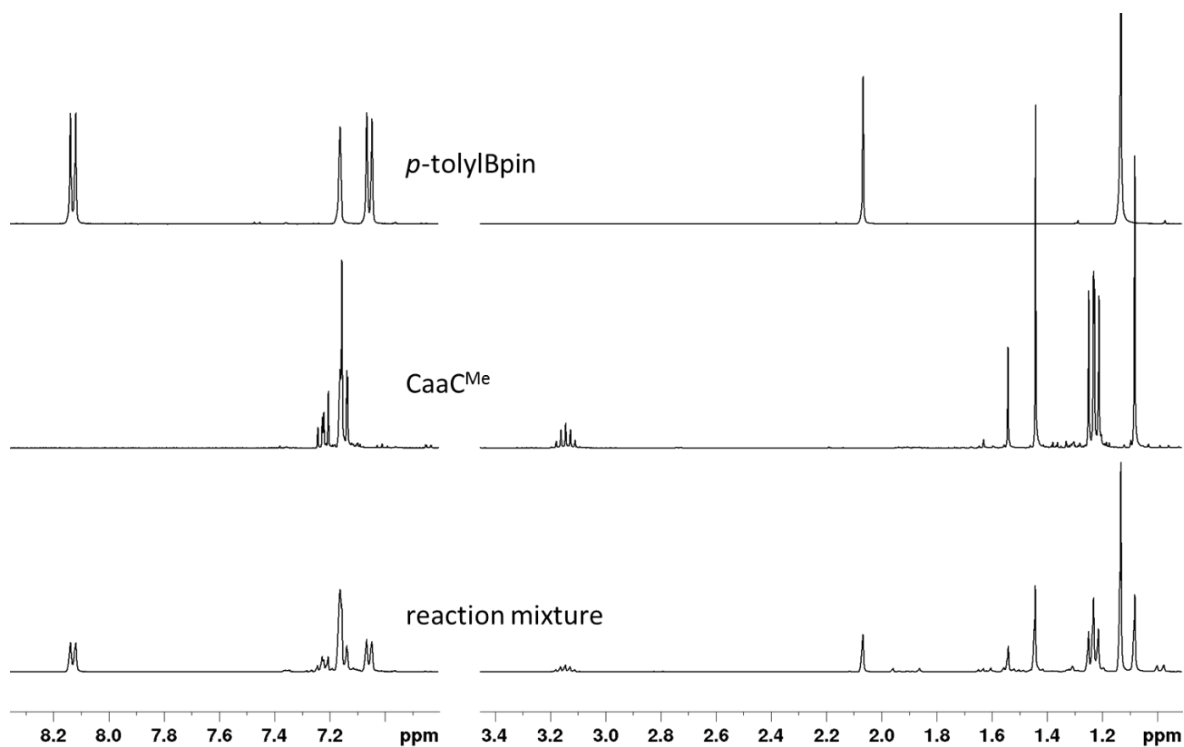


Figure 54: ^1H NMR spectra of *p*-tolylBpin (top), CaaC^{Me} (middle) and the reaction mixture of BAC2 *p*-tolylBpin• CaaC^{Me} at 25 °C after heating for 1 h at 80 °C (bottom).

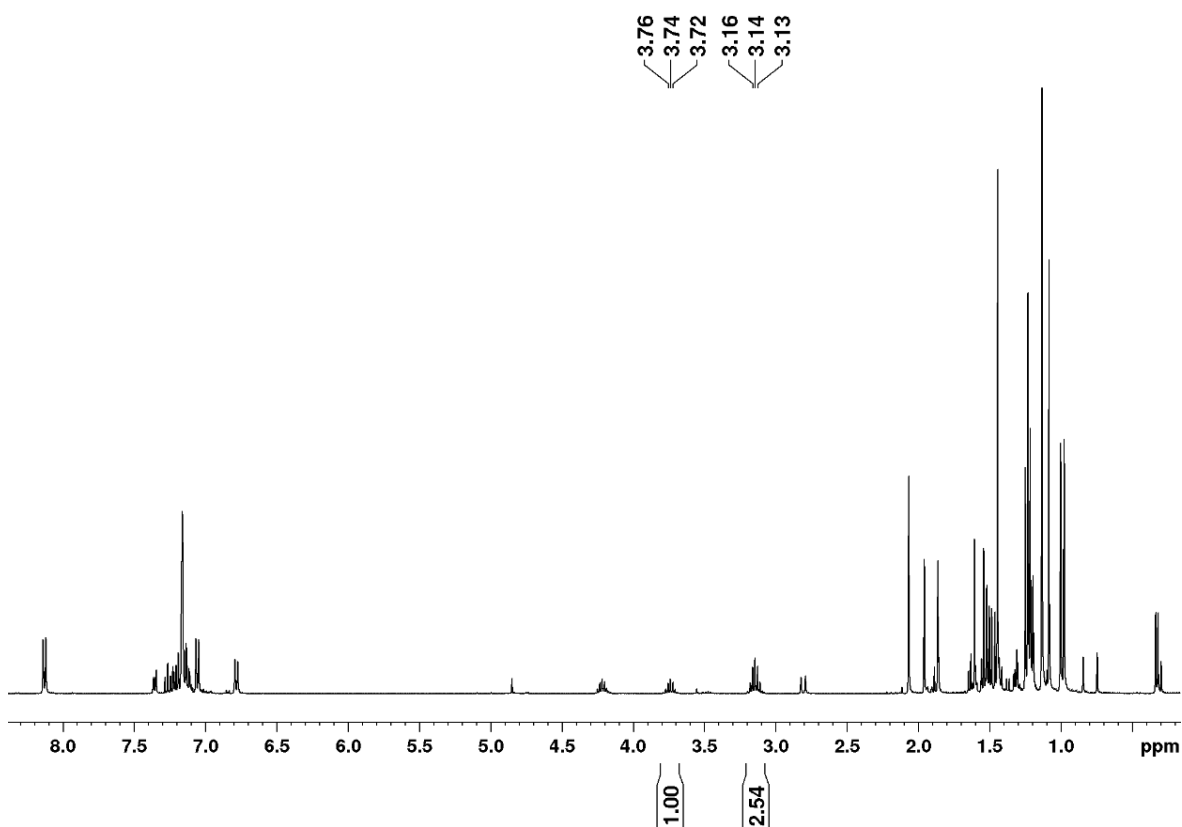
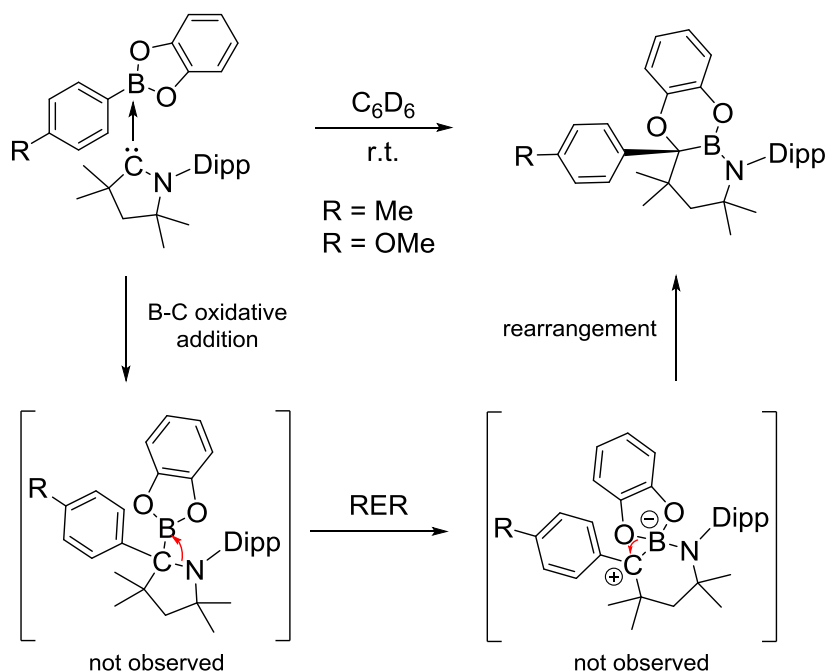


Figure 55: ^1H NMR spectrum of BCA2 recorded 24 h after the sample was heated to 80 °C (C_6D_6 at 25 °C).

These observations confirm the theory of reversible boron-carbon bond activation, as the BCA products are stable in the solid state, but at equilibrium with the starting materials in solution. The equilibrium is shifted towards the starting materials with increasing temperature, an indication of the role of entropy. This equilibrium is disadvantageous for time-consuming NMR experiments such as $^{13}\text{C}\{^1\text{H}\}$ NMR experiments. While the ^1H NMR of one sample show the signals for the BCA product exclusively, the $^{13}\text{C}\{^1\text{H}\}$ NMR showed additional signals, which could be assigned to the starting materials.

3.4.4 Ring expansion reaction at CaaC^{Me}

For the reactions of CaaC^{Me} with catecholboronate esters reactivity beyond adduct formation was found (Scheme 62). Within 24 hours in the ^1H NMR spectrum of $4\text{-MeO-C}_6\text{H}_4\text{Bcat}\cdot\text{CaaC}^{\text{Me}}$ **ADD20** two septets appeared at 3.54 and 3.87 ppm with a 1:1 ratio. In the ^{11}B NMR spectrum a new peak at 29 ppm began to grow. After 7 days, the signals for the adduct disappeared completely in the ^1H , ^{11}B as well as the $^{13}\text{C}\{^1\text{H}\}$ NMR spectra. The spectra showed complete conversion to a new compound resulting from a CaaC ring expansion reaction (RER). Heating the sample to $80\text{ }^\circ\text{C}$ overnight did not show any sign of decomposition.



Scheme 62: Ring expansion reaction (RER) of $4\text{-MeO-C}_6\text{H}_4\text{Bcat}$ and $p\text{-tolylBcat}$, respectively, and CaaC^{Me} .

Beside NMR spectroscopy, elemental analysis and HRMS, it was possible to characterize the RER products from both CaaC^{Me} adducts, $p\text{-tolylBcat}\cdot\text{CaaC}^{\text{Me}}$ **RER 1** and $4\text{-MeO-C}_6\text{H}_4\text{Bcat}\cdot\text{CaaC}^{\text{Me}}$ **RER2**, by X-ray diffraction (Figure 56).

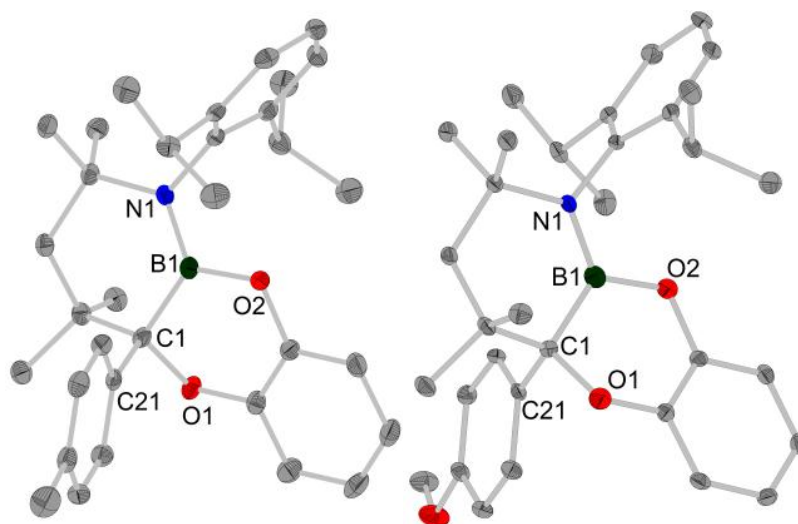


Figure 56: Molecular structures of RER products. Element (color): carbon (grey), nitrogen (blue), boron (dark green), oxygen (red). Hydrogen atoms are omitted for clarity and the thermal ellipsoids are drawn at 50% probability. Left: Molecular structure of RER1 *p*-tolylBcat•CaaC^{Me}. Selected bond lengths (Å) and angles (deg): C21-B1 2.579(2), C1-B1 1.588(2), C1-C21 1.571(2), B1-O2 1.3871(16), B1-O1 2.473(2), O1-C1 1.4787(19), N-B1 1.398(2), NB1O2 117.76(13), O2B1C1 117.26(13), C1B1N 124.98(14), NB1O2-C1C21O1 89.56(11). Right: Molecular structure of RER2 4-MeO-C₆H₄Bcat•CaaC^{Me}. Selected bond lengths (Å) and angles (deg): C21-B1 2.587(3), C1-B1 1.596(3), C1-C21 1.536(3), B1-O2 1.393(2), B1-O1 2.477(3), O1-C1 1.474(3), N-B1 1.393(3), NB1O2 118.34(17), O2B1C1 116.95(16), C1B1N 124.71(17), NB1O2-C1C21O1 77.38(18).

A sequence of steps had taken place leading to the final product (Figure 56 and Scheme 62). Thus, slow B-C oxidative addition to the CaaC^{Me} carbene-carbon atom would generate a species analogous to those discussed above. However, the enhanced Lewis acidity of the Bcat group apparently leads to rapid migration of the CaaC nitrogen atom to boron to generate a formally zwitterionic ring-expanded intermediate, which subsequently relieves the buildup of charge by rapid migration of one of the catecholates oxygens to the former carbene-carbon atom. The final product thus contains three contiguous 6-membered rings: the unsaturated arene ring of the catechol moiety, and new C₃O₂B and C₄NB rings. In both structures, the boron atom as well as the nitrogen atom are trigonal planar (sum of the angles around B = 360°, N = 359.93° and 359.73°, respectively) with all substituents in one plane, leaving the filled orbital at the nitrogen atom and the empty orbital at the boron atom aligned for interaction. The short B-N distances of 1.398(2) Å and 1.393(3) Å, respectively, are indicative of B-N multiple bond character (B-N single bond is typically 1.56 Å).

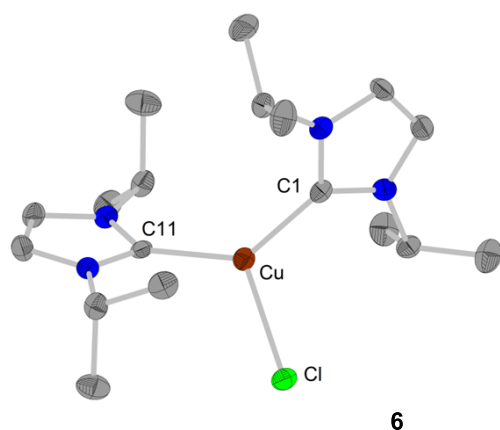
Facile B-B bond activation of B_2pin_2 , B_2neop_2 , B_2cat_2 , B_2eg_2 via oxidative addition to the carbene-carbon atom of $CaaC^{Me}$ was achieved. Whilst NHCs form adducts reversibly with aryl boronate esters, the carbene-carbon atom of $CaaC^{Me}$, which is both more nucleophilic and more electrophilic than that of an NHC, results in novel and reversible B-C oxidative addition to carbon. Thus, we have demonstrated, for the first time, the metal-free cleavage of a B-C bond in an aryl boronate ester, which leads to the intriguing possibility that we can develop organocatalytic arylation reactions of organic electrophiles. The difference in reactivity of the B-B and B-C bonds, the former oxidative addition to carbon being irreversible and the latter being reversible, likely results from differences in B-B and B-C bond strengths.

4 Summary

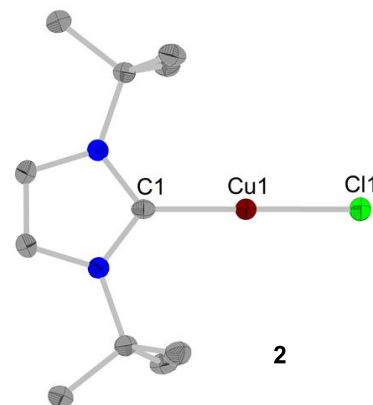
The present thesis comprises synthesis and stoichiometric model reactions of well-defined NHC-stabilized copper(I) complexes (NHC = *N*-heterocyclic carbene) in order to understand their basic reactivity in borylation and cross-coupling reactions. This also includes the investigations of the reactivity of the ligands used (NHCs and CaaCs = cyclic alkyl(amino)carbenes) with the substrates, i.e. diboron(4) esters and arylboronates, which are addressed in the second part of the thesis.

4.1 Synthesis and stoichiometric model reactions of copper(I) complexes

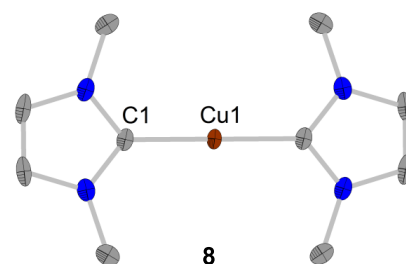
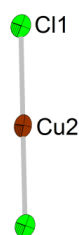
The first part of the thesis is devoted to the synthesis of NHC-stabilized copper(I) complexes and their stoichiometric model reactions in copper(I)-mediated borylation and Suzuki-Miyaura cross-coupling reactions.



As starting materials, complexes of the type $[\text{Cu}(\text{NHC})(\text{Cl})]$ with different NHC ligands (NHC = $t\text{Bu}_2\text{Im}$, $i\text{Pr}_2\text{Im}$ **2**, $i\text{Pr}_2\text{ImMe}_2$ **3**, Me_4Im **4**, Dipp_2Im , Mes_2Im) as well as chloride complexes bearing two carbene-

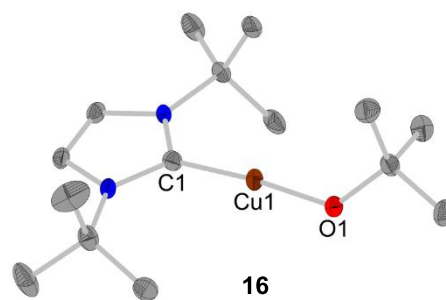


ligands $[\text{Cu}(\text{NHC})_2(\text{Cl})]$ (NHC = Me_2Im **5**, $i\text{Pr}_2\text{Im}$ **6**, $i\text{Pr}_2\text{ImMe}_2$ **7**), were synthesized from the reaction of an NHC with CuCl and characterized. From the reaction of Me_2Im with CuCl , the ionic compound $[\text{Cu}(\text{Me}_2\text{Im})_2][\text{CuCl}_2]$ **8** was obtained. The reaction of $[\text{Cu}(\text{MeCN})_4][\text{PF}_6]$ with Me_2Im afforded $[\text{Cu}(\text{Me}_2\text{Im})(\text{MeCN})][\text{PF}_6]$ **9** and $[\text{Cu}(\text{Me}_2\text{Im})_2][\text{PF}_6]$ **10**.



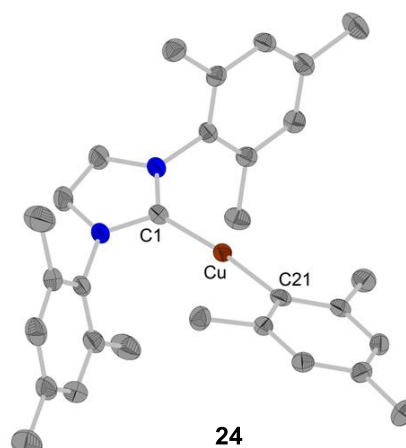
Furthermore, the highly reactive fluoride complex $[\text{Cu}(\text{Dipp}_2\text{Im})(\text{F})]$ **11** and the CaaC^{Me}-stabilized chloride complex $[\text{Cu}(\text{CaaC}^{\text{Me}})(\text{Cl})]$ **12** were also synthesized and were characterized by X-ray diffraction.

Starting from [Cu(NHC)Cl], a variety of derivatives have been synthesized. NHC-stabilized copper(I) *tert*-butoxides, which are considered to be important starting material as well as catalytic intermediates are available from the reaction with KO^tBu, namely [Cu(Dipp₂Im)(O^tBu)] **13**, [Cu(Mes₂Im)(O^tBu)] **14**,



[Cu(ⁱPr₂Im)(O^tBu)] **15** and [Cu(^tBu₂Im)(O^tBu)] **16**. Similarly, the complexes [Cu(Dipp₂Im)(OAc)], [Cu(Mes₂Im)(OAc)] and [Cu(ⁱPr₂Im)(OAc)] **17**, Cu(Dipp₂Im)(acac)] **18**, [Cu(Dipp₂Im)(hfacac)] **19**, [Cu(Dipp₂Im)DBM] **20**, [Cu(Mes₂Im)(hfacac)] **21**, [Cu(ⁱPr₂Im)(acac)] **22** and [Cu(ⁱPr₂Im)DBM] **23** have been synthesized via salt metathesis reactions. [Cu(^tBu₂Im)(O^tBu)] **16** and [Cu(ⁱPr₂Im)(OAc)] **17** were characterized by X-ray diffraction.

NHC-stabilized copper aryl complexes of the type [Cu(NHC)(Ar)] were synthesized with a wide variety of different aryl ligands (*p*-tolyl, 4-MeO-C₆H₄, Mes, C₆F₅, (4-CF₃-C₆H₄), (3,5-(CF₃)₂-C₆H₃), duryl, Dipp, C₆Me₅) and carbenes (ⁱPr₂Im, ^tBu₂Im, Mes₂Im, Dipp₂Im) using three different synthetic routes. The first route is the reaction of an NHC-stabilized copper(I) chloride complex with a Grignard reagent, the second route is the reaction of a copper(I) aryl complex with a NHCs and the third route is the reaction of an NHC-stabilized copper(I) alkoxide with an organoboronic ester. The latter reaction also allowed us to examine the important trans-metalation step involved in various catalytic processes. Using these pathways, the complexes [Cu(NHC)(Ar)] (NHC = Dipp₂Im; Ar = Mes **24**, 4-MeO-C₆H₄ **26**, *p*-tolyl **27**, C₆F₅ **30**, 4-CF₃-C₆H₄ **31**, 3,5-(CF₃)₂-C₆H₃ **33**, Dipp **35**, duryl **38**, C₆Me₅ **41**; NHC = Mes₂Im; Ar = Mes **25**, *p*-tolyl **28**, C₆F₅ **29**, 4-CF₃-C₆H₄ **32**, 3,5-(CF₃)₂-C₆H₃ **34**, Dipp **36**, duryl **39**, C₆Me₅ **42**; NHC = ^tBu₂Im; Ar = Dipp **37**, C₆Me₅ **43**; NHC = ⁱPr₂Im; Ar = duryl **40**, C₆Me₅ **44**) have been synthesized and characterized.

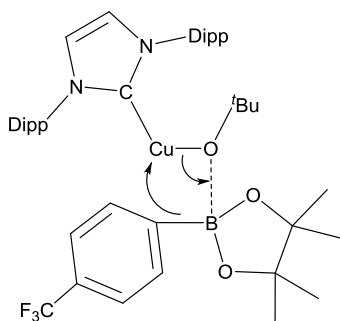


In situ VT-NMR investigations of the reaction of the fluoride complex [Cu(Dipp₂Im)(F)] with aryl boronic ester and diboron compounds reveal the high reactivity of these systems and gave some evidence for the formation of aryl and boryl complexes, respectively. However,

these reactions are overlaid with several other reaction pathways including decomposition and no well-defined product could be isolated from these mixtures. The reactions of $[\text{Cu}(\text{Dipp}_2\text{Im})(\text{O}^t\text{Bu})]$ with diboron compounds (B_2pin_2 , B_2cat_2 and B_2neop_2) also revealed that these reactions are not straightforward. Whereas the synthesis of the known copper(I) boryl complex $[\text{Cu}(\text{Dipp}_2\text{Im})(\text{Bpin})]$ was achieved, all attempts at the synthesis and isolation of $[\text{Cu}(\text{Dipp}_2\text{Im})(\text{Bneop})]$ and $[\text{Cu}(\text{Dipp}_2\text{Im})(\text{Bcat})]$ using similar conditions failed. However, using VT NMR experiments, signals indicative of the *in situ* formation of the boryl complexes were obtained. In the case of the experiments aiming at the synthesis of $[\text{Cu}(\text{Dipp}_2\text{Im})(\text{Bneop})]$, decomposition yielding $\text{Cu}(0)$, uncoordinated Dipp_2Im ligand and B_2neop_2 was observed.

Furthermore, reactions of $[\text{Cu}(\text{Dipp}_2\text{Im})(\text{Mes})]$ with B_2pin_2 , B_2cat_2 and B_2neop_2 were investigated. In the case of B_2cat_2 clean formation of the boryl complex $[\text{Cu}(\text{Dipp}_2\text{Im})(\text{Bcat})]$ and MesBcat was observed. It is noteworthy that the signals obtained in the NMR spectra are superimposable on the ones detected from the reaction of $[\text{Cu}(\text{Dipp}_2\text{Im})(\text{O}^t\text{Bu})]$ with B_2cat_2 .

The transmetalation of $4\text{-CF}_3\text{-C}_6\text{H}_4\text{Bpin}$ and $[\text{Cu}(\text{Dipp}_2\text{Im})(\text{O}^t\text{Bu})]$ was also investigated using



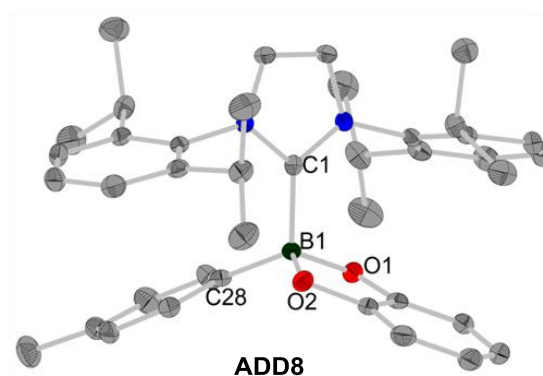
NMR spectroscopy. The spectra provide some evidence for the formation of an adduct (see left side; one signal at 7.7 ppm in the ^{11}B NMR spectra) right from the start of the reaction at $-40\text{ }^\circ\text{C}$. This adduct was stable up to a temperature of $-5\text{ }^\circ\text{C}$ and at this temperature the slow and clean formation of the aryl complex $[\text{Cu}(\text{Dipp}_2\text{Im})(4\text{-CF}_3\text{-C}_6\text{H}_4)]$ was observed.

Investigations concerning the reaction of $[\text{Cu}(\text{Dipp}_2\text{Im})(\text{Mes})]$, $[\text{Cu}(\text{Dipp}_2\text{Im})(p\text{-tolyl})]$ and $[\text{Cu}(\text{Dipp}_2\text{Im})(\text{C}_6\text{H}_5)]$ with different aryl iodides and bromides showed that all of the NHC-stabilized copper(I) aryl complexes examined have only a very low reactivity with these substrates. Low yields, long reaction times and side product formation were observed for this crucial step in cross-coupling reactions. Since this was calculated earlier (for phosphines as ligands) to be the step with the highest energy barrier for copper(I) catalyzed cross-coupling reactions, this is in good agreement with theory. Investigations on catalytic cross-coupling reactions with phosphines as ligands indicate that NHC copper complexes might form compounds which are too stable for efficient catalytic transformations.

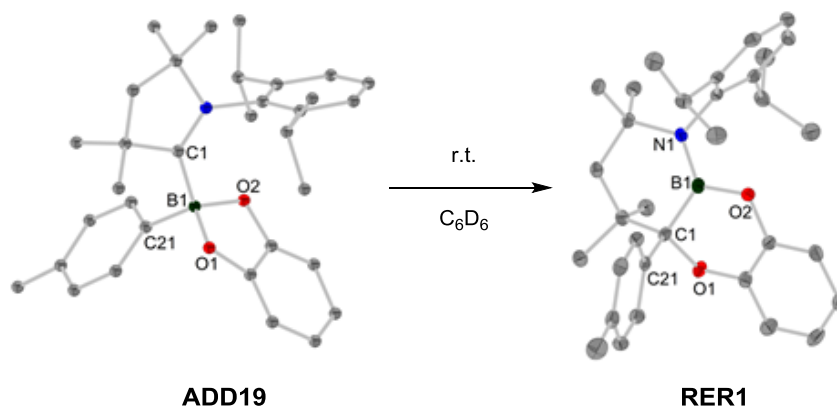
4.2 Interactions of carbenes with arylboronic esters and diboron(4) compounds

The second part of the thesis describes investigations of the reactivity of aryl boronic esters and diboron(4) esters with NHCs and CaaC^{Me} . Reversible adduct formation was observed for the reaction of NHCs and aryl boronic esters at room temperature. The Lewis acidity of the organo boronic ester and the steric demand of both the NHC and the boron compound determines whether adduct formation occurs.

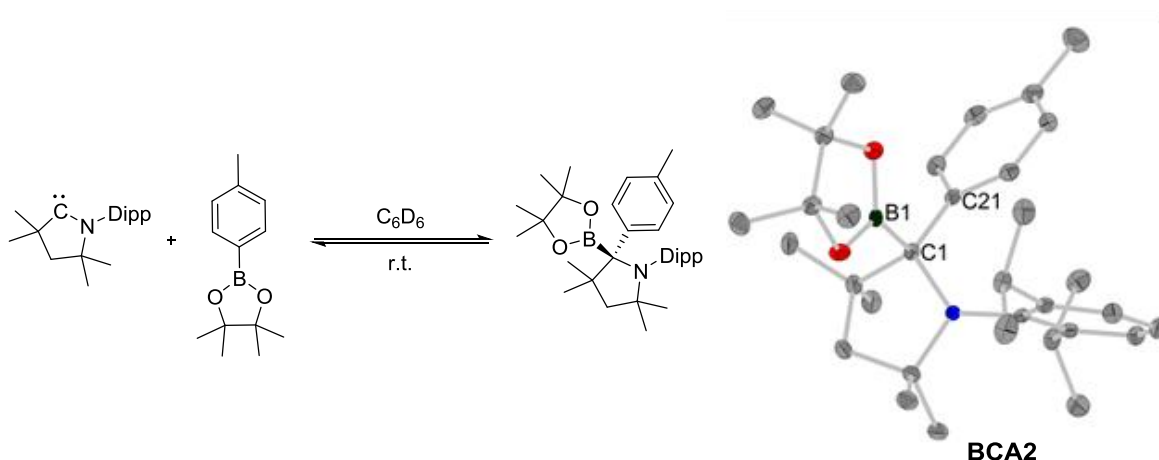
The sterically demanding NHC Dipp_2Im , for example, forms adducts with the Lewis acidic *p*-tolylBcat ester, while for the less demanding NHC $i\text{Pr}_2\text{ImMe}_2$ adduct formation with all aryl boronic esters examined ($\text{C}_6\text{H}_5\text{Bpin}$, *p*-tolylBpin, *p*-tolylBneop, *p*-tolylBcat, *p*-tolylBeg, 4-MeO- $\text{C}_6\text{H}_4\text{Bpin}$, 4-MeO- $\text{C}_6\text{H}_4\text{Bneop}$) was observed. In stability tests in solution at elevated temperatures, with and without another equivalent of NHC, no decomposition or ring-opening reactions were detected.



The outcome of the reactions of CaaC^{Me} with aryl boronic esters depends on the ester moiety used. For the reactions of CaaC^{Me} with aryl catechol boronates (4-MeO- $\text{C}_6\text{H}_4\text{Bcat}$ and *p*-tolylBcat) adduct formation and subsequent ring-opening of the five-membered CaaC^{Me} ring was observed. The product reveals three contiguous 6-membered rings and according to the X-ray crystal structure, π -bonding interactions between the nitrogen and boron atoms.

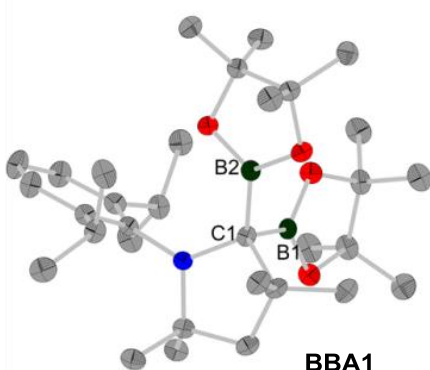


The reaction of CaaC^{Me} and aryl boronic esters of pinacol, neopentyl glycol and ethylene glycol (*p*-tolylBpin, *p*-tolylBeg, $\text{C}_6\text{H}_5\text{Bpin}$, 4-MeO- $\text{C}_6\text{H}_4\text{Bpin}$ and 4-MeO- $\text{C}_6\text{H}_4\text{Bneop}$) leads to an oxidative addition of the B-C bond to the CaaC carbene carbon atom.



No initial adduct formation was observed, and the insertion product is in solution in equilibrium with the starting materials. Many of these insertion products have been

characterized using X-ray diffraction, and NMR experiments reveal the temperature dependence of this entropically driven equilibrium.



Finally, the reaction of CaaC^{Me} with the diboron(4) compounds B_2pin_2 , B_2cat_2 , B_2neop_2 and B_2eg_2 led to oxidative addition of the B-B bond to the CaaC carbene carbon atom. All of the products are stable up to a

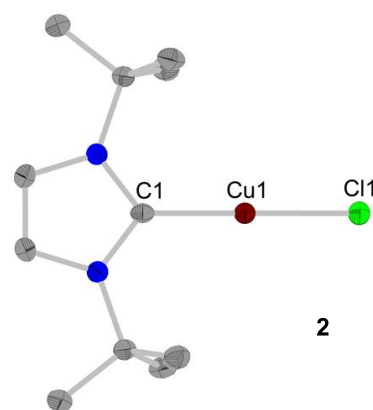
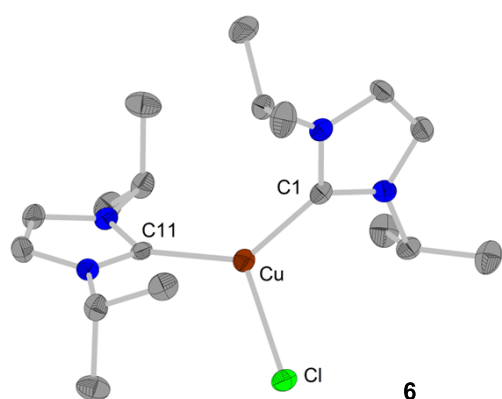
temperature of 80 °C. While adduct formation and ring expansion reactions with diboron(4) esters were also observed in earlier work for NHCs, these insertions of the CaaC carbene carbon atom into the B-B and B-C bond are remarkable and clearly demonstrate the higher nucleophilic and simultaneously higher electrophilic character of the carbene carbon atoms in CaaCs compared those of NHCs. The unique reversible B-C bond activation at carbon observed here might lead to the development of novel organocatalytic transformations, opening a new chapter in chemistry, were carbon mimics transition metals.

5 Zusammenfassung

Die dargelegte Arbeit gliedert sich in zwei Teile. In einem ersten wird die Synthese sowie stöchiometrische Modell-Reaktionen von definierten NHC-stabilisierten Kupfer(I)-Komplexen (NHC = *N*-heterocyclisches Carben) untersucht, um Einblick in das grundlegende Reaktionsverhalten in Borylierungs- und Kreuzkupplungsreaktionen zu erlangen. Der zweite Teil adressiert die Reaktivität der eingesetzten Liganden (NHCs und CaaCs = cyclische Alkyl Amino Carbene) gegenüber verwendeten sowie möglichen Substraten (Arylboronsäureester und Diboran(4)-Verbindungen).

5.1 Synthese und stöchiometrische Modell-Reaktionen von NHC-stabilisierten Kupfer(I)-Komplexen

Der erste Teil dieser Arbeit ist der Synthese von NHC-stabilisierten Kupfer(I)-Komplexen sowie den damit durchgeführten stöchiometrischen Modell-Reaktionen zu Kupfer vermittelten Borylierung und Suzuki-Miyaura Kreuzkupplungen gewidmet.



Die Ausgangsverbindungen - Komplexe vom Typ $[\text{Cu}(\text{NHC})(\text{Cl})]$ (NHC = $t\text{Bu}_2\text{Im}$, $i\text{Pr}_2\text{Im}$ **2**, $i\text{Pr}_2\text{ImMe}_2$ **3**, Me_4Im **4**, Dipp_2Im , Mes_2Im) sowie die bis-NHC

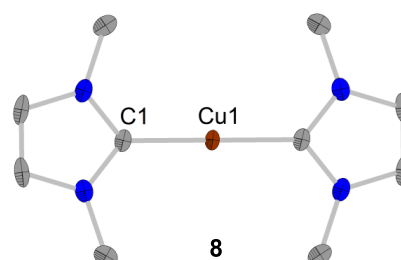
Komplexe $[\text{Cu}(\text{NHC})_2(\text{Cl})]$ (NHC = Me_2Im **5**, $i\text{Pr}_2\text{Im}$ **6**, $i\text{Pr}_2\text{ImMe}_2$ **7**) - wurden durch die Umsetzung von freiem NHC sowie Kupfer(I)chlorid erhalten, isoliert und charakterisiert.

Aus der Reaktion von Me_2Im mit CuCl wurde die Verbindung $[\text{Cu}(\text{Me}_2\text{Im})_2][\text{CuCl}_2]$ **8**

erhalten, welche aus Komplexionen aufgebaut ist. Die Reaktion von $[\text{Cu}(\text{MeCN})_4][\text{PF}_6]$ mit Me_2Im führte zur Isolierung der Verbindungen

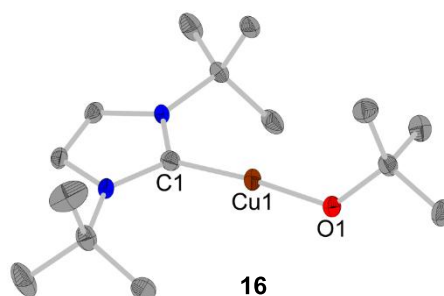
$[\text{Cu}(\text{Me}_2\text{Im})(\text{MeCN})][\text{PF}_6]$ **9** und

$[\text{Cu}(\text{Me}_2\text{Im})_2][\text{PF}_6]$ **10**.



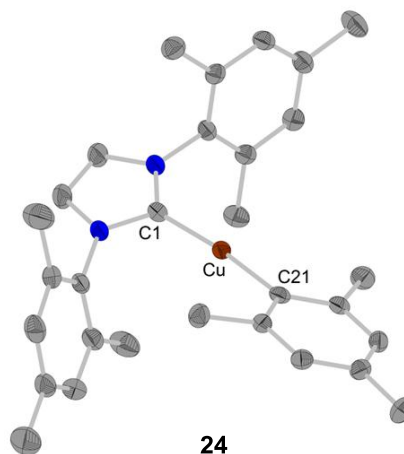
Außerdem wurde der hoch reaktive Fluorido-Komplex $[\text{Cu}(\text{Dipp}_2\text{Im})(\text{F})]$ **11** sowie der CaaC^{Me} -stabilisierte Chlorido-Komplex $[\text{Cu}(\text{CaaC}^{\text{Me}})(\text{Cl})]$ **12** synthetisiert und mittels Einkristallstrukturanalyse charakterisiert.

Ausgehend von den Chlorid-Komplexen $[\text{Cu}(\text{NHC})\text{Cl}]$ wurde eine Vielzahl an Derivaten hergestellt. NHC-stabilisierte *tert*-butoxid-Kupfer-Komplexe, welche ihrerseits ein wichtiges Ausgangsmaterial für Synthesen darstellen sowie häufig als Intermediate in katalytischen Umsetzungen aufgefasst werden,



wurden durch Umsetzung des entsprechenden Chlorido-Komplexes mit KO^tBu erhalten. Auf diesem Wege wurden die Komplexe $[\text{Cu}(\text{Dipp}_2\text{Im})(\text{O}^t\text{Bu})]$ **13**, $[\text{Cu}(\text{Mes}_2\text{Im})(\text{O}^t\text{Bu})]$ **14**, $[\text{Cu}(^i\text{Pr}_2\text{Im})(\text{O}^t\text{Bu})]$ **15** und $[\text{Cu}(^t\text{Bu}_2\text{Im})(\text{O}^t\text{Bu})]$ **16** dargestellt. In ähnlicher Weise wurden die Acetato- und Acetylacetonato-Komplexe $[\text{Cu}(\text{Dipp}_2\text{Im})(\text{OAc})]$, $[\text{Cu}(\text{Mes}_2\text{Im})(\text{OAc})]$, $[\text{Cu}(^i\text{Pr}_2\text{Im})(\text{OAc})]$ **17**, $[\text{Cu}(\text{Dipp}_2\text{Im})(\text{acac})]$ **18**, $[\text{Cu}(\text{Dipp}_2\text{Im})(\text{hfacac})]$ **19**, $[\text{Cu}(\text{Dipp}_2\text{Im})\text{DBM}]$ **20**, $[\text{Cu}(\text{Mes}_2\text{Im})(\text{hfacac})]$ **21**, $[\text{Cu}(^i\text{Pr}_2\text{Im})(\text{acac})]$ **22** und $[\text{Cu}(^i\text{Pr}_2\text{Im})\text{DBM}]$ **23** synthetisiert. Die Komplexe $[\text{Cu}(^t\text{Bu}_2\text{Im})(\text{O}^t\text{Bu})]$ **16** und $[\text{Cu}(^i\text{Pr}_2\text{Im})(\text{OAc})]$ **17** wurden mittels Einkristallstrukturanalyse charakterisiert.

Die Synthese NHC-stabilsierter Kupfer(I)-Aryl Komplexe des Typs $[\text{Cu}(\text{NHC})(\text{Ar})]$ gelang für eine Vielzahl an Aromaten (*p*-Tolyl, 4-MeO-C₆H₄, Mes, C₆F₅, (4-CF₃-C₆H₄), (3,5-(CF₃)₂C₆H₃), Duryl, Dipp, C₆Me₅) sowie NHC Liganden (^{*i*}Pr₂Im, ^{*t*}Bu₂Im, Mes₂Im, Dipp₂Im) mit drei unterschiedlichen synthetischen Ansätzen. Zum einen ausgehend von den entsprechenden NHC-stabilisierten Kupfer(I) Chlorido-Komplexen und einem Aryl-Grignard-Reagenz, unter Salz-Eliminierung, zum anderen ausgehend von Kupfer(I) Aryl-Komplexen und freiem NHC ausging. In einer dritten Route wurden Alkoxid-Kupfer(I)-Komplexe und Organoboronsäureester eingesetzt. Auf diesen Wegen wurden die Komplexe $[\text{Cu}(\text{NHC})(\text{Ar})]$ (NHC = Dipp₂Im; Ar = Mes **24**, 4-MeO-C₆H₄ **26**, *p*-Tolyl **27**, C₆F₅ **30**, 4-CF₃-C₆H₄ **31**, 3,5-(CF₃)₂-C₆H₃ **33**, Dipp **35**, Duryl **38**, C₆Me₅ **41**; NHC = Mes₂Im; Ar = Mes **25**, *p*-Tolyl **28**, C₆F₅ **29**, 4-CF₃-C₆H₄ **32**, 3,5-(CF₃)₂-C₆H₃ **34**, Dipp **36**, Duryl **39**, C₆Me₅ **42**; NHC = ^{*t*}Bu₂Im; Ar = Dipp

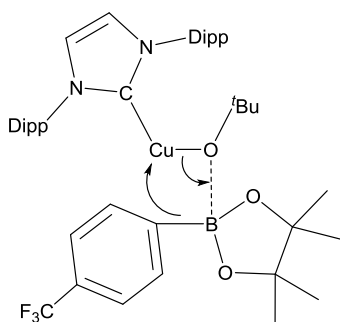


37, C₆Me₅ **43**; NHC = *i*Pr₂Im; Ar = Duryl **40**, C₆Me₅ **44**) synthetisiert und charakterisiert.

Durch *in situ* Tieftemperatur-NMR-spektroskopische Untersuchungen der Reaktionen des Fluorido-Komplexes **11** mit Arylboronsäureestern sowie Diboran(4)-Verbindungen wurde die hohe Reaktivität dieser Verbindung belegt. Die erhaltenen spektroskopischen Daten deuten auf Bildung der jeweiligen Aryl- beziehungsweise Boryl-Komplexe hin, aufgrund mehrerer Nebenreaktionen sowie Zersetzung der gewünschten Produkte wurden jedoch keine Produkte isoliert. Untersuchungen zu den Reaktionen von [Cu(Dipp₂Im)(O^tBu)] mit den Diboran(4)-Verbindungen B₂pin₂, B₂cat₂ und B₂neop₂ zeigten ebenso eine vielschichtige Reaktivität dieser Komplexe auf. Während die Synthese des Boryl-Komplexes [Cu(Dipp₂Im)(Bpin)] erfolgreich war, schlugen sämtliche Versuche zur Darstellung von Boryl-Komplexen ausgehend von B₂cat₂ und B₂neop₂ unter ähnlichen Bedingungen fehl. In Tieftemperatur-NMR Untersuchungen konnten jedoch Hinweise für die *in situ* Bildung der jeweiligen Boryl-Komplexe *in situ* erhalten werden. Im Falle der Untersuchungen zur Synthese von [Cu(Dipp₂Im)(Bneop)] wurden die Zersetzungsprodukte Cu(0), der nicht komplexierte Ligand Dipp₂Im Ligand und B₂neop₂ beobachtet.

Des weiteren wurden die Umsetzungen von [Cu(Dipp₂Im)(Mes)] mit B₂pin₂, B₂cat₂ und B₂neop₂ mittels *in situ* Tieftemperatur-NMR Untersuchungen analysiert. Hierbei konnte unter anderem die Nebenprodukt-freie Bildung des Boryl-Komplexes [Cu(Dipp₂Im)(Bcat)] und MesBcat beobachtet werden. Die Signale in den dabei erhaltenen NMR Spektren sind deckungsgleich mit den Resonanzen, die bei den Umsetzungen von [Cu(Dipp₂Im)(O^tBu)] mit B₂cat₂ beobachtet wurden.

Untersuchungen zur Transmetallierung erfolgten durch die Analyse der Umsetzung von



4-CF₃-C₆H₄Bpin mit [Cu(Dipp₂Im)(O^tBu)] mittels *in situ* Tieftemperatur-NMR Spektroskopie. Direkt zu Beginn der Reaktion bei -40 °C wurden Signale eines Adduktes (siehe Abbildung links; ein Signal im ¹¹B NMR Spektrum bei 7.7 ppm) zwischen dem Sauerstoffatom der *tert*-Butoxid-Gruppe und dem Boratom detektiert. Dieses Addukt war stabil bis zu einer

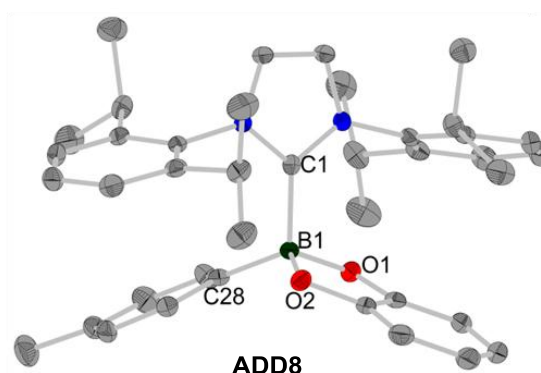
Temperatur von -5 °C, ab welcher die langsame und saubere Bildung des Aryl-Komplexes [Cu(Dipp₂Im)(4-CF₃-C₆H₄)] beobachtet wurde.

In stöchiometrischen Umsetzungen von $[\text{Cu}(\text{Dipp}_2\text{Im})(\text{Mes})]$, $[\text{Cu}(\text{Dipp}_2\text{Im})(p\text{-tolyl})]$ und $[\text{Cu}(\text{Dipp}_2\text{Im})(\text{C}_6\text{H}_5)]$ mit unterschiedlichen Aryliodiden und -bromiden zeigte sich ein sehr geringes Reaktionsvermögen. Für diesen für die Kreuzkupplung essentiellen Schritt waren lange Reaktionszeiten notwendig, zudem wurden nur äußerst geringe Ausbeuten und ein hohes Maß an Nebenprodukten beobachtet. Dies ist konform mit früheren Berechnungen, welche für diesen Schritt die höchste Energiebarriere in der Kupfer(I)-katalysierten Kreuzkupplung (mit Phosphanen als Liganden) postulierten. Untersuchungen zu katalytischen Kreuzkupplungsreaktionen mit Phosphanen als Liganden deuten ebenfalls darauf hin, dass Umsetzungen von NHC-stabilisierten Kupfer(I) Komplexen möglicherweise zu Verbindungen führen, welche zu stabil für eine effiziente Transformation sind.

5.2 Wechselwirkungen von Carbenen mit Arylboronsäureestern und Diboran(4)-Verbindungen

Der zweite Teil der Arbeit beschreibt die Untersuchungen zur Reaktivität von NHCs und CaaC^{Me} gegenüber Arylboronsäureestern und Diboran(4)-Verbindungen. Für die Umsetzungen von NHCs mit Arylboronsäureestern wurde die reversible Addukt-Bildung beobachtet. Die Lewis Azidität des Organoboronsäureesters sowie der sterische Anspruch beider Reaktionspartner bestimmten dabei, ob es zur Addukt Bildung kommt oder nicht.

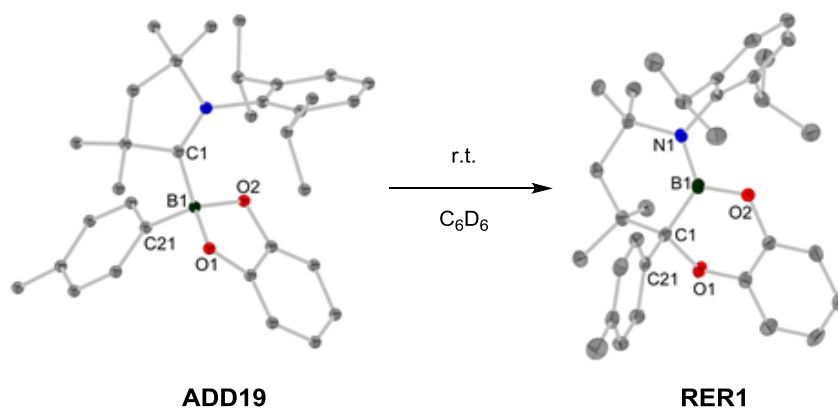
Beispielsweise kam es beim sterisch anspruchsvollen Liganden Dipp_2Im ausschließlich mit dem Lewis-sauren p -Tolyl-Bcat-Ester zur Ausbildung eines Adduktes, während das sterisch weniger anspruchsvolle Carben $i\text{Pr}_2\text{ImMe}_2$ mit allen eingesetzten Substraten (C_6H_5 -Bpin, p -Tolyl-



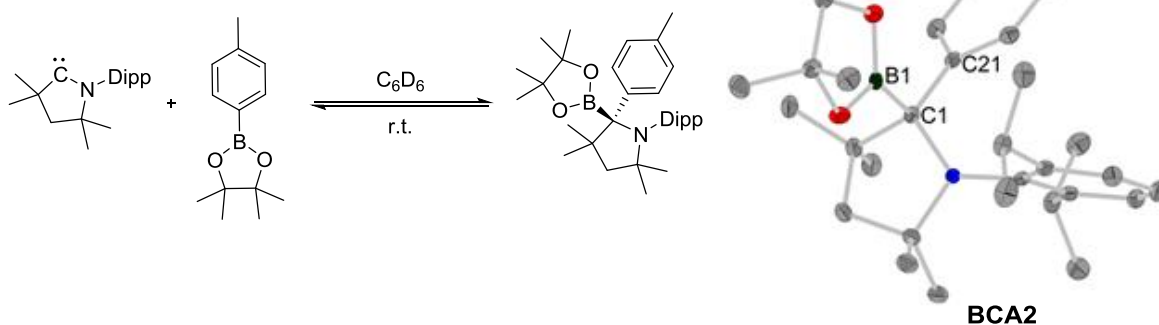
Bpin, p -Tolyl-Bneop, p -Tolyl-Bcat, p -Tolyl-Beg, 4-MeO- C_6H_4 -Bpin, 4-MeO- C_6H_4 -Bneop) ein Addukt formte. Stabilitätstests bei erhöhter Temperatur in Lösung zeigten keinerlei Tendenz zur Ringerweiterung, auch wenn ein zweites Äquivalent NHC zugesetzt wurde.

Die Ergebnisse der Reaktionen von CaaC^{Me} mit Arylboronsäureestern waren ebenfalls vom eingesetzten Ester abhängig. Bei den Umsetzungen mit Arylboronsäureestern des Brenzkatechins (4-MeO- C_6H_4 -Bcat und p -Tolyl-Bcat) wurde Addukt-Bildung mit einer

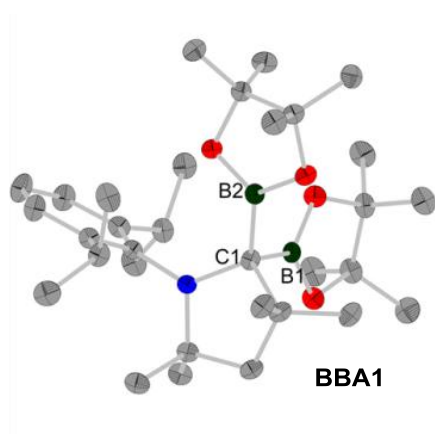
anschließenden Ringerweiterung des fünfgliedrigen CaaC^{Me} -Rings beobachtet. Einkristallstruktur-Untersuchungen der Produkte zeigten drei aneinanderhängende Sechsringe mit bindenden π -Wechselwirkungen zwischen dem Stickstoffatom und dem Boratom.



Die Reaktionen von CaaC^{Me} mit Arylboronsäureestern des Pinakols, Neopentylglykols und des Ethylenglykols (*p*-Tolyl-Bpin, *p*-Tolyl-Beg, C_6H_5 -Bpin, 4-MeO- C_6H_4 -Bpin and 4-MeO- C_6H_4 -Bneop) führten hingegen zur oxidativen Addition der jeweiligen B-C Bindung an das CaaC^{Me} Carbenkohlenstoffatom.



Es wurden keine Anzeichen für eine vorgelagerte Addukt-Bildung beobachtet. Vielmehr zeigte es sich, dass diese Produkte in Lösung im Gleichgewicht mit den Startmaterialien sind. Der Temperatur-Einfluss auf dieses Entropie-getriebene Gleichgewicht konnte in NMR-spektroskopischen Untersuchungen nachgewiesen werden. Eine Vielzahl dieser Additionsprodukte konnte mittels Einkristallstrukturanalyse charakterisiert werden.



Schließlich führten die Umsetzungen von CaaC^{Me} mit Diboran(4)-Verbindungen zur oxidativen Addition der jeweiligen B-B Bindung an das Carbenkohlenstoffatom. Die hierbei erhaltenen Produkte waren in Lösung stabil bis zu der getesteten Temperatur von 80 °C.

Während die Addukt-Bildung sowie die Ringerweiterung von NHCs mit Diboran(4)-Verbindungen bereits in vorangegangenen Arbeiten beobachtet wurden, ist die hier gefundene Insertion des Carbenkohlenstoffatoms in die B-B beziehungsweise B-C Bindung außergewöhnlich. Diese Reaktivität demonstriert auf eindrucksvolle Weise die gleichzeitig höhere Nucleophilie sowie Elektrophilie des Carbenkohlenstoffatoms in CaaCs im Vergleich zu NHCs. Die hier beobachtete, einzigartige reversible B-C Bindungsaktivierung könnte zur Entwicklung neuartiger Organokatalysatoren führen. Diese haben das Potential ein neues Kapitel in der Chemie aufzuschlagen, in welchem Kohlenstoff Übergangsmetalle nachahmt und schließlich ersetzt.

6 Experimental Section

6.1 General procedures

All manipulations, unless otherwise stated, were carried out under an atmosphere of argon using conventional Schlenk, vacuum-line and glove-box techniques. All reactions were carried out in oven-dried glassware. Solvents were purified by distillation from an appropriate drying agent (toluene, xylene, benzene, and ethers from sodium/potassium alloy with benzophenone as indicator). Halocarbons, *n*-hexane and acetonitrile were dried and deoxygenated using an Innovative Technology Inc. Pure-Solv 400 Solvent Purification System, and further deoxygenated by using the freeze-pump-thaw method.

THF- d_8 and CD_3OD were dried over 4 Å molecular sieves and distilled before usage. C_6D_6 and toluene- d_8 were dried over potassium or sodium and freshly distilled before usage. $MeCN-d_3$ was first dried over sodium hydride and distilled. Afterwards, dried over P_4O_{10} and freshly distilled.

Starting materials

All other reagents were purchased from commercial sources and were checked for purity by GC-MS and NMR spectroscopy.

The diboron reagents B_2pin_2 , B_2cat_2 and B_2neop_2 were a generous gift from AllyChem Co. Ltd.

NMR-Spectroscopy

All chemical shifts are expressed in ppm and are relative to the residual solvent peaks and external standards. The coupling constant (*J*) are stated in (Hz) without consideration of the sign. Multiplicities are abbreviated as follows: s = singlet, d = doublet, t = triplet, q = quartet, sept = septet, br = broad, m = multiplet.

^1H NMR spectroscopy: Bruker Avance 200 (200.1 MHz), Avance 400 (400.4 MHz) and Avance 500 (500.1 MHz). Solvent and lock-substance: C_6D_6 (internal standard $\text{C}_6\text{D}_5\text{H}$, $\delta = 7.16$). External standard: Tetramethylsilane.

^{11}B NMR spectroscopy: Bruker Avance 200 (64.1 MHz), Avance 400 (128.5 MHz) and Avance 500 (160.5 MHz). External standard: Boron trifluoride diethyl etherate.

^{13}C NMR spectroscopy: Bruker Avance 200 (50.3 MHz), Avance 400 (100.7 MHz) and Avance 500 (125.8 MHz). Solvent and lock-substance: C_6D_6 (internal standard C_6D_6 , $\delta = 128.06$). All $^{13}\text{C}\{^1\text{H}\}$ NMR experiments were recorded ^1H -decoupled. External standard: Tetramethylsilane.

^{31}P NMR spectroscopy: Bruker Avance 200 (81.0 MHz) and Avance 500 (202.5 MHz). Solvent and lock-substance: C_6D_6 (external standard H_3PO_4 (85% in H_2O), $\delta = 0$).

^{19}F NMR spectroscopy: Bruker Avance 200 (188.3 MHz), Avance 400 (376.6 MHz) and Avance 500 (470.8 MHz). External standard: Cl_3CF .

Elemental analysis

Elemental analyses (C, H, N) were performed at the microanalytical laboratory of the University Würzburg using a 'vario Micro cube' from ELEMENTAR.

Gas Chromatography (GCMS)

GC-MS analyses were performed using an Agilent 7890A gas chromatograph (column: HP-5MS, 30 m, \varnothing 0.25 mm, film 0.25 μm ; injector: 250 $^\circ\text{C}$; oven: 40 $^\circ\text{C}$ (2 min), 40 $^\circ\text{C}$ to 250 $^\circ\text{C}$ (20 $^\circ\text{C min}^{-1}$), 280 $^\circ\text{C}$ (5 min); carrier gas: He (1.6 mL min^{-1})) equipped with an Agilent 5975C inert mass selective detector (MSD) operating in EI mode and an Agilent 7693A as autosampler/injector; or an HP G1800A GCD System (70 eV) (column: Agilent Technologies, 'factor FOUR Silica', 30 m, \varnothing 0.25 mm, injector 280 $^\circ\text{C}$, oven 40 $^\circ\text{C}$ (2 min) 40 $^\circ\text{C}$ to 250 $^\circ\text{C}$ (20 $^\circ\text{C min}^{-1}$), 280 $^\circ\text{C}$ (5 min); carrier gas: He (1.0 mL min^{-1})), or Thermo Fisher Scientific Trace 1310 (column: TG-SQC, 15 m, \varnothing 0.25 mm, film 0.25 μm ; injector: 250 $^\circ\text{C}$; oven: 40 $^\circ\text{C}$ (2 min), 40 $^\circ\text{C}$ to 250 $^\circ\text{C}$ (20 $^\circ\text{C min}^{-1}$), 280 $^\circ\text{C}$ (5 min); carrier gas: He (1.2 mL min^{-1})) equipped

with a Thermo Fisher ISQ QD single quadrupole mass spectrometer operating in EI mode and a Thermo Fisher AL 1310 as autosampler.

Flash chromatography

Flash chromatography was performed with a Biotage Isolera Four equipped with HP-Sil or KP-Sil cartridges and a diode array UV detector.

High-Resolution Mass Spectrometry (HRMS)

The high resolution mass analysis was measured on a Thermo Scientific Exactive Plus mass spectrometer, equipped with an Orbitrap Mass Analyzer. Measurements were accomplished using an ASAP/APCI source with a corona needle, and carrier-gas (N₂) temperature of 400 °C and 250 °C, respectively. ESI mass spectrometry was performed using an HESI source with an auxiliary gas temperature of 50 °C.

Quantification and determination of the response factors:

The GC-MS quantification was done using the multiple point internal standard method. Therefore, the compounds of interest were calibrated against *n*-dodecane as an internal standard. Up to five different solutions for each compound of interest (from 0.5 mmol/L to 19 mmol/L) with internal standard (4.025 mmol/L) were prepared (Tables 14, 16, 18, 20 and 22). For the calibration, each stock solution was measured four times (Tables 15, 17, 19, 21 and 23). The compound-specific response factors were calculated according to:

$$\text{response factor} = \frac{n_{IS} * \text{peak area}(X)}{n_x * \text{peak area}(IS)}$$

The amount of a compound in a sample was determined by the ratio of its peak area to the peak area of the internal standard multiplied by the response factor and the amount of the internal standard:

$$n_x = \frac{\text{peak area}(x) * \text{response factor} * n_{IS}}{\text{peak area}(IS)}$$

Table 14: Stock solutions for the response factor determination of 4,4'-dimethyl-1,1'-biphenyl in 4.025 mM *n*-dodecane in toluene.

volume [mL]	m [mg]	n [μmol]	c (mmol/L)
100	18.8	103	1.03
10	4.60	25.2	2.52
10	7.30	40.1	4.01
10	14.6	80.0	8.01
25	72.9	400	16.0

Table 15: Response factor of 4,4'-dimethyl-1,1'-biphenyl compared to *n*-dodecane.

Concentration [mmol/l]

6 Experimental Section

measurement	1.03	2.52	4.01	8.01	16.0
1	1.364	1.336	1.250	1.285	1.344
2	1.325	1.264	1.263	1.226	1.285
3	1.301	1.263	1.214	1.245	1.302
4	1.310	1.255	1.176	1.243	1.256

average: 1.275

Table 16: Stock solutions for the response factor determination of 4-methoxy-4'-methyl-1,1'-biphenyl in 4.025 mM *n*-dodecane in toluene.

volume [mL]	m [mg]	n [μmol]	c (mmol/L)
50	10.1	50.9	1.02
10	5.10	25.7	2.57
25	19.9	100	4.00
10	15.9	80.2	8.02
10	31.6	159	15.9

Table 17: Response factor of 4-methoxy-4'-methyl-1,1'-biphenyl compared to *n*-dodecane.

measurement	Concentration [mmol/l]				
	1.02	2.57	4.00	8.02	15.9
1	2.078	1.633	1.489	1.525	1.519
2	1.940	1.662	1.437	1.445	1.616
3	1.998	1.561	1.492	1.573	1.497
4	2.026	1.669	1.451	1.520	1.527

average: 1.633

6 Experimental Section

Table 18: Stock solutions for the response factor determination of 4-methyl-4'-trifluoromethyl-1,1'-biphenyl in 4.025 mM *n*-dodecane in toluene.

volume [mL]	m [mg]	n [μ mol]	c (mmol/L)
100	11.5	48.7	0.49
50	11.7	49.5	0.99
10	9.50	25.0	4.02
10	20.0	84.7	8.47

Table 19: Response factor of 4-methyl-4'-trifluoromethyl-1,1'-biphenyl compared to *n*-dodecane.

measurement	Concentration [mmol/l]			
	0.49	0.99	4.02	8.46
1	1.907	1.471	1.340	1.355
2	2.147	1.451	1.279	1.353
3	2.091	1.511	1.314	1.376
4	2.180	1.453	1.348	1.338

average: 1.557

Table 20: Stock solutions for the response factor determination of 1,1'-biphenyl in 4.025 mM *n*-dodecane in toluene.

volume [mL]	m [mg]	n [μ mol]	c (mmol/L)
50	8.10	53.0	1.06
25	10.4	67.0	2.68
25	15.5	101	4.04
10	12.3	80.0	8.00
5	12.8	83	16.6

Table 21: Response factor of 1,1'-biphenyl compared to *n*-dodecane.

measurement	Concentration [mmol/l]				
	1.06	2.68	4.04	8.00	16.6
1	1.109	0.935	1.057	1.034	1.340
2	1.206	1.032	1.036	1.059	1.270
3	1.124	0.935	1.059	1.055	1.171

average: 1.095

Table 22: Stock solutions for the response factor determination of 4-methyl-1,1'-biphenyl in 4.025 mM *n*-dodecane in toluene.

volume [mL]	m [mg]	n [μmol]	c (mmol/L)
50	8.90	53.0	1.06
25	10.8	64.0	2.56
25	17.4	104	4.16
10	13.6	81.0	8.10
10	32.0	190	19.0

Table 23: Response factor of 4-methyl-1,1'-biphenyl compared to *n*-dodecane.

measurement	Concentration [mmol/l]				
	1.06	2.56	4.16	8.10	19.0
1	1.217	1.191	1.167	1.254	1.336
2	1.261	1.273	1.172	1.257	1.340
3	1.188	1.311	1.152	1.274	1.370
4	1.235	1.324	1.156	1.216	1.314

average: 1.251

General procedure for the copper(I)-catalyzed cross-coupling of aryl iodides with PN donor ligands

In an argon-filled glovebox, a Schlenk tube was charged with phenylboronic acid neopentyl glycol ester (23.0 mg, 121 μmol), 4-iodotoluene (26.4 mg, 121 μmol), cesium fluoride (53.6 mg, 353 μmol), copper(I) iodide (1.9 mg, 10.0 μmol) and ligand PN-1 (2.4 mg, 10.0 μmol). The tube was taken out of the glovebox and 5 mL of a 4.05 mM solution of *n*-dodecane in DMF was added before the mixture was heated for 20 h at 80 °C. After cooling to room temperature, the suspension was diluted with 2 mL ethyl acetate and filtered through a pad of Celite®. The clear solution was analyzed by GCMS using the multiple point internal standard method.

General procedure for the copper(I)-catalyzed cross-coupling of aryl iodides with Xantphos as ligand

In an argon-filled glovebox, a Schlenk tube was charged with a (1.0 mg, 10.0 μmol), Xantphos (5.8 mg, 10.0 μmol), iodobenzene (20.4 mg, 100 μmol), NaO^tBu (19.2 mg, 218 μmol), and 4-methylphenylboronic acid neopentyl glycol ester (20.5 mg, 100 μmol). The tube was taken out of the glovebox and 5 mL of a 4.95 mM solution of *n*-dodecane in toluene was added before the mixture was heated for 16 h at 80 °C. After cooling to room temperature, the suspension was quenched with 1 mL water. The organic phase analyzed by GCMS using the multiple point internal standard method.

General procedure for the *in situ* VT-NMR experiments conducted below r.t.:

In an argon-filled glovebox, a Young's-NMR tube was charged with the complex as well as the solid substrate. In a fume hood, the sample was cooled to -100 °C before precooled toluene- d_8 or THF- d_8 was added using Schlenk techniques. The sample was shaken and NMR experiments were conducted immediately.

List of VT-NMR experiments:

For each *in situ* investigation the weighed portion and the optical appearance of the sample at the beginning as well as at the end of the investigation is given.

Reaction of [Cu(Dipp₂Im)(F)] with *p*-tolylBpin in toluene-d₈: -40 – r.t.

[Cu(Dipp₂Im)(F)]: 10 mg (21.2 μmol); *p*-tolylBpin: 4.6 mg (21.2 μmol); toluene-d₈: 0.6 mL

White suspension → gel formation

Reaction of [Cu(Dipp₂Im)(F)] with *p*-tolylBneop in toluene-d₈: -40 – r.t.

[Cu(Dipp₂Im)(F)]: 10 mg (21.2 μmol); *p*-tolylBneop: 4.3 mg (21.2 μmol); toluene-d₈: 0.6 mL

White suspension → white suspension

Reaction of [Cu(Dipp₂Im)(F)] with *p*-tolylBcat in toluene-d₈: -40 – r.t.

[Cu(Dipp₂Im)(F)]: 10 mg (21.2 μmol); *p*-tolylBcat: 4.5 mg (21.2 μmol); toluene-d₈: 0.6 mL

White suspension → white suspension

Reaction of [Cu(Dipp₂Im)(F)] with *p*-tolylBpin in THF-d₈: -50 – r.t.

[Cu(Dipp₂Im)(F)]: 10 mg (21.2 μmol); *p*-tolylBpin: 4.6 mg (21.2 μmol); THF-d₈: 0.6 mL

White suspension → clear solution

Reaction of [Cu(Dipp₂Im)(F)] with *p*-tolylBneop in THF-d₈: -50 – r.t.

[Cu(Dipp₂Im)(F)]: 10 mg (21.2 μmol); *p*-tolylBneop: 4.3 mg (21.2 μmol); THF-d₈: 0.6 mL

Clear solution → clear solution

Reaction of [Cu(Dipp₂Im)(F)] with *p*-tolylBcat in THF-d₈: -50 – r.t.

[Cu(Dipp₂Im)(F)]: 10 mg (21.2 μmol); *p*-tolylBcat: 4.5 mg (21.2 μmol); THF-d₈: 0.6 mL

Clear solution → clear solution

Reaction of [Cu(Dipp₂Im)(F)] with B₂pin₂ in toluene-d₈: -50 – r.t.

[Cu(Dipp₂Im)(F)]: 10 mg (21.2 μmol); B₂pin₂: 5.4 mg (21.2 μmol); toluene-d₈: 0.6 mL

Pale yellow solution → reddish solution + black precipitate

Reaction of [Cu(Dipp₂Im)(F)] with B₂neop₂ in toluene-d₈: -50 – r.t.

[Cu(Dipp₂Im)(F)]: 10 mg (21.2 μmol); B₂neop₂: 4.8 mg (21.2 μmol); toluene-d₈: 0.6 mL

Pale yellow solution → reddish solution + black precipitate

Reaction of [Cu(Dipp₂Im)(F)] with B₂cat₂ in toluene-d₈: -50 – r.t.

[Cu(Dipp₂Im)(F)]: 10 mg (21.2 μmol); B₂cat₂: 5.0 mg (21.2 μmol); toluene-d₈: 0.6 mL

White suspension → reddish solution + black precipitate

Reaction of [Cu(Dipp₂Im)(O^tBu)] with B₂pin₂ in THF-d₈: -50 – r.t.

[Cu(Dipp₂Im)(O^tBu)]: 12 mg (22.7 μmol); B₂pin₂: 5.8 mg (22.7 μmol); THF-d₈: 0.6 mL

Clear solution → pale yellow solution

Reaction of [Cu(Dipp₂Im)(O^tBu)] with B₂neop₂ in THF-d₈: -50 – r.t.

[Cu(Dipp₂Im)(O^tBu)]: 12 mg (22.7 μmol); B₂neop₂: 5.1 mg (22.7 μmol); THF-d₈: 0.6 mL

Clear solution → black solution

Reaction of [Cu(Dipp₂Im)(O^tBu)] with B₂cat₂ in THF-d₈: -50 – r.t.

[Cu(Dipp₂Im)(O^tBu)]: 12 mg (22.7 μmol); B₂cat₂: 5.4 mg (22.7 μmol); THF-d₈: 0.6 mL

Clear solution → dark brown solution + pink oily bubbles

Reaction of [Cu(^tBu₂Im)(O^tBu)] with B₂pin₂ in toluene-d₈: -40 – r.t.

[Cu(^tBu₂Im)(O^tBu)]: 12 mg (37.9 μmol); B₂pin₂: 9.6 mg (37.9 μmol); toluene-d₈: 0.6 mL

Pale yellow solution → brown solution + black precipitate + copper mirror

Reaction of [Cu(Dipp₂Im)(O^tBu)] with 4-CF₃-C₆H₅Bpin in toluene-d₈: -40 – r.t.

[Cu(Dipp₂Im)(O^tBu)]: 16 mg (30.5 μmol); 4-CF₃-C₆H₅Bpin: 8.3 mg (30.5 μmol); toluene-d₈: 0.6 mL

Clear solution → pale yellow solution

Reaction of [Cu(Dipp₂Im)(Mes)] with B₂pin₂ in THF-d₈: -50 – r.t.

[Cu(Dipp₂Im)(Mes)]: 12 mg (21.0 μmol); B₂pin₂: 5.3 mg (21.0 μmol); THF-d₈: 0.6 mL

Clear solution → brown solution

Reaction of [Cu(Dipp₂Im)(Mes)] with B₂neop₂ in THF-d₈: -50 – r.t.

[Cu(Dipp₂Im)(Mes)]: 12 mg (21.0 μmol); B₂neop₂: 4.7 mg (21.0 μmol); THF-d₈: 0.6 mL

Clear solution → brown solution

Reaction of [Cu(Dipp₂Im)(Mes)] with B₂cat₂ in THF-d₈: -50 – r.t.

[Cu(Dipp₂Im)(Mes)]: 12 mg (21.0 μmol); B₂cat₂: 5.0 mg (21.0 μmol); THF-d₈: 0.6 mL

Clear solution → dark brown solution

Reaction of [Cu(Dipp₂Im)(DBM)] with B₂pin₂ in C₆D₆: r.t. – 60 °C

[Cu(Dipp₂Im)(DBM)]: 26.7 mg (39.3 μmol); B₂pin₂: 10.3 mg (39.3 μmol); C₆D₆: 0.6 mL

Reddish suspension → green solution + black precipitate+ copper mirror

Reaction of [Cu(Dipp₂Im)(DBM)] with B₂cat₂ in C₆D₆: r.t. – 60 °C

[Cu(Dipp₂Im)(DBM)]: 30 mg (44.4 μmol); B₂cat₂: 10.5 mg (44.4 μmol); C₆D₆: 0.6 mL

Orange solution → orange solution + brown precipitate

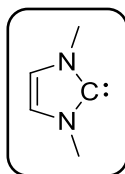
Reaction of [Cu(ⁱPr₂Im)(acac)] with B₂pin₂ in C₆D₆: r.t.

[Cu(ⁱPr₂Im)(acac)]: 15 mg (47.6 μmol); B₂pin₂: 12.0 mg (47.6 μmol); C₆D₆: 0.6 mL

Orange solution → yellow solution + black precipitate

6.2 Synthesis of known compounds

Synthesis of 1,3-dimethylimidazolin-2-ylidene^[320-321]



Step 1: Synthesis of 1,3-dimethylimidazolium iodide

To a solution of 1-methylimidazol (146 g, 1.77 mol, 142 mL) in 700 mL of toluene, methyl iodide (251 g, 1.77 mol, 110 ml) was added at room temperature. After the addition was complete, the mixture was heated to reflux for 16 h. Cooling to room temperature afforded a white precipitate which was collected by filtration, washed three times with 200 mL of *n*-hexane and dried *in vacuo*.

Yield: 392 g (1.75 mol, 99%) of a colorless solid.

¹H-NMR (400 MHz, 25 °C, D₂O): δ_{H} / ppm = 3.85 (s, 6 H, CH₃), 7.38 (s, 2 H, CHCH), 8.62 (s, 1 H, NCHN).

¹³C{¹H}-NMR (100 MHz, 25 °C, D₂O): δ_{C} / ppm = 36.0 (CH₃), 123.5 (CHCH), 136.6 (NCHN).

Step 2: Synthesis of 1,3-dimethylimidazolin-2-ylidene

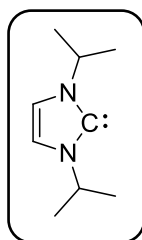
Sodium hydride (11.8 g, 491 mmol) and KO^tBu (2.50 g, 22.3 mmol, 5 mol-%) were added in small portions to a suspension of 1,3-dimethylimidazolium iodide (100 g, 446 mmol) in 700 mL of THF. The reaction mixture was stirred for 16 h at room temperature. Afterwards, the solvent was removed under reduced pressure and the crude product was purified by distillation at 75 °C under full vacuum.

Yield: 29.1 g (303 mmol, 68%) of a yellow liquid.

¹H-NMR (400 MHz, 25 °C, C₆D₆): δ_{H} / ppm = 3.43 (s, 6 H, CH₃), 6.71 (s, 2 H, CHCH).

¹³C{¹H}-NMR (100 MHz, 25 °C, C₆D₆): δ_{C} / ppm = 37.4 (CH₃), 120.2 (CHCH), 214.6 (NCN).

Synthesis of 1,3-di-*iso*-propylimidazolin-2-ylidene^[320-321]



Step 1: Synthesis of 1,3-di-*iso*-propylimidazoliumchloride

iso-Propyl amine (42.6 g, 0.72 mol, 61.8 mL) was added dropwise to a suspension of paraformaldehyde (21.6 g, 0.71 mol) in 120 mL of toluene. The temperature of the reaction mixture was kept below 40 °C during addition. The solution was stirred for a further 10 min, then cooled to 0 °C, and another equivalent of *iso*-propyl amine (42.6 g, 0.72 mol, 61.8 mL) and 6 M hydrochloric acid (120 ml, 0.72 mol) were slowly added. The solution was warmed to room temperature and 105 g of glyoxal, 40% in H₂O (0.72 mol, 82.8 ml) was added dropwise. The mixture was stirred overnight to give a dark solution. The solvent was removed under reduced pressure and the brown residue was dried *in vacuo* at 200 °C.

Yield: 112.9 g (598 mmol, 83%) of a brown solid.

¹H-NMR (400 MHz, 25 °C, D₂O): δ_{H} / ppm = 1.43 (d, 12 H, $^3J_{\text{HH}} = 7$ Hz, CHCH₃), 4.52 (sept, 2 H, $^3J_{\text{HH}} = 7$ Hz, CHCH₃), 7.47 (s, 2 H, CHCH), 8.76 (s, 1 H, NCHN).

¹³C{¹H}-NMR (100 MHz, 25 °C, D₂O): δ_{C} / ppm = 22.1 (CH₃), 53.0 (CH), 120.5 (NCCN), 132.5 (NCN).

Step 2: Synthesis of 1,3-di-*iso*-propylimidazolin-2-ylidene

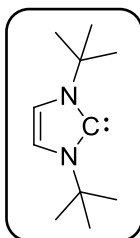
Sodium hydride (18.6 g, 776 mmol) and KO^tBu (3.98 g, 35.4 mmol, 5 mol-%) were added in small portions to a suspension of 1,3-dimethylimidazolium iodide (134 g, 706 mmol) in 800 mL of THF. The reaction mixture was stirred for 16 h at room temperature. Afterwards, the solvent was removed under reduced pressure the crude product was purified by distillation at 75 °C under full vacuum.

Yield: 78.4 g (515 mmol, 73%) of a yellow liquid.

¹H-NMR (400 MHz, 25 °C, C₆D₆): δ_{H} / ppm = 1.27 (d, 12 H, $^3J_{\text{HH}} = 7$ Hz, CHCH₃), 4.40 (sept, 2 H, $^3J_{\text{HH}} = 7$ Hz, CHCH₃), 6.63 (s, 2 H, CHCH).

$^{13}\text{C}\{^1\text{H}\}$ -NMR (100 MHz, 25 °C, C_6D_6): δ_{C} / ppm = 24.3 (CHCH₃), 52.1 (CHCH₃), 115.7 (CHCH), 211.9 (NCN).

Synthesis of 1,3-di-*tert*-butylimidazolin-2-ylidene^[322]



Step 1: Synthesis of 1,3-di-*tert*-butylimidazolium tetra fluoroborate

To a suspension of paraformaldehyde (15.0 g, 500 mmol) in 500 mL of toluene *tert*-butylamine (73.2 g, 1.00 mol, 105 mL) was added dropwise at 0 °C. The mixture was stirred for 5 min before fluoroboric acid 48% in H₂O (190 g, 1.04 mol, 136 mL) was added slowly. The mixture was allowed to warm to room temperature and 72.5 g of glyoxal, 40% in H₂O, (500 mmol, 57.4 mL) was slowly added. The solution was stirred overnight at room temperature. The precipitate was collected by filtration and washed two times with 150 mL of water and four times with 200 mL of diethyl ether. The solid was dried *in vacuo* to obtain 1,3-di-*tert*-butylimidazolium tetra fluoroborate.

Yield: 80.5 g (301 mmol, 60%) of a colorless solid.

^1H -NMR (400 MHz, 25 °C, CDCl_3): δ_{H} / ppm = 1.63 (s, 18 H, CH₃), 7.45 (s, 2 H, CHCH), 8.75 (s, 1 H, NCHN).

$^{13}\text{C}\{^1\text{H}\}$ -NMR (100 MHz, 25 °C, CDCl_3): δ_{C} / ppm = 29.7 (CH₃), 60.6 (C_q), 120.1 (NCCN), 131.8 (NCHN).

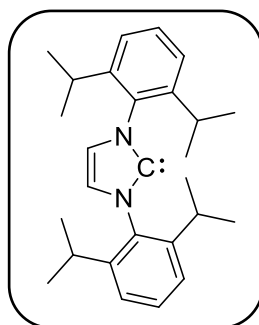
Step 2: Synthesis of 1,3-di-*tert*-butylimidazolin-2-ylidene

Sodium hydride (5.40 g, 225 mmol) and KO^tBu (0.75 g, 675 μmol , 3 mol%) were added in small portions to a suspension of 1,3-dimethylimidazolium iodide (40.0 g, 150 mmol) in 250 mL of THF. The reaction mixture was stirred for 16 h at room temperature. Afterwards, the solvent was removed under reduced pressure and the crude product was purified by distillation at 80 °C under full vacuum.

$^1\text{H-NMR}$ (400 MHz, 25 °C, C_6D_6): δ_{H} / ppm = 1.50 (s, 18 H, CH_3), 6.78 (s, 2 H, CHCH).

$^{13}\text{C}\{^1\text{H}\}\text{-NMR}$ (100 MHz, 25 °C, C_6D_6): δ_{C} / ppm = 31.7 (CH_3), 56.0 (C_q), 115.3 (NCCN), 213.0 (NCN).

Synthesis of 1,3-bis-(2,6-di-*iso*-propylphenyl)-imidazolidin-2-ylidene^[323-324]



Step 1: Synthesis of *N,N'*-(ethane-1,2-diylidene)bis(2,6-di-*iso*-propylphenylamine)

To a solution of 2,6-di-*iso*-propylaniline (197 g, 1.00 mol) and acetic acid (1.05 g, 17.5 mmol, 1.00 mL) in 500 mL of methanol 72.6 g of glyoxal 40% in H_2O (500 mmol, 57.1 mL) were added at 50 °C. The mixture was stirred overnight at room temperature. The yellow precipitate was collected by filtration and washed three times with 90 mL of methanol and dried *in vacuo*.

Yield: 156 g (414 mmol, 82%) of yellow solid.

$^1\text{H-NMR}$ (200 MHz, 25 °C, CDCl_3): δ_{H} / ppm = 1.20 (d, 24 H, $^3J_{\text{HH}} = 7$ Hz, CHCH_3), 2.93 (sept, 4 H, $^3J_{\text{HH}} = 7$ Hz, CHCH_3), 7.17 (m, 6 H, arylCH), 8.10 (s, 2 H, CHCH).

$^{13}\text{C}\{^1\text{H}\}\text{-NMR}$ (50 MHz, 25 °C, CDCl_3): δ_{C} / ppm = 23.4 (CHCH_3), 28.0 (CHCH_3), 123.2 (arylC), 125.1 (arylC), 136.7 (arylC), 148.0 (arylC), 163.1 (NC).

Step 2: Synthesis of 1,3-bis-(2,6-di-*iso*-propylphenyl)-1-H-imidazolium chloride

A suspension of *N,N'*-(ethane-1,2-diylidene)bis(2,6-di-*iso*-propylphenylamine) (128 g, 0.34 mol) and paraformaldehyde (10.3 g, 0.34 mol) in 3 L of ethyl acetate was heated to 50 °C. Under vigorous stirring, a solution of trimethylchlorosilane (43.3 mL, 0.34 mol) in 45 mL of ethyl acetate was added over a period of 60 min. After 2 h at 60 °C, the mixture was cooled to room temperature and stirred overnight. The precipitate was collected by filtration and washed three times with 200 mL of ethyl acetate and dried *in vacuo*.

Yield: 108 g (254 mmol, 74%) of a yellow powder.

¹H-NMR (200 MHz, 25 °C, CDCl₃): δ_H / ppm = 1.18 (d, 12 H, ³J_{HH} = 7 Hz, CHCH₃), 1.19 (d, 12 H, ³J_{HH} = 7 Hz, CHCH₃), 2.72 (sept, 4 H, ³J_{HH} = 7 Hz, CHCH₃), 7.12 – 7.16 (m, 4 H, *m*-CH) 7.21 (d), 7.35 7.43 (m, 2 H, *p*-CH), 11.15 (s, 1 H, NCHN).

¹³C{¹H}-NMR (50 MHz, 25 °C, CDCl₃): δ_C / ppm = 23.9, 24.4, 28.5, 123.2, 123.6, 145.7.

Step 3: Synthesis of 1,3-bis-(2,6-di-*iso*-propylphenyl)-1-H-imidazolium tetrafluoroborate

The compound 1,3-bis-(2,6-di-*iso*-propylphenyl)-1-H-imidazolium chloride (50.0 g, 117 mmol) was dissolved in the minimum amount of water (1.21 L) and, under vigorous stirring, fluoroboric acid (25.2 g, 130 mmol, 18.0 mL, 45% in water), was added. A white precipitate formed immediately, which was solubilized by the addition of 300 mL of CH₂Cl₂. The two phase system was separated and the aqueous phase was washed two times with 200 mL of CH₂Cl₂. The combined organic phases were dried over magnesium sulfate, the solvent was then removed under reduced pressure and the product was dried *in vacuo*.

Yield: 47.0 g (98.0 mmol, 84%) of a colorless solid.

¹H-NMR (200 MHz, 25 °C, CDCl₃): δ_H / ppm = 1.21 (d, 12 H, ³J_{HH} = 7 Hz, CHCH₃), 1.27 (d, 12 H, ³J_{HH} = 6.80 Hz, CHCH₃), 2.42 (sept, 4 H, ³J_{HH} = 7 Hz, CHCH₃), 7.33 (m, 4 H, *m*-CH), 7.53 (m, 2 H, *aryl*CH), 8.07 (s, 2 H, NCHCHN), 9.82 (s, 1 H, NCHN).

¹³C{¹H}-NMR (50 MHz, 25 °C, CDCl₃): δ_C / ppm = 23.8, 24.4, 28.5, 67.9, 123.2, 123.6, 145.7.

¹¹B-NMR (64 MHz, 25 °C, CDCl₃): δ_B / ppm = -1.2 (s, BF₄)

¹⁹F-NMR (188 MHz, 25 °C, CDCl₃): δ_F / ppm = -152.6 (s, BF₄).

Step 4: Synthesis of 1,3-bis-(2,6-di-*iso*-propylphenyl)-imidazolidin-2-ylidene

A Schlenk tube was charged with 1,3-bis-(2,6-di-*iso*-propylphenyl)-1-H-imidazolium tetrafluoroborate (34.5 g, 77.0 mmol), sodium hydride (3.70 g, 154 mmol), ca. 30 mg of KO^tBu and 200 mL of THF and the mixture was stirred for 16 h at room temperature. The mixture was filtered and the solid collected was washed with 50 mL of THF. The combined organic

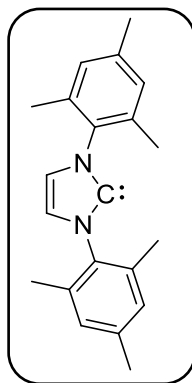
phases were concentrated under reduced pressure to ca. 20 mL. The product was precipitated by addition of 200 mL of pentane, collected by filtration and dried *in vacuo*.

Yield: 23.3 g (59.9 mmol, 77%) of a white, fluffy powder.

$^1\text{H-NMR}$ (200 MHz, 25 °C, C_6D_6): δ_{H} / ppm = 1.18 (d, 12 H, $^3J_{\text{HH}} = 7$ Hz, $^i\text{Pr-CH}_3$), 1.28 (d, 12 H, $^3J_{\text{HH}} = 7$ Hz, $^i\text{Pr-CH}_3$), 2.96 (sept, 4 H, $^3J_{\text{HH}} = 7$ Hz, $^i\text{Pr-CH}$), 6.61 (s, 4 H, CHCH), 7.15 – 7.19 (m, 4 H, $m\text{-CH}$), 7.26 – 7.33 (m, 2 H, $p\text{-CH}$).

$^{13}\text{C}\{^1\text{H}\}\text{-NMR}$ (50 MHz, 25 °C, C_6D_6): δ_{C} / ppm = 23.6 (CHCH₃), 24.8 (CHCH₃), 28.8 (CHCH₃), 121.6 (CHCH), 123.7 ($_{\text{aryl}}\text{C}$), 129.0 ($_{\text{aryl}}\text{C}$), 139.0 ($_{\text{aryl}}\text{C}$), 146.3 ($_{\text{aryl}}\text{C}$), 220.5 (NCN).

Synthesis of 1,3-bis-(2,4,6-trimethylphenyl)-imidazolidin-2-ylidene^[323-325]



Step 1: Synthesis of N,N'-(ethane-1,2-diylidene)-bis(2,4,6-trimethylphenylamine)

To a solution of 2,4,6-trimethylaniline (135 g, 1.00 mol) and acetic acid (1.05 g, 17.5 mmol, 1.00 mL) in 500 mL of methanol, glyoxal, 40% in H_2O , (72.6 g, 500 mmol, 57.1 mL) was added at 50 °C. The mixture was stirred overnight at room temperature. The yellow precipitate was collected by filtration and washed three times with 50 mL of methanol and dried *in vacuo*.

Yield: 118 g (402 mmol, 80%) of a yellow solid.

$^1\text{H-NMR}$ (200 MHz, 25 °C, C_6D_6): δ_{H} / ppm = 2.18 (s, 12 H, $o\text{-CH}_3$), 2.31 (s, 6 H, $p\text{-CH}_3$), 6.93 (s, 4 H, $m\text{-CH}$), 8.12 (s, 2 H, NCH).

Step 2: Synthesis of 1,3-bis-(2,4,6-trimethylphenyl)-imidazolium chloride

N,N'-(ethane-1,2-diylidene)-bis(2,4,6-trimethylphenylamine) (60.0 g, 200 mmol) was dissolved in 1.2 L of ethyl acetate and the solution was heated to 70 °C. Paraformaldehyde (6.21 g, 207 mmol) was added before a solution of trimethylsilyl chloride (22.3 g, 200 mmol, 26.0 mL) in 30 mL of ethyl acetate was added over 45 min. The yellow suspension was stirred for 2 h at 70 °C before it was cooled to 10 °C and filtered. The solid obtained was washed with ethyl acetate and methyl-*tert*-butyl ether and then dried *in vacuo*.

Yield: 34.0 g (100 mmol, 50%) of a colorless solid.

¹H-NMR (200 MHz, 25 °C, DMSO-*d*₆): δ_{H} / ppm = 1.25 (d, 12 H, $^3J_{\text{HH}} = 7$ Hz, *i*Pr-CH₃), 1.36 (d, 12 H, $^3J_{\text{HH}} = 7$ Hz, *i*Pr-CH₃), 3.09 (sept, 4 H, $^3J_{\text{HH}} = 7$ Hz, *i*Pr-CH), 4.41 (s, 4 H, CH₂CH₂), 7.30 – 7.62 (m, 6 H, *m*-CH), 9.63 (s, 1 H, NCHN).

¹³C{¹H}-NMR (50 MHz, 25 °C, DMSO-*d*₆): δ_{C} / ppm = 23.3 (*i*Pr-CH₃), 25.0 (*i*Pr-CH₃), 28.3 (*i*Pr-CH), 53.7 (CH₂CH₂), 124.7 (*m*-CH), 129.8 (*i*-C_q), 131.0 (*p*-CH), 146.0 (*o*-C_q), 160.0 (NCHN).

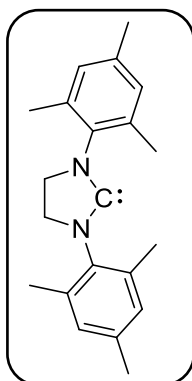
Step 3: Synthesis of 1,3-bis-(2,4,6-trimethylphenyl)-imidazolin-2-ylidene

Sodium hydride (2.15 g, 89.6 mmol) and KO^{*t*}Bu (75.0 mg, 67.5 μ mol) were added in small portions to a suspension of 1,3-bis-(2,4,6-trimethylphenyl)imidazolium chloride (14.9 g, 43.6 mmol) in 200 mL of THF. The reaction mixture was stirred for 3 d at 80 °C. Afterwards, the mixture was filtered through Celite® and concentrated under reduced pressure to ca. 30 mL. To the rapidly stirred mixture, 150 mL of *n*-hexane was added to precipitate the product, which was collected by filtration and dried *in vacuo*.

Yield: 10.2 g (33.6 mmol, 77%).

¹H-NMR (200 MHz, 25 °C, C₆D₆): δ_{H} / ppm = 2.16 (s, 18 H, CH₃), 6.49 (s, 2 H, CHCH), 6.81 (s, 4 H, *m*-CH).

¹³C{¹H}-NMR (50 MHz, 25 °C, C₆D₆): δ_{C} / ppm = 18.1 (*o*-CH₃), 21.1 (*p*-CH₃), 120.6 (CHCH), 129.1 (*o*-C_q), 135.5 (*m*-CH), 137.3 (*p*-C_q), 139.3 (*i*-C_q), 219.5 (NCN).

Synthesis of 1,3-bis-(2,4,6-trimethylphenyl)-imidazolidin-2-ylidene^[324, 326]

Step 1: Synthesis of *N,N'*-di(2,4,6-trimethylphenyl)ethane-1,2-diamine

A suspension of *N,N'*-(ethane-1,2-diylidene)bis(2,4,6-trimethylphenylamine) (3.90 g, 13.4 mmol) in 130 mL of ethyl alcohol was cooled to 0 °C and NaBH₄ (10 g, 264 mmol) was added in small portions. After stirring for 30 min, the mixture was heated to reflux for 2 h. The colorless suspension was cooled to room temperature, aqueous saturated sodium chloride was added and the suspension was stirred for a further 30 min before 150 mL of water and 120 mL of chloroform were added. The organic phase was separated and washed with a small amount of water and dried over sodium sulfate. The solvent was removed under reduced pressure affording a yellow oil.

Yield: 2.18 g (7.46 mmol, 55%) of a yellow oil.

¹H-NMR (200 MHz, 25 °C, C₆D₆): δ_H / ppm = 2.20 (s, 18 H, CH₃), 2.93 (s, 4 H, CH₂CH₂), 3.07 (br, 2 H, NH), 6.79 (s, 4 H, *m*-CH).

¹³C{¹H}-NMR (50 MHz, 25 °C, C₆D₆): δ_C / ppm = 17.1 (*o*-CH₃), 19.4 (*p*-CH₃), 48.0 (CH₂CH₂), 128.5 (*o*-C_q), 128.6 (*m*-CH), 129.9 (*p*-C_q), 142.6 (*i*-C_q).

Step 2: Synthesis of 1,3-bis-(2,4,6-trimethylphenyl)-4,5-dihydro-1-H-imidazolium chloride

A Schlenk tube charged with *N,N'*-di(2,4,6-trimethylphenyl)ethane-1,2-diamine (2.00 g, 6.75 mmol), ammonium chloride (550 mg, 10.3 mmol) and 10 mL of triethyl orthoformate was heated to 110 °C for 24 h. Afterwards, ethyl ether was added to precipitate a white solid, which was collected by filtration. The product was recrystallized from 6 mL of CH₂Cl₂ and ethyl acetate.

Yield: 1.90 g (7.46 mmol, 55%) of a white solid.

$^1\text{H-NMR}$ (200 MHz, 25 °C, CDCl_3): δ_{H} / ppm = 2.25 (s, 6 H, *p*- CH_3), 2.34 (s, 12 H, *o*- CH_3), 4.53 (s, 4 H, CH_2CH_2), 6.91 (s, 4 H, *m*-CH), 9.21 (s, 1 H, NCHN).

$^{13}\text{C}\{^1\text{H}\}$ NMR (50 MHz, 25 °C, CDCl_3): δ_{C} / ppm = 18.1 (*o*- CH_3), 21.1 (*p*- CH_3), 52.1 (CH_2CH_2), 130.1 (*o*- C_q), 130.3 (*m*-CH), 135.1 (*p*- C_q), 140.6 (*i*- C_q), 159.9 (NCHN).

Step 3: Synthesis of 1,3-bis-(2,4,6-trimethylphenyl)-imidazolidin-2-yliden

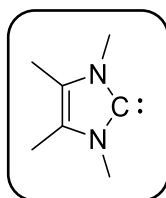
Sodium hydride (2.15 g, 89.6 mmol) and KO^tBu (75.0 mg, 67.5 μmol) were added in small portions to a suspension of 1,3-bis-(2,4,6-trimethylphenyl)-4,5-dihydro-1-H-imidazolium chloride (14.9 g, 43.6 mmol) in 200 mL of THF. The reaction mixture was stirred for 3 d at 80 °C. Afterwards, the mixture was filtered through Celite[®] and concentrated under reduced pressure to ca. 30 mL. To the rapidly stirred mixture, 150 mL of *n*-hexane was added to precipitate the product, which was collected by filtration and dried *in vacuo*.

Yield: 10.2 g (33.6 mmol, 77%) of an off-white solid.

$^1\text{H-NMR}$ (200 MHz, 25 °C, CDCl_3): δ_{H} / ppm = 2.25 (s, 6 H, *p*- CH_3), 2.34 (s, 12 H, *o*- CH_3), 4.53 (s, 4 H, CH_2CH_2), 6.91 (s, 4 H, *m*-CH), 9.21 (s, 1 H, NCHN).

$^{13}\text{C}\{^1\text{H}\}$ -NMR (50 MHz, 25 °C, CDCl_3): δ_{C} / ppm = 18.1 (*o*- CH_3), 21.1 (*p*- CH_3), 52.1 (CH_2CH_2), 130.1 (*o*- C_q), 130.3 (*m*-CH), 135.1 (*p*- C_q), 140.6 (*i*- C_q), 159.9 (NCHN).

Synthesis of 1,3,4,5-tetramethylimidazolin-2-ylidene^[327]



Step 1: Synthesis of 1,3,4,5-tetramethylimidazol-2-thione

To a solution of 1,3-dimethylthiourea (24.0 g, 150 mmol) in 250 mL of 1-hexanol 3-hydroxybutanone (100 mmol, 11.6 mL) was added and the mixture was stirred at 160 °C for 16 h. The solvent was removed under reduced pressure at 100 °C. The solid was washed

with H₂O and Et₂O. The crude product was recrystallized from EtOH/H₂O 1:1 and dried *in vacuo*.

Yield: 8.10 g (52.0 mmol, 52%) of yellowish needles.

¹H-NMR (200 MHz, 25 °C, C₆D₆): δ_H / ppm = 1.32 (s, 6 H, NCH₃), 3.15 (s, 6 H, C_qCH₃C_qCH₃).

¹³C{¹H}-NMR (100 MHz, 25 °C, CD₂Cl₂): δ_C / ppm = 8.4 (C_qCH₃C_qCH₃), 31.3 (NCH₃), 119.5 (NC_qC_qN), 163.3 (NCN).

Step 1: Synthesis of 1,3,4,5-tetramethylimidazolin-2-ylidene

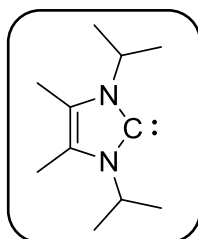
To 150 mL of THF, potassium (3.00 g, 76.8 mmol) was added as small pieces and the reaction mixture was cooled to 0 °C. The compound 1,3,4,5-tetramethylimidazol-2-thione (4.68 g, 30.0 mmol) was added and the reaction mixture was stirred for 6 h at 90 °C. The light blue suspension was filtered through Celite® and the solvent was removed under reduced pressure to obtain an off-white solid.

Yield: 1.30 g (10.8 mmol, 33%) of an off-white solid.

¹H-NMR (200 MHz, 25 °C, C₆D₆): δ_H / ppm = 1.60 (s, 6 H, NCH₃), 3.37 (s, 6 H, C_qCH₃).

¹³C{¹H}-NMR (50 MHz, 25 °C, C₆D₆): δ_C / ppm = 8.8 (C_qCH₃), 35.2 (NCH₃), 122.6 (NC_qC_qN), 213.0 (NCN).

Synthesis of 1,3-Di-*iso*-propyl-4,5-dimethylimidazolin-2-ylidene^[327]



Step 1: Synthesis of 1,3-di-*iso*-propyl-4,5-dimethylimidazol-2-thione

To a solution of 1,3-di-*iso*-propylthiourea (24.0 g, 150 mmol) in 250 mL of 1-hexanol 3-hydroxybutanone (195 mmol, 17.4 mL) was added and the mixture was stirred at 160 °C for 16 h. The solvent was removed under reduced pressure at 100 °C. The solid was washed

with H₂O and Et₂O. The crude product was recrystallized from EtOH/H₂O 1:1 and dried *in vacuo*.

Yield: 15.5 g (73.5 mmol, 49%) of a colorless needles.

¹H-NMR (200 MHz, 25 °C, C₆D₆): δ_H / ppm = 1.43 (d, 12 H, CHCH₃), 2.17 (s, 6 H, C_qCH₃C_qCH₃), 5.62 (br, 2 H, CHCH₃).

¹³C{¹H}-NMR (50 MHz, 25 °C, CD₂Cl₂): δ_C / ppm = 10.5 (C_qCH₃C_qCH₃), 21.2 (CHCH₃), 49.7 (NC_qC_qN), 121.2 (CHCH₃), 163.7 (NCN).

Step 2: Synthesis of 1,3-di-*iso*-propyl-4,5-dimethylimidazolin-2-ylidene

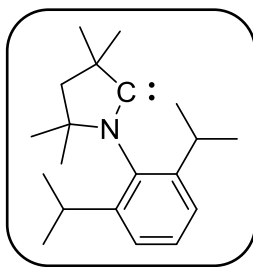
To 50 mL of THF, potassium (1.00 g, 25.6 mmol) was added as small pieces and the reaction mixture was cooled to 0 °C. The compound 1,3-di-*iso*-propyl-4,5-dimethylimidazol-2-thione (2.16 g, 10.0 mmol) was added and the reaction mixture was stirred for 6 h at 90 °C. The light blue suspension was filtered through Celite® and the solvent was removed under reduced pressure to obtain a colorless solid.

Yield: 845 mg (4.69 mmol, 47%) of a colorless solid.

Elemental analysis for [C₁₁H₂₀N₂] [180.29 g·mol⁻¹]: Calc. (obs.): 73.28 (73.34), 11.18 (11.05), 15.54 (15.62).

¹H-NMR (200 MHz, 25 °C, C₆D₆): δ_H / ppm = 1.50 (d, 12 H, ³J_{HH} = 7 Hz, CHCH₃), 1.73 (s, 6 H, C_qCH₃), 3.95 (sept, 2 H, ³J_{HH} = 7 Hz, CHCH₃).

¹³C{¹H}-NMR (50 MHz, 25 °C, C₆D₆): δ_C / ppm = 9.4 (C_qCH₃), 25.3 (CHCH₃), 49.1 (CHCH₃), 122.0 (NC_qC_qN), 208.1 (NCN).

Synthesis of 1-(2,6-di-*iso*-propylphenyl)-3,3,5,5-tetramethylpyrrolidin-2-ylidene^[328-329]**Step 1: Synthesis of lithium-di-*iso*-propylamine**

A solution of di-*iso*-propylamine (60.0 mL, 43.2 g, 427 mmol) and 175 mL of THF was cooled to -78 °C. Over 45 min, a 2.5 M of *n*BuLi (170 ml, 427 mmol) in *n*-hexane was added dropwise. The reaction mixture was warmed to room temperature and stirred for another 30 min.

Step 2: Synthesis of N-(2,6-di-*iso*-propylphenyl)-2,2,4-trimethylpent-4-en-1-imine

In a Dean-Stark apparatus 2,6-di-*iso*-propylaniline (70.1 mL, 65.9 g, 55.5 mmol), *iso*-butyraldehyde and 320 mL of toluene were heated to reflux for 72 h until 6.60 mL of water separated. The solvent was removed under reduced pressure. THF (100 mL) was added and the solution cooled to -78 °C, before the precooled LDA (see step 1) was added within 10 min. The mixture was slowly warmed to room temperature and stirred overnight. The solvent was removed under reduced pressure before 100 mL of diethylether was added. The solution was cooled to -78 °C before 3-chloro-2-methylpropene (44.0 mL, 40.4 g, 446 mmol) was added dropwise over 40 min. Warmed to room temperature the mixture was stirred for another 30 min, before the solvent was removed under reduced pressure. The crude product was dissolved in 100 mL of pentane. The insoluble byproducts were removed by filtration and washed with pentane (2 x 50 mL). The solvent was removed under reduced pressure before the crude product was purified by distillation (75 °C, 10⁻¹ mbar).

GC-MS: $m/z = 285 [M^+]; 270 [M^+ - CH_3]$

Yield: 94.46 g (330.88 mmol, 89%) of a light yellow oil.

Step 3: Synthesis of 1-(2,6-di-*iso*-propylphenyl)-2,2,4,4-tetramethyl-3,4-dihydro-2H-pyrrol-1-ium chloride

To a Schlenk tube containing N-(2,6-di-*iso*-propylphenyl)-2,2,4-trimethylpent-4-en-1-imine (13.4 g, 47.1 mmol) and 45 mL of chloroform, ethereal HCl (23.5 mL, 235 mmol) was carefully added. The tube was closed tightly before the reaction tube was heated to 62 °C (caution! overpressure!) overnight. While cooling to room temperature, a white precipitate formed from the yellow solution. The precipitate was collected by filtration, washed with diethylether (2 x 40 mL) and dried *in vacuo*.

Yield: 13.3 g (41.3 mmol, 88%) of a colorless solid.

¹H-NMR (200 MHz, 25 °C, CDCl₃): δ_H / ppm = 1.20 ppm (d, 6 H, CHCH₃), 1.34 (d, 6 H, CHCH₃), 1.55 (s, 6 H, CHC_qCH₃), 1.72 (s, 6 H, NC_qCH₃), 2.46 (s, 2 H, CH₂), 2.64 (sept, 2 H, CHCH₃), 7.31 – 7.35 (m, 2 H, *m*-CH), 7.51 (m, 1 H, *p*-CH), 10.27 (s, 1 H, NCH).

¹³C{¹H}-NMR (50 MHz, 25 °C, CDCl₃): δ_C / ppm = 22.2 (NC_qCH₃), 26.7 (CHCH₃), 28.5 (CHC_qCH₃), 29.9 (CHCH₃), 48.4 (CH₂), 49.2 (CHC_qCH₃), 83.6 (NC_qCH₃), 125.3 (*m*-CH), 128.9 (*i*-C_q), 131.9 (*p*-CH), 144.5 (*o*-C_q), 193.3 (NCH).

Step 4: Synthesis of 1-(2,6-di-*iso*-propylphenyl)-2,2,4,4-tetramethyl-3,4-dihydro-2H-pyrrol-1-ium tetra fluoroborate

The salt 1-(2,6-di-*iso*-propylphenyl)-2,2,4,4-tetramethyl-3,4-dihydro-2H-pyrrol-1-ium chloride (10.0 g 31.1 mmol), was dissolved in 50 mL of acetonitrile and sodium tetrafluoroborate (4.06 g, 36.5 mmol) was added. After 16 h at room temperature, the solvent was removed under reduced pressure. The residue was dissolved in 75 mL of DCM. The suspension was filtered and washed with 25 mL of DCM. The solvent was reduced to about 30 mL under reduced pressure before 100 mL of *n*-hexane was added to precipitate the product. The white solid was collected by filtration and dried *in vacuo*.

Yield: 9.64 g (25.8 mmol, 83%) of a colorless solid.

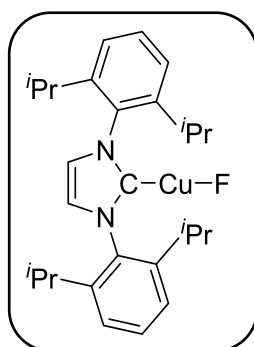
Step 5: Synthesis of 1-(2,6-di-*iso*-propylphenyl)-3,3,5,5-tetramethylpyrrolidin-2-ylidene

To 1-(2,6-di-*iso*-propylphenyl)-2,2,4,4-tetramethyl-3,4-dihydro-2H-pyrrol-1-ium tetrafluoroborate (9.50 g, 25.4 mmol) in 100 mL of benzene, a suspension of NaHMDS (4.67 g, 25.4 mmol) in 50 mL of benzene was added within 20 min. The suspension was stirred for 60 min, before the solvent was removed under reduced pressure. The crude product was dissolved in 100 mL of *n*-hexane. The insoluble byproducts were removed by filtration through Celite® and washed with 50 mL of *n*-hexane. The solvent was removed under reduced pressure before the crude product was purified by sublimation (75 °C, 10⁻² mbar).

Yield: 5.76 g (20.2 mmol, 79%) of a crystalline solid.

¹H-NMR (200 MHz, 25 °C, C₆D₆): δ_H / ppm = 1.08 (s, 6 H, NC_qCH₃), 1.22 (d, 6 H, CHCH₃), 1.24 (d, 6 H, CHCH₃), 1.44 (s, 6 H, C_qC_qCH₃), 1.54 (s, 2 H, CH₂), 3.14 (sept, 2 H, CHCH₃), 7.12 – 7.27 (m, 3 H, _{aryl}CH).

¹³C{¹H}-NMR (100 MHz, 25 °C, C₆D₆): δ_C / ppm = 21.9 (C_qC_qCH₃), 26.2 (NC_qCH₃), 28.2 (CHCH₃), 29.2 (CHCH₃), 29.5 (CHCH₃), 50.6 (CH₂), 58.2 (C_qC_qCH₃), 82.6 (NC_qCH₃), 124.3 (*m*-CH), 127.3 (*i*-C_q), 138.0 (*p*-CH), 146.2 (*o*-C_q), 313.5 (NC_qC_q).

Synthesis of [Cu(Dipp₂Im)(F)] **11**^[244]

[Cu(Dipp₂Im)(O^tBu)] (400 mg, 762 μmol) and 10 mL of toluene were added to a Schlenk-tube and triethylamine tris(hydrofluoride) (41.0 mg, 254 μmol, 41.5 μL) was added via syringe. The resulting white suspension was stirred for 6 h at room temperature after which the solvent was removed *in vacuo*. The white solid was washed with 5 mL of *n*-hexane, collected by filtration and dried *in vacuo*, to afford the title compound.

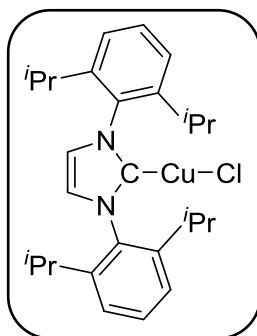
Yield: 295 mg (625 μmol, 82%) of a colorless solid.

$^1\text{H-NMR}$ (200 MHz, 25 °C, CD_2Cl_2): δ_{H} / ppm = 1.23 ppm (d, 12 H, $^3J_{\text{HH}} = 7$ Hz, CH_3), 1.30 (d, 12 H, $^3J_{\text{HH}} = 7$ Hz, CH_3), 2.57 (sept, 4 H, $^3J_{\text{HH}} = 7$ Hz, CH), 7.17 (s, 2 H, CHCH), 7.32 – 7.58 (m, 6 H, arylCH).

$^{13}\text{C}\{^1\text{H}\}$ -NMR (50 MHz, 25 °C, CD_2Cl_2): δ_{C} / ppm = 24.0 (CH_3), 24.8 (CH_3), 29.1 (CH), 123.8 (CHCH), 124.5 (arylC), 130.8 (arylC), 135.1 (arylC), 146.1 (arylC). The carbene-carbon atom was not detected.

$^{19}\text{F-NMR}$ (188.3 MHz, 25 °C, CD_2Cl_2): δ_{F} / ppm = -240.5 (s, 1 F, CuF).

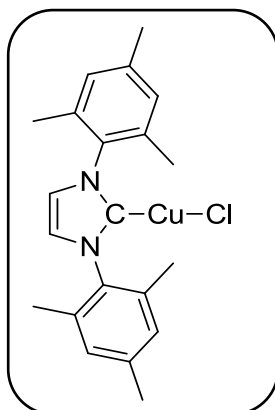
Synthesis of $[\text{Cu}(\text{Dipp}_2\text{Im})(\text{Cl})]$ ^[235]



A 1 L Schlenk flask containing 500 mL of toluene was charged with 1,3-bis-(2,6-di-*iso*-propylphenyl)-imidazoliumchloride (35.0 g, 82.3 mmol) and copper(I)oxide (6.48 g, 45.3 mmol). The reaction mixture was refluxed for 16 h and, after cooling to room temperature, the solvent was removed *in vacuo*. The residue was dissolved in CH_2Cl_2 and filtered through Celite® to afford a colorless solution which was reduced *in vacuo* to ca. 50 mL. The product was precipitated by adding 250 mL of *n*-hexane to the stirred solution. The white precipitate was collected by filtration and dried *in vacuo*.

Yield: 27.9 g (57.2 mmol, 70%) of a colorless solid.

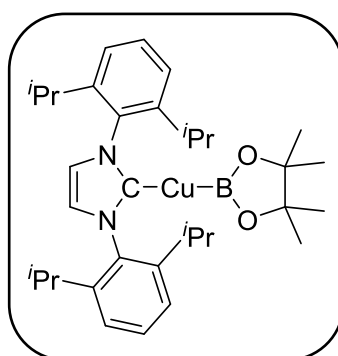
$^1\text{H-NMR}$ (200 MHz, 25 °C, CDCl_3): δ_{H} / ppm = 1.23 (d, 12 H, $^3J_{\text{HH}} = 6.90$ Hz, CHCH_3), 1.30 (d, 12 H, $^3J_{\text{HH}} = 6.90$ Hz, CHCH_3), 2.56 ppm (sept, 4 H, $^3J_{\text{HH}} = 6.90$ Hz, CHCH_3), 7.15 – 7.22 (m, 4 H, *m-CH*), 7.45 – 7.53 ppm (m, 2 H, arylCH).

Synthesis of [Cu(Mes₂Im)(Cl)]^[235]

A 1000 mL Schlenk flask containing 500 mL of toluene was charged with 1,3-bis-(2,4,6-trimethylphenyl)-imidazolium chloride (34.9 g, 102 mmol) and copper(I)oxide (8.04 g, 56.2 mmol). The reaction mixture was refluxed for 16 h, and after cooling to room temperature, the solvent was removed under reduced pressure. The residue was dissolved in THF and filtered through Celite® to afford a colorless solution which was reduced *in vacuo* to ca. 30 mL. The product was precipitated by adding 250 mL of *n*-hexane to the stirred solution. The white precipitate was collected by filtration and dried *in vacuo*.

Yield: 36.6 g (90.7 mmol, 89%) of a colorless solid.

¹H-NMR (200 MHz, 25 °C, CDCl₃): δ_H / ppm = 2.10 ppm (s, 12 H, *o*-CH₃), 2.34 (s, 6 H, *p*-CH₃), 6.99 – 7.01 (m, 4 H, arylCH), 7.05 (s, 2 H, CHCH).

Synthesis of [Cu(Dipp₂Im)(Bpin)]^[265]

A Schlenk tube was charged with [Cu(Dipp₂Im)(O^tBu)] (210 mg, 400 μmol) and bis(pinacolato)diboron (101 mg, 400 μmol) and wrapped with aluminum foil. Then, 5 mL of *n*-hexane was added and the mixture was stirred for 20 min at room temperature. The crude product was collected by filtration and dried *in vacuo*.

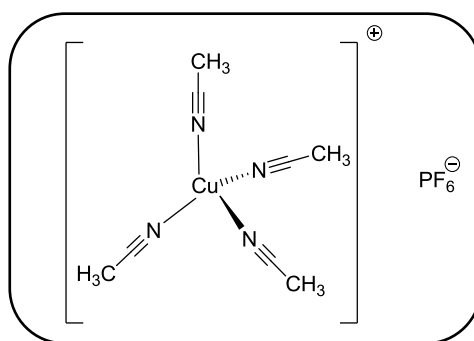
Yield: 196 mg (338 μmol , 85%) of a white solid susceptible to oxidation, hydrolysis and light.

$^1\text{H-NMR}$ (200 MHz, 25 $^\circ\text{C}$, C_6D_6): δ_{H} / ppm = 1.06 (s, 12 H, C_qCH_3), 1.09 (d, 12 H, $^3J_{\text{HH}} = 6.9$ Hz, CHCH_3), 1.48 (d, $^3J_{\text{HH}} = 6.9$ Hz, CHCH_3), 2.65 (sept, 4 H, $^3J_{\text{HH}} = 6.9$ Hz, CHCH_3), 6.22 (s, 2 H, CHCH), 7.02 – 7.07 (m, 4 H, $m\text{-CH}$), 7.12 – 7.19 (m, 2 H, $p\text{-CH}$).

$^{11}\text{B-NMR}$ (96.3 MHz, 25 $^\circ\text{C}$, C_6D_6): δ_{B} / ppm = 39.7 (br).

$^{13}\text{C}\{^1\text{H}\}\text{-NMR}$ (50 MHz, 25 $^\circ\text{C}$, C_6D_6): δ_{C} / ppm = 24.0 (CHCH_3), 25.7 (CHCH_3), 26.4 (C_qCH_3), 29.4 (CHCH_3), 79.2 (C_qCH_3), 122.3 (CHCH), 124.3 ($m\text{-CH}$), 130.5 ($p\text{-CH}$), 135.4 ($i\text{-C}_q$), 146.1 ($o\text{-C}_q$), 186.6 (NCN).

Synthesis of $[\text{Cu}(\text{MeCN})_4][\text{PF}_6]^{[330]}$



To a well stirred suspension of copper(I) oxide (4.80 g, 33.5 mmol) in 100 mL of acetonitrile, 65% HPF_6 (30.1 g, 134 mmol, 18.2 mL) in water was added carefully in small portions. Five min after the last addition, the hot solution was filtered. After 16 h, the product crystallized as colorless needles from the blue solution at -20 $^\circ\text{C}$. The solid was washed with diethyl ether and dried *in vacuo*.

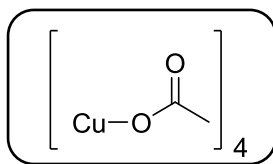
Yield: 20.7 g (55.5 mmol, 82%).

$^1\text{H-NMR}$ (200 MHz, 25 $^\circ\text{C}$, $(\text{CD}_3)_2\text{CO}$): δ_{H} / ppm = 2.27 (s, 12 H, NCCH_3).

$^{13}\text{C}\{^1\text{H}\}\text{-NMR}$ (50 MHz, 25 $^\circ\text{C}$, $(\text{CD}_3)_2\text{CO}$): δ_{C} / ppm = 1.25 (CH_3), 117.6 (NC).

$^{19}\text{F-NMR}$ (188 MHz, 25 $^\circ\text{C}$, $(\text{CD}_3)_2\text{CO}$): δ_{F} / ppm = -72.6 (d, 6F, $^1J_{\text{FP}} = 708$ Hz, PF_6).

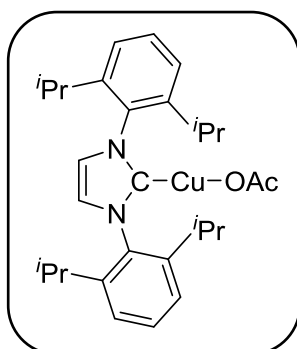
$^{31}\text{P-NMR}$ (81 MHz, 25 $^\circ\text{C}$, $(\text{CD}_3)_2\text{CO}$): δ_{P} / ppm = -144.3 (sept, 1 P, $^1J_{\text{FP}} = 708$ Hz, PF_6).

Synthesis of $[\text{Cu}^{\text{I}}(\text{OAc})_4]^{[331]}$ 

To a Schlenk tube containing copper(I) chloride (2.97 g, 30.0 mmol) suspended in 80 mL of CH_2Cl_2 , acetic acid (stored over molecular sieves) (3.00 g, 30.0 mmol, 1.71 mL) was added via syringe. After 10 min of stirring, triethylamine (3.00 g, 30.0 mmol, 4.11 mL) dissolved in 10 mL of CH_2Cl_2 , was added slowly. During 3 h of stirring at room temperature, the colorless solution turned purple and a precipitated formed. The reaction mixture was filtered and the colorless residue collected was washed with 10 mL of CH_2Cl_2 and dried *in vacuo*.

Yield: 823 mg (6.7 mmol, 22%) of a colorless solid.

$^1\text{H-NMR}$ (200 MHz, 25 °C, CD_3CN): δ_{H} / ppm = 3.60 ppm (s, 3 H, CH_3).

Synthesis of $[\text{Cu}(\text{Dipp}_2\text{Im})(\text{OAc})]^{[254]}$ 

To 150 mg of copper(I) acetate (1.22 mmol) and 474 mg of 2,6-di-iso-propyl-phenylimidazolin-2-ylidene (1.22 mmol), 10 mL of toluene were added and the reaction mixture was stirred for 12 h at room temperature. The crude mixture was filtered and the solvent was removed under reduced pressure. The white solid was washed with 5 mL of *n*-hexane and dried *in vacuo*.

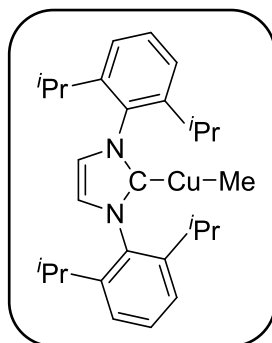
Yield: 471 mg (0.92 mmol, 75%)

$^1\text{H-NMR}$ (200 MHz, 25 °C, C_6D_6): δ_{H} / ppm = 1.07 (d, 12 H, $^3J_{\text{HH}} = 7$ Hz, $^i\text{Pr-CH}_3$), 1.44 (d, 12 H, $^3J_{\text{HH}} = 7$ Hz, $^i\text{Pr-CH}_3$), 1.91 (s, 3 H, O_2CCH_3), 2.60 (sept, 4 H, $^3J_{\text{HH}} = 7$ Hz, $^i\text{Pr-CH}$), 6.33 (s, 2 H, CHCH), 7.04 – 7.07 (m, 4 H, *m-CH*), 7.17 – 7.23 (m, 2 H, *p-CH*).

$^{13}\text{C}\{^1\text{H}\}$ -NMR (50 MHz, 25 °C, C_6D_6): δ_{C} / ppm = 23.9 (CO_2CH_3), 25.0 (CHCH_3), 29.1 (CHCH_3), 122.8 (CHCH), 124.3 (*m*-CH), 129.3 (O_2CCH_3), 130.7 (*p*-CH), 135.0 (*i*- C_q), 145.8 (*o*- C_q), 177.3 (NCN).

HRMS-ASAP (*m/z*): $[\text{M}+\text{H}]^+$ calc. for $\text{C}_{29}\text{H}_{40}\text{CuN}_2\text{O}_2$, 511.2380 found, 511.2367.

Synthesis of $[\text{Cu}(\text{Dipp}_2\text{Im})\text{Me}]$ ^[332]

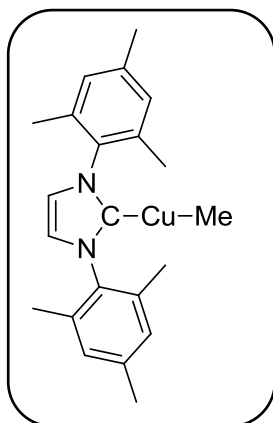


A Schlenk tube charged with $[\text{Cu}(\text{Dipp}_2\text{Im})\text{Cl}]$ (500 mg, 1.03 mmol) and 10 mL of toluene was cooled to -95 °C. Via syringe, a 0.69 M solution of methyllithium (1.5 mL, 1.03 mmol) in diethylether was added dropwise. The mixture was warmed to room temperature and stirred for 6 h and then stored at -30 °C overnight. After warming again to 20 °C, the suspension was filtered through Celite® and the solvent was removed under reduced pressure. The resulting white solid was dried *in vacuo*.

Yield: 100 mg (0.21 mmol, 20%) of a colorless solid.

^1H -NMR (300 MHz, 25 °C, C_6D_6): δ_{H} / ppm = -0.49 (s, 3 H, Cu-CH_3), 1.10 (d, 12 H, $^3\text{J}_{\text{HH}} = 7$ Hz, CHCH_3), 1.44 (d, 12 H, $^3\text{J}_{\text{HH}} = 7$ Hz, CHCH_3), 2.68 (sept, 4 H, $^3\text{J}_{\text{HH}} = 7$ Hz, CHCH_3), 6.26 (s, 2 H, CHCH), 7.08 (m, 4 H, *m*-CH), 7.21 (m, 2 H, *p*-CH).

$^{13}\text{C}\{^1\text{H}\}$ -NMR (75 MHz, 25 °C, C_6D_6): δ_{C} / ppm = -12.5 (Cu-CH_3), 23.8 (CHCH_3), 25.0 (CHCH_3), 29.0 (CHCH_3), 122.0 (CHCH), 124.1 (*m*-CH), 130.4 (*p*-CH), 135.5 (*i*- C_q), 145.9 (*o*- C_q). The resonance of the carbene-carbon atom was not detected.

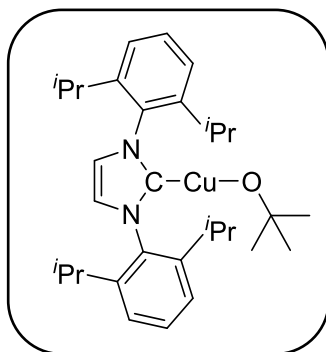
Synthesis of $[\text{Cu}(\text{Mes}_2\text{Im})\text{Me}]$ ^[332]

A Schlenk tube charged with $[\text{Cu}(\text{Mes}_2\text{Im})\text{Cl}]$ (500 mg, 1.24 mmol) in 10 mL of toluene was cooled to $-95\text{ }^\circ\text{C}$. Via syringe, a 0.69 M solution of methyllithium (1.8 mL, 1.24 mmol) in diethylether was added dropwise. The mixture was warmed to room temperature and stirred for 6 h and then stored at $-30\text{ }^\circ\text{C}$ overnight. After warming again to $20\text{ }^\circ\text{C}$ the suspension was filtered through Celite[®] and the solvent was removed under reduced pressure. The resulting white solid was dried *in vacuo*.

Yield: 382 mg (0.99 mmol, 80%) of a colorless solid.

¹H-NMR (300 MHz, $25\text{ }^\circ\text{C}$, C_6D_6): $\delta_{\text{H}} / \text{ppm} = -0.35$ (s, 3 H, Cu-CH₃), 2.05 (s, 12 H, *o*-CH₃), 2.07 (s, 6 H, *p*-CH₃), 6.02 (s, 2 H, CHCH), 6.70 (m, 4 H, *m*-CH).

¹³C{¹H}-NMR (75 MHz, $25\text{ }^\circ\text{C}$, C_6D_6): $\delta_{\text{C}} / \text{ppm} = -12.0$ (Cu-CH₃), 18.0 (*o*-CH₃), 21.1 (*p*-CH₃), 120.9 (CHCH), 129.5 (*o*-C_q), 134.8 (*m*-CH), 136.2 (*i*-C_q), 138.8 (*p*-C_q), 184.6 (NCN).

Synthesis of $[\text{Cu}(\text{Dipp}_2\text{Im})(\text{O}^t\text{Bu})]$ ^[245, 252]

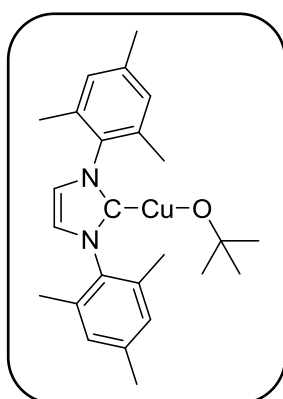
To a mixture of $[\text{Cu}(\text{Dipp}_2\text{Im})(\text{Cl})]$ (1.10 g, 2.05 mmol) and KO^tBu (230 mg, 2.05 mmol) 15 mL of THF were added and the reaction mixture was stirred for 1.5 h at room temperature.

The brown suspension was filtered through a plug of Celite® and the solvent was removed under reduced pressure to afford a white solid.

Yield: 806 mg (1.53 mmol, 75%) of a colorless solid.

¹H-NMR (300 MHz, 25 °C, C₆D₆): δ_H / ppm = 1.07 (d, 12 H, ³J_{HH} = 7 Hz, CHCH₃), 1.33 (s, 9 H, C_q(CH₃)₃), 1.41 (d, 12 H, ³J_{HH} = 7 Hz, CHCH₃), 2.60 (sept, 4 H, ³J_{HH} = 7 Hz, CHCH₃), 7.05 – 7.09 (m, 4 H, *m*-CH), 7.18 – 7.26 (m, 2 H, *p*-CH).

Synthesis of [Cu(Mes₂Im)(O^tBu)]^[245, 252]

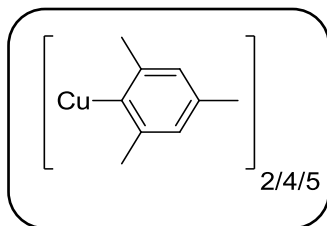


To a mixture of [Cu(Mes₂Im)(Cl)] (1.10 g, 2.05 mmol) and KO^tBu (230 mg, 2.05 mmol), 15 mL of THF were added and the reaction mixture was stirred for 1.5 h at room temperature. The brown suspension was filtered through a plug of Celite® and solvent was removed under reduced pressure to afford a white solid.

Yield: 300 mg (680 μmol, 68%) of an off-white solid.

¹H-NMR (300 MHz, 25 °C, C₆D₆): δ_H / ppm = 1.32 (s, 9 H, C_q(CH₃)₃), 1.98 (s, 12 H, *o*-CH₃), 2.11 (s, 6 H, *p*-CH₃), 6.09 (s, 2 H, CHCH), 6.72 (s, 4 H, *m*-CH).

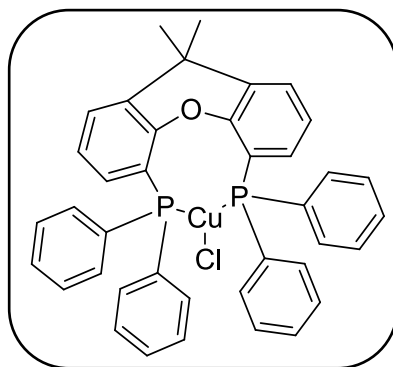
HRMS-ASAP (m/z): [M]⁺ calc. for C₂₅H₃₃CuN₂O, 441.1962 found, 441.1956.

Synthesis of $[\text{Cu}^{\text{I}}(\text{Mes})]$ ^[257]

A suspension of copper(I) chloride (0.37 g, 3.77 mmol) in 25 mL of THF was cooled to $-20\text{ }^{\circ}\text{C}$ and a 1.98 M solution of mesitylmagnesium bromide (1.90 mL, 3.77 mmol) in THF was added via cannula. The solution was then slowly warmed to room temperature and 30 mL of 1,4-dioxane was added. After 2 h, the suspension was filtered through Celite[®] and the solvent was removed under reduced pressure. The solid was dissolved in toluene and 1,4-dioxane was added to confirm the absence of magnesium salts. The solvent was evaporated to dryness and the residue was washed with *n*-hexane to afford mesitylcopper(I) as a light yellow solid.

Yield: 550 mg (3.0 mmol, 80%) of a yellow solid.

¹H-NMR (200 MHz, $25\text{ }^{\circ}\text{C}$, C_6D_6): δ_{H} / ppm = 1.90-2.02 (m, 3 H, *p*- CH_3), 2.93 (s, 6 H, *o*- CH_3), 6.59 – 6.68 (m, 2 H, *m*-CH).

Synthesis of $[\text{Cu}(\text{Xantphos})\text{Cl}]$ ^[291-292]

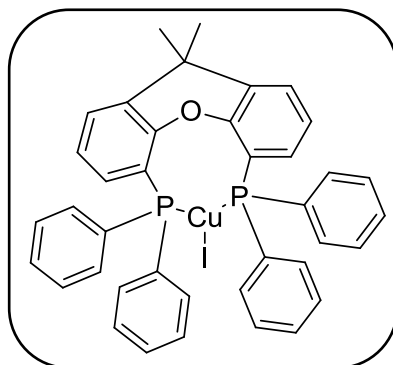
A Schlenk tube charged with CuCl (50 mg, 505 μmol) and 10 mL of acetonitrile was heated to $60\text{ }^{\circ}\text{C}$. Xantphos (300 mg, 518 μmol) was added and the reaction mixture was stirred for 2 h at $60\text{ }^{\circ}\text{C}$. The white suspension was filtered, the solid was washed with 7 mL acetonitrile and the solvent was removed from the filtrate under reduced pressure to afford a white solid.

Yield: 270 mg (398 μmol , 79%) of a white solid.

$^1\text{H-NMR}$ (200 MHz, 25 °C, C_6D_6): δ_{H} / ppm = 1.29 (s, 6 H, CH_3), 6.64 – 6.76 (m, 4 H, arylCH), 6.89 – 7.04 (m, 14 H, arylCH), 7.58 – 7.68 (m, 8 H, arylCH).

$^{31}\text{P-NMR}$ (202.5 MHz, 25 °C, C_6D_6): δ_{P} / ppm = -19.0 (s).

Synthesis of $[\text{Cu}(\text{Xantphos})\text{I}]^{[291]}$



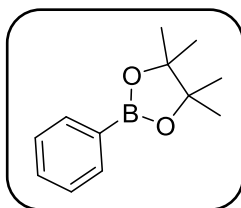
A Schlenk tube charged with CuI (250 mg, 1.31 mmol) and 10 mL of acetonitrile was heated to 60 °C. Xantphos (900 mg, 1.55 mmol) was added and the reaction mixture was stirred for 2 h at 60 °C. The white suspension was filtered, the solid was washed with 7 mL of acetonitrile and the solvent was removed from the filtrate under reduced pressure to afford a white solid.

Yield: 900 mg (1.17 mmol, 89%) of a white solid.

$^1\text{H-NMR}$ (200 MHz, 25 °C, C_6D_6): δ_{H} / ppm = 1.29 (s, 6 H, CH_3), 6.64 – 6.76 (m, 4 H, arylCH), 6.89 – 7.04 (m, 14 H, arylCH), 7.58 – 7.68 (m, 8 H, arylCH).

$^{31}\text{P-NMR}$ (202.5 MHz, 25 °C, C_6D_6): δ_{P} / ppm = -18.5 (s).

Synthesis of $\text{C}_6\text{H}_5\text{Bpin}^{[151]}$



A Schlenk tube was charged with bromobenzene (3.85 g, 24.5 mmol), bis(pinacolato)diboron (9.33 g, 36.8 mmol), KO^tBu (4.12 g, 36.8 mmol), copper(I)iodide (470 mg, 2.45 mmol), tri-*n*-butylphosphine (850 mg, 4.20 mmol), 75 mL of THF and the reaction

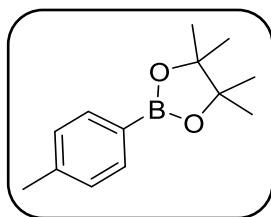
mixture was stirred at room temperature overnight. The resulting black suspension was filtered through a plug of Celite® in air and the solid was washed two times with 50 mL of THF. The solvent was removed from the filtrate using a rotary evaporator to obtain a colorless residue. The product was purified by flash chromatography using *n*-hexane:diethylether 9:1 as eluant.

Yield: 2.70 g (13.2 mmol, 54%) of a colorless oil.

¹H-NMR (200 MHz, 25 °C, C₆D₆): δ_H / ppm = 1.13 (s, 12 H, CH₃), 7.21 – 7.25 (m, 3 H, *m+p*-CH), 8.12-8.17 (m, 2 H, *o*-CH).

¹¹B-NMR (96 MHz, 25 °C, C₆D₆): δ_B / ppm = 31.3 (s).

Synthesis of *p*-tolylBpin^[151]



A Schlenk tube was charged with 4-bromotoluene (3.92 g, 22.9 mmol), bis(pinacolato)diboron (9.72 g, 34.4 mmol), KO^tBu (3.86 g, 34.4 mmol), copper(I)iodide (440 mg, 2.31 mmol), tri-*n*-butylphosphine (790 mg, 3.91 mmol), 75 mL of THF and the reaction mixture was stirred at room temperature overnight. The resulting black suspension was filtered through a plug of Celite® in air and the solid was washed two times with 50 mL of THF. The solvent was removed from the filtrate using a rotary evaporator to obtain a yellow residue. The product was purified by flash chromatography using *n*-hexane: diethylether 9:1 as eluant.

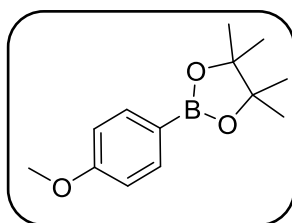
Yield: 2.80 g (12.8 mmol, 56%) of a yellow oil.

¹H-NMR (200 MHz, 25 °C, C₆D₆): δ_H / ppm = 1.13 (s, 12 H, CH₃), 2.07 (s, 3 H, _{aryl}CH₃), 7.05 (d, 2 H, ³J_{HH} = 8 Hz, *m*-CH), 8.11 (d, 2 H, ³J_{HH} = 8 Hz, *o*-CH).

¹¹B-NMR (96 MHz, 25 °C, C₆D₆): δ_B / ppm = 31.4 (s).

¹³C{¹H}-NMR (50 MHz, 25 °C, C₆D₆): δ_C / ppm = 21.7 (_{aryl}CH₃), 25.0 (C_qCH₃), 83.6 (C_q), 129.0 (*o*-CH), 135.6 (*m*-CH), 141.5 (*p*-CH).

Synthesis of 4-MeO-C₆H₄Bpin^[151]



A Schlenk tube was charged with 4-bromoanisole (3.93 g, 21.0 mmol), bis(pinacolato)diboron (8.00 g, 31.5 mmol), KO^tBu (3.53 g, 31.5 mmol), copper(I)iodide (400 mg, 2.10 mmol), tri-*n*-butylphosphine (550 mg, 2.72 mmol), 75 mL of THF and the reaction mixture was stirred at room temperature overnight. The resulting black suspension was filtered through a plug of Celite® in air and the solid was washed two times with 50 mL of THF. The solvent was removed from the filtrate using a rotary evaporator to obtain a light yellow residue. The product was purified by flash chromatography using *n*-hexane: diethylether 9:1 as eluant.

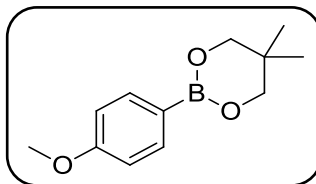
Yield: 2.78 g (11.9 mmol, 57%) of a light yellow oil.

¹H-NMR (200 MHz, 25 °C, C₆D₆): δ_H / ppm = 1.14 (s, 12 H, CH₃), 3.24 (s, 3 H, arylCH₃), 6.79 – 6.86 (m, 2 H, arylCH_m), 8.08-8.15 (m, 2 H, arylCH_o).

¹¹B-NMR (96 MHz, 25 °C, C₆D₆): δ_B / ppm = 31.2 (s, B).

¹³C{¹H}-NMR (50 MHz, 25 °C, C₆D₆): δ_C / ppm = 25.0 (C_qCH₃), 54.6 (OCH₃), 83.5 (C_q), 113.9 (*o*-CH), 137.2 (*m*-CH), 162.9 (*p*-CH).

Synthesis of 4-MeO-C₆H₄Bneop^[23, 333]



A solution of B(OMe)₃ (5 mL, 4.72 g, 44.2 mmol) in 20 mL of THF was cooled to -40 °C and a 2.8 M solution of 4-MeO-C₆H₄MgBr (8.10 mL, 22.1 mmol) in THF was added slowly. The white suspension was warmed to room temperature and the solvent removed under reduced pressure. To the residue, 20 mL of toluene and neopentyl glycol (2.92 g, 26.5 mmol) was added and the suspension was heated to reflux for 5 h. After cooling to room

temperature the reaction mixture was filtered and washed two times with 10 mL of toluene. The liquid fractions were combined and the solvent removed under reduced pressure. The crude product was purified by flash chromatography using *n*-hexane: diethylether 9:1 as eluant.

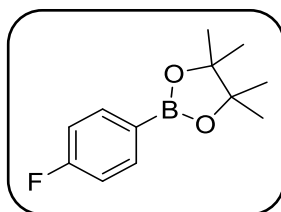
Yield: 3.60 g (15.3 mmol, 69%) of an off-white solid.

¹H-NMR (400 MHz, 25 °C, C₆D₆): δ_H / ppm = 0.60 (s, 6 H, OCH₂C_qCH₃), 3.28 (s, 3 H, OCH₃), 3.43 (s, 4 H, OCH₂C_q), 6.91 (d, 2 H, ³J_{HH} = 9 Hz, arylCH), 8.21 (d, 2 H, ³J_{HH} = 9 Hz, arylCH).

¹¹B-NMR (64 MHz, 25 °C, C₆D₆): δ_B / ppm = 27.3 (s).

¹³C{¹H}-NMR (100 MHz, 25 °C, C₆D₆): δ_C / ppm = 21.7 (OCH₂C_qCH₃), 31.6 (OCH₂C_qCH₃), 54.6 (OCH₃), 712.1 (OCH₂C_qCH₃), 113.8 (*o*-CH), 136.4 (*m*-CH), 162.6 (NCN).

Synthesis of 4-F-C₆H₄Bpin^[23, 334-335]



A solution of B(OMe)₃ (5.11 mL, 4.68 g, 50.0 mmol) in 20 mL of THF was cooled to -40 °C and a 5.11 M solution of 4-F-C₆H₄MgBr (9.00 mL, 46.0 mmol) in THF was added slowly. The white suspension was warmed to room temperature and the solvent removed under reduced pressure. To the residue, 20 mL of toluene and pinacol (7.43 g, 63.0 mmol) was added and the suspension was heated to reflux for 16 h. After cooling to room temperature, the reaction mixture was filtered and the solid washed two times with 10 mL of toluene. The liquid fractions were combined and the solvent removed under reduced pressure. The crude product was purified by flash chromatography using *n*-hexane: diethylether 9:1 as eluant.

Yield: 2.96 g (13.3 mmol, 29%) of a colorless oil.

¹H-NMR (400 MHz, 25 °C, C₆D₆): δ_H / ppm = 1.10 (s, 12 H, OC_qCH₃), 6.81 – 6.86 (m, 2 H, arylCH), 7.94 – 7.98 (m, 2 H, arylCH).

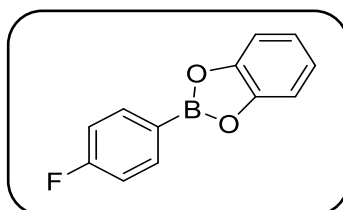
¹¹B-NMR (64 MHz, 25 °C, C₆D₆): δ_B / ppm = 30.8 (s).

$^{13}\text{C}\{^1\text{H}\}$ -NMR (50 MHz, 25 °C, C_6D_6): δ_{C} / ppm = 25.0 (OC_qCH_3), 83.9 (OC_qCH_3), 115.3 (d, $^2J_{\text{CF}}$ = 20 Hz, *m*-CH), 125.6 (br, *i*- C_q), 137.7 (d, $^3J_{\text{CF}}$ = 8 Hz, *o*-CH), 165.7 (d, $^1J_{\text{CF}}$ = 250 Hz, *p*-CH).

^{19}F -NMR (188 MHz, 25 °C, C_6D_6): δ_{F} / ppm = -108.1 – -108.0 (m).

HRMS-ASAP (m/z): $[\text{M}+\text{H}]^+$ calc. for $\text{C}_{12}\text{H}_{16}\text{BFO}_2$, 223.1300 found, 223.1296.

Synthesis of 4-F- $\text{C}_6\text{H}_4\text{Bcat}$ ^[23, 335]



A solution of $\text{B}(\text{OMe})_3$ (5.11 mL, 4.68 g, 50.0 mmol) in 20 mL of THF was cooled to -40 °C and a 5.11 M solution of 4-F- $\text{C}_6\text{H}_4\text{MgBr}$ (6.00 mL, 30.7 mmol) in THF was added slowly. The white suspension was warmed to room temperature and the solvent removed under reduced pressure. To the residue, 20 mL of toluene and catechol (6.60 g, 60.0 mmol) were added and the suspension was heated to reflux for 16 h. After cooling to room temperature, the reaction mixture was filtered and the solid was washed two times with 10 mL of toluene. The liquid fractions were combined and the solvent removed under reduced pressure. The crude product was purified by flash chromatography using *n*-hexane:diethylether 9:1 as eluant.

Yield: 2.80 g (13.3 mmol, 43%) of an off-white solid.

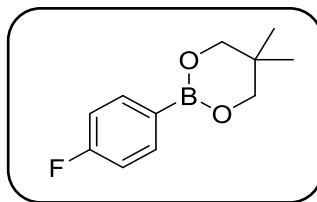
^1H -NMR (400 MHz, 25 °C, C_6D_6): δ_{H} / ppm = 6.77 – 6.81 (m, 2 H, $_{\text{aryl}}\text{CH}$), 6.81 – 6.84 (m, 2 H, $_{\text{aryl}}\text{CH}$), 7.04 – 7.09 (m, 2 H, $_{\text{aryl}}\text{CH}$), 7.87 – 7.90 (m, 2 H, $_{\text{aryl}}\text{CH}$).

^{11}B -NMR (64 MHz, 25 °C, C_6D_6): δ_{B} / ppm = 31.9 (s).

$^{13}\text{C}\{^1\text{H}\}$ -NMR (50 MHz, 25 °C, C_6D_6): δ_{C} / ppm = 112.8 ($^{\text{cat}}\text{CH}$), 115.8 (d, $^2J_{\text{CF}}$ = 21 Hz, *m*-CH), 123.1 ($^{\text{cat}}\text{CH}$), 137.7 (d, $^3J_{\text{CF}}$ = 8 Hz, *o*-CH), 149.0 ($^{\text{cat}}\text{C}_q$), 166.1 (d, $^1J_{\text{CF}}$ = 252 Hz, *p*-CH).

^{19}F -NMR (188 MHz, 25 °C, C_6D_6): δ_{F} / ppm = -106.1 – -106.0 (m).

HRMS-ASAP (m/z): $[\text{M}+\text{H}]^+$ calc. for $\text{C}_{12}\text{H}_8\text{BFO}_2$, 215.0674 found, 215.0672.

Synthesis of 4-F-C₆H₄Bneop^[23, 333, 335]


A solution of B(OMe)₃ (5.11 mL, 4.68 g, 50.0 mmol) in 20 mL of THF was cooled to -40 °C and a 5.11 M solution of 4-F-C₆H₄MgBr (5.00 mL, 25.6 mmol) in THF was added slowly. The white suspension was warmed to room temperature and the solvent removed under reduced pressure. To the residue, 20 mL of toluene and neopentyl glycol (5.42 g, 52.0 mmol) was added and the suspension was heated to reflux for 16 h. After cooling to room temperature, the reaction mixture was filtered and the solid was washed two times with 10 mL of toluene. The liquid fractions were combined and the solvent removed under reduced pressure. The crude product was purified by flash chromatography using *n*-hexane:diethylether 9:1 as eluant.

Yield: 1.40 g (6.73 mmol, 26%) of a yellow solid.

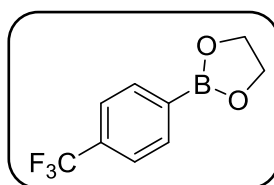
¹H-NMR (400 MHz, 25 °C, C₆D₆): δ_H / ppm = 0.57 (s, 6 H, OCH₂C_qCH₃), 3.36 (s, 4 H, OCH₂C_qCH₃), 6.90 – 6.95 (m, 2 H, _{aryl}CH), 8.02-8.06 (m, 2 H, _{aryl}CH).

¹¹B-NMR (64 MHz, 25 °C, C₆D₆): δ_B / ppm = 26.7 (s).

¹³C{¹H}-NMR (50 MHz, 25 °C, C₆D₆): δ_C / ppm = 21.6 (OCH₂CH₃), 31.5, 72.1 (OCH₂CH₃), 115.0 (d, ²J_{CF} = 20 Hz, *m*-CH), 136.8 (d, ³J_{CF} = 8 Hz, *o*-CH) 165.5 (d, ¹J_{CF} = 247 Hz, *p*-C_q).

¹⁹F-NMR (188 MHz, 25 °C, C₆D₆): δ_F / ppm = -109.5 – -109.5 (m).

HRMS-ASAP (m/z): [M+H]⁺ calc. for C₁₁H₁₄BFO₂, 209.1144 found, 209.1141.

Synthesis of 4-F-C₆H₄Beg^[336]


A solution of B(OMe)₃ (5.11 mL, 4.68 g, 50.0 mmol) in 20 mL of THF was cooled to -40 °C and a 5.11 M solution of 4-F-C₆H₄MgBr (5.00 mL, 25.6 mmol) in THF was added slowly. The

white suspension was warmed to room temperature and the solvent removed under reduced pressure. To the residue, 20 mL of toluene and ethylene glycol (3.34 g, 3.00 mL, 53.8 mmol) was added and the suspension was heated to reflux for 16 h. After cooling to room temperature, the reaction mixture was filtered and the solid was washed two times with 10 mL of toluene. The liquid fractions were combined and the solvent removed under reduced pressure. The crude product was purified by flash chromatography using *n*-hexane:diethylether 9:1 as eluant.

Yield: 545 mg (3.28 mmol, 13%) of a yellow solid.

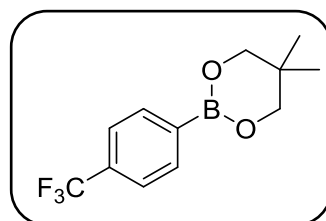
¹H-NMR (200 MHz, 25 °C, C₆D₆): δ_H / ppm = 3.62 (s, 4 H, CH₂), 6.84 (m, 2 H, *aryl*CH), 7.91 (m, 2 H, *aryl*CH).

¹¹B-NMR (64 MHz, 25 °C, C₆D₆): δ_B / ppm = 31.4 (s).

¹³C{¹H}-NMR (50 MHz, 25 °C, CDCl₃): δ_C / ppm = 65.9 (CH₂), 115.4 (d, J_{CF} = 21 Hz, *m*-CH) 137.7 (d, J_{CF} = 8 Hz, *o*-CH).

¹⁹F-NMR (188 MHz, 25 °C, C₆D₆): δ_F / ppm = -107.8 – -107.9 (m).

Synthesis of 4-CF₃-C₆H₄Bneop^[337]



A solution of B(OMe)₃ (5.11 mL, 4.68 g, 50.0 mmol) in 20 mL of THF was cooled to -40 °C and a 5.09 M solution of 4-CF₃-C₆H₄MgBr (5.00 mL, 25.5 mmol) in THF was added slowly. The white suspension was warmed to room temperature and the solvent removed under reduced pressure. To the residue, 20 mL of toluene and neopentyl glycol (5.21 g, 50.0 mmol) was added and the suspension was heated to reflux for 16 h. After cooling to room temperature, the reaction mixture was filtered and the solid was washed two times with 10 mL of toluene. The liquid fractions were combined and the solvent removed under reduced pressure. The crude product was purified by flash chromatography using *n*-hexane:diethylether 9:1 as eluant.

Yield: 2.11 g (8.19 mmol, 32%) of an off-white solid.

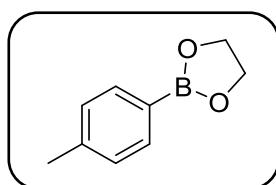
$^1\text{H-NMR}$ (400 MHz, 25 °C, CDCl_3): δ_{H} / ppm = 0.54 (s, 6 H, CH_3), 3.33 (s, 4 H, CH_2), 7.46 (m, 2 H, $_{\text{aryl}}\text{CH}$), 8.04 (m, 2 H, $_{\text{aryl}}\text{CH}$).

$^{11}\text{B-NMR}$ (64 MHz, 25 °C, C_6D_6): δ_{B} / ppm = 26.3 (s).

$^{13}\text{C}\{^1\text{H}\}\text{-NMR}$ (50 MHz, 25 °C, THF-d_8): δ_{C} / ppm = 21.9 (CH_3), 32.5 (C_qCH_2), 73.0 (C_qCH_2), 124.8 (q, $^1J_{\text{FC}} = 4$ Hz, CF_3), 125.5 (d, $^3J_{\text{CF}} = 271$ Hz, $m\text{-CH}$), 132.8 (d, $^2J_{\text{CF}} = 32$ Hz, $p\text{-C}_q$), 135.1 ($o\text{-CH}$).

$^{19}\text{F-NMR}$ (188 MHz, 25 °C, C_6D_6): δ_{F} / ppm = -63.7 (s, CF_3).

Synthesis of *p*-tolylBeg^[336, 338]



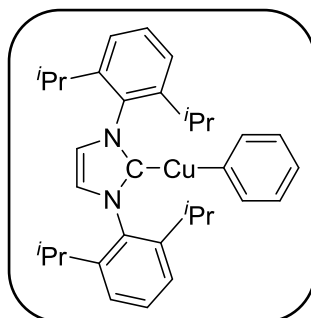
A solution of $\text{B}(\text{OMe})_3$ (5.11 mL, 4.68 g, 50.0 mmol) in 20 mL of THF was cooled to -40 °C and a 4.15 M solution of 4- $\text{CH}_3\text{-C}_6\text{H}_4\text{MgBr}$ (6.16 mL, 25.5 mmol) in THF was added slowly. The white suspension was warmed to room temperature and the solvent removed under reduced pressure. To the residue, 20 mL of toluene and ethylene glycol (3.34 g, 3.00 mL, 53.8 mmol) was added and the suspension was heated to reflux for 16 h. After cooling to room temperature, the reaction mixture was filtered and the solid was washed two times with 10 mL of toluene. The liquid fractions were combined and the solvent removed under reduced pressure. The crude product was purified by flash chromatography using *n*-hexane: diethylether 9:1 as eluant.

Yield: 496 mg (3.06 mmol, 12%) of an off-white solid.

$^1\text{H-NMR}$ (200 MHz, 25 °C, C_6D_6): δ_{H} / ppm = 2.08 (s, 3 H, CH_3), 3.67 (s, 4 H, CH_2), 7.07 (m, 2 H, $_{\text{aryl}}\text{CH}$), 8.10 (d, 2 H, $_{\text{aryl}}\text{CH}$).

$^{11}\text{B-NMR}$ (64 MHz, 25 °C, C_6D_6): δ_{B} / ppm = 32.0 (s).

$^{13}\text{C}\{^1\text{H}\}\text{-NMR}$ (50 MHz, 25 °C, CDCl_3): δ_{C} / ppm = 21.9 (CH_3), 66.1 (CH_2), 128.8 ($m\text{-CH}$), 135.0 ($o\text{-CH}$), 141.8($p\text{-C}_q$).

Synthesis of $[\text{Cu}(\text{Dipp}_2\text{Im})(\text{C}_6\text{H}_5)]$ ^[253, 332]

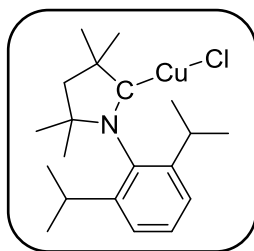
To a suspension of $[\text{Cu}(\text{Dipp}_2\text{Im})(\text{O}^t\text{Bu})]$ (1.10 g, 2.10 mmol) in 50 mL of toluene *p*-tolylpinacolborane (428 mg, 2.10 mmol) was added via syringe and the solution was stirred for 2 h at room temperature. The reaction mixture was concentrated to ca. 10 mL under reduced pressure and 60 mL of *n*-hexane were added to afford a white precipitate. The solid was collected by filtration and dried *in vacuo*.

Yield: 790mg (1.49 mmol, 71%) of a colorless solid.

¹H-NMR (200 MHz, 25 °C, C₆D₆): δ_{H} / ppm = 1.11 (d, 12 H, ³J_{HH} = 7 Hz, CHCH₃), 1.43 (d, 12 H, ³J_{HH} = 7 Hz, CHCH₃), 2.66 (sept, 4 H, ³J_{HH} = 7 Hz, CHCH₃), 6.29 (s, 2 H, CHCH), 6.84 – 6.94 (m, 2 H, *m*-CH), 7.07 – 7.11 (m, 4 H, *m*^{Dipp}-CH), 7.20 – 7.28 (m, 2 H, *p*^{Dipp}-CH), 7.53 – 7.58 (m, 2 H, *o*-CH).

¹³C{¹H}-NMR (50 MHz, 25 °C, C₆D₆): δ_{C} / ppm = 23.7 (CHCH₃), 25.2 (CHCH₃), 29.1 (CHCH₃), 112.7 (*m*-CH), 122.0 (CHCH), 124.2 (*m*^{Dipp}-CH), 130.5 (*p*^{Dipp}-CH), 135.3 (*i*^{Dipp}-C_q), 141.2 (*o*-CH), 145.9 (*o*^{Dipp}-C_q), 155.7 (*i*-C), 158.0 (OC_q). The resonance of the carbene-carbon atom was not detected.

HRMS-ASAP (*m/z*): [M + H]⁺ calc. for C₃₃H₄₁CuN₂, 529.2639 found, 529.2636.

Synthesis of $[\text{Cu}(\text{CaaC}^{\text{Me}})][\text{Cl}]$ ^[339] 12

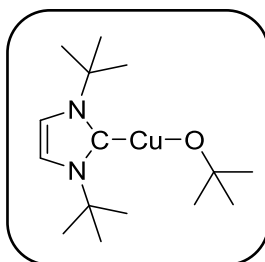
To copper(I) chloride (30 mg, 303 μmol) and CaaC^{Me} (86 mg, 303 μmol) 7 mL of THF was added. The solution was stirred for 4 h at room temperature, before the solvent was removed under reduced pressure. The crude product was washed with 3 mL of *n*-hexane.

Yield: 50 mg (130 μmol , 43%) of a colorless solid.

$^1\text{H-NMR}$ (400 MHz, 25 $^\circ\text{C}$, CD_3CN): δ_{H} / ppm = 0.78 (s, 6 H, $\text{C}_q\text{C}_q\text{CH}_3$), 1.06 (d, 6 H, $^3J_{\text{HH}} = 7$ Hz, CHCH_3), 1.18 (s, 6 H, NC_qCH_3), 1.34 (s, 2 H, CH_2), 1.39 (d, 6 H, $^3J_{\text{HH}} = 7$ Hz, CHCH_3), 2.65 (sept, 2 H, CHCH_3), 6.96 – 7.00 (m, 2 H, *m-CH*), 7.08 – 7.11 (m, 1 H, *p-CH*).

$^{13}\text{C}\{^1\text{H}\}$ NMR (100 MHz, 25 $^\circ\text{C}$, CD_3CN): δ_{C} / ppm = 22.4 (CHCH_3), 27.2 (CHCH_3), 28.3 ($\text{C}_q\text{C}_q\text{CH}_3$), 28.6 (NC_qCH_3), 29.3 (CHCH_3), 49.1 ($\text{C}_q\text{C}_q\text{CH}_3$), 53.9 (NC_qCH_2), 80.9 (NC_qCH_3), 124.9 (*m-C_q*), 130.1 (*p-C_q*), 134.3 (*i-C_q*), 145.3 (*o-C_q*), 249.6 (CuC_q).

HRMS-ASAP (*m/z*): $[\text{M} - \text{Cl}]^+$ calc. for $\text{C}_{20}\text{H}_{31}\text{CuNCl}$, 348.1747 found, 348.1742.

Synthesis of $[\text{Cu}(\text{tBu}_2\text{Im})(\text{O}^t\text{Bu})]$ ^[253] 16

To a mixture of $[\text{Cu}(\text{tBu}_2\text{Im})(\text{Cl})]$ (500 mg, 1.79 mmol) and freshly sublimed KO^tBu (200 mg, 1.79 mmol), 22 mL of THF were added and the reaction mixture was stirred overnight at room temperature. The solvent was removed under reduced pressure. The beige solid was suspended in 10 mL of toluene and filtered through Celite[®]. The solvent was removed under reduced pressure. The crude product was washed with 10 mL of *n*-hexane und dried *in vacuo*.

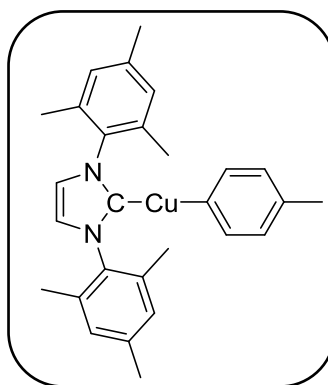
Yield: 380 mg (1.20 mmol, 67%) of a white solid.

$^1\text{H-NMR}$ (200 MHz, 25 °C, C_6D_6): $\delta_{\text{H}} / \text{ppm} = 1.48$ (s, 18 H, $\text{C}(\text{CH}_3)_3$), 1.85 (s, 9 H, $\text{OC}(\text{CH}_3)_3$), 6.47 (s, 2 H, CHCH).

$^{13}\text{C}\{^1\text{H}\}$ NMR (50 MHz, 25 °C, C_6D_6): $\delta_{\text{C}} / \text{ppm} = 31.8$ ($\text{C}(\text{CH}_3)_3$), 37.4 ($\text{OC}(\text{CH}_3)_3$), 57.5 (C_q), 69.2 (OC_q), 115.9 (CHCH), 176.6 (NCN).

HRMS-ASAP (m/z): $[\text{M} + \text{H}]^+$ calc. for $\text{C}_{15}\text{H}_{29}\text{CuN}_2\text{O}$, 317.1649 found 317.1654.

Synthesis of $[\text{Cu}(\text{Mes}_2\text{Im})(p\text{-tolyl})]$ ^[261] **26**



To a suspension of $[\text{Cu}(\text{Mes}_2\text{Im})(\text{Cl})]$ (1.52 g, 3.77 mmol) in 25 mL of THF, a 1.98 M solution of *p*-tolylmagnesium bromide (1.90 mL, 3.77 mmol) in THF was added dropwise. After stirring for 1 h at room temperature, 10 mL of 1,4-dioxane was added to precipitate the magnesium salts. The suspension was filtered and the solvent was removed under reduced pressure to obtain an off-white solid, which was dissolved in toluene. Then 1 mL of 1,4-dioxane was added and the solution stirred for 1 h at room temperature. As nothing precipitated, the solvent was removed under reduced pressure and the residue was washed with 5 mL of *n*-hexane and dried *in vacuo*.

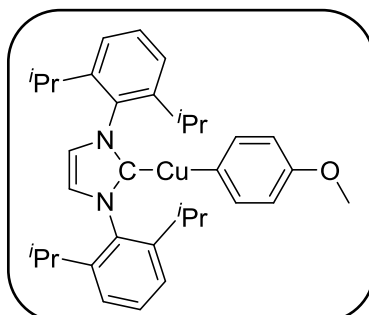
Yield: 1.32 g (2.87 mmol, 76%) of a beige solid.

$^1\text{H-NMR}$ (200 MHz, 25 °C, C_6D_6): $\delta_{\text{H}} / \text{ppm} = 2.02$ (s, 12 H, $o^{\text{Mes}}\text{-CH}_3$), 2.09 (s, 6 H, $p^{\text{Mes}}\text{-CH}_3$), 2.22 (s, 3 H, $p\text{-CH}_3$), 6.02 (s, 2 H, CHCH), 6.72 (s, 4 H, $m^{\text{Mes}}\text{-CH}$), 7.08 – 7.13 (m, 2 H, $m\text{-CH}$), 7.72 – 7.76 (m, 2 H, $o\text{-CH}$).

$^{13}\text{C}\{^1\text{H}\}$ -NMR (50 MHz, 25 °C, C_6D_6): $\delta_{\text{C}} / \text{ppm} = 18.0$ ($o^{\text{Mes}}\text{-CH}_3$), 21.1 ($p^{\text{Mes}}\text{-CH}_3$), 21.8 ($p\text{-CH}_3$), 121.3 (CHCH), 127.3 ($_{\text{aryl}}\text{CH}$), 129.6 ($m^{\text{Mes}}\text{-CH}$), 132.6 ($_{\text{aryl}}\text{C}_q$), 134.8 ($o^{\text{Mes}}\text{-C}_q$), 136.1 ($_{\text{aryl}}\text{CH}$), 139.0 ($p^{\text{Mes}}\text{-C}_q$), 142.2 ($_{\text{aryl}}\text{C}_q$), 161.5 ($i^{\text{Mes}}\text{-C}_q$), 184.3 (NCN).

HRMS-ASAP (m/z): [M + H]⁺ calc. for C₂₈H₃₁CuN₂, 459.1856 found, 459.1855.

Synthesis of [Cu(Dipp₂Im)(4-MeO-C₆H₄)]^[260, 340] **28**



To a suspension of [Cu(Dipp₂Im)(O^tBu)] (1.10 g, 2.10 mmol) in 50 mL of toluene, 4-methoxyphenyl-pinacolborane (492 mg, 2.10 mmol) was added via syringe and the solution was stirred for 2 h at room temperature. The reaction mixture was concentrated to ca. 10 mL under reduced pressure and 60 mL of *n*-hexane were added to afford a white precipitate. The solid was collected by filtration and dried *in vacuo*.

Yield: 1.02 g (1.82 mmol 87%) of a colorless solid.

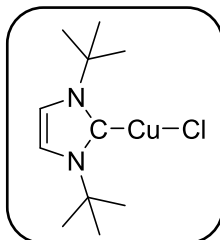
¹H-NMR (200 MHz, 25 °C, C₆D₆): δ_H / ppm = 1.11 (d, 12 H, ³J_{HH} = 7 Hz, CHCH₃), 1.43 (d, 12 H, ³J_{HH} = 7 Hz, CHCH₃), 2.66 (sept, 4 H, ³J_{HH} = 7 Hz, CHCH₃), 3.39 (s, 3 H, OCH₃), 6.29 (s, 2 H, CHCH), 6.89 – 6.93 (m, 2 H, *m*-CH), 7.07 – 7.11 (m, 4 H, *m*^{Dipp}-CH), 7.20 – 7.28 (m, 2 H, *p*^{Dipp}-CH), 7.53 – 7.58 (m, 2 H, *o*-CH).

¹³C{¹H}-NMR (50 MHz, 25 °C, C₆D₆): δ_C / ppm = 23.7 (CHCH₃), 25.2 (CHCH₃), 29.1 (CHCH₃), 54.4 (OCH₃), 112.7 (*m*-CH), 122.2 (CHCH), 124.2 (*m*^{Dipp}-CH), 130.5 (*p*^{Dipp}-CH), 135.3 (*i*^{Dipp}-C_q), 141.2 (*o*-C_q), 145.9 (*o*^{Dipp}-C_q), 155.7 (*i*-C_q), 158.0 (OC_q), 186.2 (NCN).

HRMS-ASAP (m/z): [M + H]⁺ calc. for C₃₄H₄₃CuN₂O, 559.2744 found, 559.2741.

6.3 Synthesis of new compounds

Synthesis of [Cu(^tBu₂Im)Cl] 1



A Schlenk tube containing copper(I) chloride (2.91 g, 29.4 mmol) and 1,3-di-*tert*-butylimidazolin-2-ylidene (5.25 g, 29.4 mmol) was cooled to -110 °C. THF (20 mL) was added slowly down the side of the cooled Schlenk tube. The mixture was slowly warmed to room temperature and stirred for 30 min before being heated to 50 °C for 1 h. The solvent of the yellow suspension was removed under reduced pressure. The crude product was washed with 20 mL of *n*-hexane and dried *in vacuo* to obtain a colorless solid.

Yield: 6.90 g (24.7 mmol, 84%) of a colorless solid which is susceptible to oxidation and hydrolysis.

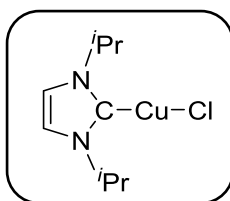
Elemental analysis for [C₁₁H₂₀ClCuN₂] [403.74 g/mol]: Calc. (obs.) C 47.31 (47.14), H 7.22 (7.64), N 10.03 (9.98).

¹H-NMR (300 MHz, 25 °C, C₆D₆): δ_H / ppm = 1.41 (s, 18 H, CH₃), 6.50 (s, 2 H, CHCH).

¹³C{¹H}-NMR (75 MHz, 25 °C, C₆D₆): δ_C / ppm = 31.9 (CH₃), 57.7 (C_q), 116.6 (CHCH), 174.1 (NCN).

HRMS-ASAP (m/z): [M]⁺ calc. for C₁₁H₂₀ClCuN₂, 278.0606 found, 278.0603.

Synthesis of [Cu(*i*Pr₂Im)Cl] 2



A Schlenk tube containing copper(I) chloride (3.00 g, 10.1 mmol) and 25 mL of THF was cooled to -110 °C. Via syringe, 1,3-di-*iso*-propylimidazolin-2-ylidene (4.61 g, 30.3 mmol, 4.61 mL) was added dropwise. The mixture was slowly warmed to room temperature and stirred for 12 h. The solvent of the grey suspension was removed under reduced pressure. The crude product was washed with 20 mL of *n*-hexane and dried *in vacuo* to obtain a grey solid.

Yield: 6.60 g (26.3 mmol, 87%) of a solid which is susceptible to oxidation and hydrolysis.

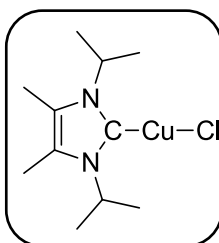
Elemental analysis for [C₉H₁₆ClCuN₂] [251.24 g/mol]: Calc. (obs.) C 43.03 (42.77), H 6.42 (6.11), N 11.15 (11.00).

¹H-NMR (300 MHz, 25 °C, C₆D₆): δ_H / ppm = 0.93 (d, 12 H, ³J_{HH} = 7 Hz, CHCH₃), 4.34 (sept, 2 H, ³J_{HH} = 7 Hz, CHCH₃), 6.25 (s, 2 H, CHCH).

¹³C{¹H}-NMR (75 MHz, 25 °C, C₆D₆): δ_C / ppm = 23.5 (CHCH₃), 53.6 (CHCH₃), 117.0 (CHCH), 174.5 (NCN).

HRMS-ASAP (m/z): [2 M]⁺ calc. for C₉H₁₆ClCuN₂, 502.0572 found 502.0554.

Synthesis of [Cu(*i*Pr₂ImMe₂)Cl] 3



A Schlenk tube containing copper(I) chloride (297 mg, 3.00 mmol) and 1,3-di-*iso*-propyl-4,5-dimethylimidazolin-2-ylidene (540 mg, 3.00 mmol) was cooled to -110 °C. THF (5 mL) was added slowly down the side of the cooled Schlenk tube. The mixture was slowly warmed to room temperature and stirred for 16 h. The solvent of the brownish suspension

was removed under reduced pressure. The crude product was washed with 10 mL of *n*-hexane and dried *in vacuo* to obtain a colorless solid.

Yield: 630 mg (2.25 mmol, 75%) of an off-white solid which is susceptible to oxidation and hydrolysis.

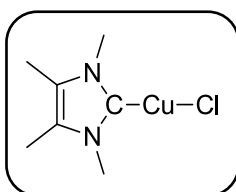
Elemental analysis for [C₁₁H₂₀CuN₄Cl] [279.29 g/mol]: Calc. (obs.) C 47.31 (47.10), H 7.22 (7.52), N 10.03 (9.71).

¹H-NMR (200 MHz, 25 °C, C₆D₆): δ_H / ppm = 1.33 (d, 12 H, ³J_{HH} = 7 Hz, CHCH₃), 1.37 (s, 6 H, C_qCH₃), 3.86 (sept, 2 H, ³J_{HH} = 7 Hz, CHCH₃).

¹³C{¹H}-NMR (100 MHz, 25 °C, C₆D₆): δ_C / ppm = 8.6 (C_qCH₃), 24.3 (CHCH₃), 50.2 (CHCH₃), 123.4 (C_qC_q), 170.0 (NCN).

HRMS-ASAP (m/z): [M - Cl]⁺ calc. for C₁₁H₂₀CuN₂, 243.0917 found, 243.0915.

Synthesis of [Cu(Me₄Im)Cl] 4



A Schlenk tube containing copper(I) chloride (198 mg, 2.00 mmol) and 1,3,4,5-tetramethylimidazolin-2-ylidene (248 mg, 2.00 mmol) was cooled to -110 °C. THF (5 mL) was added slowly down the side of the cooled Schlenk tube glass. The mixture was slowly warmed to room temperature and stirred for 16 h. The solvent of the white suspension was removed under reduced pressure. The crude product was washed with 10 mL of *n*-hexane and dried *in vacuo* to obtain a colorless solid.

Yield: 295 mg (1.32 mmol, 66%) of an off-white solid which is susceptible to oxidation and hydrolysis.

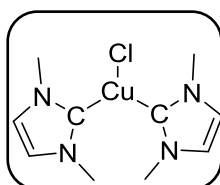
Elemental analysis for [C₇H₁₂CuN₂Cl] [223.18 g/mol]: Calc. (obs.) C 37.67 (38.04), H 5.42 (5.47), N 12.55 (12.70).

¹H-NMR (200 MHz, 25 °C, C₆D₆): δ_H / ppm = 1.17 (s, 6 H, C_qCH₃), 2.83 (s, 6 H, NCH₃).

$^{13}\text{C}\{^1\text{H}\}$ -NMR (100 MHz, 25 °C, C_6D_6): δ_{C} / ppm = 8.2 (C_qCH_3), 34.9 (NCH_3), 124.4 (C_qC_q), 175.2 (NCN).

HRMS-ASAP (m/z): $[\text{M} - \text{Cl}]^+$ calc. for $\text{C}_7\text{H}_{12}\text{CuN}_2$, 187.0291 found, 187.0285.

Synthesis of $[\text{Cu}(\text{Me}_2\text{Im})_2\text{Cl}]$ 5



To a suspension of copper(I) chloride (250 mg, 2.52 mmol) in 7 mL of THF, 1,3-dimethylimidazol-2-ylidene (485 mg, 5.05 mmol, 485 μL) was added via syringe. The yellow reaction mixture was stirred for 1 h at room temperature. The solvent was removed under reduced pressure and the crude product was washed with 10 mL of *n*-hexane and dried *in vacuo* to obtain a light grey powder.

Yield: 413 mg (1.42 mmol, 56%) of a grey powder susceptible to oxidation and hydrolysis.

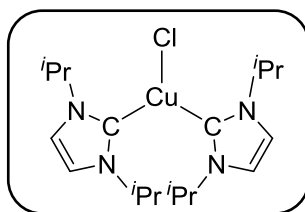
Elemental analysis for $[\text{C}_{10}\text{H}_{16}\text{ClCuN}_4]$ [291.26 g/mol]: Calc. (obs.) C 41.24 (40.96), H 5.54 (5.67), N 19.24 (18.67).

Although the present results are outside the range viewed as established for analyzed purity, they are provided to illustrate the best values obtained to date. In addition, the ^1H and the $^{13}\text{C}\{^1\text{H}\}$ NMR spectra as given in Figure 119 and Figure 120 provide evidence for the purity of the compound.

^1H -NMR (300 MHz, 25 °C, CD_3CN): δ_{H} / ppm = 3.80 (s, 6 H, CH_3), 7.01 (s, 2 H, CHCH).

$^{13}\text{C}\{^1\text{H}\}$ -NMR (75 MHz, 25 °C, CD_3CN): δ_{C} / ppm = 38.1 (CH_3), 122.3 (CHCH), 183.8 (NCN).

HRMS-ASAP (m/z): $[\text{M}]^+$ calc. for $\text{C}_{10}\text{H}_{16}\text{CuN}_4\text{Cl}$, 290.0354 found, 290.0344.

Synthesis of $[\text{Cu}(\text{iPr}_2\text{Im})_2\text{Cl}]$ 6

To a suspension of copper(I) chloride (250 mg, 2.52 mmol) in 10 mL of THF, 1,3-di-*iso*-propylimidazolin-2-ylidene (769 mg, 5.05 mmol, 769 μL) was added at room temperature. The grey-green reaction mixture was stirred for 1.5 h at room temperature before the solvent was removed under reduced pressure. The crude product was washed with 10 mL of *n*-hexane and dried *in vacuo* to obtain a light grey powder.

Yield: 665 mg (1.65 mmol, 65%) of a light grey solid which is susceptible to oxidation and hydrolysis.

Elemental analysis for $[\text{C}_{18}\text{H}_{32}\text{ClCuN}_4]$ [403.74 g/mol]: Calc. (obs.) C 53.58 (54.21), H 7.99 (8.02), N 13.89 (13.97).

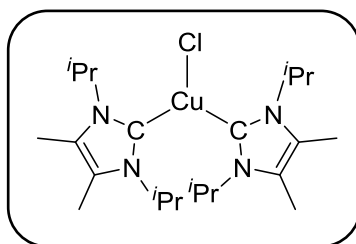
Although the present results are outside the range viewed as established for analyzed purity, they are provided to illustrate the best values obtained to date. In addition, the ^1H and the $^{13}\text{C}\{^1\text{H}\}$ NMR spectra as given in Figure 121 and Figure 122 provide evidence for the purity of the compound.

^1H -NMR (300 MHz, 25 $^\circ\text{C}$, C_6D_6): δ_{H} / ppm = 1.22 (d, 24 H, $^3J_{\text{HH}} = 7$ Hz, CHCH_3), 5.36 (sept, 4 H, $^3J_{\text{HH}} = 7$ Hz, CHCH_3), 6.46 (s, 4 H, CHCH).

$^{13}\text{C}\{^1\text{H}\}$ NMR (75 MHz, 25 $^\circ\text{C}$, C_6D_6): δ_{C} / ppm = 23.7 (CHCH_3), 52.2 (CHCH_3), 115.5 (CHCH), 184.7 (NCN).

HRMS-ASAP (m/z): $[\text{M}]^+$ calc. for $\text{C}_{18}\text{H}_{32}\text{CuN}_4\text{Cl}$, 402.1606 found, 402.1593.

Synthesis of $[\text{Cu}(\text{iPr}_2\text{ImMe}_2)_2\text{Cl}]$ 7



At room temperature, 5 mL of THF was added to a Schlenk tube containing copper(I) chloride (99 mg, 1.00 mmol) and 1,3-di-*iso*-propyl-4,5-dimethylimidazolin-2-ylidene (360 mg, 2.00 mmol). The mixture was stirred for 16 h. The solvent of the brownish suspension was removed under reduced pressure. The crude product was washed with 10 mL of *n*-hexane and dried *in vacuo* to obtain a colorless solid.

Yield: 320 mg (0.70 mmol, 70%) of an off-white solid which is susceptible to oxidation and hydrolysis.

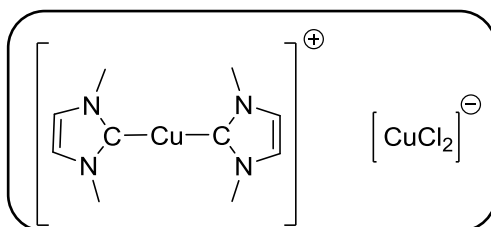
Elemental analysis for $[\text{C}_{22}\text{H}_{40}\text{CuN}_4\text{Cl}]$ [459.59 g/mol]: Calc. (obs.) C 57.50 (57.23), H 8.77 (8.62), N 12.19 (12.05).

$^1\text{H-NMR}$ (200 MHz, 25 °C, C_6D_6): δ_{H} / ppm = 1.50 (d, 24 H, $^3J_{\text{HH}} = 7$ Hz, CHCH_3), 1.68 (s, 12 H, (C_qCH_3)), 5.17 (br, 4 H, CHCH_3).

$^{13}\text{C}\{^1\text{H}\}$ NMR (100 MHz, 25 °C, C_6D_6): δ_{C} / ppm = 9.6 (C_qCH_3), 23.3 (CHCH_3), 51.8 (CHCH_3), 123.0 (C_qC_q), 183.9 (NCN).

HRMS-ASAP (m/z): $[\text{M} - \text{Cl}]^+$ calc. for $\text{C}_{22}\text{H}_{40}\text{CuN}_4$, 423.2543 found, 423.2539.

Synthesis of $[\text{Cu}(\text{Me}_2\text{Im})_2]^+[\text{CuCl}_2]^-$ 8



A Schlenk tube containing copper(I) chloride (1.00 g, 10.1 mmol) and 25 mL of THF was cooled to -110 °C. Via syringe, 1,3-dimethylimidazolin-2-ylidene (970 mg, 10.1 mmol, 970 μL) was added dropwise. The mixture was slowly warmed to room temperature and stirred

for 12 h. The solvent of the grey suspension was removed under reduced pressure. The crude product was washed with 20 mL of *n*-hexane and dried *in vacuo* to obtain a grey solid.

Yield: 1.68 g (8.61 mmol, 85%) of a grey powder susceptible to oxidation and hydrolysis.

Elemental analysis for $[\text{C}_5\text{H}_9\text{ClCuN}_2]$ [195.13 g/mol]: Calc. (obs.) C 30.78 (31.54), H 4.13 (4.46), N 14.36 (14.66).

Although the present results are outside the range viewed as established for analyzed purity, they are provided to illustrate the best values obtained to date. In addition, the ^1H and the $^{13}\text{C}\{^1\text{H}\}$ NMR spectra as given in Figure 123 and Figure 124 provide evidence for the purity of the compound.

$^1\text{H-NMR}$ (300 MHz, 25 °C, C_6D_6): $\delta_{\text{H}} / \text{ppm} = 2.70$ (s, 6 H, CH_3), 5.52 (s, 2 H, CHCH).

$^{13}\text{C}\{^1\text{H}\}\text{-NMR}$ (75 MHz, 25 °C, CD_3CN): $\delta_{\text{C}} / \text{ppm} = 38.5$ (CH_3), 123.1 (CHCH), 177.8 (NCN).

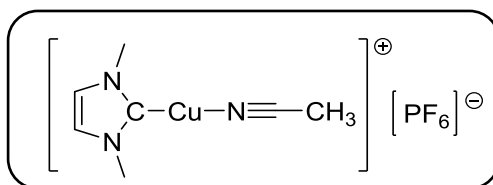
$^{31}\text{P-NMR}$ (202.5 MHz, 25 °C, CD_3CN): $\delta_{\text{P}} / \text{ppm} = -144.6$ (sept, 1 P, $^1J_{\text{PF}} = 706$ Hz, PF_6).

$^{19}\text{F-NMR}$ (188.3 MHz, 25 °C, CD_3CN): $\delta_{\text{F}} / \text{ppm} = -72.9$ (d, 6 F, $^1J_{\text{FP}} = 706$ Hz, PF_6).

HRMS-ASAP (m/z): $[\text{M}]^+$ calc. for $\text{C}_{10}\text{H}_{16}\text{CuN}_4$, 255.0665 found, 255.0662.

HRMS-ASAP (m/z): $[\text{M}]^-$ calc. for CuCl_2 , 132.8668 found, 132.8668.

Synthesis of $[\text{Cu}(\text{Me}_2\text{Im})(\text{MeCN})][\text{PF}_6]$ 9



Tetrakis(acetonitrile)copper(I) hexafluorophosphate (300 mg, 800 μmol) in 7 mL of THF was cooled to -110 °C. Via syringe, 1,3-dimethylimidazol-2-ylidene (77.3 mg, 10.1 mmol, 77.3 μL) was added dropwise before the suspension was warmed to room temperature. After 5 min the reaction mixture turned from yellow to grey and the solvent was removed under reduced pressure. The crude product was washed with 5 mL of *n*-hexane and dried *in vacuo* to obtain a grey powder.

Yield: 189 mg (0.62 mmol, 78%) of a light grey powder susceptible to oxidation and hydrolysis.

Elemental analysis for $[\text{C}_7\text{H}_{11}\text{CuN}_3\text{F}_6\text{P}]$ [345.70 g/mol]: Calc. (obs.) C 24.32 (24.70), H 3.21 (3.03), N 12.16 (12.22).

$^1\text{H-NMR}$ (300 MHz, 25 °C, CD_3CN): δ_{H} / ppm = 1.97 (s, 3 H, CNCH_3), 3.79 (s, 6H, CH_3), 7.06 (s, 2H, CHCH).

$^{13}\text{C}\{^1\text{H}\}$ -NMR (75 MHz, 25 °C, CD_3CN): δ_{C} / ppm = 38.3 (CH_3), 123.1 (CHCH). The resonance of the carbene-carbon atom was not detected.

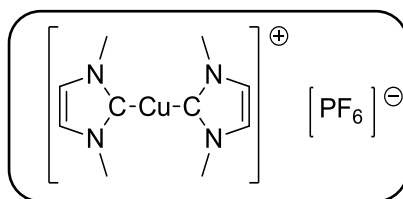
$^{31}\text{P-NMR}$ (202.5 MHz, 25 °C, CD_3CN): δ_{P} / ppm = -144.6 (sept, 1 P, $^1J_{\text{PF}} = 706$ Hz, PF_6).

$^{19}\text{F-NMR}$ (188 MHz, 25 °C, CD_3CN): δ_{F} / ppm = -72.9 (d, 6 F, $^1J_{\text{FP}} = 706$ Hz, PF_6).

HRMS-ESI (m/z): $[\text{M}]^-$ calc. for PF_6 , 144.9636 found, 144.9633.

HRMS-ESI (m/z): $[\text{M}]^+$ calc. for $\text{C}_7\text{H}_{11}\text{CuN}_3$, 200.0244 found, 200.0237.

Synthesis of $[\text{Cu}(\text{Me}_2\text{Im})_2][\text{PF}_6]$ 10



To a suspension of tetrakis(acetonitrile)copper(I) hexafluorophosphate (300 mg, 800 μmol) in 7 mL of THF, 1,3-dimethylimidazol-2-ylidene (154 mg, 1.60 mmol, 154 μL) was added via syringe. The green-grey reaction mixture was stirred for 30 min at room temperature before the solvent was removed under reduced pressure. The crude product was washed with 10 mL of *n*-hexane and dried *in vacuo* to obtain a grey powder.

Yield: 165 mg (0.41 mmol, 51%) of a grey powder susceptible to oxidation and hydrolysis.

Elemental analysis for $[\text{C}_{10}\text{H}_{16}\text{CuN}_4\text{F}_6\text{P}]$ [400.78 g/mol]: Calc. (obs.) C 29.97 (30.32), H 4.02 (3.80), N 13.98 (14.14).

$^1\text{H-NMR}$ (300 MHz, 25 °C, CD_3CN): δ_{H} / ppm = 3.83 (s, 6 H, CH_3), 7.10 (s, 2 H, CHCH).

$^{13}\text{C}\{^1\text{H}\}$ -NMR (75 MHz, 25 °C, CD_3CN): δ_{C} / ppm = 38.5 (CH_3), 123.3 (CHCH). The resonance of the carbene-carbon atom was not detected.

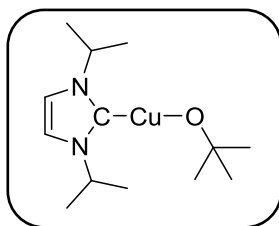
$^{31}\text{P-NMR}$ (202.5 MHz, 25 °C, CD_3CN): δ_{P} / ppm = -144.6 (sept, $^1J_{\text{PF}} = 706$ Hz, PF_6).

^{19}F -NMR (188 MHz, 25 °C, CD_3CN): δ_{F} / ppm = -72.9 (d, 6 F, $^1J_{\text{FP}} = 706$ Hz, PF_6).

HRMS-ESI (m/z): $[\text{M}]^-$ calc. for PF_6 , 144.9636 found, 144.9633.

HRMS-ESI (m/z): $[\text{M}]^+$ calc. for $\text{C}_{10}\text{H}_{16}\text{CuN}_4$, 255.0665 found, 255.0656.

Synthesis of $[\text{Cu}(\text{iPr}_2\text{Im})(\text{O}^t\text{Bu})]$ 15



To a mixture of $[\text{Cu}(\text{iPr}_2\text{Im})(\text{Cl})]$ (200 mg, 796 μmol) and KO^tBu (90.0 mg, 796 μmol) 10 mL of THF were added and the yellow reaction mixture was stirred for 16 h at room temperature. The solvent was removed under reduced pressure. Toluene (10 mL) was added and the suspension filtered through Celite[®]. The solvent was removed under reduced pressure and the crude product was washed with 10 mL of *n*-hexane. The resulting yellow solid was dried *in vacuo*.

Yield: 58 mg (231 μmol , 29%) of a yellow solid.

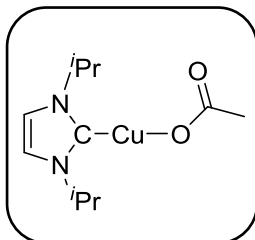
Elemental analysis for $[\text{C}_{13}\text{H}_{25}\text{CuN}_2\text{O}]$ [288.90 g/mol]: Calc. (obs.) C 54.05 (54.55), H 8.72 (8.59), N 9.70 (9.34).

^1H -NMR (200 MHz, 25 °C, C_6D_6): δ_{H} / ppm = 0.99 (d, 12 H, $^3J_{\text{HH}} = 7$ Hz, CHCH_3), 1.79 (s, 9 H, $\text{C}(\text{CH}_3)_3$), 4.66 (sept, 2 H, $^3J_{\text{HH}} = 7$ Hz, CHCH_3), 6.25 (s, 2 H, CHCH).

$^{13}\text{C}\{^1\text{H}\}$ NMR (50 MHz, 25 °C, C_6D_6): δ_{C} / ppm = 23.4 (CHCH_3), 36.6 ($\text{C}(\text{CH}_3)_3$), 53.2 (CHCH_3), 69.1 (OC_q), 116.3 (CHCH), 177.5 (NCN).

HRMS-ASAP (m/z): $[\text{M} + \text{H}]^+$ calc. for $\text{C}_{13}\text{H}_{25}\text{CuN}_2\text{O}$, 289.1336 found, 289.1333.

Synthesis of [Cu(*i*Pr₂Im)(OAc)] 17



Copper(I) acetate (150 mg, 1.22 mmol) was suspended in 10 mL of toluene and 1,3-di-*iso*-propyl-imidazolin-2-ylidene (186 mg, 1.22 mmol, 186 μ L) was added. The red reaction mixture was stirred for 12 h before it was filtered through Celite[®]. Afterwards, the solvent was removed under reduced pressure. The crude product was washed with *n*-hexane and dried *in vacuo* to obtain a beige solid.

Yield: 106 mg (0.39 mmol, 32%) of a beige solid which is which is susceptible to oxidation and hydrolysis.

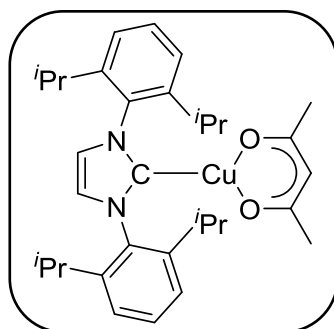
Elemental analysis for [C₁₁H₁₉CuN₂O₂] [274.83 g/mol]: Calc. (obs.) C 48.07 (48.52), H 6.97 (6.94), N 10.19 (9.73).

¹H-NMR (400 MHz, 25 °C, C₆D₆): δ_{H} / ppm = 0.96 (d, 12 H, ³J_{HH} = 7 Hz, CHCH₃), 2.58 (br, 3 H, O₂CCH₃), 4.49 (sept, 2 H, ³J_{HH} = 7 Hz, CHCH₃), 6.23 (s, 2 H, CHCH).

¹³C{¹H}-NMR (100 MHz, 25 °C, C₆D₆): δ_{C} / ppm = 23.1 (C_qCH₃), 23.3 (CHCH₃), 53.3 (CHCH₃), 116.9 (CHCH), 174.5 (NCN), 176.1 (br, C_qCH₃).

HRMS-ASAP (m/z): [M+H]⁺ calc. for C₁₁H₁₉CuN₂O₂, 275.0815 found, 275.0806.

Synthesis of [Cu(Dipp₂Im)(acac)] 18



Acetylacetone (38.0 mg, 380 μ mol, 39 μ L) was added to a stirred solution of [Cu(Dipp₂Im)(O^{*t*}Bu)] (200 mg, 380 μ mol) in 5 mL of THF. The solution turned yellow

immediately. After 16 h at room temperature, the solvent was removed under reduced pressure. The product was dried *in vacuo*.

Yield: 125 mg (227 μmol , 60%) of a yellow solid.

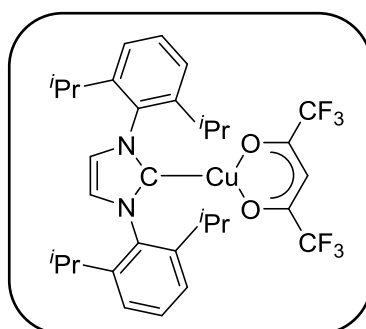
Elemental analysis for $[\text{C}_{32}\text{H}_{43}\text{CuN}_2\text{O}_2]$ [551.25 g/mol]: Calc. (obs.) C 69.72 (69.32), H 7.86 (8.04), N 5.08 (4.74).

$^1\text{H-NMR}$ (200 MHz, 25 °C, C_6D_6): δ_{H} / ppm = 1.15 (d, 12 H, $^3J_{\text{HH}} = 7$ Hz, CHCH_3), 1.54 (d, 12 H, $^3J_{\text{HH}} = 7$ Hz, CHCH_3), 1.70 (s, 6 H, C_qCH_3), 2.91 (sept, 4 H, $^3J_{\text{HH}} = 7$ Hz, CHCH_3), 5.05 (s, 1 H, C_qCHC_q), 6.40 (s, 2 H, CHCH), 7.05 – 7.12 (m, 6 H, $_{\text{aryl}}\text{CH}$).

$^{13}\text{C}\{^1\text{H}\}$ NMR (100 MHz, 25 °C, C_6D_6): δ_{C} / ppm = 24.3, 24.4, 28.2, 29.0, 98.9, 121.7, 124.0, 130.1, 136.3, 146.3, 187.1 (NCN), 188.4 (OC_q).

HRMS-ASAP (m/z): $[\text{M} + \text{H}]^+$ calc. for $\text{C}_{32}\text{H}_{43}\text{CuN}_2\text{O}_2$, 551.2693 found, 551.2682.

Synthesis of $[\text{Cu}(\text{Dipp}_2\text{Im})(\text{hfacac})]$ 19



Hexafluoroacetylacetone (79.0 mg, 380 μmol , 54 μL) was added to a stirred solution of $[\text{Cu}(\text{Dipp}_2\text{Im})(\text{O}^t\text{Bu})]$ (200 mg, 380 μmol) in 5 mL of THF. The solution turned orange immediately. After 16 h at room temperature, the solvent was removed under reduced pressure. The product was dried *in vacuo*.

Yield: 120 mg (182 μmol , 48%) of an orange solid.

Elemental analysis for $[\text{C}_{32}\text{H}_{40}\text{CuF}_6\text{N}_2\text{O}_2]$ [551.25 g/mol]: Calc. (obs.) C 58.31 (59.80), H 5.66 (5.82), N 4.25 (4.53).

Although the present results are outside the range viewed as established for analyzed purity, they are provided to illustrate the best values obtained to date. In addition, the ^1H ,

$^{13}\text{C}\{^1\text{H}\}$ and the ^{19}F NMR spectra as given in Figure 125, Figure 126 and Figure 127 provide evidence for the purity of the compound.

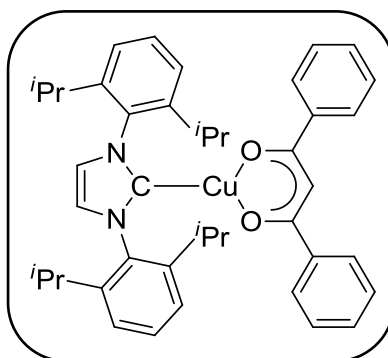
$^1\text{H-NMR}$ (200 MHz, 25 °C, C_6D_6): δ_{H} / ppm = 1.09 (d, 12 H, $^3J_{\text{HH}} = 7$ Hz, CHCH_3), 1.41 (d, 12 H, $^3J_{\text{HH}} = 7$ Hz, CHCH_3), 2.72 (sept, 4 H, $^3J_{\text{HH}} = 7$ Hz, CHCH_3), 5.80 (s, 1 H, C_qCHC_q), 6.36 (s, 2 H, CHCH), 7.04 – 7.06 (m, 4 H, arylCH), 7.12 – 7.14 (m, 2 H, arylCH).

$^{13}\text{C}\{^1\text{H}\}$ NMR (100 MHz, 25 °C, C_6D_6): δ_{C} / ppm = 24.1, 24.2, 29.0, 88.9, 118.4 (q, $^1J_{\text{CF}} = 215$ Hz, CF_3), 122.4, 124.3, 130.6, 135.6, 146.1, 176.3 (q, $^2J_{\text{CF}} = 25$ Hz, OC_q), 184.4 (NCN).

$^{19}\text{F-NMR}$ (188 MHz, 25 °C, C_6D_6): δ_{F} / ppm = -76.5 (s, CF_3).

HRMS-ASAP (m/z): $[\text{M}]^+$ calc. for $\text{C}_{32}\text{H}_{37}\text{CuF}_6\text{N}_2\text{O}_2$, 658.2050 found, 658.2040.

Synthesis of $[\text{Cu}(\text{Dipp}_2\text{Im})(\text{DBM})]$ 20



Dibenzoylmethane (85.0 mg, 380 μmol) was added to a stirred solution of $[\text{Cu}(\text{Dipp}_2\text{Im})(\text{O}^t\text{Bu})]$ (200 mg, 380 μmol) in 5 mL of THF. The solution turned orange immediately. After 16 h at room temperature, the solvent was removed under reduced pressure. The product was dried *in vacuo*.

Yield: 185 mg (274 μmol , 72%) of an orange solid.

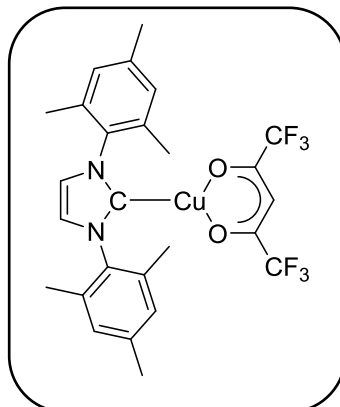
Elemental analysis for $[\text{C}_{42}\text{H}_{47}\text{CuN}_2\text{O}_2]$ [675.40 g/mol]: Calc. (obs.) C 74.69 (74.60), H 7.01 (6.92), N 4.15 (3.95).

$^1\text{H-NMR}$ (200 MHz, 25 °C, C_6D_6): δ_{H} / ppm = 1.17 (d, 12 H, $^3J_{\text{HH}} = 7$ Hz, CHCH_3), 1.59 (d, 12 H, $^3J_{\text{HH}} = 7$ Hz, CHCH_3), 2.93 (sept, 4 H, $^3J_{\text{HH}} = 7$ Hz, CHCH_3), 6.42 (s, 2 H, CHCH), 6.52 (s, 1 H, C_qCHC_q), 7.03 – 7.12 (m, 6 H, arylCH), 7.19 – 7.23 (m, 6 H, arylCH), 7.87 – 7.91 (m, 4 H, arylCH).

$^{13}\text{C}\{^1\text{H}\}$ NMR (100 MHz, 25 °C, C_6D_6): δ_{C} / ppm = 24.2, 24.6, 29.1, 93.2, 121.8, 124.1, 127.5, 128.0, 129.6, 130.2, 136.2, 143.1, 146.2, 183.7 (OC_q), 186.8 (NCN).

HRMS-ASAP (m/z): $[M + H]^+$ calc. for $C_{42}H_{47}CuN_2O_2$, 675.3006 found, 675.2985.

Synthesis of $[Cu(Mes_2Im)(hfacac)]$ 21



To a Schlenk tube charged with $[Cu(Mes_2Im)(Cl)]$ (202 mg, 499 μ mol) and KO^tBu (56 mg, 499 μ mol), 5 mL of THF was added, before hexafluoroacetylacetone (103 mg, 499 μ mol, 70 μ L) was added via syringe. After 2 h at room temperature the orange reaction mixture was filtered through Celite[®]. The solvent was removed under reduced pressure and the product was dried *in vacuo*.

Yield: 80 mg (139 μ mol, 28%) of an orange solid.

Elemental analysis for $[C_{26}H_{25}CuF_6N_2O_2]$ [575.03 g/mol]: Calc. (obs.) C 54.31 (52.65), H 4.38 (4.99), N 4.87 (5.95).

Although the present results are outside the range viewed as established for analyzed purity, they are provided to illustrate the best values obtained to date. In addition, the 1H , $^{13}C\{^1H\}$ and the ^{19}F NMR spectra as given in Figure 128, Figure 129 and Figure 130 provide evidence for the purity of the compound.

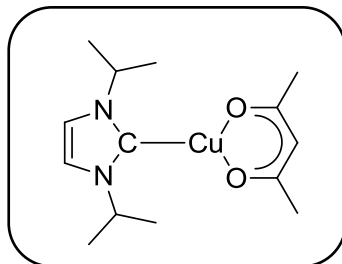
1H -NMR (400 MHz, 25 $^\circ$ C, C_6D_6): δ_H / ppm = 2.01 (s, 12 H, *o*-CH₃), 2.02 (s, 6 H, *p*-CH₃), 5.86 (br, 1 H, C_qCHC_q), 6.06 (s, 2 H, NCHCHN), 6.68 (s, 4 H, *m*-CH).

$^{13}C\{^1H\}$ NMR (100 MHz, 25 $^\circ$ C, C_6D_6): δ_C / ppm = 17.6 (*o*-CH₃), 21.0 (*p*-CH₃), 89.0 (br, C_qCH), 118.5 (br, q, CF₃), 121.4 (NCHCHN), 129.5 (*m*-CH), 135.1 (*o*-C_q), 136.1 (*i*-C_q), 139.3 (*p*-C_q), 176.3 (br, OC_q), 182.4 (NC_qN).

^{19}F -NMR (366 MHz, 25 $^\circ$ C, C_6D_6): δ_F / ppm = -76.4 (s, CF₃).

HRMS-ASAP (m/z): $[M]^+$ calc. for $C_{26}H_{25}CuN_2O_2F_6$, 574.1111 found, 574.1106.

Synthesis of [Cu(ⁱPr₂Im)(acac)] 22



To a Schlenk tube charged with [Cu(ⁱPr₂Im)(Cl)] (125 mg, 498 μmol) and KO^tBu (56 mg, 498 μmol), 5 mL of THF was added, before acetylacetonate (47 mg, 498 μmol, 52 μL) was added via syringe. After 1 h at room temperature, the yellow reaction mixture was filtered through Celite®. The solvent was removed under reduced pressure and the product was dried *in vacuo*.

Yield: 85 mg (270 μmol, 54%) of a yellow solid.

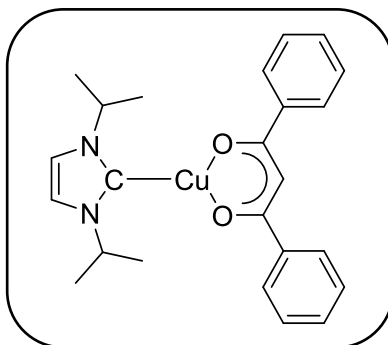
Elemental analysis for [C₁₄H₂₃CuN₂O₂] [314.90 g/mol]: Calc. (obs.) C 53.40 (53.82), H 7.36 (7.29), N 8.90 (9.18).

¹H-NMR (200 MHz, 25 °C, C₆D₆): δ_H / ppm = 1.02 (d, 12 H, ³J_{HH} = 7 Hz, CHCH₃), 2.12 (s, 6 H, C_qCH₃), 4.89 (sept, 2 H, ³J_{HH} = 7 Hz, CHCH₃), 5.57 (s, 1 H, C_qCHC_q), 6.21 (s, 2 H, CHCH).

¹³C{¹H} NMR (100 MHz, 25 °C, C₆D₆): δ_C / ppm = 23.5, 28.8, 52.9, 99.6, 115.6, 180.4 (NCN), 189.5 (OC_q).

HRMS-ASAP (m/z): [M + H]⁺ calc. for C₁₄H₂₄CuN₂O₂, 315.1128 found, 315.1123.

Synthesis of [Cu(ⁱPr₂Im)(DBM)] 23



To a Schlenk tube charged with [Cu(ⁱPr₂Im)(Cl)] (125 mg, 498 μmol) and KO^tBu (56 mg, 498 μmol) and dibenzoylmethane (112 mg, 498 μmol), 5 mL of THF was added. After 1 h at

room temperature, the bright orange reaction mixture was filtered through Celite®. The solvent was removed under reduced pressure and the product was dried *in vacuo*.

Yield: 30 mg (68 μmol , 14%) of an orange slurry solid.

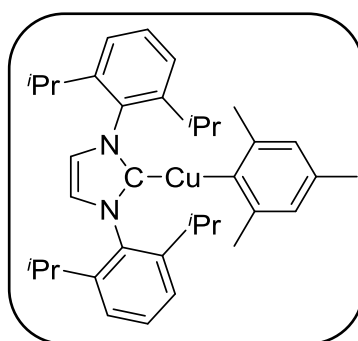
Elemental analysis for $[\text{C}_{24}\text{H}_{27}\text{CuN}_2\text{O}_2]$ [439.04 g/mol]: Calc. (obs.) C 65.66 (65.68), H 6.20 (6.07), N 6.38 (5.54).

$^1\text{H-NMR}$ (200 MHz, 25 °C, C_6D_6): δ_{H} / ppm = 1.06 (d, 12 H, $^3J_{\text{HH}} = 7$ Hz, CHCH_3), 4.81 (sept, 2 H, $^3J_{\text{HH}} = 7$ Hz, CHCH_3), 6.34 (s, 2 H, CHCH), 6.95 (s, 1 H, C_qCHC_q) 7.18 – 7.28 (m, 6 H, arylCH), 8.19-8.22 (m, 4 H, arylCH).

$^{13}\text{C}\{^1\text{H}\}$ NMR (100 MHz, 25 °C, C_6D_6): δ_{C} / ppm = 23.5, 53.1, 93.8, 116.2, 127.7, 128.3, 129.8, 143.9, 178.8 (NCN), 184.8 (OC_q).

HRMS-ASAP (m/z): $[\text{M} + \text{H}]^+$ calc. for $\text{C}_{24}\text{H}_{27}\text{CuN}_2\text{O}_2$, 439.1441 found, 439.1437.

Synthesis of $[\text{Cu}(\text{Dipp}_2\text{Im})(\text{Mes})]$ 24



A solution of 1,3-bis-(2,6-di-*iso*-propylphenyl)imidazolin-2-ylidene (4.15 g, 10.7 mmol) in 30 mL of toluene was transferred to a solution of mesitylcopper(I) (1.96 mg, 10.7 mmol) in 100 mL of toluene via cannula and the solution was stirred overnight at room temperature. The solvent was removed under reduced pressure to obtain the crude product, which was washed with *n*-hexane and dried *in vacuo*.

Yield: 3.45 g (8.88 mmol, 83%) of an off-white solid.

Elemental analysis for $[\text{C}_{36}\text{H}_{47}\text{CuN}_2]$ [571.32 g/mol]: Calc. (obs.) C 75.68 (76.28), H 8.29 (8.44), N 4.90 (5.32).

Although the present results are outside the range viewed as established for analyzed purity, they are provided to illustrate the best values obtained to date. In addition, the ^1H

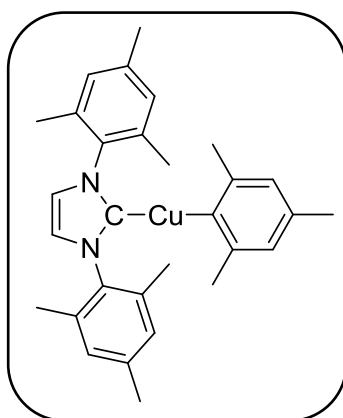
and the $^{13}\text{C}\{^1\text{H}\}$ NMR spectra as given in Figure 131 and Figure 132 provide evidence for the purity of the compound.

$^1\text{H-NMR}$ (200 MHz, 25 °C, C_6D_6): $\delta_{\text{H}} / \text{ppm} = 1.10$ (d, 12 H, $^3J_{\text{HH}} = 7$ Hz, CHCH_3), 1.37 (d, 12 H, $^3J_{\text{HH}} = 7$ Hz, CHCH_3), 2.08 (s, 6 H, $m\text{-CH}_3$), 2.30 (s, 3 H, $p\text{-CH}_3$), 2.63 (sept, 4 H, $^3J_{\text{HH}} = 7$ Hz, CHCH_3), 6.31 (s, 2 H, CHCH), 6.91 (s, 2 H, $m\text{-CH}$), 7.08 – 7.12 (m, 4 H, $m^{\text{Dipp-CH}}$), 7.23 – 7.31 (m, 2 H, $p\text{-CH}$).

$^{13}\text{C}\{^1\text{H}\}$ NMR (50 MHz, 25 °C, C_6D_6): $\delta_{\text{C}} / \text{ppm} = 21.7$ ($p\text{-CH}_3$), 23.8 (CHCH_3), 25.1 (CHCH_3), 28.0 ($m\text{-CH}_3$), 29.1 (CHCH_3), 122.1 (CHCH), 124.2 ($m^{\text{Dipp-CH}}$), 124.6 ($m\text{-C}_q$), 130.4 ($p^{\text{Dipp-CH}}$), 132.9 ($p\text{-C}_q$), 135.6 ($i^{\text{Dipp-C}_q}$), 146.1 ($o^{\text{Dipp-C}_q}$), 147.2 (arylCH), 163.3 (arylCH), 186.4 (NCN).

HRMS-ASAP (m/z): $[\text{M} + \text{H}]^+$ calc. for $\text{C}_{36}\text{H}_{48}\text{CuN}_2$, 571.3108 found, 571.3101.

Synthesis of $[\text{Cu}(\text{Mes}_2\text{Im})(\text{Mes})]$ 25



A solution of 1,3-bis-(2,4,6-trimethylphenyl)imidazolin-2-ylidene (498 mg, 1.64 mmol) in 10 mL of toluene was transferred to a solution of mesitylcopper(I) (300 mg, 10.7 mmol) in 10 mL of toluene via cannula and the reaction was stirred overnight at room temperature. The solvent was removed under reduced pressure to obtain the crude product, which was washed with *n*-hexane and dried *in vacuo*.

Yield: 604 mg (1.24 mmol, 75%) of an off-white solid.

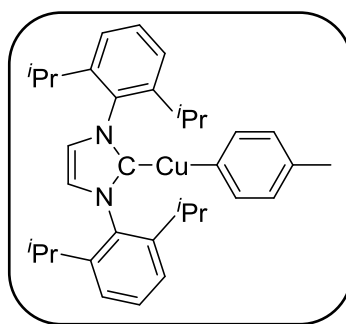
Elemental analysis for $[\text{C}_{30}\text{H}_{35}\text{CuN}_2]$ [487.16 g/mol]: Calc. (obs.) C 73.96 (73.62), H 7.24 (7.44), N 5.75 (6.04).

$^1\text{H-NMR}$ (200 MHz, 25 °C, C_6D_6): $\delta_{\text{H}} / \text{ppm} = 2.02$ (s, 12 H, $o^{\text{Mes-CH}_3}$), 2.12 (s, 6 H, $p^{\text{Mes-CH}_3}$), 2.30 (s, 6 H, $o\text{-CH}_3$), 2.31 (s, 3 H, $p\text{-CH}_3$), 6.04 (s, 2 H, CHCH), 6.75 (s, 4 H, $m^{\text{Mes-CH}}$), 6.94 (s, 2 H, $m\text{-CH}$).

$^{13}\text{C}\{^1\text{H}\}$ NMR (50 MHz, 25 °C, C_6D_6): $\delta_{\text{C}} / \text{ppm} = 17.8$ ($o^{\text{Mes-CH}_3}$), 21.0 ($p^{\text{Mes-CH}_3}$), 21.7 ($p\text{-CH}_3$), 28.3 ($o\text{-CH}_3$), 121.1 (CHCH), 124.6 ($m\text{-CH}$), 129.4 ($m^{\text{Mes-CH}}$), 132.8 (arylCH), 135.1 ($o^{\text{Mes-CH}}$), 136.2 ($i^{\text{Mes-C}_q}$), 139.1 ($p^{\text{Mes-C}_q}$), 147.2 (arylCH), 164.0 ($i\text{-C}_q$), 184.7 (NCN).

HRMS-ASAP (m/z): $[\text{M} + \text{H}]^+$ calc. for $\text{C}_{30}\text{H}_{35}\text{CuN}_2$, 487.2169 found, 487.2159.

Synthesis of $[\text{Cu}(\text{Dipp}_2\text{Im})(p\text{-tolyl})]$ 27



To a suspension of $[\text{Cu}(\text{Dipp}_2\text{Im})(\text{O}^t\text{Bu})]$ (1.10 g, 2.10 mmol) in 50 mL of toluene p -tolyl-pinacolborane (458 mg, 2.10 mmol) and was added via syringe and the solution was stirred for 2 h at room temperature. The reaction mixture was concentrated to ca. 10 mL under reduced pressure and 60 mL of n -hexane were added to afford a white precipitate. The solid was collected by filtration and dried *in vacuo*.

Yield: 0.88 g (1.62 mmol, 77%) of a colorless solid.

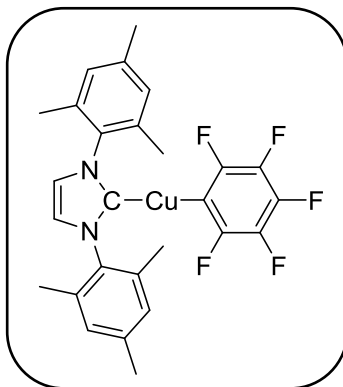
Elemental analysis for $[\text{C}_{34}\text{H}_{43}\text{CuN}_2]$ [543.28 g/mol]: Calc. (obs.) C 75.17 (74.85), H 7.98 (7.86), N 5.16 (5.14).

$^1\text{H-NMR}$ (200 MHz, 25 °C, C_6D_6): $\delta_{\text{H}} / \text{ppm} = 1.10$ (d, 12 H, $^3J_{\text{HH}} = 7$ Hz, CHCH₃), 1.42 (d, 12 H, $^3J_{\text{HH}} = 7$ Hz, CHCH₃), 2.21 (s, 3 H, $p\text{-CH}_3$), 2.66 (sept, 4 H, $^3J_{\text{HH}} = 7$ Hz, CHCH₃), 6.29 (s, 2 H, CHCH), 7.06 – 7.10 (m, 6 H, $m\text{-CH} + m^{\text{Dipp-CH}}$), 7.19 – 7.27 (m, 2 H, $p^{\text{Dipp-CH}}$), 7.57 – 7.61 (m, 2 H, $o\text{-CH}$).

$^{13}\text{C}\{^1\text{H}\}$ NMR (50 MHz, 25 °C, C_6D_6): δ_{C} / ppm = 21.8 (CH_3), 23.7 (CHCH_3), 25.2 (CHCH_3), 29.0 (CHCH_3), 122.3 (CHCH), 124.2 ($m^{\text{Dipp-CH}}$), 127.2 ($_{\text{aryl}}\text{CH}$), 130.5 ($p^{\text{Dipp-CH}}$), 132.4 ($_{\text{aryl}}\text{CH}$), 135.3 ($i^{\text{Dipp-Cq}}$), 140.8 ($o\text{-Cq}$), 145.9 ($o\text{-Dipp-Cq}$), 161.4 ($i\text{-Cq}$), 186.0 (NCN).

HRMS-ASAP (m/z): $[\text{M} + \text{H}]^+$ calc. for $\text{C}_{33}\text{H}_{43}\text{CuN}_2$, 543.2795 found, 543.2793.

Synthesis of $[\text{Cu}(\text{Mes}_2\text{Im})(\text{C}_6\text{F}_5)]$ 29



To a suspension of $[\text{Cu}(\text{Mes}_2\text{Im})(\text{Cl})]$ (1.45 g, 3.60 mmol) in 20 mL of THF, a 1.23 M solution of $\text{C}_6\text{F}_5\text{MgBr}$ (2.92 mL, 3.60 mmol) in THF was added dropwise. After stirring for 1 h at room temperature, 15 mL of 1,4-dioxane was added to precipitate the magnesium salts. The suspension was filtered and the solvent was removed under reduced pressure to obtain a beige solid, which was dissolved in toluene. Then 1 mL of 1,4-dioxane was added and the solution was stirred for 1 h at room temperature. As nothing precipitated, the solvent was removed under reduced pressure and the residue was washed with 5 mL of *n*-hexane and dried *in vacuo*.

Yield: 503 mg (0.94 mmol, 26%) of a light grey solid.

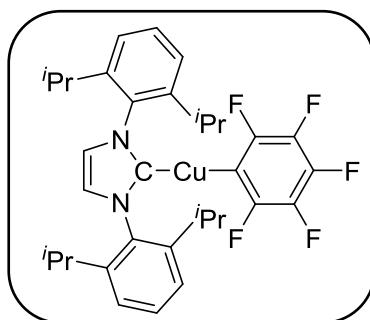
Elemental analysis for $[\text{C}_{27}\text{H}_{24}\text{CuF}_5\text{N}_2]$ [535.04 g/mol]: Calc. (obs.) C 60.61 (60.57), H 4.52 (4.57), N 5.24 (5.36).

$^1\text{H-NMR}$ (200 MHz, 25 °C, C_6D_6): δ_{H} / ppm = 1.99 (s, 12 H, $o\text{-CH}_3$), 2.06 (s, 6 H, $p\text{-CH}_3$), 6.04 (s, 2 H, CHCH), 6.71 (s, 4 H, $m\text{-CH}$).

$^{13}\text{C}\{^1\text{H}\}$ NMR (50 MHz, 25 °C, C_6D_6): δ_{C} / ppm = 17.7 ($o\text{-CH}_3$), 21.0 ($p\text{-CH}_3$), 121.8 (CHCH), 129.6 ($m^{\text{Mes-CH}}$), 134.7 ($o^{\text{Mes-Cq}}$), 135.6 ($i\text{-Cq}$), 139.5 ($p^{\text{Mes-Cq}}$), 148.9-149.2 (m, $m\text{-CF}$), 151.1 – 151.4 ($m+o\text{-CF}$), 181.5 (NCN).

^{19}F -NMR (188 MHz, 25 °C, C_6D_6): δ_{F} / ppm = -112.0 (m, 2 F, *o*-F), -160.9 (m, 1 F, *p*-F), -163.3 (m, 2 F, *m*-F).

Synthesis of $[\text{Cu}(\text{Dipp}_2\text{Im})(\text{C}_6\text{F}_5)]$ 30



To a suspension of $[\text{Cu}(\text{Dipp}_2\text{Im})(\text{Cl})]$ (1.40 g, 2.87 mmol) in 20 mL of THF, a 1.23 M solution of $\text{C}_6\text{F}_5\text{MgBr}$ (2.33 mL, 2.87 mmol) in THF was added dropwise. After stirring for 1 h at room temperature, 10 mL of 1,4-dioxane was added to precipitate the magnesium salts. The suspension was filtered and the solvent was removed under reduced pressure to obtain a beige solid, which was dissolved in toluene. Then, 1 mL of 1,4-dioxane was added and the solution was stirred for 1 h at room temperature. The solvent was removed under reduced pressure and the residue was washed with 5 mL of *n*-hexane and dried *in vacuo*.

Yield: 1.15 g (1.86 mmol, 65%) of a beige solid.

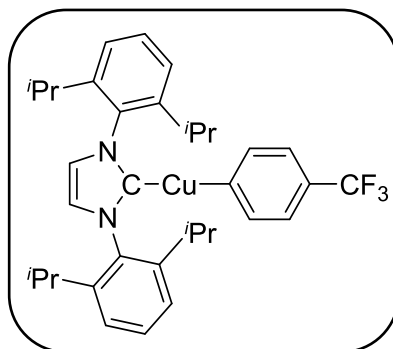
Elemental analysis for $[\text{C}_{33}\text{H}_{36}\text{CuF}_5\text{N}_2]$ [619.20 g/mol]: Calc. (obs.) C 64.01 (63.89), H 5.86 (5.83), N 4.52 (4.66).

^1H -NMR (200 MHz, 25 °C, C_6D_6): δ_{H} / ppm = 1.09 (d, 12 H, $^3J_{\text{HH}} = 7$ Hz, CHCH_3), 1.40 (d, 12 H, $^3J_{\text{HH}} = 7$ Hz, CHCH_3), 2.59 (sept, 4 H, $^3J_{\text{HH}} = 7$ Hz, CHCH_3), 6.30 (s, 2 H, CHCH), 7.04 – 7.08 (m, 4 H, *m*-CH), 7.16 – 7.24 (m, 2 H, *p*-CH).

$^{13}\text{C}\{^1\text{H}\}$ NMR (50 MHz, 25 °C, C_6D_6): δ_{C} / ppm = 23.6 (CHCH_3), 24.8 (CHCH_3), 28.9 (CHCH_3), 122.5 (CHCH), 124.1 (*m*^{Dipp}-CH), 130.7 (*p*^{Dipp}-CH), 134.6 (*i*^{Dipp}-C_q), 145.7 (*o*^{Dipp}-C_q), 183.1 (NCN). The carbon atoms of the fluorinated phenyl substituent were not detected.

^{19}F -NMR (188 MHz, 25 °C, C_6D_6): δ_{F} / ppm = -112.3 (m, 2 F, *o*-CF), -160.9 (m, 1 F, *p*-CF), -163.4 (m, 2 F, *m*-CF).

HRMS-ASAP (m/z): $[\text{M}]^+$ calc. for $\text{C}_{33}\text{H}_{36}\text{CuF}_5\text{N}_2$, 618.2089 found, 618.2084.

Synthesis of $[\text{Cu}(\text{Dipp}_2\text{Im})(4\text{-CF}_3\text{-C}_6\text{H}_4)]$ 31

To a suspension of $[\text{Cu}(\text{Dipp}_2\text{Im})(\text{Cl})]$ (1.60 g, 3.28 mmol) in 20 mL of THF, a 1.05 M solution of $4\text{-CF}_3\text{-C}_6\text{H}_4\text{MgBr}$ (3.12 mL, 3.28 mmol) in THF was added dropwise. After stirring for 1 h at room temperature 10 mL of 1,4-dioxane was added to precipitate the magnesium salts. The suspension was filtered and the solvent was removed under reduced pressure to obtain a beige solid, which was dissolved in toluene. Then, 1 mL of 1,4-dioxane was added and the solution was stirred for 1 h at room temperature. The solvent was removed under reduced pressure and the residue was washed with 5 mL of *n*-hexane and dried *in vacuo*.

Yield: 826 mg (1.38 mmol, 42%) of a light reddish solid.

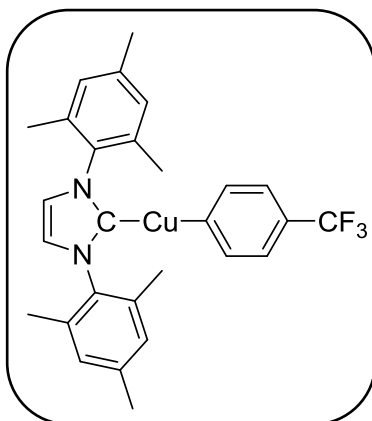
Elemental analysis for $[\text{C}_{34}\text{H}_{40}\text{CuF}_3\text{N}_2]$ [597.25 g/mol]: Calc. (obs.) C 68.38 (68.39), H 6.75 (7.03), N 4.69 (4.94).

$^1\text{H-NMR}$ (200 MHz, 25 °C, C_6D_6): δ_{H} / ppm = 1.09 (d, 12 H, $^3J_{\text{HH}} = 7$ Hz, CHCH_3), 1.36 (d, 12 H, $^3J_{\text{HH}} = 7$ Hz, CHCH_3), 2.58 (sept, 4 H, $^3J_{\text{HH}} = 7$ Hz, CHCH_3), 6.27 (s, 2 H, CHCH), 7.04 – 7.09 (m, 4 H, $m^{\text{Dipp-CH}}$), 7.16 – 7.24 (m, 2 H, $p^{\text{Dipp-CH}}$), 7.38 – 7.42 (m, 2 H, $o\text{-CH}$) 7.54 – 7.59 (m, 2 H, $m\text{-CH}$).

$^{13}\text{C}\{^1\text{H}\}$ NMR (100 MHz, 25 °C, C_6D_6): δ_{C} / ppm = 23.7 (CHCH_3), 25.1 (CHCH_3), 29.0 (CHCH_3), 122.0 (q, $^1J_{\text{CF}} = 4$ Hz, CF_3), 122.6 (CHCH), 124.3 ($m^{\text{Dipp-CH}}$), 126.1 (q, $^2J_{\text{CF}} = 31$ Hz, $p\text{-C}_q$), 130.7 ($p^{\text{Dipp-CH}}$), 135.0 ($i^{\text{Dipp-C}_q}$), 140.5 ($_{\text{aryl}}\text{CH}$), 145.9 ($o^{\text{Dipp-C}_q}$), 171.9 ($i\text{-C}_q$), 185.0 (NCN).

$^{19}\text{F-NMR}$ (188 MHz, 25 °C, C_6D_6): δ_{F} / ppm = -61.6 (s, CF_3).

HRMS-ASAP (m/z): $[\text{M} + \text{H}]^+$ calc. for $\text{C}_{34}\text{H}_{40}\text{CuF}_3\text{N}_2$, 597.2512 found, 597.2510.

Synthesis of [Cu(Mes₂Im)(4-CF₃-C₆H₄)] 32

To a suspension of [Cu(Mes₂Im)(Cl)] (1.68 g, 4.16 mmol) in 20 mL of THF, a 1.05 M solution of (4-CF₃-C₆H₄)MgBr (3.38 mL, 3.28 mmol) in THF was added dropwise. After stirring for 1 h at room temperature, 10 mL of 1,4-dioxane was added to precipitate the magnesium salts. The suspension was filtered and the solvent was removed under reduced pressure to obtain a beige solid, which was dissolved in toluene. Then 1 mL of 1,4-dioxane was added and the solution stirred for 1 hour at room temperature. The solvent was removed under reduced pressure and the residue was washed with 5 mL of *n*-hexane and dried *in vacuo*.

Yield: 1.90 g (3.70 mmol, 89%) of a light brown solid.

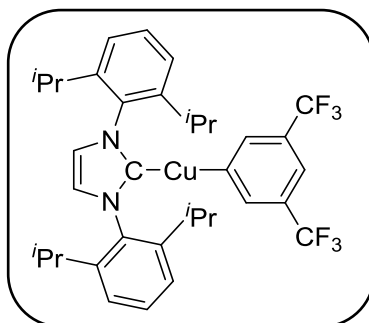
Elemental analysis for [C₂₈H₂₈CuF₃N₂] [513.09 g/mol]: Calc. (obs.) C 65.55 (65.88), H 5.50 (5.24), N 5.46 (5.69).

¹H-NMR (200 MHz, 25 °C, C₆D₆): δ_H / ppm = 1.99 (s, 12 H, *o*-CH₃), 2.08 (s, 6 H, *p*^{Mes}-CH₃), 6.01 (s, 2 H, CHCH), 6.71 (s, 4 H, *m*^{Mes}-CH), 7.40 – 7.44 (m, 2 H, *m*-CH), 7.67 – 7.72 (m, 2 H, *o*-CH).

¹³C{¹H}-NMR (50 MHz, 25 °C, C₆D₆): δ_C / ppm = 17.7 (*o*-CH₃), 20.9 (*p*-CH₃), 121.3 (CHCH), 121.8 (q, ¹J_{CF} = 3.92 Hz, CF₃), 129.4 (*m*^{Mes}-CH), 134.6 (*o*^{Mes}-CH), 135.7 (*i*-C_q), 139.1 (*p*^{Mes}-C_q), 140.4 (arylCH), 172.0 (arylC_q), 183.3 (NCN).

¹⁹F-NMR (188 MHz, 25 °C, C₆D₆): δ_F / ppm = -61.5 (s, CF₃).

HRMS-ASAP (m/z): [M]⁺ calc. for C₂₈H₂₈CuF₃N₂, 513.1573 found, 513.1569.

Synthesis of [Cu(Dipp₂Im)(3,5-(CF₃)₂-C₆H₃)] 33

To a suspension of [Cu(Dipp₂Im)(Cl)] (1.50 g, 3.47 mmol) in 25 mL of THF, a 1.05 M solution of (3,5-(CF₃)₂-C₆H₃)MgBr (3.30 mL, 3.47 mmol) in THF was added dropwise. After stirring for 1 h at room temperature 10 mL of 1,4-dioxane was added to precipitate the magnesium salts. The suspension was filtered and the solvent was removed under reduced pressure to obtain a beige solid, which was dissolved in toluene. Then, 1 mL of 1,4-dioxane was added and the solution was stirred for 1 h at room temperature. The solvent was removed under reduced pressure and the residue was washed with 5 mL of *n*-hexane and dried *in vacuo*.

Yield: 1.74 g (2.62 mmol, 75%) of a beige solid.

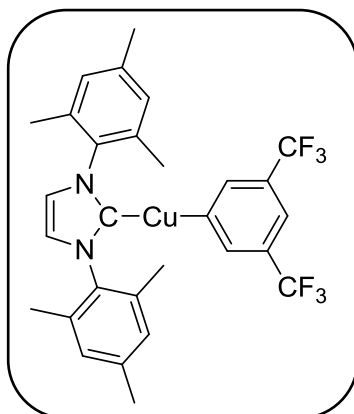
Elemental analysis for [C₃₅H₃₉CuF₆N₂] [665.25 g/mol]: Calc. (obs.) C 63.19 (63.07), H 5.91 (5.86), N 4.21 (4.26).

¹H-NMR (200 MHz, 25 °C, C₆D₆): δ_H / ppm = 1.06 (d, 12 H, ³J_{HH} = 7 Hz, CHCH₃), 1.31 (d, 12 H, ³J_{HH} = 7 Hz, CHCH₃), 2.55 (sept, 4 H, ³J_{HH} = 7 Hz, CHCH₃), 6.26 (s, 2 H, CHCH), 7.04 – 7.08 (m, 4 H, *m*^{Dipp}-CH), 7.20 – 7.28 (m, 2 H, *p*^{Dipp}-CH), 7.64 (br, 1 H, *p*-CH) 7.87 (br, 2 H, *m*-CH).

¹³C{¹H} NMR (50 MHz, 25 °C, C₆D₆): δ_C / ppm = 23.6 (CHCH₃), 25.0 (CHCH₃), 29.0 (CHCH₃), 117.9 (q, ¹J_{CF} = 4 Hz, CF₃), 122.6 (CHCH), 123.1 (*aryl*CH), 124.3 (*m*^{Dipp}-CH), 126.8 (*aryl*CH), 130.8 (*p*^{Dipp}-CH), 135.0 (*i*^{Dipp}-CH), 139.5 (br, *m*-C_q), 145.8 (*o*^{Dipp}-CH), 168.2 (*i*-C_q), 184.4 (NCN).

¹⁹F-NMR (188 MHz, 25 °C, C₆D₆): δ_F / ppm = -62.1 (s, CF₃).

HRMS-ASAP (m/z): [M+H]⁺ calc. for C₃₅H₃₉CuF₆N₂, 665.2386 found, 665.2386.

Synthesis of $[\text{Cu}(\text{Mes}_2\text{Im})(3,5\text{-(CF}_3)_2\text{-C}_6\text{H}_3)]$ 34

To a suspension of $[\text{Cu}(\text{Mes}_2\text{Im})(\text{Cl})]$ (1.34 g, 3.32 mmol) in 20 mL of THF, a 1.05 M solution of $(3,5\text{-(CF}_3)_2\text{-C}_6\text{H}_3)\text{MgBr}$ (3.16 mL, 3.32 mmol) in THF was added dropwise. After stirring for 1 h at room temperature, 15 mL of 1,4-dioxane was added to precipitate the magnesium salts. The suspension was filtered and the solvent was removed under reduced pressure to obtain a beige solid, which was dissolved in toluene. Then, 1 mL of 1,4-dioxane was added and the solution stirred for 1 h at room temperature. The was removed under reduced pressure and the residue was washed with 5 mL of *n*-hexane and dried *in vacuo*.

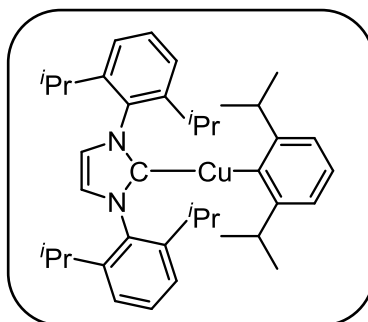
Yield: 1.07 g (1.84 mmol, 56%) of a beige solid.

Elemental analysis for $[\text{C}_{29}\text{H}_{27}\text{CuF}_6\text{N}_2]$ [581.09 g/mol]: Calc. (obs.) C 59.94 (59.80), H 4.68 (4.66), N 4.82 (4.49).

$^1\text{H-NMR}$ (200 MHz, 25 °C, C_6D_6): δ_{H} / ppm = 1.94 (s, 12 H, *o*- CH_3), 2.12 (s, 6 H, *p*- CH_3), 6.00 (s, 2 H, *CHCH*), 6.73 (s, 4 H, *m*^{Mes}-CH), 7.67 (br, 1 H, *p*-CH), 7.93 (m, 2 H, *o*-CH).

$^{13}\text{C}\{^1\text{H}\}$ -NMR (50 MHz, 25 °C, C_6D_6): δ_{C} / ppm = 17.6 (*o*^{Mes}- CH_3), 20.1 (*p*^{Mes}- CH_3), 117.9 (q, $^1J_{\text{CF}} = 4$ Hz, CF_3), 121.5 (*CHCH*), 129.7 (*m*^{Mes}-CH), 134.7 (*o*^{Mes}- C_q), 135.7 (*i*- C_q), 139.7 (*p*^{Mes}- C_q), 168.5, 183.0 (NCN).

$^{19}\text{F-NMR}$ (188 MHz, 25 °C, C_6D_6): δ_{F} / ppm = -62.1 (s, CF_3).

Synthesis of [Cu(Dipp₂Im)(Dipp)] 35

To a suspension of [Cu(Dipp₂Im)Cl] (1.50 g, 3.28 mmol) in 10 mL of THF, a 0.55 M solution of 2,6-di-*iso*-propyl-phenyl magnesium bromide (6.0 mL, 3.28 mmol) in THF was added dropwise. After stirring for 24 h at room temperature, 2 mL of 1,4-dioxane was added to precipitate the magnesium salts. The milky suspension was filtered through Celite® and the solvent was removed under reduced pressure to obtain a white solid, which was dissolved in toluene. Then, 1 mL of 1,4-dioxane was added and the solution was stirred for 1 h at room temperature. The solvent was removed under reduced pressure and the residue was washed with 6 mL of *n*-hexane and dried *in vacuo*.

Yield: 850 mg (1.42 mmol, 42%) of a colorless solid.

Elemental analysis for [C₃₉H₅₃CuN₂] [613.41 g/mol]: Calc. (obs.) C 76.36 (75.89), H 8.71 (9.47), N 4.57 (4.76).

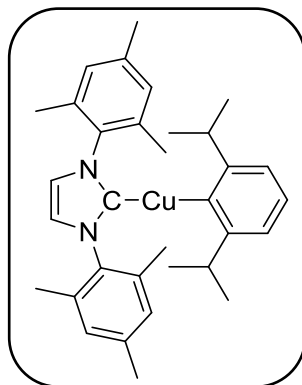
Although the present results are outside the range viewed as established for analyzed purity, they are provided to illustrate the best values obtained to date. In addition, the ¹H and the ¹³C{¹H} NMR spectra as given in Figure 133 and Figure 134 provide evidence for the purity of the compound.

¹H-NMR (200 MHz, 25 °C, C₆D₆): δ_H / ppm = 1.10 (d, 12 H, ³J_{HH} = 7 Hz, ^{Dipp}-CHCH₃), 1.12 (d, 12 H, ³J_{HH} = 7 Hz, ^{Dipp}-CHCH₃), 1.38 (d, 12 H, ³J_{HH} = 7 Hz, ^{Dipp}-CHCH₃), 2.38 (sept, 2 H, ³J_{HH} = 7 Hz, ^{Dipp}-CHCH₃), 2.64 (sept, 4 H, ³J_{HH} = 7 Hz, ^{Dipp}-CHCH₃), 6.33 (s, 2 H, CHCH), 7.09-7.13 (m, 6 H, *m*-CH), 7.23-7.34 (m, 3 H, *p*-CH).

¹³C{¹H} NMR (50 MHz, 25 °C, C₆D₆): δ_C / ppm = 24.0 (^{Dipp}-CHCH₃), 25.0 (^{Dipp}-CHCH₃), 26.3 (^{Dipp}-CHCH₃), 29.1 (^{Dipp}-CHCH₃), 41.4 (CHCH₃), 120.0 (arylCH), 122.2 (CHCH), 124.4 (*m*^{Dipp}-CH), 125.4 (arylCH), 130.4 (*p*^{Dipp}-CH), 135.5 (*i*^{Dipp}-C_q), 145.8 (*o*^{Dipp}-C_q), 158.9 (*i*-C_q), 166.4 (arylCH), 185.8 (NCN).

HRMS-ASAP (m/z): $[M + H]^+$ calc. for $C_{39}H_{53}CuN_2$, 613.3578 found 613.3573.

Synthesis of $[Cu(Mes_2Im)(Dipp)]$ 36



To a suspension of $[Cu(Mes_2Im)Cl]$ (1.51 g, 3.74 mmol) in 10 mL of THF, a 0.55 M solution of 2,6-di-*iso*-propyl-phenyl magnesium bromide (6.8 mL, 3.74 mmol) in THF was added dropwise. After stirring for 16 h at room temperature, 2 mL of 1,4-dioxane was added to precipitate the magnesium salts. The grey suspension was filtered through Celite® and the solvent was removed under reduced pressure to obtain a greenish solid, which was dissolved in toluene. Then, 1 mL of 1,4-dioxane was added and the solution was stirred for 1 h at room temperature. The solvent was removed under reduced pressure and the residue was washed with 6 mL of *n*-hexane and dried *in vacuo*.

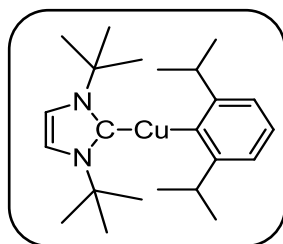
Yield: 1.04 g (1.97 mmol, 52%) of a light green solid.

Elemental analysis for $[C_{33}H_{41}CuN_2]$ [529.25 g/mol]: Calc. (obs.) C 74.89 (74.64), H 7.81 (8.13), N 5.29 (5.18).

1H -NMR (200 MHz, 25 °C, C_6D_6): δ_H / ppm = 1.20 (d, 12 H, $^3J_{HH} = 7$ Hz, $CHCH_3$), 2.00 (s, 12 H, $o^{Mes}-CH_3$), 2.14 (s, 6 H, $p^{Mes}-CH_3$), 2.67 (sept, 2 H, $^3J_{HH} = 7$ Hz, $CHCH_3$), 6.03 (s, 2 H, $CHCH$), 6.76 (s, 4 H, $m^{Mes}-CH$), 7.12-7.16 (m, 2 H, $m-CH$), 7.24-7.31 (m, 1 H, $p-CH$).

$^{13}C\{^1H\}$ NMR (50 MHz, 25 °C, C_6D_6): δ_C / ppm = 17.8 ($o^{Mes}-CH_3$), 21.1 ($p^{Mes}-CH_3$), 24.3 ($CHCH_3$), 26.0 ($CH(CH_3)$), 41.5 ($CHCH_3$), 121.2 ($CHCH$), 124.2 ($m-CH$), 125.1 ($p-CH$), 129.5 ($m^{Mes}-CH$), 135.1 ($o^{Mes}-C_q$), 136.0 ($i^{Mes}-C_q$), 139.2 ($p^{Mes}-C_q$), 158.6 ($o-C_q$), 166.8 ($i-C_q$), 183.8 (NCN).

HRMS-ASAP (m/z): $[M + H]^+$ calc. for $C_{33}H_{42}CuN_2$, 529.2639 found 529.2637.

Synthesis of [Cu(^tBu₂Im)(Dipp)] 37

To a suspension of [Cu(Dipp₂Im)Cl] (1.00 g, 3.58 mmol) in 10 mL of THF, a 0.55 M solution of 2,6-di-*iso*-propyl-phenyl magnesium bromide (6.5 mL, 3.58 mmol) in THF was added dropwise. After stirring for 48 h at room temperature, 2 mL of 1,4-dioxane was added to precipitate the magnesium salts. The milky suspension was filtered through Celite® and the solvent was removed under reduced pressure to obtain a white solid, which was dissolved in toluene. Then, 1.5 mL of 1,4-dioxane was added and the solution was stirred for 1 h at room temperature. The solvent was removed under reduced pressure and the residue was washed with 6 mL of *n*-hexane and dried *in vacuo*.

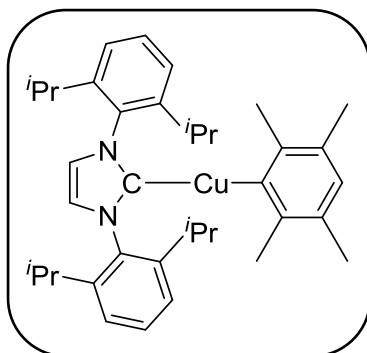
Yield: 726 mg (1.79 mmol, 50%) of a yellow solid.

Elemental analysis for [C₂₃H₇₃CuN₂] [405.11 g/mol]: Calc. (obs.) C 68.19 (67.68), H 9.21 (9.21), N 6.92 (6.96).

¹H-NMR (200 MHz, 25 °C, C₆D₆): δ_H/ ppm = 1.52 (s, 18 H, C(CH₃)₃), 1.61 (d, 12 H, ³J_{HH} = 7 Hz, CHCH₃), 3.76 (sept, 2 H, ³J_{HH} = 7 Hz, CHCH₃), 6.40 (s, 2 H, CHCH), 7.34 – 7.39 (m, 2 H, *m*-CH), 7.44 – 7.51 (m, 1 H, *p*-CH).

¹³C{¹H} NMR (50 MHz, 25 °C, C₆D₆): δ_C/ ppm = 26.0 (CHCH₃), 31.9 (C(CH₃)₃), 42.5 (CHCH₃), 57.7 (C_q), 115.6 (CHCH), 120.6 (arylCH), 125.5 (arylCH), 158.6 (arylC_q), 166.0 (arylC_q), 180.1 (NCN).

HRMS-ASAP (m/z): [M + H]⁺ calc. for C₂₃H₃₇CuN₂, 405.2326 found, 405.2321.

Synthesis of [Cu(Dipp₂Im)(duryl)] 38

To a suspension of [Cu(Dipp₂Im)Cl] (1.50 g, 3.28 mmol) in 10 mL of THF, a 0.59 M solution of pentamethyl-phenyl magnesium bromide (5.6 mL, 3.28 mmol) in THF was added dropwise. After stirring for 24 h at room temperature, 2 mL of 1,4-dioxane was added to precipitate the magnesium salts. The milky suspension was filtered through Celite® and the solvent was removed under reduced pressure to obtain a white solid, which was dissolved in toluene. Then, 1.5 mL of 1,4-dioxane was added and the solution was stirred for 1 h at room temperature. The solvent was removed under reduced pressure and the residue was washed with 6 mL of *n*-hexane and dried *in vacuo*.

Yield: 1.13 g (1.93 mmol, 59%) of a light brown solid.

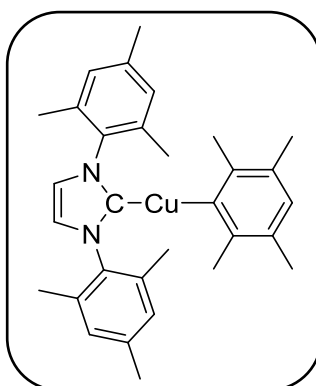
Elemental analysis for [C₃₇H₄₉CuN₂] [585.36 g/mol]: Calc. (obs.) C 75.92 (76.27), H 8.44 (8.63), N 4.79 (4.95).

Although the present results are outside the range viewed as established for analyzed purity, they are provided to illustrate the best values obtained to date. In addition, the ¹H and the ¹³C{¹H} NMR spectra as given in Figure 135 and Figure 136 provide evidence for the purity of the compound.

¹H-NMR (200 MHz, 25 °C, C₆D₆): δ_H / ppm = 1.12 (d, 12 H, ³J_{HH} = 7 Hz, CHCH₃), 1.38 (d, 12 H, ³J_{HH} = 7 Hz, CHCH₃), 2.01 (s, 6 H, *o*-CH₃), 2.27 (s, 6 H, *m*-CH₃), 2.65 (sept, 2 H, ³J_{HH} = 7 Hz, CHCH₃), 6.33 (s, 2 H, CHCH), 6.77 (s, 1 H, *p*-CH), 7.11 – 7.15 (m, 4 H, *m*^{Dipp}-CH), 7.26 – 7.33 (m, 2 H, *p*^{Dipp}-CH).

¹³C{¹H} NMR (50 MHz, 25 °C, C₆D₆): δ_C / ppm = 21.0 (*m*-CH₃), 23.9 (CHCH₃), 25.1 (CHCH₃), 25.3 (*o*-CH₃), 29.1 (CHCH₃), 122.1 (CHCH), 124.2 (*m*^{Dipp}-CH), 128.8 (*m*-C_q), 130.1 (*p*^{Dipp}-CH), 130.4 (*p*-CH), 135.7 (*o*-C_q), 143.0 (*i*^{Dipp}-C_q), 146.2 (*o*^{Dipp}-C_q), 168.9 (*i*-C_q), 186.4 (NCN).

HRMS-ASAP (m/z): [M + H]⁺ calc. for C₃₇H₄₉CuN₂, 585.3265 found 585.3270.

Synthesis of [Cu(Mes₂Im)(duryl)] 39

To a suspension of [Cu(Mes₂Im)Cl] (1.50 g, 3.72 mmol) in 10 mL of THF, a 0.59 M solution of 2,3,5,6-tetramethyl-phenyl magnesium bromide (6.3 mL, 3.72 mmol) in THF was added dropwise. After stirring for 48 h at room temperature, 2 mL of 1,4-dioxane was added to precipitate the magnesium salts. The milky suspension was filtered through Celite® and the solvent was removed under reduced pressure to obtain a white solid, which was dissolved in toluene. Then, 1.5 mL of 1,4-dioxane was added and the solution was stirred for 1 h at room temperature. The solvent was removed under reduced pressure and the residue was washed with 6 mL of *n*-hexane and dried *in vacuo*.

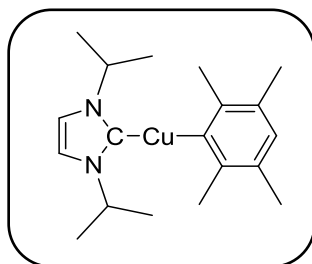
Yield: 520 mg (1.04 mmol, 30%) of a white solid.

Elemental analysis for [C₃₁H₃₇CuN₂] [501.20 g/mol]: Calc. (obs.) C 74.29 (74.05), H 7.44 (7.48), N 5.59 (5.61).

¹H-NMR (200 MHz, 25 °C, C₆D₆): δ_H / ppm = 2.04 (s, 12 H, *o*^{Mes}-CH₃), 2.14 (s, 6 H, *p*^{Mes}-CH₃), 2.24 (s, 6 H, *o*-CH₃), 2.29 (s, 6 H, *m*-CH₃), 6.05 (s, 2 H, CHCH), 6.78 (s, 4 H, *m*^{Mes}-CH), 6.79 (s, 1 H, *p*-CH).

¹³C{¹H} NMR (50 MHz, 25 °C, C₆D₆): δ_C / ppm = 17.9 (*o*^{Mes}-CH₃), 21.0 (*p*^{Mes}-CH₃), 21.1 (*m*-CH₃), 25.6 (*o*-CH₃), 121.1 (CHCH), 128.4 (*p*-CH), 128.8 (*m*^{Mes}-CH), 130.1 (arylC_q), 135.2 (*o*^{Mes}-C_q), 136.3 (*i*^{Mes}-C_q), 139.1 (*p*^{Mes}-C_q), 143.0 (arylC_q), 170.0 (*i*-C_q), 184.7 (NCN).

HRMS-ASAP (m/z): [M + H]⁺ calc. for C₃₂H₃₉CuN₂, 501.2326 found 501.2325.

Synthesis of [Cu(ⁱPr₂Im)(duryl)] 40

To a suspension of [Cu(ⁱPr₂Im)Cl] (1.50 g, 5.97 mmol) in 10 mL of THF, a 0.59 M solution of 2,3,5,6-tetramethyl-phenyl magnesium bromide (10.1 mL, 5.97 mmol) in THF was added dropwise. After stirring for 48 h at room temperature, 2 mL of 1,4-dioxane was added to precipitate the magnesium salts. The yellow suspension was filtered through Celite® and the solvent was removed under reduced pressure to obtain a white solid, which was dissolved in toluene. Then, 1.5 mL of 1,4-dioxane was added and the solution was stirred for 1 h at room temperature. The solvent was removed under reduced pressure and the residue was washed with 6 mL of *n*-hexane and dried *in vacuo*.

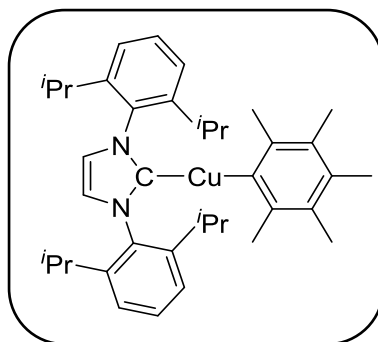
Yield: 855 mg (2.45 mmol, 41%) of a beige solid.

Elemental analysis for [C₁₉H₂₉CuN₂] [349.00 g/mol]: Calc. (obs.) C 65.39 (65.82), H 8.38 (8.68), N 8.03 (8.42).

¹H-NMR (200 MHz, 25 °C, C₆D₆): δ_H / ppm = 1.07 (d, 12 H, ³J_{HH} = 7 Hz, CHCH₃), 2.47 (s, 6 H, *o*-CH₃), 3.00 (s, 6 H, *m*-CH₃), 4.70 (sept, 2 H, ³J_{HH} = 7 Hz, CHCH₃), 6.17 (s, 2 H, CHCH), 7.00 (s, 1 H, *p*-CH).

¹³C{¹H} NMR (50 MHz, 25 °C, C₆D₆): δ_C / ppm = 21.2 (*m*-CH₃), 23.7 (CHCH₃), 27.1 (*o*-CH₃), 53.2 (CHCH₃), 116.2 (CHCH), 129.2 (*p*-CH), 130.8 (_{aryl}C_q), 142.8 (_{aryl}C_q), 170.0 (*i*-C_q), 179.4 (NCN).

HRMS-ASAP (m/z): [M + H]⁺ calc. for C₁₉H₂₉CuN₂, 349.1700 found 349.1703.

Synthesis of [Cu(Dipp₂Im)(C₆Me₅)] 41

To a suspension of [Cu(Dipp₂Im)Cl] (1.00 g, 2.19 mmol) in 10 mL of THF, a 0.38 M solution of pentamethyl-phenyl magnesium bromide (5.82 mL, 2.19 mmol) in THF was added dropwise. After stirring for 5 h at room temperature, 3.5 mL of 1,4-dioxane was added to precipitate the magnesium salts. The yellow suspension was filtered through Celite® and the solvent was removed under reduced pressure to obtain a white solid, which was dissolved in toluene. Then, 3 mL of 1,4-dioxane was added and the solution was stirred for 1 h at room temperature. The solvent was removed under reduced pressure and the residue was washed with 5 mL of *n*-hexane and dried *in vacuo*.

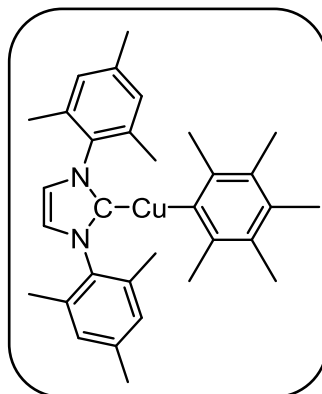
Yield: 728 mg (1.25 mmol, 57%) of a beige solid.

Elemental analysis for [C₃₈H₅₁CuN₂] [599.39 g/mol]: Calc. (obs.) C 76.15 (75.72), H 8.58 (8.71), N 4.67 (4.65).

¹H-NMR (200 MHz, 25 °C, C₆D₆): δ_H/ ppm = 1.12 (d, 12 H, ³J_{HH} = 7 Hz, CHCH₃), 1.38 (d, 12 H, ³J_{HH} = 7 Hz, CHCH₃), 2.06 (s, 6 H, *o*-CH₃), 2.22 (s, 3 H, *p*-CH₃), 2.23 (s, 6 H, *m*-CH₃), 2.65 (sept, 4 H, ³J_{HH} = 7 Hz, CHCH₃), 6.33 (s, 2 H, CHCH), 7.10 – 7.14 (m, 4 H, *m*-CH), 7.25 – 7.30 (m, 2 H, *p*-CH).

¹³C{¹H} NMR (50 MHz, 25 °C, C₆D₆): δ_C/ ppm = 16.5 (*p*-CH₃), 17.2 (*m*-CH₃), 23.9 (CHCH₃), 25.1 (CHCH₃), 27.3 (*o*-CH₃), 29.1 (CHCH₃), 122.1 (CHCH), 124.2 (*m*^{Dipp}-CH), 128.7 (*p*^{Dipp}-CH), 130.0 (*p*-C_q), 130.4 (*i*^{Dipp}-C_q), 135.7 (arylC_q), 142.5 (arylC_q), 146.2 (*o*^{Dipp}-C_q), 186.6 (NCN).

HRMS-ASAP (m/z): [M + H]⁺ calc. for C₃₈H₅₁CuN₂, 599.3421 found 599.3413.

Synthesis of [Cu(Mes₂Im)(C₆Me₅)] 42

To a suspension of [Cu(Mes₂Im)Cl] (1.00 g, 2.48 mmol) in 10 mL of THF a 0.38 M solution of pentamethyl-phenyl magnesium bromide (6.59 mL, 2.48 mmol) in THF was added dropwise. After stirring for 5 h at room temperature, 3.5 mL of 1,4-dioxane was added to precipitate the magnesium salts. The yellow suspension was filtered through Celite[®] and the solvent was removed under reduced pressure to obtain a white solid, which was dissolved in toluene. Then, 3 mL of 1,4-dioxane was added and the solution was stirred for 1.5 h at room temperature. The suspension was filtered through Celite[®] and the solvent was removed under reduced pressure. The residue was washed with 5 mL of *n*-hexane and dried *in vacuo*.

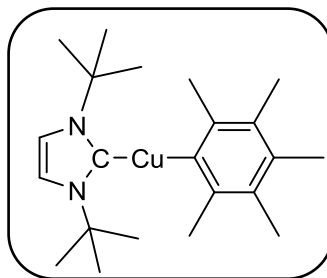
Yield: 343 mg (0.666 mmol, 27%) of a beige solid.

Elemental analysis for [C₃₂H₃₉CuN₂] [515.22 g/mol]: Calc. (obs.) C 74.60 (74.32), H 7.63 (7.59), N 5.44 (5.43).

¹H-NMR (400 MHz, 25 °C, C₆D₆): δ_H / ppm = 2.04 (s, 12 H, *o*^{Mes}-CH₃), 2.14 (s, 6 H, *p*^{Mes}-CH₃), 2.23 (s, 3 H, *p*-CH₃), 2.26 (s, 6 H, *o*-CH₃), 2.32 (s, 6 H, *m*-CH₃), 6.06 (s, 2 H, CHCH), 6.78 (s, 4 H, *m*^{Mes}-CH).

¹³C{¹H} NMR (100 MHz, 25 °C, C₆D₆): δ_C / ppm = 16.5 (*p*-CH₃), 17.2 (*m*-CH₃), 17.9 (*m*^{Mes}-CH₃), 21.1 (*p*^{Mes}-CH₃), 27.6 (*o*-CH₃), 121.1 (CHCH), 128.8 (arylC_q), 129.4 (*m*^{Mes}-CH), 130.0 (arylC_q), 135.2 (*o*^{Mes}-C_q), 136.3 (*i*^{Mes}-C_q), 139.1 (*p*^{Mes}-C_q), 142.5 (arylC_q), 166.0 (*i*-C_q), 184.9 (NCN).

HRMS-ASAP (m/z): [M + H]⁺ calc. for C₃₂H₃₉CuN₂, 515.2482 found 515.2488.

Synthesis of $[\text{Cu}(\text{tBu}_2\text{Im})(\text{C}_6\text{Me}_5)]$ 43

To a suspension of $[\text{Cu}(\text{tBu}_2\text{Im})\text{Cl}]$ (1.00 g, 3.58 mmol) in 10 mL of THF, a 0.38 M solution of pentamethyl-phenyl magnesium bromide (9.52 mL, 3.58 mmol) in THF was added dropwise. After stirring for 5 h at room temperature, 3.5 mL of 1,4-dioxane was added to precipitate the magnesium salts. The light brown suspension was filtered through Celite[®] and the solvent was removed under reduced pressure to obtain a white solid, which was dissolved in toluene. Then, 3 mL of 1,4-dioxane was added and the solution was stirred for 1 h at room temperature. The solvent was removed under reduced pressure and the residue was washed with 5 mL of *n*-hexane and dried *in vacuo*.

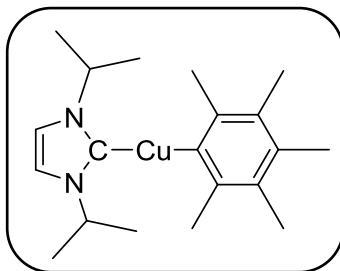
Yield: 680 mg (1.74 mmol, 49%) of a beige solid.

Elemental analysis for $[\text{C}_{22}\text{H}_{35}\text{CuN}_2]$ [391.08 g/mol]: Calc. (obs.) C 67.57 (67.21), H 9.02 (8.97), N 7.16 (6.97).

¹H-NMR (200 MHz, 25 °C, C₆D₆): δ_{H} / ppm = 1.52 (s, 18 H, C(CH₃)₃), 2.39 (s, 3 H, *p*-CH₃), 2.44 (s, 6 H, *o*-CH₃), 3.02 (s, 3 H, *m*-CH₃), 6.39 (s, 2 H, CHCH).

¹³C{¹H} NMR (50 MHz, 25 °C, C₆D₆): δ_{C} / ppm = 16.6 (*p*-CH₃), 17.4 (*m*-CH₃), 28.9 (*o*-CH₃), 31.9 (C(CH₃)₃), 57.7 (C(CH₃)₃), 115.5 (CHCH), 128.4 (_{aryl}C_q), 130.1 (_{aryl}C_q), 142.2 (_{aryl}C_q), 165.5 (_{aryl}C_q), 180.5 (NCN).

HRMS-ASAP (m/z): [M + H]⁺ calc. for C₂₂H₃₅CuN₂, 391.2169 found 391.2173.

Synthesis of $[\text{Cu}(\text{iPr}_2\text{Im})(\text{C}_6\text{Me}_5)]$ 44

To a suspension of $[\text{Cu}(\text{iPr}_2\text{Im})\text{Cl}]$ (1.00 g, 3.98 mmol) in 10 mL of THF, a 0.38 M solution of pentamethyl-phenyl magnesium bromide (10.58 mL, 5.97 mmol) in THF was added dropwise. After stirring for 12 h at room temperature, 3.5 mL of 1,4-dioxane was added to precipitate the magnesium salts. The grey suspension was filtered through Celite® and the solvent was removed under reduced pressure to obtain a white solid, which was dissolved in toluene. Then, 3 mL of 1,4-dioxane was added and the solution was stirred for 1.5 h at room temperature. The suspension was filtered through Celite® and the solvent was removed under reduced pressure. The residue was washed with 5 mL of *n*-hexane and dried *in vacuo*.

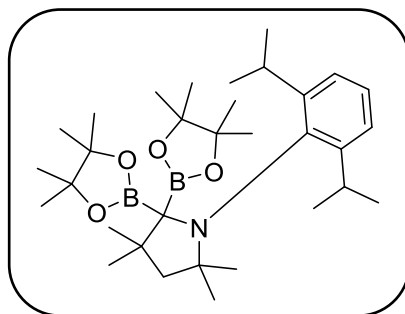
Yield: 444 mg (1.22 mmol, 31%) of a white solid.

Elemental analysis for $[\text{C}_{20}\text{H}_{31}\text{CuN}_2]$ [363.03 g/mol]: Calc. (obs.) C 66.17 (66.19), H 8.61 (8.59), N 7.72 (7.57).

$^1\text{H-NMR}$ (200 MHz, 25 °C, C_6D_6): δ_{H} / ppm = 1.04 (d, 12 H, $^3J_{\text{HH}} = 7$ Hz, CHCH_3), 2.37 (s, 3 H, *p*- CH_3), 2.44 (s, 6 H, *o*- CH_3), 3.09 (s, 6 H, *m*- CH_3), 4.71 (sept, 2 H, $^3J_{\text{HH}} = 7$ Hz, CHCH_3), 6.14 (s, 2 H, CHCH).

$^{13}\text{C}\{^1\text{H}\}$ NMR (50 MHz, 25 °C, C_6D_6): δ_{C} / ppm = 16.7 (*p*- CH_3), 17.5 (*m*- CH_3), 23.6 (CHCH_3), 29.1 (*o*- CH_3), 53.1 (CHCH_3), 116.1 (CHCH), 129.5 ($_{\text{aryl}}\text{C}_q$), 142.4 ($_{\text{aryl}}\text{C}_q$), 149.8 ($_{\text{aryl}}\text{C}_q$), 166.5 ($_{\text{aryl}}\text{C}_q$), 179.7 (NCN).

HRMS-ASAP (m/z): $[\text{M} + \text{H}]^+$ calc. for $\text{C}_{20}\text{H}_{32}\text{CuN}_2$, 363.1856 found 363.1860.

Synthesis of BBA B₂pin₂•CaaC^{Me}[301] BBA1

To B₂pin₂ (45 mg, 175 μmol) and CaaC^{Me} (50 mg, 175 μmol) 3 mL of C₆D₆ was added. After 14 h at room temperature the solvent was removed under reduced pressure. The residue was washed with 5 mL of *n*-hexane and dried *in vacuo*.

Yield: 29 mg (54 μmol, 31%) of a white solid.

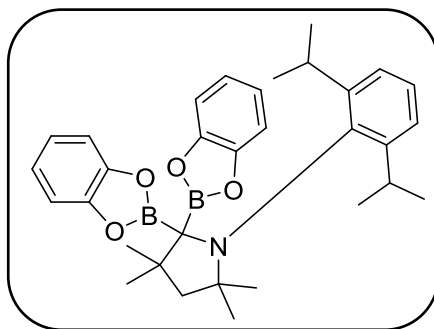
Elemental analysis for [C₃₂H₅₅B₂NO₄] [539.41 g/mol] Calc. (obs.): C 71.25 (71.25), H 10.28 (10.32), N 2.60 (2.67).

¹H-NMR (400 MHz, 25 °C, C₆D₆): δ_H / ppm = 0.95 (s, 6 H, OC_qCH₃), 1.09 (s, 6 H, OC_qCH₃), 1.11 (s, 6 H, OC_qCH₃), 1.16 (s, 6 H, OC_qCH₃), 1.26 (s, 3 H, NC_qCH₃), 1.37 (d, 3 H, ³J_{HH} = 7 Hz, CHCH₃), 1.37 (d, 3 H, ³J_{HH} = 7 Hz, CHCH₃), 1.41 (d, 3 H, ³J_{HH} = 7 Hz, CHCH₃), 1.42 (d, 3 H, ³J_{HH} = 7 Hz, CHCH₃), 1.46 (s, 3 H, NC_qCH₃), 1.59 (s, 3 H, C_qC_qCH₃), 1.82 (s, 3 H, C_qC_qCH₃), 1.83 (d, 1 H, ¹J_{HH} = 12 Hz, C_qCH₂), 2.7 (d, 1 H, ¹J_{HH} = 12 Hz, C_qCH₂), 3.50 (sept, 1 H, ³J_{HH} = 7 Hz, CHCH₃), 4.27 (sept, ³J_{HH} = 7 Hz, CHCH₃), 7.26 (s, 3H, arylCH).

¹¹B-NMR (128 MHz, 25 °C, C₆D₆): δ_B / ppm = 31.6 (s).

¹³C{¹H}-NMR (100 MHz, 25 °C, C₆D₆): δ_C / ppm = 24.3 (OC_qCH₃), 24.5 (CHCH₃), 24.7 (CHCH₃), 25.2 (OC_qCH₃), 26.4 (OC_qCH₃), 26.7 (CHCH₃), 27.1 (OC_qCH₃), 27.4 (NC_qCH₃), 27.6 (CHCH₃), 27.8 (CHCH₃), 28.8 (CHCH₃), 30.1 (NC_qCH₃), 30.2 (C_qC_qCH₃), 31.2 (C_qC_qCH₃), 44.1 (BC_qC_q), 56.8 (NC_qCH₂), 62.6 (NC_qCH₂), 82.6 (OC_q), 83.3 (OC_q), 124.3 (*m*^{Dipp}-CH), 124.5 (*m*^{Dipp}-CH), 126.4 (*p*^{Dipp}-CH), 140.8 (*i*^{Dipp}-CH), 152.5 (*o*^{Dipp}-CH), 153.5 (*o*^{Dipp}-CH).

HRMS-ASAP (m/z): [M + H]⁺ calc. for C₃₂H₅₅B₂NO₄, 540.4390 found 540.4388.

Synthesis of BBA B₂cat₂•CaaC^{Me}[301] BBA2


To B₂cat₂ (42 mg, 175 μmol) and CaaC^{Me} (50 mg, 175 μmol) 3 mL of C₆D₆ was added. After 15 h at room temperature the solvent was removed under reduced pressure. The residue was washed with 5 mL of *n*-hexane and dried *in vacuo*.

Yield: 16 mg (31 μmol, 18%) of an off-white solid.

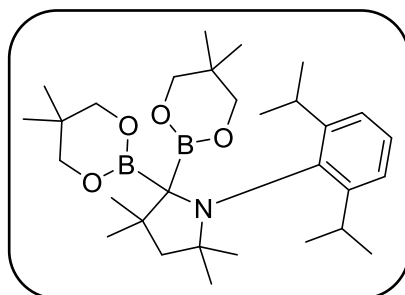
Elemental analysis for [C₃₂H₃₉B₂NO₄] [523.28 g/mol] Calc. (obs.): C 73.45 (71.57), H 7.51 (7.50), N 2.68 (2.78).

¹H-NMR (400 MHz, 25 °C, C₆D₆): δ_H / ppm = 0.85 (d, 6 H, ³J_{HH} = 7 Hz, CHCH₃), 1.29 (d, 6 H, ³J_{HH} = 7 Hz, CHCH₃), 1.47 (s, 6 H, NC_qCH₃), 1.64 (s, 6 H, C_qC_qCH₃), 2.38 (s, 2 H, NC_qCH₂), 3.97 (sept, 2 H, ³J_{HH} = 7 Hz, CHCH₃), 6.64 – 6.68 (m, 4 H, aryl^{cat}-CH), 6.81 – 6.85 (m, 4 H, aryl^{cat}-CH), 7.18 – 7.20 (m, 2 H, *m*^{Dipp}-CH), 7.26 – 7.30 (m, 1 H, *p*^{Dipp}-CH).

¹¹B-NMR (128 MHz, 25 °C, C₆D₆): δ_B / ppm = 34.2 (s).

¹³C{¹H}-NMR (100 MHz, 25 °C, C₆D₆): δ_C / ppm = 24.5 (CHCH₃), 25.3 (CHCH₃), 28.1 (C_qC_qCH₃), 28.4 (CHCH₃), 30.8 (NC_qCH₃), 43.6 (C_qC_qCH₃), 56.5 (NC_qCH₂), 63.7 (NC_qCH₂), 112.8 (aryl^{cat}-CH), 123.1 (aryl^{cat}-CH), 124.7 (*m*^{Dipp}-CH), 127.5 (*p*^{Dipp}-CH), 139.4 (*i*^{Dipp}-C_q), 148.1 (aryl^{cat}-C_q), 153.4 (*o*^{Dipp}-C_q).

HRMS-ASAP (m/z): [M + H]⁺ calc. for C₃₂H₃₉B₂NO₄, 524.3138 found 524.3132.

Synthesis of BBA B₂neop₂•CaaC^{Me}[301] BBA3

To B₂neop₂ (40 mg, 175 μmol) and CaaC^{Me} (50 mg, 175 μmol) 3 mL of C₆D₆ was added. After 3 h at room temperature the solvent was removed under reduced pressure. The residue was washed with 5 mL of *n*-hexane and dried *in vacuo*.

Yield: 40 mg (78 μmol, 45%) of an off-white solid.

Elemental analysis for [C₃₀H₅₂B₂NO₄] [511.35 g/mol] Calc. (obs.): C 70.46 (70.38), H 10.05 (10.04), N 2.74 (2.82)

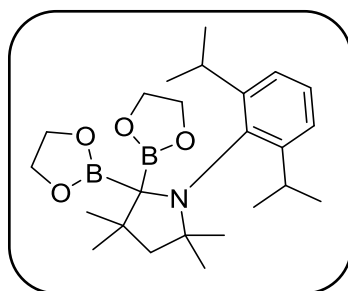
¹H-NMR (400 MHz, 25 °C, C₆D₆): δ_H / ppm = 0.69 (s, 12 H, OCH₂C_qCH₃), 1.30 (d, 6 H, ³J_{HH} = 7 Hz, CHCH₃), 1.41 (s, 6 H, NC_qCH₃), 1.47 (d, 6 H, ³J_{HH} = 7 Hz, CHCH₃), 1.76 (s, 6 H, C_qC_qCH₃), 2.30 (s, 2 H, NC_qCH₂), 3.33 (m, 8 H, OCH₂), 4.11 (sept, 2 H, ³J_{HH} = 7 Hz, CHCH₃), 7.29 (s, 3 H, arylCH).

¹¹B-NMR (128 MHz, 25 °C, C₆D₆): δ_B / ppm = 29.2 (s).

¹³C{¹H}-NMR (100 MHz, 25 °C, C₆D₆): δ_C / ppm = 23.0 (OCH₂C_qCH₃), 25.0 (CHCH₃), 26.4 (CHCH₃), 28.1 (CHCH₃), 29.1 (C_qC_qCH₃), 30.9 (NC_qCH₃), 31.1 (OCH₂C_qCH₃), 42.8 (C_qC_qCH₃), 57.5 (NC_qCH₂), 62.4 (NC_qCH₃), 71.3 (OCH₂), 124.1 (*m*^{Dipp}-CH), 126.0 (*p*^{Dipp}-CH), 142.3 (*i*^{Dipp}-C_q), 153.1 (*o*^{Dipp}-C_q).

¹³C{¹H}[¹¹B]-NMR (75 MHz, 25 °C, C₆D₆): δ_C / ppm = 64.1 (BC_q).

HRMS-ASAP (m/z): [M + H]⁺ calc. for C₃₀H₅₁B₂NO₄, 512.4077 found 512.4074.

Synthesis of BBA B₂eg₂•CaaC^{Me}[301] BBA4

To B₂eg₂ (22 mg, 155 μmol) and CaaC^{Me}(43 mg, 147 μmol) 3 mL of toluene was added. After 17 h at room temperature the solvent was removed under reduced pressure. The residue was washed with 1 mL of *n*-hexane and dried *in vacuo*.

Yield: 22 mg (51 μmol, 33%) of a white solid.

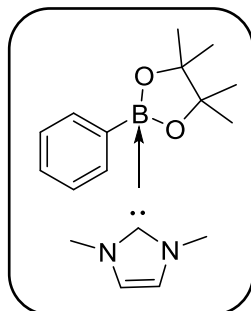
Elemental analysis for [C₂₄H₃₉B₂NO₄] [427.19 g/mol] Calc. (obs.): C 67.48 (67.00), H 9.20 (9.30), N 3.28 (3.00).

¹H-NMR (400 MHz, 25 °C, C₆D₆): δ_H / ppm = 1.23 (d, 6 H, ³J_{HH} = 7 Hz, CHCH₃), 1.37 (s, 6 H, C_qC_qCH₃), 1.41 (d, 6 H, ³J_{HH} = 7 Hz, CHCH₃), 1.63 (br, 6 H, NC_qCH₃), 2.24 (br, 2 H, NC_qCH₂), 3.55 (s, 8 H, OCH₂), 4.04 (sept, 2 H, ³J_{HH} = 7, CHCH₃), 7.24 (s, 3H, arylCH).

¹¹B-NMR (128 MHz, 25 °C, C₆D₆): δ_B / ppm = 33.2 (s).

¹³C{¹H}-NMR (100 MHz, 25 °C, C₆D₆): δ_C / ppm = 24.5 (CHCH₃), 26.0 (CHCH₃), 28.0 (CHCH₃), 28.0 (NC_qCH₃), 30.6 (C_qC_qCH₃), 42.6 (C_qC_qCH₃), 56.6 (NC_qCH₂), 63.0 (NC_qCH₃), 65.1 (OCH₂), 124.3 (*m*^{Dipp}-CH), 126.8 (*p*^{Dipp}-CH), 140.5 (*i*^{Dipp}-C_q), 153.4 (*o*^{Dipp}-C_q).

HRMS-ASAP (m/z): [M + H]⁺ calc. for C₂₄H₃₉B₂NO₄, 428.3138 found, 428.3135.

Synthesis of C₆H₅Bpin•Me₂Im ADD1

To a solution of phenylBpin (150 mg, 730 μmol) in 5 mL of toluene, Me₂Im (104 mg, 730 μmol) was added. After 16 h at room temperature the solvent was removed under reduced pressure. The residue was washed with 5 mL of *n*-hexane and dried *in vacuo*.

Yield: 96 mg (300 μmol , 41%) of a white solid.

Elemental analysis for [C₁₇H₂₅BN₂O₂] [300.21 g/mol] Calc. (obs.): C 68.01 (68.58), H 8.39 (8.87), N 9.33 (9.58).

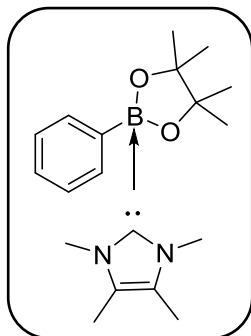
Although the present results are outside the range viewed as established for analyzed purity, they are provided to illustrate the best values obtained to date. In addition, the ¹H, ¹¹B, and the ¹³C{¹H} NMR spectra as given in Figure 137, Figure 138 and Figure 139 provide evidence for the purity of the compound.

¹H-NMR (200 MHz, 25 °C, C₆D₆): δ_{H} / ppm = 1.33 (br, 12 H, OC_qCH₃), 3.50 (s, 6 H, NCH₃), 5.51 (s, 2 H, NCHCHN), 7.22 – 7.29 (m, 1 H, *p*-CH), 7.39 – 7.47 (m, 2 H, *o*-CH), 7.90 – 7.94 (m, 2 H, *m*-CH).

¹¹B-NMR (64 MHz, 25 °C, C₆D₆): δ_{B} / ppm = 4.5 (s).

¹³C{¹H}-NMR (100 MHz, 25 °C, C₆D₆): δ_{C} / ppm = 25.4 (br. OC_qCH₃), 26.4 (br. OC_qCH₃), 35.9 (NCH₃), 79.2 (OC_qCH₃), 120.1 (NCHCHN), 125.7 (*p*-CH), 127.7 (*m*-CH), 132.0 (*o*-CH), 154.2 (br, *i*-C_q), 169.1 (br, NCN).

HRMS-ASAP (m/z): [M]⁺ calc. for C₁₇H₂₅BN₂O₂, 300.2004 found 300.1999.

Synthesis of C₆H₅Bpin•Me₄Im ADD2

To a solution of phenylBpin (150 mg, 730 μmol) in 5 mL of toluene, Me₄Im (91 mg, 730 μmol) was added. After 16 h at room temperature the solvent was removed under reduced pressure. The residue was washed with 5 mL of *n*-hexane and dried *in vacuo*.

Yield: 179 mg (540 μmol , 74%) of a white solid.

Elemental analysis for [C₁₉H₂₉BN₂O₂] [328.26 g/mol] Calc. (obs.): C 69.52 (68.66), H 8.91 (8.99), N 8.53 (8.23).

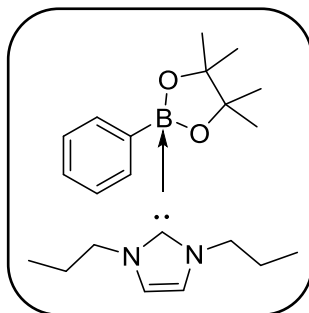
Although the present results are outside the range viewed as established for analyzed purity, they are provided to illustrate the best values obtained to date. In addition, the ¹H, ¹¹B, and the ¹³C{¹H} NMR spectra as given in Figure 140, Figure 141 and Figure 142 provide evidence for the purity of the compound.

¹H-NMR (200 MHz, 25 °C, C₆D₆): δ_{H} / ppm = 1.10 (s, 6 H, Im-CH₃), 1.29 (br, 6 H, OC_qCH₃), 1.47 (br, 6 H, OC_qCH₃), 3.59 (s, 6 H, NCH₃), 7.22 – 7.26 (m, 1 H, *p*-CH), 7.42 – 7.50 (m, 2 H, *m*-CH), 8.00 – 8.04 (m, 2 H, *o*-CH).

¹¹B-NMR (64 MHz, 25 °C, C₆D₆): δ_{B} / ppm = 4.6 (s).

¹³C{¹H}-NMR (100 MHz, 25 °C, C₆D₆): δ_{C} / ppm = 7.6 (NC_qCH₃), 25.6 (OC_qCH₃), 26.6 (OC_qCH₃), 32.4 (NCH₃), 79.2 (OC_qCH₃), 123.3 (NCHCHN), 125.5 (*p*-CH), 127.4 (*m*-CH), 132.0(*o*-CH), 155.2 (br, *i*-C_q), 166.9 (br, NCN).

HRMS-ASAP (m/z): [M]⁺ calc. for C₁₉H₂₉BN₂O₂, 328.2317 found 328.2305.

Synthesis of $C_6H_5Bpin \bullet ^nPr_2Im$ ADD3

To a solution of phenylBpin (150 mg, 730 μ mol) in 5 mL of toluene, nPr_2Im (104 mg, 730 μ mol) was added. After 17 h at room temperature the solvent was removed under reduced pressure. The residue was washed with 5 mL of *n*-hexane and dried *in vacuo*.

Yield: 78 mg (220 μ mol, 30%) of a white solid.

Elemental analysis for $[C_{21}H_{33}BN_2O_2]$ [356.32 g/mol] Calc. (obs.): C 70.79 (71.01), H 9.34 (9.74), N 7.86 (7.88).

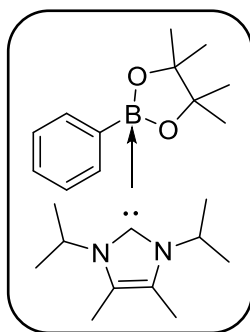
1H -NMR (400 MHz, 25 $^{\circ}C$, C_6D_6): δ_H / ppm = 0.68 (t, 6 H, $^3J_{HH} = 7$ Hz, $NCH_2CH_2CH_3$), 1.24 (br, 6 H, OC_qCH_3), 1.36 – 1.45 (m, 10 H, $CH_2CHCH_3 + OC_qCH_3$), 4.22 (t, 4 H, $^3J_{HH} = 7$ Hz, $CH_2CH_2CH_3$), 5.86 (s, 2 H, $NCHCHN$), 7.21 – 7.25 (m, 1 H, *p*-CH), 7.39 – 7.43 (m, 2 H, *m*-CH), 7.91 – 7.93 (m, 2 H, *o*-CH).

^{11}B -NMR (128 MHz, 25 $^{\circ}C$, C_6D_6): δ_B / ppm = 4.8 (s).

$^{13}C\{^1H\}$ -NMR (100 MHz, 25 $^{\circ}C$, C_6D_6): δ_C / ppm = 11.0 ($CH_2CH_2CH_3$), 24.3 ($CH_2CH_2CH_3$), 25.8 (OC_qCH_3), 26.6 (OC_qCH_3), 49.8 ($CH_2CH_2CH_3$), 79.2 (OC_q), 118.9 ($NCHCHN$), 125.6 (*p*-CH), 127.4 (*m*-CH), 132.2 (*o*-CH), 155.1 (br, *i*- C_q), 168.9 (br, NCN).

HRMS-ASAP (m/z): $[M]^+$ calc. for $C_{21}H_{32}BN_2O_2$, 355.2551 found 355.2538.

Synthesis of $C_6H_5Bpin \bullet iPr_2ImMe_2$ ^[300] ADD4



To phenylBpin (150 mg, 730 μ mol) and iPr_2ImMe_2 (132 mg, 730 μ mol), 5 mL of toluene was added. After 16 h at room temperature the solvent was removed under reduced pressure. The residue was washed with 5 mL of *n*-hexane and dried *in vacuo*.

Yield: 97 mg (210 μ mol, 29%) of a white solid.

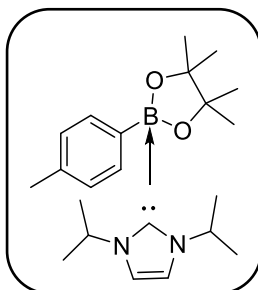
1H -NMR (200 MHz, 25 $^\circ$ C, C_6D_6): δ_H / ppm = 1.14 (d, 12 H, $^3J_{HH}$ = 6 Hz, CHCH₃), 1.33 (br, 12 H, OC_qCH₃), 1.52 (br, 6 H, NC_qCH₃), 6.52 (br, 2 H, CHCH₃), 7.23 – 7.30 (m, 1 H, *p*-CH), 7.40 – 7.47 (m, 2 H, *m*-CH), 7.95 – 7.99 (m, 2 H, *o*-CH).

^{11}B -NMR (64 MHz, 25 $^\circ$ C, C_6D_6): δ_B / ppm = 5.0(s).

$^{13}C\{^1H\}$ -NMR (100 MHz, 25 $^\circ$ C, C_6D_6): δ_C / ppm = 10.0 (NC_qCH₃), 21.5 (CHCH₃), 26.2 (OC_qCH₃), 26.5 (OC_qCH₃), 48.6 (CHCH₃), 79.0 (OC_qCH₃), 124.2 (br, NC_qCH₃), 125.4 (*p*-CH), 127.4 (*o*-CH), 132.3 (*m*-CH), 155.8 (br, *i*-CH), 167.5 (br, NCN).

HRMS-ASAP (*m/z*): [M]⁺ calc. for C₂₃H₃₇BN₂O₂, 384.2943 found 384.2929.

Synthesis of *p*-tolylBpin $\bullet iPr_2Im$ ADD5



To a solution of *p*-tolylBpin (150 mg, 0.68 mmol) in 20 mL of toluene, iPr_2Im (106 μ L, 106 mg, 0.68 mmol) was added. After 18 h at room temperature the solvent was removed under reduced pressure. The residue was washed with 5 mL of *n*-hexane and dried *in vacuo*.

Yield: 89 mg (240 μmol , 35%) of a yellow solid.

Elemental analysis for $[\text{C}_{22}\text{H}_{35}\text{BN}_2\text{O}_2]$ [370.34 g/mol] Calc. (obs.): C 71.35 (70.79), H 9.53 (9.55), N 7.56 (7.71).

Although the present results are outside the range viewed as established for analyzed purity, they are provided to illustrate the best values obtained to date. In addition, the ^1H , ^{11}B , and the $^{13}\text{C}\{^1\text{H}\}$ NMR spectra as given in Figure 143, Figure 144 and Figure 145 provide evidence for the purity of the compound.

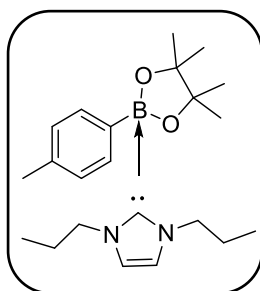
$^1\text{H-NMR}$ (200 MHz, 25 $^\circ\text{C}$, C_6D_6): δ_{H} / ppm = 0.96 (d, 12 H, $^3J_{\text{HH}} = 7$ Hz, CHCH_3), 1.34 (br, 12 H, OC_qCH_3), 2.29 (s, 3 H, $p^{\text{tolyl}}\text{-CH}_3$), 6.10 (s, 2 H, NCHCHN), 6.17 (br, 2 H, CHCH_3), 7.22 – 7.26 (m, 2 H, $o\text{-CH}$), 7.81 – 7.85 (m, 2 H, $m\text{-CH}$).

$^{11}\text{B-NMR}$ (64 MHz, 25 $^\circ\text{C}$, C_6D_6): δ_{B} / ppm = 5.3 (s).

$^{13}\text{C}\{^1\text{H}\}\text{-NMR}$ (100 MHz, 25 $^\circ\text{C}$, C_6D_6): δ_{C} / ppm = 21.6 ($p\text{-CH}_3$), 23.1 (OC_qCH_3), 26.3 (br, CHCH_3), 48.6 (CHCH_3), 79.1 (OC_qCH_3), 115.6 (NCHCHN), 132.3 ($m\text{-CH}$), 133.6 ($o\text{-CH}$), 134.2 ($p\text{-C}_q$), 151.3 (br, $i\text{-C}_q$), 168.0 (br, NCN).

HRMS-ASAP (m/z): $[\text{M}]^+$ calc. for $\text{C}_{22}\text{H}_{35}\text{BN}_2\text{O}_2$, 370.2786 found 370.2783.

Synthesis of $p\text{-tolylBpin}\bullet^n\text{Pr}_2\text{Im ADD6}$



To a solution of $p\text{-tolylBpin}$ (150 mg, 0.68 mmol) in 20 mL of toluene, $^n\text{Pr}_2\text{Im}$ (106 μL , 106 mg, 0.68 mmol) was added. After 17 h at room temperature the solvent was removed under reduced pressure. The residue was washed with 5 mL of $n\text{-hexane}$ and dried *in vacuo*.

Yield: 42 mg (114 μmol , 17%) of a white solid.

Elemental analysis for $[\text{C}_{22}\text{H}_{35}\text{BN}_2\text{O}_2]$ [370.34 g/mol] Calc. (obs.): C 71.35 (71.47), H 9.53 (8.90), N 7.56 (7.46).

Although the present results are outside the range viewed as established for analyzed purity, they are provided to illustrate the best values obtained to date. In addition, the ^1H , ^{11}B , and the $^{13}\text{C}\{^1\text{H}\}$ NMR spectra as given in Figure 146, Figure 147 and Figure 148 provide evidence for the purity of the compound.

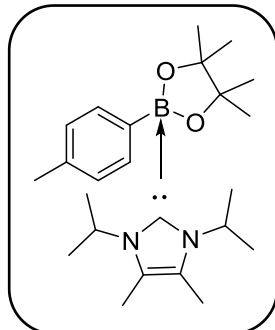
$^1\text{H-NMR}$ (200 MHz, 25 °C, C_6D_6): $\delta_{\text{H}} / \text{ppm} = 0.69$ (t, 6 H, $^3J_{\text{HH}} = 7$ Hz, $\text{CH}_2\text{CH}_2\text{CH}_3$), 1.33 (br, 12 H, OC_qCH_3), 1.37 – 1.52 (m, 4 H, $\text{CH}_2\text{CH}_2\text{CH}_3$), 2.28 (s, 3 H, $p\text{-CH}_3$), 4.22 (t, 4 H, $^3J_{\text{HH}} = 7$ Hz, $\text{CH}_2\text{CH}_2\text{CH}_3$), 5.86 (s, 2 H, NCHCHN), 7.24 – 7.28 (m, 2 H, $o\text{-CH}$), 7.84 – 7.88 (m, 2 H, $m\text{-CH}$).

$^{11}\text{B-NMR}$ (64 MHz, 25 °C, C_6D_6): $\delta_{\text{B}} / \text{ppm} = 5.4$ (s).

$^{13}\text{C}\{^1\text{H}\}\text{-NMR}$ (100 MHz, 25 °C, C_6D_6): $\delta_{\text{C}} / \text{ppm} = 11.0$ ($\text{CH}_2\text{CH}_2\text{CH}_3$), 21.6 ($p\text{-CH}_3$), 24.3 ($\text{CH}_2\text{CH}_2\text{CH}_3$), 26.1 (OC_qCH_3), 49.9 ($\text{CH}_2\text{CH}_2\text{CH}_3$), 79.2 (OC_qCH_3), 118.9 (NCHCHN), 128.2 ($o\text{-CH}$), 132.3 ($m\text{-CH}$), 134.3 ($p\text{-C}_q$), 169.5 (br, NCN).

HRMS-ASAP (m/z): $[\text{M} - \text{H}]^+$ calc. for $\text{C}_{22}\text{H}_{35}\text{BN}_2\text{O}_2$, 369.2708 found 369.2703.

Synthesis of $p\text{-tolylBpin}\cdot^i\text{Pr}_2\text{ImMe}_2$ ^[300] ADD7



To $p\text{-tolylBpin}$ (150 mg, 680 μmol) and $^i\text{Pr}_2\text{ImMe}_2$ (124 mg, 680 μmol) 5 mL of toluene was added. After 16 h at room temperature the solvent was removed under reduced pressure. The residue was washed with 5 mL of $n\text{-hexane}$ and dried *in vacuo*.

Yield: 56 mg (140 μmol , 21%) of a white solid.

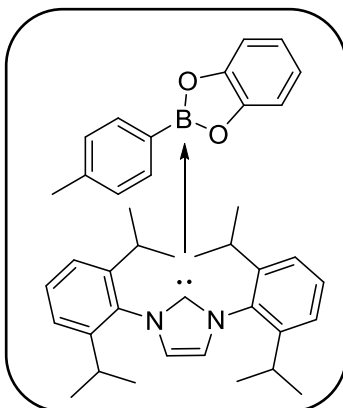
$^1\text{H-NMR}$ (200 MHz, 25 °C, C_6D_6): $\delta_{\text{H}} / \text{ppm} = 1.19$ (br, 12 H, CHCH_3), 1.33 (s, 12 H, OC_qCH_3), 1.52 (s, 6 H, NC_qCH_3), 2.27 (s, 3 H, $p\text{-CH}_3$), 6.50 (br, 2 H, CHCH_3), 7.22 – 7.26 (m, 2 H, $o\text{-CH}$), 7.90 – 7.94 (m, 2 H, $m\text{-CH}$).

$^{11}\text{B-NMR}$ (64 MHz, 25 °C, C_6H_6): $\delta_{\text{B}} / \text{ppm} = 6.1$ (s).

$^{13}\text{C}\{^1\text{H}\}$ -NMR (100 MHz, 25 °C, C_6D_6): $\delta_{\text{C}} / \text{ppm} = 21.6$ ($p\text{-CH}_3$), 23.1 (OC_qCH_3), 26.3 (br, CHCH_3), 48.6 (CHCH_3), 79.1 (OC_qCH_3), 115.6 (NCHCHN), 132.3 ($m\text{-CH}$), 133.6 ($o\text{-CH}$), 134.2 ($p\text{-C}_q$), 151.3 (br, $i\text{-C}_q$), 168.0 (br, NCN).

HRMS-ASAP (m/z): $[\text{M}]^+$ calc. for $\text{C}_{24}\text{H}_{39}\text{BN}_2\text{O}_2$, 398.3099 found 398.3096.

Synthesis of $p\text{-tolylBcat}\cdot\text{Dipp}_2\text{Im ADD8}$



To $p\text{-tolylBcat}$ (150 mg, 710 μmol) and Mes_2Im (277 mg, 710 μmol) 5 mL of toluene was added. After 3 h at room temperature the solvent was removed under reduced pressure. The residue was washed with 5 mL of $n\text{-hexane}$ and dried *in vacuo*.

Yield: 240 mg (400 μmol , 56%) of a white solid.

Elemental analysis for $[\text{C}_{40}\text{H}_{47}\text{BN}_2\text{O}_2]$ [598.64 g/mol] Calc. (obs.): C 80.26 (79.58), H 7.91 (7.99), N 4.68 (4.80).

Although the present results are outside the range viewed as established for analyzed purity, they are provided to illustrate the best values obtained to date. In addition, the ^1H , ^{11}B , and the $^{13}\text{C}\{^1\text{H}\}$ NMR spectra as given in Figure 149, Figure 150 and Figure 151 provide evidence for the purity of the compound.

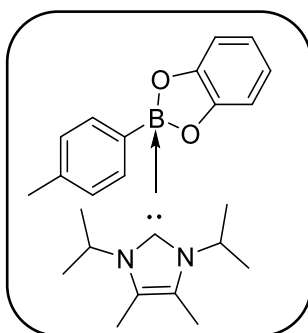
^1H -NMR (400 MHz, 25 °C, C_6D_6): $\delta_{\text{H}} / \text{ppm} = 0.94$ (d, 12 H, $^3J_{\text{HH}} = 7$ Hz, CHCH_3), 1.14 (d, 12 H, $^3J_{\text{HH}} = 7$ Hz, CHCH_3), 2.16 (s, 3 H, $p^{\text{tolyl}}\text{-CH}_3$), 2.71 (sept, 2 H, $^3J_{\text{HH}} = 7$ Hz, CHCH_3), 6.32 (s, 2 H, NCHCHN), 6.38 – 6.42 (m, 2 H, $\text{aryl}^{\text{cat}}\text{-CH}$), 6.52 – 6.56 (m, 2 H, $\text{aryl}^{\text{cat}}\text{-CH}$), 6.87 – 6.89 (m, 2 H, $\text{aryl}^{\text{tolyl}}\text{-CH}$), 7.06 – 7.08 (m, 4 H, $m^{\text{Dipp}}\text{-CH}$), 7.19 – 7.21 (m, 2 H, $\text{aryl}^{\text{tolyl}}\text{CH}$), 7.22 – 7.26 (m, 2 H, $p^{\text{Dipp}}\text{CH}$).

^{11}B -NMR (128 MHz, 25 °C, C_6D_6): $\delta_{\text{B}} / \text{ppm} = 8.8$ (s).

$^{13}\text{C}\{^1\text{H}\}$ -NMR (100 MHz, 25 °C, C_6D_6): δ_{C} / ppm = 21.4 ($p^{\text{tolyl}}\text{-CH}_3$), 22.0 (CHCH_3), 26.3 (CHCH_3), 29.3 (CHCH_3), 109.2 ($_{\text{aryl}^{\text{cat}}}\text{-CH}$), 118.0 ($_{\text{aryl}^{\text{cat}}}\text{-CH}$), 123.9 ($m^{\text{Dipp}}\text{-CH}$), 124.0 (NCHCHN), 130.3 ($p^{\text{Dipp}}\text{-CH}$), 132.5 ($m^{\text{tolyl}}\text{-CH}$), 134.6 ($o^{\text{tolyl}}\text{-CH}$), 135.2 ($i^{\text{Dipp}}\text{-C}_q$), 145.6 ($o^{\text{Dipp}}\text{-C}_q$), 153.9 ($_{\text{aryl}^{\text{cat}}}\text{-CH}$), 166.6 (br, NCN).

HRMS-ASAP (m/z): $[\text{M} + \text{H}]^+$ calc. for $\text{C}_{40}\text{H}_{47}\text{BN}_2\text{O}_2$, 599.3803 found 599.3785.

Synthesis of $p\text{-tolylBcat}\cdot i\text{Pr}_2\text{ImMe}_2^{[300]}$ ADD9



To $p\text{-tolylBcat}$ (150 mg, 710 μmol) and $i\text{Pr}_2\text{ImMe}_2$ (129 mg, 710 μmol) 5 mL of toluene was added. After 3 h at room temperature the solvent was removed under reduced pressure. The residue was washed with 5 mL of $n\text{-hexane}$ and dried *in vacuo*.

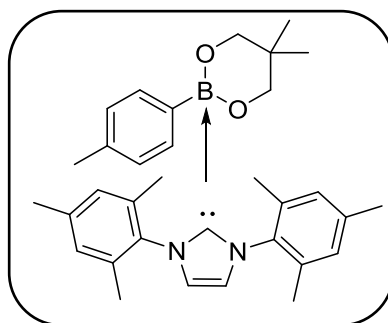
Yield: 180 mg (460 μmol , 65%) of a white solid.

^1H -NMR (200 MHz, 25 °C, C_6D_6): δ_{H} / ppm = 1.04 (d, 12 H, $^3J_{\text{HH}} = 7$ Hz, CHCH_3), 1.50 (s, 6 H, NC_qCH_3), 2.26 (s, 3 H, $p^{\text{tolyl}}\text{-CH}_3$), 5.84 (sept, 2 H, $^3J_{\text{HH}} = 7$ Hz, CHCH_3), 6.86 – 6.92 (m, 2 H, $_{\text{aryl}^{\text{cat}}}\text{-CH}$), 7.02 – 7.08 (m, 2 H, $_{\text{aryl}^{\text{cat}}}\text{-CH}$), 7.19 – 7.23 (m, 2 H, $o^{\text{tolyl}}\text{-CH}$), 7.62 – 7.66 (m, 2 H, $m^{\text{tolyl}}\text{-CH}$).

^{11}B -NMR (64 MHz, 25 °C, C_6D_6): δ_{B} / ppm = 10.3 (s).

$^{13}\text{C}\{^1\text{H}\}$ -NMR (100 MHz, 25 °C, C_6D_6): δ_{C} / ppm = 8.3 (C_qCH_3), 10.1 (CHCH_3), 21.4 ($p\text{-CH}_3$), 50.3 (NC_qCH_3), 109.3 ($_{\text{aryl}^{\text{cat}}}\text{-CH}$), 118.7 ($_{\text{aryl}^{\text{cat}}}\text{-CH}$), 125.2 ($\text{NC}_q\text{C}_q\text{N}$), 128.6 ($m^{\text{tolyl}}\text{-CH}$), 132.6 ($o^{\text{tolyl}}\text{-CH}$), 136.1 ($p^{\text{tolyl}}\text{-CH}$), 146.3 (br, $i^{\text{tolyl}}\text{-C}_q$) 154.7 (OC_q), 162.2 (br, NCN).

HRMS-ASAP (m/z): $[\text{M} + \text{H}]^+$ calc. for $\text{C}_{24}\text{H}_{31}\text{BN}_2\text{O}_2$, 391.2551 found 391.2539.

Synthesis of *p*-tolylBneop•Mes₂Im ADD10

To *p*-tolylBneop (150 mg, 730 μmol) and Mes₂Im (223 mg, 730 μmol) 5 mL of toluene was added. After 16 h at room temperature the solvent was removed under reduced pressure. The residue was washed with 5 mL of *n*-hexane and dried *in vacuo*.

Yield: 282 mg (550 μmol , 75%) of a white solid.

Elemental analysis for [C₃₃H₄₁BN₂O₂] [508.51 g/mol] Calc. (obs.): C 77.95 (77.79), H 8.13 (8.21), N 5.51 (5.69)

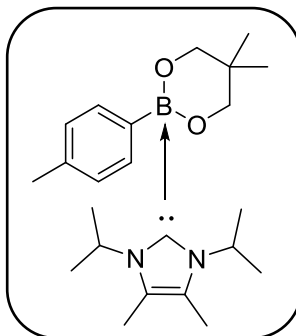
¹H-NMR (200 MHz, 25 °C, C₆D₆): δ_{H} / ppm = 0.70 (s, 6 H, OCH₂C_qCH₃), 2.09 (s, 12 H, *o*^{Mes}-CH₃), 2.17 (s, 6 H, *p*^{Mes}-CH₃), 2.24 (s, 3 H, *p*^{tolyl}-CH₃), 3.38 (s, 4 H, OCH₂), 6.07 (s, 2 H, NCHCHN), 6.79 (s, 4 H, *m*^{Mes}-CH), 7.05 – 7.08 (m, 2 H, *o*^{tolyl}-CH), 7.58 – 7.62 (d, 2 H, *m*^{tolyl}-CH).

¹¹B-NMR (64 MHz, 25 °C, C₆D₆): δ_{B} / ppm = 10.2 (s).

¹³C{¹H}-NMR(100 MHz, 25 °C, C₆D₆): δ_{C} / ppm = 18.1 (*o*-CH₃), 21.1 (*p*^{Mes}-CH₃), 21.7 (*p*^{tolyl}-CH₃), 23.2 (OCH₂C_qCH₃), 32.7 (OCH₂C_qCH₃), 72.2 (OCH₂C_qCH₃), 121.5 (NCHCHN), 128.8 (*m*^{Mes}-CH), 134.7 (*o*^{Mes}-C_q), 135.6 (*o*^{tolyl}-CH), 136.2 (*i*^{Mes}-C_q), 137.2 (*p*^{Mes}-C_q), 138.2 (*m*^{tolyl}-CH), 140.4 (br, *i*^{tolyl}-C_q), 182.8 (br, NCN).

HRMS-ASAP (m/z): [M + H]⁺ calc. for C₃₃H₄₂BN₂O₂, 509.3334 found 509.3319.

Synthesis of *p*-tolylBneop•ⁱPr₂ImMe₂^[300] ADD11



To *p*-tolylBneop (150 mg, 730 μmol) and ⁱPr₂ImMe₂ (132 mg, 730 μmol) 5 ml of toluene was added. After 16 h at room temperature the solvent was removed under reduced pressure. The residue was washed with 5 mL of *n*-hexane and dried *in vacuo*.

Yield: 141 mg (360 μmol, 49%) of a white solid.

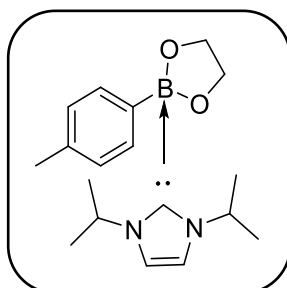
¹H-NMR (200 MHz, 25 °C, C₆D₆): δ_H / ppm = 1.00 (s, 6 H, OCH₂CH₃), 1.24 (d, 12 H, ³J_{HH} = 7 Hz, CHCH₃), 1.61 (br, 6 H, NC_qCH₃), 2.26 (s, 3 H, *p*-CH₃), 3.65 (s, 4 H, OCH₂CH₃), 5.89 (br, 2 H, CHCH₃), 7.22 – 7.26 (m, 2 H, *o*-CH), 7.92 – 7.96 (m, 2 H, *m*-CH).

¹¹B-NMR (200 MHz, 25 °C, C₆D₆): δ_B / ppm = 10.6 (s).

¹³C{¹H}-NMR (100 MHz, 25 °C, C₆D₆): δ_C / ppm = 9.8 (NC_qCH₃), 21.6 (*p*-CH₃), 22.7 (br, OCH₂C_qCH₃), 23.0 (br, OCH₂C_qCH₃), 32.8 (OCH₂C_qCH₃), 48.5 (NCHCH₃), 73.4 (OCH₂C_qCH₃), 124.0 (NC_qC_qN), 133.5 (*o*-CH), 136.3 (*i*-C_q).

HRMS-ASAP (m/z): [M + H]⁺ calc. for C₂₃H₃₇BN₂O₂, 385.3021 found 385.3015.

Synthesis of *p*-tolylBeg•ⁱPr₂Im ADD12



To a solution of *p*-tolylBeg (100 mg, 0.61 mmol) in 5 mL of toluene, ⁱPr₂Im (94 mg, 0.61 mmol) was added. After 4 h at room temperature the solvent was removed under reduced pressure. The residue was washed with 5 mL of *n*-hexane and dried *in vacuo*.

Yield: 86 mg (273 μmol , 45%) of a white solid.

Elemental analysis for $[\text{C}_{18}\text{H}_{27}\text{BN}_2\text{O}_2]$ [314.23 g/mol] Calc. (obs.): C 68.80 (67.55), H 8.66 (8.39), N 8.91 (8.20)

Although the present results are outside the range viewed as established for analyzed purity, they are provided to illustrate the best values obtained to date. In addition, the ^1H , ^{11}B , and the $^{13}\text{C}\{^1\text{H}\}$ NMR spectra as given in Figure 152, Figure 153 and Figure 154 provide evidence for the purity of the compound.

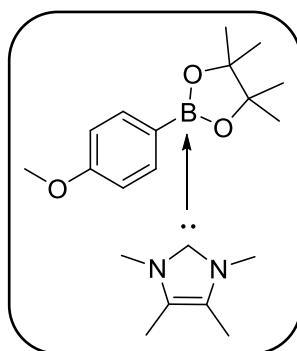
$^1\text{H-NMR}$ (400 MHz, 25 $^\circ\text{C}$, C_6D_6): δ_{H} / ppm = 0.96 (d, 12 H, $^3J_{\text{HH}} = 7$ Hz, CHCH_3), 2.29 (s, 3 H, C_qCH_3), 4.02 (br, 2 H, OCH_2), 4.23 (br, 2 H, OCH_2), 6.01 (sept, 2 H, $^3J_{\text{HH}} = 7$ Hz, CHCH_3), 6.17 (s, 2 H, NCHCHN), 7.25 – 7.26 (m, 2 H, arylCH), 7.72 – 7.74 (m, 2 H, arylCH).

$^{11}\text{B-NMR}$ (128 MHz, 25 $^\circ\text{C}$, C_6D_6): δ_{B} / ppm = 6.6 (s).

$^{13}\text{C}\{^1\text{H}\}$ -NMR (100 MHz, 25 $^\circ\text{C}$, C_6D_6): δ_{C} / ppm = 21.6 ($p\text{-CH}_3$), 23.3 (CHCH_3), 49.2 (CHCH_3), 65.8 ($\text{OCH}_2\text{CH}_2\text{O}$), 115.8 (NCHCHN), 128.7 ($m\text{-C}_q$), 132.6 ($p\text{-C}_q$), 134.9 ($o\text{-C}_q$), 166.2 (NCN).

HRMS-ASAP (m/z): $[\text{M} + \text{H}]^+$ calc. for $\text{C}_{18}\text{H}_{27}\text{BN}_2\text{O}_2$, 315.2238 found, 315.2234.

Synthesis of 4-MeO-C₆H₄Bpin•Me₄Im ADD13



To 4-MeO-C₆H₄Bpin (100 mg, 420 μmol) and Me₄Im (53 mg, 420 μmol) 5 mL of toluene was added. After 2 h at room temperature the solvent was removed under reduced pressure. The residue was washed with 5 mL of *n*-hexane and dried *in vacuo*.

Yield: 79 mg (190 μmol , 28%) of a white solid.

Elemental analysis for $[\text{C}_{20}\text{H}_{31}\text{BN}_2\text{O}_3]$ [358.28g/mol] Calc. (obs.): C 67.05 (66.00), H 8.72 (8.68), N 7.82 (7.67)

Although the present results are outside the range viewed as established for analyzed purity, they are provided to illustrate the best values obtained to date. In addition, the ^1H , ^{11}B , and the $^{13}\text{C}\{^1\text{H}\}$ NMR spectra as given in Figure 155, Figure 156 and Figure 157 provide evidence for the purity of the compound.

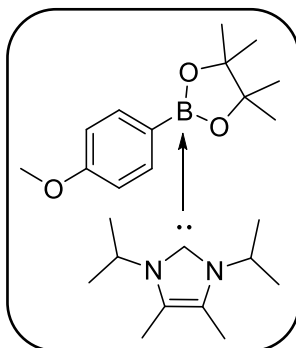
$^1\text{H-NMR}$ (400 MHz, 25 °C, C_6D_6): δ_{H} / ppm = 1.14 (s, 6 H, NC_qCH_3), 1.29 (br, 6 H, OC_qCH_3), 1.47 (br, 6 H, OC_qCH_3), 3.44 (s, 3 H, OCH_3), 3.59 (s, 6 H, NCH_3), 7.07 (d, 2 H, $^3J_{\text{HH}} = 9$ Hz, arylCH), 7.90 (d, 2 H, $^3J_{\text{HH}} = 9$ Hz, arylCH).

$^{11}\text{B-NMR}$ (128 MHz, 25 °C, C_6D_6): δ_{B} / ppm = 4.6 (s).

$^{13}\text{C}\{^1\text{H}\}$ -NMR (100 MHz, 25 °C, C_6D_6): δ_{C} / ppm = 7.6 (NC_qCH_3), 25.6 (br, OC_qCH_3), 26.7 (br, OC_qCH_3), 32.5 (NCH_3), 54.7 (OCH_3), 79.2 (OC_q), 113.2 ($\text{NC}_q\text{C}_q\text{N}$), 123.3 ($m\text{-CH}$), 133.0 ($o\text{-CH}$), 147.0 (br, $i\text{-C}_q$), 158.6 ($p\text{-CH}$), 167.3 (br, NCN).

HRMS-ASAP (m/z): $[\text{M} + \text{H}]^+$ calc. for $\text{C}_{20}\text{H}_{31}\text{BN}_2\text{O}_3$, 359.2500 found 359.2500.

Synthesis of 4-MeO-C₆H₄Bpin•ⁱPr₂Im Me₂^[300] ADD14



To 4-MeO-C₆H₄Bpin (100 mg, 420 μmol) and ⁱPr₂Im^{Me} (77 mg, 420 μmol), 5 mL of toluene was added. After 2 h at room temperature, the solvent was removed under reduced pressure. The residue was washed with 5 mL of *n*-hexane and dried *in vacuo*. Yield: 90 mg (220 μmol , 53%) of a white solid.

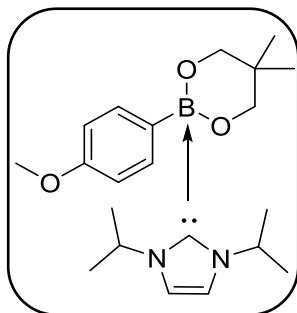
$^1\text{H-NMR}$ (400 MHz, 25 °C, C_6D_6): δ_{H} / ppm = 1.27 (br, 24 H, CHCH_3 and OC_qCH_3), 1.55 (br, 6 H, NC_qCH_3), 3.39 (br, 3 H, OCH_3), 7.00 (br, 2 H, $o\text{-CH}$), 7.95 (br, 2 H, $m\text{-CH}$).

$^{11}\text{B-NMR}$ (128 MHz, 25 °C, C_6D_6): δ_{B} / ppm = 5.5.

$^{13}\text{C}\{^1\text{H}\}$ -NMR (100 MHz, 25 °C, C_6D_6): δ_{C} / ppm = 9.7 (br, NC_qCH_3), 22.7 (br, CHCH_3), 25.9 (br, OC_qCH_3), 48.7 (br, CHCH_3), 78.5 (br, OC_qCH_3), 113.4 (br, $o\text{-CH}$), 123.7 (br, $\text{NC}_q\text{C}_q\text{N}$), 134.4 (br, $m\text{-CH}$).

HRMS-ASAP (m/z): $[\text{M}]^+$ calc. for $\text{C}_{24}\text{H}_{39}\text{BN}_2\text{O}_3$, 414.3048 found 414.3049.

Synthesis of 4-MeO- $\text{C}_6\text{H}_4\text{Bneop}\bullet^i\text{Pr}_2\text{Im}$ ADD15



To a solution of 4-MeO- $\text{C}_6\text{H}_4\text{Bneop}$ (150 mg, 680 μmol) in 5 mL of toluene, $^i\text{Pr}_2\text{Im}$ (105 mg, 680 μmol) was added. After 16 h at room temperature the solvent was removed under reduced pressure. The residue was washed with 5 mL of *n*-hexane and dried *in vacuo*.

Yield: 70 mg (190 μmol , 28%) of a beige solid.

Elemental analysis for $[\text{C}_{21}\text{H}_{33}\text{BN}_2\text{O}_2]$ [372.32 g/mol] Calc. (obs.): C 67.75 (66.85), H 8.93 (8.85), N 7.52 (7.08).

Although the present results are outside the range viewed as established for analyzed purity, they are provided to illustrate the best values obtained to date. In addition, the ^1H , ^{11}B , and the $^{13}\text{C}\{^1\text{H}\}$ NMR spectra as given in Figure 158, Figure 159 and Figure 160 provide evidence for the purity of the compound.

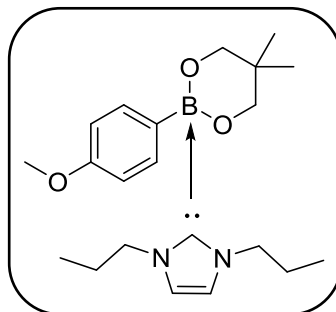
^1H -NMR (400 MHz, 25 °C, C_6D_6): δ_{H} / ppm = 1.01 (d, 12 H, $^3J_{\text{HH}} = 7$ Hz, CHCH_3), 1.13 (s, 6 H, $\text{OCH}_2\text{C}_q\text{CH}_3$), 3.45 (s, 3 H, OCH_3), 3.72 (s, 4 H, $\text{OCH}_2\text{C}_q\text{CH}_3$), 6.10 (br, 2 H, CHCH_3), 6.30 (s, 2 H, NCHCHN), 7.03 (d, 2 H, $^3J_{\text{HH}} = 8$, $_{\text{aryl}}\text{CH}$), 7.80 (d, 2 H, $^3J_{\text{HH}} = 8$ Hz, $_{\text{aryl}}\text{CH}$).

^{11}B -NMR (64 MHz, 25 °C, C_6D_6): δ_{B} / ppm = 3.3 (s).

$^{13}\text{C}\{^1\text{H}\}$ -NMR (100 MHz, 25 °C, C_6D_6): δ_{C} / ppm = 23.5 (NCHCH_3), 23.5 ($\text{OCH}_2\text{C}_q\text{CH}_3$), 33.3 ($\text{OCH}_2\text{C}_q\text{CH}_3$), 49.0 (NCHCH_3), 54.6 (OCH_3), 73.7 ($\text{OCH}_2\text{C}_q\text{CH}_3$), 113.3 ($o\text{-CH}$), 116.5 (br, NCHCHN), 133.8 ($m\text{-CH}$), 143.1 (br, $i\text{-C}_q$), 158.9 ($p\text{-C}_q\text{O}$), 168.4 (br, NCN).

HRMS-ASAP (m/z): $[M + H]^+$ calc. for $C_{21}H_{33}BN_2O_3$, 373.2657 found 373.2653.

Synthesis of 4-MeO-C₆H₄Bneop•ⁿPr₂Im ADD16



To a solution of 4-MeO-C₆H₄Bneop (150 mg, 680 μ mol) in 5 mL of toluene, ⁿPr₂Im (105 mg, 680 μ mol) was added. After 16 h at room temperature the solvent was removed under reduced pressure. The residue was washed with 5 mL of *n*-hexane and dried *in vacuo*.

Yield: 84 mg (220 μ mol, 32%) of a white solid.

Elemental analysis for $[C_{21}H_{33}BN_2O_3]$ [372.32g/mol] Calc. (obs.): C 67.75 (66.83), H 8.93 (8.92), N 7.52 (7.10)

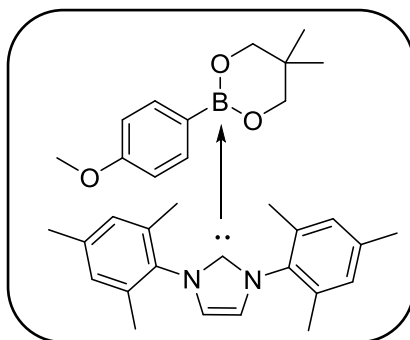
Although the present results are outside the range viewed as established for analyzed purity, they are provided to illustrate the best values obtained to date. In addition, the ¹H, ¹¹B, and the ¹³C{¹H} NMR spectra as given in Figure 161, Figure 162 and Figure 163 provide evidence for the purity of the compound.

¹H-NMR (200 MHz, 25 °C, C₆D₆): δ_H / ppm = 0.70 (t, 6 H, ³J_{HH} = 7 Hz, NCH₂CH₂CH₃), 1.11 (s, 6 H, OCH₂C_qCH₃), 1.43 (sext, 4 H, ³J_{HH} = 7 Hz, NCH₂CH₂CH₃), 3.44 (s, 3 H, C_qOCH₃), 3.69 (br, 4 H, OCH₂C_qCH₃), 4.16 (m, 4 H, NCH₂CH₂CH₃), 6.12 (s, 2 H, NCHCHN), 7.04 (m, 2 H, arylCH), 7.82 (m, 2 H, arylCH).

¹¹B-NMR (64 MHz, 25 °C, C₆D₆): δ_B / ppm = 2.5 (s).

¹³C{¹H}-NMR (100 MHz, 25 °C, C₆D₆): δ_C / ppm = 11.0 (NCH₂CH₂CH₃), 23.5 (OCH₂C_qCH₃), 24.5 (NCH₂CH₂CH₃), 33.3 (OCH₂C_qCH₃), 50.0 (OCH₃), 54.7 (NCH₂CH₂CH₃), 73.3 (OCH₂C_qCH₃), 113.3 (NCHCHN), 119.6 (*m*-CH), 134.0 (*o*-CH), 143.3 (br, *i*-C_q), 159.0 (*p*-C_qO), 167.9 (br, NCN).

HRMS-ASAP (m/z): $[M]^+$ calc. for $C_{21}H_{33}BN_2O_3$, 372.2579 found 372.2574.

Synthesis of 4-MeO-C₆H₄Bneop•Mes₂Im ADD17

To 4-MeO-C₆H₄Bneop (150 mg, 680 μmol) and Mes₂Im (206 mg, 680 μmol) 5 mL of toluene was added. After 1 h at room temperature the solvent was removed under reduced pressure. The residue was washed with 5 mL of *n*-hexane and dried *in vacuo*.

Yield: 211 mg (400 μmol, 59%) of a white solid.

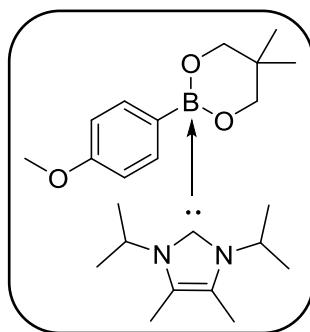
Elemental analysis for [C₃₃H₄₁BN₂O₂] [524.50g/mol] Calc. (obs.): C 75.57 (75.22), H 7.88 (7.75), N 5.34 (5.19)

¹H-NMR (400 MHz, 25 °C, C₆D₆): δ_H / ppm = 0.71 (s, 6 H, OCH₂C_qCH₃), 2.10 (s, 12 H, *o*-CH₃), 2.16 (s, 6 H, *p*-CH₃), 3.39 (s, 4 H, OCH₂C_qCH₃), 3.40 (s, 3 H, OCH₃), 6.06 (s, 2 H, NCHCHN), 6.79 (s, 4 H, *m*^{Mes}-CH), 6.86 (d, 2 H, ³J_{HH} = 9 Hz, *aryl*CH), 7.70 (d, 2 H, ³J_{HH} = 9 Hz, *aryl*CH).

¹¹B-NMR (128 MHz, 25 °C, C₆D₆): δ_B / ppm = 9.1 (s).

¹³C{¹H}-NMR (100 MHz, 25 °C, C₆D₆): δ_C / ppm = 18.1, 21.1, 23.3, 32.8, 54.6, 72.2, 112.9 (*m*-CH), 121.5 (NCHCHN), 128.8 (*m*^{Mes}-CH), 135.6 (*aryl*C_q), 135.7 (*o*-CH), 137.1 (*aryl*C_q), 138.2 (*aryl*C_q), 159.7 (*p*-C_qO), 182.2 (br, NCN).

HRMS-ASAP (m/z): [M + H]⁺ calc. for C₃₃H₄₁BN₂O₃, 525.3283 found 525.3277.

Synthesis of 4-MeO-C₆H₄Bneop•ⁱPr₂ImMe₂^[300] ADD18


To 4-MeO-C₆H₄Bneop (150 mg, 680 μmol) and ⁱPr₂ImMe₂ (122 mg, 680 μmol) 5 mL of toluene was added. After 3 h at room temperature the solvent was removed under reduced pressure. The residue was washed with 5 mL of *n*-hexane and dried *in vacuo*.

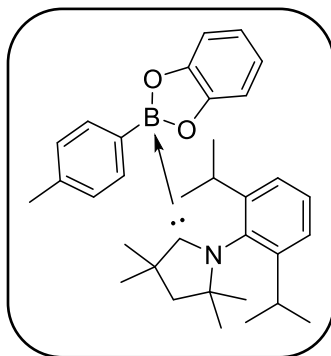
Yield: 101 mg (250 μmol, 35%) of a white solid.

¹H-NMR (400 MHz, 25 °C, C₆D₆): δ_H / ppm = 0.93 (br, 6 H, OCH₂C_qCH₃), 1.29 (d, 12 H, ³J_{HH} = 6 Hz, CHCH₃), 1.64 (br, 6 H, NC_qCH₃), 3.39 (s, 3 H, OCH₃), 3.61 (s, 4 H, OCH₂C_qCH₃), 5.42 (br, 2 H, CHCH₃), 6.99 – 7.01 (m, 2 H, *o*-CH), 7.99 – 8.01 (m, 2 H, *m*-CH).

¹¹B-NMR (128 MHz, 25 °C, C₆D₆): δ_B / ppm = 3.8.

¹³C{¹H}-NMR (100 MHz, 25 °C, C₆D₆): δ_C / ppm = 9.5 (NC_qCH₃), 22.7 (CHCH₃), 23.1 (br, OCH₂C_qCH₃), 32.5 (OCH₂C_qCH₃), 48.5 (br, CHCH₃), 54.6 (OCH₃), 73.1 (OCH₂C_qCH₃), 113.4 (*o*-CH), 123.6 (NC_qC_qN), 135.0 (*m*-CH), 157.6 (*p*-C_q), 160.5 (OC_q).

HRMS-ASAP (m/z): [M]⁺ calc. for C₂₃H₃₇BN₂O₃, 400.2892 found 400.2873.

Synthesis of *p*-tolylBcat•CaaC^{Me}[300] ADD19

To *p*-tolylBcat (150 mg, 710 μmol) and CaaC^{Me} (128 mg, 710 μmol) 5 mL of toluene was added. After 3 h at room temperature the solvent was removed under reduced pressure. The residue was washed with 5 mL of *n*-hexane and dried *in vacuo*.

Yield: 180 mg (360 μmol , 51%) of a white solid.

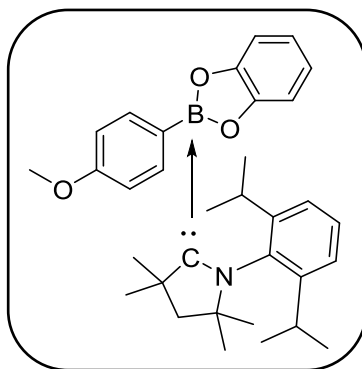
Elemental analysis for $[\text{C}_{33}\text{H}_{42}\text{BNO}_2]$ [497.53 g/mol] Calc. (obs.): C 79.99 (80.34), H 8.54 (8.67), N 2.83 (3.01).

$^1\text{H-NMR}$ (400 MHz, 25 $^\circ\text{C}$, C_6D_6): δ_{H} / ppm = 0.89 (s, 6 H, NC_qCH_3), 1.08 (d, 6 H, $^3J_{\text{HH}} = 7$ Hz, CHCH_3), 1.18 (d, 6 H, $^3J_{\text{HH}} = 7$ Hz, CHCH_3), 1.37 (s, 2 H, NC_qCH_2), 1.40 (s, 6 H, $\text{C}_q\text{C}_q\text{CH}_3$), 2.21 (s, 3 H, *p*- CH_3), 2.77 (sept, 2 H, $^3J_{\text{HH}} = 7$ Hz, CHCH_3), 6.63 – 6.68 (m, 4 H, arylCH), 7.00 (d, 2 H, *m*^{Dipp}-CH), 7.07 (d, 2 H, $^3J_{\text{HH}} = 8$ Hz, *o*^{tolyl}-CH), 7.12 – 7.14 (m, 1 H, *p*^{Dipp}-CH), 7.59 (d, 2 H, $^3J_{\text{HH}} = 8$ Hz, *m*^{tolyl}-CH).

$^{11}\text{B-NMR}$ (128 MHz, C_6D_6 , 25 $^\circ\text{C}$): δ_{B} / ppm = 9.3.

$^{13}\text{C}\{^1\text{H}\}$ -NMR (100 MHz, 25 $^\circ\text{C}$, C_6D_6): δ_{C} / ppm = 21.5 (*p*^{tolyl}- CH_3), 25.3 (CHCH_3), 25.7 (CHCH_3), 28.6 ($\text{C}_q\text{C}_q\text{CH}_3$), 29.5 (NC_qCH_3), 29.7 (NC_qCH_3), 52.0 (NC_qCH_2), 53.6 ($\text{C}_q\text{C}_q\text{CH}_3$), 80.1 (NC_qCH_3), 109.3 ($\text{aryl}^{\text{cat}}\text{CH}$), 118.3 ($\text{aryl}^{\text{cat}}\text{CH}$), 125.4 (*m*^{Dipp}-CH), 128.2 (*o*^{tolyl}-CH), 129.6 (*p*^{Dipp}-CH), 132.6 (*m*^{tolyl}-CH), 134.5 (*i*^{Dipp}- C_q), 135.5 (*p*^{tolyl}- C_q), 145.3 (*o*^{Dipp}- C_q), 154.0 (OC_q), 228.8 (br, NC_qB).

HRMS-ASAP (m/z): $[\text{M} + \text{H}]^+$ calc. for $\text{C}_{33}\text{H}_{42}\text{BNO}_2$, 496.3381 found 496.3364.

Synthesis of 4-MeO-C₆H₄Bcat•CaaC^{Me}[300] ADD20

To 4-MeO-C₆H₄Bcat (81 mg, 357 μmol) and CaaC^{Me} (102 mg, 357 μmol), 5 mL of toluene was added. After 2 h at room temperature, the solvent was removed under reduced pressure. The residue was washed with 5 mL of *n*-hexane and dried *in vacuo*.

Yield: 83 mg (162 μmol, 45%) of a yellow solid.

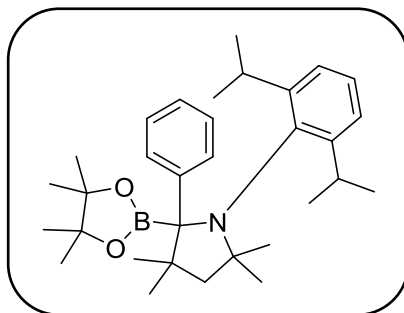
Elemental analysis for [C₃₃H₄₂BNO₃+C₆D₆] [511.51 + 84.15 g/mol] Calc. (obs.): C 78.64 (79.06), H 9.14 (9.16), N 2.35 (2.71).

¹H-NMR (400 MHz, 25 °C, C₆D₆): δ_H / ppm = 0.89 (s, 6 H, NC_qCH₃), 1.07 (d, 6 H, ³J_{HH} = 7 Hz, CHCH₃), 1.18 (d, 6 H, ³J_{HH} = 7 Hz, CHCH₃), 1.38 (s, 2 H, CH₂), 1.41 (s, 6 H, C_qC_qCH₃), 2.75 (sept, ³J_{HH} = 7 Hz, 2 H, CHCH₃), 3.40 (s, 3 H, OCH₃), 6.65 – 6.70 (m, 4 H, _{aryl}^{cat}CH), 6.84 – 6.86 (m, 2 H, *o*^{anisol}CH), 6.98 – 7.00 (m, 2 H, *m*^{Dipp}-CH), 7.11 – 7.13 (m, 1 H, *p*^{Dipp}-CH), 7.53 – 7.56 (m, 2 H, *m*^{anisol}CH).

¹¹B-NMR (128 MHz, 25 °C, C₆D₆): δ_B / ppm = 9.2.

¹³C{¹H}-NMR (100 MHz, 25 °C, C₆D₆): δ_C / ppm = 25.2 (CHCH₃), 25.7 (CHCH₃), 28.6 (C_qCH₃), 29.5 (CHCH₃), 29.6 (C_qCH₃), 52.1 (CH₂), 53.6 (C_qC_qCH₃), 54.6 (OCH₃), 80.1 (NC_qCH₃), 109.3 (_{aryl}^{cat}CH), 113.2 (*o*^{anisol}CH), 118.3 (_{aryl}^{cat}CH), 125.4 (*m*^{Dipp}-CH), 129.6 (*m*^{Dipp}-CH), 133.6 (*m*^{anisol}CH), 134.5 (*i*^{Dipp}-C_q), 145.3 (*o*^{Dipp} C_q), 154.0 (OC_q), 159.3 (*p*^{anisol}-C_q), 228.9 (NC_qB).

HRMS-ASAP (m/z): [M + H]⁺ calc. for C₃₃H₄₂BNO₃, 512.3331 found 512.3322.

Synthesis of BCA $C_6H_5Bpin \cdot CaaC^{Me[300]}$ BCA1

To phenylBpin (36 mg, 175 μ mol) and $CaaC^{Me}$ (50 mg, 175 μ mol) 4 mL of toluene was added. After 3 h at room temperature the solvent was removed under reduced pressure. The residue was washed with 2 mL of *n*-hexane and dried *in vacuo*.

Yield: 32 mg (65 μ mol, 37%) of a white solid.

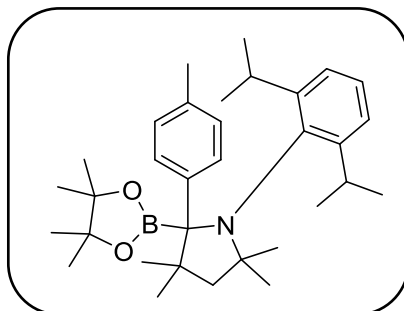
Elemental analysis for $[C_{32}H_{48}BNO_2]$ [489.55 g/mol] Calc. (obs.): C 78.51 (78.67), H 9.88 (9.85), N 2.86 (2.94).

1H -NMR (400 MHz, 25 $^\circ$ C, C_6D_6): δ_H / ppm = 0.24 (d, 3 H, $^3J_{HH} = 7$ Hz, $CHCH_3$), 0.97 (s, 6 H, OC_qCH_3), 0.99 (s, 6 H, OC_qCH_3), 1.16 (s, 3 H, $C_qC_qCH_3$), 1.19 (d, 3 H, $^3J_{HH} = 7$ Hz, $CHCH_3$), 1.42 (d, 3 H, $^3J_{HH} = 7$ Hz, $CHCH_3$), 1.47 (d, 3 H, $^3J_{HH} = 7$ Hz, $CHCH_3$), 1.49 (s, 3 H, $C_qC_qCH_3$), 1.58 (s, 3 H, NC_qCH_3), 1.83 (s, 3 H, NC_qCH_3), 1.86 (d, 1 H, $^2J_{HH} = 12$ Hz, NC_qCH_2), 2.78 (d, 1 H, $^2J_{HH} = 12$ Hz, NC_qCH_2), 3.67 (sept, 1 H, $^3J_{HH} = 7$ Hz, $CHCH_3$), 4.20 (sept, 1 H, $^3J_{HH} = 7$ Hz, $CHCH_3$), 6.85 – 6.88 (m, 1 H, $p^{tolyl}-CH$), 6.94 – 6.98 (m, 2 H $\sigma^{tolyl}-CH$), 7.07 – 7.09 (m, 1 H, $m^{Dipp}-CH$), 7.21 – 7.26 (m, 3 H, $p^{Dipp}-CH+m^{tolyl}-CH$), 7.31 – 7.34 (m, 1 H, $m^{Dipp}-CH$).

^{11}B -NMR (128 MHz, 25 $^\circ$ C, C_6D_6): δ_B / ppm = 32.4.

$^{13}C\{^1H\}$ -NMR (100 MHz, 25 $^\circ$ C, C_6D_6): δ_C / ppm = 24.2 ($CHCH_3$), 25.1 ($CHCH_3$), 25.4 ($CHCH_3$), 25.8 (OC_qCH_3), 27.8 ($CHCH_3$), 28.4 (NC_qCH_3), 29.1 (NC_qCH_3), 30.6 ($C_qC_qCH_3$), 31.8 ($C_qC_qCH_3$), 43.5 ($C_qC_qCH_3$), 57.9 (C_qCH_2), 61.1 (NC_qCH_2), 83.7 (OC_qC_qO), 125.3 ($m^{Dipp}-CH$), 125.5 ($m^{Dipp}-CH$), 125.7 ($p^{phenyl}-CH$), 127.1 ($p^{Dipp}-CH$), 128.6 ($\sigma^{phenyl}-CH$), 129.9 ($m^{phenyl}-CH$), 135.5 ($p^{phenyl}C_q$), 137.9 ($i^{phenyl}C_q$), 140.7 ($i^{Dipp}C_q$), 152.7 ($\sigma^{Dipp}C_q$), 154.8 ($\sigma^{Dipp}C_q$).

HRMS-ASAP (m/z): $[M + H]^+$ calc. for $C_{32}H_{49}BNO_2$, 490.3851 found, 490.3843.

Synthesis of BCA *p*-tolylBpin•CaaC^{Me}[300] BCA2

To *p*-tolylBpin (100 mg, 460 μmol) and CaaC^{Me} (131 mg, 460 μmol) 5 mL of toluene was added. After 14 h at room temperature the solvent was removed under reduced pressure. The residue was washed with 5 mL of *n*-hexane and dried *in vacuo*.

Yield: 124 mg (246 μmol , 54%) of a white solid.

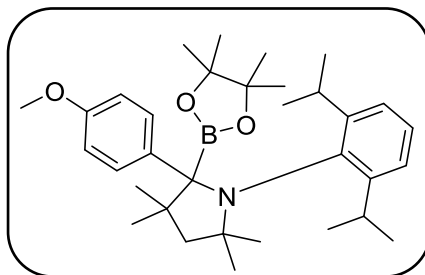
Elemental analysis for [C₃₃H₅₀BNO₂] [503.57 g/mol] Calc. (obs.): C 78.71 (78.87), H 10.01 (10.50), N 2.78 (2.88).

¹H-NMR (400 MHz, 25 °C, C₆D₆): δ_{H} / ppm = 0.33 (d, 3 H, ³J_{HH} = 7 Hz, CHCH₃), 0.98 (s, 6 H, OC_qCH₃), 1.00 (s, 6 H, OC_qCH₃), 1.19 (s, 3 H, C_qC_qCH₃), 1.22 (d, 3 H, ³J_{HH} = 7 Hz, CHCH₃), 1.46 (d, 3 H, ³J_{HH} = 7 Hz, CHCH₃), 1.50 (d, 3 H, ³J_{HH} = 7 Hz, CHCH₃), 1.52 (s, 3 H, C_qC_qCH₃), 1.60 (s, 3 H, NC_qCH₃), 1.86 (s, 3 H, NC_qCH₃), 1.87 (d, 1 H, ²J_{HH} = 12 Hz, NC_qCH₂), 1.96 (s, 3 H, *p*^{tolyl}-CH₃), 2.81 (d, 1 H, ²J_{HH} = 12 Hz, NC_qCH₂), 3.74 (sept, 1 H, ³J_{HH} = 7 Hz, CHCH₃), 4.22 (sept, 1 H, ³J_{HH} = 7 Hz, CHCH₃), 6.77 – 6.79 (m, 2 H, *o*^{tolyl}-CH), 7.11 – 7.13 (m, 1 H, *m*^{Dipp}-CH), 7.17 – 7.19 (m, 2 H, *m*^{tolyl}-CH), 7.24 – 7.28 (m, 1 H, *p*^{Dipp}-CH), 7.34 – 7.36 (m, 1 H, *m*^{Dipp}-CH).

¹¹B-NMR (128 MHz, 25 °C, C₆D₆): δ_{B} / ppm = 32.3.

¹³C{¹H}-NMR (100 MHz, 25 °C, C₆D₆): δ_{C} / ppm = 20.8 (*p*^{tolyl}-CH₃), 24.2 (CHCH₃), 25.1 (CHCH₃), 25.4 (CHCH₃), 25.9 (OC_qCH₃), 25.9 (OC_qCH₃), 27.7 (CHCH₃), 27.8 (CHCH₃), 27.9 (CHCH₃), 28.4 (NC_qCH₃), 29.2 (NC_qCH₃), 30.7 (C_qC_qCH₃), 31.8 (C_qC_qCH₃), 43.6 (C_qC_qCH₃), 57.9 (C_qCH₂), 61.1 (NC_qCH₂), 70.9 (BC_qC_q), 83.7 (OC_qC_qO), 125.2 (*m*^{Dipp}-CH), 125.5 (*m*^{Dipp}-CH), 127.2 (*p*^{Dipp}-CH), 127.9 (*o*^{tolyl}-CH), 129.8 (*m*^{tolyl}-CH), 134.2 (*p*^{tolyl}-C_q), 139.8 (*i*^{tolyl}-C_q), 140.9 (*i*^{Dipp}-C_q), 152.7 (*o*^{Dipp}-C_q), 154.9 (*o*^{Dipp}-C_q).

HRMS-ASAP (m/z): [M + H]⁺ calc. for C₃₃H₅₁BNO₂, 504.4007 found, 504.3997.

Synthesis of BCA 4-MeO-C₆H₄Bpin•CaaC^{Me}[300] BCA3


To 4-MeO-C₆H₄Bpin (150 mg, 639 μ mol) and CaaC^{Me} (182 mg, 639 μ mol), 5 mL of toluene was added. After 12 h at room temperature, the solvent was removed under reduced pressure. The residue was washed with 5 mL of *n*-hexane and dried *in vacuo*.

Yield: 143 mg (275 μ mol, 43%) of a light yellow solid.

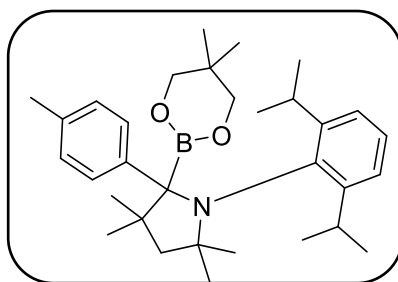
Elemental analysis for [C₃₃H₅₀BNO₃] [519.58 g/mol] Calc. (obs.): C 76.29 (75.45), H 9.70 (10.13), N 2.70 (2.42).

¹H-NMR (400 MHz, 25 °C, C₆D₆): δ_{H} / ppm = 0.38 (d, 3 H, ³J_{HH} = 7 Hz, CHCH₃), 0.99 (s, 6 H, OC_qCH₃), 1.01 (s, 6 H, OC_qCH₃), 1.19 (s, 3 H, C_qC_qCH₃), 1.22 (d, 3 H, ³J_{HH} = 7 Hz, CHCH₃), 1.46 (d, 3 H, ³J_{HH} = 7 Hz, CHCH₃), 1.49 (d, 3 H, ³J_{HH} = 7 Hz, CHCH₃), 1.52 (s, 3 H, C_qC_qCH₃), 1.60 (s, 3 H, NC_qCH₃), 1.85 (s, 3 H, NC_qCH₃), 1.88 (d, 1 H, ²J_{HH} = 12 Hz, NC_qCH₂), 2.82 (d, 1 H, ²J_{HH} = 12 Hz, NC_qCH₂), 3.15 (s, 3 H, OCH₃), 3.77 (sept, 1 H, ³J_{HH} = 7 Hz, CHCH₃), 4.20 (sept, 1 H, ³J_{HH} = 7 Hz, CHCH₃), 6.58 – 6.62 (m, 2 H, *o*^{anisol}-CH), 7.12 – 7.14 (m, 1 H, *m*^{Dipp}-CH), 7.18 – 7.20 (m, 2 H, *m*^{anisol}-CH), 7.24 – 7.28 (m, 1 H, *p*^{Dipp}-CH), 7.34 – 7.36 (m, 1 H, *m*^{Dipp}-CH).

¹¹B-NMR (128 MHz, 25 °C, C₆D₆): δ_{B} / ppm = 32.8.

¹³C{¹H}-NMR (100 MHz, 25 °C, C₆D₆): δ_{C} / ppm = 24.3 (CHCH₃), 25.1 (CHCH₃), 25.4 (CHCH₃), 25.8 (OC_qCH₃), 26.0 (OC_qCH₃), 27.7 (CHCH₃), 27.8 (CHCH₃), 28.0 (CHCH₃), 28.5 (NC_qCH₃), 29.2 (NC_qCH₃), 30.7 (C_qC_qCH₃), 31.7 (C_qC_qCH₃), 43.7 (C_qC_qCH₃), 54.4 (*p*^{anisol}-CH₃), 58.0 (NC_qCH₂), 61.1 (NC_qCH₃), 70.6 (br, BC_qC_q), 83.6 (OC_qCH₃), 112.6 (*o*^{anisol}-CH), 125.2 (*m*^{Dipp}-CH), 125.5 (*m*^{Dipp}-CH), 127.3 (*p*^{Dipp}-CH), 130.9 (*m*^{anisol}-CH), 135.0 (*i*^{anisol}-C_q), 140.9 (*i*^{Dipp}-CH), 152.7 (*o*^{Dipp}-CH), 155.0 (*o*^{Dipp}-CH), 157.5 (*p*^{anisol}-C_q).

HRMS-ASAP (m/z): [M + H]⁺ calc. for C₃₃H₅₀BNO₃, 520.3957 found 520.3947.

Synthesis of BCA *p*-tolylBneop•CaaC^{Me}[300] BCA4

To *p*-tolylBneop (36 mg, 175 μ mol) and CaaC^{Me} (50 mg, 175 μ mol) 3 mL of toluene was added. After 3 h at room temperature the solvent was removed under reduced pressure. The residue was washed with 2 mL of *n*-hexane and dried *in vacuo*.

Yield: 31 mg (63 μ mol, 36%) of a white solid.

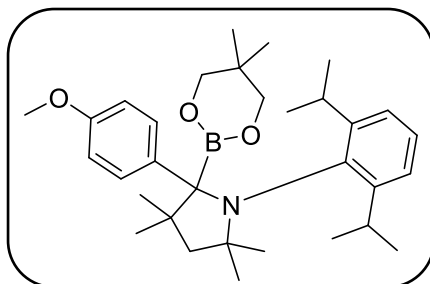
Elemental analysis for [C₃₂H₄₈BNO₂] [489.55 g/mol] Calc. (obs.): C 78.51 (77.01), H 9.88 (9.40), N 2.86 (3.24).

¹H-NMR (400 MHz, 25 °C, C₆D₆): δ_{H} / ppm = 0.38 (d, 3 H, ³J_{HH} = 7 Hz, CHCH₃), 0.54 (s, 6 H, OCH₂C_qCH₃), 1.23 (d, 3 H, ³J_{HH} = 7 Hz, CHCH₃), 1.28 (s, 3 H, NC_qCH₃), 1.38 (d, 3 H, ³J_{HH} = 7 Hz, CHCH₃), 1.47 (s, 3 H, NC_qCH₃), 1.48 (d, 3 H, ³J_{HH} = 7 Hz, CHCH₃), 1.66 (s, 3 H, C_qC_qCH₃), 1.87 (s, 3 H, C_qC_qCH₃), 1.92 (d, 1 H, (d, 3 H, ¹J_{HH} = 12 Hz, NC_qCH₂), 2.03 (s, 3 H, *p*^{tolyl}-CH₃), 2.94 (d, 1 H, ¹J_{HH} = 12 Hz, NC_qCH₂), 3.19 – 3.29 (m, 4 H, OCH₂), 3.76 (sept, 1 H, ³J_{HH} = 7 Hz, CHCH₃), 4.14 (sept, 1 H, ³J_{HH} = 7 Hz, CHCH₃), 6.81 – 6.83 (m, 2 H, *o*^{tolyl}-CH), 7.13 – 7.15 (m, 2 H, *m*^{tolyl}-CH), 7.18 – 7.23 (m, 1 H, *m*^{Dipp}-CH), 7.28 – 7.32 (m, 1 H, *p*^{Dipp}-CH), 7.34 – 7.36 (m, 1 H, *m*^{Dipp}-CH).

¹¹B-NMR (128 MHz, 25 °C, C₆D₆): δ_{B} / ppm = 27.2.

¹³C{¹H}-NMR (100 MHz, 25 °C, C₆D₆): δ_{C} / ppm = 20.8 (*p*^{tolyl}-CH₃), 22.9 (OCH₂C_qCH₃), 24.3 (CHCH₃), 25.4 (CHCH₃), 25.9 (CHCH₃), 26.5 (CHCH₃), 27.9 (CHCH₃), 28.0 (CHCH₃), 29.3 (C_qC_qCH₃), 29.5 (C_qC_qCH₃), 30.6 (OCH₂C_qCH₃), 31.0 (NC_qCH₃), 31.4 (NC_qCH₃), 43.3 (C_qC_qCH₃), 58.2 (NC_qCH₂), 61.5 (NC_qCH₂), 71.6 (OCH₂), 74.4 (BC_qC_q), 125.1 (*m*^{Dipp}-CH), 125.4 (*m*^{Dipp}-CH), 127.3 (*p*^{Dipp}-CH), 127.6 (*o*^{tolyl}-CH), 130.5 (*m*^{tolyl}-CH), 133.8 (*p*^{tolyl}-C_q), 140.5 (*i*^{tolyl}-C_q), 141.3 (*j*^{Dipp}-C_q), 152.7 (*o*^{Dipp}-C_q), 155.4 (*o*^{Dipp}-C_q).

HRMS-ASAP (m/z): [M + H]⁺ calc. for C₃₂H₄₉BNO₂, 490.3851 found 490.3841.

Synthesis of BCA 4-MeO-C₆H₄Bneop•CaaC^{Me}[300] BCA5


To 4-MeO-C₆H₄Bneop (150 mg, 680 μmol) and CaaC^{Me} (194 mg, 680 μmol) 5 mL of toluene was added. After 3 h at room temperature the solvent was removed under reduced pressure. The residue was washed with 5 mL of *n*-hexane and dried *in vacuo*.

Yield: 130 mg (260 μmol, 38%) of a white solid.

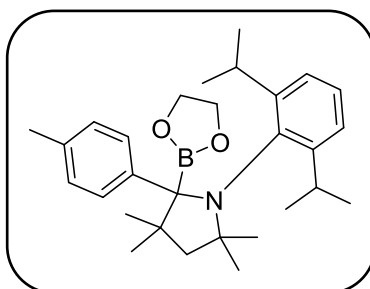
Elemental analysis for [C₃₂H₄₈BNO₃] [505.55 g/mol] Calc. (obs.): C 76.03 (75.61), H 9.57 (9.51), N 2.77 (2.55).

¹H-NMR (400 MHz, 25 °C, C₆D₆): δ_H / ppm = 0.42 (d, 3 H, ³J_{HH} = 7 Hz, CHCH₃), 0.55 (s, 6 H,), 1.22 (d, 3 H, ³J_{HH} = 7 Hz, CHCH₃), 1.28 (s, 3 H, C_qC_qCH₃), 1.38 (d, 3 H, ³J_{HH} = 7 Hz, CHCH₃), 1.47 (s, 3 H, C_qC_qCH₃), 1.48 (d, 3 H, ³J_{HH} = 7 Hz, CHCH₃), 1.66 (s, 3 H, NC_qCH₃), 1.87 (s, 3 H, NC_qCH₃), 1.93 (d, 1 H, ¹J_{HH} = 12 Hz, NC_qCH₂), 2.95 (d, 1 H, ¹J_{HH} = 12 Hz, NC_qCH₂), 3.21 (s, 3 H, OCH₃), 3.25 (m, 4 H, OCH₂), 3.78 (sept, 1 H, ³J_{HH} = 7 Hz, CHCH₃), 4.13 (sept, 1 H, ³J_{HH} = 7 Hz, CHCH₃), 6.61 – 6.63 (m, 2 H, _{aryl}CH), 7.13 – 7.18 (m, 3 H, _{aryl}CH and *p*^{Dipp}-CH), 7.27 – 7.36 (m, 2 H, *m*^{Dipp}-CH).

¹¹B-NMR (128 MHz, 25 °C, C₆D₆): δ_B / ppm = 29.4.

¹³C{¹H}-NMR (100 MHz, 25 °C, C₆D₆): δ_C / ppm = 22.9 (OCH₂C_qCH₃), 24.4 (CHCH₃), 25.9 (CHCH₃), 26.2 (CHCH₃), 26.5 (CHCH₃), 28.0 (CHCH₃), 29.2 (NC_qCH₃), 29.5 (NC_qCH₃), 30.6 (OCH₂C_q), 31.0 (C_qC_qCH₃), 31.4 (C_qC_qCH₃), 43.3 (BC_qC_q), 54.5 (OCH₃), 54.6 (OCH₃), 58.2 (NC_qCH₂), 61.5 (NC_q), 71.7 (OCH₂), 73.9 (br, BC_q), 112.4 (*m*^{anisol}-CH), 125.1 (*m*^{Dipp}-CH), 125.5 (*m*^{Dipp}-CH), 127.3 (*p*^{Dipp}-CH), 131.5 (*o*^{anisol}-CH), 135.7 (*i*^{anisol}-CH), 141.3 (*i*^{Dipp}-C_q), 152.6 (*o*^{Dipp}-CH), 155.4 (*o*^{Dipp}-CH), 157.3 (OC_q).

HRMS-ASAP (m/z): [M + H]⁺ calc. for C₃₂H₄₈BNO₃, 506.3800 found 506.3792.

Synthesis of BCA *p*-tolylBeg•CaaC^{Me}[300] BCA6

To *p*-tolylBeg (100 mg, 0.61 mmol) and CaaC^{Me} (176 mg, 0.62 mmol) 5 mL of toluene was added. After 4 h at room temperature the solvent was removed under reduced pressure to yield a viscous oil. The residue was washed with 5 mL of *n*-hexane and dried *in vacuo*.

Yield: 97 mg (171 μ mol, 28%) of a white solid.

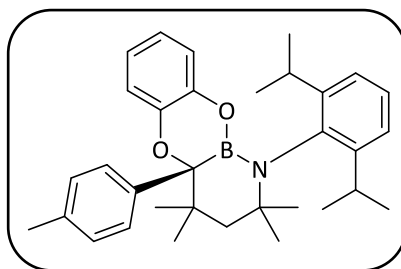
Elemental analysis for [C₂₉H₄₂BNO₂] [447.47 g/mol] Calc. (obs.): C 77.84 (77.21), H 9.46 (9.34), N 3.13 (2.92).

¹H-NMR (400 MHz, 25 °C, C₆D₆): δ_{H} / ppm = 0.39 (d, 3 H, ³J_{HH} = 7 Hz, CHCH₃), 1.23 (d, 3 H, ³J_{HH} = 7 Hz, CHCH₃), 1.27 (d, 3 H, ³J_{HH} = 7 Hz, CHCH₃), 1.30 (s, 3 H, C_qC_qCH₃), 1.44 (d, 3 H, ³J_{HH} = 7 Hz, CHCH₃), 1.44 (s, 3 H, C_qC_qCH₃), 1.56 (s, 3 H, NC_qCH₃), 1.63 (s, 3 H, NC_qCH₃), 2.03 (d, 1 H, ²J_{HH} = 12 Hz, NC_qCH₂), 2.04 (s, 3 H, *p*^{tolyl}-CH₃), 2.69 (d, 1 H, ²J_{HH} = 12 Hz, NC_qCH₂), 3.49 (s, 4 H, OCH₂), 3.78 (sept, 1 H, ³J_{HH} = 7 Hz, CHCH₃), 4.07 (sept, 1 H, ³J_{HH} = 7 Hz, CHCH₃), 6.84 – 6.86 (m, 2 H, *o*^{tolyl}-CH), 7.13 – 7.16 (m, 1 H, *m*^{Dipp}-CH), 7.16 – 7.18 (m, 2 H, *o*^{tolyl}-CH), 7.25 – 7.29 (m, 1 H, *p*^{Dipp}-CH), 7.29 – 7.32 (m, 1 H, *m*^{Dipp}-CH).

¹¹B-NMR (128 MHz, 25 °C, C₆D₆): δ_{B} / ppm = 33.8.

¹³C{¹H}-NMR (100 MHz, 25 °C, C₆D₆): δ_{C} / ppm = 20.8 (*p*^{tolyl}-CH₃), 24.4 (CHCH₃), 24.9 (CHCH₃), 25.7 (CHCH₃), 25.7 (CHCH₃), 28.1 (CHCH₃), 28.1 (NC_qCH₃), 28.7 (NC_qCH₃), 28.8 (CHCH₃), 30.9 (C_qC_qCH₃), 31.1 (C_qC_qCH₃), 43.4 (C_qC_qCH₃), 57.0 (NC_qCH₂), 61.8 (NC_qCH₂), 65.2 (OCH₂), 71.4 (BC_qC_q), 125.1 (*m*^{Dipp}-CH), 125.3 (*m*^{Dipp}-CH), 127.4 (*p*^{Dipp}-CH), 130.0 (*m*^{tolyl}-CH), 134.5 (*p*^{tolyl}-C_q), 140.6 (*i*^{tolyl}-C_q), 141.1 (*i*^{Dipp}-C_q), 152.7 (*o*^{Dipp}-C_q), 155.0 (*o*^{Dipp}-C_q).

HRMS-ASAP (m/z): [M + H]⁺ calc. for C₂₉H₄₃BNO₂, 448.3381 found, 448.3375.

Synthesis of RER *p*-tolylBcat•CaaC^{Me[300]} RER1

A saturated solution of 15 mg of *p*-tolylBcat•CaaC^{Me} in 1 mL of C₆D₆ was slowly evaporated (12 days) under an argon atmosphere at room temperature. RER *p*-tolylBcat•CaaC^{Me} was obtained quantitatively as a crystalline powder.

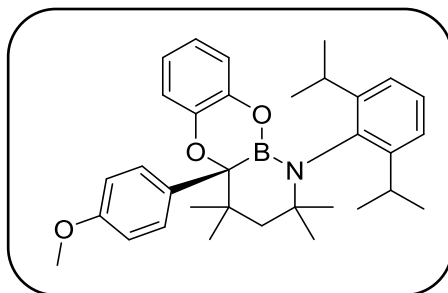
Elemental analysis for [C₃₃H₄₂BNO₂] [497.53 g/mol] Calc. (obs.): C 79.99 (79.79), H 8.54 (8.56), N 2.83 (2.72).

¹H-NMR (400 MHz, 25 °C, C₆D₆): δ_H / ppm = 0.91 (s, 3 H, NC_qCH₃), 1.04 (d, 3 H, ³J_{HH} = 7 Hz, CHCH₃), 1.13 (s, 3 H, C_qC_qCH₃), 1.16 (s, 3 H, NC_qCH₃), 1.28 (d, 3 H, ³J_{HH} = 7 Hz, CHCH₃), 1.30 (d, 3 H, ³J_{HH} = 7 Hz, CHCH₃), 1.35 (d, 1 H, ²J_{HH} = 15 Hz, C_qCH₂), 1.47 (d, 3 H, ³J_{HH} = 7 Hz, CHCH₃), 1.79 (s, 3 H, C_qC_qCH₃), 1.97 (s, 3 H, *p*-CH₃), 2.11 (d, ²J_{HH} = 15 Hz, C_qCH₂), 3.54 (sept, 1 H, ³J_{HH} = 7 Hz, CHCH₃), 3.90 (sept, 1 H, ³J_{HH} = 7 Hz, CHCH₃), 6.35 – 6.40 (m, 2 H, arylCH), 6.61 – 6.65 (m, 1 H, arylCH), 6.94 – 6.96 (m, 2 H, *o*^{tolyl}-CH), 7.06 – 7.09 (m, 1 H, aryl^{cat}CH), 7.17 – 7.19 (m, 1 H, *p*^{Dipp}-CH), 7.21 – 7.25 (m, 2 H, *m*^{Dipp}-CH), 7.69 – 7.71 (m, 2 H, *m*^{tolyl}-CH).

¹¹B-NMR (128 MHz, 25 °C, C₆D₆): δ_B / ppm = 29.1.

¹³C{¹H}-NMR (100 MHz, 25 °C, C₆D₆): δ_C / ppm = 20.9 (*p*^{tolyl}-CH₃), 22.3 (CHCH₃), 22.8 (CHCH₃), 26.1 (CHCH₃), 26.5 (CHCH₃), 26.7 (NC_qCH₃), 27.3 (NC_qCH₃), 28.4 (C_qC_qCH₃), 29.5 (CHCH₃), 30.1 (CHCH₃), 32.2 (C_qC_qCH₃), 37.9 (C_qC_qCH₃), 50.5 (C_qCH₂), 57.8 (NC_qCH₃), 79.1 (NC_qC_q), 118.6 (aryl^{cat}CH), 118.9 (aryl^{cat}CH), 121.9 (aryl^{cat}CH), 122.4 (aryl^{cat}CH), 123.7 (*m*^{Dipp}-CH), 124.4 (*p*^{Dipp}-CH), 128.6 (*o*^{tolyl}-CH), 128.8 (*m*^{tolyl}-CH), 135.4 (*i*^{Dipp}-C_q), 136.7 (*p*^{tolyl}-CH), 138.2 (*i*^{tolyl}-CH), 143.5 (OC_q), 146.1 (OC_q), 148.5 (*o*^{Dipp}-C_q), 149.0 (*o*^{Dipp}-C_q).

HRMS-ASAP (m/z): [M + H]⁺ calc. for C₃₃H₄₂BNO₂, 496.3381 found 496.3364.

Synthesis of RER 4-MeO-C₆H₄Bcat•CaaC^{Me}[300] RER2


A saturated solution of 15 mg of 4-MeO-C₆H₄Bcat•CaaC^{Me} in 1 mL of C₆D₆ was slowly evaporated (14 days) under an argon atmosphere at room temperature. RER 4-MeO-C₆H₄Bcat•CaaC^{Me} was obtained quantitatively as a crystalline powder.

Elemental analysis for [C₃₃H₄₂BNO₃+C₆D₆] [511.51 + 84.15 g/mol] Calc. (obs.): C 78.64 (78.95), H 9.14 (9.63), N 2.35 (2.14).

¹H-NMR (400 MHz, 25 °C, C₆D₆): δ_H / ppm = 0.93 (s, 3 H, NC_qCH₃), 1.04 (d, 3 H, ³J_{HH} = 7 Hz, CHCH₃), 1.12 (s, 3 H, C_qC_qCH₃), 1.16 (s, 3 H, NC_qCH₃), 1.28 (d, 3 H, ³J_{HH} = 7 Hz, CHCH₃), 1.30 (d, 3 H, ³J_{HH} = 7 Hz, CHCH₃), 1.36 (d, 1 H, ²J_{HH} = 15 Hz, C_qCH₂), 1.43 (d, 3 H, ³J_{HH} = 7 Hz, CHCH₃), 1.79 (s, 3 H, C_qC_qCH₃), 2.10 (d, 1 H, ²J_{HH} = 15 Hz, C_qCH₂), 3.17 (s, 3 H, OCH₃), 3.54 (sept, 1 H, ³J_{HH} = 7 Hz, CHCH₃), 3.87 (sept, 1 H, ³J_{HH} = 7 Hz, CHCH₃), 6.37 – 6.42 (m, 2 H, aryl^{CH}), 6.62 – 6.67 (m, 1 H, aryl^{CH}), 6.76 – 6.79 (m, 2 H, o^{tolyl}-CH), 7.06 – 7.09 (m, 1 H, aryl^{cat}CH), 7.16 – 7.19 (m, 1 H, p^{Dipp}-CH), 7.22 – 7.24 (m, 2 H, m^{Dipp}-CH), 7.70 – 7.74 (m, 2 H, m^{tolyl}-CH).

¹¹B-NMR (128 MHz, 25 °C, C₆D₆): δ_B / ppm = 28.9.

¹³C{¹H}-NMR (100 MHz, 25 °C, C₆D₆): δ_C / ppm = 22.3 (CHCH₃), 22.8 (CHCH₃), 26.1 (CHCH₃), 26.4 (CHCH₃), 26.6 (NC_qCH₃), 27.2 (NC_qCH₃), 28.4 (C_qC_qCH₃), 29.5 (CHCH₃), 30.1 (CHCH₃), 32.2 (C_qC_qCH₃), 38.0 (C_qC_qCH₃), 50.5 (C_qCH₂), 54.6 (OCH₃), 57.8 (NC_qCH₃), 78.9 (NC_qC_q), 113.4 (o^{ansiol}-CH), 118.6 (aryl^{cat}CH), 118.9 (aryl^{cat}CH), 121.9 (aryl^{cat}CH), 122.4 (aryl^{cat}CH), 123.6 (m^{Dipp}-CH), 124.4 (p^{Dipp}-CH), 129.9 (m^{ansiol}-CH), 132.9 (j^{ansiol}-C_q), 135.4 (j^{Dipp}-C_q), 143.5 (OC_q), 146.1 (OC_q), 148.5 (o^{Dipp}-C_q), 149.0 (o^{Dipp}-C_q), 159.1 (p^{ansiol}-C_q).

HRMS-ASAP (m/z): [M + H]⁺ calc. for C₃₃H₄₂BNO₃, 512.3331 found 512.3322.

7 Crystallographic data

Crystals suitable for single crystal X-ray diffraction were selected, coated in perfluoropolyether oil, and mounted on MiTeGen sample holders. The data were collected on Bruker X8 Apex-2 instruments with a CCD area detector using either mirror- or graphite-monochromated MoK α radiation ($\lambda = 0.71073 \text{ \AA}$). Both instruments are equipped with open flow N₂ Cryoflex II (Bruker) devices and measurements were performed at 100 K. For data reduction, the Bruker Apex2 or Apex3 software suites (Bruker AXS) were used.

Table 24: Crystallographic data for compound 1: [Cu(^tBu₂Im)Cl]

[Cu(^t Bu ₂ Im)Cl] 1	
Identification code	ae003_a
Empirical formula	C ₁₁ H ₂₀ ClCuN ₂
Formula weight [g/mol]	279.28
Temperature [K]	100(2)
Wavelength [Å]	0.71073
Crystal system	monoclinic
Space group	C2/c
Unit cell dimensions	a = 10.8229(9) Å b = 11.6435(11) Å c = 11.0027(9) Å β = 107.335(2)°
Volume [Å ³]	1323.5(2)
Z	4
Density (calculated) [g/cm ³]	1.402
Absorption coefficient [mm ⁻¹]	1.824
F(000)	584
θ range [°]	2.64 - 27.02
No. of reflections collected	4386
No. of unique reflections	1435 [R _{int} = 0.0202]
Observed reflections [I > 2σ(I)]	1246
Data / restraints / parameters	1435 / 0 / 73
Goof	0.812
Final R indices [I > 2σ(I)]	R ₁ = 0.0266, wR ₂ = 0.0926
R indices (all data)	R ₁ = 0.0311, wR ₂ = 0.1003
Largest diff. peak and hole [e Å ⁻³]	0.658 and -0.396
Diffractometer	Bruker Smart Apex 2

Table 25: Crystallographic data for compound 2: [Cu(ⁱPr₂Im)Cl]

[Cu(ⁱ Pr ₂ Im)Cl] 2	
Identification code	ae001_a
Empirical formula	C ₉ H ₁₆ ClCuN ₂
Formula weight [g/mol]	251.23
Temperature [K]	100(2)
Wavelength [Å]	0.71073
Crystal system	monoclinic
Space group	<i>P</i> 2 ₁ / <i>c</i>
Unit cell dimensions	a = 10.2944(5) Å b = 9.8798(5) Å c = 12.1082(6) Å β = 109.8560(10)°
Volume [Å ³]	1158.27(10)
Z	4
Density (calculated) [g/cm ³]	1.441
Absorption coefficient [mm ⁻¹]	2.076
F(000)	520
θ range [°]	2.10 - 26.07
No. of reflections collected	14729
No. of unique reflections	2298 [R _{int} = 0.0242]
Observed reflections [I > 2σ(I)]	2189
Data / restraints / parameters	2298 / 0 / 122
Goof	1.066
Final R indices [I > 2σ(I)]	R ₁ = 0.0203, wR ₂ = 0.0542
R indices (all data)	R ₁ = 0.0218, wR ₂ = 0.0550
Largest diff. peak and hole [e Å ⁻³]	0.375 and -0.233
Diffractometer	Bruker Smart Apex 2

Table 26: Crystallographic data for compound 3: [Cu(ⁱPr₂ImMe₂)Cl]

[Cu(ⁱ Pr ₂ ImMe ₂)Cl] 3	
Identification code	ae096_a
Empirical formula	C ₁₁ H ₂₀ ClCuN ₂
Formula weight [g/mol]	279.28
Temperature [K]	100(2)
Wavelength [Å]	0.71073
Crystal system	tetragonal
Space group	<i>P</i> 4 ₃ 2 ₁ 2
Unit cell dimensions	a = 7.9930(17) Å b = 7.9930(17) Å c = 20.607(4) Å
Volume [Å ³]	1316.5(6)
Z	4
Density (calculated) [g/cm ³]	1.409
Absorption coefficient [mm ⁻¹]	1.834
F(000)	584
θ range [°]	2.733 - 26.091
No. of reflections collected	13329 [R _{int} = 0.0893]
No. of unique reflections	1304
Observed reflections [I > 2σ(I)]	1227
Data / restraints / parameters	1304 / 0 / 74
Goof	1.107
Final R indices [I > 2σ(I)]	R ₁ = 0.0304, wR ₂ = 0.0822
R indices (all data)	R ₁ = 0.0320, wR ₂ = 0.0829
Largest diff. peak and hole [e Å ⁻³]	0.352 and -0.782
Diffractometer	Bruker Smart Apex 2

Table 27: Crystallographic data for compound 4: [Cu(Me₄Im)Cl]

[Cu(Me ₄ Im)Cl] 4	
Identification code	ae099_a
Empirical formula	C ₇ H ₁₂ ClCuN ₂
Formula weight [g/mol]	233.18
Temperature [K]	100(2)
Wavelength [Å]	0.71073
Crystal system	monoclinic
Space group	<i>P</i> 2 ₁ / <i>c</i>
Unit cell dimensions	a = 8.2580(8) Å b = 15.8530(11) Å c = 7.7508(5) Å β = 115.996(2)°
Volume [Å ³]	912.03(12)
Z	4
Density (calculated) [g/cm ³]	1.625
Absorption coefficient [mm ⁻¹]	2.625
F(000)	456
θ range [°]	2.570 - 26.024
No. of reflections collected	11651
No. of unique reflections	1799 [R _{int} = 0.0329]
Observed reflections [I > 2σ(I)]	1633
Data / restraints / parameters	1799 / 0 / 104
Goof	1.083
Final R indices [I > 2σ(I)]	R ₁ = 0.0227, wR ₂ = 0.0570
R indices (all data)	R ₁ = 0.0264, wR ₂ = 0.0586
Largest diff. peak and hole [e Å ⁻³]	0.400 and -0.292
Diffractometer	Bruker Smart Apex 2

Table 28: Crystallographic data for compound 6: [Cu(¹Pr₂Im)₂Cl]

[Cu(¹ Pr ₂ Im) ₂ Cl] 6	
Identification code	ae002_a
Empirical formula	C ₁₈ H ₃₂ ClCuN ₄
Formula weight [g/mol]	403.47
Temperature [K]	100(2)
Wavelength [Å]	0.71073
Crystal system	orthorhombic
Space group	<i>P</i> 2 ₁ 2 ₁ 2 ₁
Unit cell dimensions	a = 9.3953(19) Å b = 10.1716(18) Å c = 21.326(5) Å
Volume [Å ³]	2038.1(7)
Z	4
Density (calculated) [g/cm ³]	1.315
Absorption coefficient [mm ⁻¹]	1.210
F(000)	856
θ range [°]	1.91 - 26.85
No. of reflections collected	12480
No. of unique reflections	4277 [R _{int} = 0.0688]
Observed reflections [I > 2σ(I)]	3064
Data / restraints / parameters	4277 / 0 / 225
Goof	0.974
Final R indices [I > 2σ(I)]	R ₁ = 0.0455, wR ₂ = 0.0799
R indices (all data)	R ₁ = 0.0766, wR ₂ = 0.0901
Largest diff. peak and hole [e Å ⁻³]	0.490 and -0.360
Diffractometer	Bruker Smart Apex 2

Table 29: Crystallographic data for compound 7 [Cu(ⁱPr₂ImMe₂)₂(Cl)]

[Cu(ⁱ Pr ₂ ImMe ₂) ₂ (Cl)] 7	
Identification code	ae212_a
Empirical formula	C ₂₆ H ₄₀ ClCuN ₄ O
Formula weight [g/mol]	531.67
Temperature [K]	100(2)
Wavelength [Å]	0.71073
Crystal system	Triclinic
Space group	<i>P</i> -1
Unit cell dimensions	a = 10.4578(13) Å b = 12.1452(15) Å c = 13.451(2) Å α = 63.824(4)° β = 67.123(3)° γ = 74.874(3)°
Volume [Å ³]	1404.4(3)
Z	2
Density (calculated) [g/cm ³]	1.238
Absorption coefficient [mm ⁻¹]	0.896
F(000)	556
θ range [°]	1.778 - 26.232
No. of reflections collected	16781
No. of unique reflections	5609 [R _{int} = 0.0273]
Observed reflections [I > 2σ (I)]	4602
Data / restraints / parameters	5609 / 122 / 356
Goof	1.026
Final R indices [I > 2σ (I)]	R ₁ = 0.0414, wR ₂ = 0.0979
R indices (all data)	R ₁ = 0.0561, wR ₂ = 0.1067
Largest diff. peak and hole [e Å ⁻³]	1.698 and -0.743
Diffractometer	Bruker Smart Apex 2

Table 30: Crystallographic data for compound 8: [Cu(Me₂Im)Cl]

[Cu(Me ₂ Im)Cl] 8	
Identification code	ae008_a
Empirical formula	C ₅ H ₁₆ ClCuN ₂
Formula weight [g/mol]	195.125
Temperature [K]	100(2)
Wavelength [Å]	0.71073
Crystal system	monoclinic
Space group	C2/m
Unit cell dimensions	a = 14.996(3) Å b = 6.2266(15) Å c = 8.0416(19) Å β = 111.107(6)°
Volume [Å ³]	700.5(3)
Z	4
Density (calculated) [g/cm ³]	1.850
Absorption coefficient [mm ⁻¹]	3.403
F(000)	392
θ range [°]	2.72 - 26.87
No. of reflections collected	4578
No. of unique reflections	820 [R _{int} = 0.0380]
Observed reflections [I > 2σ(I)]	773
Data / restraints / parameters	820 / 0 / 59
Goof	1.793
Final R indices [I > 2σ(I)]	R ₁ = 0.0213, wR ₂ = 0.0551
R indices (all data)	R ₁ = 0.0229, wR ₂ = 0.0555
Largest diff. peak and hole [e Å ⁻³]	0.357 and -0.263
Diffractometer	Bruker Smart Apex 2

Table 31: Crystallographic data for compound 11: [Cu(Dipp₂Im)F]

[Cu(Dipp ₂ Im)F] 11	
Identification code	ds129
Empirical formula	C ₂₇ H ₃₆ CuFN ₂
Formula weight [g/mol]	471.12
Temperature [K]	100(2)
Wavelength [Å]	0.71073
Crystal system	monoclinic
Space group	C2/c
Unit cell dimensions	a = 22.617(2) Å b = 8.9917(9) Å c = 16.6343(17) Å β = 115.905(3)°
Volume [Å ³]	3042.9(5)
Z	4
Density (calculated) [g/cm ³]	1.028
Absorption coefficient [mm ⁻¹]	0.737
F(000)	1000
θ range [°]	2.00 - 26.05
No. of reflections collected	18962
No. of unique reflections	3000 [R _{int} = 0.0443]
Observed reflections [I > 2σ(I)]	2563
Data / restraints / parameters	3000 / 0 / 147
Goof	1.064
Final R indices [I > 2σ(I)]	R ₁ = 0.0404, wR ₂ = 0.1002
R indices (all data)	R ₁ = 0.0480, wR ₂ = 0.1033
Largest diff. peak and hole [e Å ⁻³]	0.513 and -0.306
Diffractometer	Bruker Smart Apex 2

Table 32: Crystallographic data for compound 12: [Cu(CaaC^{Me})(Cl)]

[Cu(CaaC ^{Me})(Cl)] 12	
Identification code	ae227_a
Empirical formula	C ₂₀ H ₃₁ ClCuN
Formula weight [g/mol]	384.45
Temperature [K]	100(2)
Wavelength [Å]	0.71073
Crystal system	Monoclinic
Space group	<i>P</i> 2 ₁ / <i>n</i>
Unit cell dimensions	a = 10.6742(9) Å b = 10.0310(8) Å c = 18.8758(15) Å β = 90.011(4)°
Volume [Å ³]	2021.1(3)
Z	4
Density (calculated) [g/cm ³]	1.263
Absorption coefficient [mm ⁻¹]	1.213
F(000)	816
θ range [°]	2.158 - 26.423
No. of reflections collected	21937
No. of unique reflections	4151 [R _{int} = 0.0398]
Observed reflections [I > 2σ (I)]	3557
Data / restraints / parameters	4151 / 0 / 216
Goof	1.074
Final R indices [I > 2σ (I)]	R ₁ = 0.0424, wR ₂ = 0.1066
R indices (all data)	R ₁ = 0.0514, wR ₂ = 0.1112
Largest diff. peak and hole [e Å ⁻³]	1.159 and -0.578
Diffractometer	Bruker Smart Apex 2

Table 33: Crystallographic data for compound 16 [Cu(^tBu₂Im)(O^tBu)]

[Cu(^t Bu ₂ Im)(O ^t Bu)] 16	
Identification code	ae207-1_a
Empirical formula	C ₁₅ H ₂₉ CuN ₂ O
Formula weight [g/mol]	316.94
Temperature [K]	100(2)
Wavelength [Å]	0.71073
Crystal system	Monoclinic
Space group	<i>P</i> 2 ₁ / <i>c</i>
Unit cell dimensions	a = 13.4799(17) Å b = 15.6013(19) Å c = 16.538(2) Å β = 104.506(3)°
Volume [Å ³]	3367.2(7)
Z	8
Density (calculated) [g/cm ³]	1.250
Absorption coefficient [mm ⁻¹]	1.293
F(000)	1360
θ range [°]	1.560 - 26.399
No. of reflections collected	50992
No. of unique reflections	6882 [R _{int} = 0.1096]
Observed reflections [I > 2σ (I)]	4451
Data / restraints / parameters	6882 / 0 / 361
Goof	1.000
Final R indices [I > 2σ (I)]	R ₁ = 0.0424, wR ₂ = 0.0784
R indices (all data)	R ₁ = 0.0961, wR ₂ = 0.0931
Largest diff. peak and hole [e Å ⁻³]	0.810 and -0.500
Diffractometer	Bruker Smart Apex 2

Table 34: Crystallographic data for compound 17: [Cu(ⁱPr₂Im)(OAc)]

[Cu(ⁱ Pr ₂ Im)(OAc)] 17	
Identification code	Ae025_a
Empirical formula	C ₁₁ H ₁₉ CuN ₂ O ₂
Formula weight [g/mol]	274.82
Temperature [K]	100(2)
Wavelength [Å]	0.71073
Crystal system	Triclinic
Space group	<i>P</i> -1
Unit cell dimensions	a = 9.3560(5) Å b = 12.0931(6) Å c = 12.1272(6) Å α = 76.550(4)° β = 88.732(2)° γ = 84.509(2)°
Volume [Å ³]	1328.35(12)
Z	4
Density (calculated) [g/cm ³]	1.374
Absorption coefficient [mm ⁻¹]	1.633
F(000)	576
θ range [°]	1.73 - 26.11
No. of reflections collected	23911
No. of unique reflections	5250 [R _{int} = 0.0281]
Observed reflections [I > 2σ (I)]	4364
Data / restraints / parameters	5250 / 0 / 299
Goof	1.021
Final R indices [I > 2σ (I)]	R ₁ = 0.0249, wR ₂ = 0.0567
R indices (all data)	R ₁ = 0.0374, wR ₂ = 0.0619
Largest diff. peak and hole [e Å ⁻³]	0.334 and -0.273
Diffractometer	Bruker Smart Apex 2

Table 35: Crystallographic data for compound 18: [Cu(Dipp₂Im)(acac)]

[Cu(Dipp ₂ Im)(acac)] 18	
Identification code	ae103_a
Empirical formula	C ₃₂ H ₄₃ CuN ₂ O ₂
Formula weight [g/mol]	551.22
Temperature [K]	100(2)
Wavelength [Å]	0.71073
Crystal system	orthorhombic
Space group	<i>Pnma</i>
Unit cell dimensions	a = 16.3507(10) Å b = 17.1657(10) Å c = 10.6638(6) Å
Volume [Å ³]	2993.0(3)
Z	4
Density (calculated) [g/cm ³]	1.223
Absorption coefficient [mm ⁻¹]	0.759
F(000)	1176
θ range [°]	2.248 - 26.044
No. of reflections collected	37165 [R _{int} = 0.0500]
No. of unique reflections	3060
Observed reflections [I > 2σ(I)]	2375
Data / restraints / parameters	3060 / 0 / 187
GooF	1.028
Final R indices [I > 2σ(I)]	R ₁ = 0.0310, wR ₂ = 0.0763
R indices (all data)	R ₁ = 0.0471, wR ₂ = 0.0845
Largest diff. peak and hole [e Å ⁻³]	0.359 and -0.455
Diffractometer	Bruker Smart Apex 2

Table 36: Crystallographic data for compound 19: [Cu(Dipp₂Im)(hfacac)]

[Cu(Dipp ₂ Im)(hfacac)] 19	
Identification code	ae0092_a
Empirical formula	C ₃₂ H ₃₇ CuF ₆ N ₂ O ₂
Formula weight [g/mol]	659.17
Temperature [K]	100(2)
Wavelength [Å]	0.71073
Crystal system	monoclinic
Space group	<i>P</i> 2 ₁ / <i>n</i>
Unit cell dimensions	a = 10.610(5) Å b = 39.269(16) Å c = 15.980(7) Å β = 105.465(13)°
Volume [Å ³]	6417(5)
Z	8
Density (calculated) [g/cm ³]	1.365
Absorption coefficient [mm ⁻¹]	0.746
F(000)	2736
θ range [°]	1.420 - 26.316
No. of reflections collected	62974 [R _{int} = 0.0707]
No. of unique reflections	12828
Observed reflections [I > 2σ(I)]	10587
Data / restraints / parameters	12828 / 12 / 792
Goof	1.080
Final R indices [I > 2σ(I)]	R ₁ = 0.0599, wR ₂ = 0.1498
R indices (all data)	R ₁ = 0.0741, wR ₂ = 0.1569
Largest diff. peak and hole [e Å ⁻³]	1.975 and -0.962
Diffractionmeter	Bruker Smart Apex 2

Table 37: Crystallographic data for compound 20: [Cu(Dipp₂Im)(DBM)]

[Cu(Dipp ₂ Im)(DBM)] 20	
Identification code	ae101_a
Empirical formula	C ₄₂ H ₄₇ CuN ₂ O ₂
Formula weight [g/mol]	675.35
Temperature [K]	100(2)
Wavelength [Å]	0.71073
Crystal system	Monoclinic
Space group	<i>P</i> 2 ₁ / <i>n</i>
Unit cell dimensions	a = 13.4962(8) Å b = 16.2826(10) Å c = 16.5250(10) Å β = 90.246(2)°
Volume [Å ³]	3631.4(4)
Z	4
Density (calculated) [g/cm ³]	1.235
Absorption coefficient [mm ⁻¹]	0.638
F(000)	1432
θ range [°]	1.756 - 26.144
No. of reflections collected	47351 [R _{int} = 0.0309]
No. of unique reflections	7232
Observed reflections [I > 2σ(I)]	6235
Data / restraints / parameters	7232 / 27 / 474
Goof	1.034
Final R indices [I > 2σ(I)]	R ₁ = 0.0344, wR ₂ = 0.0861
R indices (all data)	R ₁ = 0.0417, wR ₂ = 0.0906
Largest diff. peak and hole [e Å ³]	0.673 and -0.721
Diffractometer	Bruker Smart Apex 2

Table 38: Crystallographic data for compound 21: [Cu(Mes₂Im)(hfacac)]

[Cu(Mes ₂ Im)(hfacac)] 21	
Identification code	ae173_a
Empirical formula	C ₂₆ H ₂₅ CuF ₆ N ₂ O ₂
Formula weight [g/mol]	575.02
Temperature [K]	100(2)
Wavelength [Å]	0.71073
Crystal system	Monoclinic
Space group	<i>P</i> 2 ₁ / <i>c</i>
Unit cell dimensions	a = 8.3748(8) Å b = 16.1229(15) Å c = 19.0665(16) Å β = 97.623(3)°
Volume [Å ³]	2551.7(4)
Z	4
Density (calculated) [g/cm ³]	1.497
Absorption coefficient [mm ⁻¹]	0.926
F(000)	1176
θ range [°]	1.660 - 26.077
No. of reflections collected	17914
No. of unique reflections	5039 [R _{int} = 0.0350]
Observed reflections [I > 2σ (I)]	3783
Data / restraints / parameters	5039 / 0 / 340
Goof	1.008
Final R indices [I > 2σ (I)]	R ₁ = 0.0374, wR ₂ = 0.0779
R indices (all data)	R ₁ = 0.0617, wR ₂ = 0.0866
Largest diff. peak and hole [e Å ⁻³]	0.395 and -0.413
Diffractometer	Bruker Smart Apex 2

Table 39: Crystallographic data for compound 23: [Cu(ⁱPr₂Im)(DBM)]

[Cu(ⁱ Pr ₂ Im)(DBM)] 23	
Identification code	ae215_a
Empirical formula	C ₂₄ H ₂₇ CuN ₂ O ₂
Formula weight [g/mol]	439.01
Temperature [K]	100(2)
Wavelength [Å]	0.71073
Crystal system	Monoclinic
Space group	<i>P</i> 2 ₁ / <i>c</i>
Unit cell dimensions	a = 17.1889(12) Å b = 10.5700(7) Å c = 36.668(3) Å β = 96.129(2)°
Volume [Å ³]	6624.1(8)
Z	12
Density (calculated) [g/cm ³]	1.321
Absorption coefficient [mm ⁻¹]	1.010
F(000)	2760
θ range [°]	1.718 - 26.432
No. of reflections collected	66500
No. of unique reflections	13597 [R _{int} = 0.0320]
Observed reflections [I > 2σ (I)]	11202
Data / restraints / parameters	13597 / 0 / 826
Goof	1.015
Final R indices [I > 2σ (I)]	R ₁ = 0.0449, wR ₂ = 0.0968
R indices (all data)	R ₁ = 0.0582, wR ₂ = 0.1030
Largest diff. peak and hole [e Å ⁻³]	1.336 and -1.388
Diffractometer	Bruker Smart Apex 2

Table 40: Crystallographic data for compound 24: [Cu(Dipp₂Im)Mes]

[Cu(Dipp ₂ Im)Mes] 24	
Identification code	ds119
Empirical formula	C ₃₆ H ₄₇ CuN ₂
Formula weight [g/mol]	571.30
Temperature [K]	100(2)
Wavelength [Å]	0.71073
Crystal system	monoclinic
Space group	C2/c
Unit cell dimensions	a = 20.1599(13) Å b = 15.8111(10) Å c = 23.232(2) Å β = 113.516(2)°
Volume [Å ³]	6790.3(8)
Z	8
Density (calculated) [g/cm ³]	1.118
Absorption coefficient [mm ⁻¹]	0.667
F(000)	2448
θ range [°]	1.69 - 26.05
No. of reflections collected	36189
No. of unique reflections	6699 [R _{int} = 0.0327]
Observed reflections [I > 2σ(I)]	5689
Data / restraints / parameters	6699 / 0 / 374
GooF	1.034
Final R indices [I > 2σ(I)]	R ₁ = 0.0375, wR ₂ = 0.0948
R indices (all data)	R ₁ = 0.0467, wR ₂ = 0.1006
Largest diff. peak and hole [e Å ³]	0.640 and -0.401
Diffractionmeter	Bruker Smart Apex 2

Table 41: Crystallographic data for compound 25: [Cu(Mes₂Im)(Mes)]

[Cu(Mes ₂ Im)(Mes)] 25	
Identification code	ds124
Empirical formula	C ₃₀ H ₃₅ CuN ₂
Formula weight [g/mol]	324.76
Temperature [K]	103(2)
Wavelength [Å]	0.71073
Crystal system	monoclinic
Space group	<i>P</i> 2 ₁ / <i>c</i>
Unit cell dimensions	a = 16.8089(12) Å b = 14.3508(11) Å c = 22.4757(17) Å β = 96.002(2)°
Volume [Å ³]	5391.9(7)
Z	8
Density (calculated) [g/cm ³]	1.200
Absorption coefficient [mm ⁻¹]	0.829
F(000)	2064
θ range [°]	1.22 - 26.09
No. of reflections collected	67818
No. of unique reflections	10655 [R _{int} = 0.0530]
Observed reflections [I > 2σ(I)]	7935
Data / restraints / parameters	10655 / 0 / 613
Goof	1.015
Final R indices [I > 2σ(I)]	R ₁ = 0.0350, wR ₂ = 0.0781
R indices (all data)	R ₁ = 0.0601, wR ₂ = 0.0889
Largest diff. peak and hole [e Å ⁻³]	0.381 and -0.302
Diffractometer	Bruker Smart Apex 2

Table 42: Crystallographic data for compound 29: [Cu(Mes₂Im)(C₆F₅)]

[Cu(Mes ₂ Im)(C ₆ F ₅)] 29	
Identification code	ae020_a
Empirical formula	C ₃₄ H ₃₀ CuF ₅ N ₂
Formula weight [g/mol]	625.14
Temperature [K]	100(2)
Wavelength [Å]	0.71073
Crystal system	monoclinic
Space group	C2/c
Unit cell dimensions	a = 8.4625(19) Å b = 22.966(5) Å c = 15.900(4) Å β = 99.738(6)°
Volume [Å ³]	3045.6(12)
Z	4
Density (calculated) [g/cm ³]	1.363
Absorption coefficient [mm ⁻¹]	0.773
F(000)	1288
θ range [°]	1.773 - 26.023
No. of reflections collected	9817 [R _{int} = 0.0442]
No. of unique reflections	2943
Observed reflections [I > 2σ(I)]	2102
Data / restraints / parameters	2943 / 33 / 200
Goof	1.025
Final R indices [I > 2σ(I)]	R ₁ = 0.0567, wR ₂ = 0.1335
R indices (all data)	R ₁ = 0.0854, wR ₂ = 0.1490
Largest diff. peak and hole [e Å ⁻³]	0.919 and -0.508
Diffractometer	Bruker Smart Apex 2

Table 43: Crystallographic data for compound 30: [Cu(Dipp₂Im)(C₆F₅)]

[Cu(Dipp ₂ Im)(C ₆ F ₅)] 30	
Identification code	ae022_a
Empirical formula	C ₃₃ H ₃₆ CuF ₅ N ₂
Formula weight [g/mol]	619.19
Temperature [K]	100(2)
Wavelength [Å]	0.71073
Crystal system	monoclinic
Space group	C2/c
Unit cell dimensions	a = 10.8260(6) b = 20.3149(12) c = 14.1343(8) β = 98.945(2)
Volume [Å ³]	3070.7(3)
Z	4
Density (calculated) [g/cm ³]	1.339
Absorption coefficient [mm ⁻¹]	0.766
F(000)	1288
θ range [°]	2.00 - 26.04
No. of reflections collected	30468
No. of unique reflections	3042 [R _{int} = 0.0733]
Observed reflections [I > 2σ(I)]	2318
Data / restraints / parameters	3042 / 0 / 192
Goof	1.060
Final R indices [I > 2σ(I)]	R ₁ = 0.0337, wR ₂ = 0.0592
R indices (all data)	R ₁ = 0.0610, wR ₂ = 0.0684
Largest diff. peak and hole [e Å ⁻³]	0.297 and -0.323
Diffractometer	Bruker Smart Apex 2

Table 44: Crystallographic data for compound 33: [Cu(Dipp₂Im)(3,5-(CF₃)₂-C₆H₄)]

[Cu(Dipp ₂ Im)(3,5-(CF ₃) ₂ -C ₆ H ₄)] 33	
Identification code	ae019_a
Empirical formula	C ₂₀ H ₂₀ CuF ₃ N ₂
Formula weight [g/mol]	408.92
Temperature [K]	296(2)
Wavelength [Å]	0.71073
Crystal system	monoclinic
Space group	<i>P</i> 2 ₁ / <i>n</i>
Unit cell dimensions	a = 24.796(5) Å b = 12.142(3) Å c = 24.932(7) Å β = 107.435(8)°
Volume [Å ³]	7161(3)
Z	16
Density (calculated) [g/cm ³]	1.517
Absorption coefficient [mm ⁻¹]	1.255
F(000)	3360
θ range [°]	1.88 - 22.72
No. of reflections collected	9799
No. of unique reflections	6858 [R _{int} = 0.0568]
Observed reflections [I > 2σ(I)]	2900
Data / restraints / parameters	6858 / 244 / 871
Goof	0.829
Final R indices [I > 2σ(I)]	R ₁ = 0.0668, wR ₂ = 0.1514
R indices (all data)	R ₁ = 0.1547, wR ₂ = 0.1772
Largest diff. peak and hole [e Å ⁻³]	0.700 and -0.356
Diffractometer	Bruker Smart Apex 2

Table 45: Crystallographic data for compound 37: [Cu(^tBu₂Im)(Dipp)]

[Cu(^t Bu ₂ Im)(Dipp)] 37	
Identification code	ae028_a
Empirical formula	C ₂₉ H ₄₃ CuN ₂
Formula weight [g/mol]	483.19
Temperature [K]	100(2)K
Wavelength [Å]	0.71073A
Crystal system	orthorhombic
Space group	<i>Pnma</i>
Unit cell dimensions	a = 17.8110(3) Å b = 16.6825(7) Å c = 9.2669(6) Å
Volume [Å ³]	2753.5(2)
Z	4
Density (calculated)[g/cm ³]	1.166
Absorption coefficient[mm ⁻¹]	0.811
F(000)	1040
θ range [°]	2.287 - 26.039
No. of reflections collected	32479
No. of unique reflections	2808 [R _{int} = 0.0530]
Observed reflections [I>2σ(I)]	2462
Data / restraints / parameters	2808 / 0 / 182
Goof	1.249
Final R indices[I>2σ(I)]	R ₁ = 0.0439, wR ₂ = 0.0932
R indices (all data)	R ₁ = 0.0523, wR ₂ = 0.0959
Largest diff. peak and hole [eÅ ³]	0.448 and -0.918
Diffractometer	Bruker Smart Apex2

Table 46: Crystallographic data for compound 40: [Cu(ⁱPr₂Im)(duryl)]

[Cu(ⁱ Pr ₂ Im)(duryl)] 40	
Identification code	ae193_a
Empirical formula	C ₁₉ H ₂₉ CuN ₂
Formula weight [g/mol]	348.98
Temperature [K]	100(2)
Wavelength [Å]	0.71073
Crystal system	Orthorhombic
Space group	<i>P</i> 2 ₁ 2 ₁ 2 ₁
Unit cell dimensions	a = 9.433(5) Å b = 12.479(6) Å c = 16.510(9) Å
Volume [Å ³]	1943.6(17)
Z	4
Density (calculated) [g/cm ³]	1.193
Absorption coefficient [mm ⁻¹]	1.123
F(000)	744
θ range [°]	2.046 - 26.119
No. of reflections collected	12803
No. of unique reflections	3860 [R _{int} = 0.0308]
Observed reflections [I > 2σ (I)]	3093
Data / restraints / parameters	3860 / 0 / 207
Goof	1.041
Final R indices [I > 2σ (I)]	R ₁ = 0.0357, wR ₂ = 0.0737
R indices (all data)	R ₁ = 0.0544, wR ₂ = 0.0803
Largest diff. peak and hole [e Å ⁻³]	0.279 and -0.198
Diffractometer	Bruker Smart Apex 2

Table 47: Crystallographic data for compound 42: [Cu(Mes₂Im)(C₆Me₅)]

[Cu(Mes ₂ Im)(C ₆ Me ₅)] 42	
Identification code	ae196_a
Empirical formula	C ₃₂ H ₃₉ CuN ₂
Formula weight [g/mol]	515.19
Temperature [K]	100(2)
Wavelength [Å]	0.71073
Crystal system	Monoclinic
Space group	<i>P</i> 2 ₁ / <i>n</i>
Unit cell dimensions	a = 12.5957(13) Å b = 14.5702(15) Å c = 15.9675(16) Å β = 105.712(3)°
Volume [Å ³]	2820.9(5)
Z	4
Density (calculated) [g/cm ³]	1.213
Absorption coefficient [mm ⁻¹]	0.796
F(000)	1096
θ range [°]	1.836 - 26.105
No. of reflections collected	36349
No. of unique reflections	5591 [R _{int} = 0.0338]
Observed reflections [I > 2σ (I)]	4959
Data / restraints / parameters	5591 / 0 / 327
Goof	1.032
Final R indices [I > 2σ (I)]	R ₁ = 0.0282, wR ₂ = 0.0716
R indices (all data)	R ₁ = 0.0339, wR ₂ = 0.0748
Largest diff. peak and hole [e Å ⁻³]	0.313 and -0.254
Diffractometer	Bruker Smart Apex 2

Table 48: Crystallographic data for compound 45: [Cu(Xantphos)(I)(MeCN)]

[Cu(Xantphos)(I)(MeCN)] 45	
Identification code	ae088_a
Empirical formula	C ₄₃ H ₃₈ CuIN ₂ OP ₂
Formula weight [g/mol]	851.13
Temperature [K]	100(2)
Wavelength [Å]	0.71073
Crystal system	triclinic
Space group	<i>P</i> -1
Unit cell dimensions	a = 9.1582(5) Å b = 11.6716(6) Å c = 18.2977(10) Å α = 80.818(2)° β = 80.072(2)° γ = 77.867(2)°
Volume [Å ³]	1868.02(17)
Z	2
Density (calculated) [g/cm ³]	1.513
Absorption coefficient [mm ⁻¹]	1.533
F(000)	860
θ range [°]	2.003 - 26.078
No. of reflections collected	24780
No. of unique reflections	7397 [R _{int} = 0.0565]
Observed reflections [<i>I</i> > 2σ(<i>I</i>)]	6261
Data / restraints / parameters	7397 / 0 / 455
Goof	1.043
Final R indices [<i>I</i> > 2σ (<i>I</i>)]	R ₁ = 0.0444, wR ₂ = 0.1125
R indices (all data)	R ₁ = 0.0540, wR ₂ = 0.1187
Largest diff. peak and hole [e Å ⁻³]	2.301 and -0.858
Diffractometer	Bruker Smart Apex 2

Table 49: Crystallographic data for compound 46: [Cu(Xantphos)(Cl)(MeCN)]

[Cu(Xantphos)(Cl)(MeCN)] 46	
Identification code	ae077_a
Empirical formula	C ₄₃ H ₃₈ ClCuN ₂ OP ₂
Formula weight [g/mol]	759.68
Temperature [K]	100(2)
Wavelength [Å]	0.71073
Crystal system	triclinic
Space group	<i>P</i> -1
Unit cell dimensions	a = 9.1673(3) Å b = 11.3603(4) Å c = 18.2225(7) Å α = 80.3780(10)° β = 80.2380(10)° γ = 77.0640(10)°
Volume [Å ³]	1806.24(11)
Z	2
Density (calculated) [g/cm ³]	1.397
Absorption coefficient [mm ⁻¹]	0.805
F(000)	788
θ range [°]	2.289 - 26.061
No. of reflections collected	23474
No. of unique reflections	7130 [R _{int} = 0.0429]
Observed reflections [$I > 2\sigma(I)$]	5828
Data / restraints / parameters	7130 / 0 / 455
Goof	1.047
Final R indices [$I > 2\sigma(I)$]	R ₁ = 0.0374, wR ₂ = 0.0841
R indices (all data)	R ₁ = 0.0500, wR ₂ = 0.0904
Largest diff. peak and hole [eÅ ³]	0.571 and -0.429
Diffractometer	Bruker Smart Apex 2

Table 50: Crystallographic data for compound 47: [Cu(Xantphos)(MeCN-oligomer)]

[Cu(Xantphos)(MeCN-oligomer)] 47	
Identification code	ae094_a
Empirical formula	C ₄₇ H ₄₂ CuN ₄ OP ₂
Formula weight [g/mol]	816.59
Temperature [K]	100(2)
Wavelength [Å]	0.71073
Crystal system	monoclinic
Space group	C2/c
Unit cell dimensions	a = 20.508(13) Å b = 17.066(11) Å c = 23.997(15) Å β = 103.76(2)°
Volume [Å ³]	8158(9)
Z	8
Density (calculated) [g/cm ³]	1.310
Absorption coefficient [mm ⁻¹]	0.655
F(000)	3352
θ range [°]	1.571 - 26.307
No. of reflections collected	49963
No. of unique reflections	8096 [R _{int} = 0.0918]
Observed reflections [I > 2σ(I)]	6877
Data / restraints / parameters	8096 / 2 / 530
Goof	1.050
Final R indices [I > 2σ(I)]	R ₁ = 0.0441, wR ₂ = 0.1180
R indices (all data)	R ₁ = 0.0522, wR ₂ = 0.1247
Largest diff. peak and hole [e Å ⁻³]	0.852 and -0.593
Diffractometer	Bruker Smart Apex 2

Table 51: Crystallographic data for compound BBA1: B₂pin₂•CaaC^{Me}[301]

B ₂ pin ₂ •CaaC ^{Me} BBA1	
Identification code	ae185_a
Empirical formula	C ₃₂ H ₅₅ B ₂ NO ₄
Formula weight [g/mol]	539.39
Temperature [K]	100(2)
Wavelength [Å]	0.71073
Crystal system	Triclinic
Space group	<i>P</i> -1
Unit cell dimensions	a = 10.8403(14) Å b = 10.8459(14) Å c = 15.907(2) Å α = 91.467(4)° β = 103.418(4)° γ = 116.778(4)°
Volume [Å ³]	1605.8(4)
Z	2
Density (calculated) [g/cm ³]	1.116
Absorption coefficient [mm ⁻¹]	0.070
F(000)	592
θ range [°]	2.127 - 26.172
No. of reflections collected	20966
No. of unique reflections	6392 [R _{int} = 0.0568]
Observed reflections [I > 2σ (I)]	4836
Data / restraints / parameters	6392 / 0 / 368
Goof	1.028
Final R indices [I > 2σ (I)]	R ₁ = 0.0563, wR ₂ = 0.1469
R indices (all data)	R ₁ = 0.0763, wR ₂ = 0.1630
Largest diff. peak and hole [e Å ⁻³]	0.477 and -0.352
Diffractometer	Bruker Smart Apex 2

Table 52: Crystallographic data for compound BBA2: B₂cat₂•CaaC^{Me}[301]

B ₂ cat ₂ •CaaC ^{Me} BBA2	
Identification code	ae184_a
Empirical formula	C ₃₂ H ₃₉ B ₂ NO ₄
Formula weight [g/mol]	523.26
Temperature [K]	100(2)
Wavelength [Å]	0.71073
Crystal system	Monoclinic
Space group	<i>P</i> 2 ₁ / <i>n</i>
Unit cell dimensions	a = 14.325(2) Å b = 12.0505(18) Å c = 17.419(3) Å β = 113.316(4)°
Volume [Å ³]	2761.3(7)
Z	4
Density (calculated) [g/cm ³]	1.259
Absorption coefficient [mm ⁻¹]	0.080
F(000)	1120
θ range [°]	1.567 - 26.116
No. of reflections collected	33371
No. of unique reflections	5462 [R _{int} = 0.0486]
Observed reflections [I > 2σ (I)]	4633
Data / restraints / parameters	5462 / 0 / 360
Goof	1.039
Final R indices [I > 2σ (I)]	R ₁ = 0.0393, wR ₂ = 0.0959
R indices (all data)	R ₁ = 0.0481, wR ₂ = 0.1020
Largest diff. peak and hole [e Å ⁻³]	0.340 and -0.254
Diffractometer	Bruker Smart Apex 2

Table 53: Crystallographic data for compound BBA3: B₂neop₂•CaaC^{Me}[301]

B ₂ neop ₂ •CaaC ^{Me} BBA3	
Identification code	AE189
Empirical formula	C ₃₀ H ₅₁ B ₂ NO ₄
Formula weight [g/mol]	511.33
Temperature [K]	100(2)
Wavelength [Å]	0.71073
Crystal system	Orthorhombic
Space group	<i>Pna</i> 2 ₁
Unit cell dimensions	a = 19.384(2) Å b = 10.3921(13) Å c = 15.1929(19) Å
Volume [Å ³]	3060.5(7)
Z	4
Density (calculated) [g/cm ³]	1.110
Absorption coefficient [mm ⁻¹]	0.071
F(000)	1120
θ range [°]	2.101 - 26.423
No. of reflections collected	39145
No. of unique reflections	6267 [R _{int} = 0.0407]
Observed reflections [I > 2σ (I)]	5907
Data / restraints / parameters	6267 / 1 / 346
Goof	1.022
Final R indices [I > 2σ (I)]	R ₁ = 0.0345, wR ₂ = 0.0877
R indices (all data)	R ₁ = 0.0377, wR ₂ = 0.0902
Largest diff. peak and hole [e Å ⁻³]	0.226 and -0.156
Diffractometer	Bruker Smart Apex 2

Table 54: Crystallographic data for compound BBA4: B₂eg₂•CaaC^{Me}[301]

B ₂ eg ₂ CaaC ^{Me} BBA4	
Identification code	ae182_a
Empirical formula	C ₂₄ H ₃₉ B ₂ NO ₄
Formula weight [g/mol]	427.18
Temperature [K]	100(2)
Wavelength [Å]	0.71073
Crystal system	Triclinic
Space group	<i>P</i> -1
Unit cell dimensions	a = 9.5144(9) Å b = 15.1352(14) Å c = 18.5970(17) Å α = 113.046(2)° β = 95.252(2)° γ = 95.926(2)°
Volume [Å ³]	2425.5(4)
Z	4
Density (calculated) [g/cm ³]	1.170
Absorption coefficient [mm ⁻¹]	0.076
F(000)	928
θ range [°]	1.202 - 26.039
No. of reflections collected	21765
No. of unique reflections	9509 [R _{int} = 0.0253]
Observed reflections [I > 2σ (I)]	7022
Data / restraints / parameters	9509 / 0 / 575
Goof	1.011
Final R indices [I > 2σ (I)]	R ₁ = 0.0428, wR ₂ = 0.0945
R indices (all data)	R ₁ = 0.0685, wR ₂ = 0.1066
Largest diff. peak and hole [e Å ⁻³]	0.291 and -0.265
Diffractometer	Bruker Smart Apex 2

Table 55: Crystallographic data for compound ADD3: phenylBpin•ⁿPr₂Im

phenylBpin• ⁿ Pr ₂ Im ADD3	
Identification code	ae107_a
Empirical formula	C ₂₁ H ₃₃ BN ₂ O ₂
Formula weight [g/mol]	356.30
Temperature [K]	100(2)
Wavelength [Å]	0.71073
Crystal system	Monoclinic
Space group	C2/c
Unit cell dimensions	a = 21.506(3) Å b = 15.792(2) Å c = 14.4078(19) Å β = 123.334(4)°
Volume [Å ³]	4088.2(10)
Z	8
Density (calculated) [g/cm ³]	1.158
Absorption coefficient [mm ⁻¹]	0.073
F(000)	1552
θ range [°]	1.717 - 26.218
No. of reflections collected	24540
No. of unique reflections	4119 [R _{int} = 0.0212]
Observed reflections [I > 2σ (I)]	3502
Data / restraints / parameters	4119 / 3 / 251
Goof	1.022
Final R indices [I > 2σ (I)]	R ₁ = 0.0452, wR ₂ = 0.1159
R indices (all data)	R ₁ = 0.0543, wR ₂ = 0.1248
Largest diff. peak and hole [e Å ⁻³]	0.650 and -0.685
Diffractometer	Bruker Smart Apex 2

Table 56: Crystallographic data for compound ADD4: phenylBpin•iPr₂ImMe₂^[300]

phenylBpin•iPr ₂ ImMe ₂ ADD4	
Identification code	ae104_a
Empirical formula	C ₂₃ H ₃₇ BN ₂ O ₂
Formula weight [g/mol]	384.35
Temperature [K]	100(2)
Wavelength [Å]	0.71073
Crystal system	Monoclinic
Space group	<i>P</i> 2 ₁ / <i>n</i>
Unit cell dimensions	a = 9.3185(8) Å b = 14.3021(11) Å c = 16.9995(13) Å β = 92.300(2)°
Volume [Å ³]	2263.8(3)
Z	4
Density (calculated) [g/cm ³]	1.128
Absorption coefficient [mm ⁻¹]	0.070
F(000)	840
θ range [°]	1.861 - 26.157
No. of reflections collected	27301
No. of unique reflections	4523 [R _{int} = 0.0592]
Observed reflections [I > 2σ (I)]	3296
Data / restraints / parameters	4523 / 0 / 263
Goof	1.016
Final R indices [I > 2σ (I)]	R ₁ = 0.0420, wR ₂ = 0.0938
R indices (all data)	R ₁ = 0.0701, wR ₂ = 0.1058
Largest diff. peak and hole [e Å ⁻³]	0.228 and -0.232
Diffractometer	Bruker Smart Apex 2

Table 57: Crystallographic data for compound ADD5: *p*-tolylBpin•ⁱPr₂Im

<i>p</i> -tolylBpin• ⁱ Pr ₂ Im ADD5	
Identification code	ae044_a
Empirical formula	C ₂₂ H ₃₅ BN ₂ O ₂
Formula weight [g/mol]	370.33
Temperature [K]	100(2)
Wavelength [Å]	0.71073
Crystal system	triclinic
Space group	<i>P</i> -1
Unit cell dimensions	a = 9.272(3) Å b = 10.653(4) Å c = 12.084(4) Å α = 106.437(11)° β = 101.149(12)° γ = 98.034(11)°
Volume [Å ³]	1098.9(7)
Z	2
Density (calculated) [g/cm ³]	1.119
Absorption coefficient [mm ⁻¹]	0.070
F(000)	404
θ range [°]	2.037 - 26.205
No. of reflections collected	10997
No. of unique reflections	4333 [R _{int} = 0.0402]
Observed reflections [I > 2σ(I)]	3173
Data / restraints / parameters	4333 / 0 / 253
Goof	1.034
Final R indices [I > 2σ(I)]	R ₁ = 0.0482, wR ₂ = 0.1145
R indices (all data)	R ₁ = 0.0721, wR ₂ = 0.1296
Largest diff. peak and hole [e Å ⁻³]	0.272 and -0.210
Diffractometer	Bruker Smart Apex 2

Table 58: : Crystallographic data for compound ADD6: *p*-tolylBpin•ⁿPr₂Im

tolyBpin• ⁿ Pr ₂ Im ADD6	
	ae105_a
Empirical formula	C ₂₂ H ₃₅ BN ₂ O ₂
Formula weight [g/mol]	370.33
Temperature [K]	100(2)
Wavelength [Å]	0.71073
Crystal system	Triclinic
Space group	<i>P</i> -1
Unit cell dimensions	a = 7.7372(19) Å b = 11.568(3) Å c = 12.363(3) Å α = 83.794(7)° β = 85.228(7)° γ = 77.956(7)°
Volume [Å ³]	1073.7(5)
Z	2
Density (calculated) [g/cm ³]	1.146
Absorption coefficient [mm ⁻¹]	0.072
F(000)	404
θ range [°]	1.808 - 26.174
No. of reflections collected	14204
No. of unique reflections	4296 [R _{int} = 0.0254]
Observed reflections [I > 2σ (I)]	3493
Data / restraints / parameters	4296 / 0 / 261
Goof	1.037
Final R indices [I > 2σ (I)]	R ₁ = 0.0376, wR ₂ = 0.0918
R indices (all data)	R ₁ = 0.0486, wR ₂ = 0.0983
Largest diff. peak and hole [e Å ⁻³]	0.297 and -0.210
Diffractometer	Bruker Smart Apex 2

Table 59: Crystallographic data for compound ADD7: *p*-tolylBpin•Pr₂ImMe₂^[300]

<i>p</i> -tolylBpin•Pr ₂ ImMe ₂ ADD7	
Identification code	ae112_a
Empirical formula	C ₂₄ H ₃₉ BN ₂ O ₂
Formula weight [g/mol]	398.38
Temperature [K]	100(2)
Wavelength [Å]	0.71073
Crystal system	Monoclinic
Space group	<i>P</i> 2 ₁ / <i>n</i>
Unit cell dimensions	a = 13.1638(7) Å b = 11.2503(6) Å c = 15.8830(10) Å β = 97.214(2)°
Volume [Å ³]	2333.6(2)
Z	4
Density (calculated) [g/cm ³]	1.134
Absorption coefficient [mm ⁻¹]	0.070
F(000)	872
θ range [°]	1.896 - 26.077
No. of reflections collected	14887
No. of unique reflections	4607 [R _{int} = 0.0305]
Observed reflections [I > 2σ (I)]	3657
Data / restraints / parameters	4607 / 0 / 273
Goof	1.037
Final R indices [I > 2σ (I)]	R ₁ = 0.0419, wR ₂ = 0.0974
R indices (all data)	R ₁ = 0.0562, wR ₂ = 0.1056
Largest diff. peak and hole [e Å ⁻³]	0.263 and -0.211
Diffractometer	Bruker Smart Apex 2

Table 60: Crystallographic data for compound ADD8: *p*-tolylBcat•Dipp₂Im

<i>p</i> -tolylBcat•Dipp ₂ Im ADD8	
Identification code	ae132_a
Empirical formula	C ₄₀ H ₄₇ BN ₂ O ₂
Formula weight [g/mol]	598.60
Temperature [K]	100(2)
Wavelength [Å]	0.71073
Crystal system	Orthorhombic
Space group	<i>Pbca</i>
Unit cell dimensions	a = 15.8941(19) Å b = 20.172(2) Å c = 22.127(3) Å
Volume [Å ³]	7094.1(14)
Z	8
Density (calculated) [g/cm ³]	1.121
Absorption coefficient [mm ⁻¹]	0.068
F(000)	2576
θ range [°]	1.873 - 26.062
No. of reflections collected	71721
No. of unique reflections	6996 [R _{int} = 0.0538]
Observed reflections [I > 2σ (I)]	5855
Data / restraints / parameters	6996 / 0 / 415
Goof	1.006
Final R indices [I > 2σ (I)]	R ₁ = 0.0382, wR ₂ = 0.0932
R indices (all data)	R ₁ = 0.0488, wR ₂ = 0.1009
Largest diff. peak and hole [e Å ⁻³]	0.324 and -0.263
Diffractometer	Bruker Smart Apex 2

Table 61: Crystallographic data for compound ADD9: *p*-tolylBcat•Pr₂ImMe₂^[300]

<i>p</i> -tolylBcat•Pr ₂ ImMe ₂ ADD9	
Identification code	ae142_a
Empirical formula	C ₂₄ H ₃₁ BN ₂ O ₂
Formula weight [g/mol]	390.32
Temperature [K]	100(2)
Wavelength [Å]	0.71073
Crystal system	Triclinic
Space group	<i>P</i> -1
Unit cell dimensions	a = 9.1708(9) Å b = 9.7560(10) Å c = 13.3012(13) Å α = 69.560(2)° β = 77.404(3)° γ = 81.188(3)°
Volume [Å ³]	1084.43(19)
Z	2
Density (calculated) [g/cm ³]	1.195
Absorption coefficient [mm ⁻¹]	0.075
F(000)	420
θ range [°]	1.660 - 26.099
No. of reflections collected	9420
No. of unique reflections	4270 [R _{int} = 0.0236]
Observed reflections [I > 2σ (I)]	3399
Data / restraints / parameters	4270 / 0 / 269
Goof	1.041
Final R indices [I > 2σ (I)]	R ₁ = 0.0452, wR ₂ = 0.1068
R indices (all data)	R ₁ = 0.0606, wR ₂ = 0.1160
Largest diff. peak and hole [e Å ⁻³]	0.308 and -0.278
Diffractometer	Bruker Smart Apex 2

Table 62: Crystallographic data for compound ADD10: *p*-tolylBneop•Mes₂Im

<i>p</i> -tolylBneop•Mes ₂ Im ADD10	
Identification code	ae138_a
Empirical formula	C ₃₃ H ₄₁ BN ₂ O ₂
Formula weight [g/mol]	508.49
Temperature [K]	100(2)
Wavelength [Å]	0.71073
Crystal system	Monoclinic
Space group	<i>P</i> 2 ₁
Unit cell dimensions	a = 8.3730(10) Å b = 18.758(2) Å c = 18.778(2) Å β = 97.429(3)°
Volume [Å ³]	2924.4(6)
Z	4
Density (calculated) [g/cm ³]	1.155
Absorption coefficient [mm ⁻¹]	0.071
F(000)	1096
θ range [°]	2.171 - 26.133
No. of reflections collected	38738
No. of unique reflections	11665 [R _{int} = 0.0355]
Observed reflections [I > 2σ (I)]	11157
Data / restraints / parameters	11665 / 1 / 703
Goof	1.039
Final R indices [I > 2σ (I)]	R ₁ = 0.0308, wR ₂ = 0.0783
R indices (all data)	R ₁ = 0.0329, wR ₂ = 0.0797
Largest diff. peak and hole [e Å ⁻³]	0.207 and -0.186
Diffractometer	Bruker Smart Apex 2

Table 63: Crystallographic data for compound ADD 11: *p*-tolylBneop•ⁱPr₂ImMe₂^[300]

<i>p</i> -tolylBneop• ⁱ Pr ₂ ImMe ₂ ADD11	
Identification code	ae118_a
Empirical formula	C ₂₃ H ₃₇ BN ₂ O ₂
Formula weight [g/mol]	384.35
Temperature [K]	100(2)
Wavelength [Å]	0.71073
Crystal system	Monoclinic
Space group	<i>P</i> 2 ₁ / <i>c</i>
Unit cell dimensions	a = 16.1248(7) Å b = 9.1135(4) Å c = 15.9267(7) Å β = 105.3820(10)°
Volume [Å ³]	2256.64(17)
Z	4
Density (calculated) [g/cm ³]	1.131
Absorption coefficient [mm ⁻¹]	0.071
F(000)	840
θ range [°]	2.591 - 26.032
No. of reflections collected	14451
No. of unique reflections	4445 [R _{int} = 0.0339]
Observed reflections [I > 2σ (I)]	3382
Data / restraints / parameters	4445 / 0 / 262
Goof	1.046
Final R indices [I > 2σ (I)]	R ₁ = 0.0407, wR ₂ = 0.0908
R indices (all data)	R ₁ = 0.0588, wR ₂ = 0.0989
Largest diff. peak and hole [e Å ⁻³]	0.285 and -0.207
Diffractometer	Bruker Smart Apex 2

Table 64: Crystallographic data for compound ADD13: 4-MeO-C₆H₄Bneop•Me₄Im

4-MeO-C ₆ H ₄ Bneop•Me ₄ Im ADD13	
Identification code	ae140_a
Empirical formula	C ₁₉ H ₂₉ BN ₂ O ₃
Formula weight [g/mol]	344.25
Temperature [K]	100(2)
Wavelength [Å]	0.71073
Crystal system	Monoclinic
Space group	<i>P</i> 2 ₁ / <i>c</i>
Unit cell dimensions	a = 10.2091(12) Å b = 12.3401(15) Å c = 15.1434(18) Å β = 98.424(4)°
Volume [Å ³]	1887.2(4)
Z	4
Density (calculated) [g/cm ³]	1.212
Absorption coefficient [mm ⁻¹]	0.081
F(000)	744
θ range [°]	2.017 - 26.027
No. of reflections collected	11778
No. of unique reflections	3703 [R _{int} = 0.0419]
Observed reflections [I > 2σ (I)]	3073
Data / restraints / parameters	3703 / 0 / 233
Goof	1.012
Final R indices [I > 2σ (I)]	R ₁ = 0.0421, wR ₂ = 0.1097
R indices (all data)	R ₁ = 0.0535, wR ₂ = 0.1184
Largest diff. peak and hole [e Å ⁻³]	0.335 and -0.338
Diffractometer	Bruker Smart Apex 2

Table 65: Crystallographic data for compound ADD14: 4-MeO-C₆H₄Bpin•ⁱPr₂ImMe₂^[300]

4-MeO-C ₆ H ₄ Bpin• ⁱ Pr ₂ ImMe ₂ ADD14	
Identification code	ae130_a
Empirical formula	C ₂₄ H ₃₉ BN ₂ O ₃
Formula weight [g/mol]	414.38
Temperature [K]	100(2)
Wavelength [Å]	0.71073
Crystal system	Monoclinic
Space group	<i>P</i> 2 ₁ / <i>c</i>
Unit cell dimensions	a = 11.4110(15) Å b = 13.1057(17) Å c = 16.9599(18) Å β = 109.951(7)°
Volume [Å ³]	2384.1(5)
Z	4
Density (calculated) [g/cm ³]	1.154
Absorption coefficient [mm ⁻¹]	0.074
F(000)	904
θ range [°]	1.899 - 26.081
No. of reflections collected	14409
No. of unique reflections	4714 [R _{int} = 0.0496]
Observed reflections [I > 2σ (I)]	3530
Data / restraints / parameters	4714 / 0 / 282
Goof	1.005
Final R indices [I > 2σ (I)]	R ₁ = 0.0573, wR ₂ = 0.1506
R indices (all data)	R ₁ = 0.0775, wR ₂ = 0.1657
Largest diff. peak and hole [e Å ⁻³]	0.379 and -0.353
Diffractometer	Bruker Smart Apex 2

Table 66: Crystallographic data for compound ADD15: 4-MeO-C₆H₄Bneop•iPr₂Im

4-MeO-C ₆ H ₄ Bneop•iPr ₂ Im ADD15	
Identification code	ae148_a
Empirical formula	C ₂₁ H ₃₃ BN ₂ O ₃
Formula weight [g/mol]	372.30
Temperature [K]	100(2)
Wavelength [Å]	0.71073
Crystal system	Monoclinic
Space group	<i>Pc</i>
Unit cell dimensions	a = 7.8813(7) Å b = 12.0832(10) Å c = 11.3196(9) Å β = 93.791(2)°
Volume [Å ³]	1075.62(16)
Z	2
Density (calculated) [g/cm ³]	1.150
Absorption coefficient [mm ⁻¹]	0.075
F(000)	404
θ range [°]	1.685 - 26.048
No. of reflections collected	7335
No. of unique reflections	3665 [R _{int} = 0.0219]
Observed reflections [I > 2σ (I)]	3439
Data / restraints / parameters	3665 / 2 / 251
Goof	1.025
Final R indices [I > 2σ (I)]	R ₁ = 0.0318, wR ₂ = 0.0765
R indices (all data)	R ₁ = 0.0346, wR ₂ = 0.0784
Largest diff. peak and hole [e Å ⁻³]	0.183 and -0.195
Diffractometer	Bruker Smart Apex 2

Table 67: Crystallographic data for compound ADD16: 4-MeO-C₆H₄Bneop•ⁿPr₂Im

4-MeO-C ₆ H ₄ Bneop• ⁿ Pr ₂ Im ADD16	
Identification code	ae143_a
Empirical formula	C ₂₁ H ₃₃ BN ₂ O ₃
Formula weight [g/mol]	372.30
Temperature [K]	100(2)
Wavelength [Å]	0.71073
Crystal system	Monoclinic
Space group	<i>P</i> 2 ₁ / <i>c</i>
Unit cell dimensions	a = 10.0079(6) Å b = 13.7237(8) Å c = 15.3685(9) Å β = 90.753(2)°
Volume [Å ³]	2110.6(2)
Z	4
Density (calculated) [g/cm ³]	1.172
Absorption coefficient [mm ⁻¹]	0.077
F(000)	808
θ range [°]	1.990 - 26.046
No. of reflections collected	22423
No. of unique reflections	4169 [R _{int} = 0.0246]
Observed reflections [I > 2σ (I)]	3693
Data / restraints / parameters	4169 / 0 / 249
Goof	1.038
Final R indices [I > 2σ (I)]	R ₁ = 0.0350, wR ₂ = 0.0826
R indices (all data)	R ₁ = 0.0407, wR ₂ = 0.0861
Largest diff. peak and hole [e Å ⁻³]	0.321 and -0.214
Diffractometer	Bruker Smart Apex 2

Table 68: Crystallographic data for compound ADD18: 4-MeO-C₆H₄Bneop•ⁱPr₂ImMe₂^[300]

4-MeO-C ₆ H ₄ Bneop• ⁱ Pr ₂ ImMe ₂ ADD18	
Identification code	ae137_a
Empirical formula	C ₂₃ H ₃₇ BN ₂ O ₃
Formula weight [g/mol]	400.35
Temperature [K]	100(2)
Wavelength [Å]	0.71073
Crystal system	Monoclinic
Space group	<i>P</i> 2 ₁ / <i>n</i>
Unit cell dimensions	a = 8.3984(4) Å b = 14.3014(7) Å c = 19.2534(9) Å β = 101.8150(10)°
Volume [Å ³]	2263.51(19)
Z	4
Density (calculated) [g/cm ³]	1.175
Absorption coefficient [mm ⁻¹]	0.076
F(000)	872
θ range [°]	1.788 - 26.068
No. of reflections collected	29014
No. of unique reflections	4487 [R _{int} = 0.0309]
Observed reflections [I > 2σ (I)]	3813
Data / restraints / parameters	4487 / 0 / 271
Goof	1.027
Final R indices [I > 2σ (I)]	R ₁ = 0.0375, wR ₂ = 0.0900
R indices (all data)	R ₁ = 0.0465, wR ₂ = 0.0947
Largest diff. peak and hole [e Å ⁻³]	0.325 and -0.239
Diffractometer	Bruker Smart Apex 2

Table 69: Crystallographic data for compound ADD19: *p*-tolylBcat•CaaC^{Me}[300]

<i>p</i> -tolylBcat•CaaC ^{Me} ADD19	
Identification code	ae117_a
Empirical formula	C ₃₃ H ₄₂ BNO ₂
Formula weight [g/mol]	495.48
Temperature [K]	100(2)
Wavelength [Å]	0.71073
Crystal system	Triclinic
Space group	<i>P</i> -1
Unit cell dimensions	a = 10.8750(4) Å b = 15.4367(6) Å c = 26.8007(11) Å α = 73.4300(10)° β = 80.5800(10)° γ = 86.6210(10)°
Volume [Å ³]	4253.8(3)
Z	6
Density (calculated) [g/cm ³]	1.161
Absorption coefficient [mm ⁻¹]	0.070
F(000)	1608
θ range [°]	1.777 - 26.130
No. of reflections collected	30514
No. of unique reflections	16905 [R _{int} = 0.0324]
Observed reflections [I > 2σ (I)]	10787
Data / restraints / parameters	16905 / 2232 / 1140
Goof	1.023
Final R indices [I > 2σ (I)]	R ₁ = 0.0549, wR ₂ = 0.1106
R indices (all data)	R ₁ = 0.1018, wR ₂ = 0.1294
Largest diff. peak and hole [e Å ⁻³]	0.378 and -0.264
Diffractometer	Bruker Smart Apex 2

Table 70: Crystallographic data for compound ADD24: C₆H₅Bpin-ⁱPr₂Im

C ₆ H ₅ Bpin- ⁱ Pr ₂ Im ADD24	
Identification code	ae045_a
Empirical formula	C ₂₁ H ₃₃ BN ₂ O ₂
Formula weight [g/mol]	356.30
Temperature [K]	100(2)
Wavelength [Å]	0.71073
Crystal system	monoclinic
Space group	<i>P</i> 2 ₁ / <i>n</i>
Unit cell dimensions	a = 9.505(3) Å b = 14.587(5) Å c = 15.216(5) Å β = 92.677(9)°
Volume [Å ³]	2107.4(12)
Z	4
Density (calculated) [g/cm ³]	1.127
Absorption coefficient [mm ⁻¹]	0.072
F(000)	780
θ range [°]	2.476 - 26.281
No. of reflections collected	34397
No. of unique reflections	4219 [R _{int} = 0.1753]
Observed reflections [I > 2σ(I)]	2050
Data / restraints / parameters	4219 / 0 / 244
Goof	0.984
Final R indices [I > 2σ(I)]	R ₁ = 0.0616, wR ₂ = 0.1103
R indices (all data)	R ₁ = 0.1665, wR ₂ = 0.1444
Largest diff. peak and hole [e Å ⁻³]	0.264 and -0.257
Diffractometer	Bruker Smart Apex 2

Table 71: Crystallographic data for compound ADD25: *p*-tolylBpin•Me₄Im

tolylBpin•Me ₄ Im ADD25	
Identification code	ae106_a
Empirical formula	C ₂₀ H ₃₁ BN ₂ O ₂
Formula weight [g/mol]	342.28
Temperature [K]	100(2)
Wavelength [Å]	0.71073
Crystal system	Monoclinic
Space group	<i>P</i> 2 ₁ / <i>c</i>
Unit cell dimensions	a = 11.0467(8) Å b = 16.8082(12) Å c = 10.9076(8) Å β = 98.776(2)°
Volume [Å ³]	2001.6(3)
Z	4
Density (calculated) [g/cm ³]	1.136
Absorption coefficient [mm ⁻¹]	0.072
F(000)	744
θ range [°]	1.865 - 26.040
No. of reflections collected	14330
No. of unique reflections	3957 [R _{int} = 0.0451]
Observed reflections [I > 2σ (I)]	2819
Data / restraints / parameters	3957 / 0 / 235
Goof	1.027
Final R indices [I > 2σ (I)]	R ₁ = 0.0459, wR ₂ = 0.1020
R indices (all data)	R ₁ = 0.0746, wR ₂ = 0.1147
Largest diff. peak and hole [e Å ⁻³]	0.273 and -0.226
Diffractometer	Bruker Smart Apex 2

Table 72: Crystallographic data for compound ADD26: *p*-tolylBcat•ⁱPr₂Im

<i>p</i> -tolylBcat• ⁱ Pr ₂ Im ADD26	
Identification code	ae116_a
Empirical formula	C ₂₂ H ₂₇ BN ₂ O ₂
Formula weight [g/mol]	362.26
Temperature [K]	100(2)
Wavelength [Å]	0.71073
Crystal system	Triclinic
Space group	<i>P</i> -1
Unit cell dimensions	a = 7.9855(6) Å b = 9.9187(7) Å c = 13.9502(10) Å α = 76.504(2)° β = 81.627(3)° γ = 68.274(2)°
Volume [Å ³]	995.96(13)
Z	2
Density (calculated) [g/cm ³]	1.208
Absorption coefficient [mm ⁻¹]	0.076
F(000)	388
θ range [°]	1.504 - 26.080
No. of reflections collected	12963
No. of unique reflections	3937 [R _{int} = 0.0195]
Observed reflections [I > 2σ (I)]	3351
Data / restraints / parameters	3937 / 0 / 249
Goof	1.031
Final R indices [I > 2σ (I)]	R ₁ = 0.0399, wR ₂ = 0.0965
R indices (all data)	R ₁ = 0.0486, wR ₂ = 0.1019
Largest diff. peak and hole [e Å ⁻³]	0.304 and -0.287
Diffractometer	Bruker Smart Apex 2

Table 73: Crystallographic data for compound ADD27: *p*-tolylBpin•Me₂Im

<i>p</i> -tolylBpin•Me ₂ Im ADD27	
Identification code	ae121_a
Empirical formula	C ₁₈ H ₂₇ BN ₂ O ₂
Formula weight [g/mol]	314.22
Temperature [K]	100(2)
Wavelength [Å]	0.71073
Crystal system	Orthorhombic
Space group	<i>Pbca</i>
Unit cell dimensions	a = 12.5921(6) Å b = 16.2773(8) Å c = 17.5311(8) Å
Volume [Å ³]	3593.3(3)
Z	8
Density (calculated) [g/cm ³]	1.162
Absorption coefficient [mm ⁻¹]	0.075
F(000)	1360
θ range [°]	2.323 - 26.068
No. of reflections collected	28501
No. of unique reflections	3545 [R _{int} = 0.0363]
Observed reflections [I > 2σ (I)]	2987
Data / restraints / parameters	3545 / 0 / 215
Goof	1.046
Final R indices [I > 2σ (I)]	R ₁ = 0.0399, wR ₂ = 0.0967
R indices (all data)	R ₁ = 0.0502, wR ₂ = 0.1035
Largest diff. peak and hole [e Å ⁻³]	0.347 and -0.294
Diffractometer	Bruker Smart Apex 2

Table 74: Crystallographic data for compound ADD28: *p*-tolylBcat•Mes₂Im

<i>p</i> -tolylBcat•Mes ₂ Im ADD28	
Identification code	ae123new_a
Empirical formula	C ₃₄ H ₃₅ BN ₂ O ₂
Formula weight [g/mol]	514.45
Temperature [K]	100(2)
Wavelength [Å]	0.71073
Crystal system	Tetragonal
Space group	<i>P</i> -4
Unit cell dimensions	a = 13.699(2) Å b = 13.699(2) Å c = 14.996(3) Å
Volume [Å ³]	2814.2(10)
Z	4
Density (calculated) [g/cm ³]	1.214
Absorption coefficient [mm ⁻¹]	0.074
F(000)	1096
θ range [°]	1.358 - 26.089
No. of reflections collected	26960
No. of unique reflections	5565 [R _{int} = 0.0741]
Observed reflections [I > 2σ (I)]	5104
Data / restraints / parameters	5565 / 1110 / 451
Goof	1.101
Final R indices [I > 2σ (I)]	R ₁ = 0.0688, wR ₂ = 0.1646
R indices (all data)	R ₁ = 0.0752, wR ₂ = 0.1685
Largest diff. peak and hole [e Å ⁻³]	0.286 and -0.258
Diffractometer	Bruker Smart Apex 2

Table 75: Crystallographic data for compound BCA1: C₆H₅Bpin•CaaC^{Me}[300]

C ₆ H ₅ Bpin•CaaC ^{Me} BCA1	
Identification code	ae146_a
Empirical formula	C ₃₂ H ₄₈ BNO ₂
Formula weight [g/mol]	489.52
Temperature [K]	100(2)
Wavelength [Å]	0.71073
Crystal system	Monoclinic
Space group	<i>P</i> 2 ₁ / <i>c</i>
Unit cell dimensions	a = 9.7150(8) Å b = 30.000(2) Å c = 9.9729(8) Å β = 100.016(3)°
Volume [Å ³]	2862.3(4)
Z	4
Density (calculated) [g/cm ³]	1.136
Absorption coefficient [mm ⁻¹]	0.068
F(000)	1072
θ range [°]	2.129 - 26.094
No. of reflections collected	29936
No. of unique reflections	5652 [R _{int} = 0.0571]
Observed reflections [I > 2σ (I)]	4028
Data / restraints / parameters	5652 / 0 / 337
Goof	1.017
Final R indices [I > 2σ (I)]	R ₁ = 0.0442, wR ₂ = 0.0924
R indices (all data)	R ₁ = 0.0744, wR ₂ = 0.1054
Largest diff. peak and hole [e Å ⁻³]	0.260 and -0.233
Diffractometer	Bruker Smart Apex 2

Table 76: Crystallographic data for compound BCA2: *p*-tolylBpin•CaaC^{Me}[300]

<i>p</i> -tolylBpin•CaaC ^{Me} BCA2	
Identification code	ae178_a
Empirical formula	C ₃₃ H ₅₀ BNO ₂
Formula weight [g/mol]	503.55
Temperature [K]	100(2)
Wavelength [Å]	0.71073
Crystal system	Triclinic
Space group	<i>P</i> -1
Unit cell dimensions	a = 9.5885(6) Å b = 10.0172(5) Å c = 15.5522(8) Å α = 83.322(2)° β = 88.508(2)° γ = 80.195(2)°
Volume [Å ³]	1461.95(14)
Z	2
Density (calculated) [g/cm ³]	1.144
Absorption coefficient [mm ⁻¹]	0.069
F(000)	552
θ range [°]	1.318 - 26.081
No. of reflections collected	16182
No. of unique reflections	5776 [R _{int} = 0.0224]
Observed reflections [I > 2σ (I)]	4781
Data / restraints / parameters	5776 / 0 / 347
Goof	1.028
Final R indices [I > 2σ (I)]	R ₁ = 0.0391, wR ₂ = 0.0914
R indices (all data)	R ₁ = 0.0501, wR ₂ = 0.0976
Largest diff. peak and hole [e Å ⁻³]	0.328 and -0.253
Diffractometer	Bruker Smart Apex 2

Table 77: Crystallographic data for compound BCA3: 4-MeO-C₆H₄Bpin•CaaC^{Me}[300]

4-MeO-C ₆ H ₄ Bpin•CaaC ^{Me} BCA3	
Identification code	ae145_a
Empirical formula	C ₃₃ H ₅₀ BNO ₃
Formula weight [g/mol]	519.55
Temperature [K]	100(2)
Wavelength [Å]	0.71073
Crystal system	Triclinic
Space group	<i>P</i> -1
Unit cell dimensions	a = 9.6473(10) Å b = 10.0527(11) Å c = 15.4868(16) Å α = 84.791(4)° β = 89.900(4)° γ = 79.846(4)°
Volume [Å ³]	1472.1(3)
Z	2
Density (calculated) [g/cm ³]	1.172
Absorption coefficient [mm ⁻¹]	0.073
F(000)	568
θ range [°]	1.320 - 26.095
No. of reflections collected	12907
No. of unique reflections	5825 [R _{int} = 0.0260]
Observed reflections [I > 2σ (I)]	4652
Data / restraints / parameters	5825 / 0 / 356
Goof	1.025
Final R indices [I > 2σ (I)]	R ₁ = 0.0415, wR ₂ = 0.0927
R indices (all data)	R ₁ = 0.0562, wR ₂ = 0.1006
Largest diff. peak and hole [e Å ⁻³]	0.265 and -0.218
Diffractionmeter	Bruker Smart Apex 2

Table 78: Crystallographic data for compound BCA4: *p*-tolylBneop•CaaC^{Me}[300]

<i>p</i> -tolylBneop•CaaC ^{Me} BCA4	
Identification code	ae124_a
Empirical formula	C ₃₂ H ₄₈ BNO ₂
Formula weight [g/mol]	489.52
Temperature [K]	100(2)
Wavelength [Å]	0.71073
Crystal system	Triclinic
Space group	<i>P</i> -1
Unit cell dimensions	a = 9.8357(4) Å b = 9.9522(4) Å c = 15.3271(6) Å α = 80.0710(10)° β = 86.8750(10)° γ = 84.6270(10)°
Volume [Å ³]	1470.23(10)
Z	2
Density (calculated) [g/cm ³]	1.106
Absorption coefficient [mm ⁻¹]	0.067
F(000)	536
θ range [°]	1.350 - 26.034
No. of reflections collected	19322
No. of unique reflections	5780 [R _{int} = 0.0236]
Observed reflections [I > 2σ (I)]	5078
Data / restraints / parameters	5780 / 0 / 336
Goof	1.033
Final R indices [I > 2σ (I)]	R ₁ = 0.0379, wR ₂ = 0.0934
R indices (all data)	R ₁ = 0.0436, wR ₂ = 0.0976
Largest diff. peak and hole [e Å ⁻³]	0.307 and -0.220
Diffractometer	Bruker Smart Apex 2

Table 79: Crystallographic data for compound BCA5: 4-MeO-C₆H₄Bneop•CaaC^{Me}[300]

4-MeO-C ₆ H ₄ Bneop•CaaC ^{Me} BCA5	
Identification code	ae120_a
Empirical formula	C ₃₂ H ₄₈ BNO ₃
Formula weight [g/mol]	505.52
Temperature [K]	100(2)
Wavelength [Å]	0.71073
Crystal system	Monoclinic
Space group	<i>P</i> 2 ₁ / <i>c</i>
Unit cell dimensions	a = 9.5768(5) Å b = 15.2176(8) Å c = 19.8696(11) Å β = 95.547(2)°
Volume [Å ³]	2882.2(3)
Z	4
Density (calculated) [g/cm ³]	1.165
Absorption coefficient [mm ⁻¹]	0.072
F(000)	1104
θ range [°]	1.688 - 26.059
No. of reflections collected	21962
No. of unique reflections	5686 [R _{int} = 0.0373]
Observed reflections [I > 2σ (I)]	4326
Data / restraints / parameters	5686 / 0 / 345
Goof	1.011
Final R indices [I > 2σ (I)]	R ₁ = 0.0407, wR ₂ = 0.0891
R indices (all data)	R ₁ = 0.0605, wR ₂ = 0.0989
Largest diff. peak and hole [e Å ⁻³]	0.275 and -0.211
Diffractometer	Bruker Smart Apex 2

Table 80: Crystallographic data for compound BCA6: *p*-tolylBeg•CaaC^{Me}[300]

<i>p</i> -tolylBeg•CaaC ^{Me} BCA6	
Identification code	ae175_a
Empirical formula	C ₂₉ H ₄₂ BNO ₂
Formula weight [g/mol]	447.44
Temperature [K]	100(2)
Wavelength [Å]	0.71073
Crystal system	Monoclinic
Space group	<i>C</i> 2/ <i>c</i>
Unit cell dimensions	a = 16.0964(10) Å b = 13.4282(8) Å c = 24.8642(18) Å β = 106.393(2)°
Volume [Å ³]	5155.8(6)
Z	8
Density (calculated) [g/cm ³]	1.153
Absorption coefficient [mm ⁻¹]	0.070
F(000)	1952
θ range [°]	2.010 - 26.074
No. of reflections collected	21581
No. of unique reflections	5091 [R _{int} = 0.0317]
Observed reflections [I > 2σ (I)]	3924
Data / restraints / parameters	5091 / 0 / 307
Goof	1.040
Final R indices [I > 2σ (I)]	R ₁ = 0.0408, wR ₂ = 0.0963
R indices (all data)	R ₁ = 0.0582, wR ₂ = 0.1053
Largest diff. peak and hole [e Å ⁻³]	0.295 and -0.237
Diffractometer	Bruker Smart Apex 2

Table 81: Crystallographic data for compound RER1: *p*-tolylBcat•CaaC^{Me}[300]

RER <i>p</i> -tolylBcat•CaaC ^{Me} RER1	
Identification code	ae109_a
Empirical formula	C ₃₃ H ₄₂ BNO ₂
Formula weight [g/mol]	495.48
Temperature [K]	100(2)
Wavelength [Å]	0.71073
Crystal system	Monoclinic
Space group	<i>P</i> 2 ₁ / <i>c</i>
Unit cell dimensions	a = 10.8306(11) Å b = 15.3619(18) Å c = 17.9016(17) Å β = 106.930(3)°
Volume [Å ³]	2849.4(5)
Z	4
Density (calculated) [g/cm ³]	1.155
Absorption coefficient [mm ⁻¹]	0.070
F(000)	1072
θ range [°]	1.781 - 26.040
No. of reflections collected	20424
No. of unique reflections	5616 [R _{int} = 0.0403]
Observed reflections [I > 2σ (I)]	4071
Data / restraints / parameters	5616 / 0 / 343
Goof	1.019
Final R indices [I > 2σ (I)]	R ₁ = 0.0420, wR ₂ = 0.0901
R indices (all data)	R ₁ = 0.0678, wR ₂ = 0.1016
Largest diff. peak and hole [e Å ⁻³]	0.216 and -0.242
Diffractometer	Bruker Smart Apex 2

Table 82: Crystallographic data for compound RER2: ansiolBcat•CaaC^{Me}[300]

RER ansiolBcat•CaaC ^{Me} RER2	
Identification code	AE235_a
Empirical formula	C ₃₆ H ₄₅ BNO ₃
Formula weight [g/mol]	550.54
Temperature [K]	100(2)
Wavelength [Å]	0.71073
Crystal system	Triclinic
Space group	<i>P</i> -1
Unit cell dimensions	a = 9.4131(11) Å b = 10.9130(13) Å c = 16.1481(18) Å α = 74.405(4)° β = 78.850(4)° γ = 74.715(4)°
Volume [Å ³]	1527.8(3)
Z	2
Density (calculated) [g/cm ³]	1.197
Absorption coefficient [mm ⁻¹]	0.074
F(000)	594
θ range [°]	1.321 - 26.408
No. of reflections collected	14532
No. of unique reflections	6257 [R _{int} = 0.0482]
Observed reflections [I > 2σ (I)]	4291
Data / restraints / parameters	6257 / 36 / 407
Goof	1.035
Final R indices [I > 2σ (I)]	R ₁ = 0.0537, wR ₂ = 0.1187
R indices (all data)	R ₁ = 0.0880, wR ₂ = 0.1349
Largest diff. peak and hole [e Å ³]	0.276 and -0.249
Diffractometer	Bruker Smart Apex 2

Table 83: Crystallographic data for compound 4-F-C₆H₅Beg

4-F-C ₆ H ₅ Beg	
Identification code	ae166_a
Empirical formula	C ₈ H ₈ BFO ₂
Formula weight [g/mol]	165.95
Temperature [K]	100(2)
Wavelength [Å]	0.71073
Crystal system	Orthorhombic
Space group	<i>Fdd2</i>
Unit cell dimensions	a = 11.1816(19) Å b = 13.076(2) Å c = 10.7598(18) Å
Volume [Å ³]	1573.2(5)
Z	8
Density (calculated) [g/cm ³]	1.401
Absorption coefficient [mm ⁻¹]	0.112
F(000)	688
θ range [°]	3.055 - 26.048
No. of reflections collected	1698
No. of unique reflections	691 [R _{int} = 0.0143]
Observed reflections [I > 2σ (I)]	659
Data / restraints / parameters	691 / 1 / 57
Goof	1.135
Final R indices [I > 2σ (I)]	R ₁ = 0.0255, wR ₂ = 0.0639
R indices (all data)	R ₁ = 0.0279, wR ₂ = 0.0652
Largest diff. peak and hole [e Å ³]	0.137 and -0.161
Diffractometer	Bruker Smart Apex 2

Table 84: Crystallographic data for compound 4-F-C₆H₅Beg

4-F-C ₆ H ₅ Beg	
Identification code	ae209_a
Empirical formula	C ₈ H ₈ BFO ₂
Formula weight [g/mol]	165.95
Temperature [K]	100(2)
Wavelength [Å]	0.71073
Crystal system	Monoclinic
Space group	C2/c
Unit cell dimensions	a = 11.2280(14) Å b = 10.6893(13) Å c = 7.4248(9) Å β = 118.481(3)°
Volume [Å ³]	783.27(17)
Z	4
Density (calculated) [g/cm ³]	1.407
Absorption coefficient [mm ⁻¹]	0.112
F(000)	344
θ range [°]	2.809 - 26.346
No. of reflections collected	4990
No. of unique reflections	807 [R _{int} = 0.0201]
Observed reflections [I > 2σ (I)]	733
Data / restraints / parameters	807 / 0 / 57
Goof	1.081
Final R indices [I > 2σ (I)]	R ₁ = 0.0306, wR ₂ = 0.0802
R indices (all data)	R ₁ = 0.0334, wR ₂ = 0.0825
Largest diff. peak and hole [e Å ⁻³]	0.234 and -0.257
Diffractometer	Bruker Smart Apex 2

Table 85: Crystallographic data for compound 4-MeO-C₆H₄Bneop

4-MeO-C ₆ H ₄ Bneop	
Identification code	ae128_a
Empirical formula	C ₁₂ H ₁₇ BO ₃
Formula weight [g/mol]	220.06
Temperature [K]	100(2)
Wavelength [Å]	0.71073
Crystal system	Orthorhombic
Space group	<i>P</i> 2 ₁ 2 ₁ 2 ₁
Unit cell dimensions	a = 6.5530(9) Å b = 9.4754(12) Å c = 19.250(2) Å
Volume [Å ³]	1195.3(3)
Z	4
Density (calculated) [g/cm ³]	1.223
Absorption coefficient [mm ⁻¹]	0.085
F(000)	472
θ range [°]	2.116 - 25.983
No. of reflections collected	3888
No. of unique reflections	2111 [R _{int} = 0.0247]
Observed reflections [I > 2σ (I)]	1874
Data / restraints / parameters	2111 / 0 / 148
Goof	1.055
Final R indices [I > 2σ (I)]	R ₁ = 0.0358, wR ₂ = 0.0836
R indices (all data)	R ₁ = 0.0423, wR ₂ = 0.0870
Largest diff. peak and hole [e Å ⁻³]	0.150 and -0.225
Diffractometer	Bruker Smart Apex 2

Table 86: Crystallographic data for compound 4-CF₃-C₆H₅Bneop

4-CF ₃ -C ₆ H ₅ Bneop	
Identification code	ae214_a
Empirical formula	C ₁₂ H ₁₄ BF ₃ O ₂
Formula weight [g/mol]	258.04
Temperature [K]	100(2)
Wavelength [Å]	0.71073
Crystal system	Triclinic
Space group	<i>P</i> -1
Unit cell dimensions	a = 6.0347(8) Å b = 9.2244(12) Å c = 11.7949(15) Å α = 77.158(4)° β = 82.811(4)° γ = 72.456(4)°
Volume [Å ³]	609.19(14)
Z	2
Density (calculated) [g/cm ³]	1.407
Absorption coefficient [mm ⁻¹]	0.122
F(000)	268
θ range [°]	1.774 - 26.419
No. of reflections collected	8236
No. of unique reflections	2511 [R _{int} = 0.0318]
Observed reflections [I >2σ(I)]	2087
Data / restraints / parameters	2511 / 42 / 193
Goof	1.015
Final R indices [I >2σ(I)]	R ₁ = 0.0418, wR ₂ = 0.1067
R indices (all data)	R ₁ = 0.0516, wR ₂ = 0.1133
Largest diff. peak and hole [e Å ⁻³]	0.324 and -0.266
Diffractometer	Bruker Smart Apex 2

Table 87: Crystallographic data for compound 4-CF₃-C₆H₅Beg

4-CF ₃ -C ₆ H ₅ Beg	
Identification code	ae203_a
Empirical formula	C ₉ H ₈ BF ₃ O ₂
Formula weight [g/mol]	215.96
Temperature [K]	100(2)
Wavelength [Å]	0.71073
Crystal system	Monoclinic
Space group	<i>P</i> 2 ₁ / <i>c</i>
Unit cell dimensions	a = 10.977(2) Å b = 14.533(3) Å c = 5.6699(11) Å β = 96.585(4)°
Volume [Å ³]	898.6(3)
Z	4
Density (calculated) [g/cm ³]	1.596
Absorption coefficient [mm ⁻¹]	0.149
F(000)	440
θ range [°]	1.867 - 26.436
No. of reflections collected	5483
No. of unique reflections	1839 [R _{int} = 0.0217]
Observed reflections [I > 2σ (I)]	1589
Data / restraints / parameters	1839 / 0 / 136
Goof	1.048
Final R indices [I > 2σ (I)]	R ₁ = 0.0335, wR ₂ = 0.0819
R indices (all data)	R ₁ = 0.0398, wR ₂ = 0.0857
Largest diff. peak and hole [e Å ⁻³]	0.358 and -0.253
Diffractometer	Bruker Smart Apex 2

Table 88: Crystallographic data for compound 4-CF₃-C₆H₅Bpin

4-CF ₃ -C ₆ H ₅ Bpin	
Identification code	ae199_a (twin5)
Empirical formula	C ₁₃ H ₁₆ BF ₃ O ₂
Formula weight [g/mol]	272.07
Temperature [K]	100(2)
Wavelength [Å]	0.71073
Crystal system	Triclinic
Space group	<i>P</i> -1
Unit cell dimensions	a = 8.3839(7) Å b = 8.7381(7) Å c = 10.3523(8) Å α = 107.514(2)° β = 105.682(2)° γ = 97.260(2)°
Volume [Å ³]	678.27(9)
Z	2
Density (calculated) [g/cm ³]	1.332
Absorption coefficient [mm ⁻¹]	0.114
F(000)	284
θ range [°]	2.182 - 26.427
No. of reflections collected	2775
No. of unique reflections	2775 [R _{int} = 0.0364]
Observed reflections [I > 2σ (I)]	2538
Data / restraints / parameters	2775 / 69 / 205
Goof	1.067
Final R indices [I > 2σ (I)]	R ₁ = 0.0356, wR ₂ = 0.0956
R indices (all data)	R ₁ = 0.0391, wR ₂ = 0.0986
Largest diff. peak and hole [e Å ⁻³]	0.344 and -0.172
Diffractometer	Bruker Smart Apex 2

Table 89: Crystallographic data for compound *p*-tolylBeg

<i>p</i> -tolylBeg	
Identification code	ae179_a
Empirical formula	C ₉ H ₁₁ BO ₂
Formula weight [g/mol]	161.99
Temperature [K]	100(2)
Wavelength [Å]	0.71073
Crystal system	Monoclinic
Space group	C2/c
Unit cell dimensions	a = 7.4769(6) Å b = 11.3831(8) Å c = 10.3537(8) Å β = 101.470(2)°
Volume [Å ³]	863.61(11)
Z	4
Density (calculated) [g/cm ³]	1.246
Absorption coefficient [mm ⁻¹]	0.084
F(000)	344
θ range [°]	3.306 - 26.420
No. of reflections collected	5624
No. of unique reflections	900 [R _{int} = 0.0168]
Observed reflections [I > 2σ (I)]	830
Data / restraints / parameters	900 / 0 / 58
Goof	1.062
Final R indices [I > 2σ (I)]	R ₁ = 0.0325, wR ₂ = 0.0861
R indices (all data)	R ₁ = 0.0351, wR ₂ = 0.0889
Largest diff. peak and hole [e Å ⁻³]	0.287 and -0.244
Diffractometer	Bruker Smart Apex 2

Table 90: Crystallographic data for compound C₆F₅Bpin

C ₆ F ₅ Bpin	
Identification code	ae210_a
Empirical formula	C ₁₂ H ₁₂ BF ₅ O ₂
Formula weight [g/mol]	294.03
Temperature [K]	100(2)
Wavelength [Å]	0.71073
Crystal system	Orthorhombic
Space group	<i>P</i> 2 ₁ 2 ₁ 2 ₁
Unit cell dimensions	a = 10.5323(14) Å b = 18.053(3) Å c = 20.390(3) Å
Volume [Å ³]	3877.0(9)
Z	12
Density (calculated) [g/cm ³]	1.511
Absorption coefficient [mm ⁻¹]	0.147
F(000)	1800
θ range [°]	1.507 - 26.373
No. of reflections collected	14671
No. of unique reflections	7876 [R _{int} = 0.0449]
Observed reflections [I > 2σ (I)]	5489
Data / restraints / parameters	7876 / 0 / 553
Goof	1.014
Final R indices [I > 2σ (I)]	R ₁ = 0.0486, wR ₂ = 0.0864
R indices (all data)	R ₁ = 0.0918, wR ₂ = 0.0999
Largest diff. peak and hole [e Å ⁻³]	0.291 and -0.232
Diffractometer	Bruker Smart Apex 2

8 Appendix

8.1 Abbreviations

General

ADD	adduct
BBA	boron-boron bond activation
BCA	boron-carbon bond activation
h	hour(s)
min	minute(s)
r.t.	room temperature
RER	ring expansion reaction
xs	excess (of reagent)
eq.	equivalent

Solvents

C ₆ D ₆	deuterated benzene
DCM	dichloromethane
DMF	dimethylformamide
Et ₂ O	diethylether
MeCN	acetonitrile
MeOH	methanol
THF	tetrahydrofuran

Substituents and chemical moieties

{B(NDippCH) ₂ }	1,3-bis(2,6-di- <i>iso</i> -propylphenyl)-1,3-dihydro-1,3,2-diazaborole
9-BBN	9-borabicyclo-(3,3,1)-nonane
Ar	aryl
<i>p</i> -anisyl	<i>para</i> -methoxyphenyl (4-MeO-C ₆ H ₄ -)

B ₂ pin ₂	bis(pinacolato)diboron
B ₂ cat ₂	bis(catecholato)diboron
B ₂ neop ₂	bis(neopentylglycolato)diboron
B ₂ eg ₂	bis(ethylen glycolato)diboron
cat	catecholato
Cy	cyclohexyl
DABCO	1,4-diazabicyclo-(2,2,2)-octane
dmab	1,2-di(methylamino)benzene
dbab	1,2-di(benzylamino)benzene
DBM	dibenzoylmethane
Dipp	2,6-di- <i>iso</i> -propylphenyl
duryl	2,3,5,6-tetramethyl-phenyl
eg	ethylen glycolato
Et	ethyl
Hal	halogen
Hfacac	hexafluoroacetylacetonate
Im	Imidazole (2,6-diazacyclopenta-2,4-diene)
L	coordinating ligand
M	transition metal
Me	methyl
Mes	mesityl (2,4,6-trimethylphenyl)
MeO	methoxy
neop	neopentyl glycolato
OTf	triflate/OSO ₂ CF ₃
<i>i</i> Pr	<i>iso</i> -propyl
<i>n</i> Pr	<i>n</i> -propyl
Ph	phenyl
pin	pinacolato
R	generalized organic group

^t Bu	<i>tert</i> -butyl
^t BuO	<i>tert</i> -butoxy
<i>p</i> -tolyl	<i>para</i> -tolyl (4-methylphenyl)
TMS	trimethylsilyl
Xantphos	4,5-bis(diphenylphosphino)-9,9-dimethylxanthene

Carbenes

Me ₂ Im	1,3-dimethylimidazolin-2-ylidene
ⁿ Pr ₂ Im	1,3-di- <i>n</i> -propylimidazolin-2-ylidene
ⁱ Pr ₂ Im	1,3-di- <i>iso</i> -propylimidazolin-2-ylidene
^t Bu ₂ Im	1,3-di- <i>tert</i> -butylimidazolin-2-ylidene
Cy ₂ Im	1,3-dicyclohexylimidazolin-2-ylidene
Mes ₂ Im	1,3-dimesitylimidazolin-2-ylidene
Me ₄ Im	1,3,4,5-tetramethylimidazolin-2-ylidene
ⁱ Pr ₂ ImMe ₂	1,3-di- <i>iso</i> -propyl-4,5-dimethylimidazolin-2-ylidene
Dipp ₂ Im	1,3-(2,6-di- <i>iso</i> -propylphenyl)imidazolin-2-ylidene
Caac ^{Me}	1-(2,6-di- <i>iso</i> -propylphenyl)-2,2,4,4-tetramethyl-pyrrolidine

Spectroscopy / Spectrometry

δ	chemical shift, expressed in ppm
ASAP	atmospheric solids analysis probe
COSY	correlation spectroscopy
HMBC	heteronuclear multiple-bond correlation
HSQC	heteronuclear single quantum coherence
IR	infrared
m/z	mass-to-charge ratio
NMR	nuclear magnetic resonance
ⁿ J _{AB}	n-bond coupling between nuclei A and B, expressed in Hz

NOESY	nuclear Overhauser effect spectroscopy
s, d, t, sept, br, m	singlet, doublet, triplet, septet, broad, multiplet
ppm	parts per million

Symbols and non-SI units

Å	Ångström, $1 \text{ Å} = 10^{-10} \text{ m} = 100 \text{ pm}$
c	concentration, mol dm^{-3}
M	molar concentration, $1 \text{ M} = 1 \text{ mol dm}^{-3}$
mol%	percentage by amount

8.2 List of compounds

Compound 1:	[Cu(^t Bu ₂ Im)Cl]
Compound 2:	[Cu(ⁱ Pr ₂ Im)Cl]
Compound 3:	[Cu(ⁱ Pr ₂ ImMe ₂)Cl]
Compound 4:	[Cu(Me ₄ Im)Cl]
Compound 5:	[Cu(Me ₂ Im) ₂ Cl]
Compound 6:	[Cu(ⁱ Pr ₂ Im) ₂ Cl]
Compound 7:	[Cu(ⁱ Pr ₂ ImMe ₂) ₂ Cl]
Compound 8:	[Cu(Me ₂ Im) ₂] ⁺ [CuCl ₂] ⁻
Compound 9:	[Cu(Me ₂ Im)(MeCN)][PF ₆]
Compound 10:	[Cu(Me ₂ Im) ₂][PF ₆]
Compound 11:	[Cu(Dipp ₂ Im)(F)]
Compound 12:	[Cu(CaaC ^{Me})(Cl)]
Compound 13:	[Cu(Dipp ₂ Im)(O ^t Bu)]
Compound 14:	[Cu(Mes ₂ Im)(O ^t Bu)]
Compound 15:	[Cu(ⁱ Pr ₂ Im)(O ^t Bu)]
Compound 16:	[Cu(^t Bu ₂ Im)(O ^t Bu)]
Compound 17:	[Cu(ⁱ Pr ₂ Im)(OAc)]
Compound 18:	[Cu(Dipp ₂ Im)(acac)]
Compound 19:	[Cu(Dipp ₂ Im)(hfacac)]
Compound 20:	[Cu(Dipp ₂ Im)(DBM)]
Compound 21:	[Cu(Mes ₂ Im)(hfacac)]
Compound 22:	[Cu(ⁱ Pr ₂ Im)(acac)]
Compound 23:	[Cu(ⁱ Pr ₂ Im)(DBM)]

Compound 24:	[Cu(Dipp ₂ Im)(Mes)]
Compound 25:	[Cu(Mes ₂ Im)(Mes)]
Compound 26:	[Cu(Dipp ₂ Im)(4-MeO-C ₆ H ₄)]
Compound 27:	[Cu(Dipp ₂ Im)(<i>p</i> -tolyl)]
Compound 28:	[Cu(Mes ₂ Im)(<i>p</i> -tolyl)]
Compound 29:	[Cu(Mes ₂ Im)(C ₆ F ₅)]
Compound 30:	[Cu(Dipp ₂ Im)(C ₆ F ₅)]
Compound 31:	[Cu(Dipp ₂ Im)(4-CF ₃ -C ₆ H ₄)]
Compound 32:	[Cu(Mes ₂ Im)(4-CF ₃ -C ₆ H ₄)]
Compound 33:	[Cu(Dipp ₂ Im)(3,5-(CF ₃) ₂ -C ₆ H ₃)]
Compound 34:	[Cu(Mes ₂ Im)(3,5-(CF ₃) ₂ -C ₆ H ₃)]
Compound 35:	[Cu(Dipp ₂ Im)(Dipp)]
Compound 36:	[Cu(Mes ₂ Im)(Dipp)]
Compound 37:	[Cu(^t Bu ₂ Im)(Dipp)]
Compound 38:	[Cu(Dipp ₂ Im)(duryl)]
Compound 39:	[Cu(Mes ₂ Im)(duryl)]
Compound 40:	[Cu(ⁱ Pr ₂ Im)(duryl)]
Compound 41:	[Cu(Dipp ₂ Im)(C ₆ Me ₅)]
Compound 42:	[Cu(Mes ₂ Im)(C ₆ Me ₅)]
Compound 43:	[Cu(^t Bu ₂ Im)(C ₆ Me ₅)]
Compound 44:	[Cu(ⁱ Pr ₂ Im)(C ₆ Me ₅)]
Compound 45:	[Cu(Xantphos)(I)(MeCN)]
Compound 46:	[Cu(Xantphos)(Cl)(MeCN)]

Compound 47:	[Cu(Xantphos)(MeCN) ₄]
Compound BBA1:	B ₂ pin ₂ •CaaC ^{Me} [301]
Compound BBA2:	B ₂ cat ₂ •CaaC ^{Me} [301]
Compound BBA3:	B ₂ neop ₂ •CaaC ^{Me} [301]
Compound BBA4:	B ₂ eg ₂ •CaaC ^{Me} [301]
Compound ADD1:	C ₆ H ₅ Bpin•Me ₂ Im
Compound ADD2:	C ₆ H ₅ Bpin•Me ₄ Im
Compound ADD3:	C ₆ H ₅ Bpin• ⁿ Pr ₂ Im
Compound ADD4:	C ₆ H ₅ Bpin• ⁱ Pr ₂ ImMe ₂ ^[300]
Compound ADD5:	<i>p</i> -tolylBpin• ⁱ Pr ₂ Im
Compound ADD6:	<i>p</i> -tolylBpin• ⁿ Pr ₂ Im
Compound ADD7:	<i>p</i> -tolylBpin• ⁱ Pr ₂ ImMe ₂ ^[300]
Compound ADD8:	<i>p</i> -tolylBcat•Dipp ₂ Im
Compound ADD9:	<i>p</i> -tolylBcat• ⁱ Pr ₂ ImMe ₂ ^[300]
Compound ADD10:	<i>p</i> -tolylBneop•Mes ₂ Im
Compound ADD11:	<i>p</i> -tolylBneop• ⁱ Pr ₂ ImMe ₂ ^[300]
Compound ADD12:	<i>p</i> -tolylBeg• ⁱ Pr ₂ Im
Compound ADD13:	4-MeO-C ₆ H ₄ Bpin•Me ₄ Im
Compound ADD14:	4-MeO-C ₆ H ₄ Bpin• ⁱ Pr ₂ Im Me ₂ ^[300]
Compound ADD15:	4-MeO-C ₆ H ₄ Bneop• ⁱ Pr ₂ Im
Compound ADD16:	4-MeO-C ₆ H ₄ Bneop• ⁿ Pr ₂ Im
Compound ADD17:	4-MeO-C ₆ H ₄ Bneop•Mes ₂ Im
Compound ADD18:	4-MeO-C ₆ H ₄ Bneop• ⁱ Pr ₂ ImMe ₂ ^[300]
Compound ADD19:	<i>p</i> -tolylBcat•CaaC ^{Me} [300]

- Compound ADD20: 4-MeO-C₆H₄Bcat•CaaC^{Me[300]}
- Compound BCA1: C₆H₅Bpin•CaaC^{Me[300]}
- Compound BCA2: *p*-tolylBpin•CaaC^{Me[300]}
- Compound BCA3: 4-MeO-C₆H₄Bpin•CaaC^{Me[300]}
- Compound BCA4: *p*-tolylBneop•CaaC^{Me[300]}
- Compound BCA5: 4-MeO-C₆H₄Bneop•CaaC^{Me[300]}
- Compound BCA6: *p*-tolylBeg•CaaC^{Me[300]}
- Compound RER1: RER *p*-tolylBcat•CaaC^{Me[300]}
- Compound RER2: RER 4-MeO-C₆H₄Bcat•CaaC^{Me[300]}

8.3 Additional NMR data and crystal structures

8.3.1 Additional NMR data

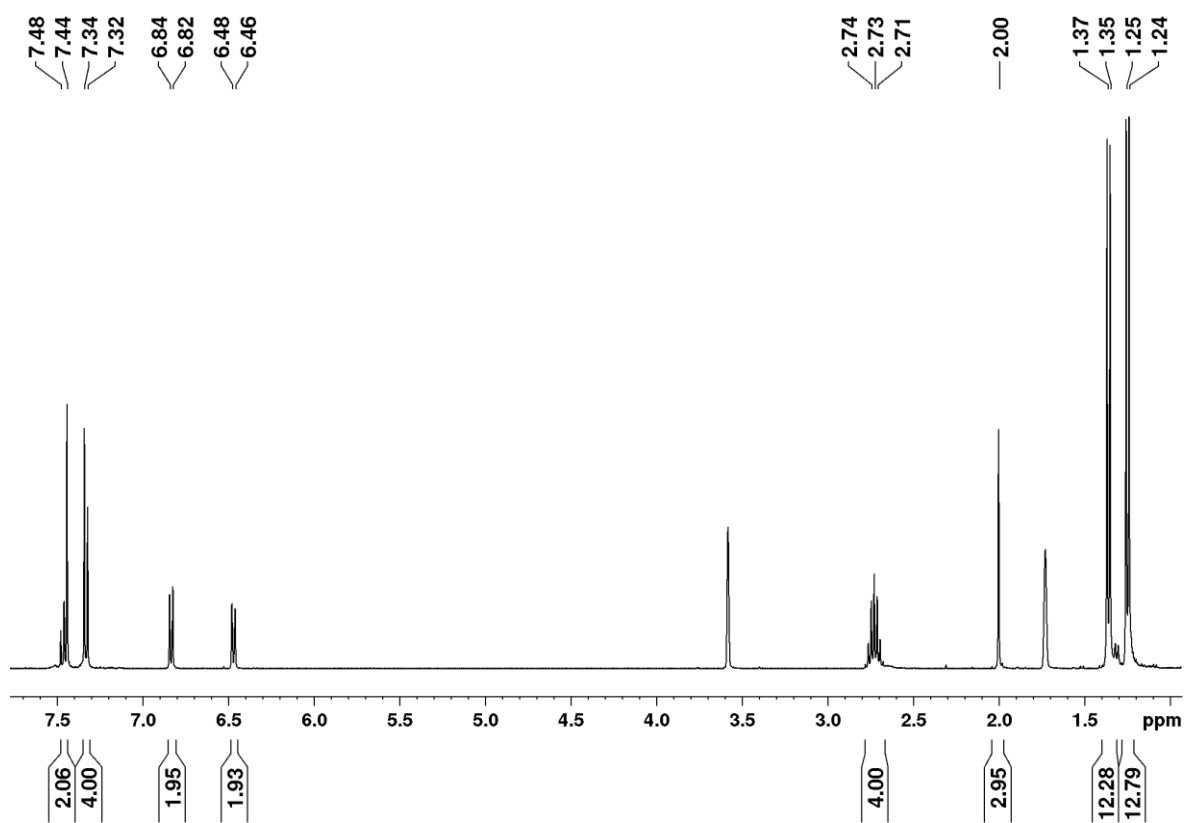
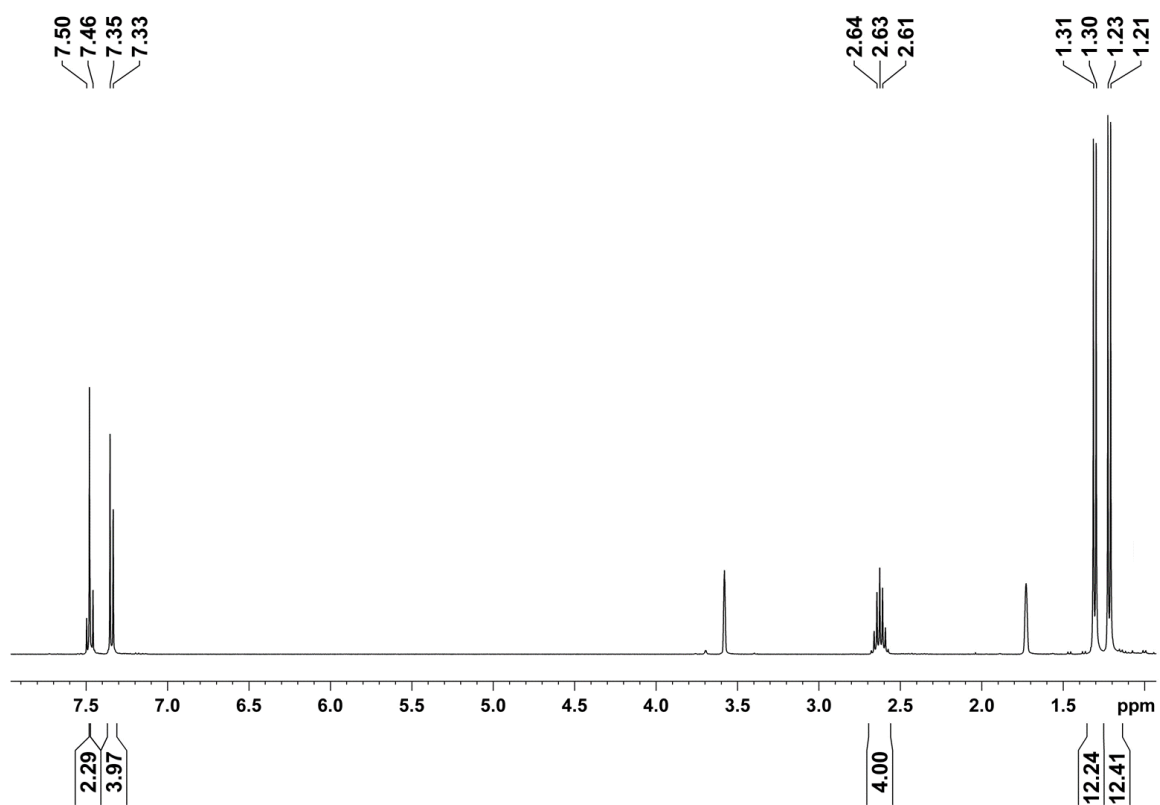
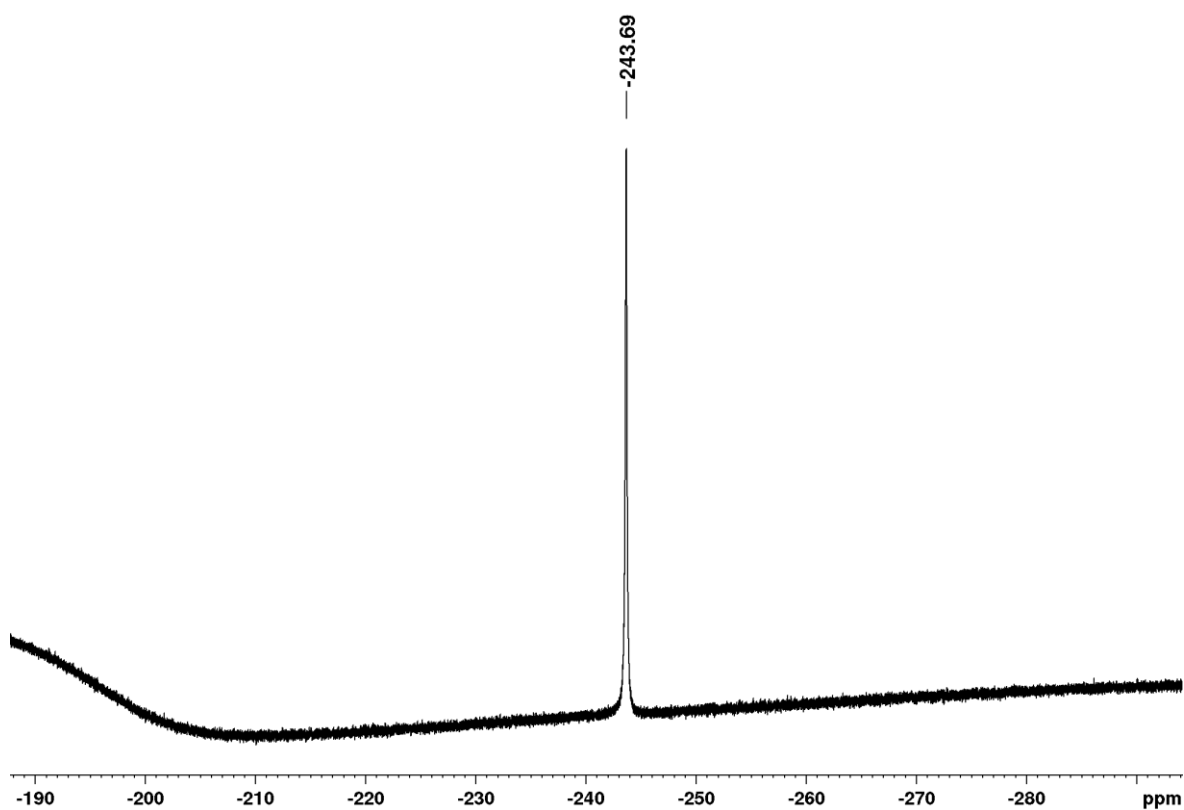
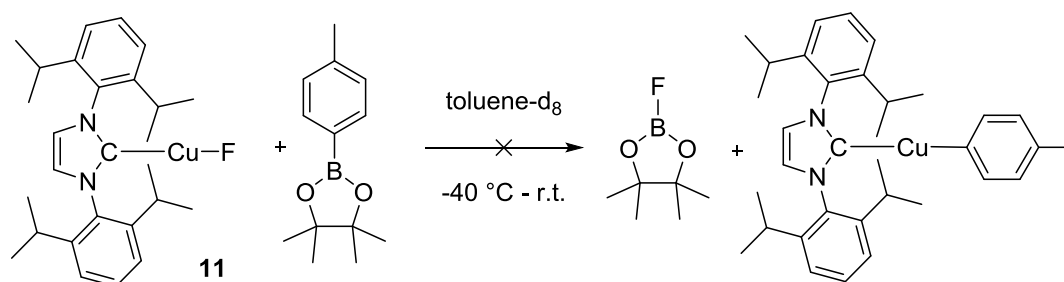


Figure 57: ^1H NMR spectrum of $[\text{Cu}(\text{Dipp}_2\text{Im})(p\text{-tolyl})]$ 27 in THF-d_8 .

Figure 58: ¹H NMR spectrum of [Cu(Dipp₂Im)(F)] 11 in THF-d₈.Figure 59: ¹⁹F NMR spectrum of [Cu(Dipp₂Im)(F)] 11 in THF-d₈.

Reaction of $[\text{Cu}(\text{Dipp}_2\text{Im})(\text{F})]$ with *p*-tolylBpin in toluene- d_8 :



The ^1H NMR spectra (Figure 60) showed broad signals, which did not sharpen at higher temperatures and could not be assigned to a specific compound. The intensity of the signals compared to the solvent residual peaks is low and reflects the observed gel formation. In the ^{11}B and ^{19}F NMR spectra (Figures 61 and 62) signals were detected at 31.4 ppm and -121.0 ppm, respectively. The boron signal matches the resonance of the starting material (31.4 ppm), while the ^{19}F NMR spectra showed that the signal for the fluoride complex (-240 ppm) is gone.

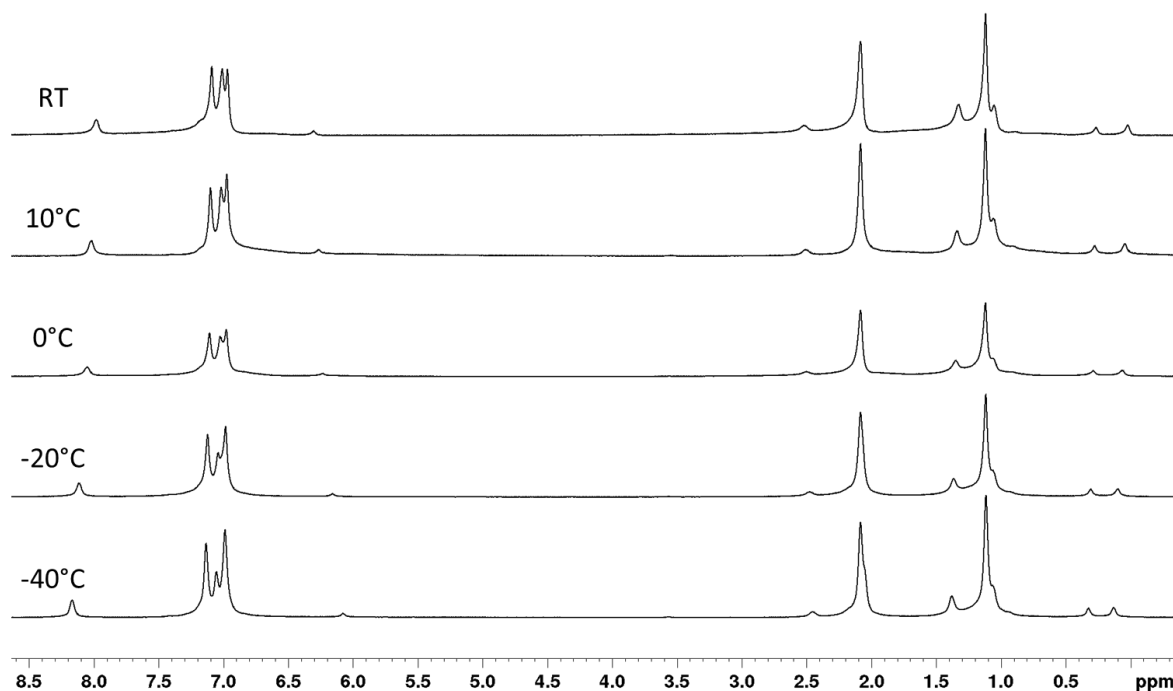


Figure 60: ^1H VT-NMR spectra of the reaction of $[\text{Cu}(\text{Dipp}_2\text{Im})\text{F}]$ with *p*-tolylBpin in toluene- d_8 .

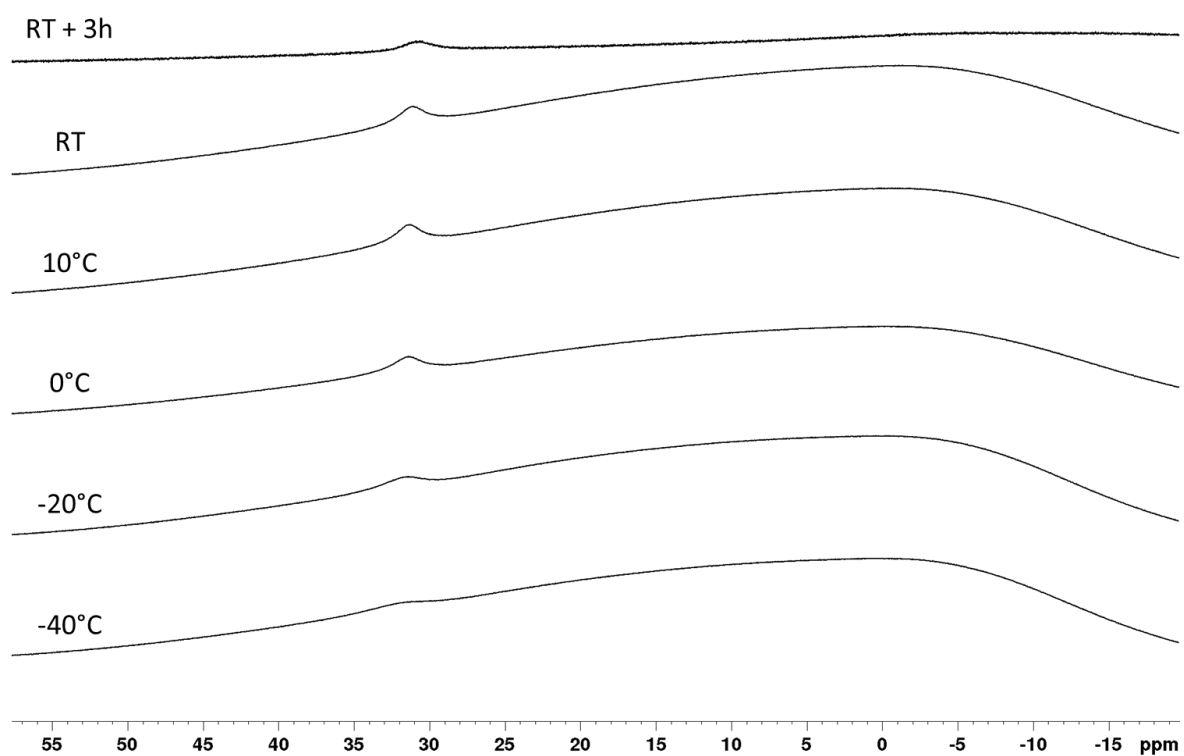


Figure 61: ^{11}B VT-NMR spectra of the reaction of $[\text{Cu}(\text{Dipp}_2\text{Im})\text{F}]$ with *p*-tolylBpin in toluene-d_8 .

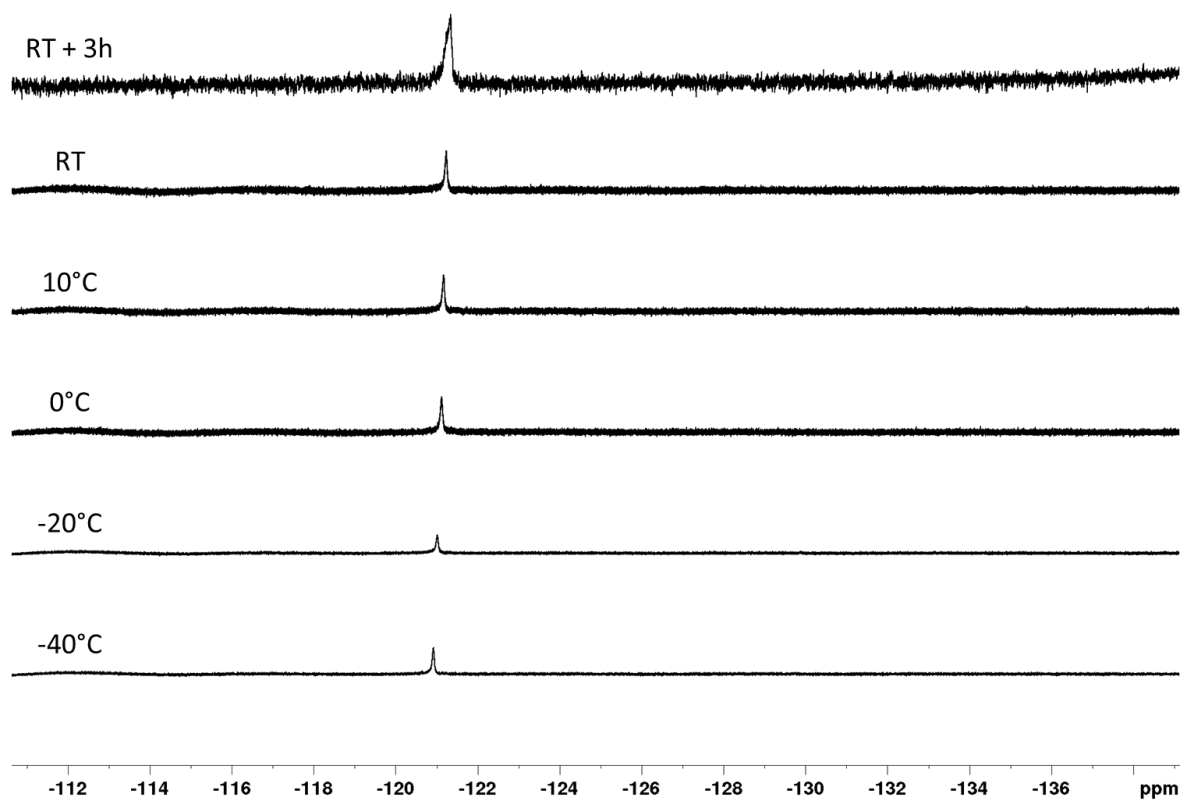
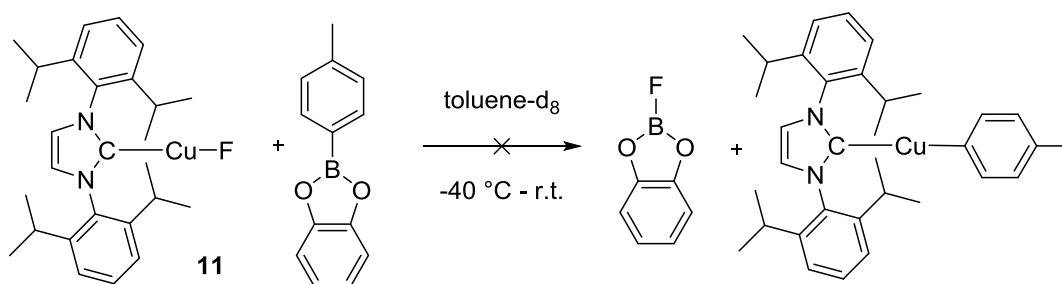


Figure 62: ^{19}F VT-NMR spectra of the reaction of $[\text{Cu}(\text{Dipp}_2\text{Im})\text{F}]$ with *p*-tolylBpin in toluene-d_8 .

Reaction of [Cu(Dipp₂Im)(F)] with *p*-tolylBcat in toluene-d₈:



The ¹H NMR spectra (Figure 63) showed broad signals at low temperature. Upon heating a temperature dependent shift and sharpening was observed for most of the signals. For the Dipp₂Im ligand, a set of signals with appropriate integral ratios, coupling patterns and resonance frequencies was detected.

In the ¹¹B NMR spectra (Figure 64) no signal was detected until the sample was kept at room temperature for 3 h, when signals with low intensities were detected at 14.6, 6.4 and -0.2 ppm.

The ¹⁹F NMR spectra (Figure 65) at -50 °C showed two signals at -122.5 and -130.8 ppm and a signal with low intensity at -129.8 ppm. Upon heating the sample, the signal at -122.5 ppm decreases and the two signals at -129.8 and 130.8 ppm appeared as septets. The coupling constants are 6.1 and 6.2 Hz, respectively. ¹⁹F{¹H} NMR spectra showed that the pattern was due to proton coupling (Figure 66). A coupling constant of 6 Hz could either be the result ³J_{HF} or a ⁴J_{HF} coupling.^[341] Two satellites around each signal were detected with a coupling of 171 Hz and 148 Hz, respectively, which could indicate ¹³C-satellites.^[341] The ¹H{¹⁹F} NMR showed two singlets for the doublet and the triplet detected at 0.05 and -0.10 ppm. The integral ratios of the two signals is 2:3.

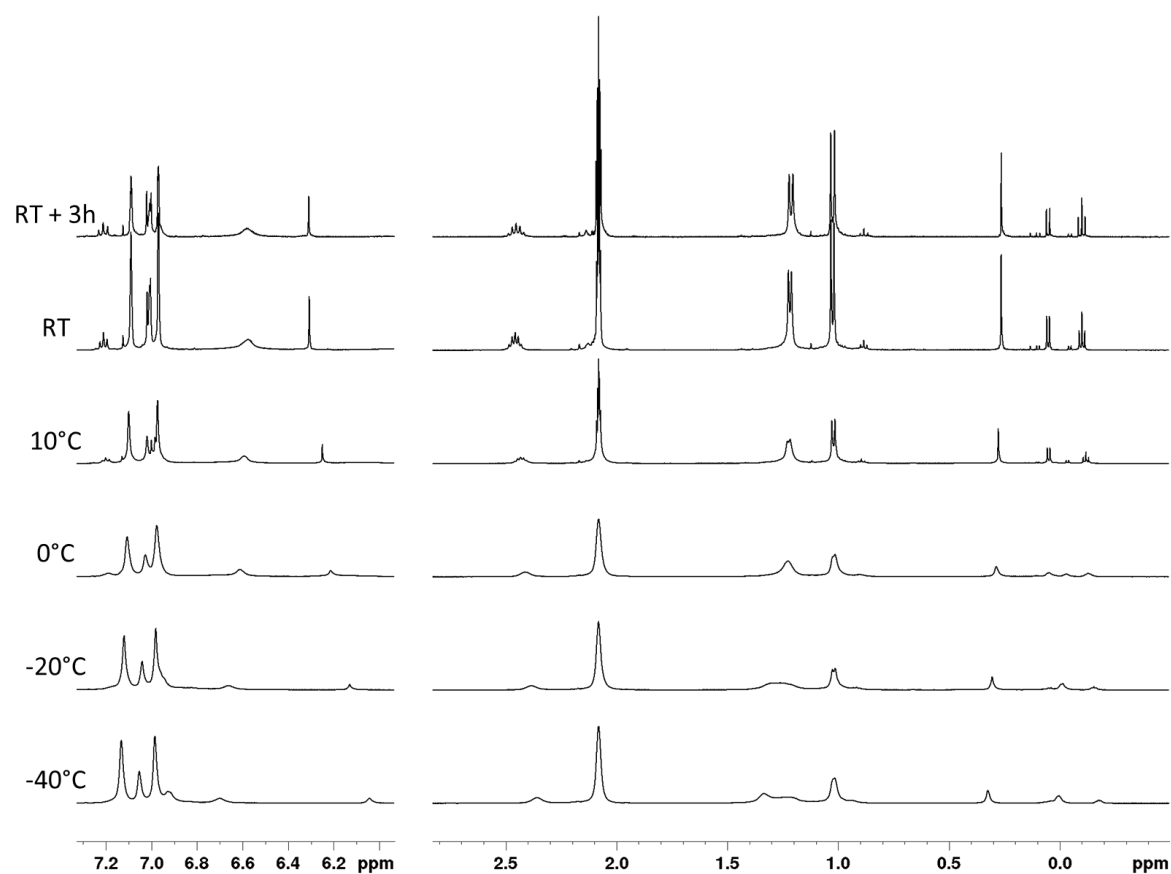


Figure 63: ^1H VT-NMR spectra of the reaction of $[\text{Cu}(\text{Dipp}_2\text{Im})\text{F}]$ with p -tolylBcat in toluene-d_8 .

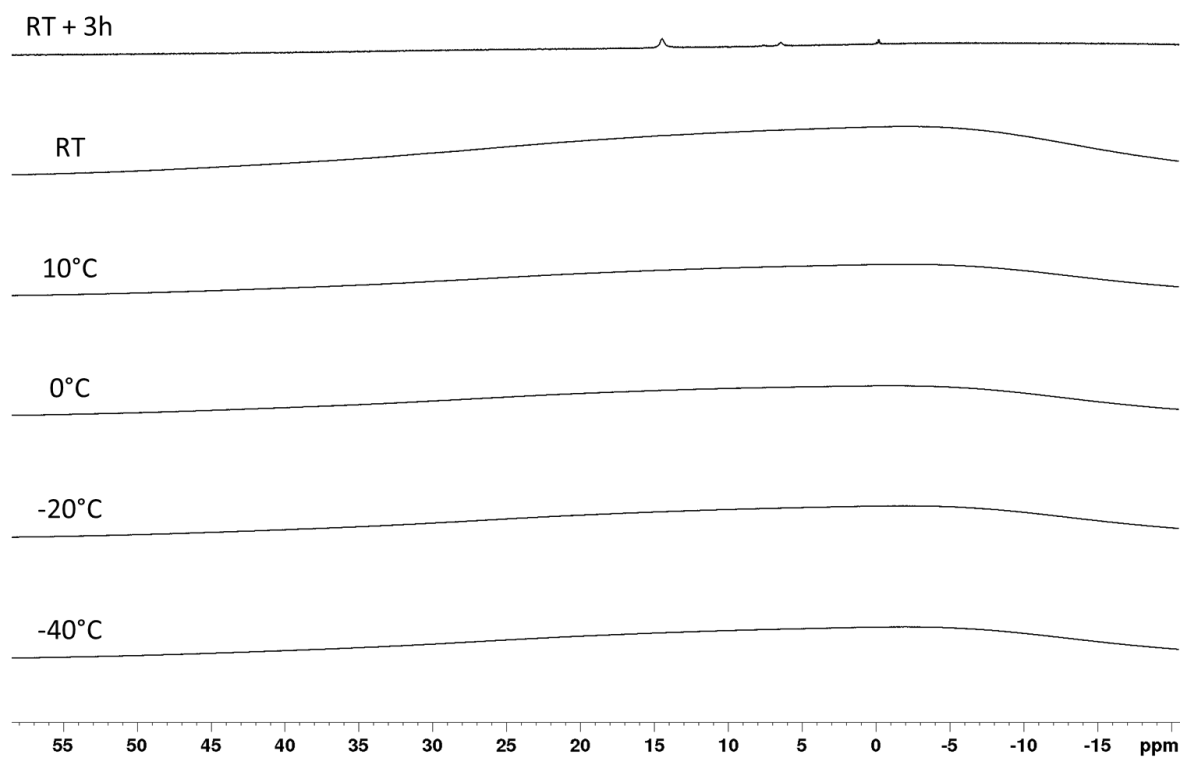


Figure 64: ^{11}B VT-NMR spectra of the reaction of $[\text{Cu}(\text{Dipp}_2\text{Im})\text{F}]$ with p -tolylBcat in toluene-d_8 .

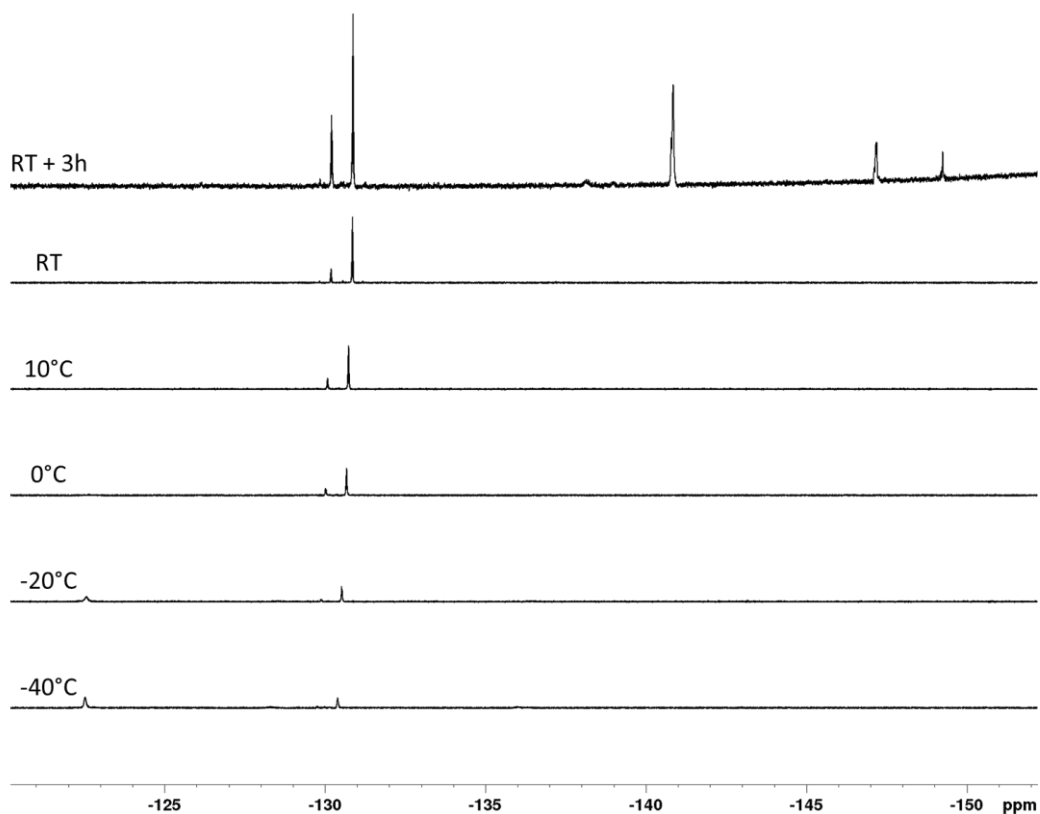


Figure 65: ^{19}F VT-NMR spectra of the reaction of $[\text{Cu}(\text{Dipp}_2\text{Im})\text{F}]$ with *p*-tolylBcat in toluene- d_8 .

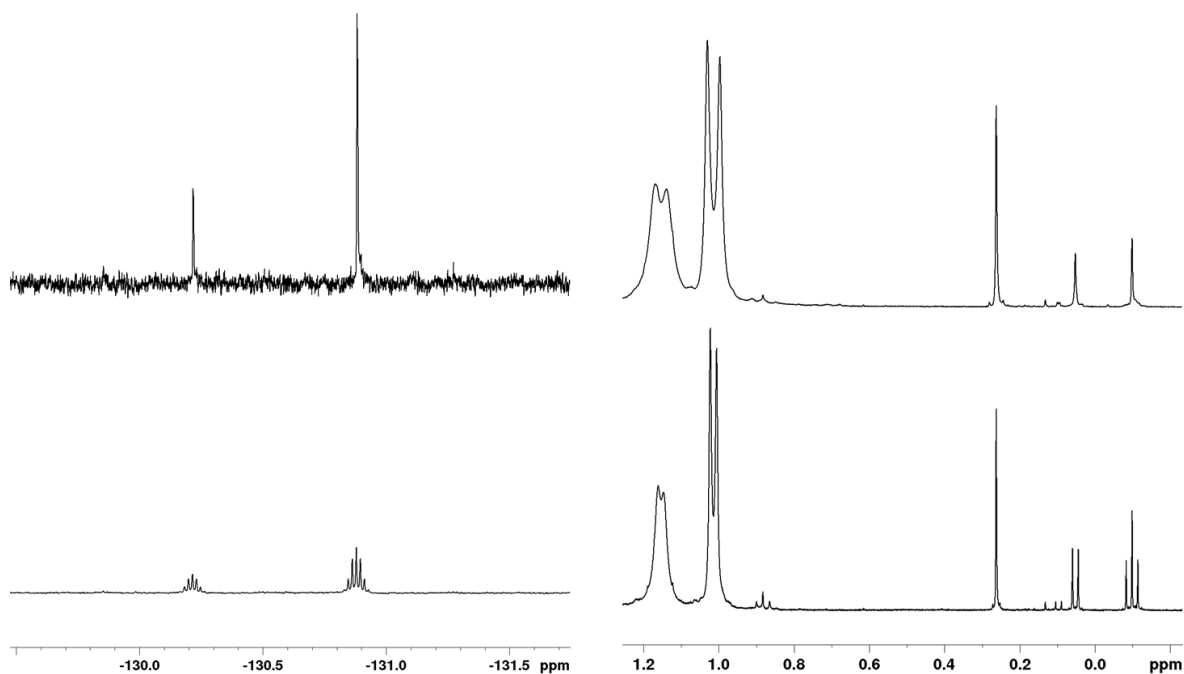
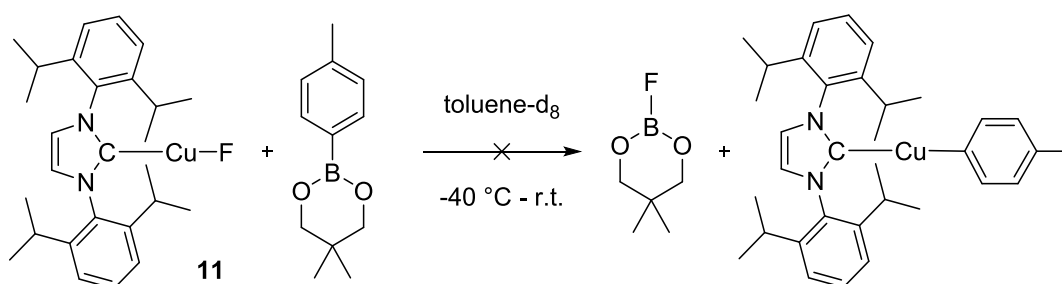


Figure 66: Left top: $^{19}\text{F}\{^1\text{H}\}$ NMR spectrum from -129.5 ppm to -131.75 ppm of the reaction of $[\text{Cu}(\text{Dipp}_2\text{Im})(\text{F})]$ with *p*-tolylBcat at room temperature. Left bottom: ^{19}F NMR spectrum from -129.5 ppm to -131.75 ppm of the reaction of $[\text{Cu}(\text{Dipp}_2\text{Im})(\text{F})]$ with *p*-tolylBcat at room temperature. Right top: $^1\text{H}\{^{19}\text{F}\}$ NMR spectrum from -0.4 ppm to 1.26 ppm of the reaction of $[\text{Cu}(\text{Dipp}_2\text{Im})(\text{F})]$ with *p*-tolylBcat at room temperature. Right bottom: ^1H NMR spectrum from -0.4 ppm to 1.26 ppm of the reaction of $[\text{Cu}(\text{Dipp}_2\text{Im})(\text{F})]$ with *p*-tolylBcat at room temperature.

Reaction of [Cu(Dipp₂Im)(F)] with *p*-tolylBneop in toluene-d₈:



The ¹H NMR spectra (Figure 67) at low temperature show broad signals which might arise from one compound. From room temperature on another set of signals grows with the same integral ratios and coupling patterns as the one observed before.

One peak at 27.1 ppm was detected in the ¹¹B NMR spectra (Figure 68) until at 10 °C another peak at 0 ppm was observed.

A resonance at -120.9 ppm was detected in the ¹⁹F NMR spectra (Figure 69) with another signal at -151.7 ppm growing in intensity from 10 °C on. After the sample was kept at room temperature for 6 h new peaks were observed between -120.9 and -151.7 ppm. A ¹⁹F{¹¹B} NMR spectrum (Figure 70) showed boron coupling for the peak at -151.7 ppm, which might indicate the formation of a FBneop species. In DMF the compound FBneop is supposed to show resonance at -150.6 ppm in the ¹⁹F NMR and at 19.1 ppm in the ¹¹B NMR spectrum.^[169] After 24 h at room temperature a broad peak was observed at 17.9 ppm in the ¹¹B NMR spectrum, which might arise from a formed FBneop species.

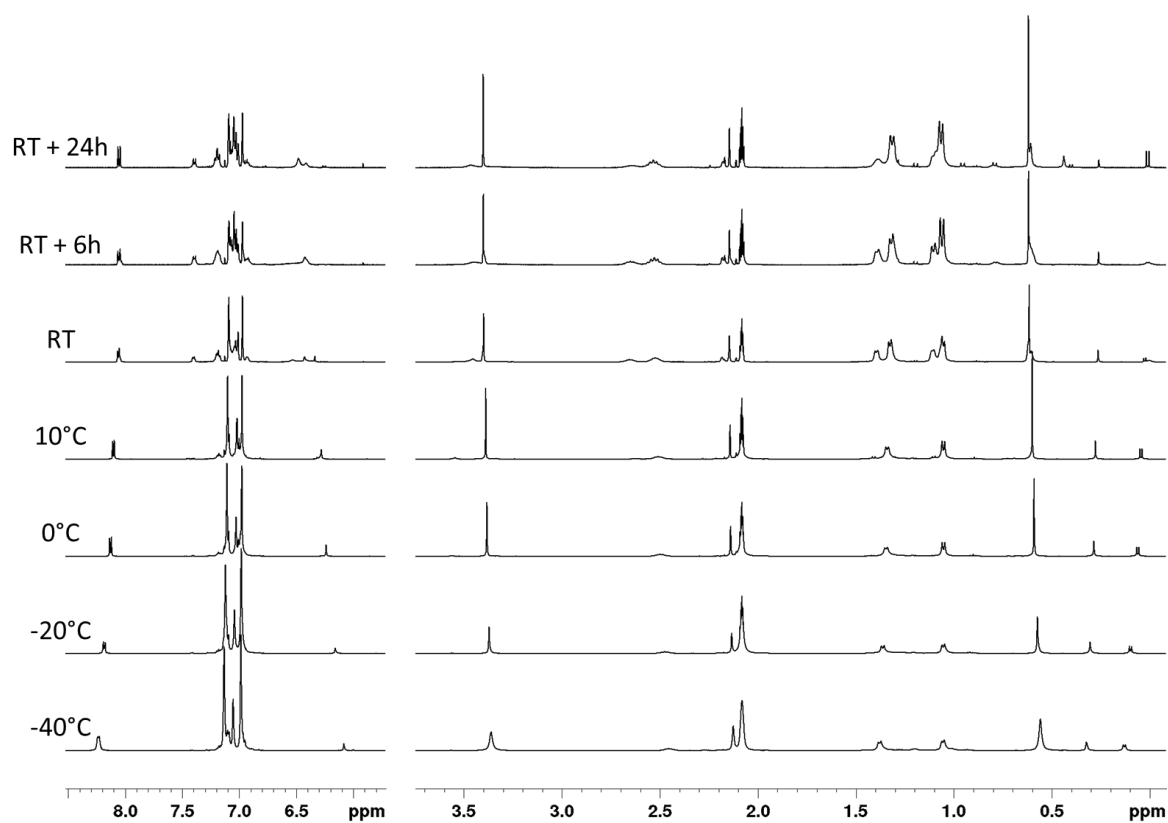


Figure 67: ^1H VT-NMR spectra of the reaction of $[\text{Cu}(\text{Dipp}_2\text{Im})\text{F}]$ with *p*-tolylBneop in toluene- d_8 .

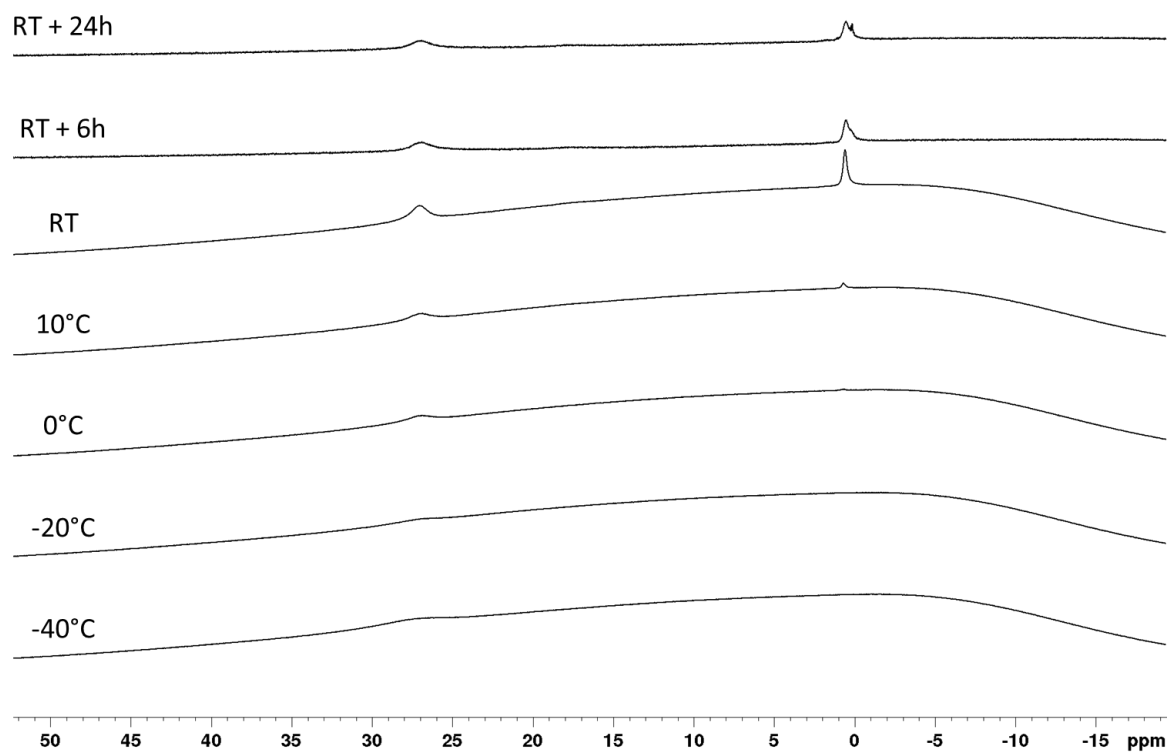


Figure 68: ^{11}B VT-NMR spectra of the reaction of $[\text{Cu}(\text{Dipp}_2\text{Im})\text{F}]$ with *p*-tolylBneop in toluene- d_8 .

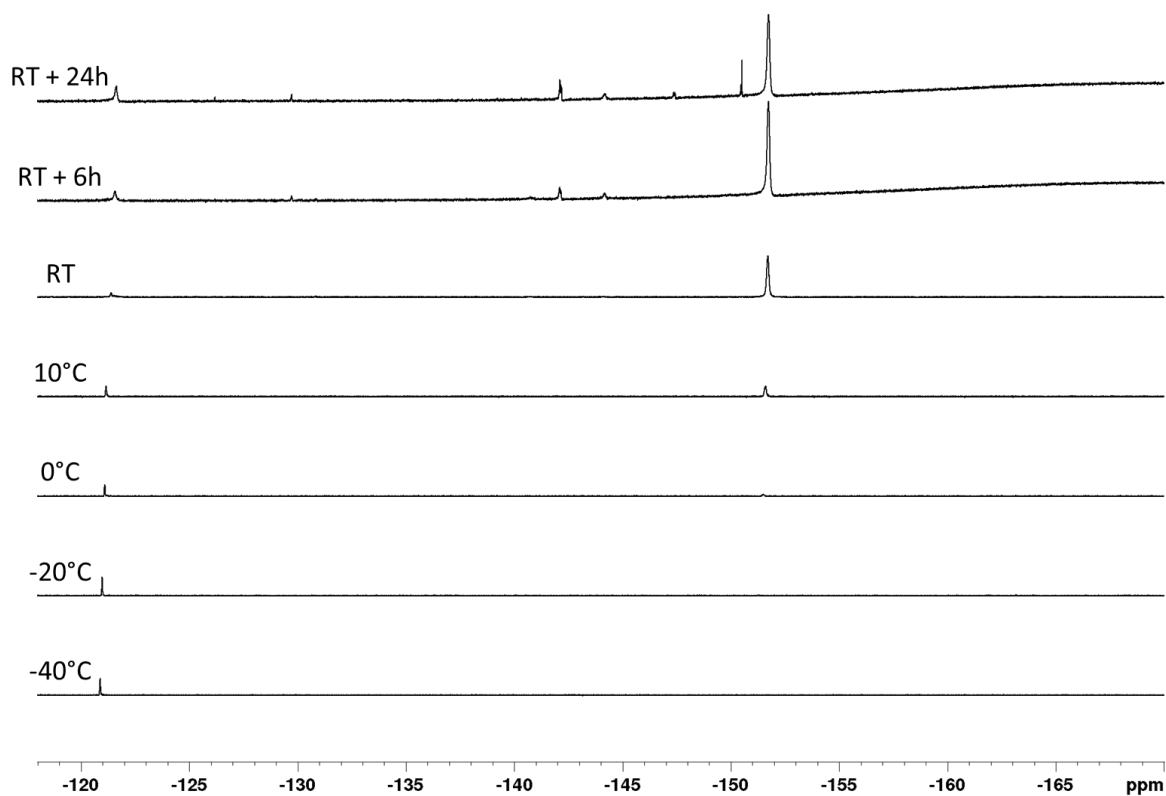


Figure 69: ^{19}F VT-NMR spectra of the reaction of $[\text{Cu}(\text{Dipp}_2\text{Im})\text{F}]$ with *p*-tolylBneop in toluene- d_8 .

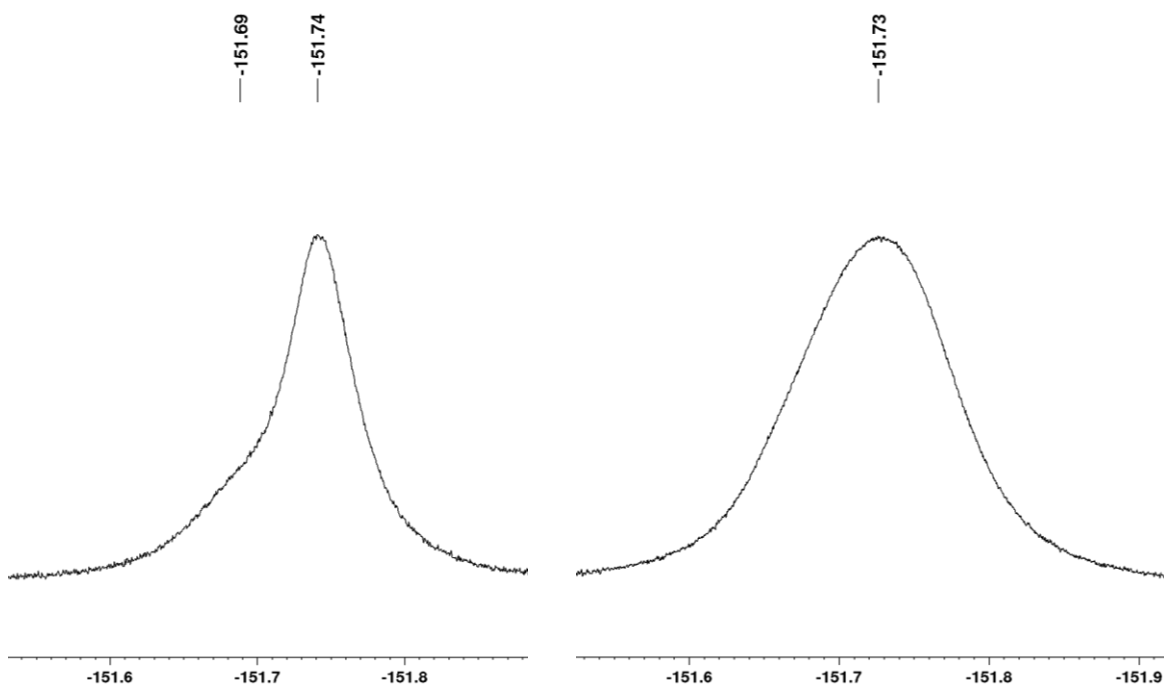
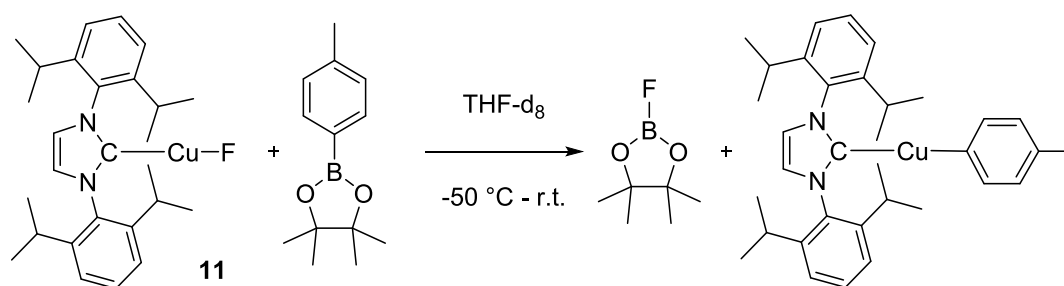


Figure 70: *In situ* Fluorine NMR spectra of the reaction of 10 with *p*-tolylBneop. Left: $^{19}\text{F}\{^{11}\text{B}\}$ NMR spectrum. Right: ^{19}F NMR spectrum.

Reaction of [Cu(Dipp₂Im)(F)] with *p*-tolylBpin in THF-d₈:



The ¹H NMR spectra (Figure 71) at low temperature showed broad signals in relatively low intensities, which could not be assigned to a specific compound. From room temperature on the intensity of the signals increased and sharper signals were detected. After 24 h at room temperature another set of signals started to appear. The coupling pattern, integral ratios as well as the chemical shifts fit those observed for the desired [Cu(Dipp₂Im)(*p*-tolyl)] complex (Figures 72 and 73).

One broad signal at 30 ppm was detected in the ¹¹B NMR spectra (Figure 74) at -50 °C. At -30 °C an additional broad signal was detected at around 7 ppm with low intensity. At room temperature a relatively sharp signal at 5 ppm and a broad signal at 20 ppm were observed. After 6 h at room temperature a broad peak at about 25 ppm and a growing signal at 5 ppm was detected, while after 24 h a peak at 31, 23 and 5 ppm was detected.

The ¹⁹F NMR spectra (Figure 75) showed three signals at -124, -133 and -140 ppm. With rising temperature the signal at -133 ppm became broader. From room temperature on the signal at -133 ppm was gone and a new peak was growing at -145 ppm.

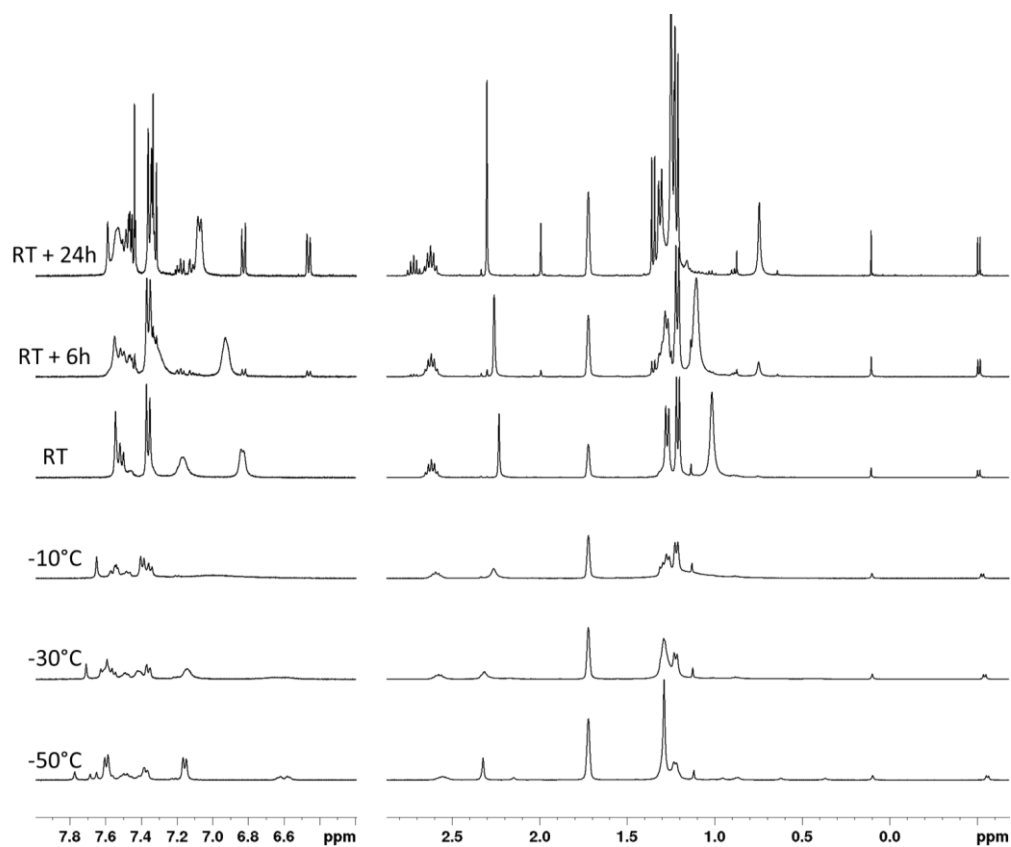


Figure 71: ^1H VT-NMR spectra of the reaction of $[\text{Cu}(\text{Dipp}_2\text{Im})\text{F}]$ with p -tolylBpin in THF-d_8 .

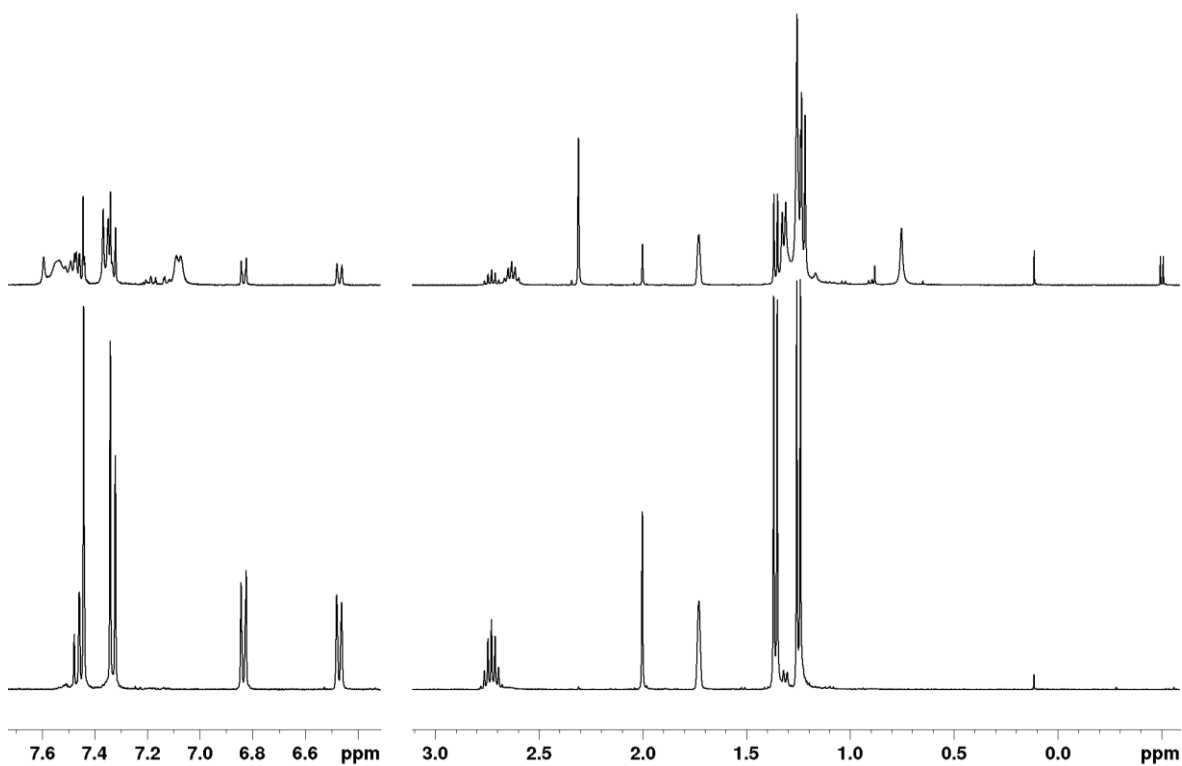


Figure 72: Comparison of the ^1H NMR spectrum of complex $[\text{Cu}(\text{Dipp}_2\text{Im})(p\text{-tolyl})]$ 27 (bottom) with *in situ* ^1H VT-NMR spectrum of the reaction of $[\text{Cu}(\text{Dipp}_2\text{Im})\text{F}]$ with p -tolylBpin in THF-d_8 at room temperature after 24 h (top).

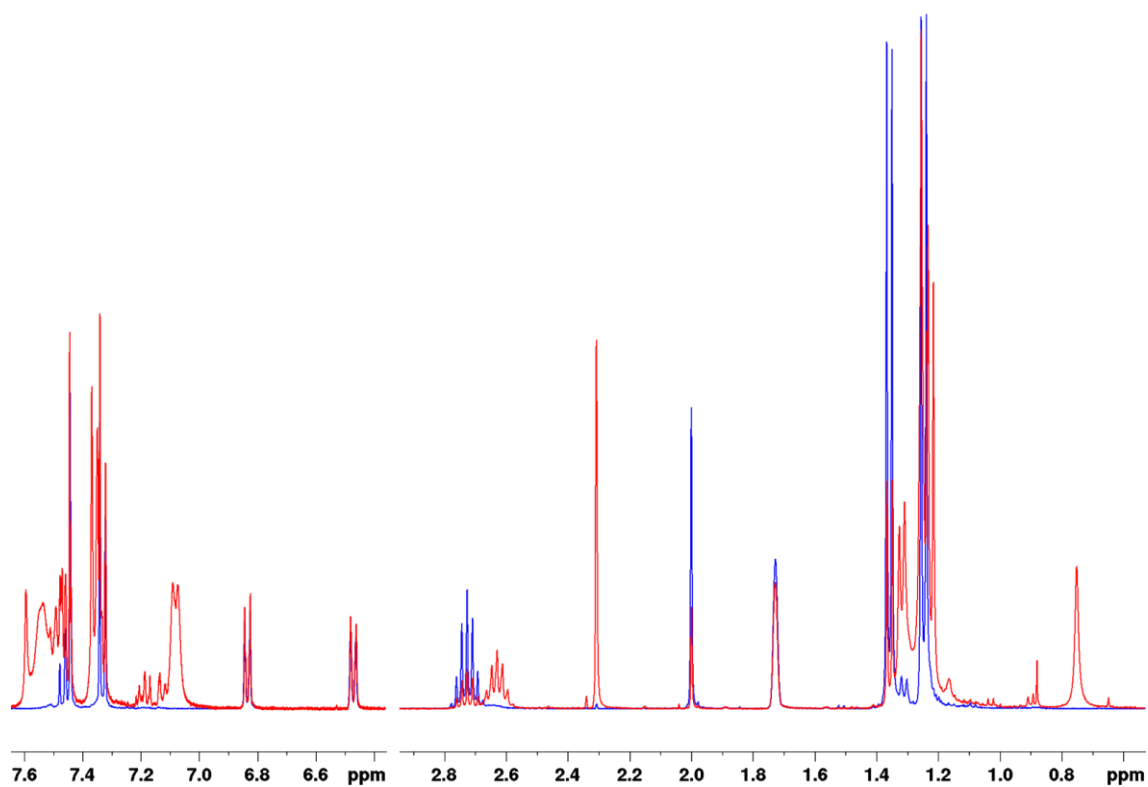


Figure 73: Overlay of the ^1H NMR spectrum of $[\text{Cu}(\text{Dipp}_2\text{Im})(p\text{-tolyl})]$ 27 (blue) and the *in situ* ^1H VT-NMR spectrum of the reaction of $[\text{Cu}(\text{Dipp}_2\text{Im})\text{F}]$ with *p*-tolylBneop in THF-d_8 at room temperature after 24 h (red).

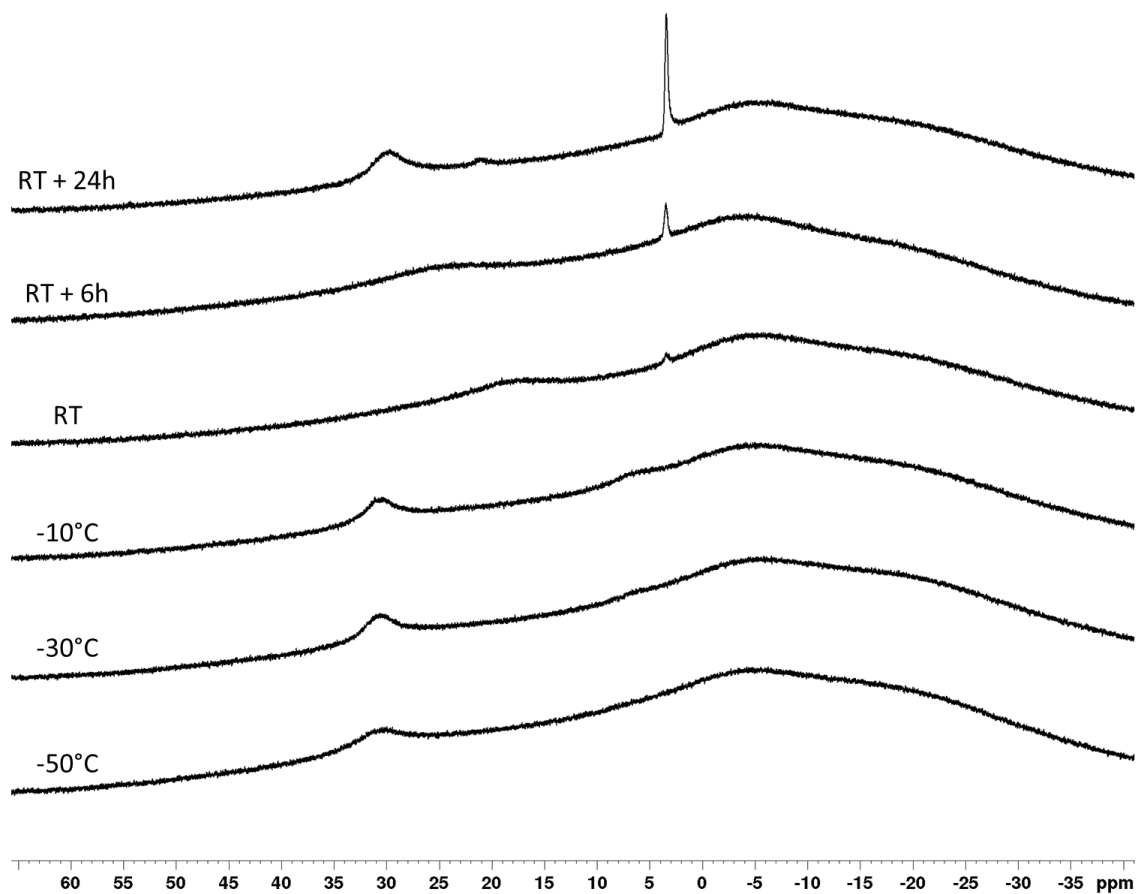


Figure 74: ^{11}B VT-NMR spectra of the reaction of $[\text{Cu}(\text{Dipp}_2\text{Im})\text{F}]$ with *p*-tolylBpin in THF-d_8 .

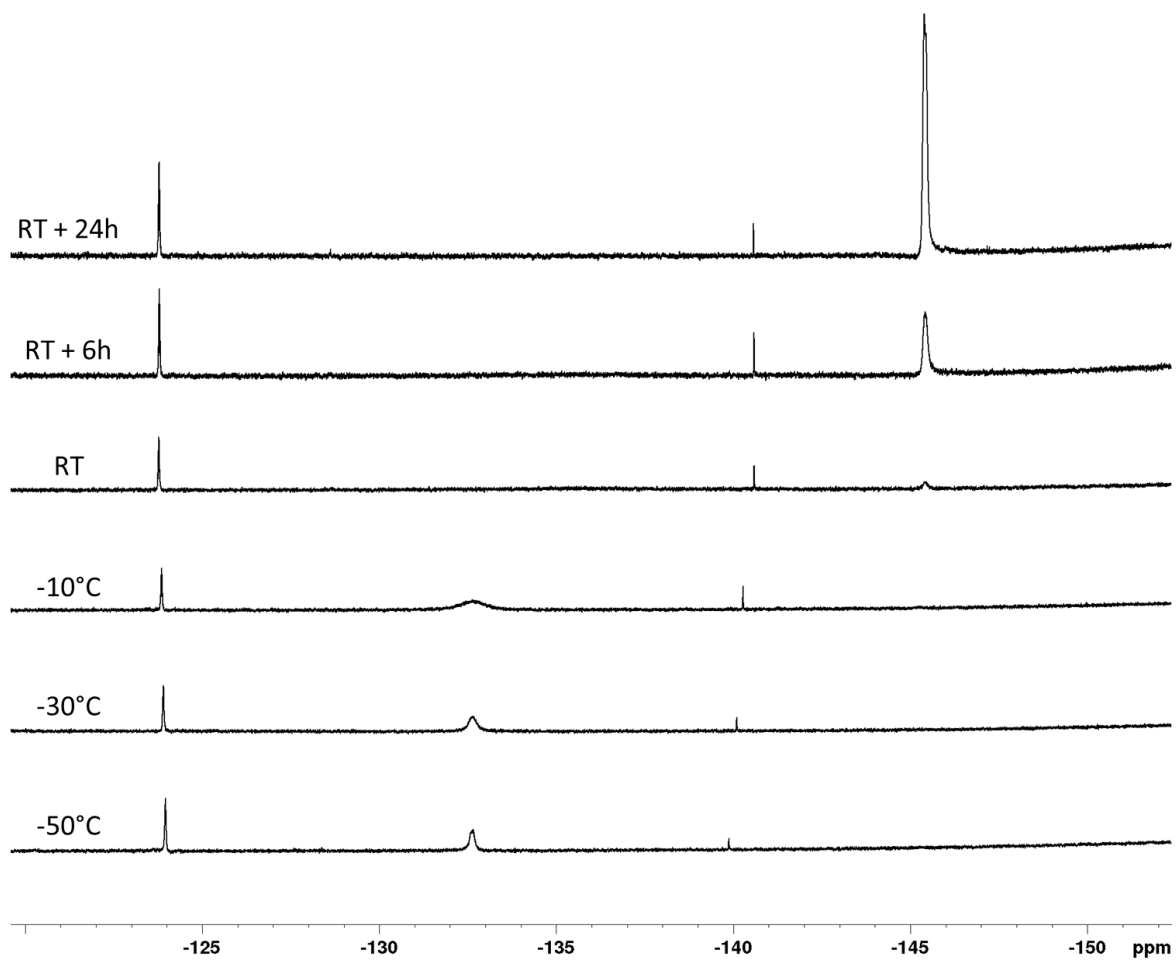
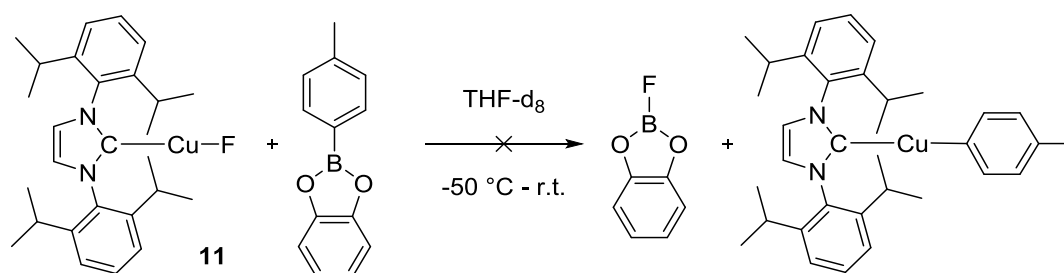


Figure 75: ^{19}F VT-NMR spectra of the reaction of $[\text{Cu}(\text{Dipp}_2\text{Im})\text{F}]$ with *p*-tolylBpin in THF-d_8 .

Reaction of [Cu(Dipp₂Im)(F)] with *p*-tolylBcat in THF-d₈:



In the ¹H NMR spectra (Figure 76) sharp signals (from -50 °C to -10 °C) for one Dipp₂Im moiety, two catecholate moieties and two *p*-tolyl moieties were detected in a 1.6:1.5:1.2:1.5:1 ratio (Figure 15). Three more signals in the aromatic region were detected which could not be assigned to specific moieties. Upon heating from -50 °C to -10 °C besides a temperature dependent shift no changes were observed. From room temperature on all signals except those found for the Dipp₂Im ligand were broadened. Within the next 24 h a shift of the aromatic protons of the Dipp₂Im ligand was observed. New sharp signals with coupling patterns typical for catecholate protons and a new singlet in the region of a *p*-methyl group were detected as well.

In the ¹¹B NMR spectra (Figure 77) two peaks with a chemical shift of 32 and 9.8 ppm were detected. When the sample was kept at room temperature multiple other peaks at 15.0, 7.0 and 0 ppm were detected over time.

One peak at -138.3 ppm was observed in the ¹⁹F NMR spectra (Figure 78), which showed a shoulder around 7 ppm downfield shifted. This shoulder might arise from a ¹⁰B-¹⁹F coupling. After 3 h at room temperature new peaks were detected at -132, -143, -150, -154 and -157 ppm. In the following 21 h the new signals were growing, especially the signal at -143 ppm.

The signal at -138.7 ppm in the ¹⁹F NMR spectrum and the singlet in the ¹¹B NMR spectrum at 9.8 ppm might arise from a fluorine adduct of *p*-tolylBcat, since Cs[(*p*-tolylBpin)(F)] was observed at -133.0 and 7.0 ppm, respectively (in DMSO).^[264] Albeit these compounds show interesting reactivity the observed signals in the ¹H NMR spectra at room temperature do not fit those of the desired complex [Cu(Dipp₂Im)(*p*-tolyl)].

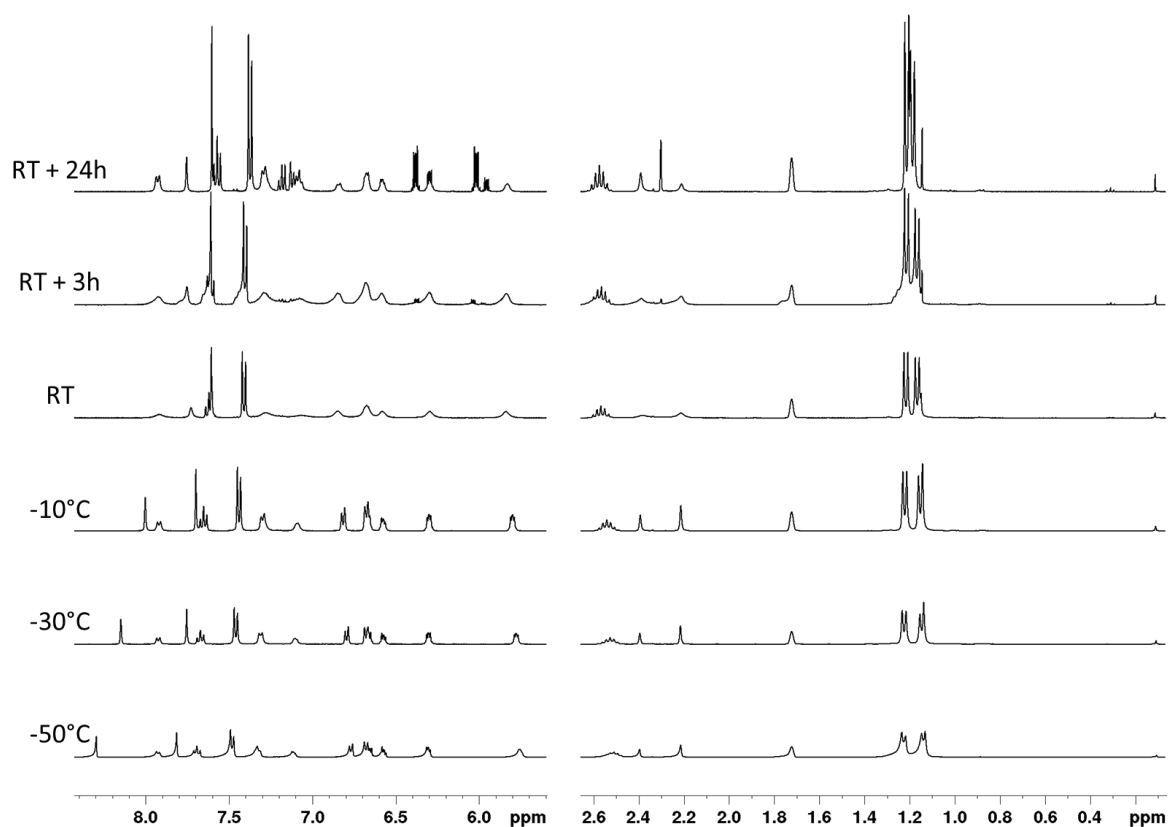


Figure 76: ^1H VT-NMR spectra of the reaction of $[\text{Cu}(\text{Dipp}_2\text{Im})\text{F}]$ with *p*-tolylBcat in THF-d_8 .

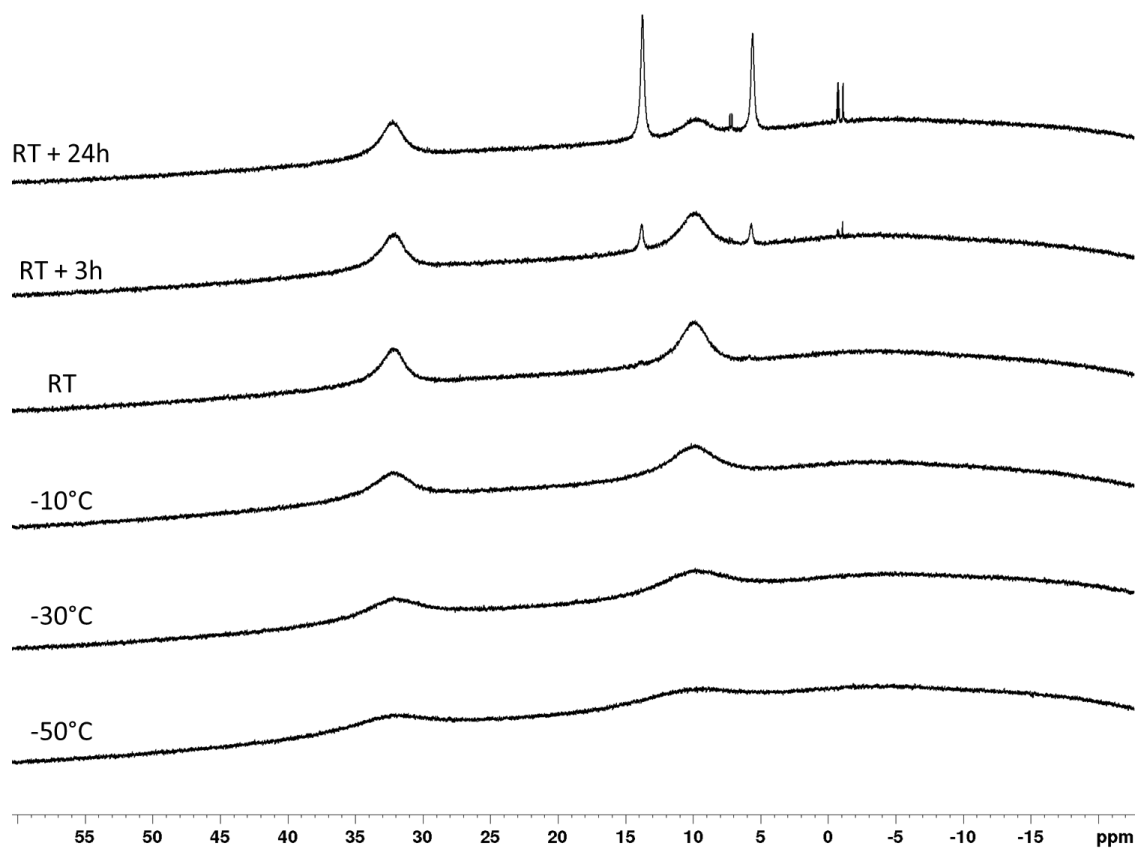


Figure 77: ^{11}B VT-NMR spectra of the reaction of $[\text{Cu}(\text{Dipp}_2\text{Im})\text{F}]$ with *p*-tolylBcat in THF-d_8 .

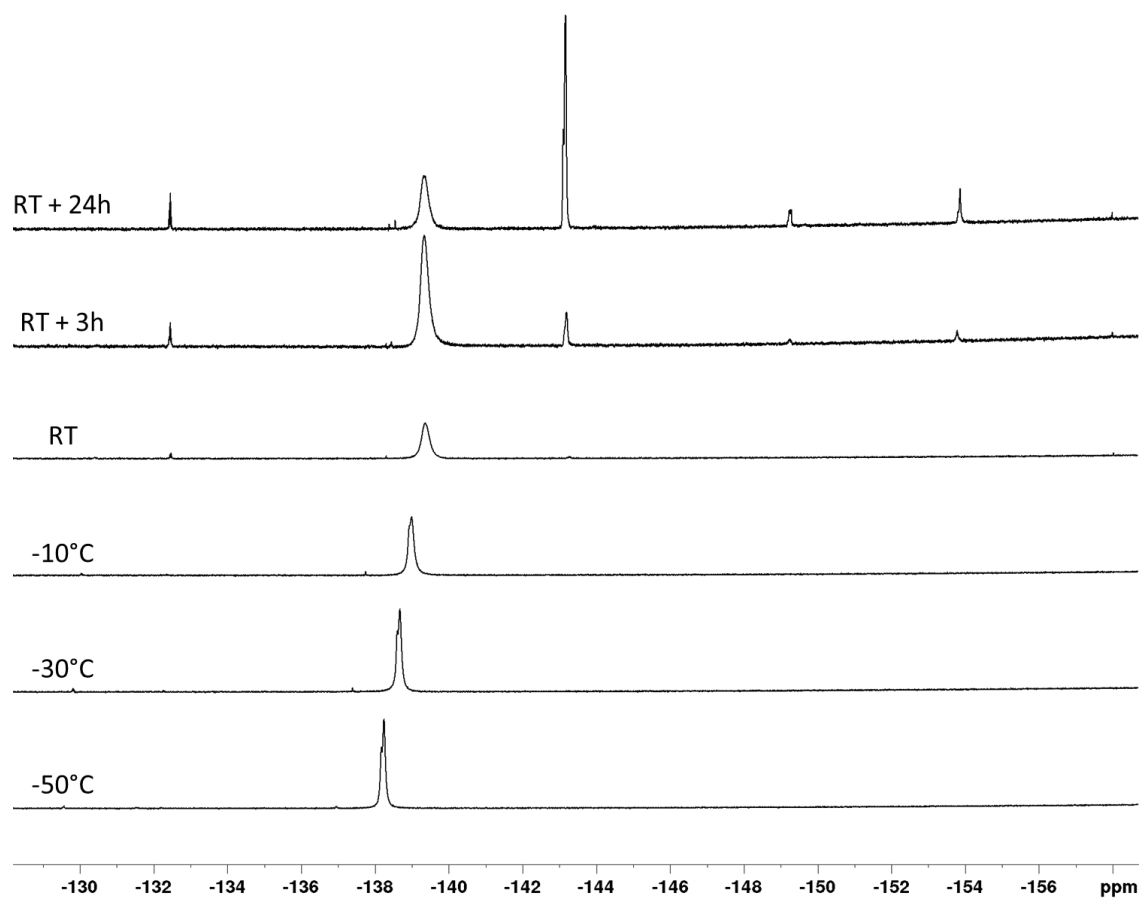
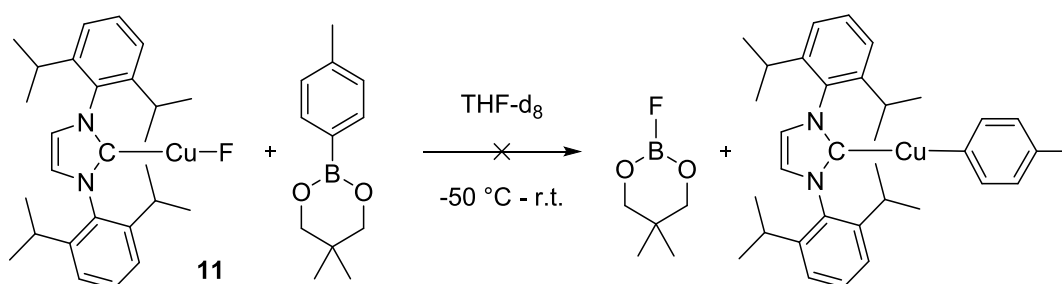


Figure 78: ^{19}F VT-NMR spectra of the reaction of $[\text{Cu}(\text{Dipp}_2\text{Im})\text{F}]$ with *p*-tolylBcat in THF-d_8 .

Reaction of [Cu(Dipp₂Im)(F)] with *p*-tolylBneop in THF-d₈:



The ¹H NMR spectra at -50 °C showed relatively sharp signals for the Dipp₂Im ligand and the methyl group of the *p*-tolyl moiety, while the signals for the neopentyl glycolate moiety and the aromatic signals of the *p*-tolyl moiety were broadened (Figure 79). At -50 °C the ratio of the Dipp₂Im moiety and the aryl boronic ester is 1:1.7, while at -30 °C a ratio of 1:2.6 was found. Heating to -10 °C showed a ratio of 1:3.3 with broad signals for the Dipp₂Im moiety and sharp signal for the aryl boronic ester. Compared with the integrals of the residual solvent peak the Dipp₂Im moiety decreases (possible precipitation?) while heating from -50 °C to -10 °C. From room temperature on signals for the desired complex [Cu(Dipp₂Im)(*p*-tolyl)] **27** were detected (Figure 80). Two set of signals of neopentyl glycolate protons were detected at 0.49 and 3.13 ppm as well as 0.98 and 3.72 ppm. In addition to that a second set of signals for the Dipp₂Im and the aryl moiety was observed (Figures 81 and 82). The ratio of the complex [Cu(Dipp₂Im)(*p*-tolyl)] **27**, the neopentyl glycolate protons at 0.49 and 0.98 ppm, respectively, and the second set of signals is 1:1.1:1.6:1.25. Three hours after the sample was heated to room temperature the ratio was 1:1.2:1.5:1.65 and did not change further within the next 24 hours.

The ¹¹B NMR spectra at -50 °C showed a broad signal between 20 and 25 ppm (Figure 83). Heating to -30 °C and -10 °C showed an additional peak with a chemical shift of -0.2 ppm. From room temperature on new peaks at 26.6 and 16.6 ppm were observed as well as the growth of the peak at -0.2 ppm. At -0.8 ppm a quartet with a coupling constant of 8.9 Hz and low intensity was observed. In ¹¹B{¹H} NMR experiments this signal did not change its coupling pattern, substantiating a B-F coupling.

Next to a broad peak at -162.9 ppm in the ¹⁹F NMR spectra three more peaks at -124.0, -139.9 and 15.2 ppm were detected (Figure 84). Significant changes in the spectra with new peaks at -144.0 (¹¹B-F boron coupled quartet J = 8.9 Hz + ¹⁰B-F signal), -147.0 and 158.0 ppm were observed, when the sample was kept at room temperature for 3 h.

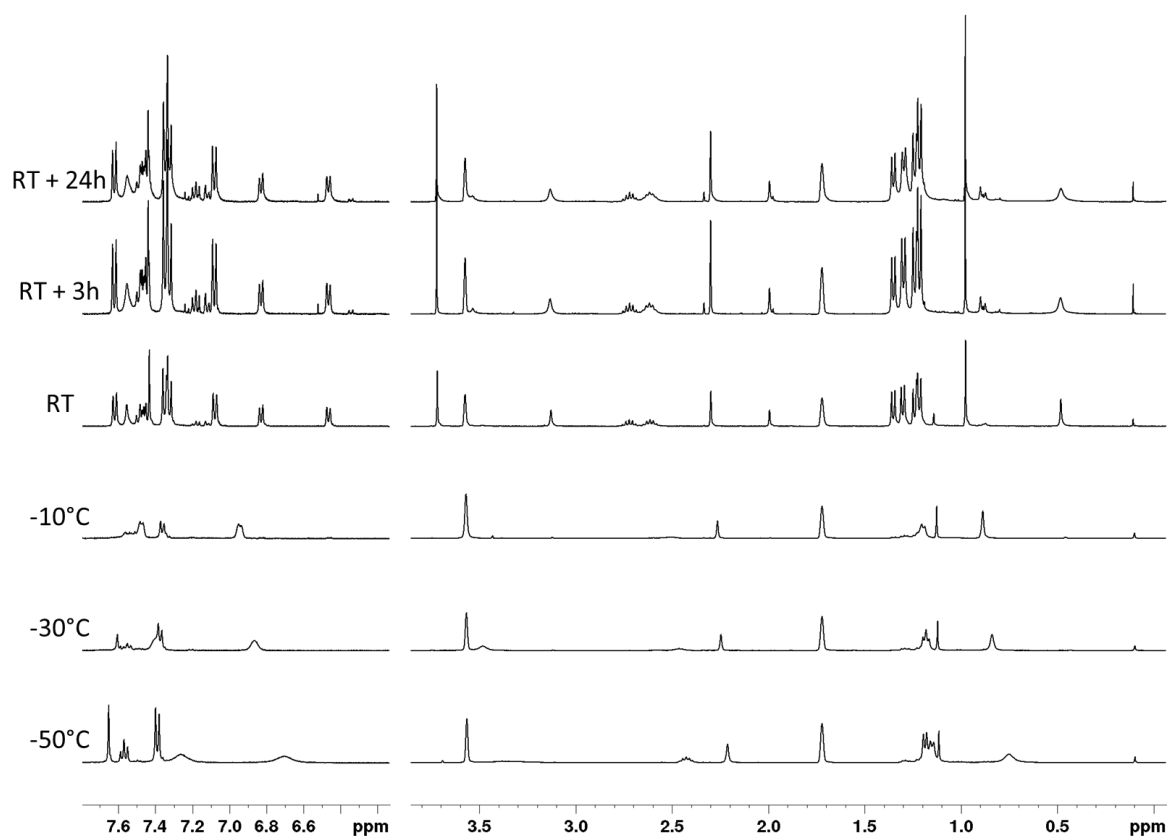


Figure 79: ^1H VT-NMR spectra of the reaction of $[\text{Cu}(\text{Dipp}_2\text{Im})\text{F}]$ with p -tolylBneop in THF-d_8 .

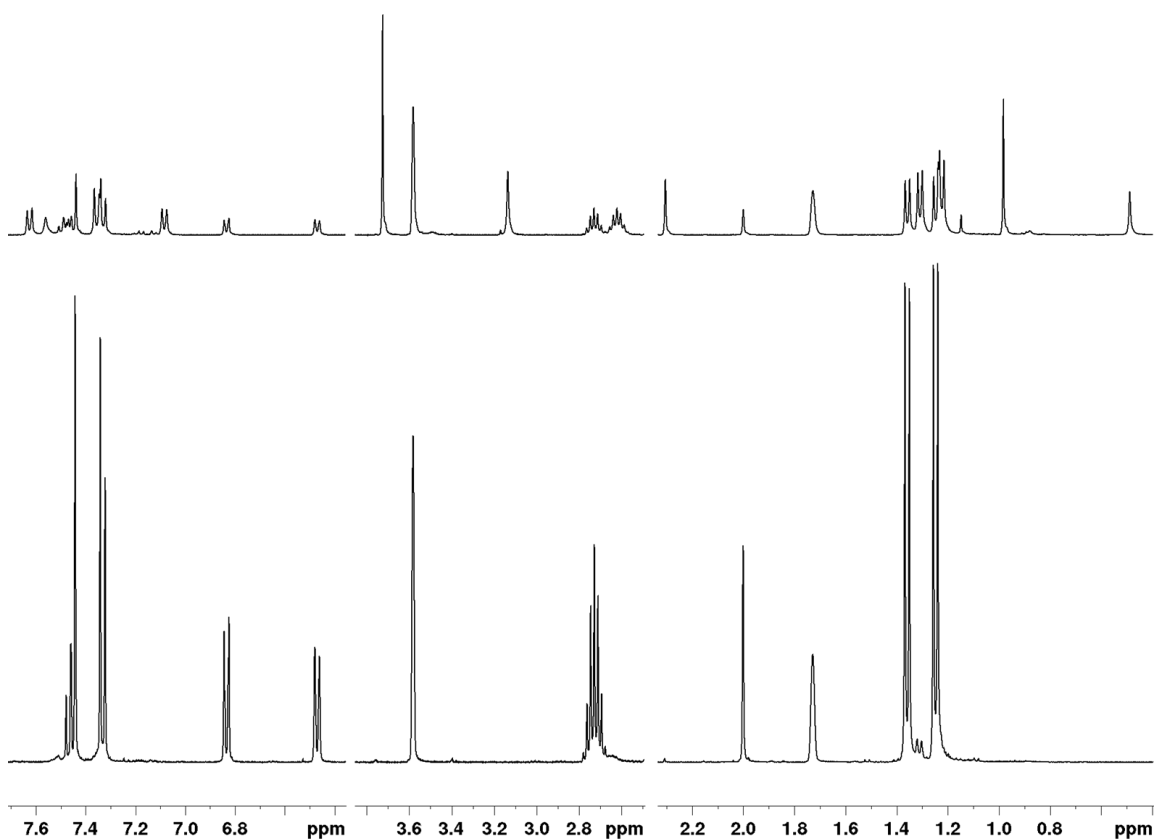
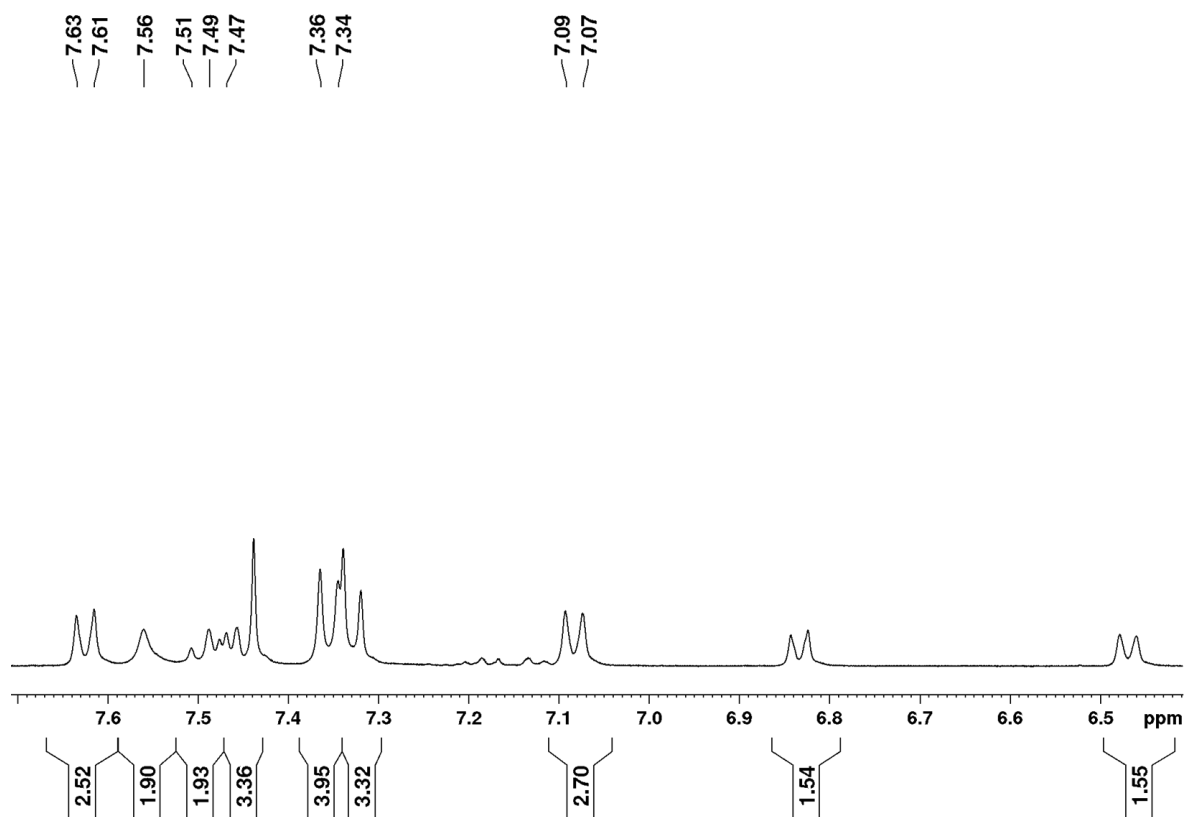
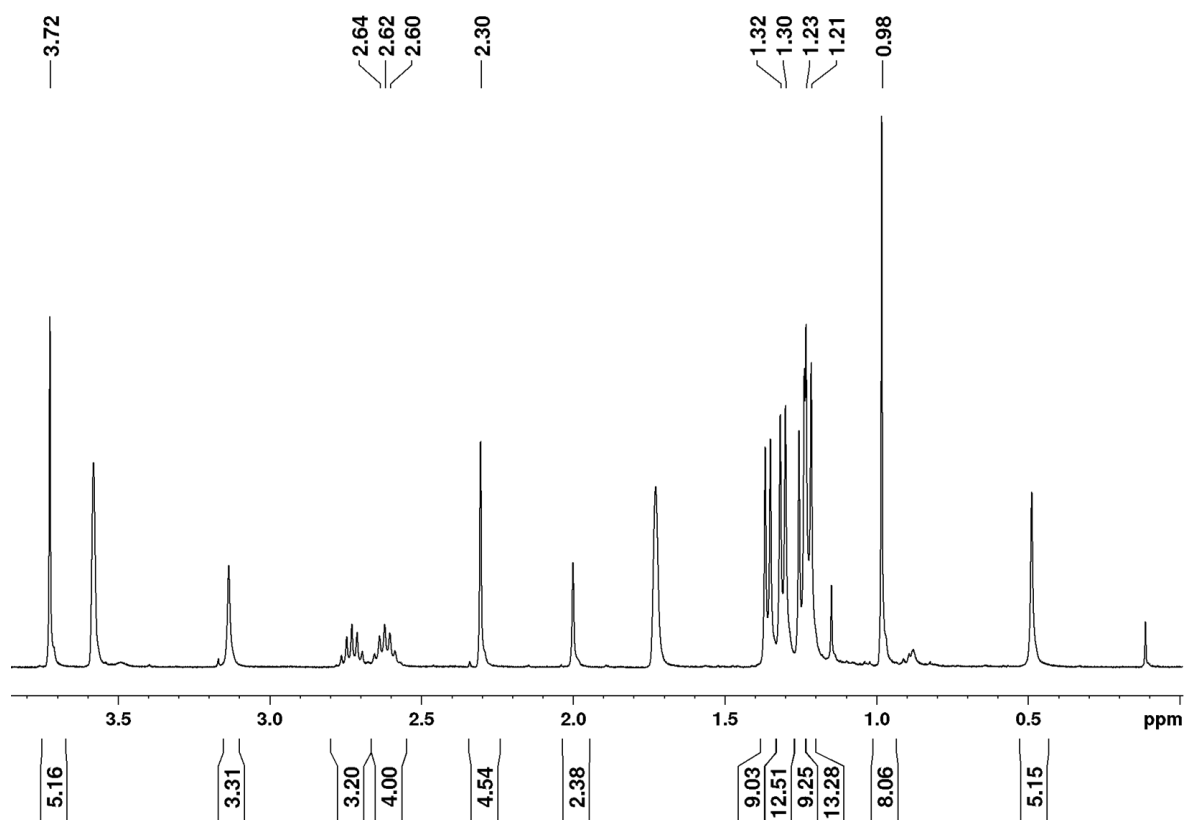


Figure 80: Comparison of the ^1H NMR spectrum of complex $[\text{Cu}(\text{Dipp}_2\text{Im})(p\text{-tolyl})]$ 27 (bottom) with *in situ* ^1H VT-NMR spectrum of the reaction of $[\text{Cu}(\text{Dipp}_2\text{Im})\text{F}]$ with p -tolylBneop in THF-d_8 at room temperature (top).



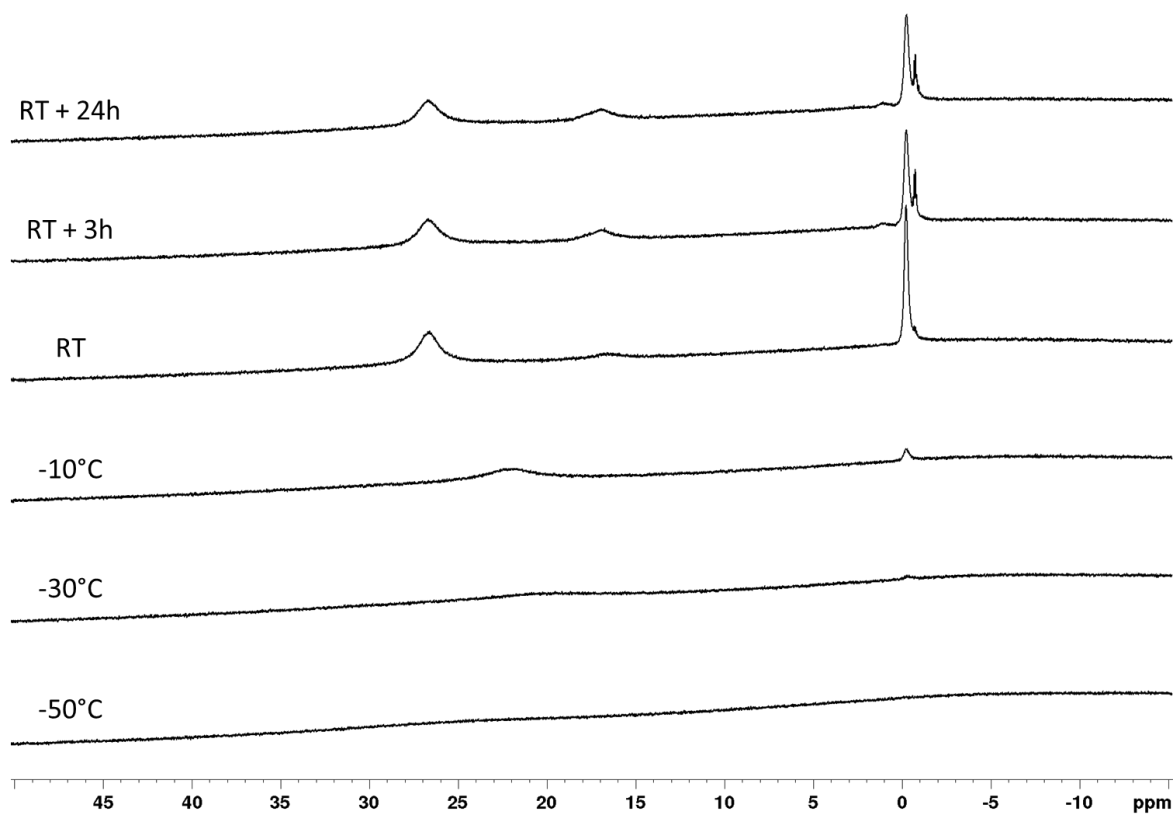


Figure 83: ^{11}B VT-NMR spectra of the reaction of $[\text{Cu}(\text{Dipp}_2\text{Im})\text{F}]$ with *p*-tolylBneop in THF-d_8 .

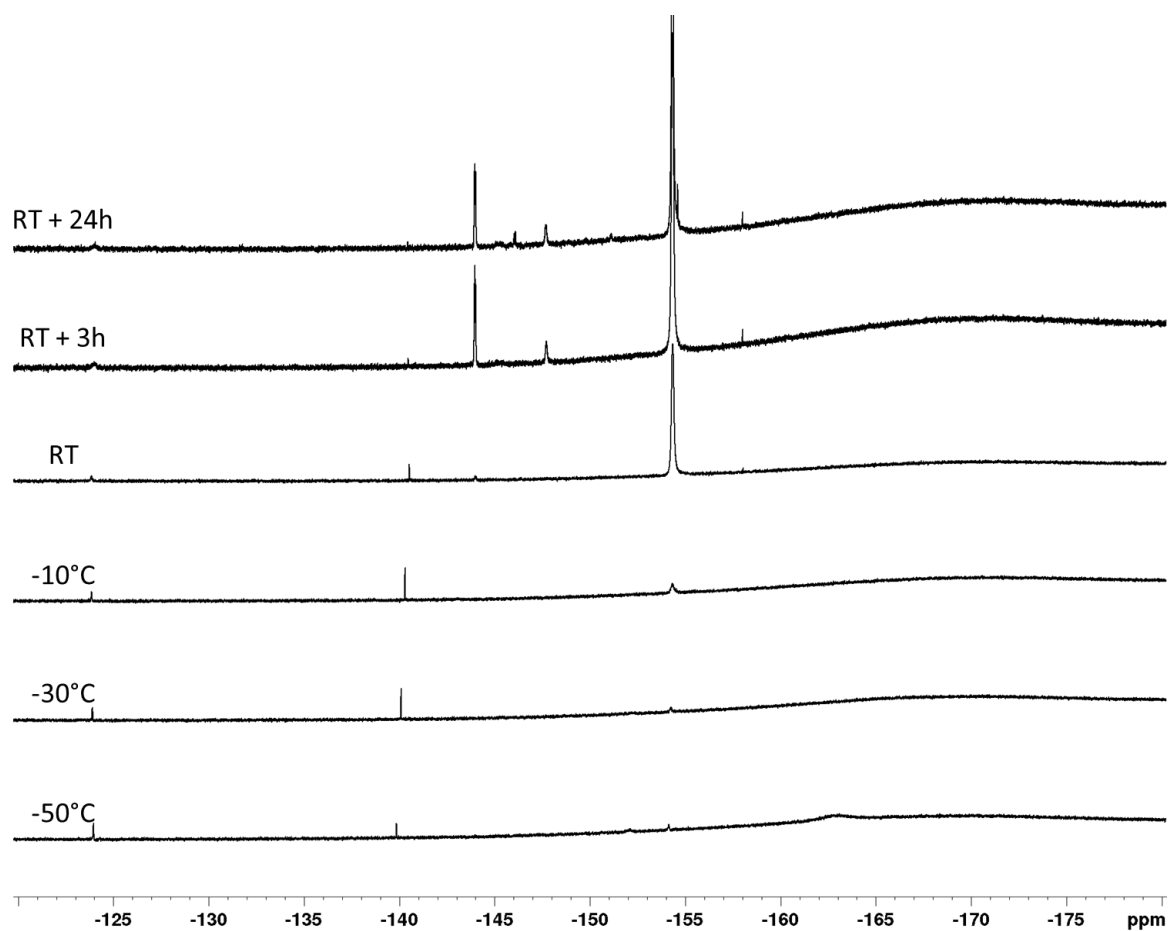
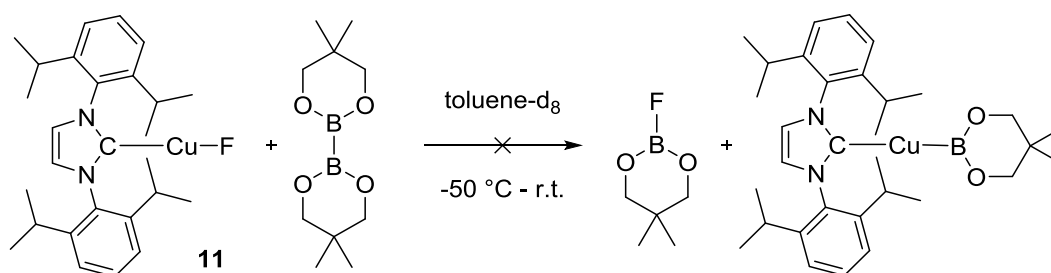


Figure 84: ^{19}F VT-NMR spectra of the reaction of $[\text{Cu}(\text{Dipp}_2\text{Im})\text{F}]$ with *p*-tolylBneop in THF-d_8 .

Reaction of [Cu(Dipp₂Im)(F)] with B₂neop₂ in toluene-d₈:



The ¹H NMR spectra at -50 °C showed relatively broad signals with low intensity (Figure 85). Two septets (2.47 and 2.59 ppm) as well as three sets for the neopentyl glycolate protons indicate the formation of multiple species. From -30 °C on the species showing the septet at 2.47 ppm is predominant. Warming to room temperature showed the formation of several additional septets in lower intensities, which could not be assigned to specific compounds. From room temperature on the predominant set of signals starts to disappear. After 24 h at room temperature three septets and at least four sets of signals for the neopentyl glycolate protons were observed, which could not be assigned to specific compounds.

The ¹¹B NMR spectra between -50 and -10 °C showed only one peak at 0.6 ppm (Figure 86). From 0 °C on a broad peak at around 17 ppm starts to appear. At room temperature two peaks at 18.0 and 17.1 ppm were detected next to signals with lower intensities at 1.5, 0.6 and 0.3 ppm. After 6 h at room temperature an additional peak at 28.0 ppm was observed.

The ¹⁹F NMR spectra showed two main peaks at a temperature of -50 °C with a chemical shift of -120.9 and -151.0 ppm (Figure 87). Two minor peaks were observed at -135.7 and -141.5 ppm. At a sample temperature of 0 °C only the two main peaks remained. Warming further to room temperature showed the disappearance of the peak at -120.9 ppm and a new peak at -144.3 ppm. After 6 h at room temperature only one peak with a chemical shift of -152.2 ppm and a ¹¹B-¹⁹F as well as a ¹⁰B-¹⁹F (as an increase in the intensity of the quartet at the left hands side – the septet was not resolved) coupling pattern was observed. The ¹¹B-¹⁹F coupling constant is 61.2 Hz.

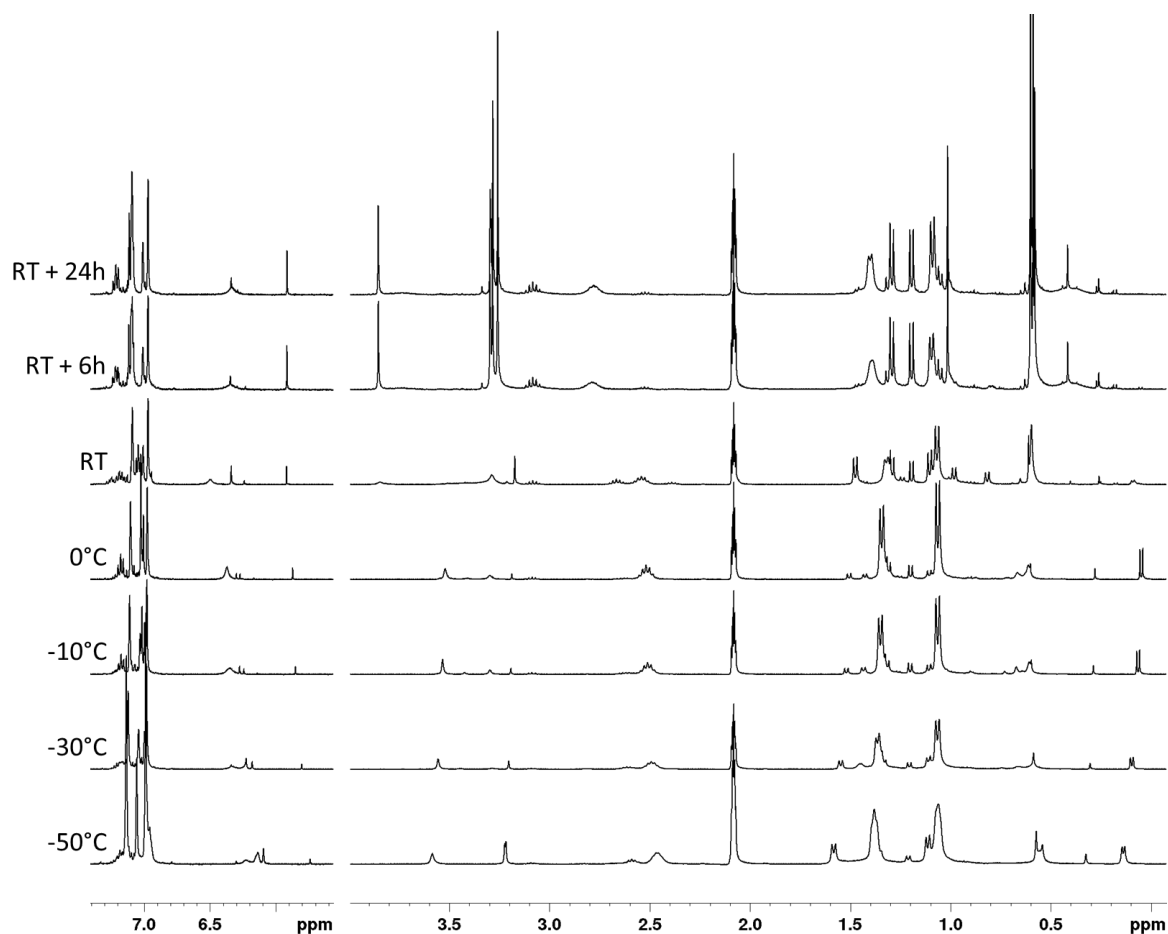


Figure 85: ^1H VT-NMR spectra of the reaction of $[\text{Cu}(\text{Dipp}_2\text{Im})\text{F}]$ with B_2neop_2 in toluene- d_8 .

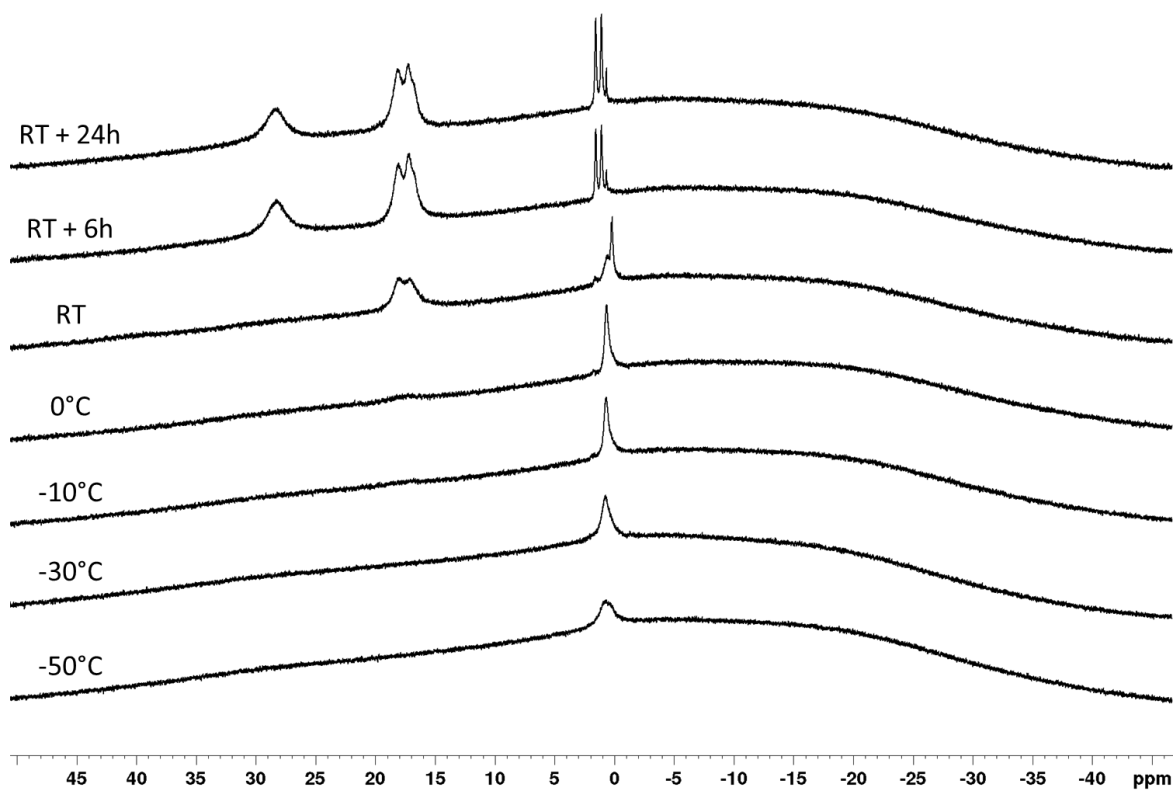


Figure 86: ^{11}B VT-NMR spectra of the reaction of $[\text{Cu}(\text{Dipp}_2\text{Im})\text{F}]$ with B_2neop_2 in toluene- d_8 .

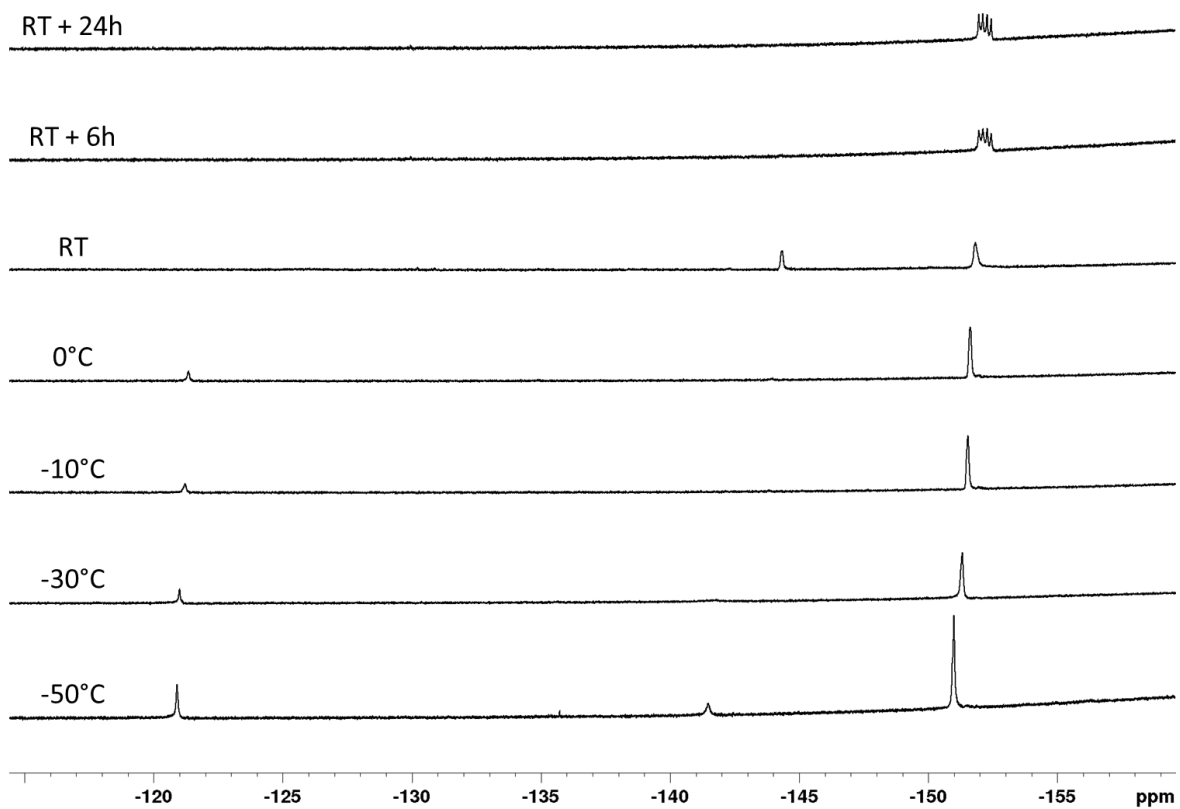
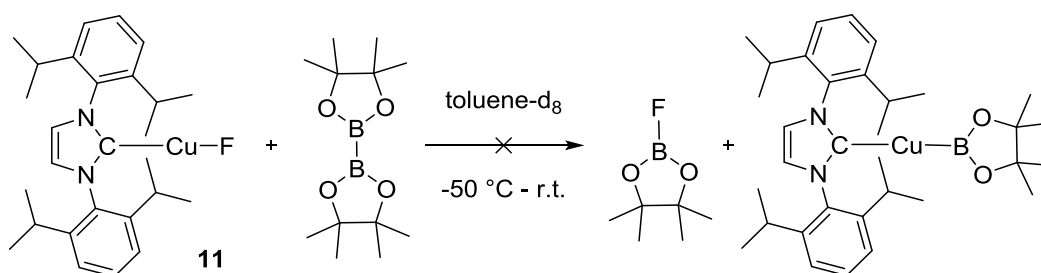


Figure 87: ^{19}F VT-NMR spectra of the reaction of $[\text{Cu}(\text{Dipp}_2\text{Im})\text{F}]$ with B_2neop_2 in toluene- d_8 .

Reaction of [Cu(Dipp₂Im)(F)] with B₂pin₂ in toluene-d₈:



Broad signals with low intensities were observed in the ¹H NMR spectra at -50 °C (Figure 88). Three broad peak between 2.46 and 2.82 ppm likely arise from three different Dipp₂Im moieties. The signal of the pinacolate protons is the most intense signal. Warming to room temperature showed no significant changes in the spectra. From room temperature on, when sharp signals were detected, one set of signals for the Dipp₂Im moiety and two overlapping peaks for two individual pinacolate protons were identified.

In the ¹¹B NMR spectra one broad peak was observed at 30.9 ppm and a minor signal was detected at 4.4 ppm (Figure 89). A possible [(B₂pin₂)(F)]⁻ adduct would show peaks at 31.4 and 5.1 ppm in THF-d₈ and at 33.9 and 5.7 ppm in MeCN-d₃.^[192] Heating afforded the growth of the peak at 4.4 ppm as well as a new peak at 21.4 ppm. Another peak at 21.8 ppm was observed from -10 °C on. After 24 h at room temperature the peak at 30.9 ppm, one signal at 20.8 ppm and two small signals at 4.4 and 4.0 ppm were detected. From room temperature on a broad signal at around 40 ppm in low intensity was observed, indicative of boryl formation.

At a temperature of -50 °C five fluorine moieties were detected in the ¹⁹F NMR spectra (Figure 90). Up to a temperature of -10 °C only two signals at -131.7 and -142.5 ppm were observed. When the sample reached a temperature of 0 °C five signals at -130.7, -131.9, -136.5 and -142.5 ppm were detected. At room temperature the disappearance of the signal at -142.5 ppm was observed. After 24 h at room temperature one quartet (J = 54 Hz) at -129.6 ppm and one proton coupled quintet (J = 6 Hz) at -132.1 ppm were detected.

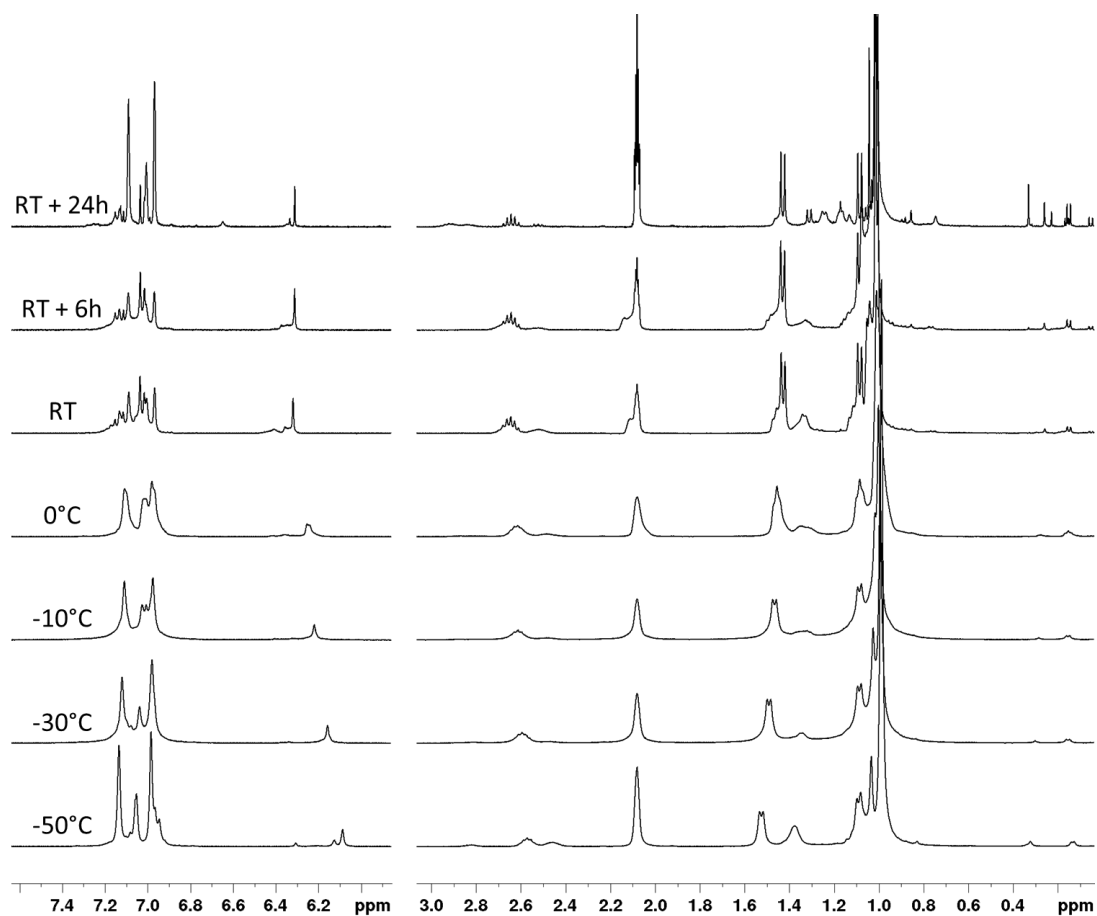


Figure 88: ^1H VT-NMR spectra of the reaction of $[\text{Cu}(\text{Dipp}_2\text{Im})\text{F}]$ with B_2pin_2 in toluene- d_8 .

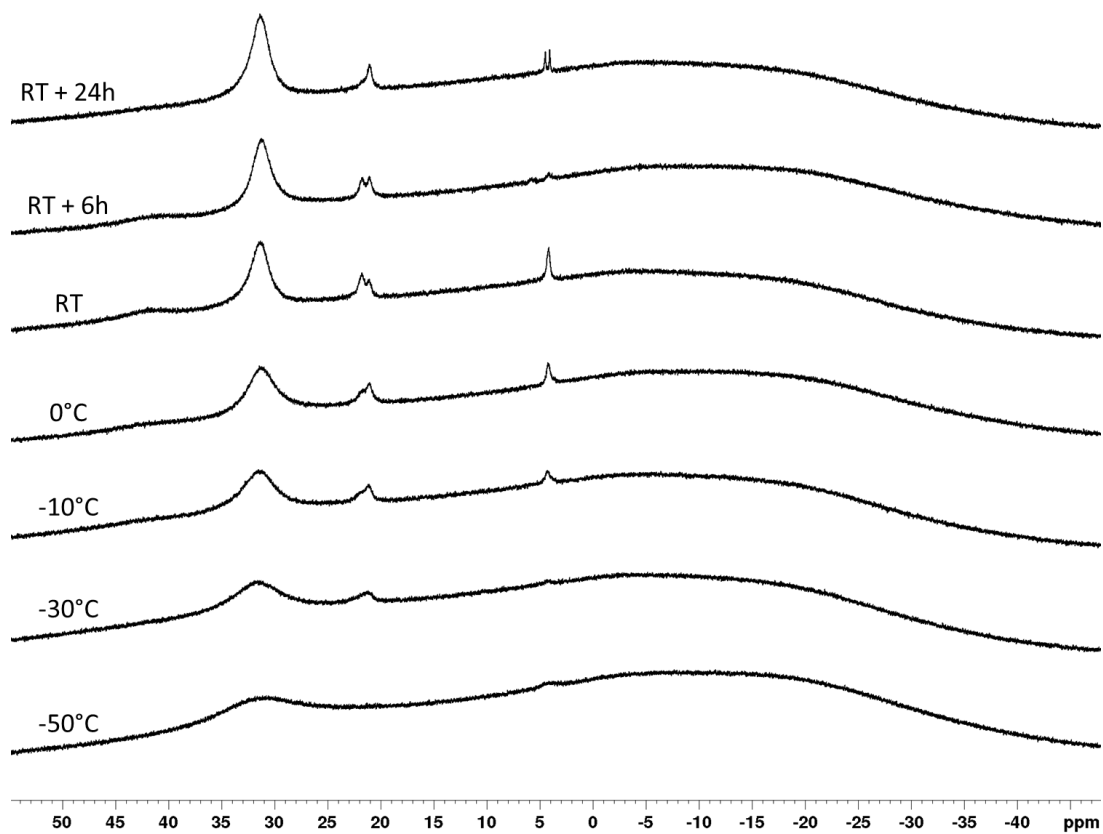


Figure 89: ^{11}B VT-NMR spectra of the reaction of $[\text{Cu}(\text{Dipp}_2\text{Im})\text{F}]$ with B_2pin_2 in toluene- d_8 .

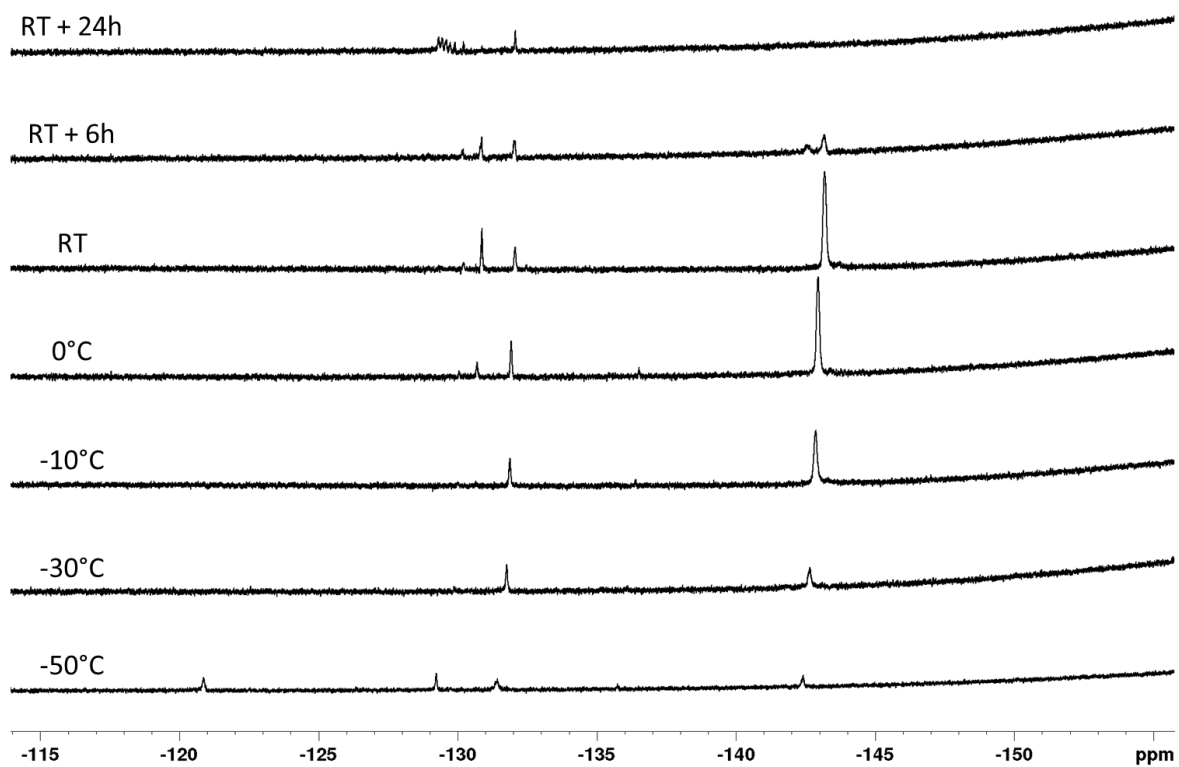
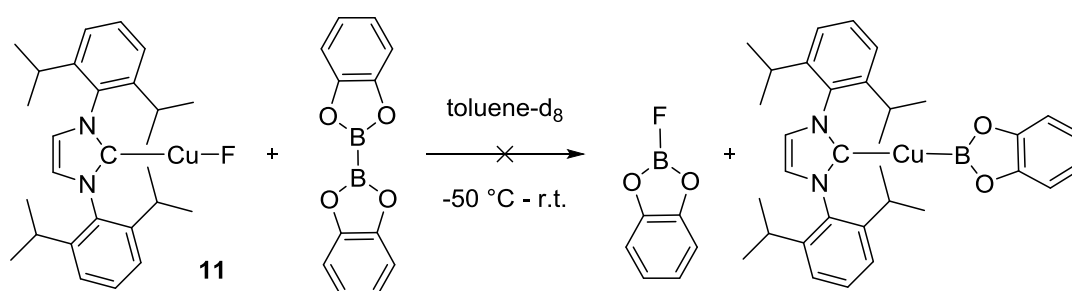


Figure 90: ^{19}F VT-NMR spectra of the reaction of $[\text{Cu}(\text{Dipp}_2\text{Im})\text{F}]$ with B_2pin_2 in toluene- d_8 .

Reaction of [Cu(Dipp₂Im)(F)] with B₂cat₂ in toluene-d₈:



The ¹H NMR spectra showed broad signals until room temperature was reached (Figure 91). Besides broad signals in the aromatic region one set of signals for the Dipp₂Im moiety and one set of signals for the catecholate protons were detected.

In the ¹¹B NMR spectra two peaks at 7.7 and 0.0 ppm were detected (Figure 92). An additional signal at 14.9 ppm was observed when the sample reached a temperature of -10 °C. From room temperature on two new signals at 31.5 and 21.4 ppm were detected and the signal at 0.0 ppm was absent.

The ¹⁹F NMR spectra showed, among others, one peak at -130.3 ppm (Figure 93). From room temperature on the peak -140.9 and later as well the signals at -135.7, -132.2, -130.9 and -130.2 ppm were detected. While the peaks at -140.9 and -135.7 ppm appeared a broadened singlets the peaks at -132.2, -130.9 and -130.2 ppm showed coupling as a quintet. In ¹⁹F{¹H} experiments these signals appear as singlets, substantiating the proton coupling nature of the pattern (Figure 94).

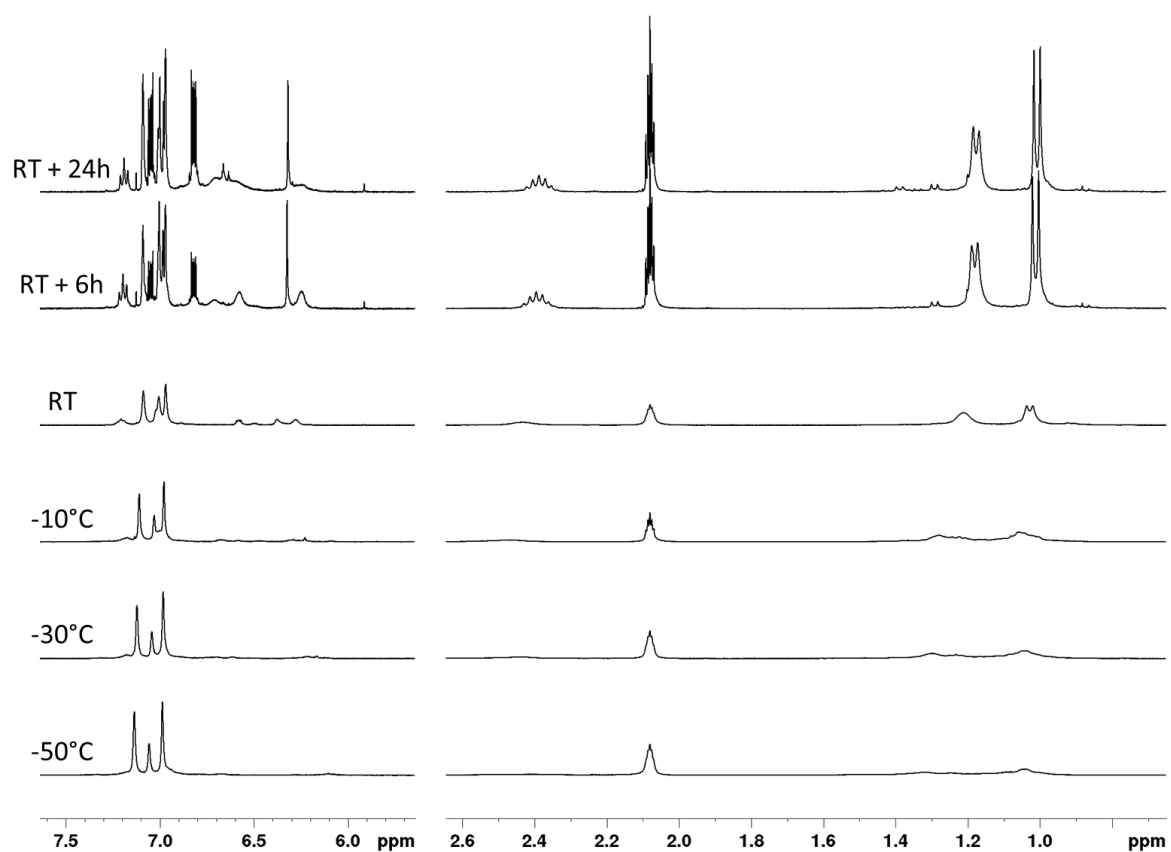


Figure 91: ^1H VT-NMR spectra of the reaction of $[\text{Cu}(\text{Dipp}_2\text{Im})\text{F}]$ with B_2cat_2 in toluene- d_8 .

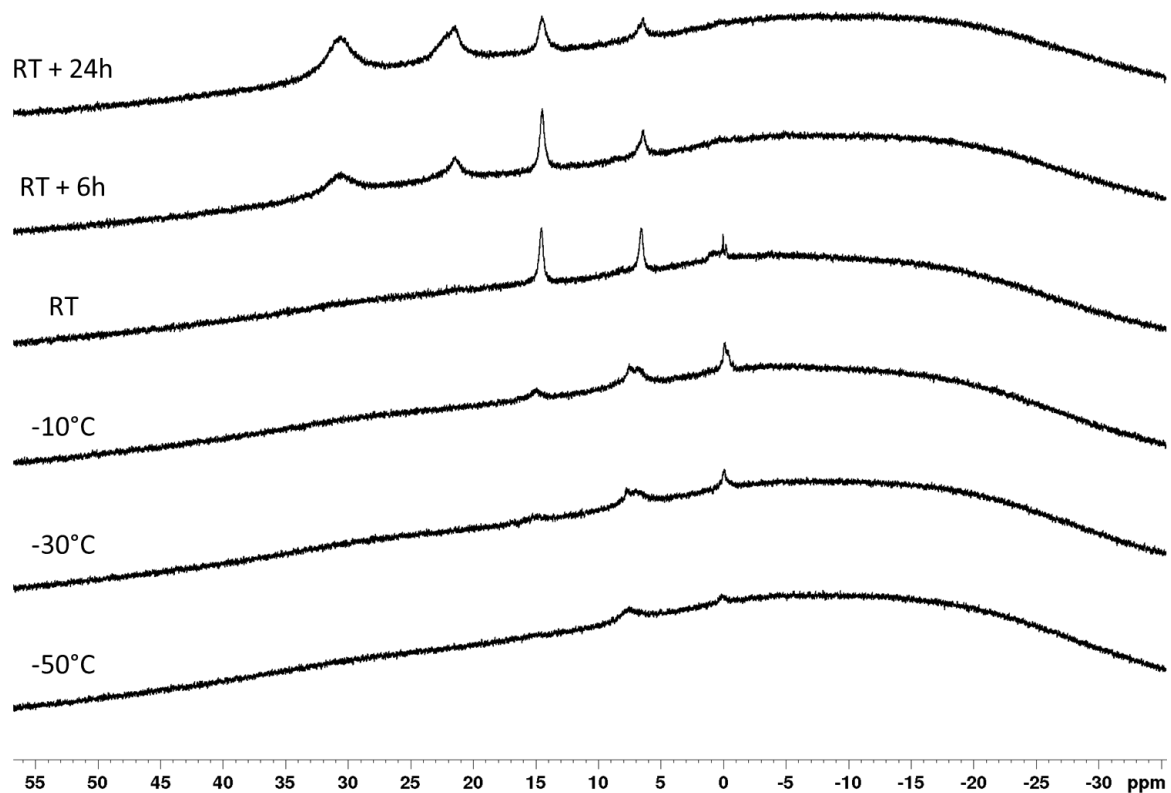


Figure 92: ^{11}B VT-NMR spectra of the reaction of $[\text{Cu}(\text{Dipp}_2\text{Im})\text{F}]$ with B_2cat_2 in toluene- d_8 .

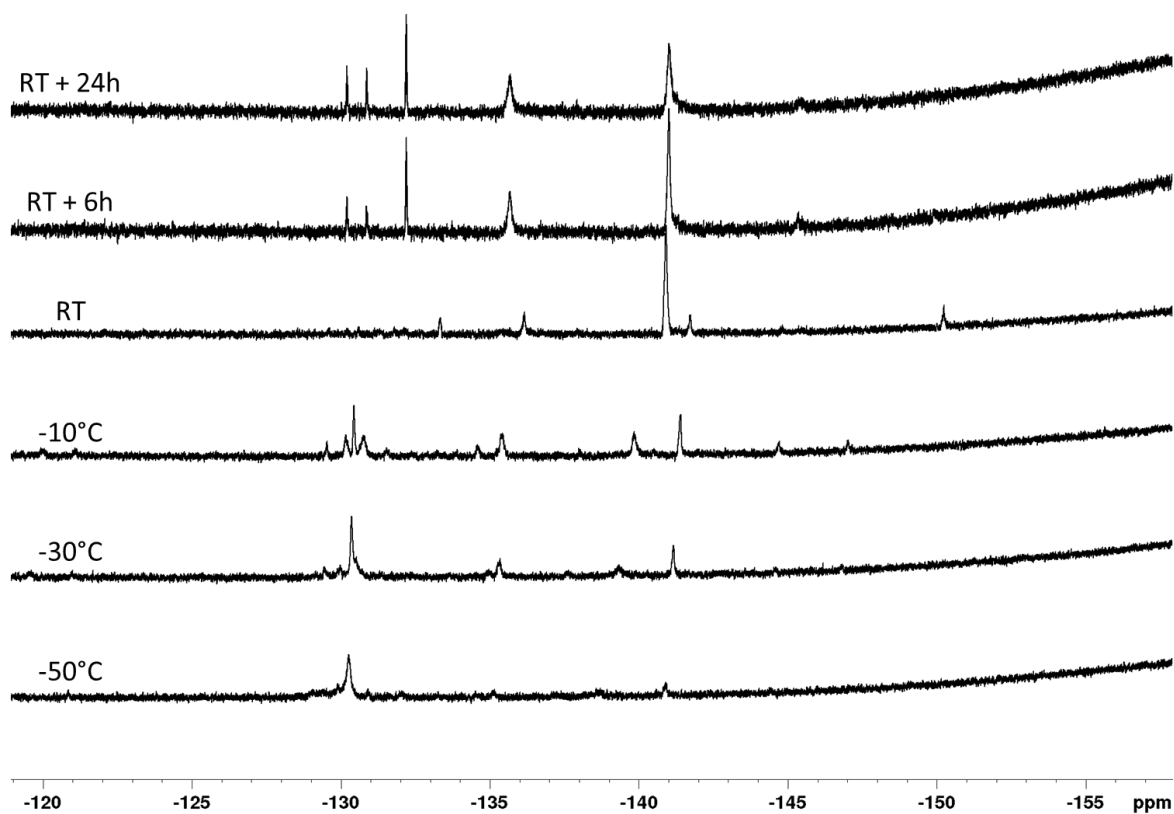


Figure 93: ^{19}F VT-NMR spectra of the reaction of $[\text{Cu}(\text{Dipp}_2\text{Im})\text{F}]$ with B_2cat_2 in toluene-d_8 .

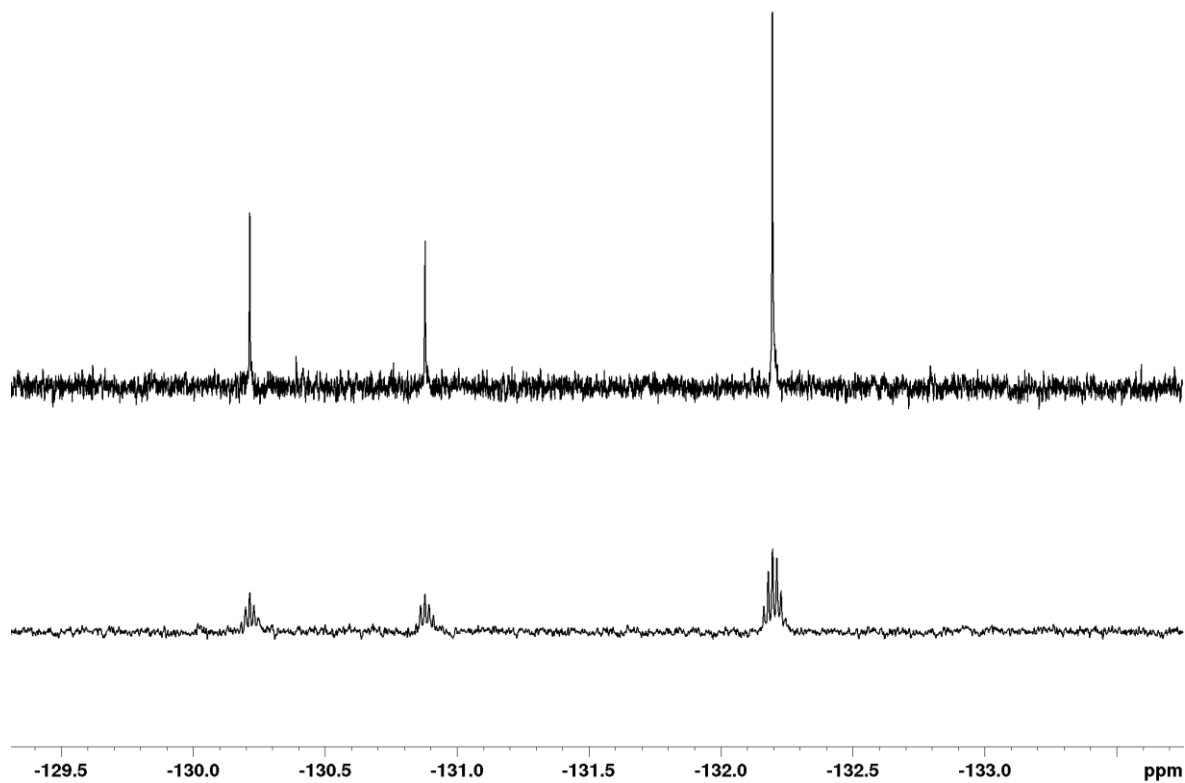
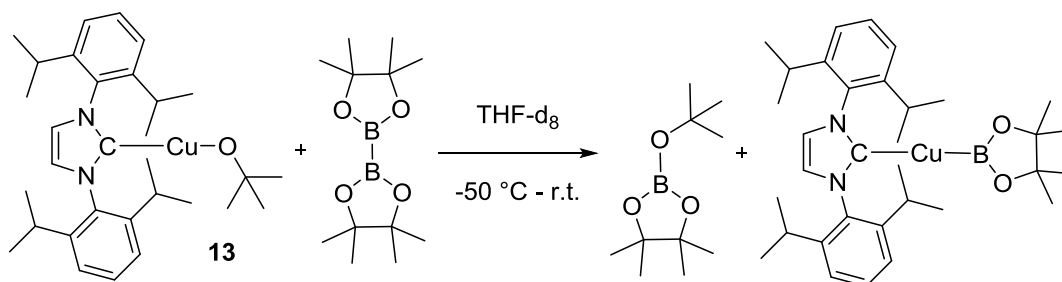


Figure 94: Comparison of the ^{19}F NMR spectrum (Bottom) of the reaction of $[\text{Cu}(\text{Dipp}_2\text{Im})\text{F}]$ with B_2cat_2 at room temperature with the $^{19}\text{F}\{^1\text{H}\}$ NMR spectrum (Top).

Reaction of $[\text{Cu}(\text{Dipp}_2\text{Im})(\text{O}^t\text{Bu})]$ with B_2pin_2 in THF-d_8 :



In the ^1H NMR spectra recorded at $-50\text{ }^\circ\text{C}$ relatively sharp signals for the NHC ligand were detected (Figure 95). The septet and the doublet signals are a little misshapen and a doubling of the NHC backbone protons as well as the *meta* protons of the Dipp moiety was observed, indicating that two similar complexes/ligands are present in solution having almost identical chemical shifts (Figure 97). In addition, five singlets between 0.64 and 1.29 ppm in a 1.5:1.5:6.4:1.5:1 ratio were observed (Figure 98). At a temperature of $-30\text{ }^\circ\text{C}$ the intensity of signals for the complex, which was detected at slightly higher field strength, increased at the expense of the other one. In addition, four singlets at 0.84, 1.19, 1.19 and 1.29 ppm were observed with a ratio of 1.2:(1.2:1.2):1 and the singlet at 0.64 ppm almost disappeared completely. At $-10\text{ }^\circ\text{C}$ only one set of signals for the Dipp_2Im moiety and one singlet at 1.19 ppm was detected besides the peaks singlets at 0.84 and 1.29 ppm. The ratio of the septet of the ligand and the singlet at 1.19 is 4:18.3, while with the singlet at 1.29 and 0.84 ppm it shows a ratio of 4:9.2 and 4:12.0, respectively (Figure 16). When warming to room temperature only a temperature dependent shift of the protons in the aromatic region was observed. After room temperature was reached slow decomposition by the formation of a new septet and the corresponding signals was observed.

While the ratio of the peaks at 0.84 and 1.29 ppm was 1:1.3 at $-10\text{ }^\circ\text{C}$, as expected for the formed byproduct $^t\text{BuOBpin}$, it changed to 1:1 24 h after warming to room temperature. This plus the fact the ratio of the septet and the singlet at 0.84 ppm is about 4:12 throughout the entire temperature range indicates that the signals at 0.84 ppm corresponds to the pinacol boronate protons of the boryl complex. Therefore, the signal at 1.19 ppm corresponds to the pinacol boronate protons of $^t\text{BuOBpin}$ byproduct and free B_2pin_2 as the ^{11}B NMR spectra suggest. This slight excess of B_2pin_2 in solution is possibly due to weighing errors. The peak at 0.64 ppm might be from an intermediate between the alkoxide complex

and the boryl complex in which both starting materials are linked via the oxygen of the alkoxide group.^[151]

The ^{11}B NMR spectrum at $-50\text{ }^\circ\text{C}$ showed the broad signal of the starting material at 30.1 ppm and another peak at 21.2 ppm belonging to the expected byproduct $^t\text{BuOBpin}$ (Figure 96).^[192] From $-30\text{ }^\circ\text{C}$ on, next to the peaks at 30.1 and 21.2 ppm, the growth of a new, broad peak at around 41 ppm was detected indicative of boryl formation. No significant changes in the spectra were observed when warming to room temperature and 24 h later. After 24 h at room temperature the chemical shifts of the three signals detected in the ^{11}B NMR spectrum are 41.5, 30.8 and 21.3 ppm.

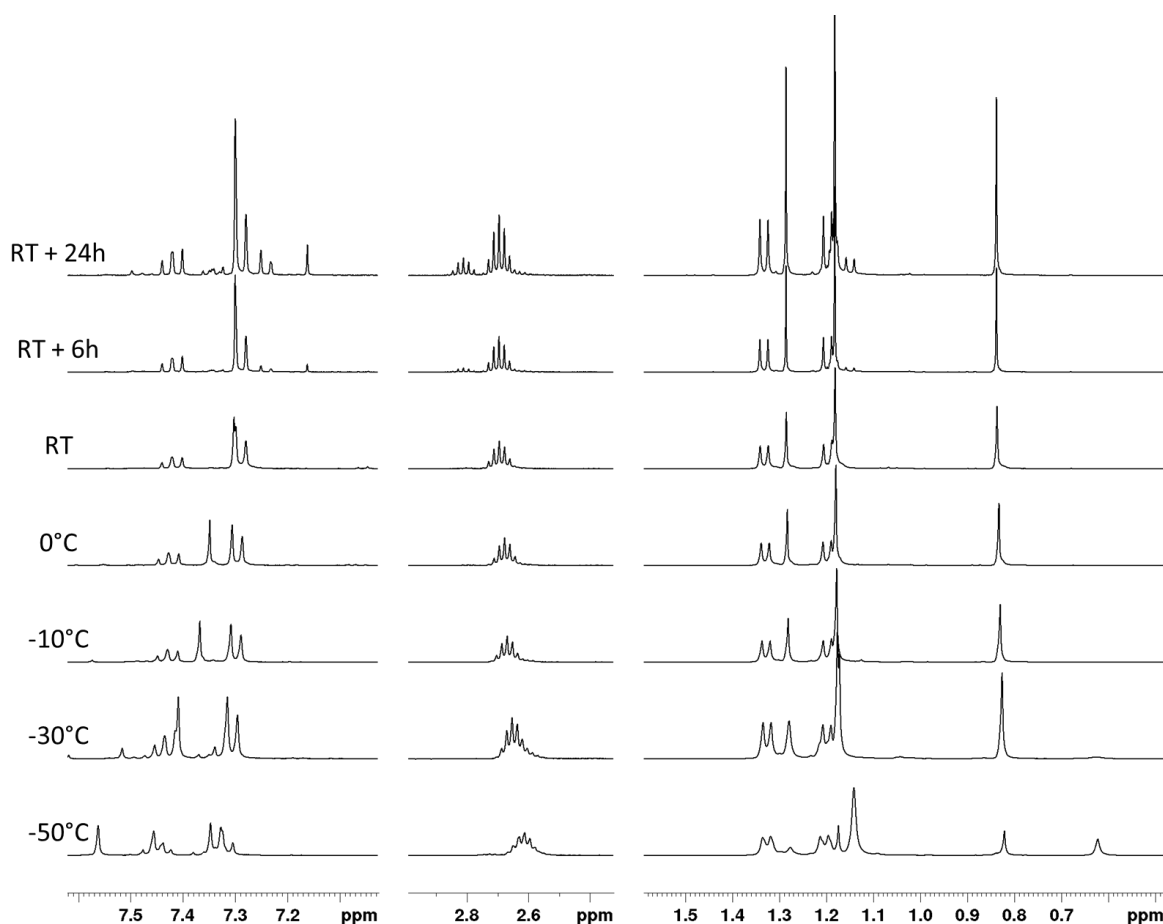


Figure 95: ^1H VT-NMR spectra of the reaction of $[\text{Cu}(\text{Dipp}_2\text{Im})(\text{O}^t\text{Bu})]$ with B_2pin_2 in THF-d_8 .

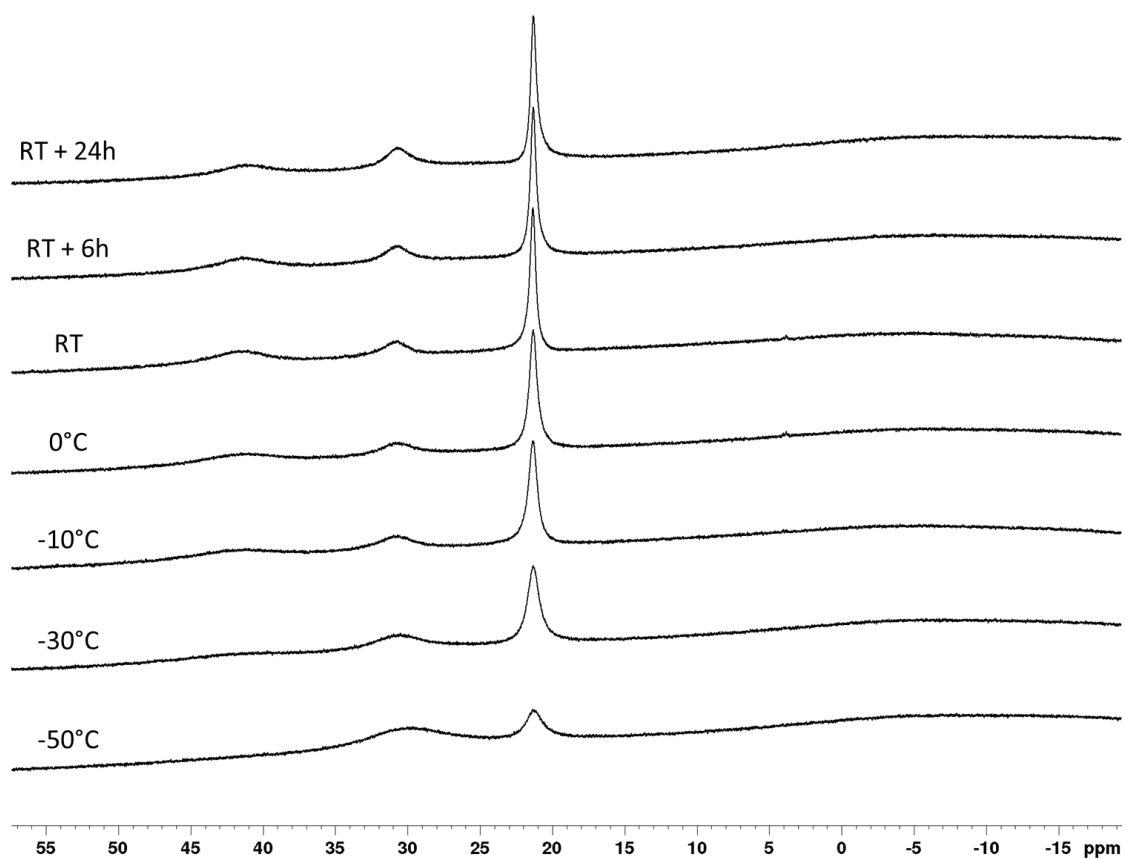


Figure 96: ^{11}B VT-NMR spectra of the reaction of $[\text{Cu}(\text{Dipp}_2\text{Im})(\text{O}'\text{Bu})]$ with B_2pin_2 in THF-d_8 .

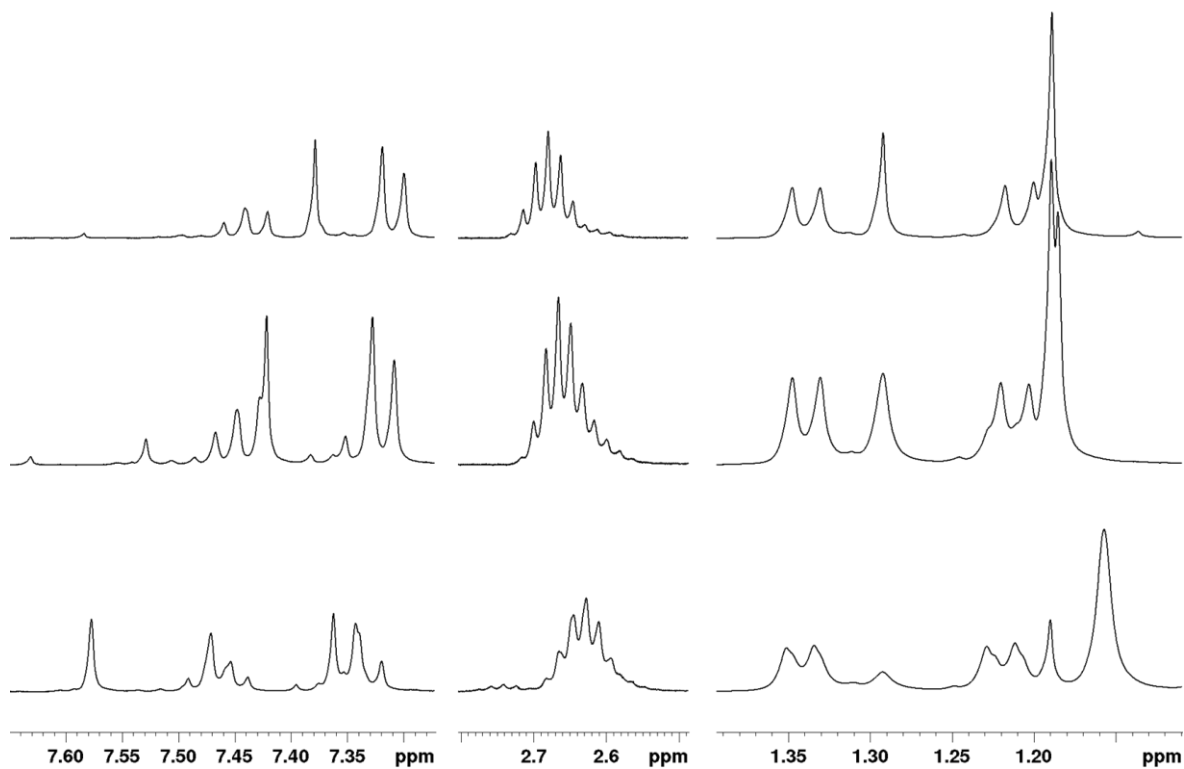


Figure 97: ^1H VT-NMR spectra of the reaction of $[\text{Cu}(\text{Dipp}_2\text{Im})(\text{O}'\text{Bu})]$ with B_2pin_2 in THF-d_8 showing two sets of signals for the Dipp_2Im ligand at almost the same chemical shift. Bottom: -50°C . Middle: -30°C . Top: -10°C .

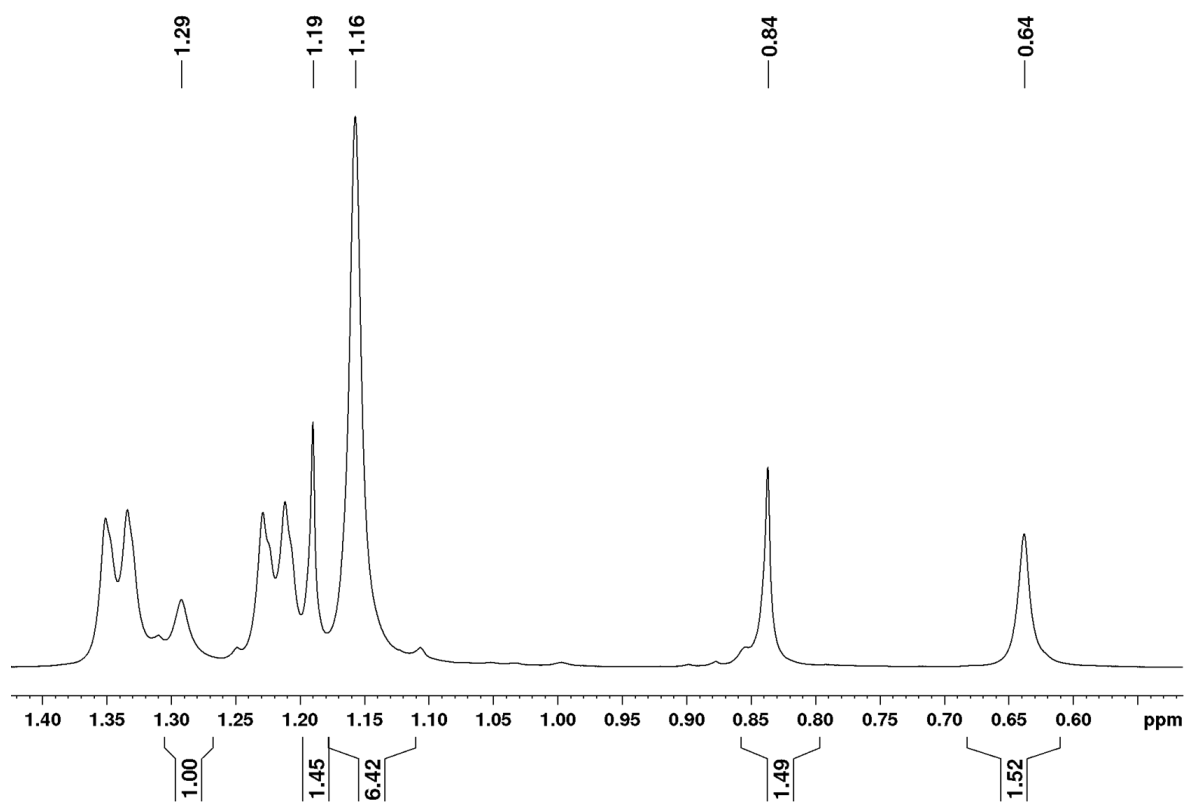
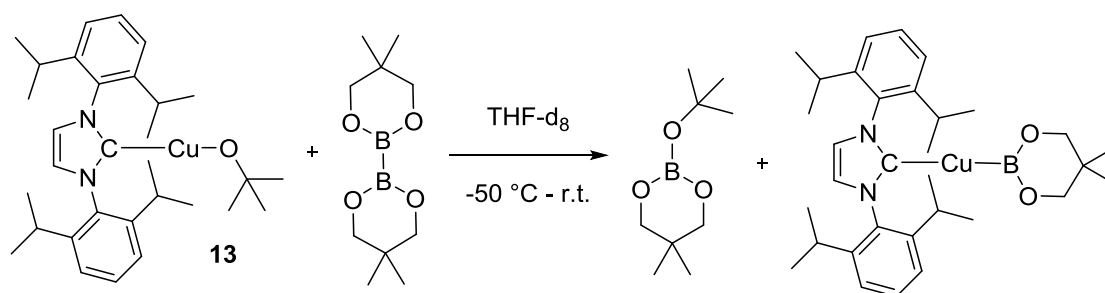


Figure 98: ^1H VT-NMR spectra of the reaction of $[\text{Cu}(\text{Dipp}_2\text{Im})(\text{O}^t\text{Bu})]$ with B_2pin_2 in THF-d_8 recorded at $-50\text{ }^\circ\text{C}$ showing the ratio of the singlets between 1.29 and 0.64 ppm.

Reaction of $[\text{Cu}(\text{Dipp}_2\text{Im})(\text{O}^t\text{Bu})]$ with B_2neop_2 in THF-d_8 :



The ^1H NMR spectra at $-50\text{ }^\circ\text{C}$ showed mostly the resonances for the Dipp_2Im ligand, while the signals for more than one the neopentyl glycol moiety (3.51/0.88 and 3.02/0.64 ppm) and the *tert*-butoxide group (broad peak at around 0.83 ppm) were detected in lower intensities (Figure 99). The protons of the *tert*-butoxide moiety gave rise to a broad signal at around 0.82 ppm (0.89 $-30\text{ }^\circ\text{C}$; 0.99 $-10\text{ }^\circ\text{C}$; 1.13 $10\text{ }^\circ\text{C}$; 1.26 r.t. (sharp signal)) ppm. In the spectrum recorded at $-30\text{ }^\circ\text{C}$, which showed sharper signals, the signals for two Dipp_2Im ligands with almost the same resonance frequencies were detected instead of one. When room temperature was reached two set of signals were assigned: one to the expected $^t\text{BuOBneop}$ byproduct and the other, growing set of signals, to free B_2neop_2 . The remaining set of signals after 24 h at room temperature were assigned to the Dipp_2Im ligand.

The ^{11}B NMR spectra showed one signal at 16.3 ppm which might correspond to the $^t\text{BuOBneop}$ byproduct (Figure 100).^[273] When a temperature of $10\text{ }^\circ\text{C}$ was reached an additional peak at 39.5 ppm, indicative of boryl formation, was detected. In the subsequent spectra the formation of a new peak with the chemical shift of free B_2neop_2 was detected, while the intensity of signal at 39.5 ppm decreased.

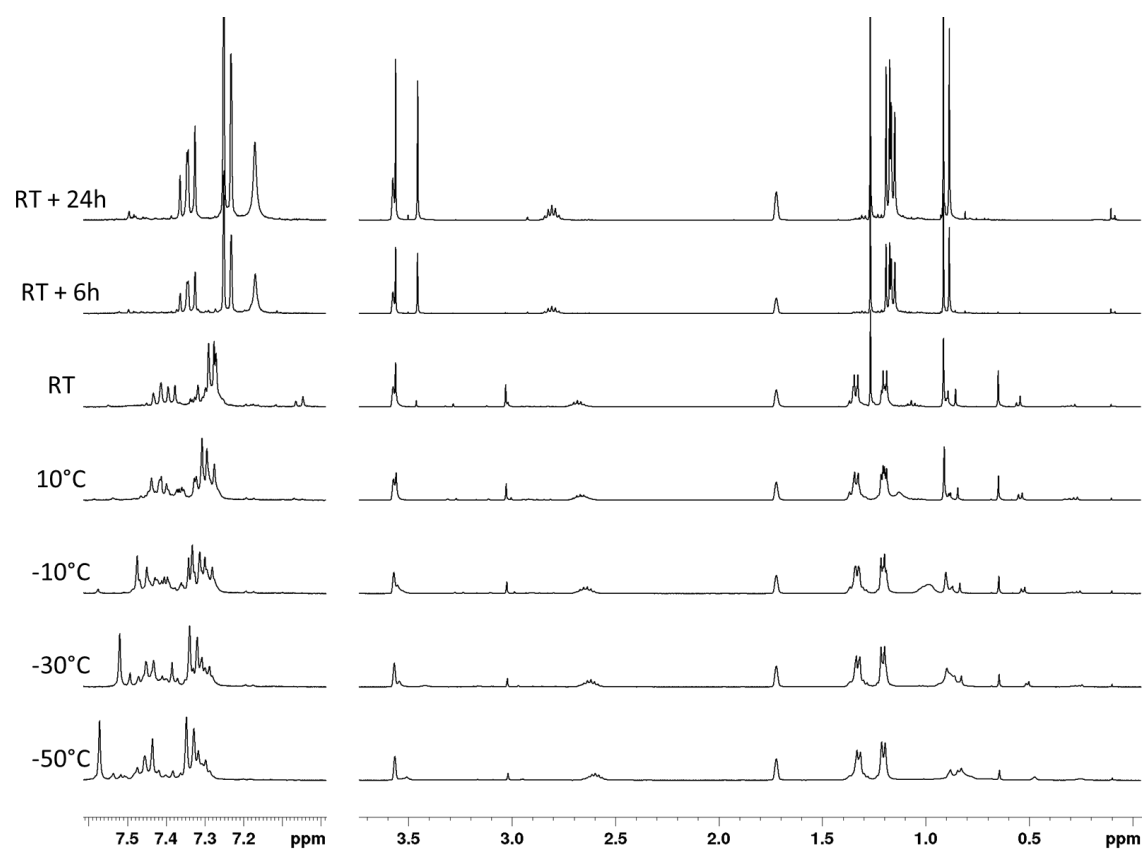


Figure 99: ^1H VT-NMR spectra of the reaction of $[\text{Cu}(\text{Dipp}_2\text{Im})(\text{O}^t\text{Bu})]$ with B_2neop_2 in THF-d_8 .

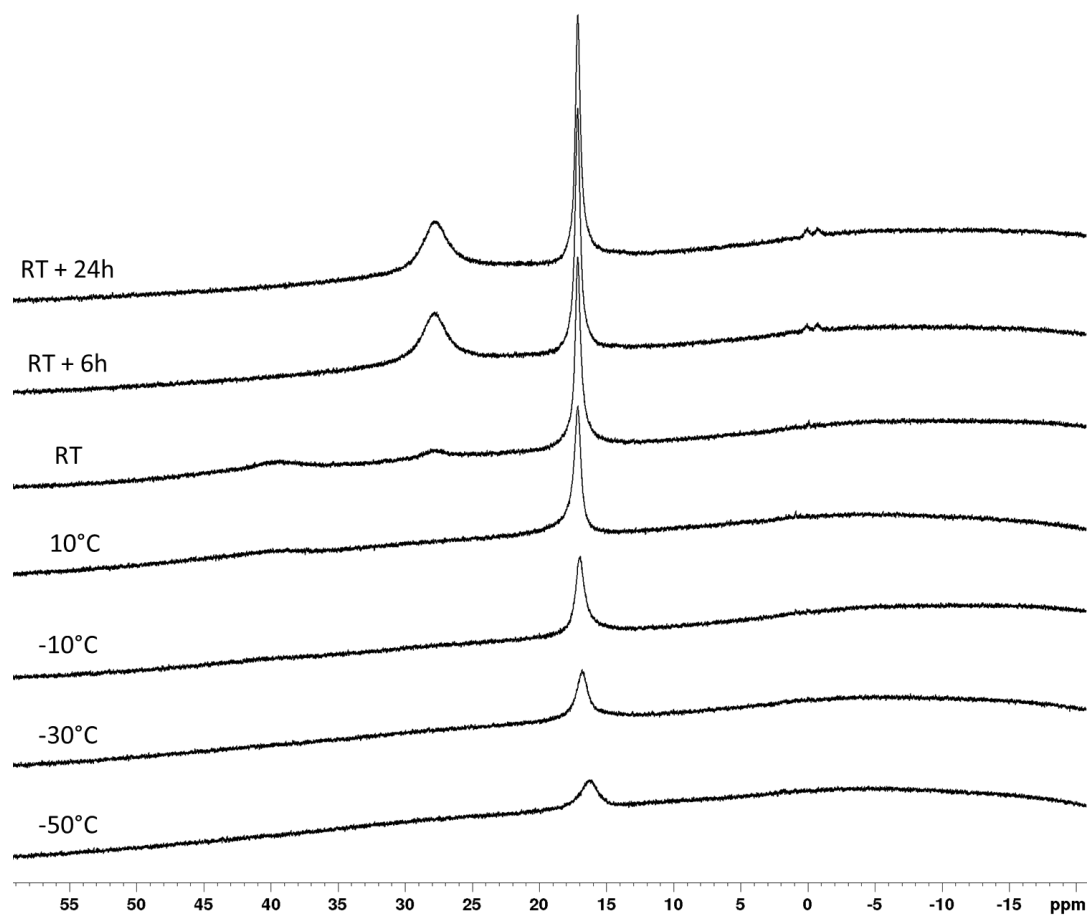
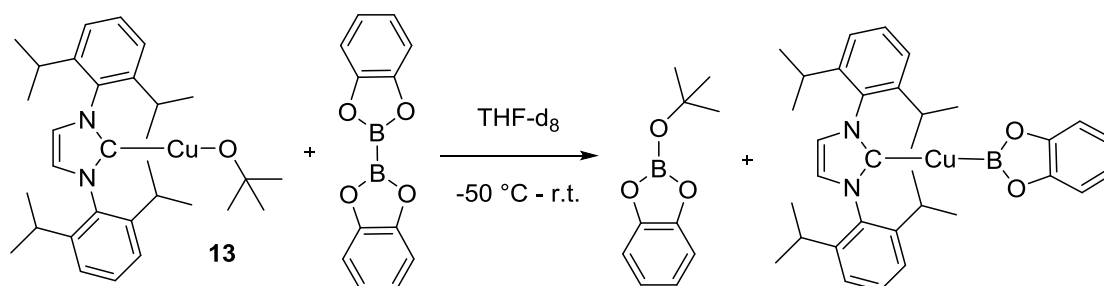


Figure 100: ^{11}B VT-NMR spectra of the reaction of $[\text{Cu}(\text{Dipp}_2\text{Im})(\text{O}^t\text{Bu})]$ with B_2neop_2 in THF-d_8 .

Reaction of $[\text{Cu}(\text{Dipp}_2\text{Im})(\text{O}^t\text{Bu})]$ with B_2cat_2 in THF-d_8 :



Two set of signals for the Dipp_2Im protons were detected in the ^1H NMR spectra at $-50\text{ }^\circ\text{C}$ (septets at 2.61 and 2.49 ppm) (Figure 101). Four singlets (ratio 7.5:1:5.6:5.8) for the *tert*-butyl group were detected at 1.25, 0.81, 0.62 and 0.38 ppm. The aromatic protons of the diboron compound showed resonance as one multiplet and a chemical shift of 6.20 ppm. The ratio of the diboron compound protons and the two septets of the Dipp_2Im protons is 1:1.25:2.0, indicating that most of the diboron compound is not in solution and thus was not detected. At $-30\text{ }^\circ\text{C}$, multiple septets were detected as well as two new sets of signals for the aromatic protons of the diboron compound. When the sample was warmed to $-10\text{ }^\circ\text{C}$ the *tert*-butyl protons were detected as one singlet at 0.81 ppm. Two new septets (and the other coupling patterns and ratios expected for the protons of a Dipp_2Im ligand) were detected at 2.83 and 2.71 ppm and two sets of signals for the catecholate protons were observed at 6.83/6.69 and 6.23/5.95 ppm. The septet at 2.83 ppm (and the corresponding signals) and the signals of the catecholate moiety at 6.23/5.95 ppm showed a ratio of 1.07:1:2.07, while the septet at 2.71 ppm (and the corresponding signals) and the signals of the catecholate moiety at 6.83/6.69 ppm showed a ratio of 1.0:1.0:2.09. The stoichiometry is indicative of two discreet complexes each bearing one ligand and one catecholate moiety. From $-30\text{ }^\circ\text{C}$ to room temperature, the singlet at 0.81 ppm and the septet at 2.83 ppm showed a ratio of 4.5:1 in all spectra, which is double what is expected for a $[\text{Cu}(\text{Dipp}_2\text{Im})(\text{O}^t\text{Bu})]$ complex. At room temperature the growth of two new sets of signals (7.06/6.95 and 6.29 ppm) of catecholate moieties (at the expense of the moiety at 6.23/5.95 ppm) and a new singlet at 1.48 ppm was observed. The ratio of the singlet at 1.48 ppm and the new aromatic catecholate protons at 7.06/6.95 ppm is 4.5:1:1 as expected for $^t\text{BuOBcat}$. Over the next 45 minutes the growth of the new peaks along with the septet at 2.71 ppm and the corresponding other resonances of the ligand as well as the catecholate

protons showing resonance at 6.83/6.69 ppm was observed at the expense of the other signals. In Figure 19 the spectrum after 44 minutes at room temperature is displayed, showing mostly the copper boryl complex and the corresponding t BuOBcat byproduct. The following 24 h showed the formation of multiple other compounds next to the described ones in varying intensities, which could not be assigned to specific compounds.

The ^{11}B NMR spectra at $-50\text{ }^\circ\text{C}$ and $-30\text{ }^\circ\text{C}$ showed one peak of low intensity and a shift of 8.2 ppm (Figure 102). At $-10\text{ }^\circ\text{C}$ the intensity of the peak multiplies and peaks at 14.5, 22.0 and 43.0 ppm were detected. Warming to room temperature showed an intensity increase of the peaks at 43.0 and 22.0 ppm at the expense of the peak at 8.2 ppm as well as the growth of the peak at 14.5 ppm. Within the next minutes the disappearance of the peak at 8.2 ppm and a new peak at 7.2 ppm was observed. (Figure 20). After 24 h at room temperature smaller peaks at 15.6, 6.1 and 5.2 ppm were detected next to the remaining peaks at 43.0, 22.0, 14.5 and 7.2 ppm.

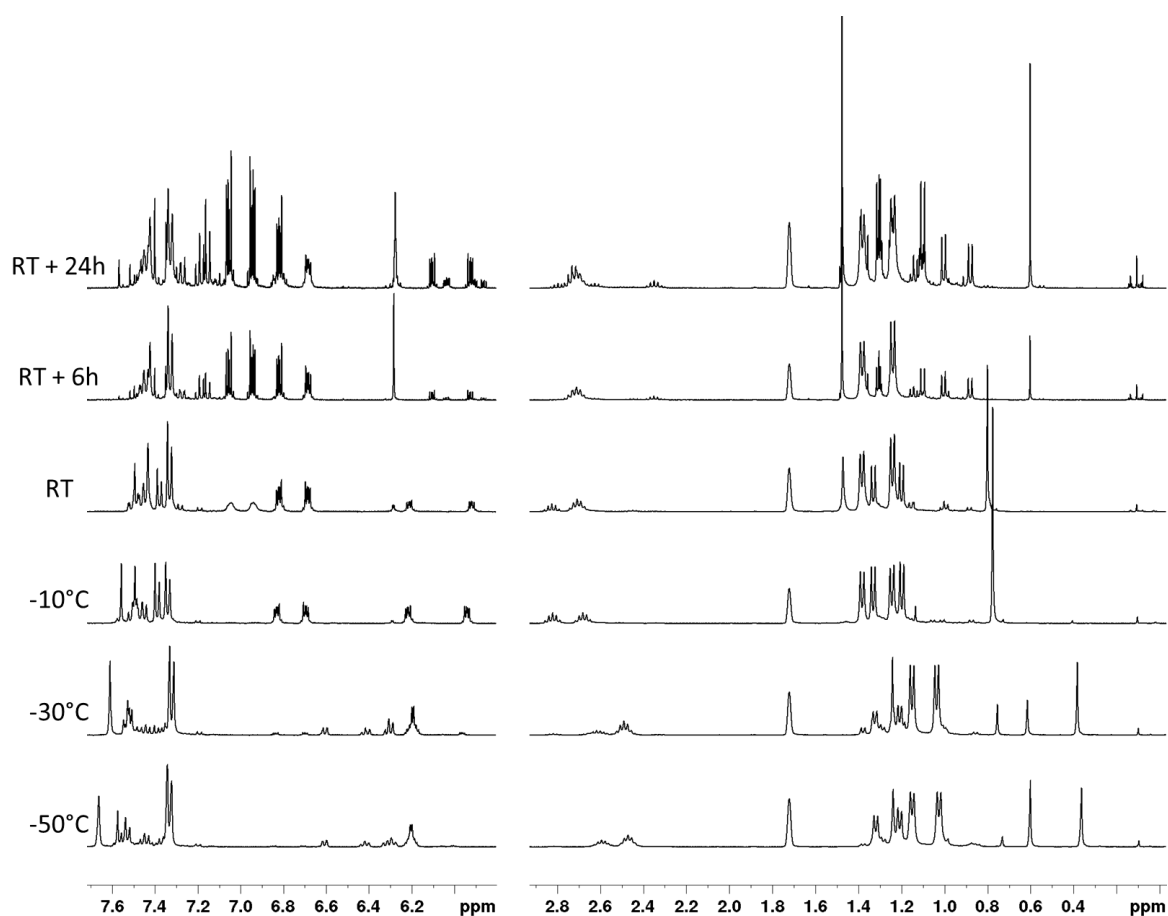


Figure 101: ^1H VT-NMR spectra of the reaction of $[\text{Cu}(\text{Dipp}_2\text{Im})(\text{O}^t\text{Bu})]$ with B_2cat_2 in THF-d_8 .

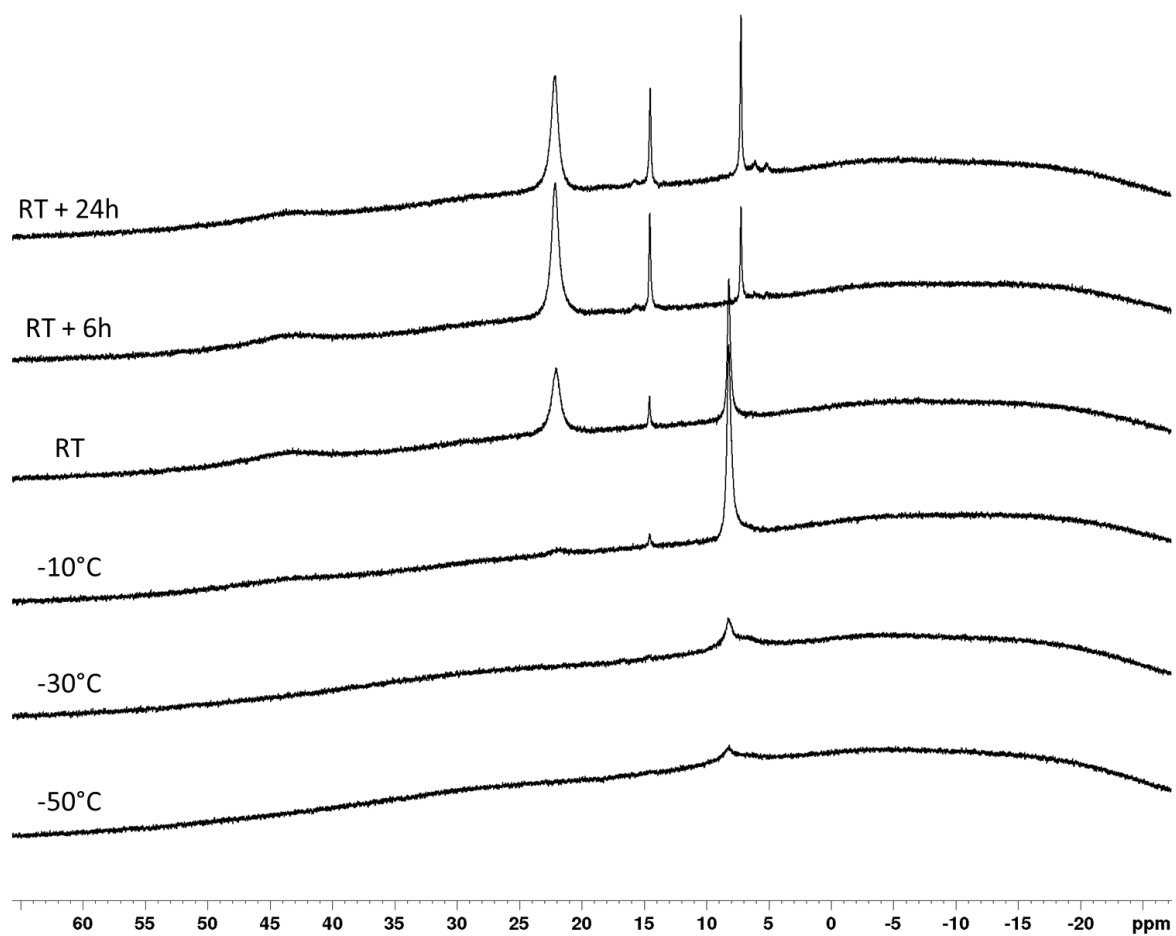
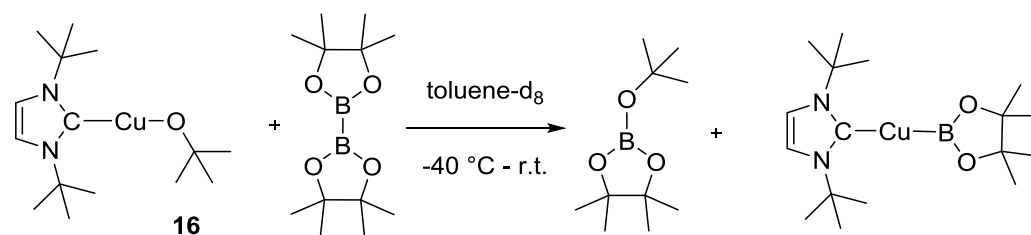


Figure 102: ^{11}B VT-NMR spectra of the reaction of $[\text{Cu}(\text{Dipp}_2\text{Im})(\text{O}^t\text{Bu})]$ with B_2catz_2 in THF-d_8 .

Reaction of $[\text{Cu}(\text{}^t\text{Bu}_2\text{Im})(\text{O}^t\text{Bu})]$ with B_2pin_2 in THF-d_8 :



The ^1H NMR spectra showed broadened signals of relatively low intensity, indicative of a precipitate. The ratios of the signals detected do not fit those expected for a ${}^t\text{Bu}_2\text{Im}$ ligand. When the sample was heated to room temperature only minor changes in the ^1H NMR spectra were observed.

In the ^{11}B NMR spectra at $-50\text{ }^\circ\text{C}$ one signal at 21.5 ppm was detected, which corresponds to the expected byproduct ${}^t\text{BuOBpin}$. The putative formed boryl complex might not be detected due to the broadness of the expected signal and low concentration in solution. From $-20\text{ }^\circ\text{C}$ on the formation of a new signal next to the signal for the byproduct was detected at 31.0 ppm. This signal likely arises from the formation of B_2pin_2 , which is formed by reductive elimination of the boryl complex. Similar reactivity was observed by Kleeberg *et al.* and a copper mirror was observed at the end of the investigation.^[271]

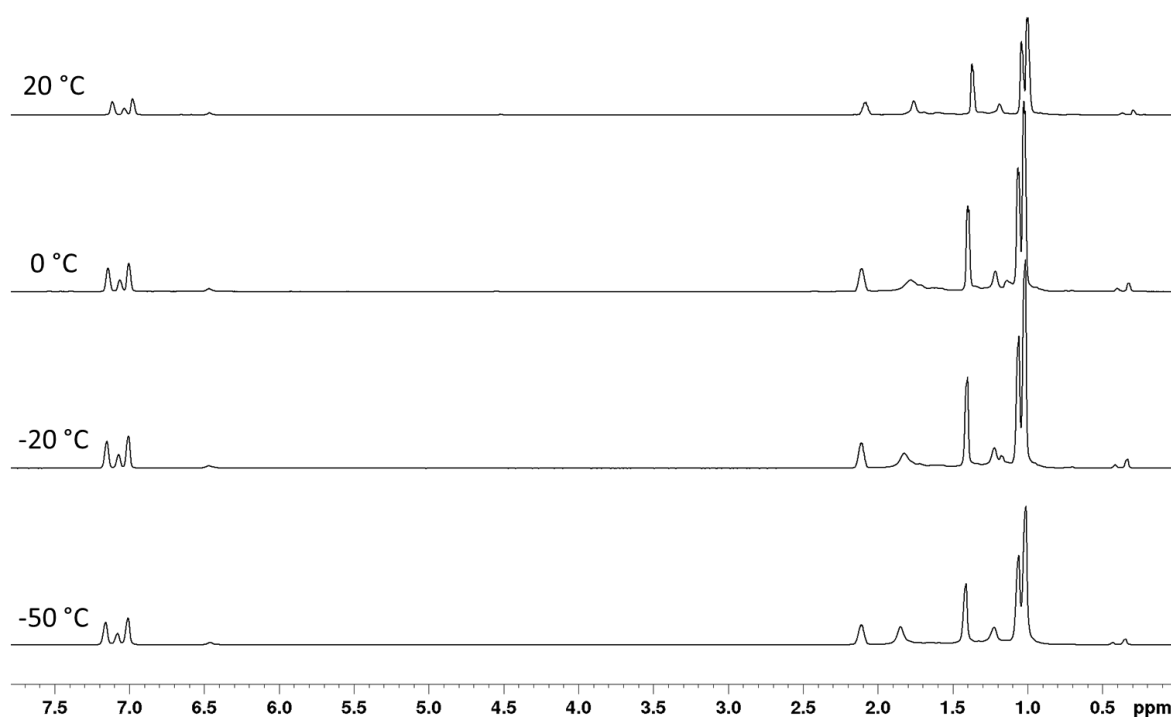


Figure 103: ^1H VT-NMR spectra of the reaction of $[\text{Cu}(\text{}^t\text{Bu}_2\text{Im})(\text{O}^t\text{Bu})]$ 16 with B_2pin_2 in toluene-d_8 .

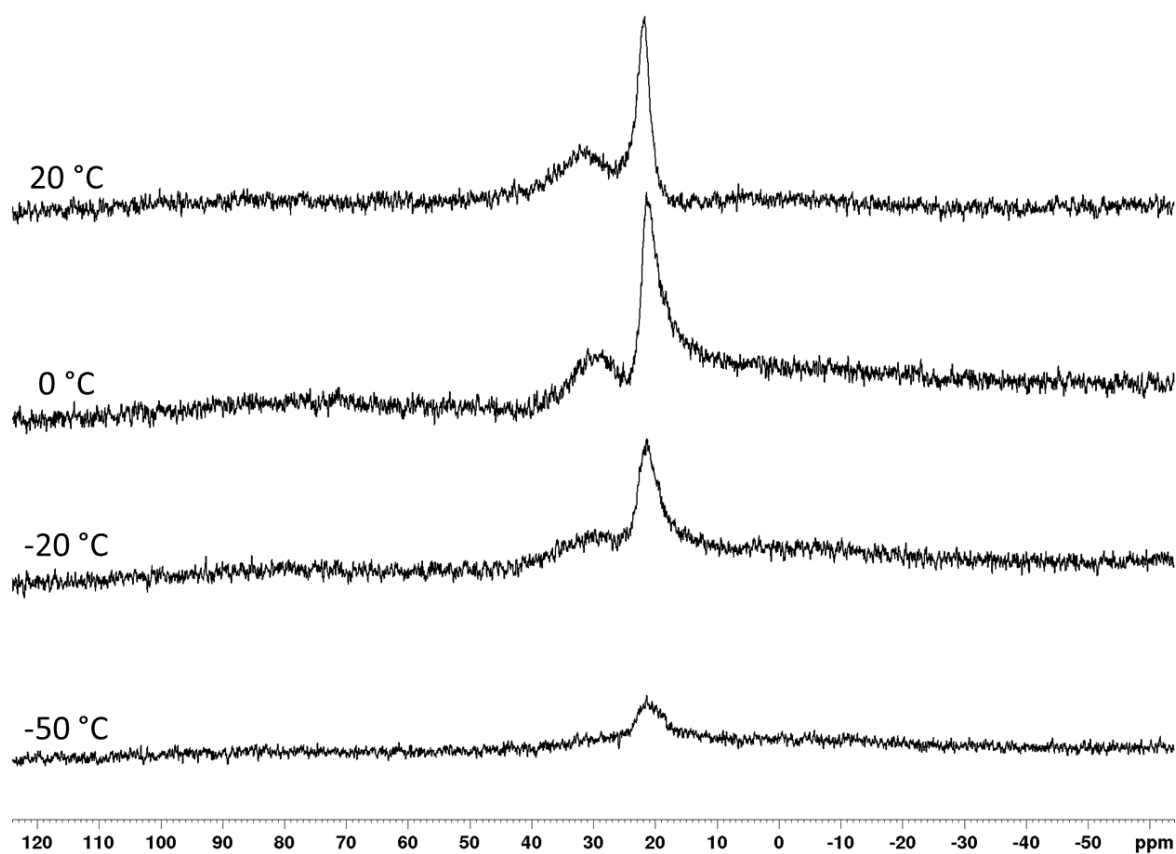
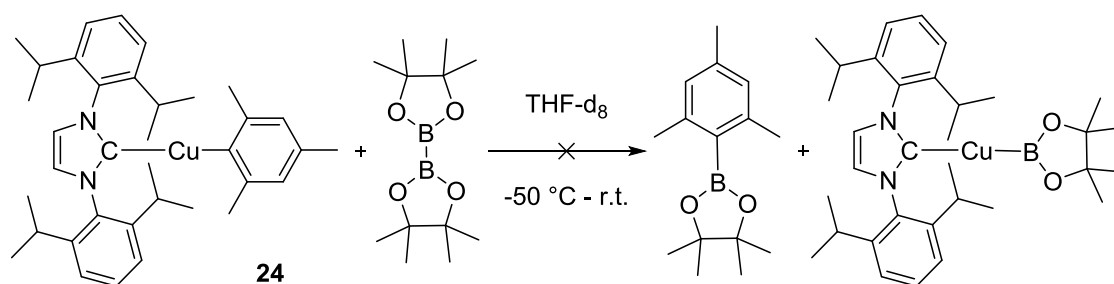


Figure 104: ^{11}B VT-NMR spectra of the reaction of $[\text{Cu}(\text{tBu}_2\text{Im})(\text{O}^t\text{Bu})]$ 16 with B_2pin_2 in toluene-d_8 .

Reaction of $[\text{Cu}(\text{Dipp}_2\text{Im})(\text{Mes})]$ with B_2pin_2 in THF-d_8 :



The ^1H NMR spectra showed the signals for the starting materials (Figure 105). Besides a temperature dependent shift, no changes were observed when warming the sample from $-50\text{ }^\circ\text{C}$ to room temperature. After 24 h at room temperature multiple new set of signals were observed, which could not be assigned to specific compounds.

At 30.8 ppm the ^{11}B NMR spectra showed the peak for the diboron compound from $-50\text{ }^\circ\text{C}$ to room temperature (Figure 106). After 6 h at room temperature another peak at 21.3 ppm was detected next to a broad peak of low intensity at around 41 ppm.

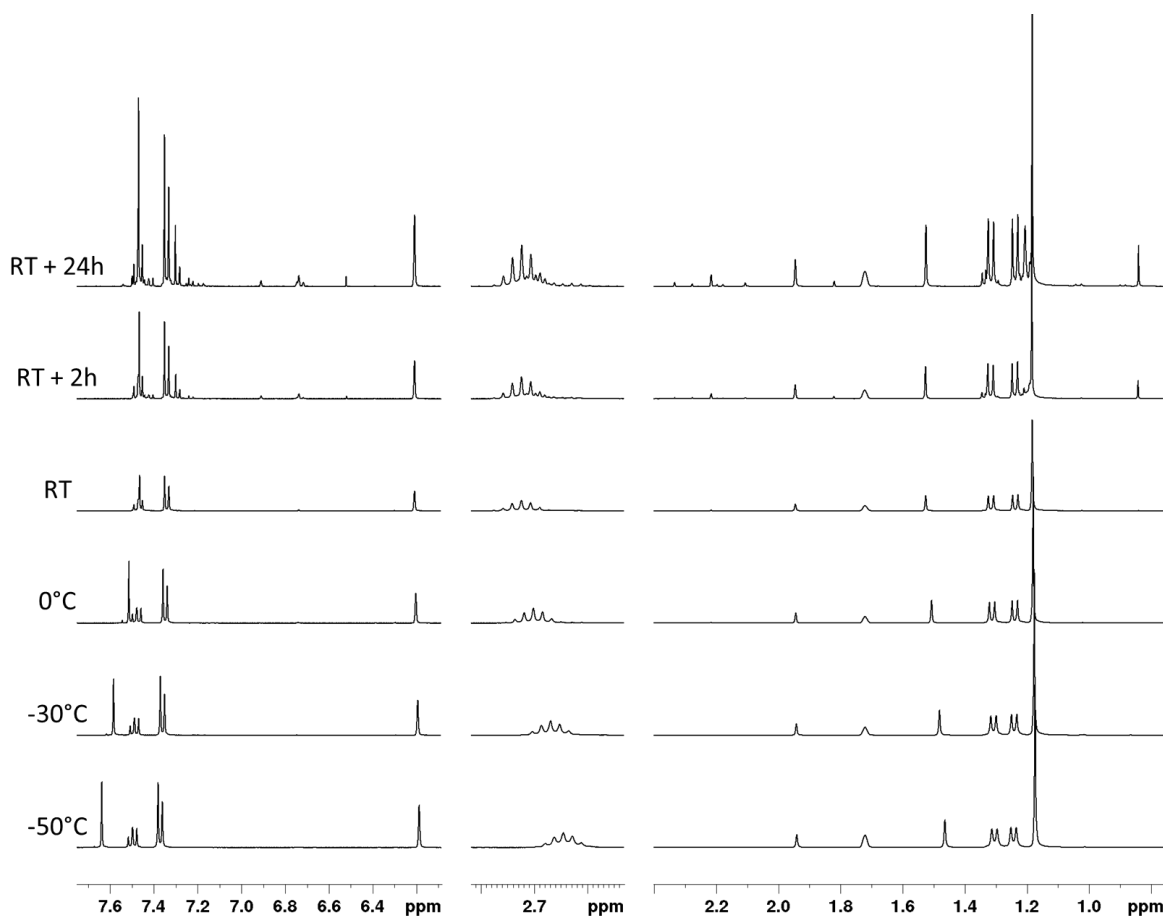


Figure 105: ^1H VT-NMR spectra of the reaction of $[\text{Cu}(\text{Dipp}_2\text{Im})(\text{Mes})]$ with B_2pin_2 in THF-d_8 .

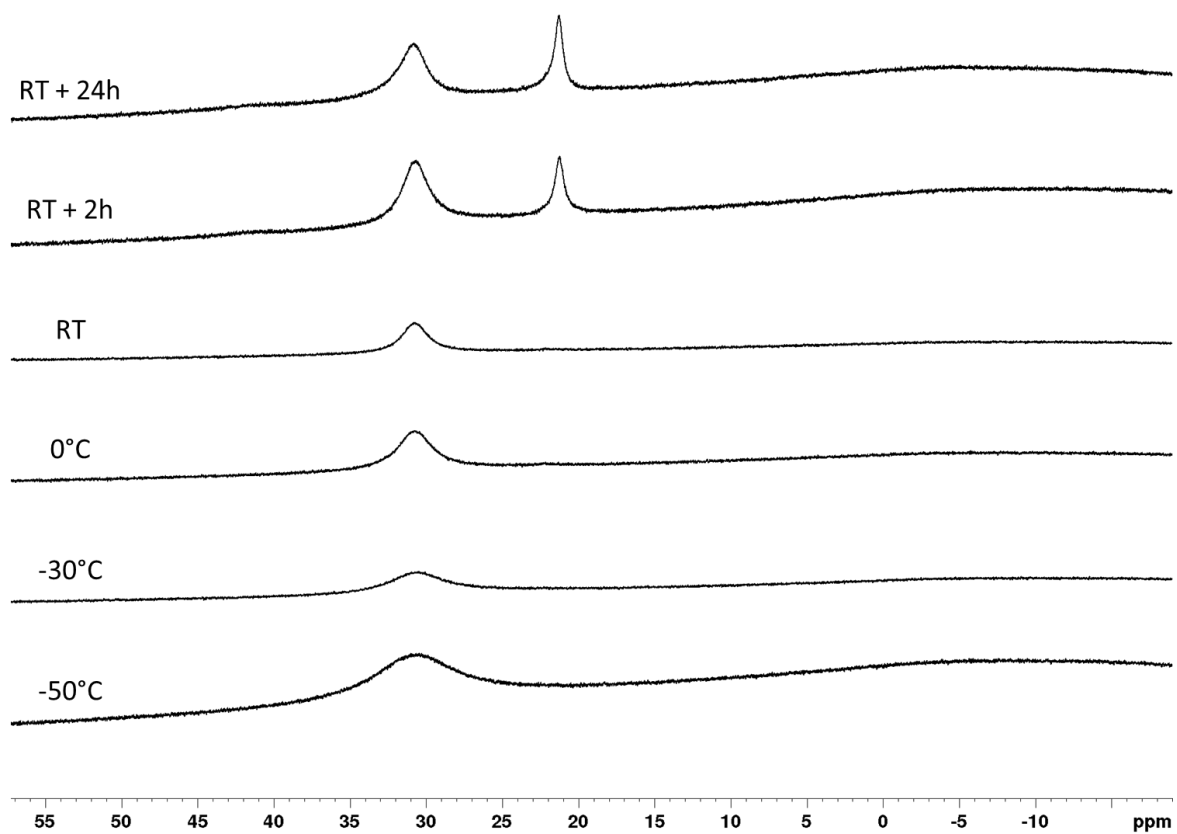
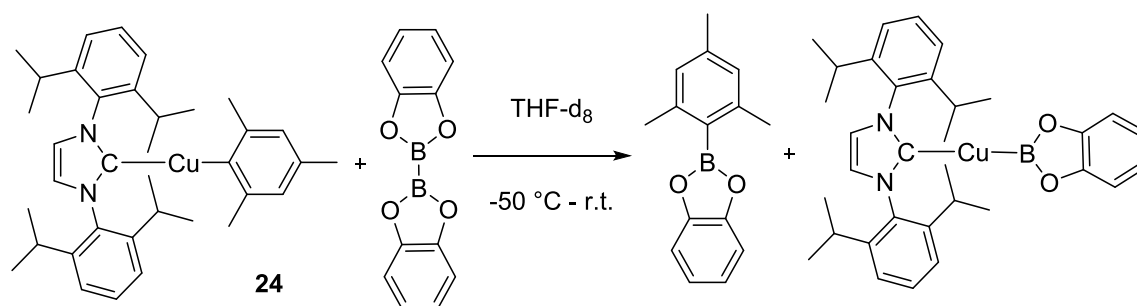


Figure 106: ^{11}B VT-NMR spectra of the reaction of $[\text{Cu}(\text{Dipp}_2\text{Im})(\text{Mes})]$ with B_2pin_2 in THF-d_8 .

Reaction of $[\text{Cu}(\text{Dipp}_2\text{Im})(\text{Mes})]$ with B_2cat_2 in THF-d_8 :



The ^1H NMR spectra at $-50\text{ }^\circ\text{C}$ showed the signals for the starting compounds (Figure 107). The ratio of the complex and the diboron compound is 1:0.35. From $-30\text{ }^\circ\text{C}$ on the growth of a new set of signals was observed. The new set of signal showed the same coupling patterns as the starting complex and the diboron compound albeit the shift are slightly different. In particular the aromatic protons of the biscatecholate diboron moiety and the methyl protons of the mesityl moiety showed significantly different chemical shifts, as one would expect for the new formed aryl boronic ester. Heating the sample accelerates the reaction. Calculated from the ratios of the mesityl protons of the different compounds the extent of reaction is 43% at a temperature of $-10\text{ }^\circ\text{C}$. After 12 hours at room temperature no signals for the methyl protons of the $[\text{Cu}(\text{Dipp}_2\text{Im})(\text{Mes})]$ complex were detected, indicating complete conversion. Albeit smaller changes in the spectra were observed after 24 hours at room temperature the formed boryl complex is relatively stable under the conditions applied.

In the ^{11}B VT-NMR spectra one broad peak was detected at $-50\text{ }^\circ\text{C}$ at 30.2 ppm (Figure 108). From $-30\text{ }^\circ\text{C}$ on an additional peak with a chemical shift of 14.5 ppm was observed in low intensity. At a temperature of $-10\text{ }^\circ\text{C}$ a new peak right next to the initial peak at 32.5 ppm indicates the formation of a new compound. From room temperature on another very broad peak was observed at 43.0 ppm, indicative of the copper-boryl formation, while the initial peak at 30.2 ppm was absent.

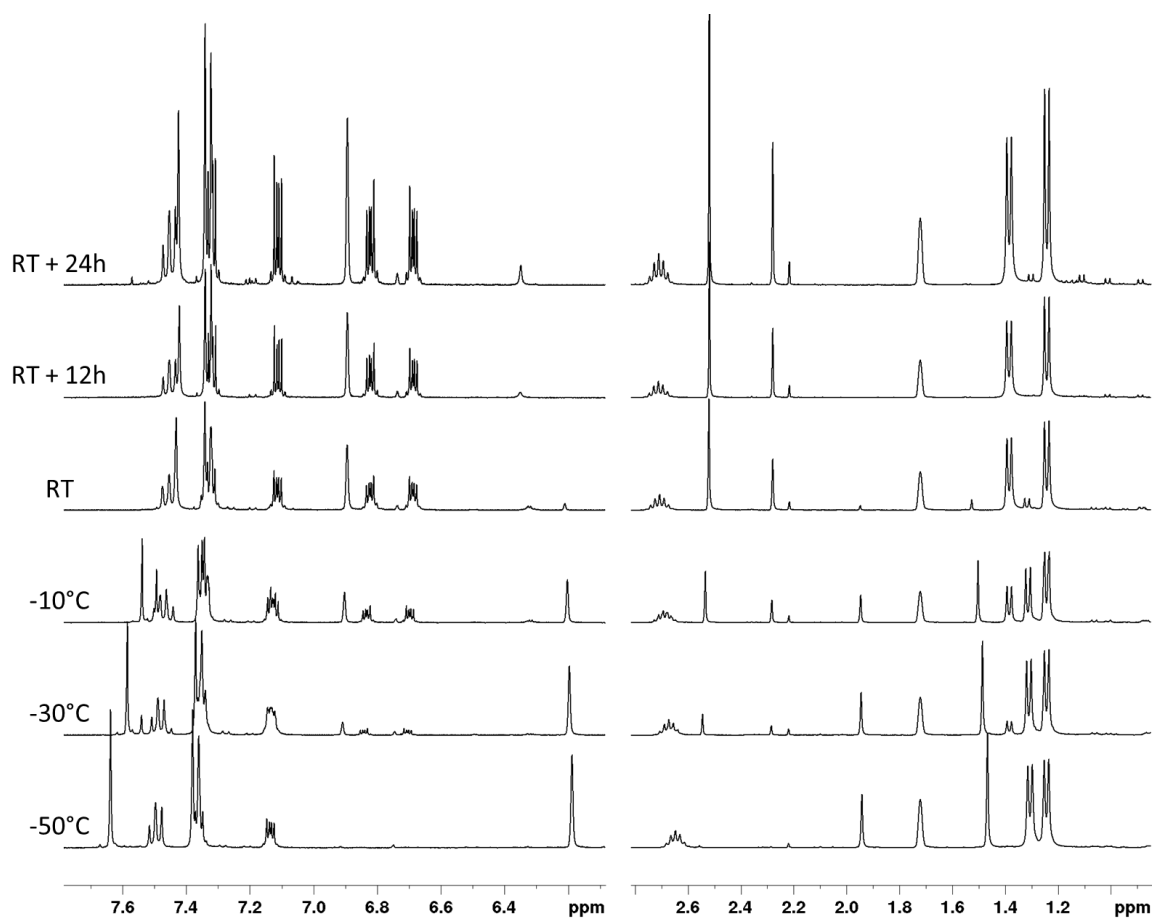


Figure 107: ^1H VT-NMR spectra of the reaction of $[\text{Cu}(\text{Dipp}_2\text{Im})(\text{Mes})]$ with B_2cat_2 in THF-d_8 .

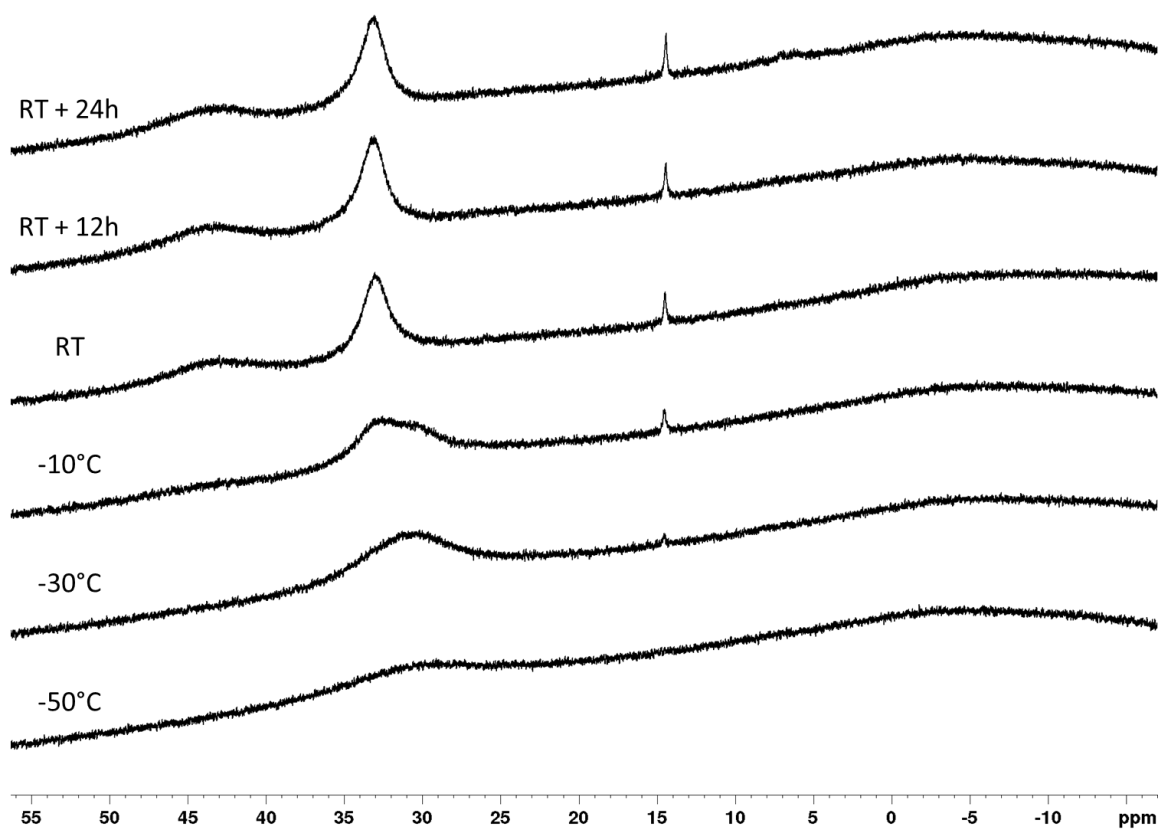
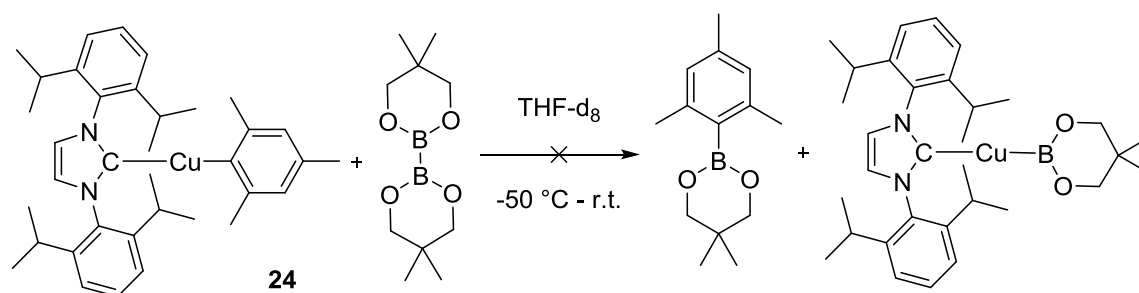


Figure 108: ^{11}B VT-NMR spectra of the reaction of $[\text{Cu}(\text{Dipp}_2\text{Im})(\text{Mes})]$ with B_2cat_2 in THF-d_8 .

Reaction of $[\text{Cu}(\text{Dipp}_2\text{Im})(\text{Mes})]$ with B_2neop_2 in THF-d_8 :



The ^1H VT-NMR spectra showed the signals for both starting materials until the sample was kept at room temperature for 24 h, when new signals started to appear (Figure 109). Albeit more than one new set of signals was observed the experiment looks promising and should be investigated at higher temperature or kept longer at room temperature to observe the new signals in higher intensities.

In the ^{11}B VT-NMR spectra the resonance for the starting material was observed at 27.7 ppm until at a temperature of 0 °C a new peak was detected with a chemical shift of 17.6 ppm (Figure 110).

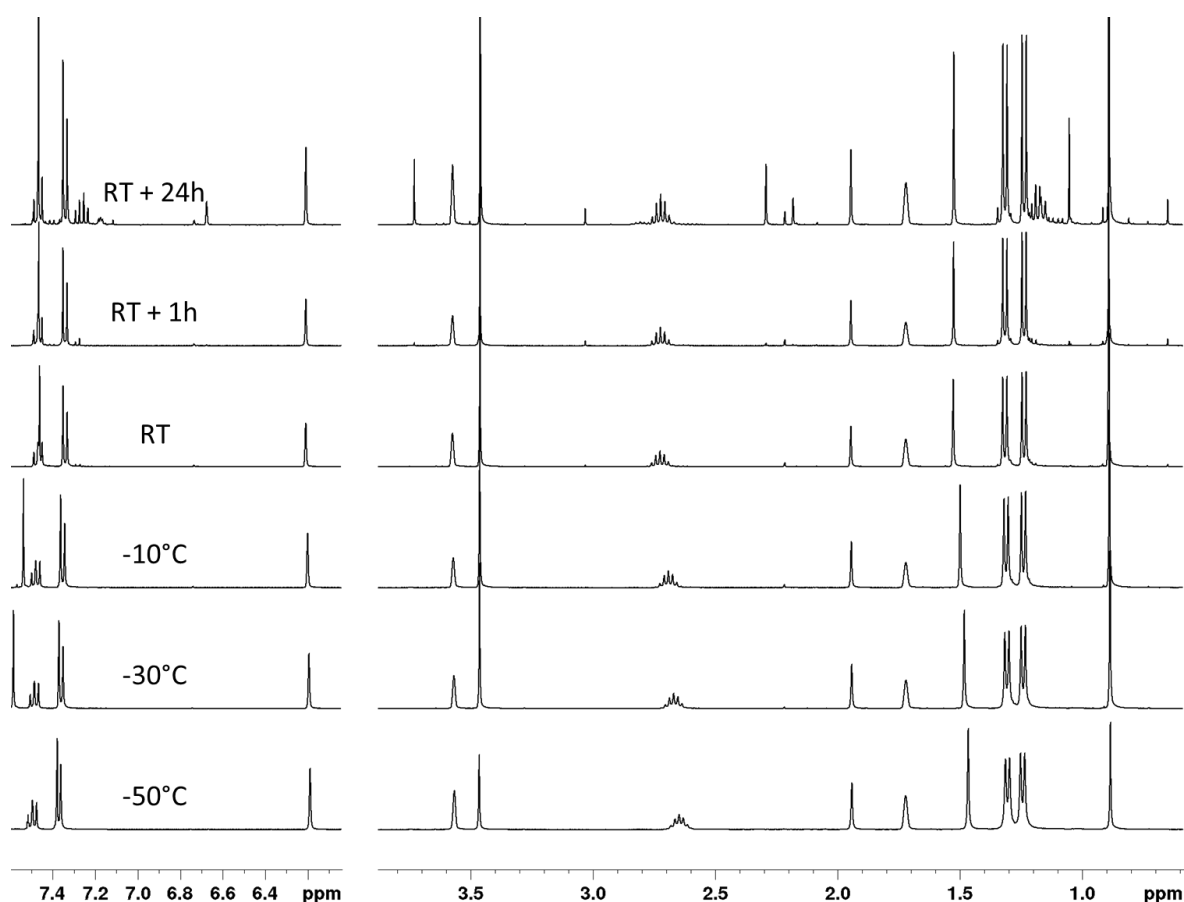


Figure 109: ^1H VT-NMR spectra of the reaction of $[\text{Cu}(\text{Dipp}_2\text{Im})(\text{Mes})]$ with B_2neop_2 in THF-d_8 .

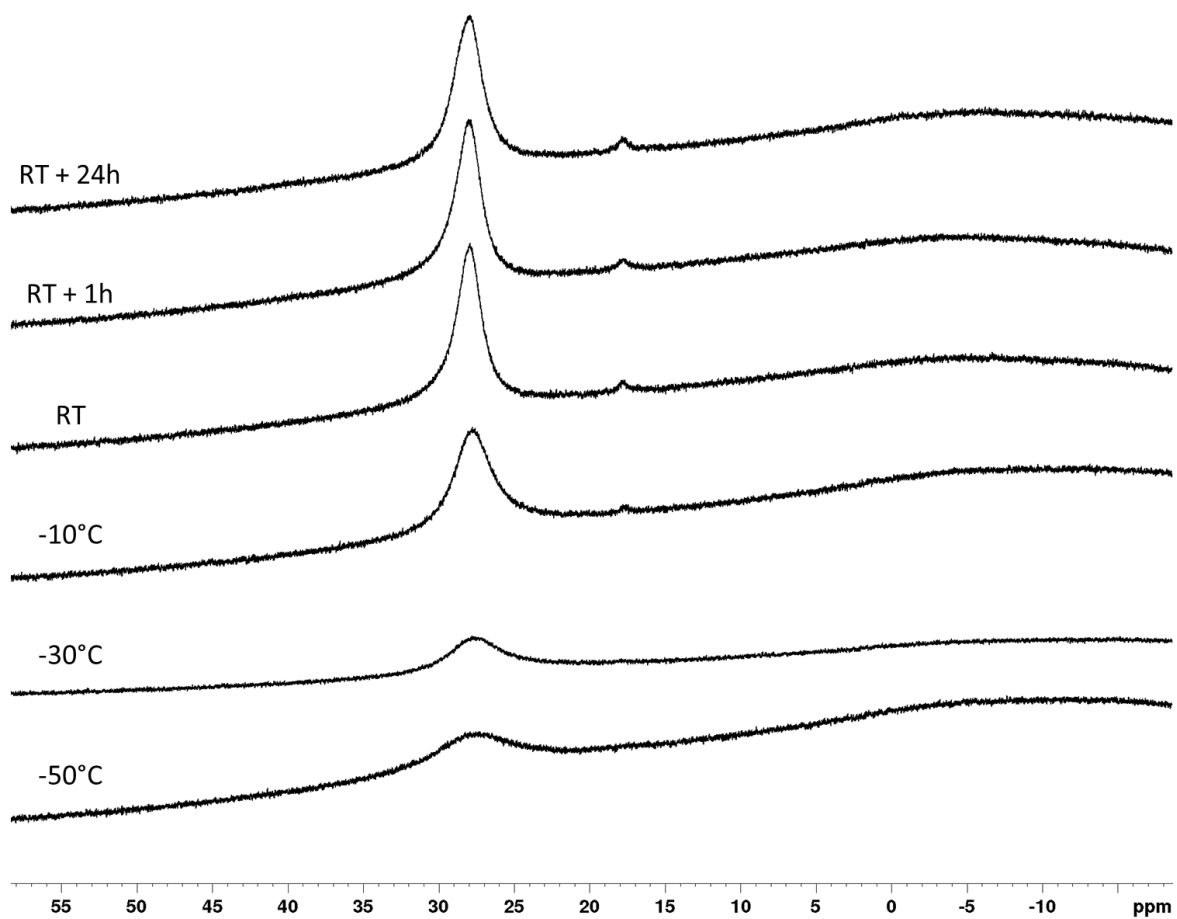
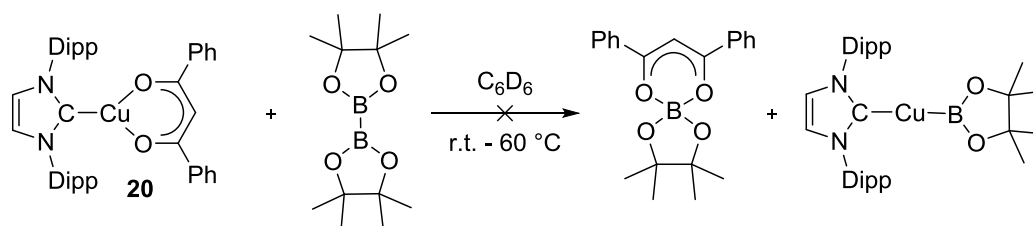


Figure 110: ^{11}B VT-NMR spectra of the reaction of $[\text{Cu}(\text{Dipp}_2\text{Im})(\text{Mes})]$ with B_2neop_2 in THF-d_8 .

Reaction of [Cu(Dipp₂Im)(DBM)] with B₂pin₂ in C₆D₆:



The reaction of complex [Cu(Dipp₂Im)(DBM)] **20** with B₂pin₂ showed only the peaks for the starting material in the ¹H as well as the ¹¹B NMR spectrum (Figures 111 and 112). The ratio of the complex and the diboron compound was 1:2.4. Heating the sample to 60 °C for 4 h afforded the growth of a new peak in the ¹¹B NMR spectra at 21.8 ppm. In the ¹H NMR spectra the ratio of the complex to the diboron compound increased to 1: 2.1 but no other changes were detected. After another 20 h at 60 °C, which turned the reddish solution into a green suspension with black precipitates and a copper mirror, no starting material in the ¹¹B NMR was detected but the intensity of peak at 21.8 ppm increased. However, no significant changes in the ¹H NMR spectrum were observed besides the fact that the ratio of the complex to the diboron compound increased to 1:1.19.

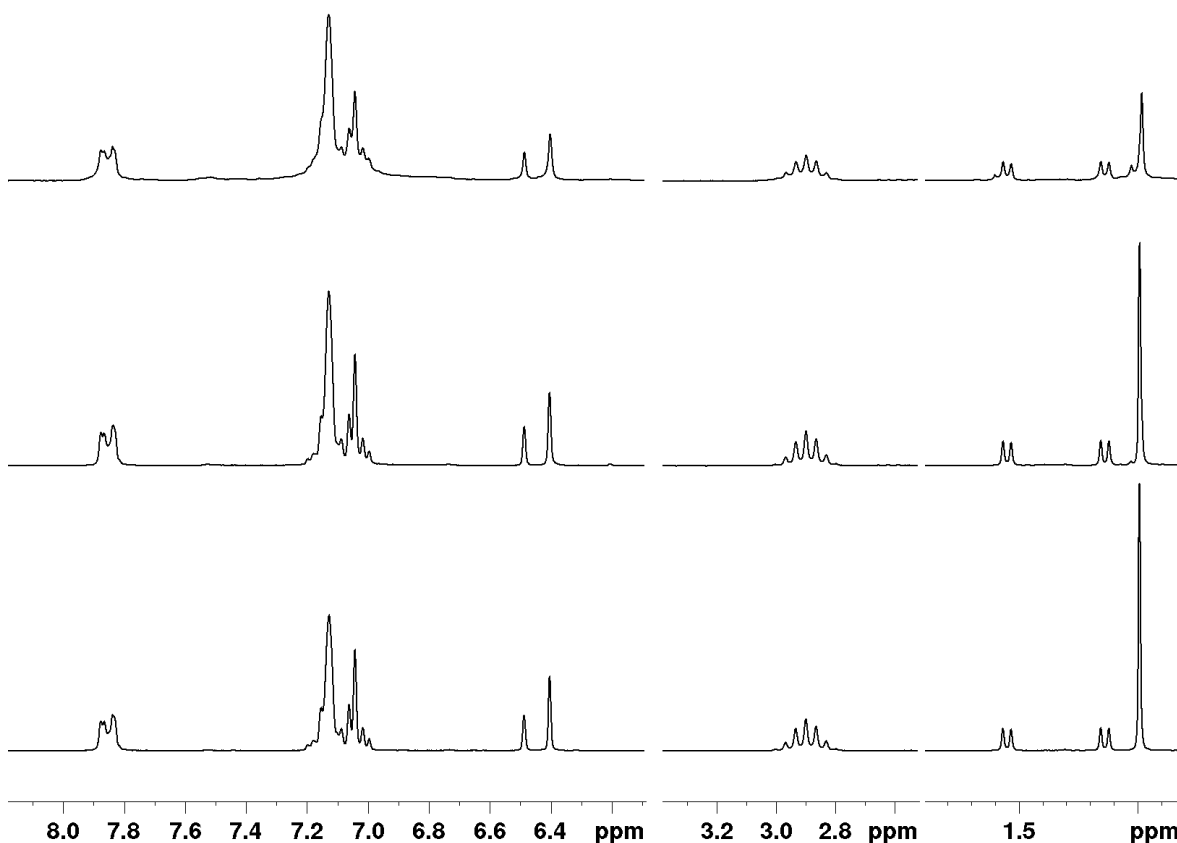


Figure 111: ¹H NMR spectra of the reaction of [Cu(Dipp₂Im)(DBM)] **20** with B₂pin₂ in C₆D₆ at r.t. Bottom: After 1 min at room temperature. Middle: After 4 h at 60 °C. Top: After 24 h at 60 °C.

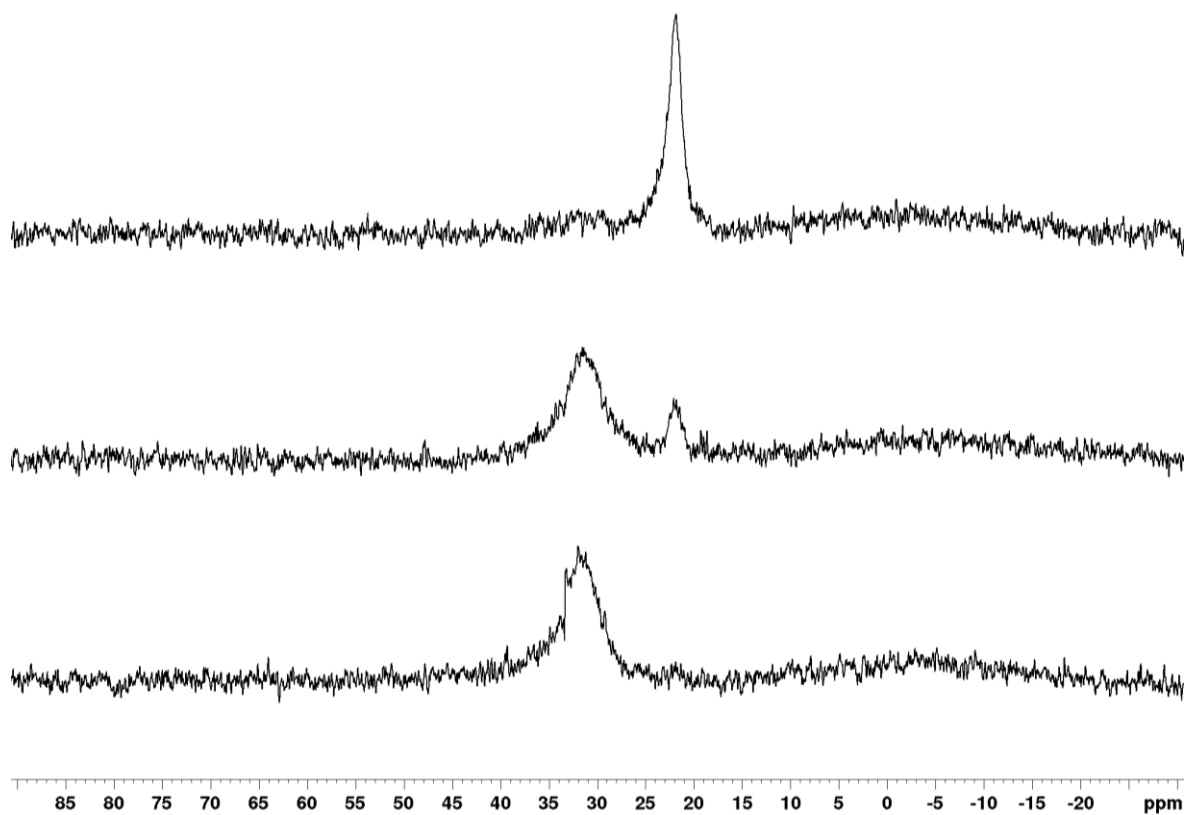
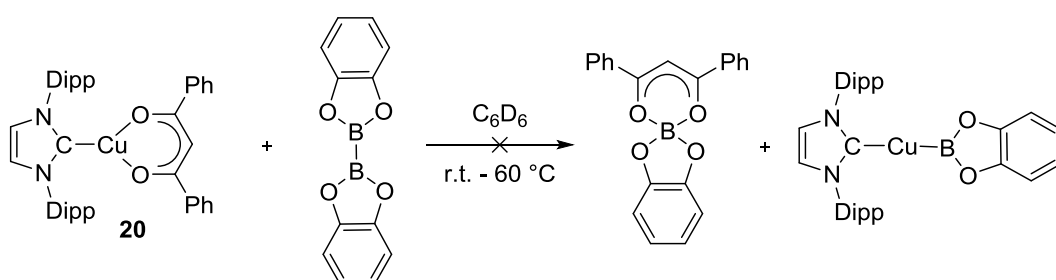


Figure 112: ^{11}B NMR spectra of the reaction of $[\text{Cu}(\text{Dipp}_2\text{Im})(\text{DBM})]$ 20 with B_2pin_2 in C_6D_6 at r.t. Bottom: After 1 min at room temperature. Middle: After 4 h at 60 °C. Top: After 24 h at 60 °C.

Reaction of [Cu(Dipp₂Im)(DBM)] with B₂cat₂ in C₆D₆:



Complex **20** and B₂cat₂ afforded an orange solution which turned into a yellow suspension within 5 min at room temperature. The ¹H NMR spectrum (see Figures 113 and 115) showed the starting complex and a new one in a 1:2.9 ratio. The ratio of two multiplets typical for the catecholate protons at 6.64 and 6.37 ppm with the new complex is 1:0.6.

The ¹¹B NMR spectrum (see Figure 114) showed two peaks at 14.7 and 10.7 ppm. Albeit [Bcat₂]⁻ moieties have been observed with chemical shifts of 15.2 ppm in CD₂Cl₂, the poor solubility of salts in C₆D₆ suggests a different species.^[342] Since the spectra did not change within the next hour at room temperature the sample was heated to 60 °C for 2 h. In the ¹H NMR spectrum a ratio of starting complex to new complex of 1:3.8 was observed and a new septet of low intensity and a chemical shift of 2.47 ppm was detected. The ¹¹B NMR spectrum remained unchanged. The next 24 h at 60 °C did not show significant changes in the ¹H and ¹¹B NMR spectra.

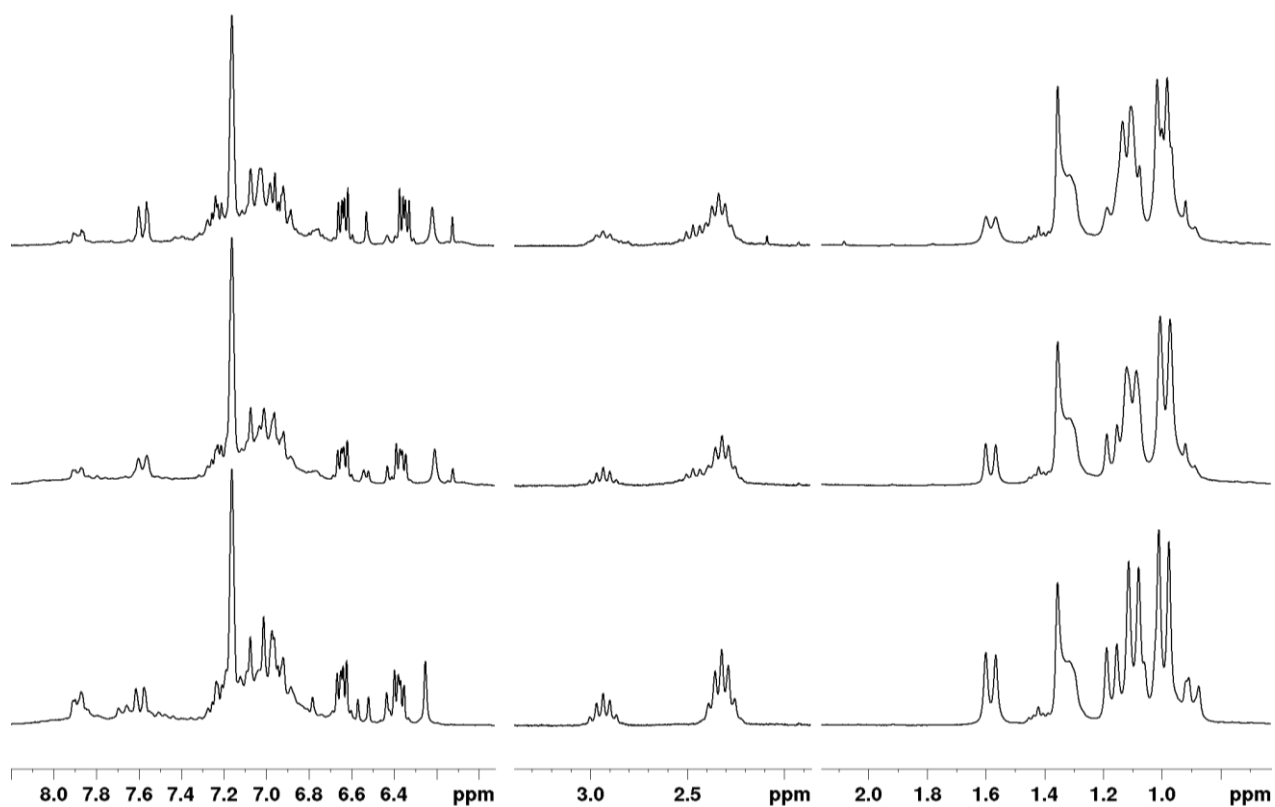


Figure 113: ^1H NMR spectra of the reaction of $[\text{Cu}(\text{Dipp}_2\text{Im})(\text{DBM})]$ 20 with B_2cat_2 in C_6D_6 at r.t. Bottom: After 3 min at room temperature. Middle: After 2 h at 60 °C. Top: After 24 h at 60 °C.

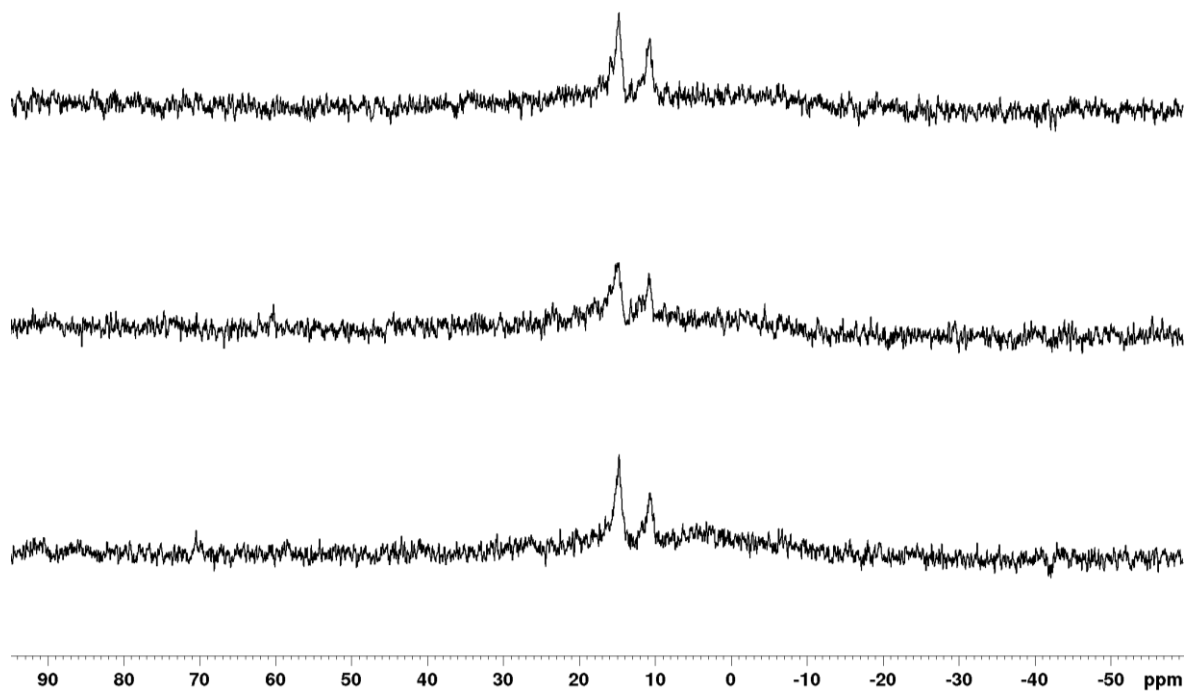


Figure 114: ^{11}B NMR spectra of the reaction of $[\text{Cu}(\text{Dipp}_2\text{Im})(\text{DBM})]$ 20 with B_2cat_2 in C_6D_6 at r.t. Bottom: After 1 min at room temperature. Middle: After 2 h at 60 °C. Top: After 24 h at 60 °C.

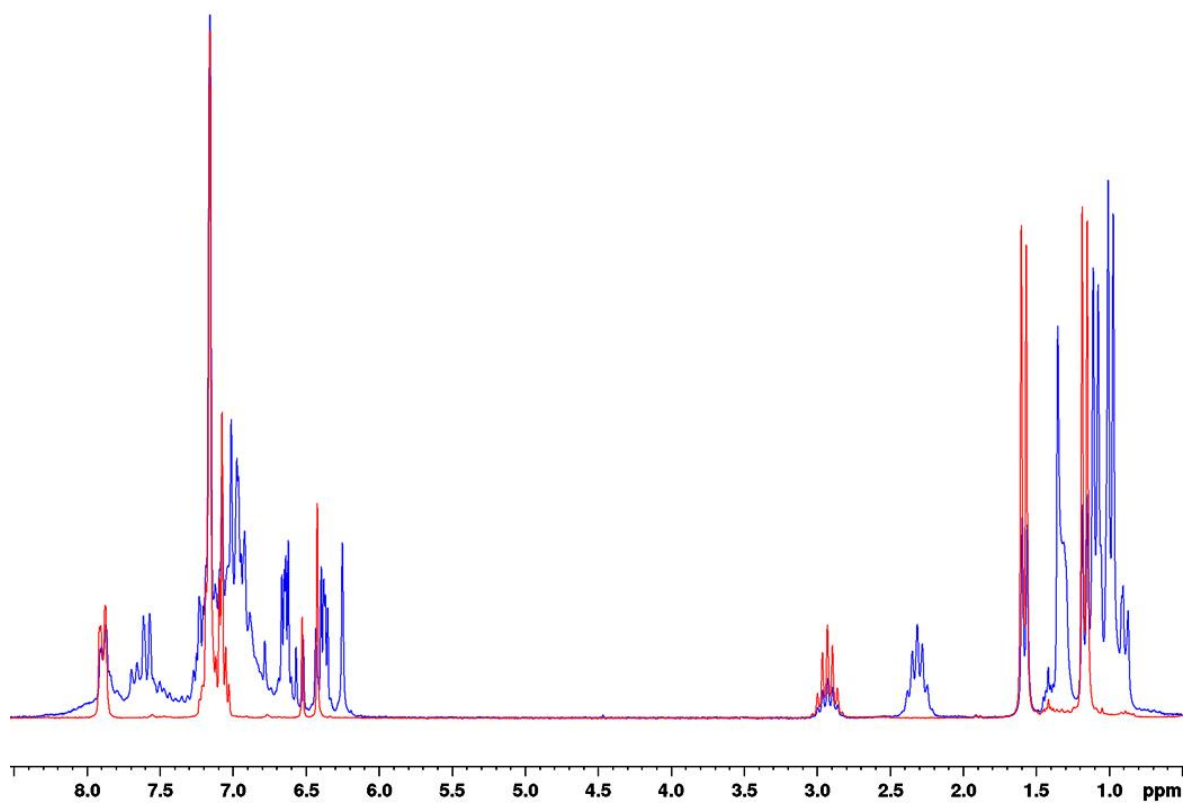
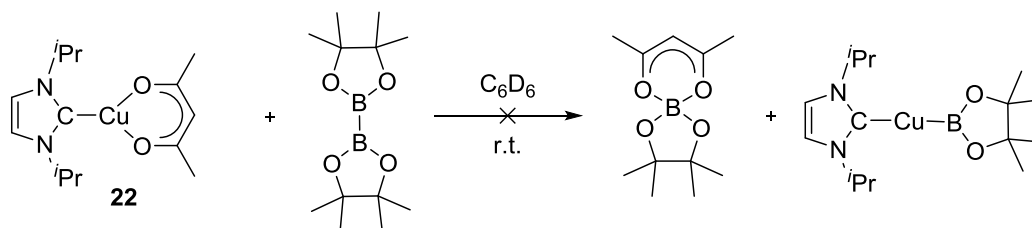


Figure 115: Overlay of the ¹H NMR spectrum of complex [Cu(Dipp₂Im)(DBM)] 20 (red) and the *in situ* ¹H NMR spectrum of the reaction of [Cu(Dipp₂Im)(DBM)] with B₂cat₂ in C₆D₆ at room temperature after 3 min (blue).

Reaction of $[\text{Cu}(i\text{Pr}_2\text{Im})(\text{acac})]$ with B_2pin_2 in C_6D_6 :



The ^1H NMR spectrum of the reddish solution after 5 minutes at room temperature showed mainly broadened signals with chemical shifts identical with those found for the starting complex $[\text{Cu}(i\text{Pr}_2\text{Im})(\text{acac})]$ **22** next to a singlet for B_2pin_2 (Figure 116). It is noteworthy that the ratio of the signals of the NHC ligand and the acac moiety was 1:0.7, indicating that complex is not intact anymore despite the fact that the resonances do match those of **22** almost perfectly (Figure 118). After 1 hour at room temperature the signals for the $i\text{Pr}_2\text{Im}$ ligand were detected as broad signals. The signals for the acac moiety almost disappeared and a new singlet at 1.50 ppm was detected. After 6 h at room temperature no signals for the acac moiety were detected. The ratio of the septet of ligand and the signal at 1.50 ppm is 1:6.3.

In the ^{11}B NMR spectrum a signal for B_2pin_2 at 31.6 ppm was detected next to a peaks at 21.8 and a sharp peak 3.6 ppm. Six hours later only the peak 21.8 ppm prevails and a new peak at 10.2 ppm was detected (Figure 117).

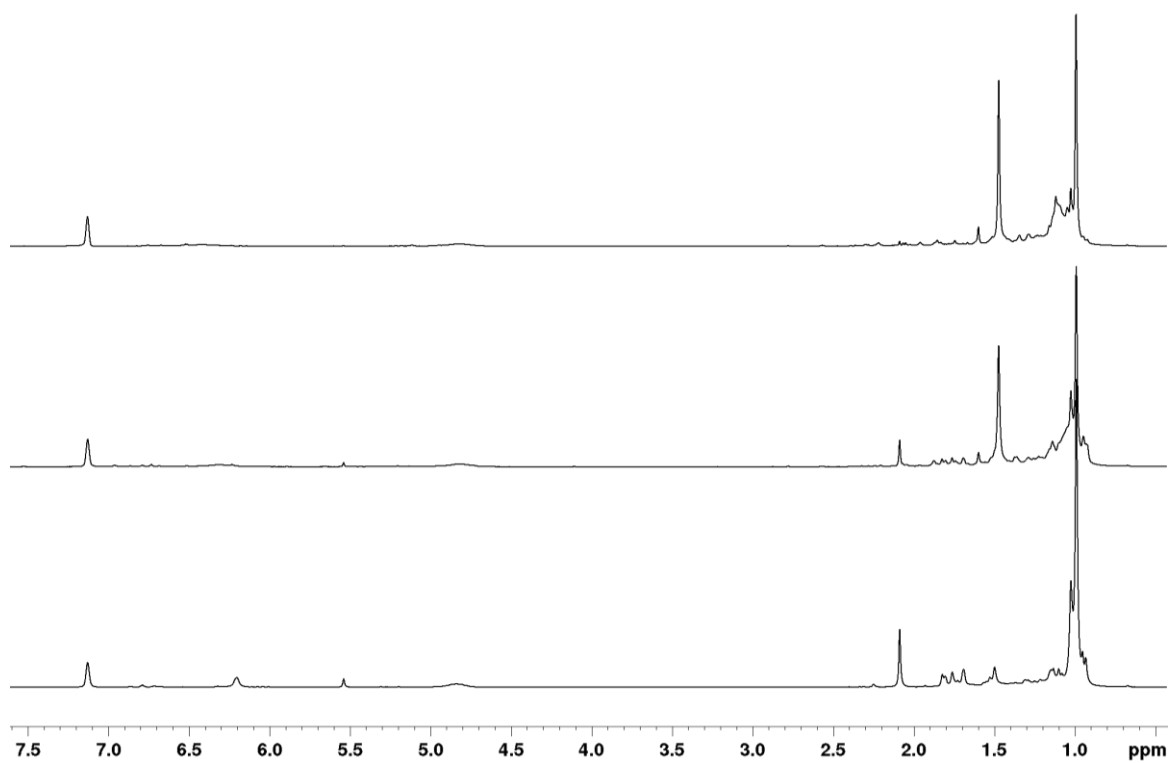


Figure 116: ^1H NMR spectra of the reaction of $[\text{Cu}(^i\text{Pr}_2\text{Im})(\text{acac})]$ 20 with B_2pin_2 in C_6D_6 at r.t. Bottom: After 5 min at room temperature. Middle: After 1 h at r.t. Top: After 6 h at r.t.

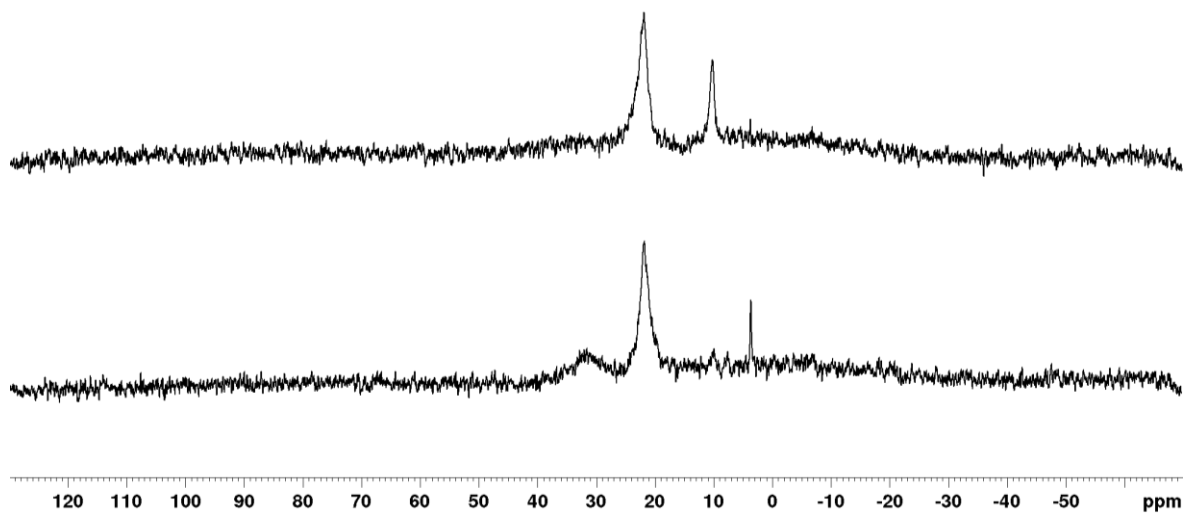


Figure 117: ^{11}B NMR spectra of the reaction of $[\text{Cu}(^i\text{Pr}_2\text{Im})(\text{acac})]$ 20 with B_2pin_2 in C_6D_6 at r.t. Bottom: After 5 min at room temperature. Top: After 6 h at r.t.

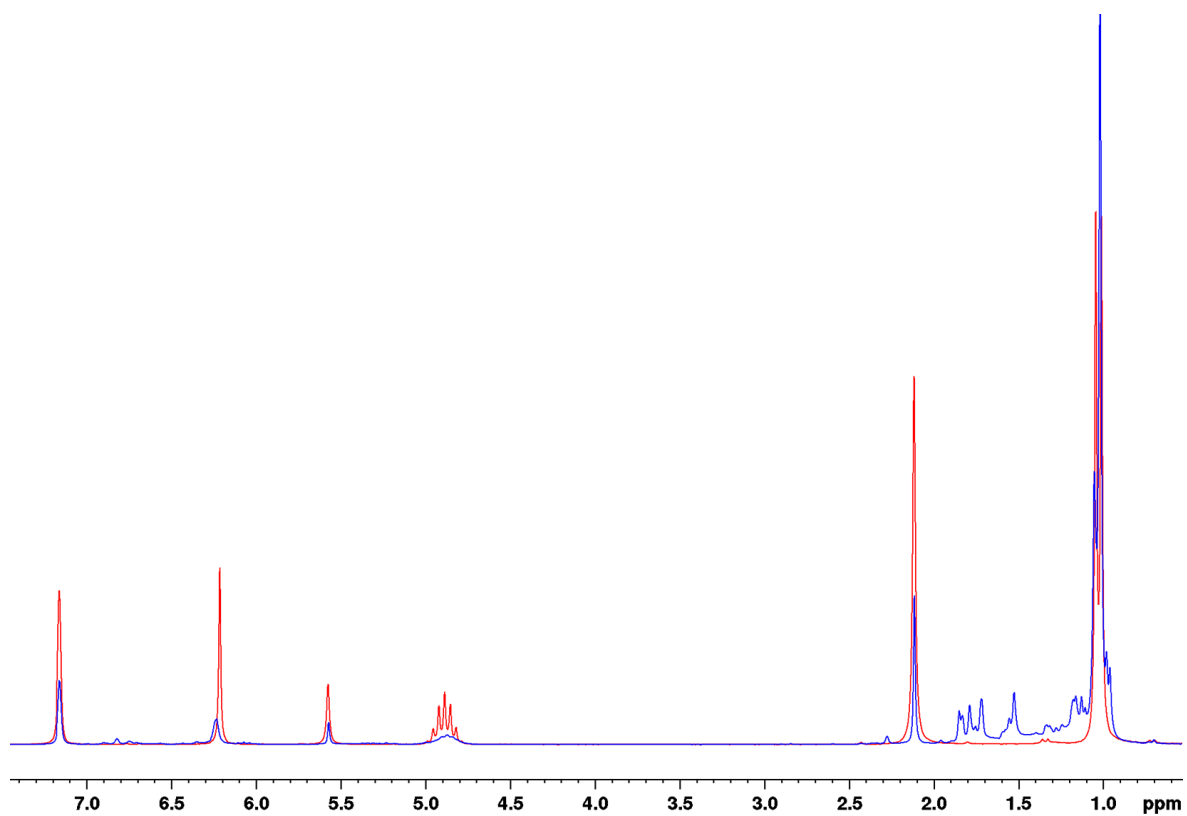


Figure 118: Overlay of the ^1H NMR spectrum of complex $[\text{Cu}(\text{iPr}_2\text{Im})(\text{acac})]$ 22 (red) and the *in situ* ^1H NMR spectrum of the reaction of $[\text{Cu}(\text{iPr}_2\text{Im})(\text{acac})]$ with B_2pin_2 in C_6D_6 at room temperature after 5 min (blue).

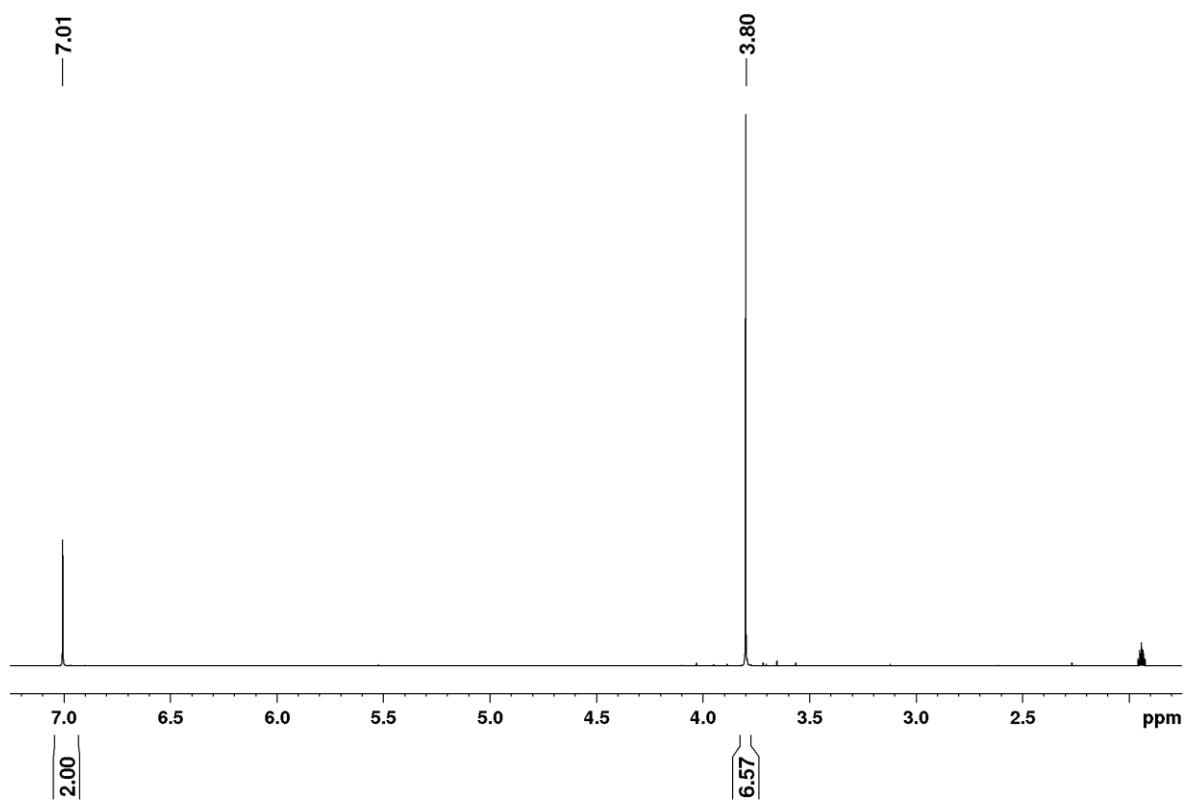


Figure 119: ^1H NMR spectrum (300 MHz) of $[\text{Cu}(\text{Me}_2\text{Im})_2\text{Cl}]$ 5 in CD_3CN .

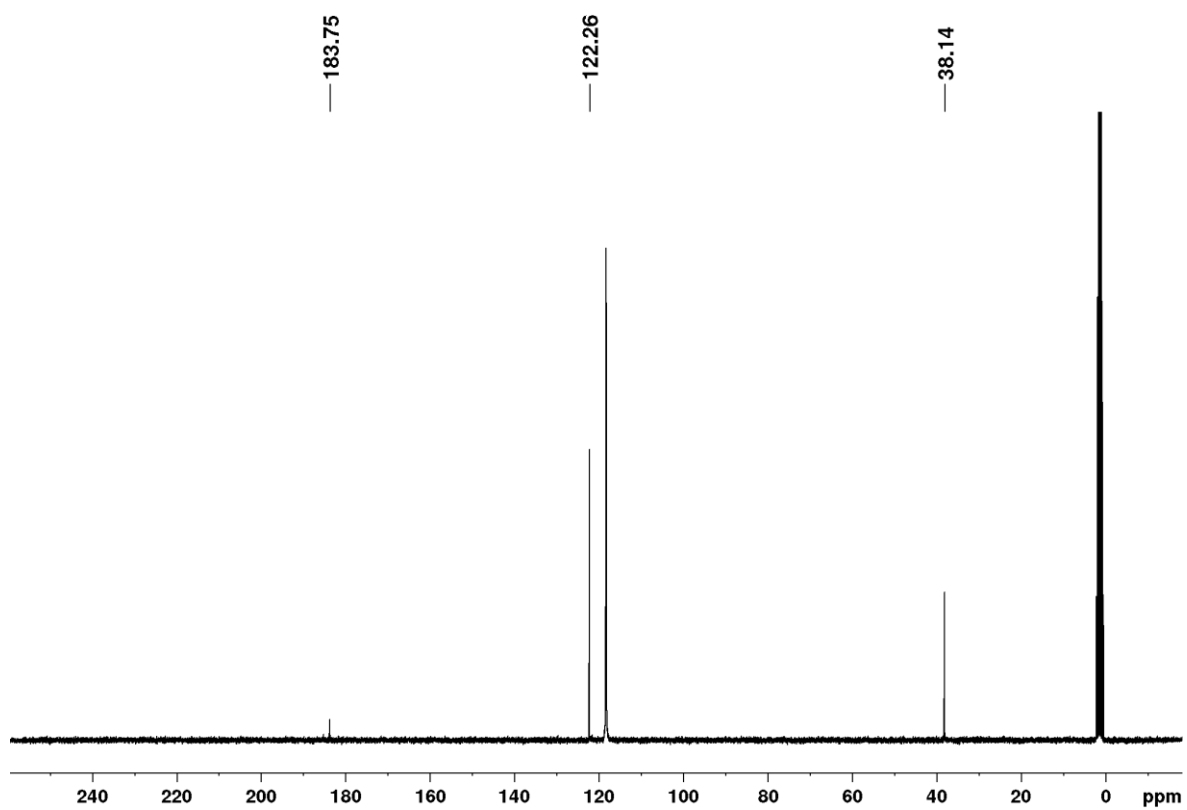
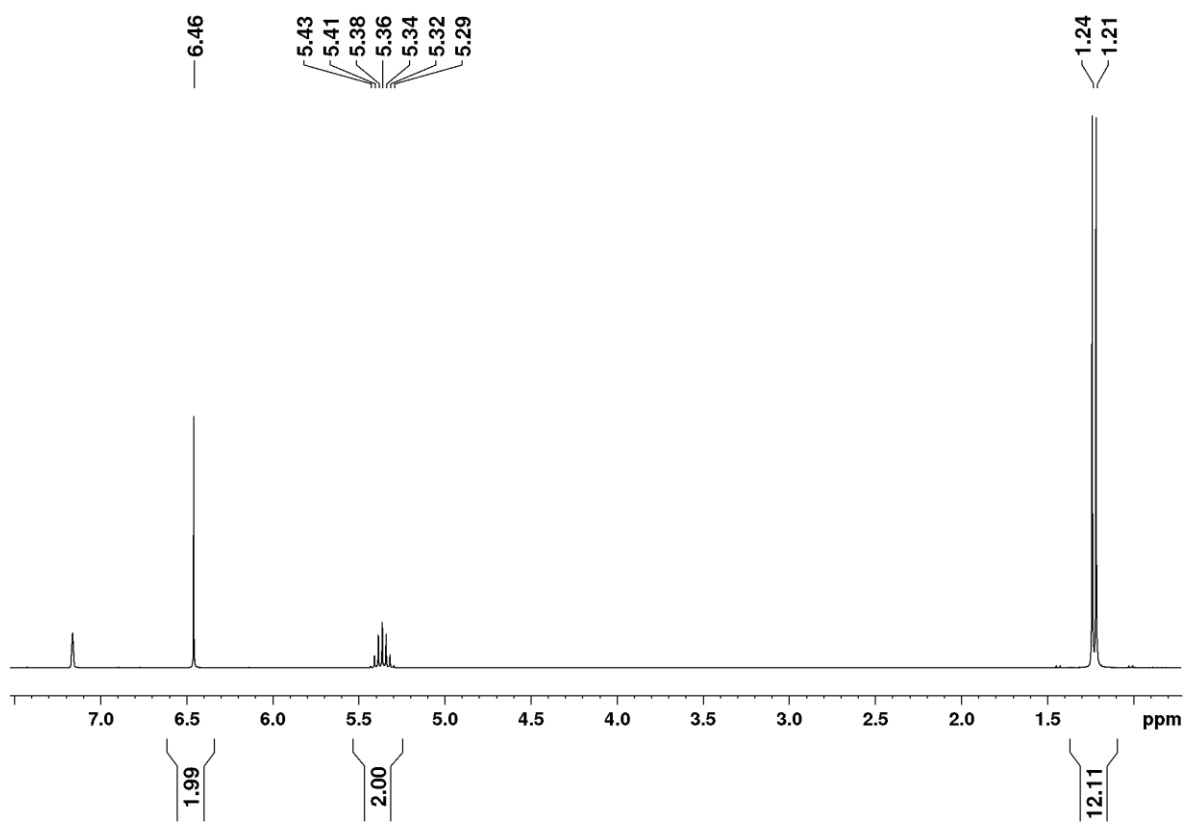
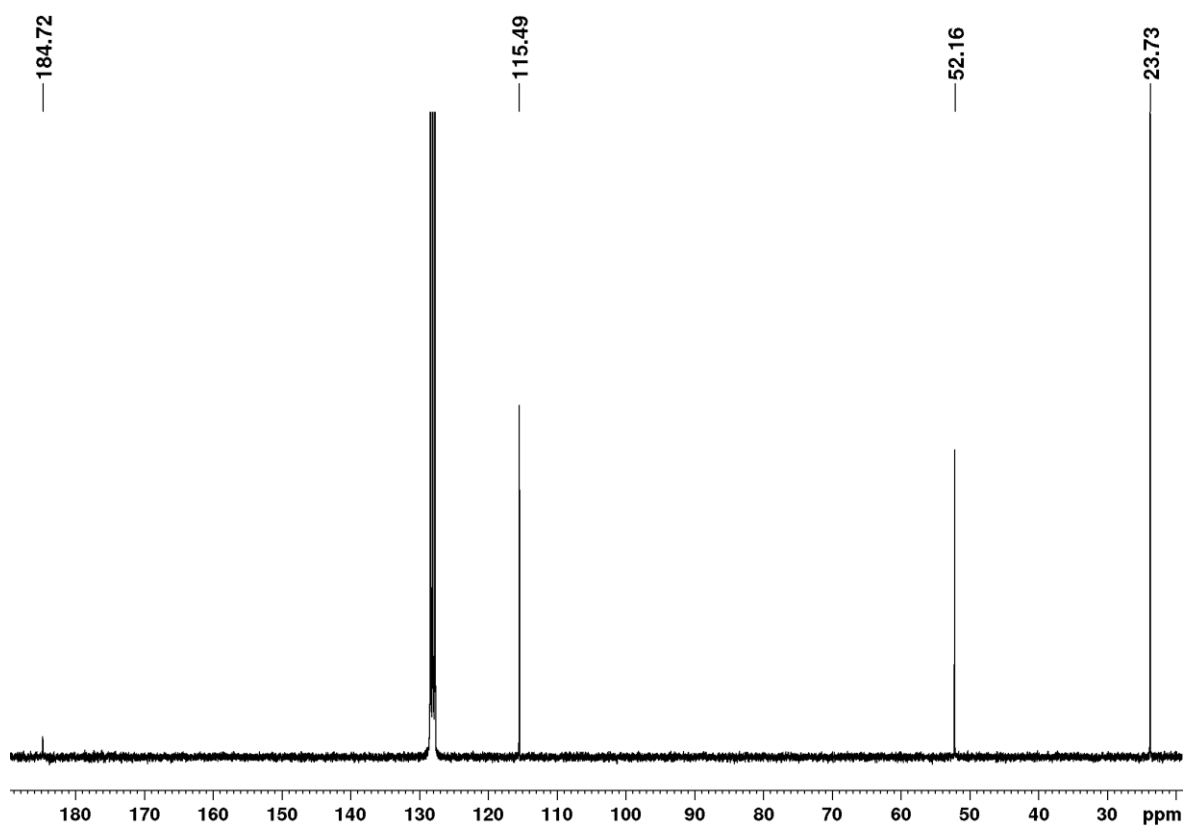


Figure 120: $^{13}\text{C}\{^1\text{H}\}$ NMR spectrum (75 MHz) of $[\text{Cu}(\text{Me}_2\text{Im})_2\text{Cl}]$ 5 in CD_3CN .

Figure 121: ^1H NMR spectrum (300 MHz) of $[\text{Cu}(\text{iPr}_2\text{Im})_2\text{Cl}]$ 6 in C_6D_6 .Figure 122: $^{13}\text{C}\{^1\text{H}\}$ NMR spectrum (75 MHz) of $[\text{Cu}(\text{iPr}_2\text{Im})_2\text{Cl}]$ 6 in C_6D_6 .

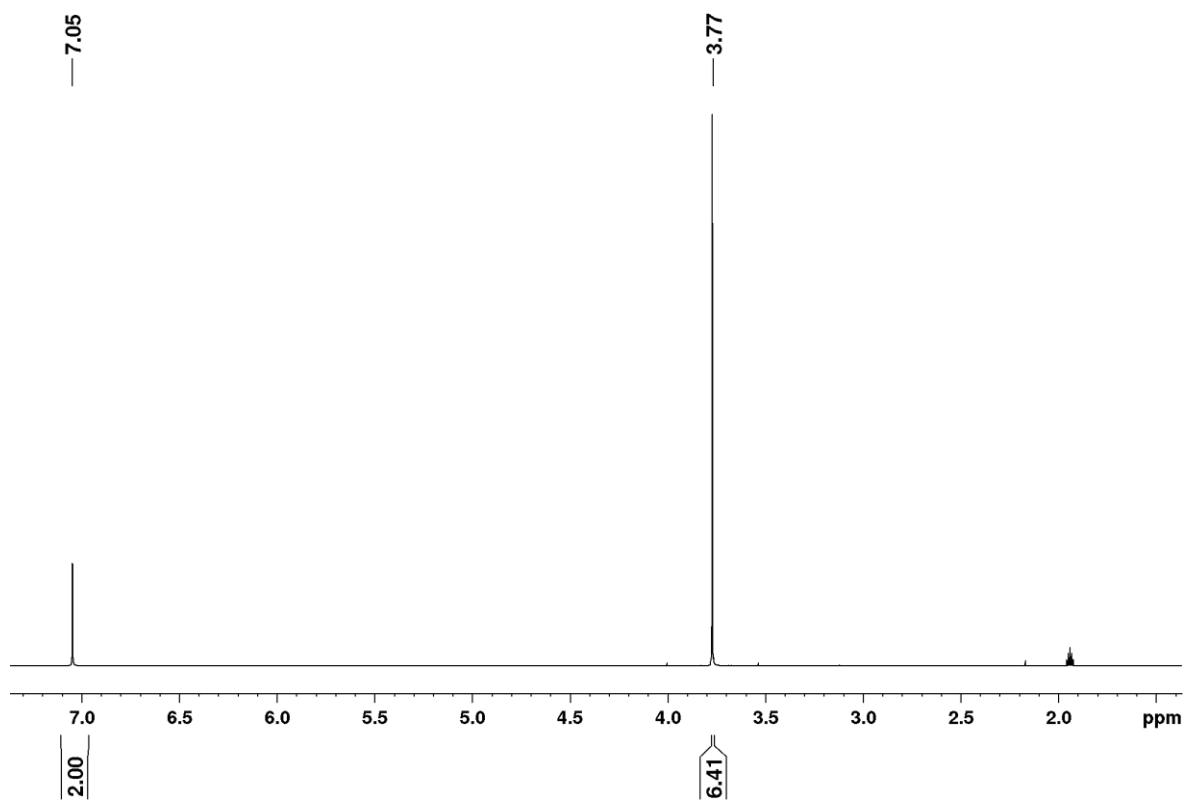


Figure 123: ^1H NMR spectrum (300 MHz) of $[\text{Cu}(\text{Me}_2\text{Im})_2]^+[\text{CuCl}_2]^-$ 8 in CD_3CN .

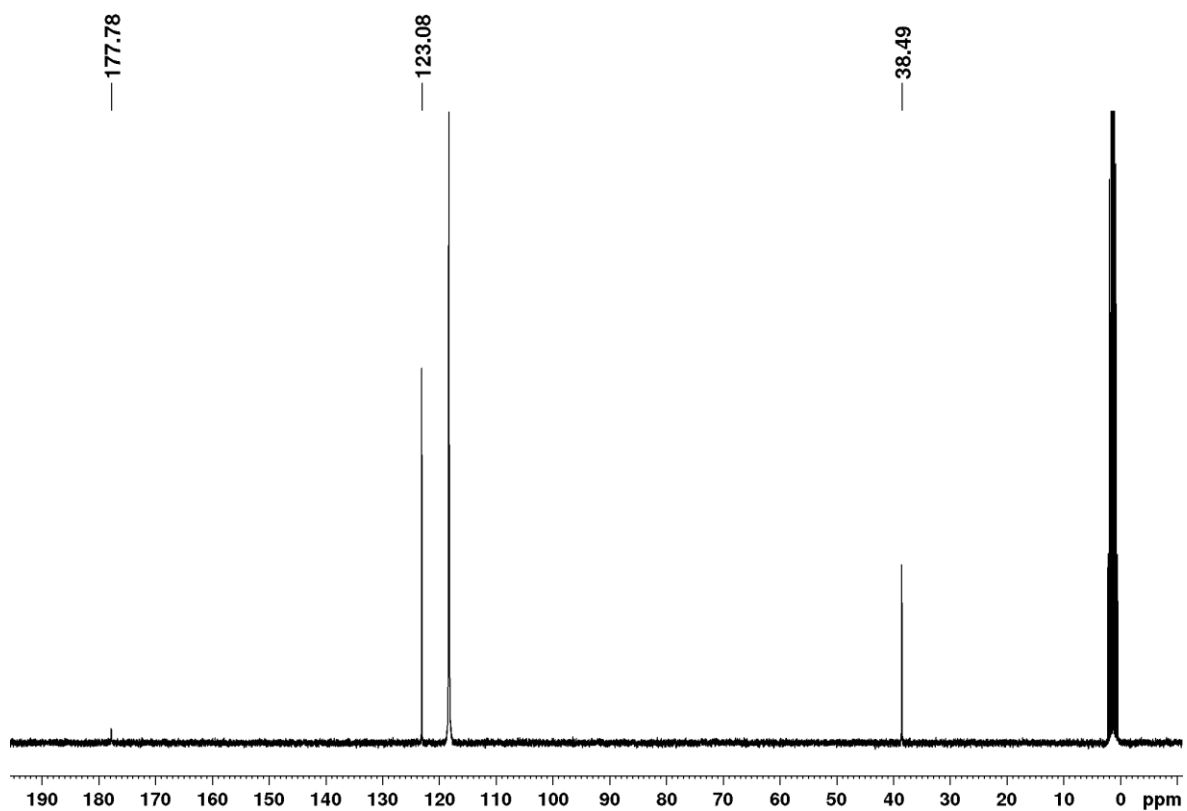


Figure 124: $^{13}\text{C}\{^1\text{H}\}$ NMR spectrum (75 MHz) of $[\text{Cu}(\text{Me}_2\text{Im})_2]^+[\text{CuCl}_2]^-$ 8 in CD_3CN .

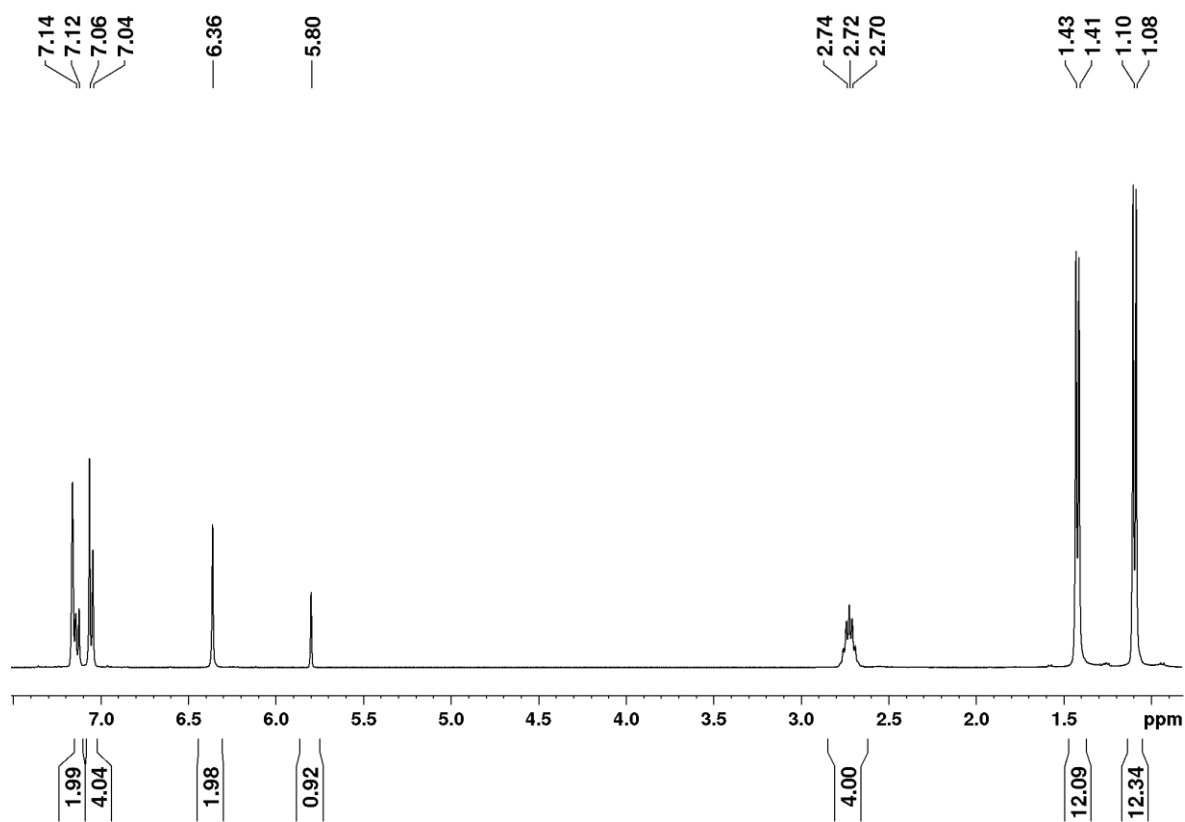


Figure 125: ^1H NMR spectrum (200 MHz) of $[\text{Cu}(\text{Dipp}_2\text{Im})(\text{hfacac})]$ 19 in C_6D_6 .

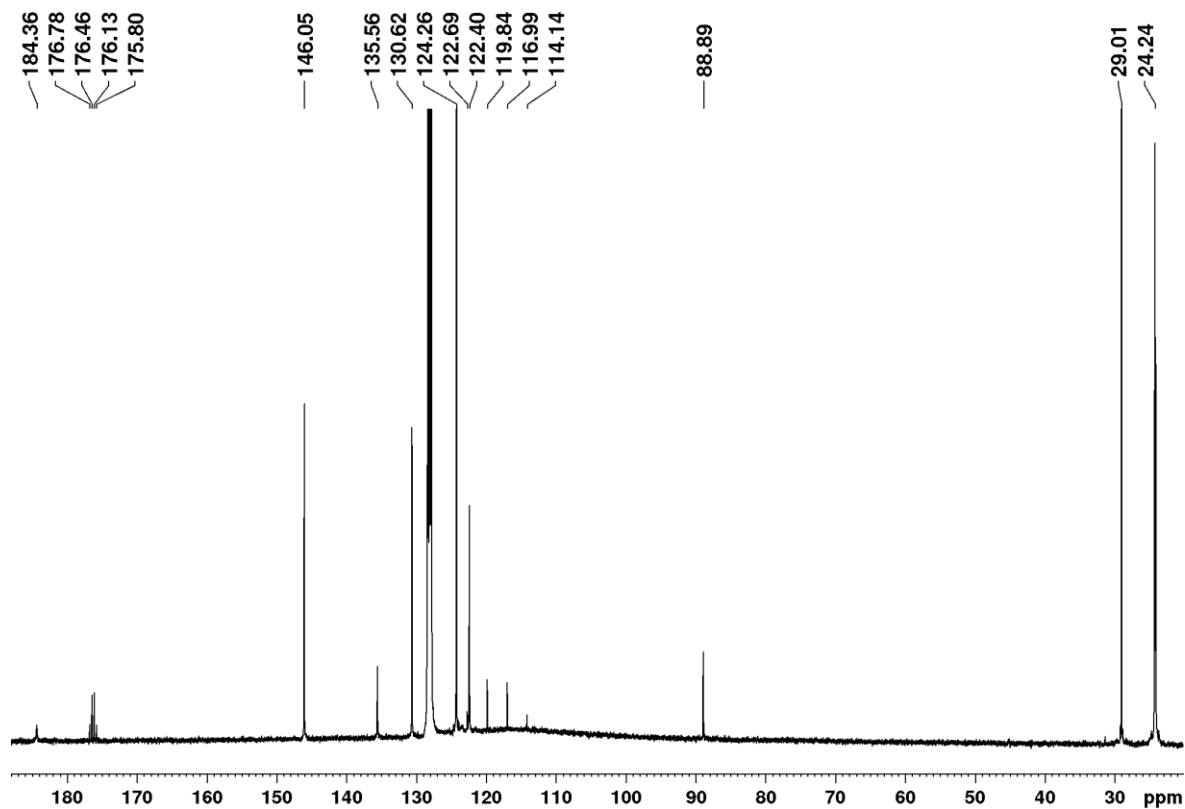


Figure 126: $^{13}\text{C}\{^1\text{H}\}$ NMR spectrum (100 MHz) of $[\text{Cu}(\text{Dipp}_2\text{Im})(\text{hfacac})]$ 19 in C_6D_6 .

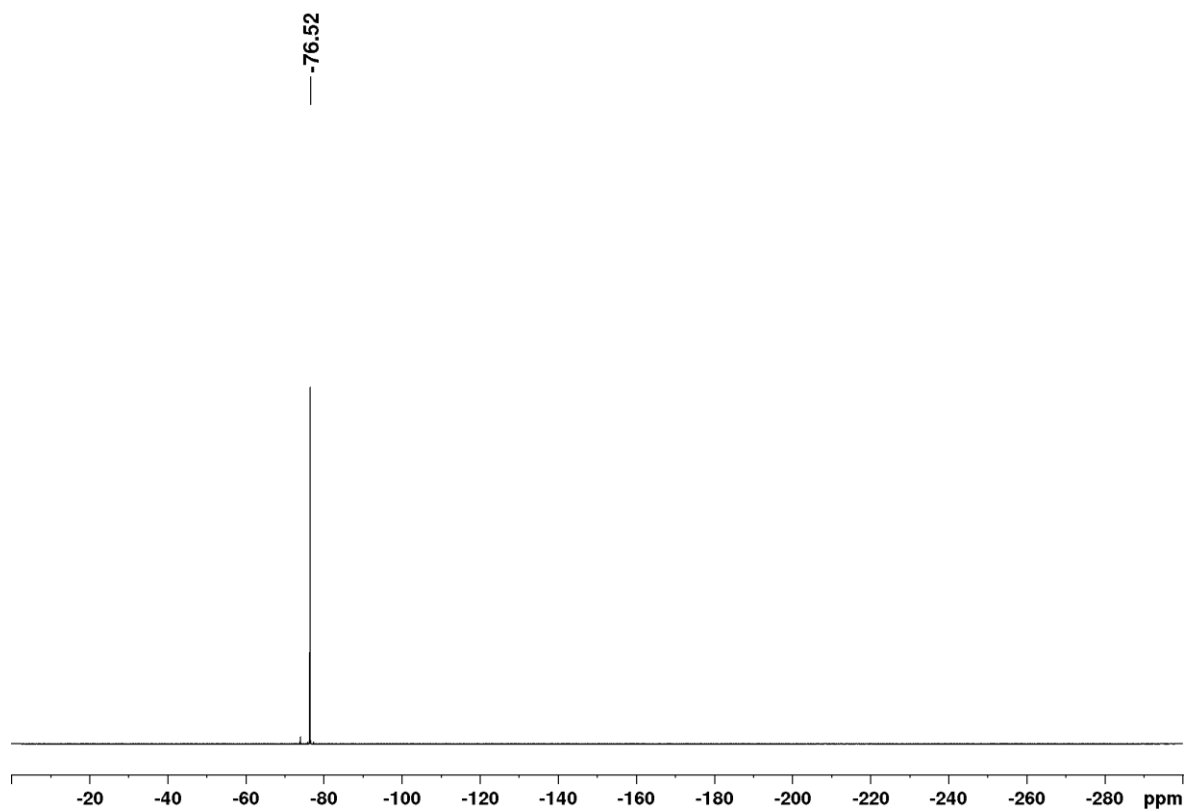


Figure 127: ^{19}F NMR spectrum (188 MHz) of $[\text{Cu}(\text{Dipp}_2\text{Im})(\text{hfacac})]$ 19 in C_6D_6 .

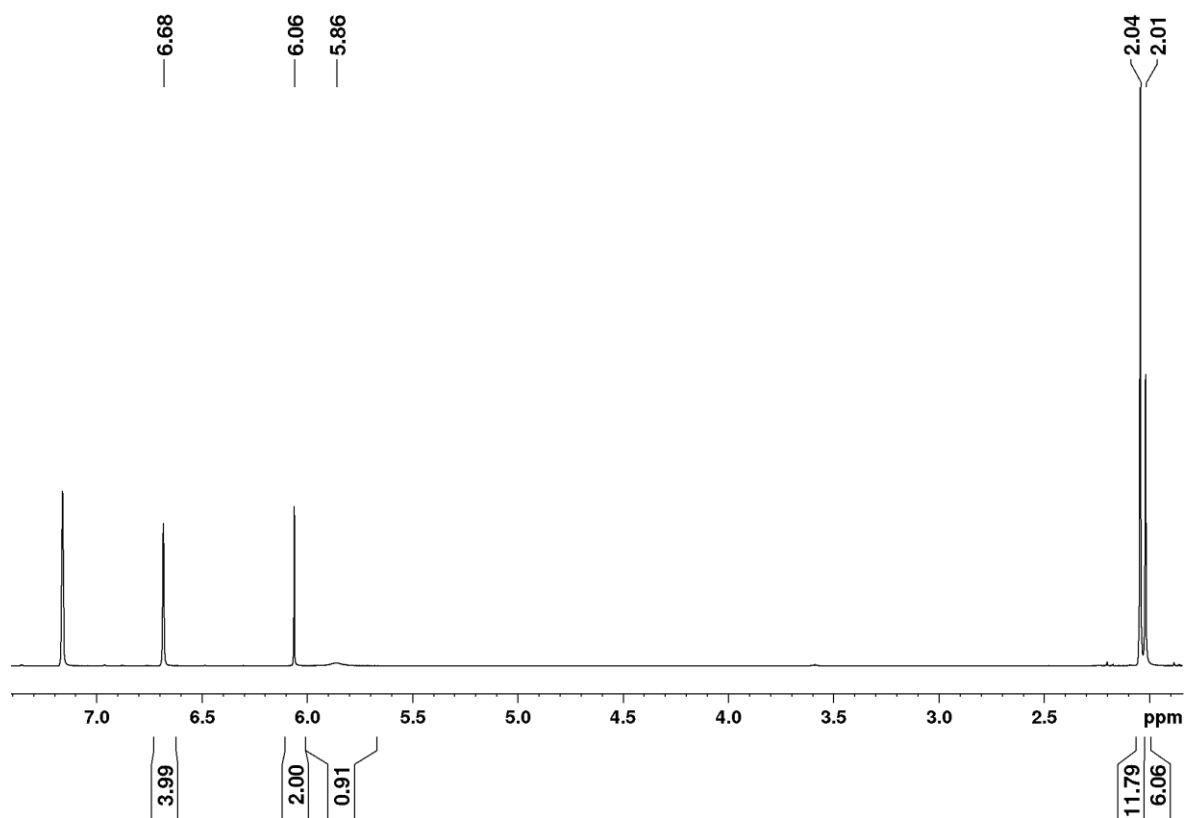


Figure 128: ^1H NMR spectrum (400 MHz) of $[\text{Cu}(\text{Mes}_2\text{Im})(\text{hfacac})]$ 21 in C_6D_6 .

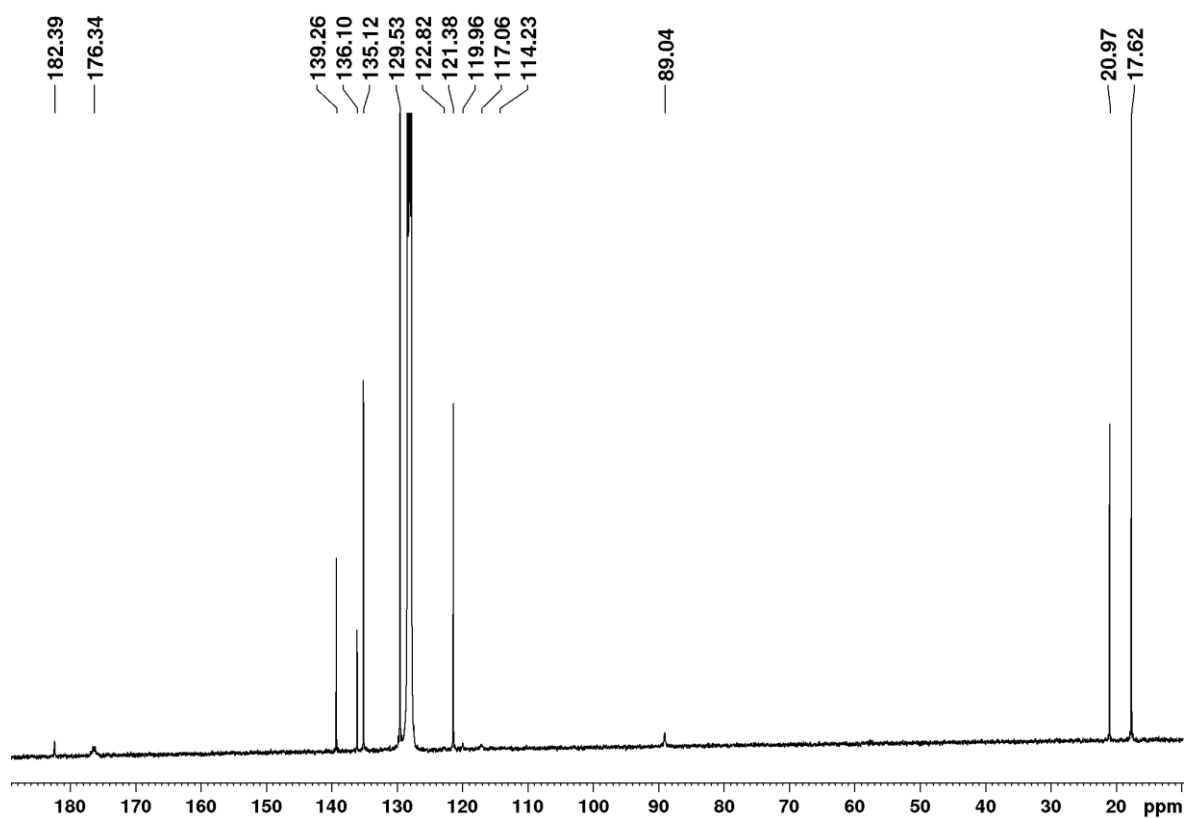


Figure 129: $^{13}\text{C}\{^1\text{H}\}$ NMR spectrum (100 MHz) of $[\text{Cu}(\text{Mes}_2\text{Im})(\text{hfacac})]$ 21 in C_6D_6 .

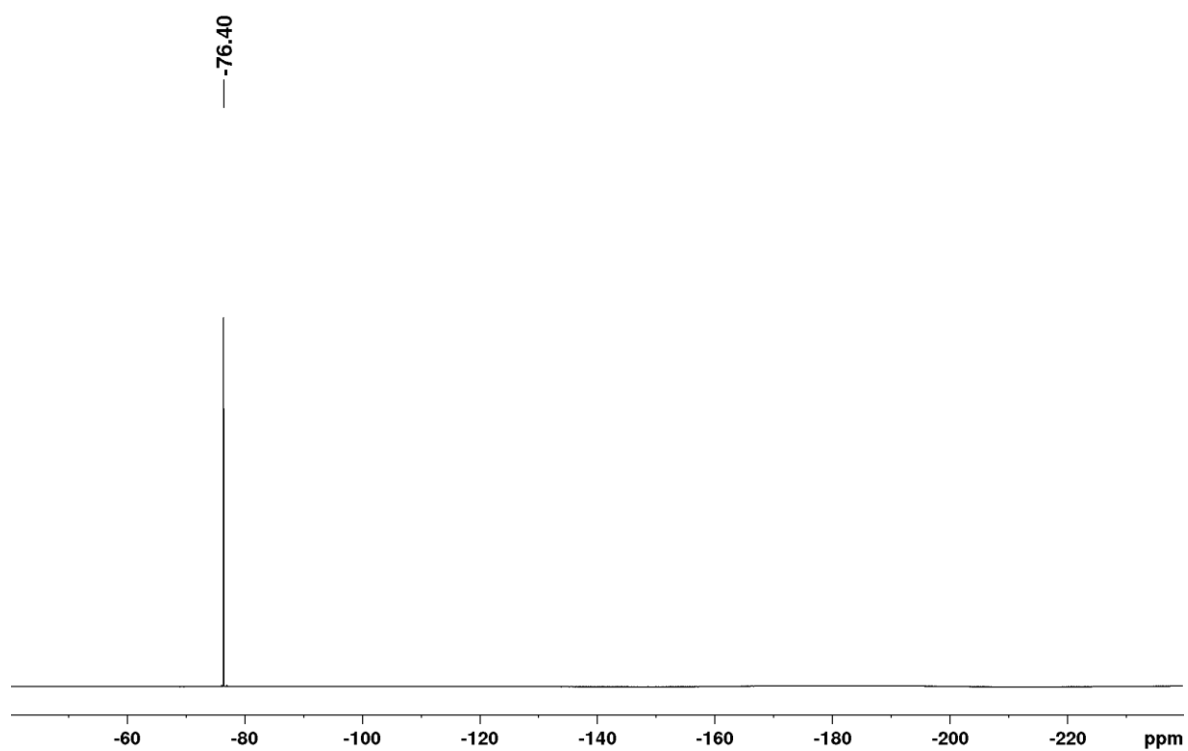
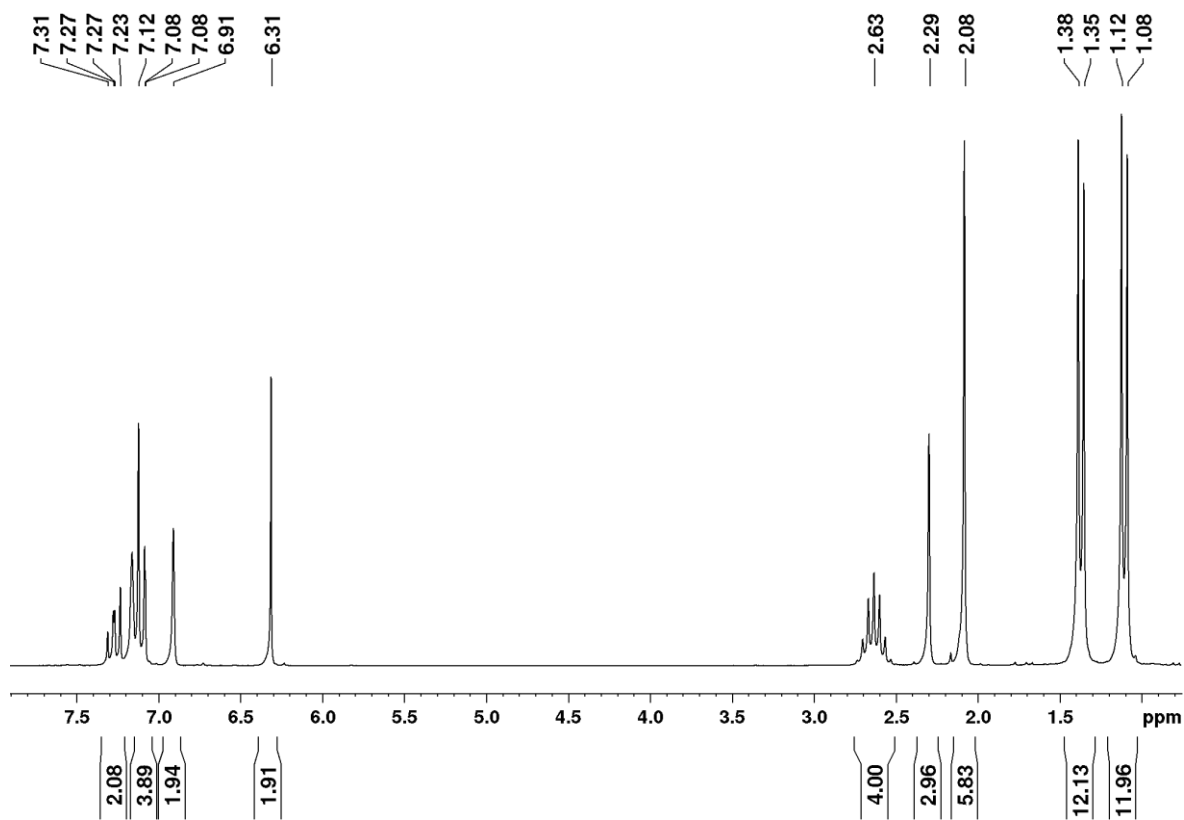
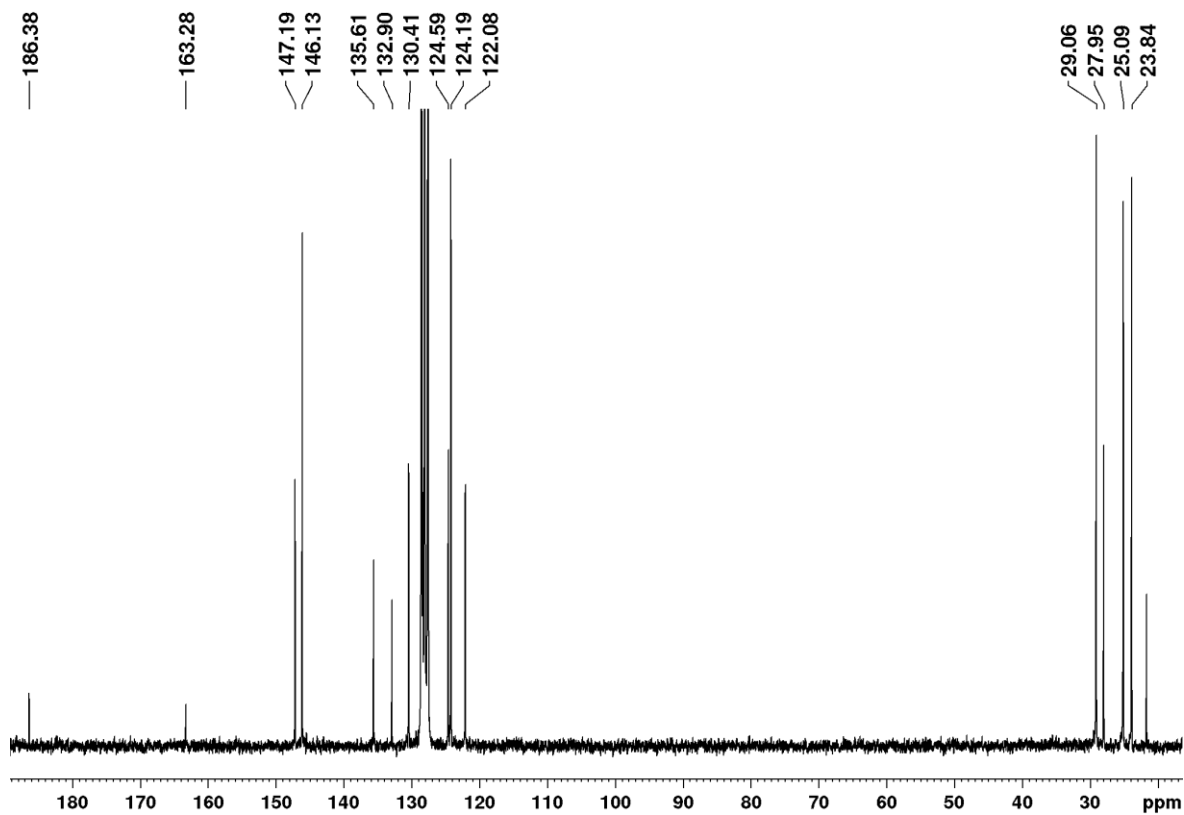
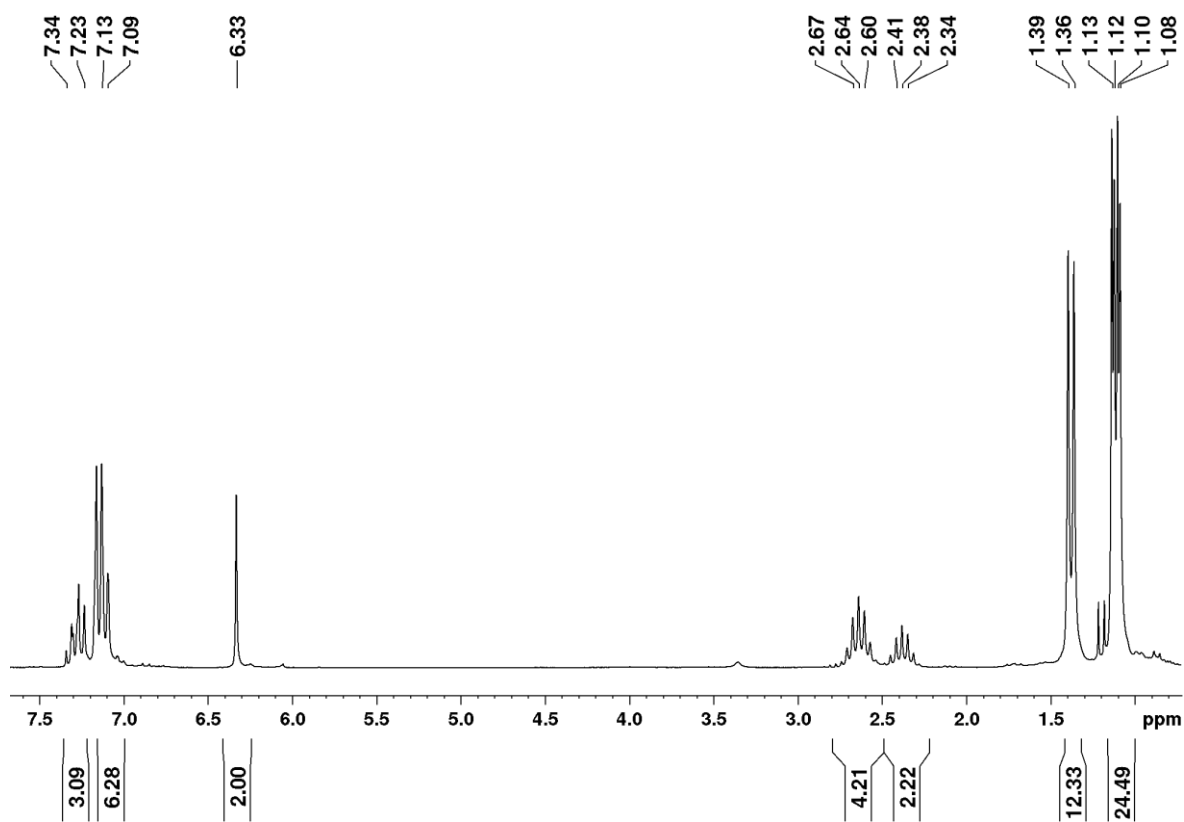
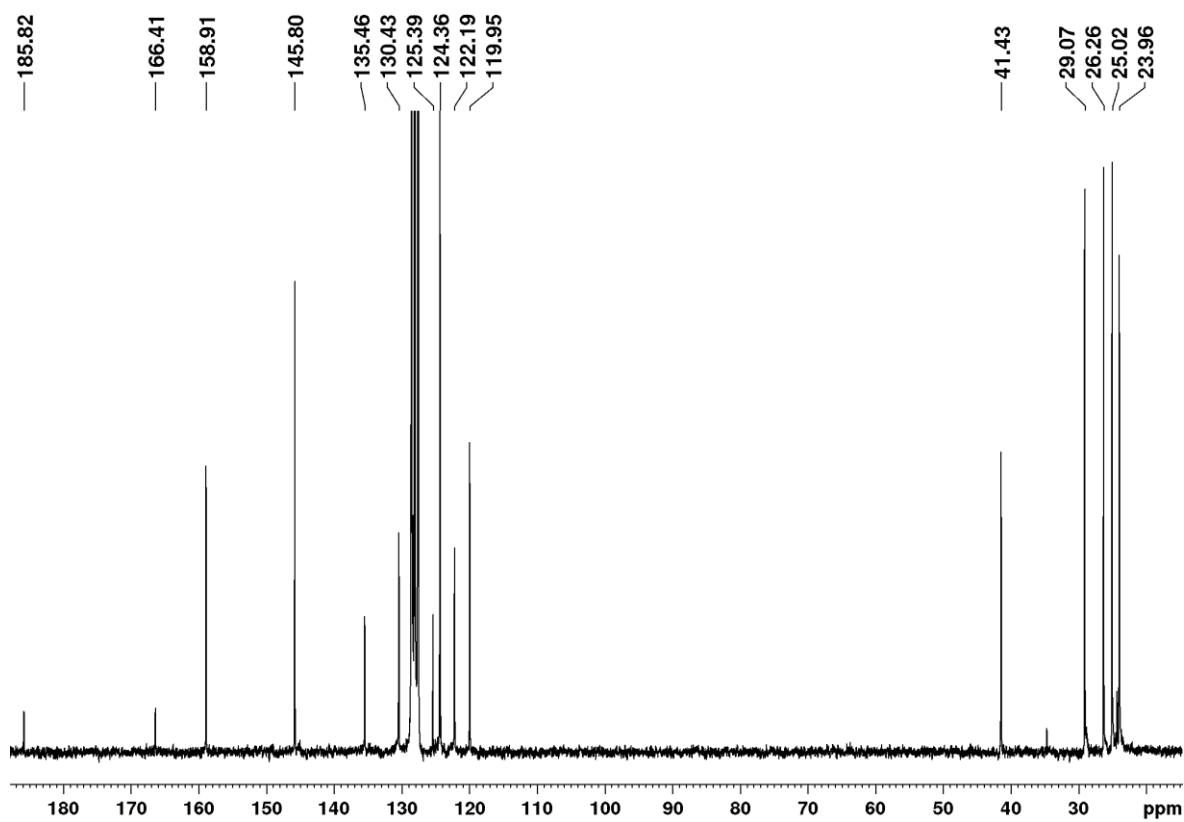
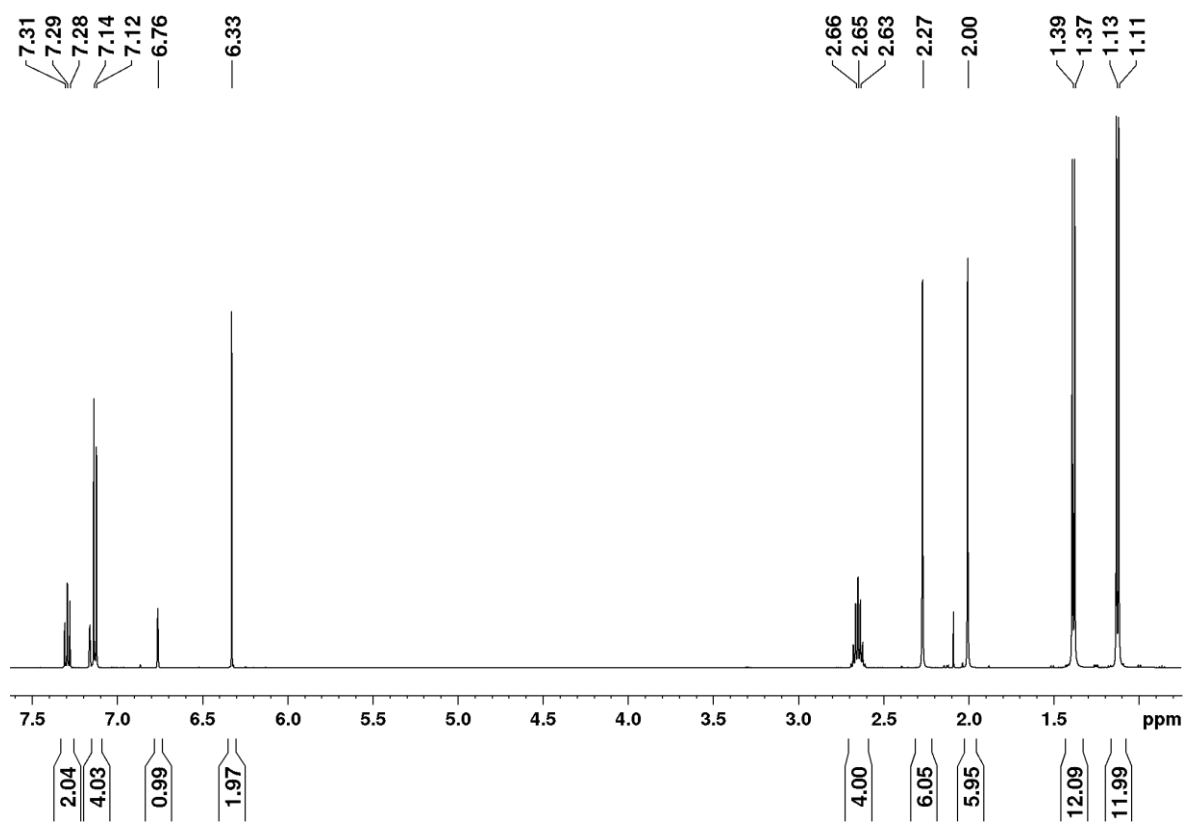
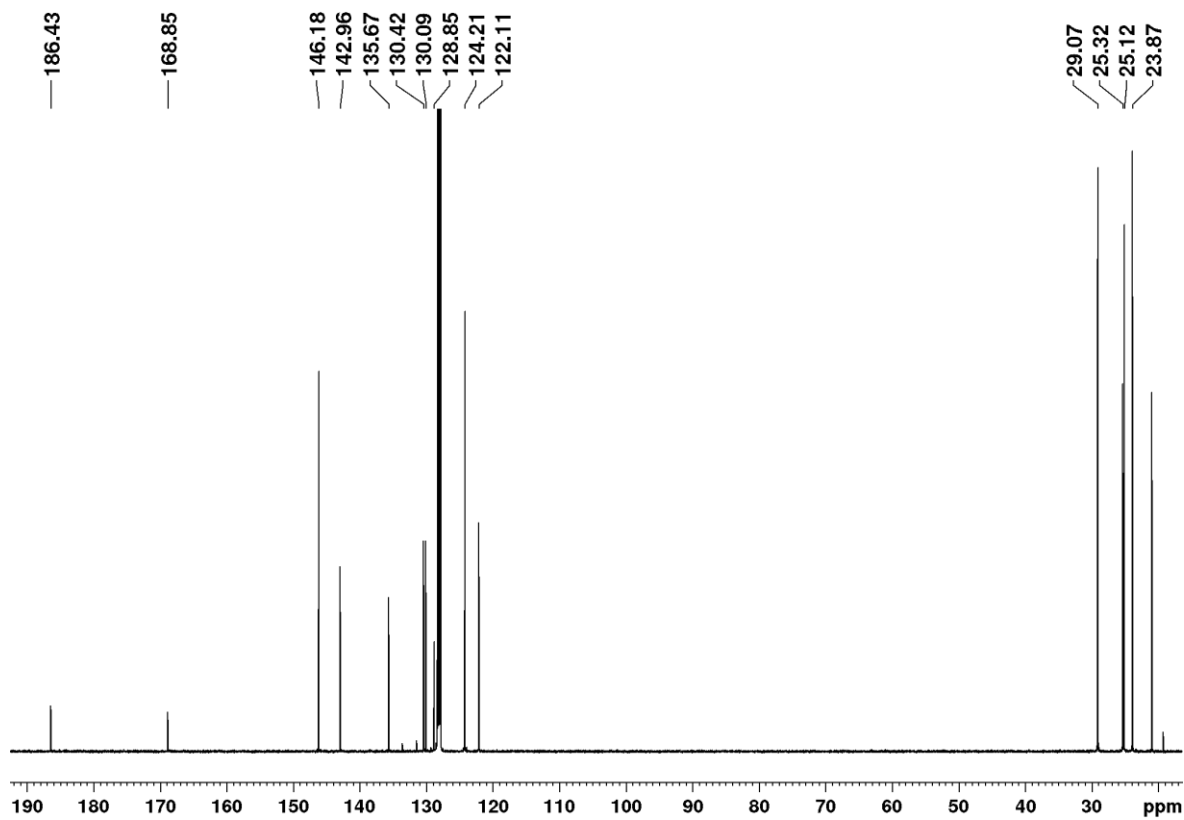


Figure 130: ^{19}F NMR spectrum (366 MHz) of $[\text{Cu}(\text{Mes}_2\text{Im})(\text{hfacac})]$ 21 in C_6D_6 .

Figure 131: ¹H NMR spectrum (200 MHz) of [Cu(Dipp₂Im)(Mes)] 24 in C₆D₆.Figure 132: ¹³C{¹H} NMR spectrum (75 MHz) of [Cu(Dipp₂Im)(Mes)] 24 in C₆D₆.

Figure 133: ^1H NMR spectrum (200 MHz) of $[\text{Cu}(\text{Dipp}_2\text{Im})(\text{Dipp})]$ 35 in C_6D_6 .Figure 134: $^{13}\text{C}\{^1\text{H}\}$ NMR spectrum (50 MHz) of $[\text{Cu}(\text{Dipp}_2\text{Im})(\text{Dipp})]$ 35 in C_6D_6 .

Figure 135: ¹H NMR spectrum (400 MHz) of [Cu(Dipp₂Im)(duryl)] 38 in C₆D₆.Figure 136: ¹³C{¹H} NMR spectrum (100 MHz) of [Cu(Dipp₂Im)(duryl)] 38 in C₆D₆.

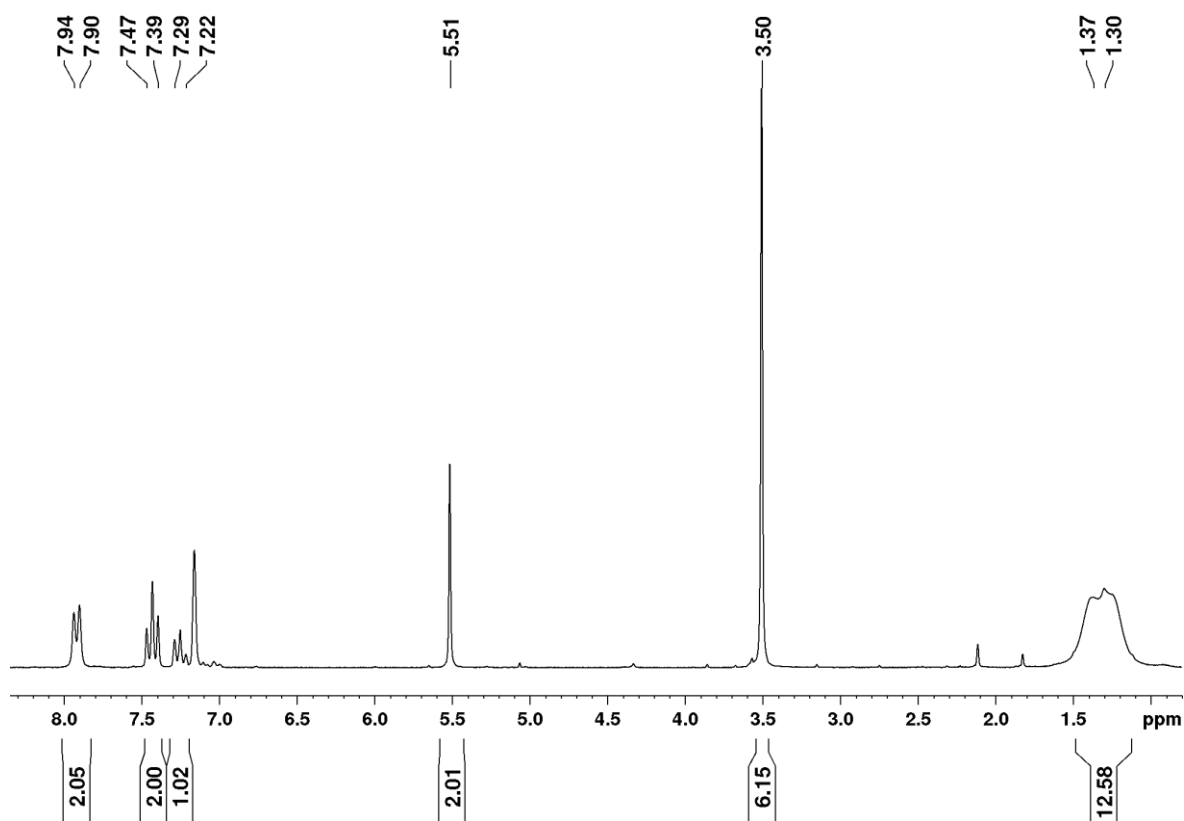


Figure 137: ^1H NMR spectrum (200 MHz) of phenylBpin•Me₂Im ADD1 in C₆D₆.

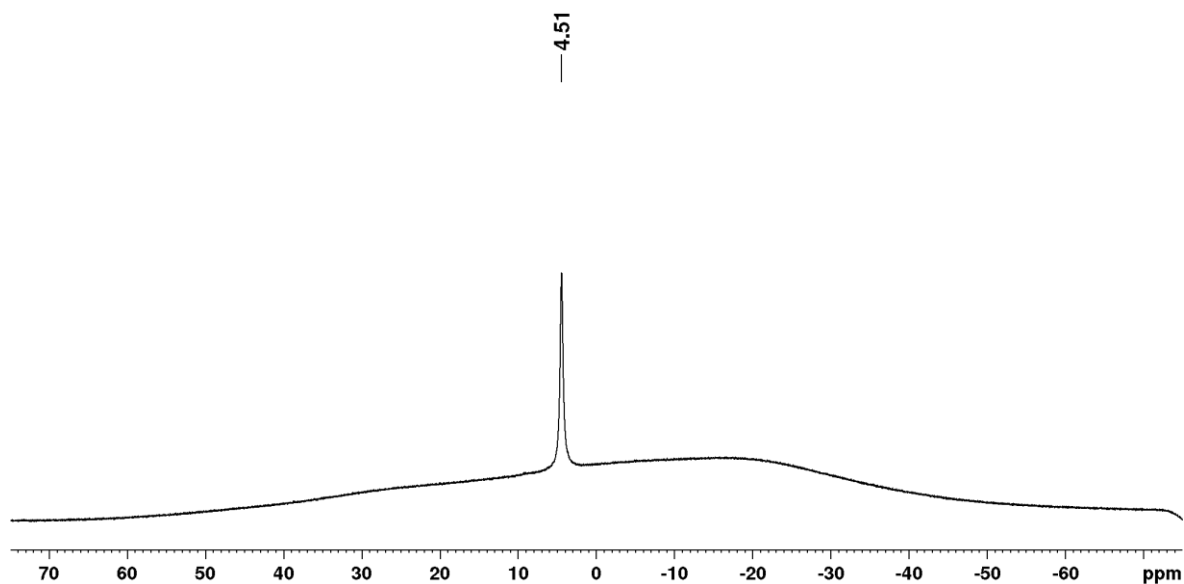
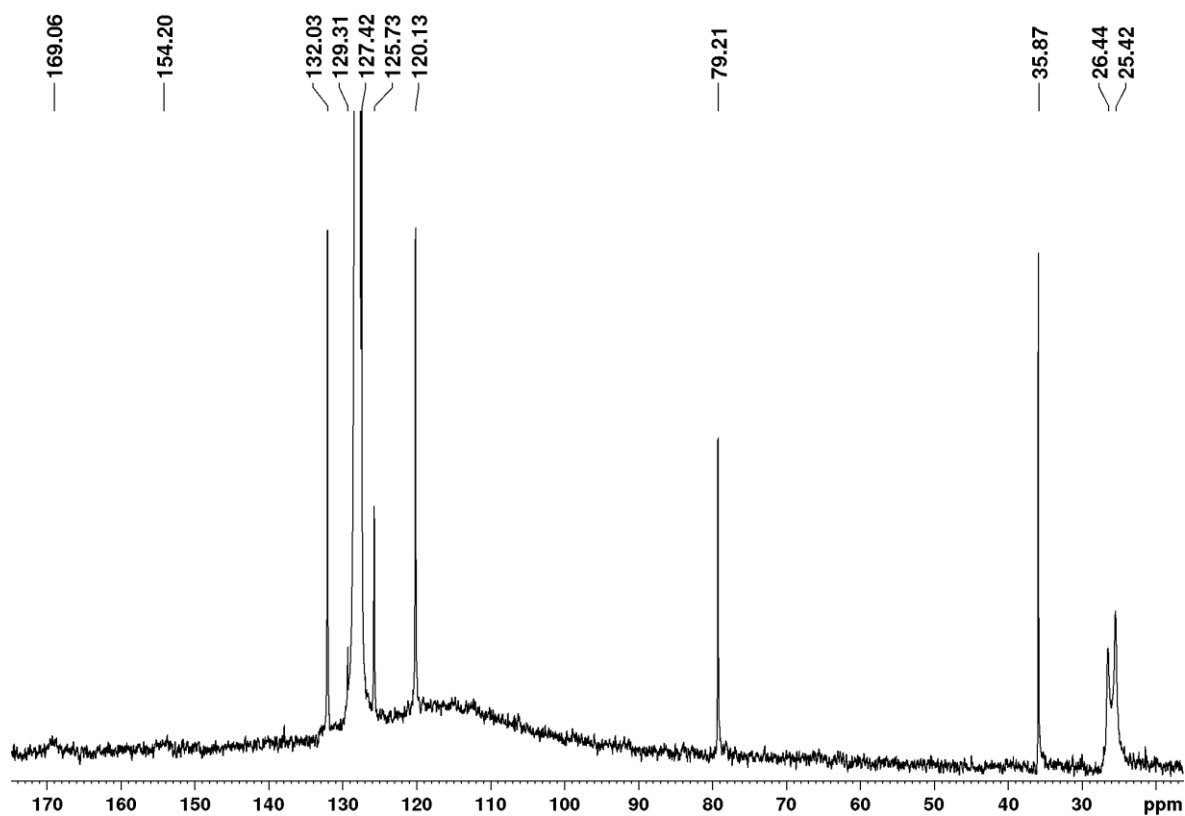
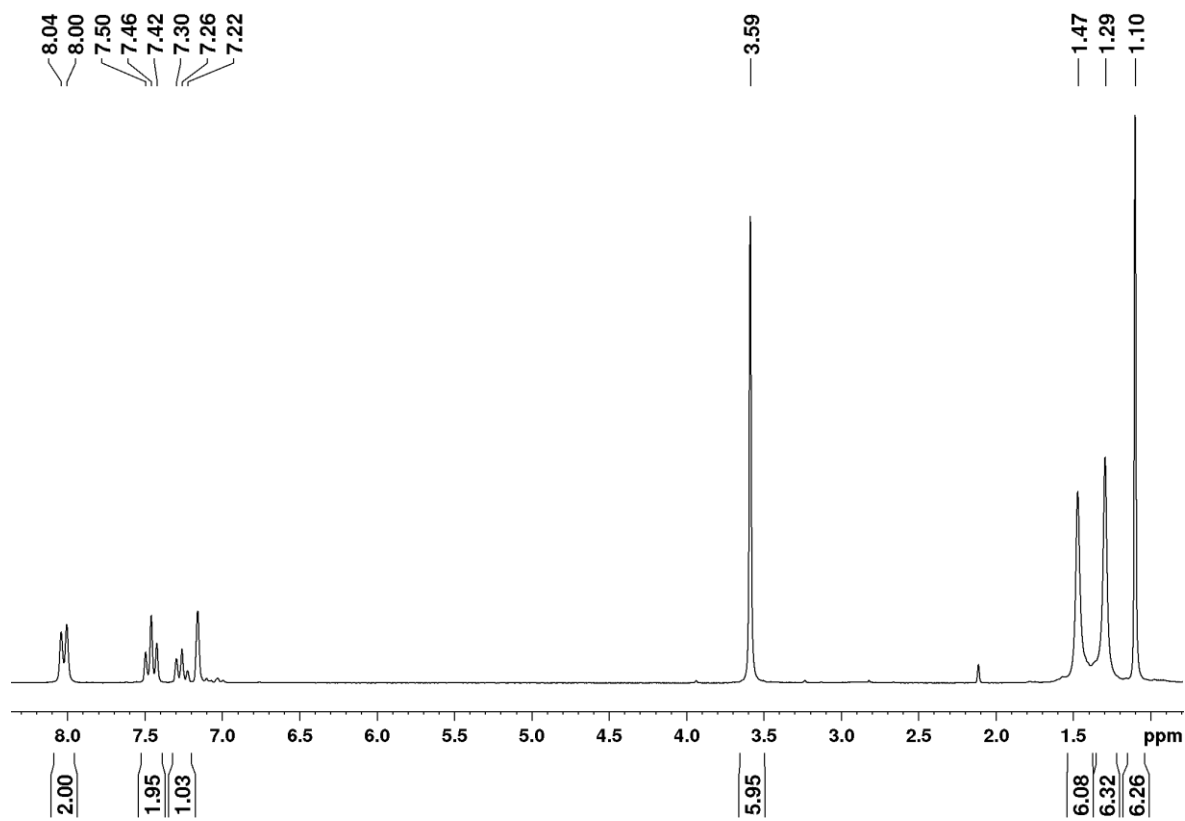


Figure 138: ^{11}B NMR spectrum (64 MHz) of phenylBpin•Me₂Im ADD1 in C₆D₆.

Figure 139: $^{13}\text{C}\{^1\text{H}\}$ NMR spectrum (100 MHz) of phenylBpin•Me₂Im ADD1 in C₆D₆.Figure 140: ^1H NMR spectrum (200 MHz) of phenylBpin•Me₄Im ADD2 in C₆D₆.

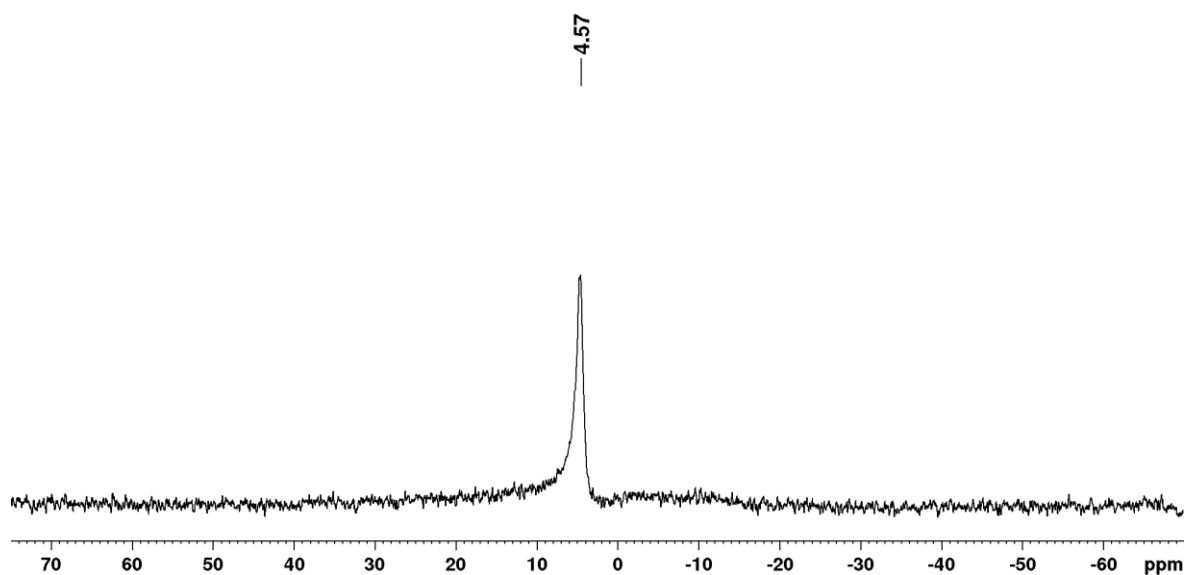


Figure 141: ^{11}B NMR spectrum (64 MHz) of phenylBpin•Me₄Im ADD2 in C₆D₆.

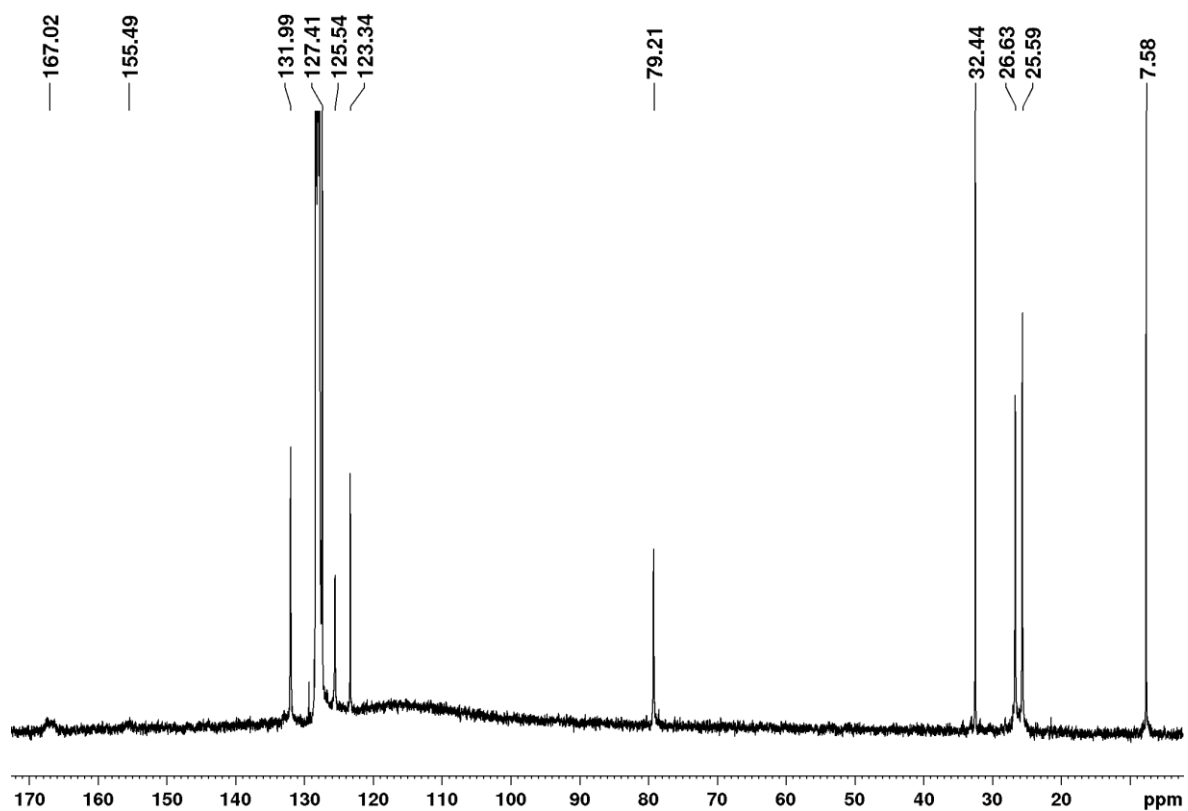


Figure 142: $^{13}\text{C}\{^1\text{H}\}$ NMR spectrum (100 MHz) of phenylBpin•Me₄Im ADD2 in C₆D₆.

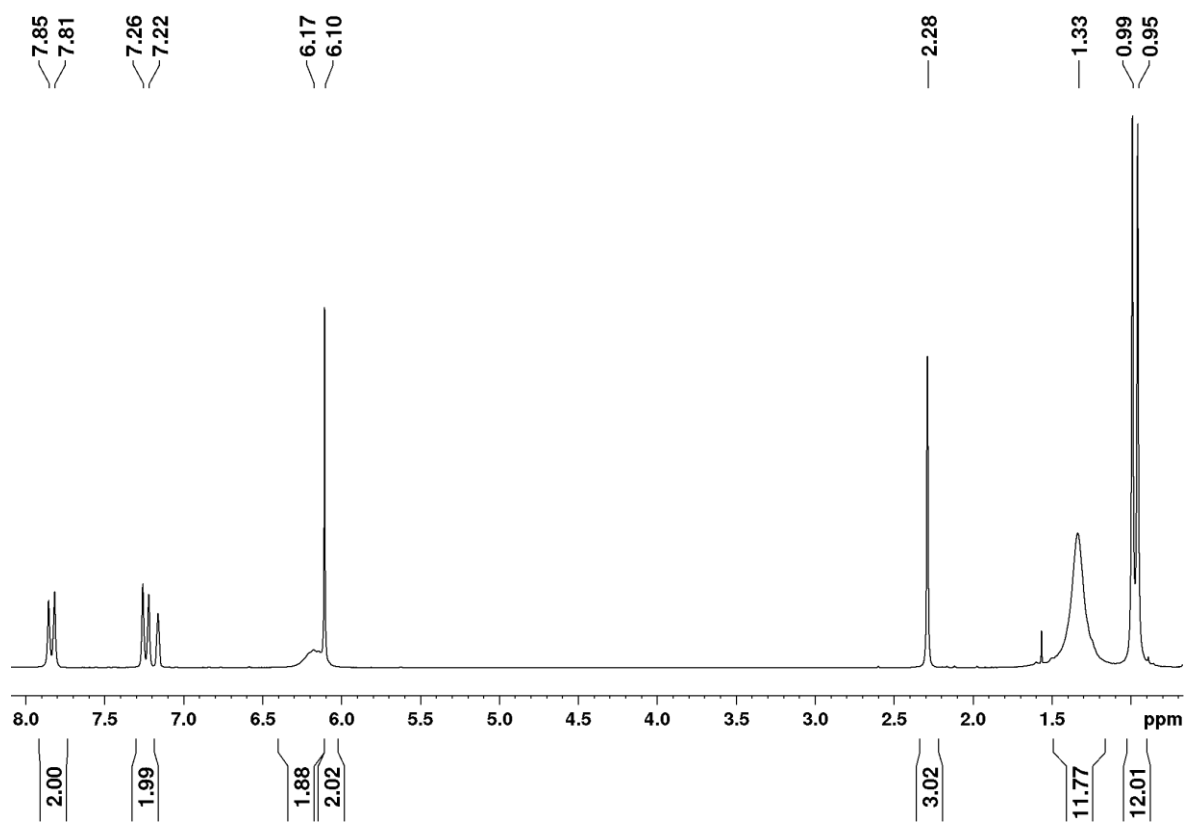


Figure 143: ^1H NMR spectrum (200 MHz) of *p*-tolylBpin• Pr_2Im Add5 in C_6D_6 .

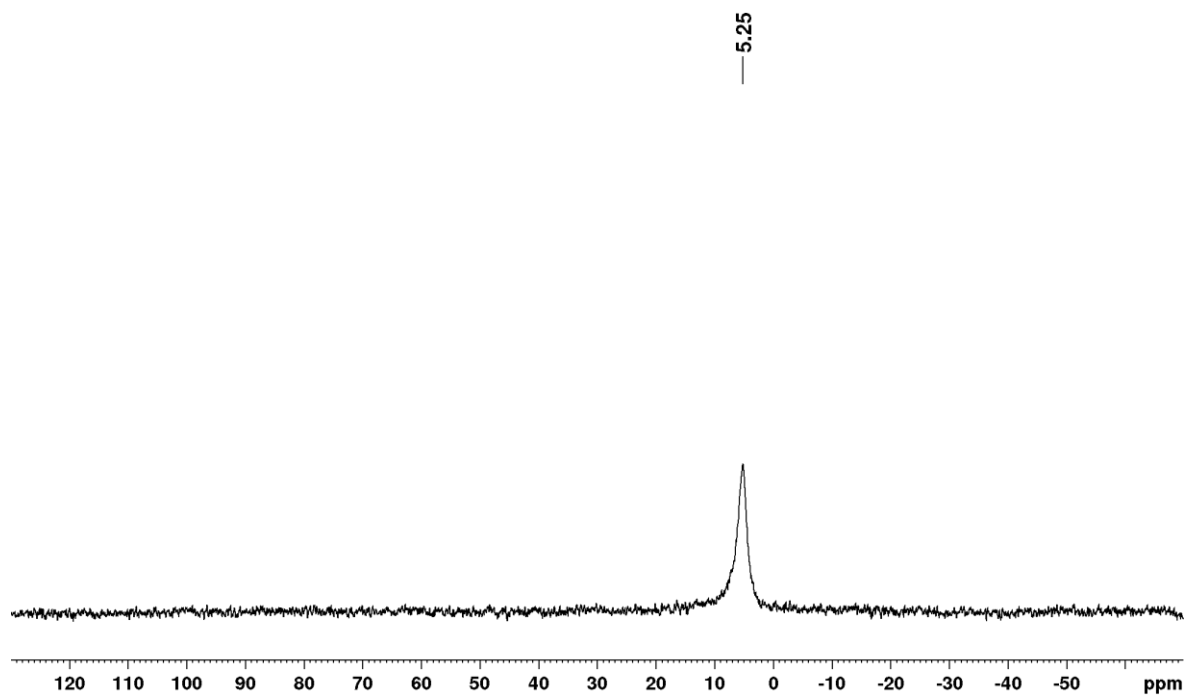
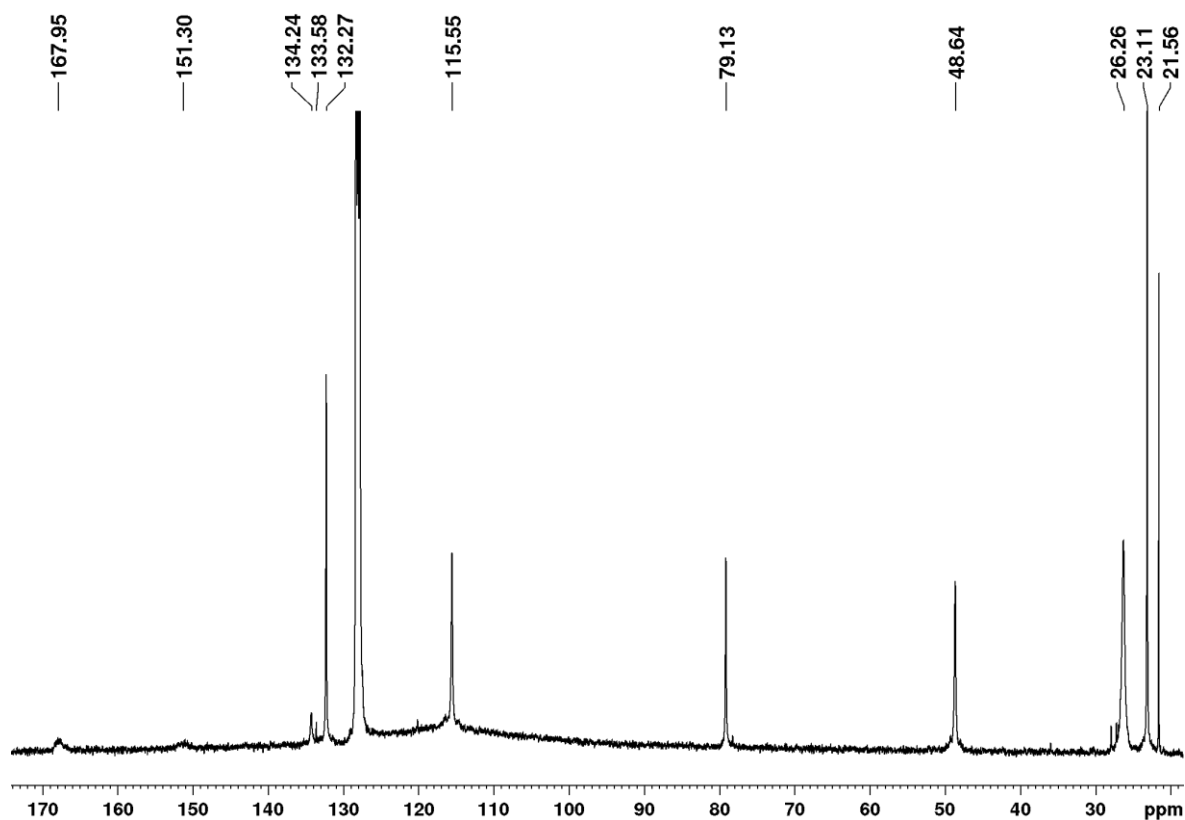
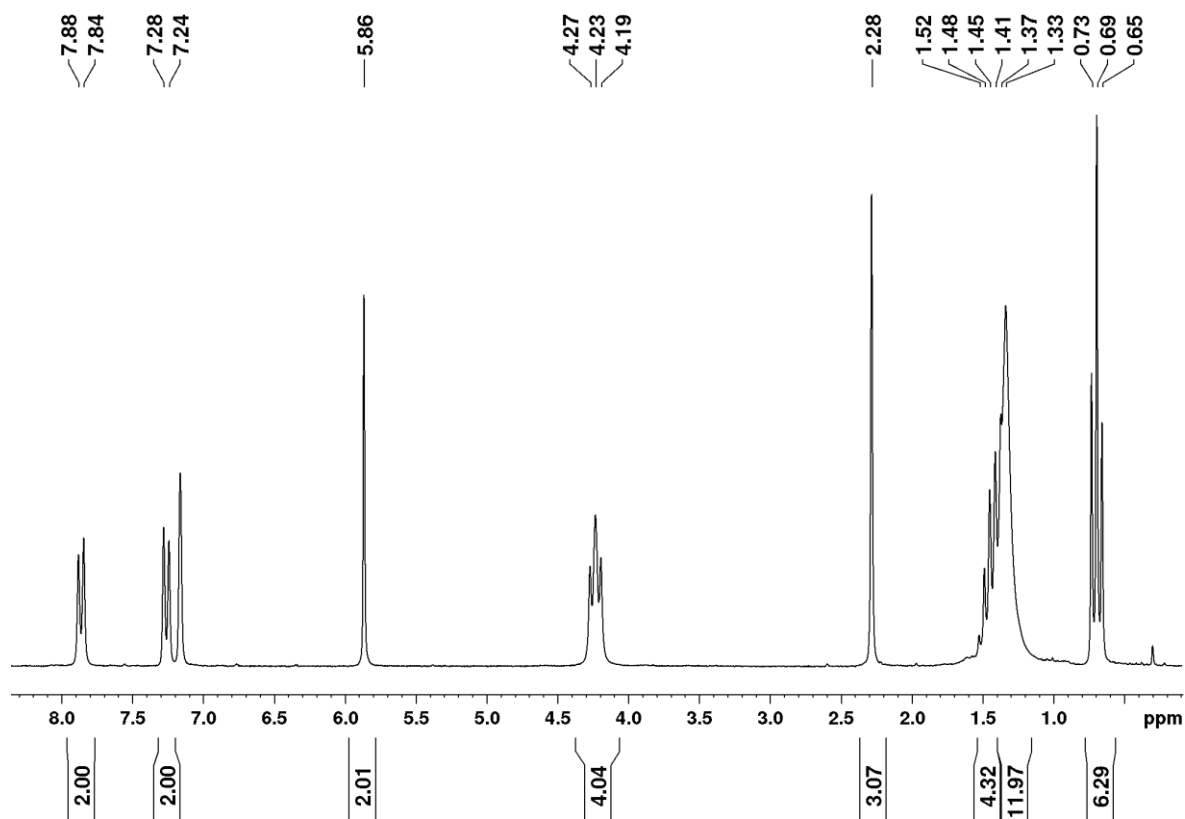


Figure 144: ^{11}B NMR spectrum (64 MHz) of *p*-tolylBpin• Pr_2Im Add5 in C_6D_6 .

Figure 145: $^{13}\text{C}\{^1\text{H}\}$ NMR spectrum (100 MHz) of *p*-tolylBpin•*i*Pr₂Im Add5 in C₆D₆.Figure 146: ^1H NMR spectrum (200 MHz) of *p*-tolylBpin•*n*Pr₂Im Add6 in C₆D₆.

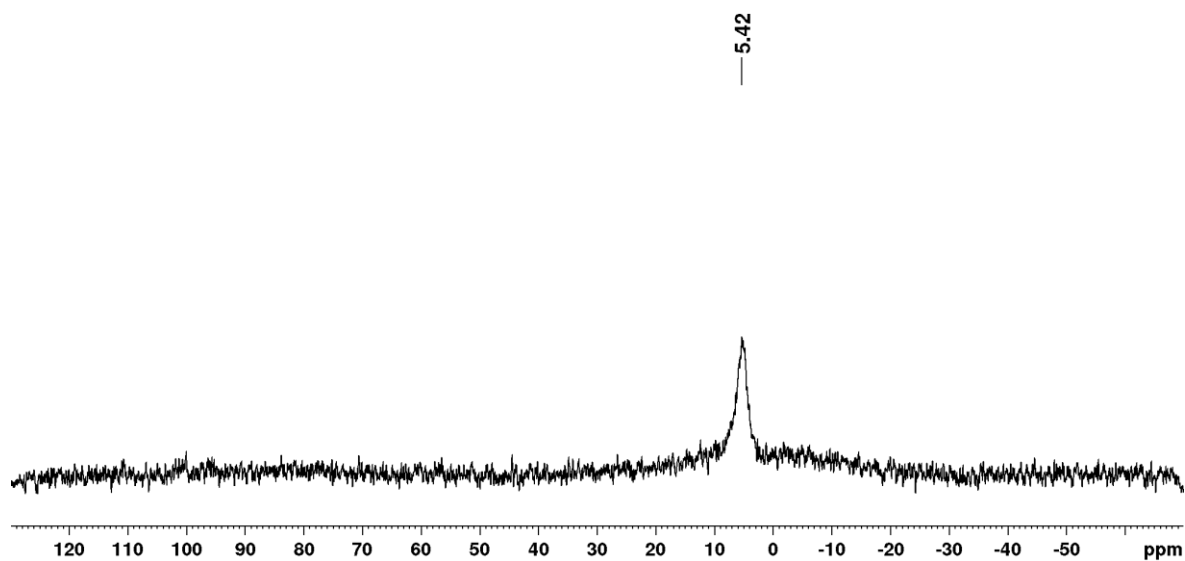


Figure 147: ^{11}B NMR spectrum (64 MHz) of *p*-tolylBpin• Pr_2Im Add6 in C_6D_6 .

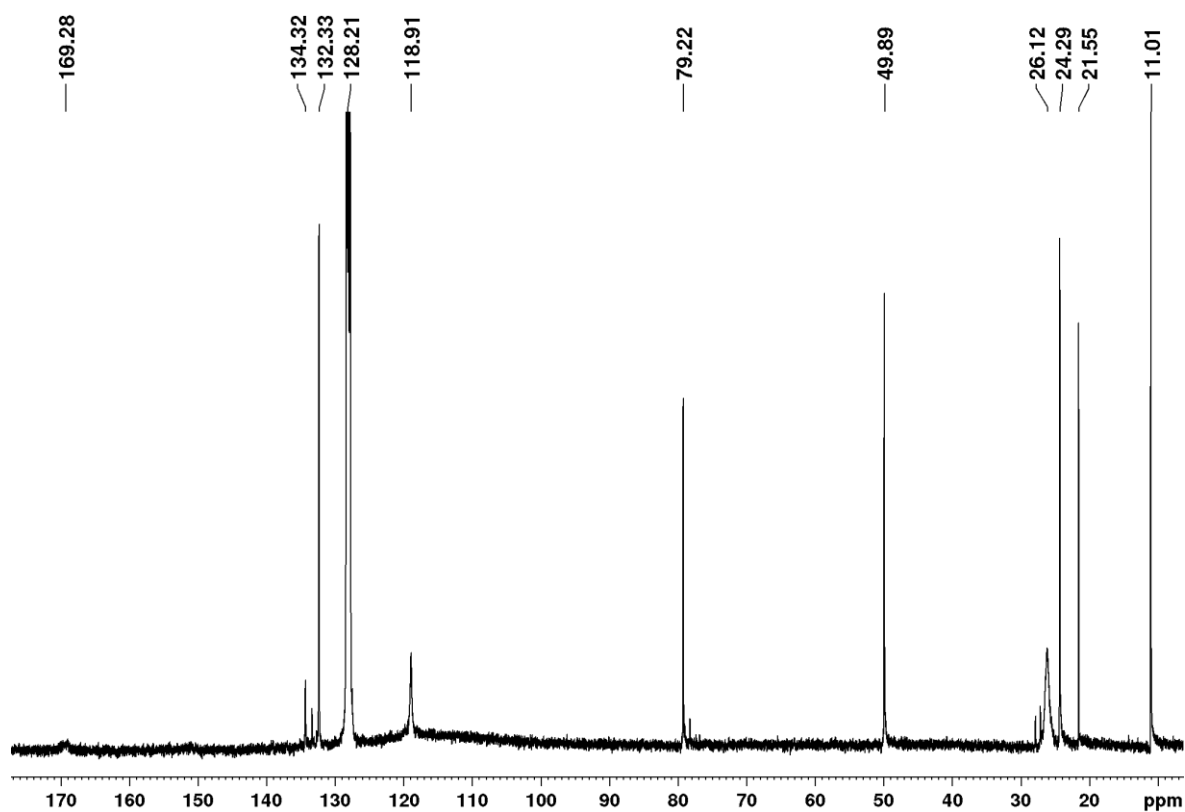
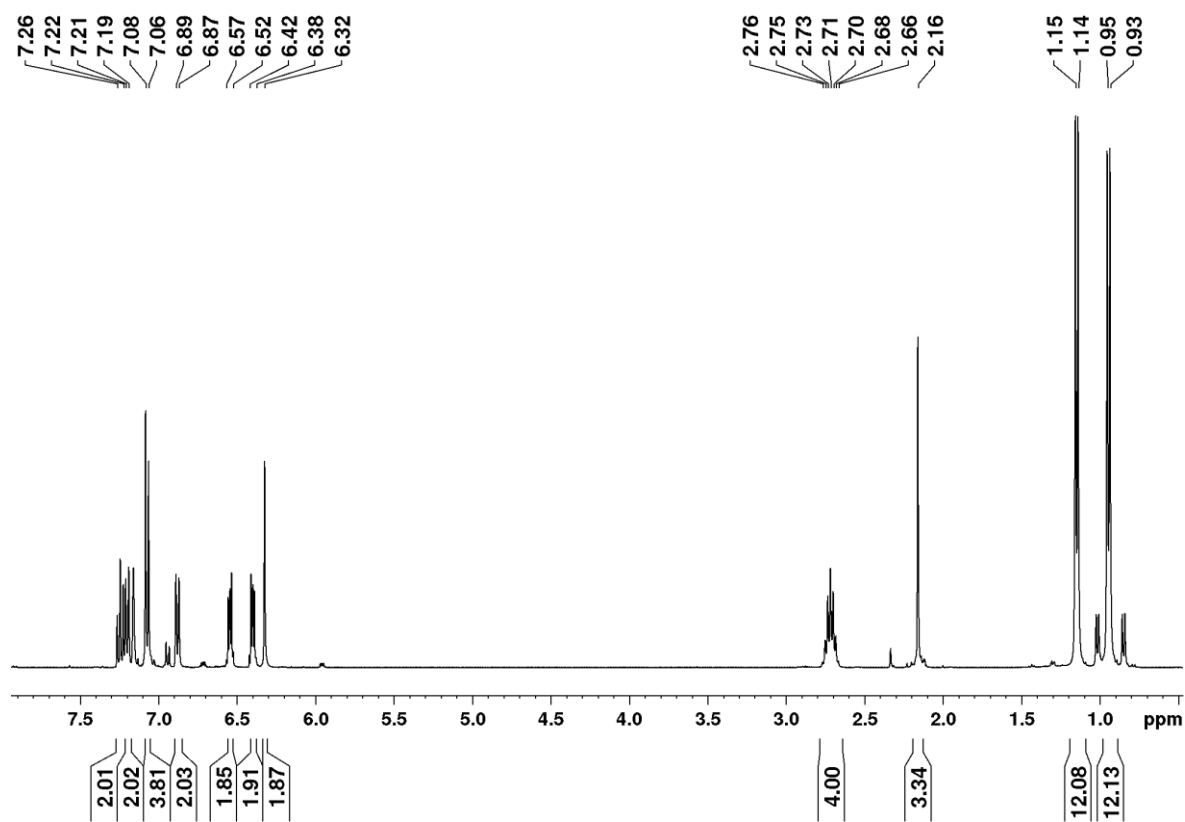
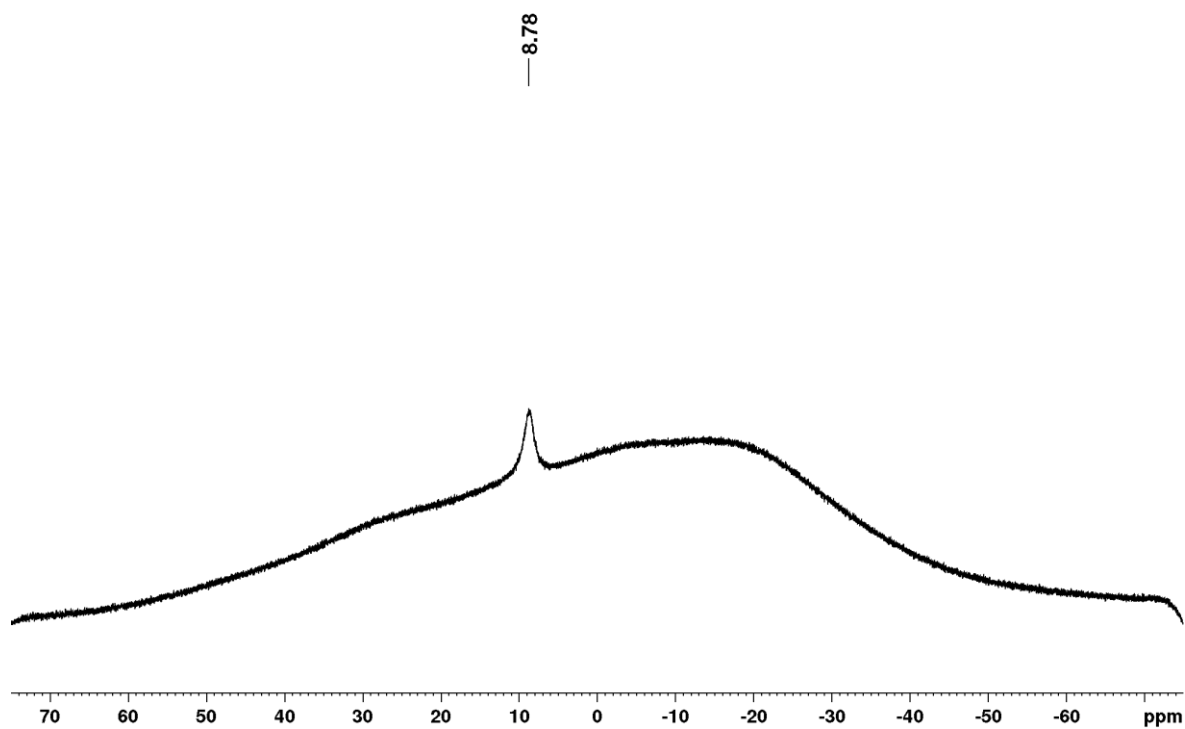
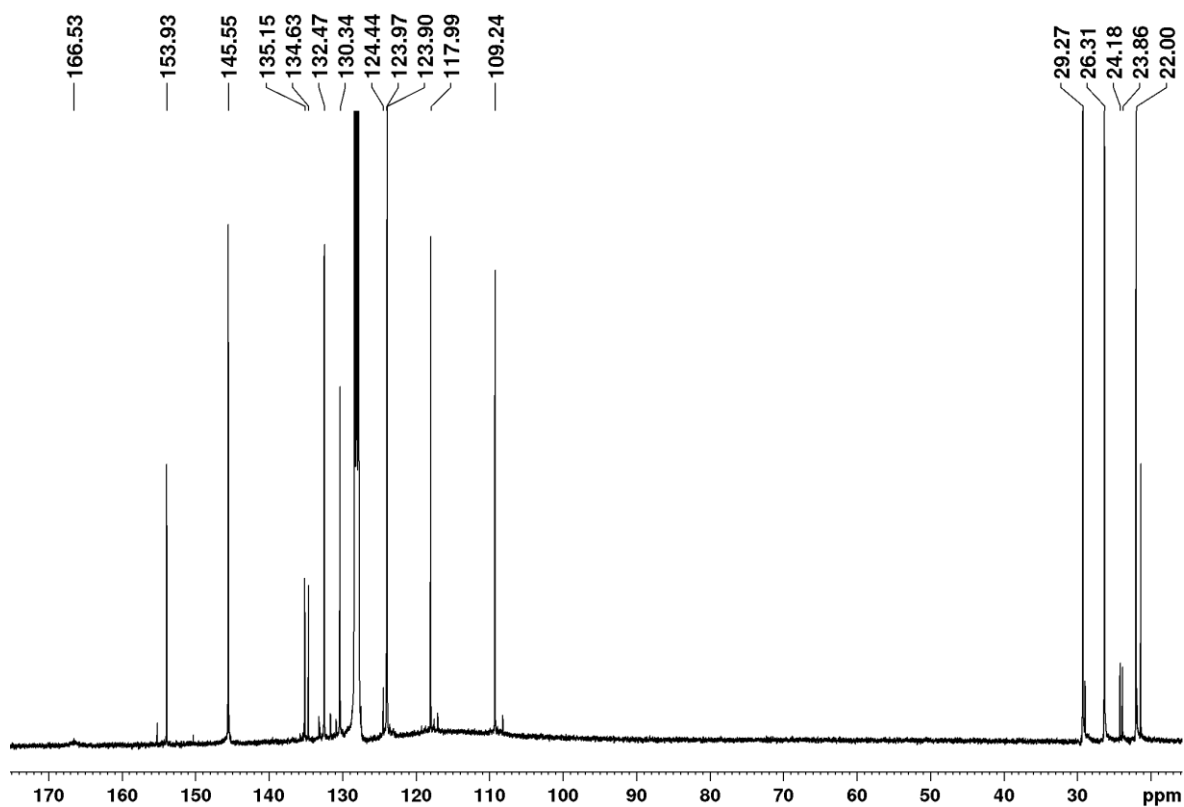
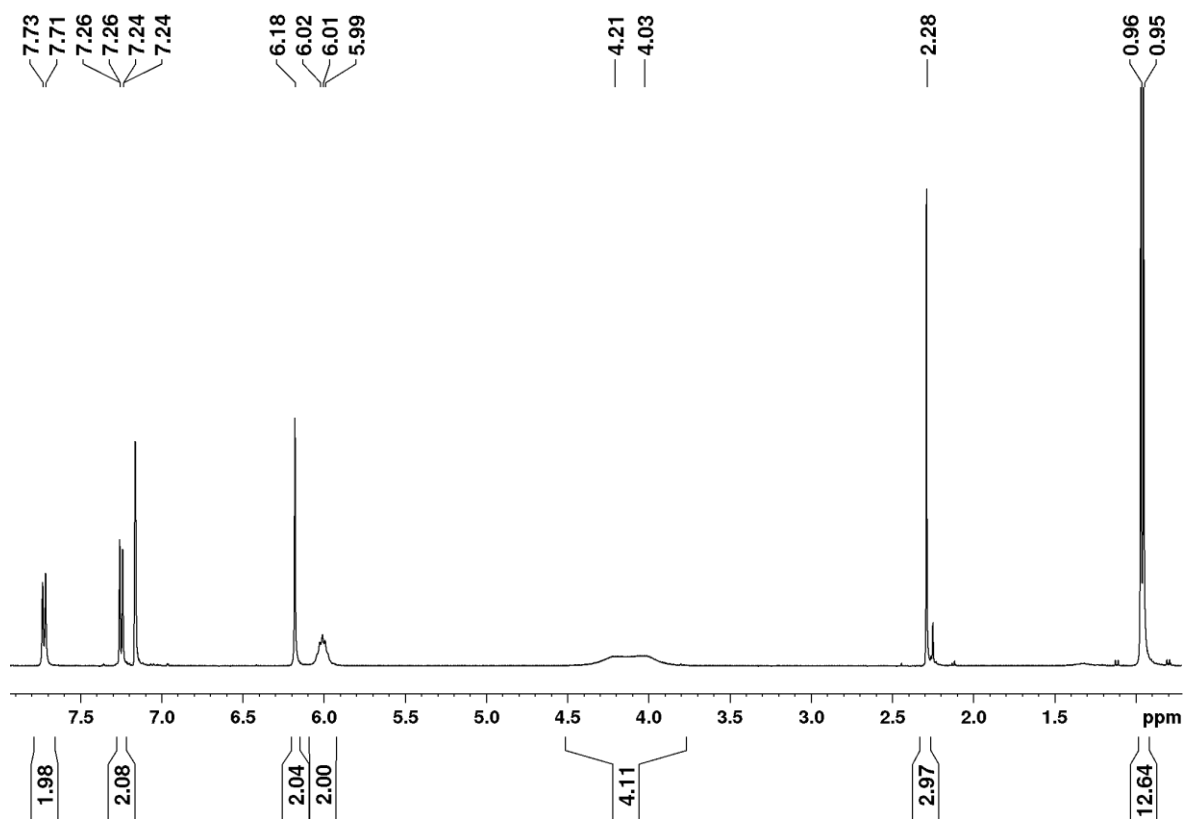


Figure 148: $^{13}\text{C}\{^1\text{H}\}$ NMR spectrum (100 MHz) of *p*-tolylBpin• Pr_2Im Add6 in C_6D_6 .

Figure 149: ^1H NMR spectrum (400 MHz) of *p*-tolylBcat•Dipp₂Im ADD8 in C₆D₆.Figure 150: ^{11}B NMR spectrum (128 MHz) of *p*-tolylBcat•Dipp₂Im ADD8 in C₆D₆.

Figure 151: $^{13}\text{C}\{^1\text{H}\}$ NMR spectrum (100 MHz) of *p*-tolylBcat•Dipp₂Im ADD8 in C_6D_6 .Figure 152: ^1H NMR spectrum (400 MHz) of *p*-tolylBcat•Pr₂Im ADD12 in C_6D_6 .

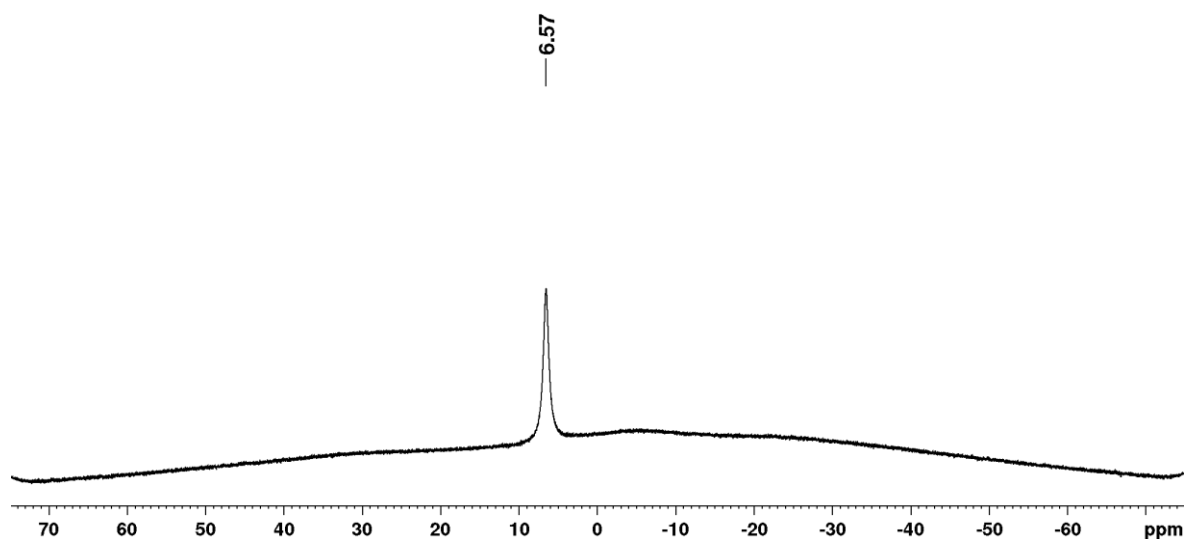


Figure 153: ^{11}B NMR spectrum (128 MHz) of *p*-tolylBeg•*i*Pr₂Im ADD12 in C₆D₆.

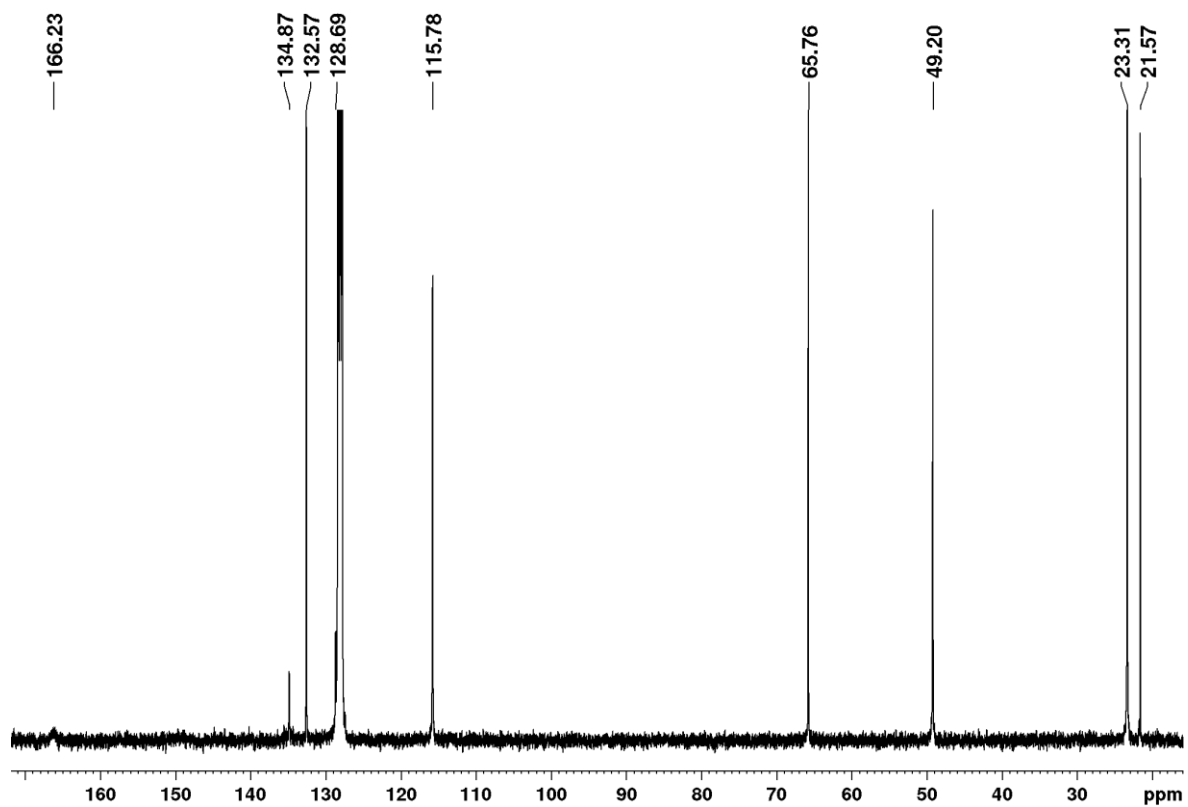


Figure 154: $^{13}\text{C}\{^1\text{H}\}$ NMR spectrum (100 MHz) of *p*-tolylBeg•*i*Pr₂Im ADD12 in C₆D₆.

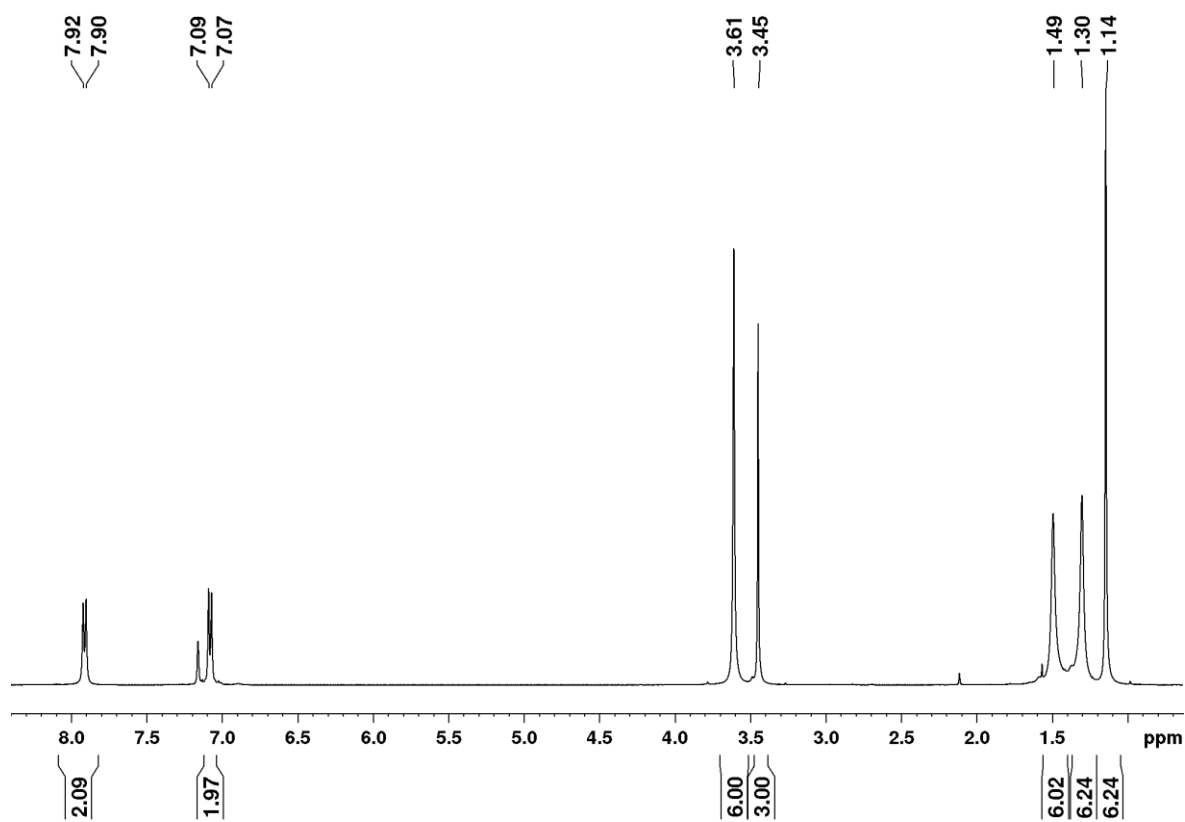


Figure 155: ^1H NMR spectrum (400 MHz) of 4-MeO-C₆H₄Bpin•Me₄Im ADD13 in C₆D₆.

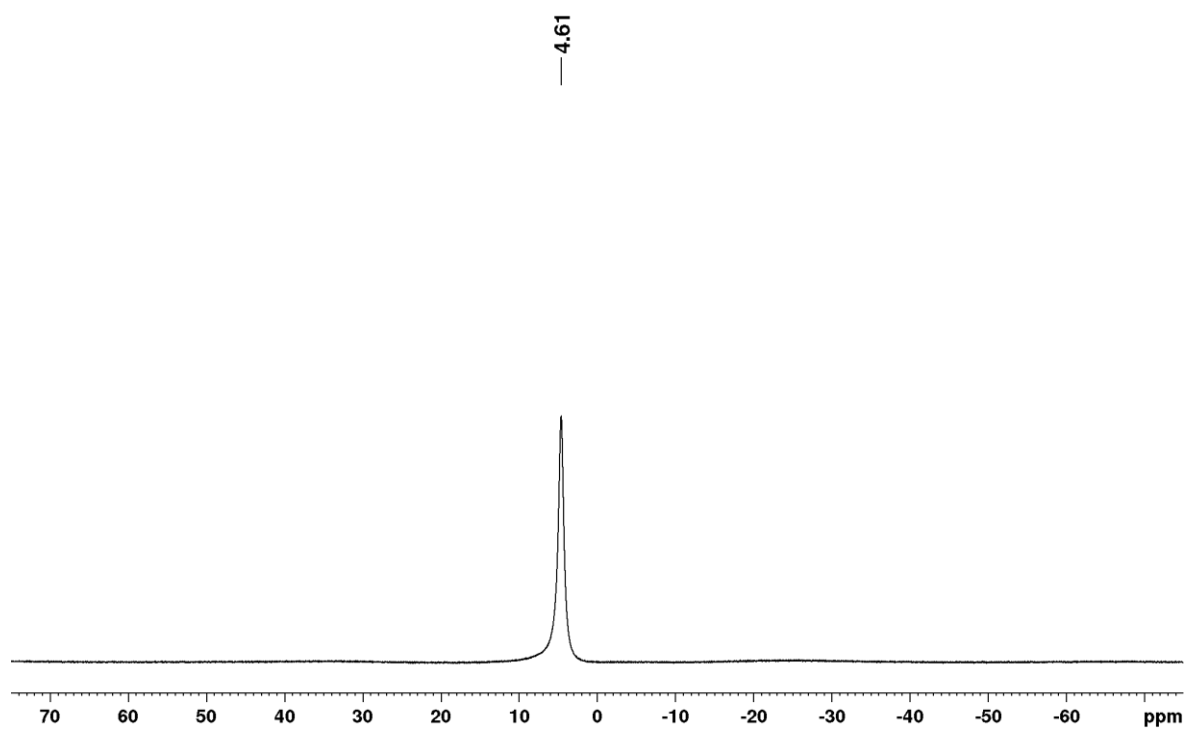
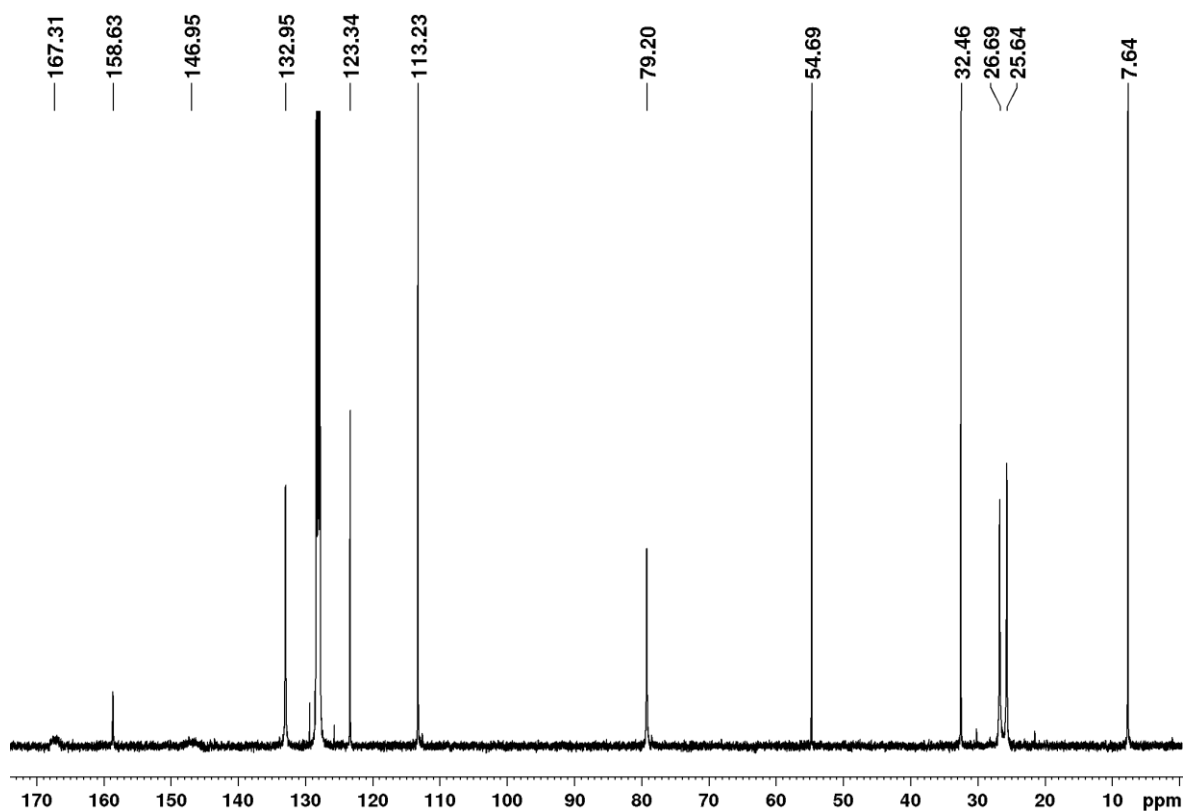
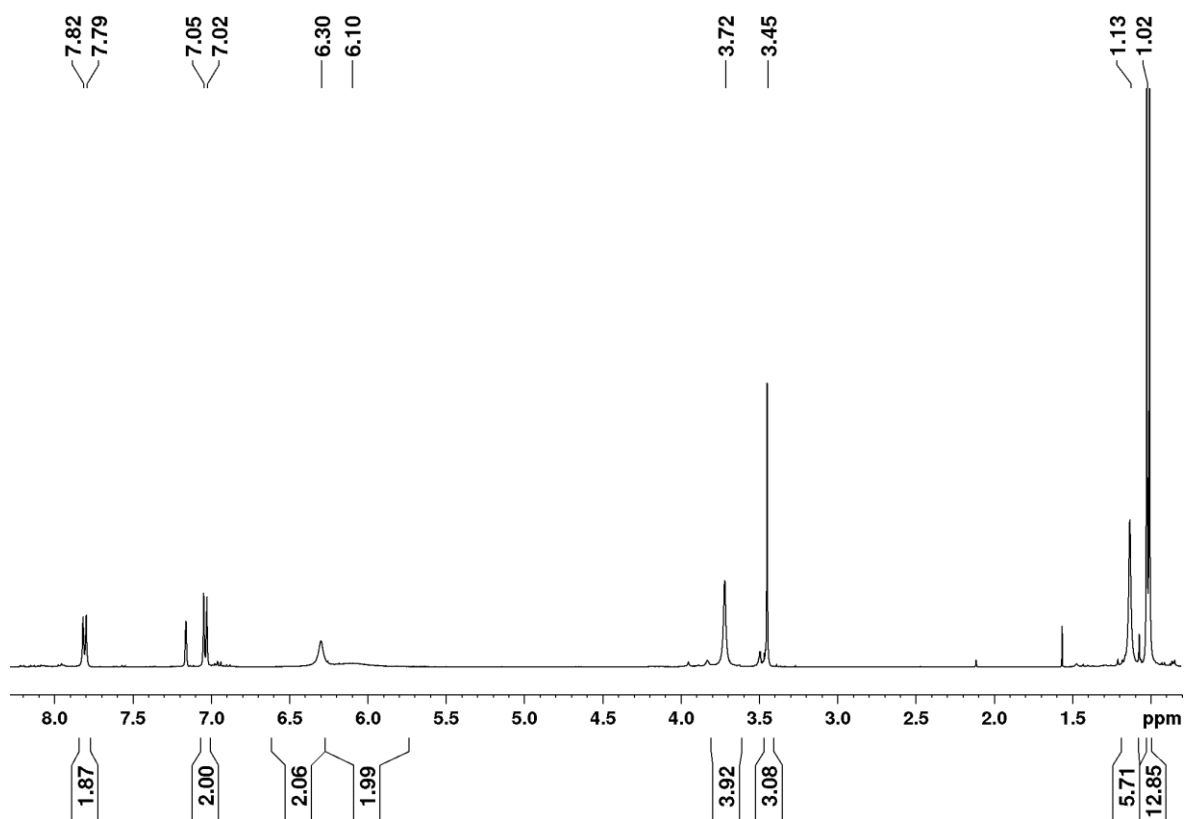


Figure 156: ^{11}B NMR spectrum (128 MHz) of 4-MeO-C₆H₄Bpin•Me₄Im ADD13 in C₆D₆.

Figure 157: $^{13}\text{C}\{^1\text{H}\}$ NMR spectrum (100 MHz) of 4-MeO-C₆H₄Bpin•Me₄Im ADD13 in C₆D₆.Figure 158: ^1H NMR spectrum (400 MHz) of 4-MeO-C₆H₄Bneop•*i*Pr₂Im ADD15 in C₆D₆.

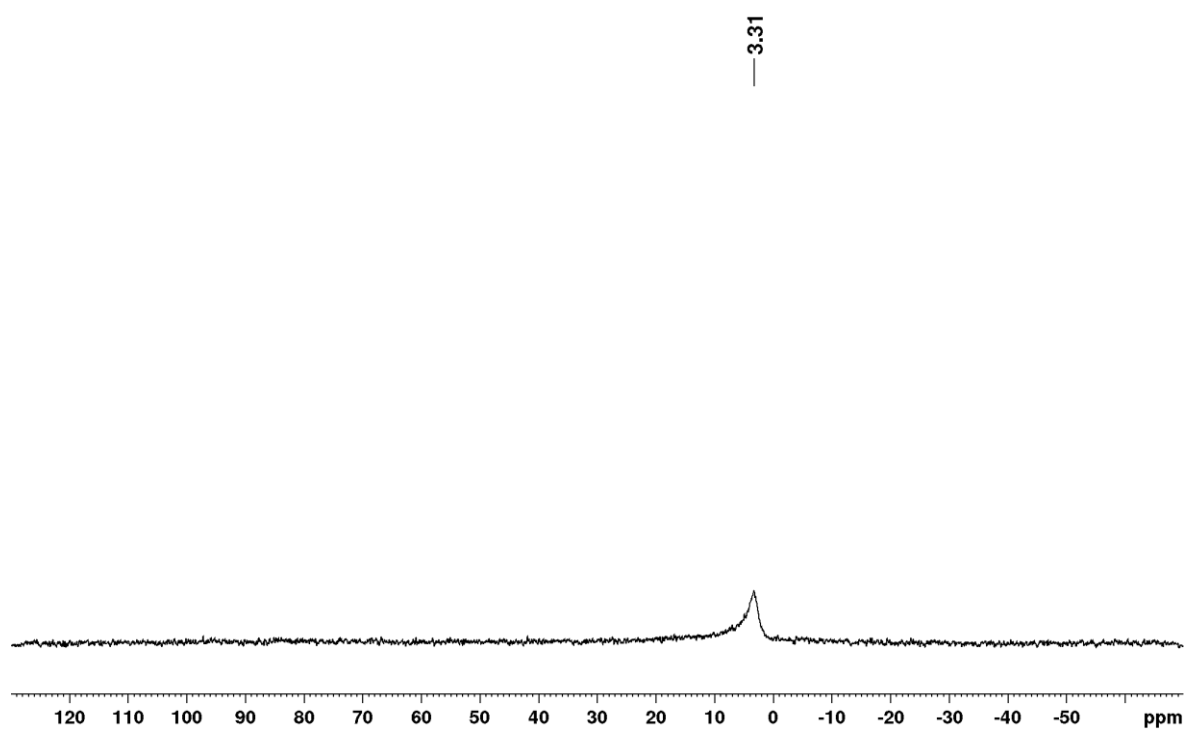


Figure 159: ^{11}B NMR spectrum (64 MHz) of 4-MeO-C₆H₄Bneop•*i*Pr₂Im ADD15 in C₆D₆.

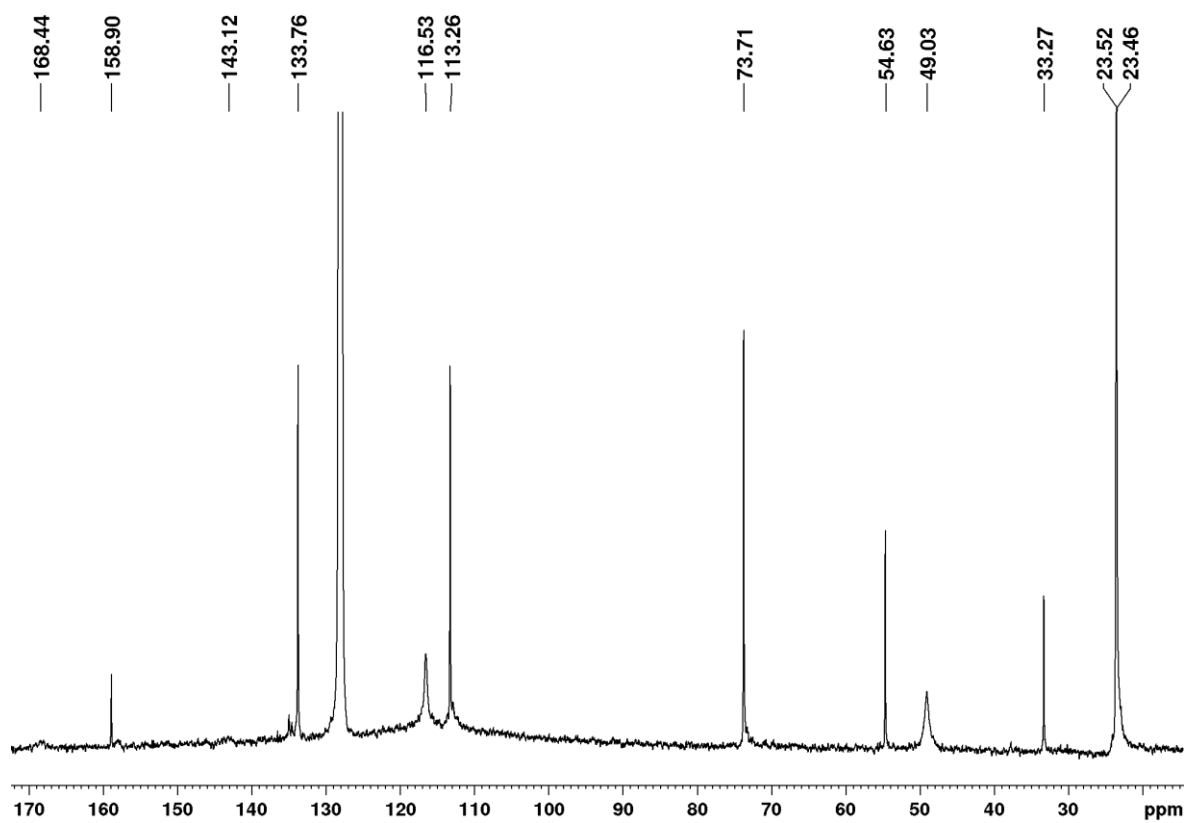


Figure 160: $^{13}\text{C}\{^1\text{H}\}$ NMR spectrum (100 MHz) of 4-MeO-C₆H₄Bneop•*i*Pr₂Im ADD15 in C₆D₆.

8 Appendix

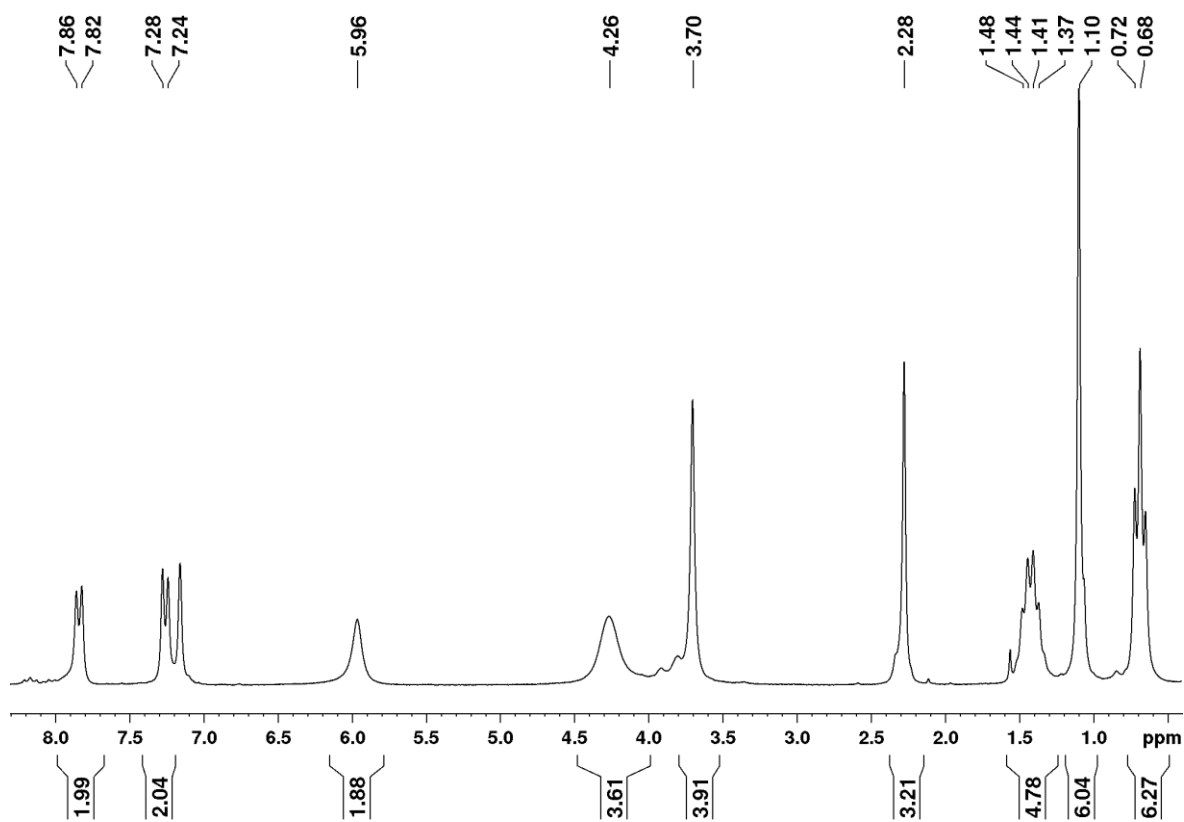


Figure 161: ^1H NMR spectrum (200 MHz) of 4-MeO-C₆H₄Bneop•ⁿPr₂Im ADD16 in C₆D₆.

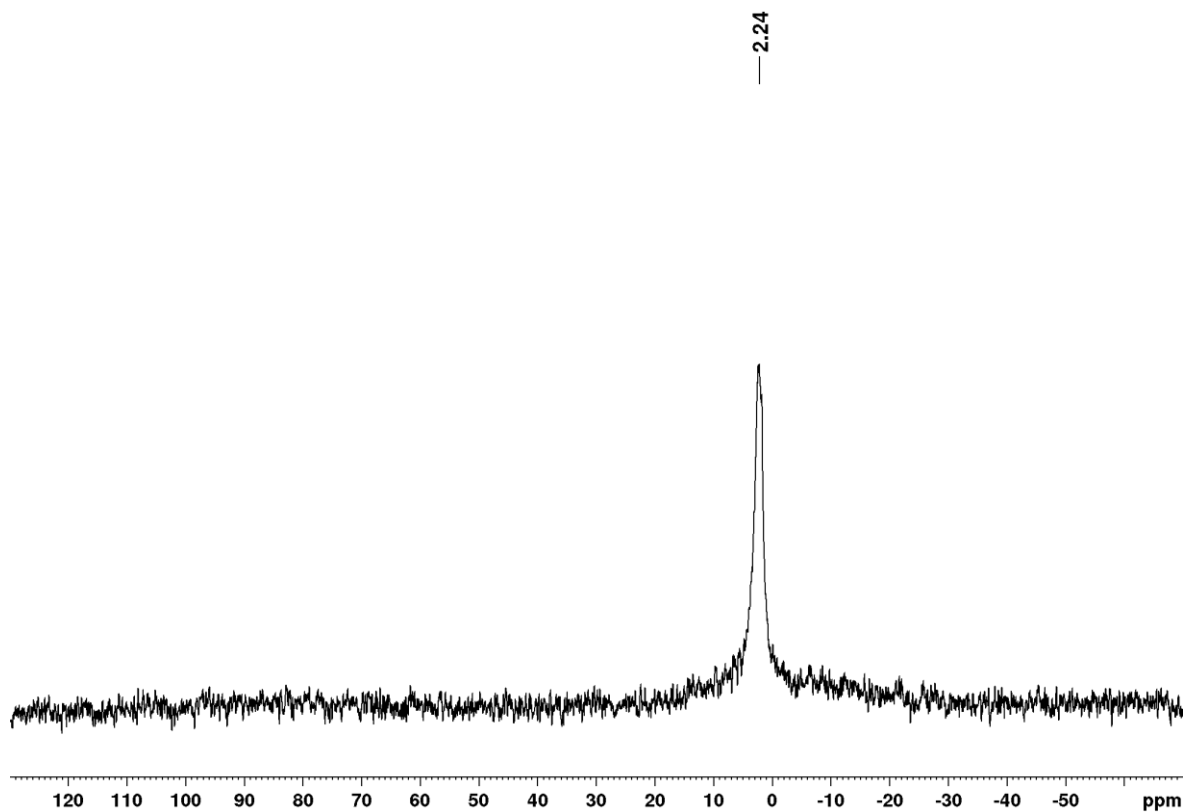


Figure 162: ^{11}B NMR spectrum (64 MHz) of 4-MeO-C₆H₄Bneop•ⁿPr₂Im ADD16 in C₆D₆.

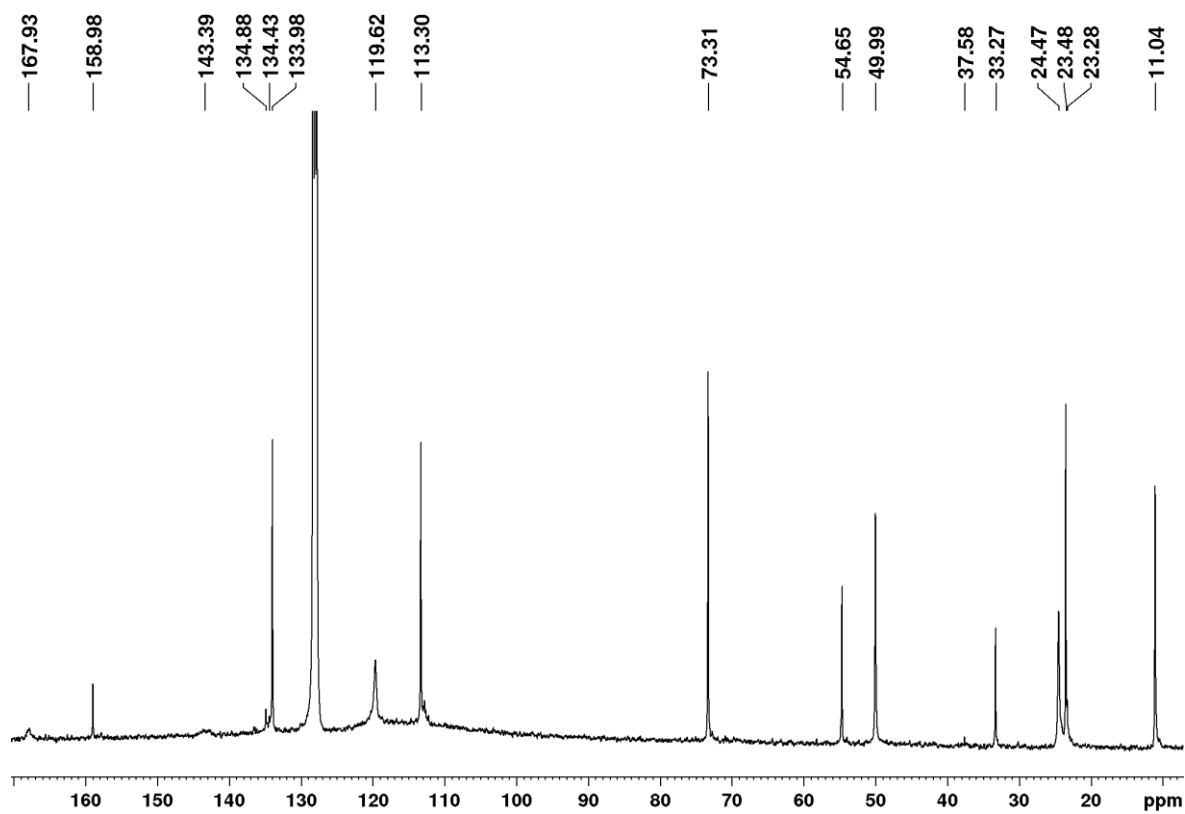


Figure 163: $^{13}\text{C}\{^1\text{H}\}$ NMR spectrum (100 MHz) of 4-MeO-C₆H₄Bneop*Pr₂Im ADD16 in C₆D₆.

8.3.2 NHC adducts of organoboronic ester

In the course of this study various adducts of aryl boronic esters and *N*-heterocyclic carbenes were synthesized and studied by X-ray diffraction for the first time. In Figures 164 to 169 the crystal structures are displayed. Table 91 summarizes important bond length and angles for comparison.

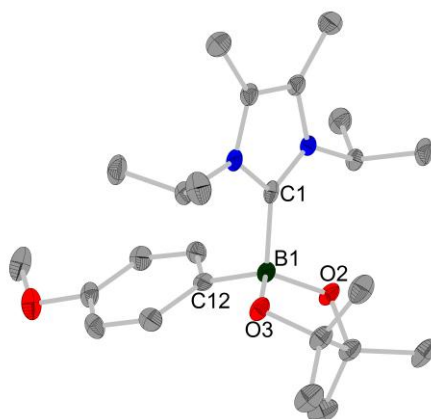


Figure 164: Molecular structure of 4-MeO-C₆H₄Bpin•Pr₂ImMe₂ ADD14. Element (color): carbon (grey), nitrogen (blue), boron (dark green), oxygen (red). Hydrogen atoms are omitted for clarity and the thermal ellipsoids are drawn at 50% probability. Selected bond lengths (Å) and angles (deg): C12-B1 1.629(2), C1-B1 1.691(3), C1-B1-C12 106.02(15), NC1N-C12B1 18.12(15), O1B1O2-C1B1C12 87.65(11).

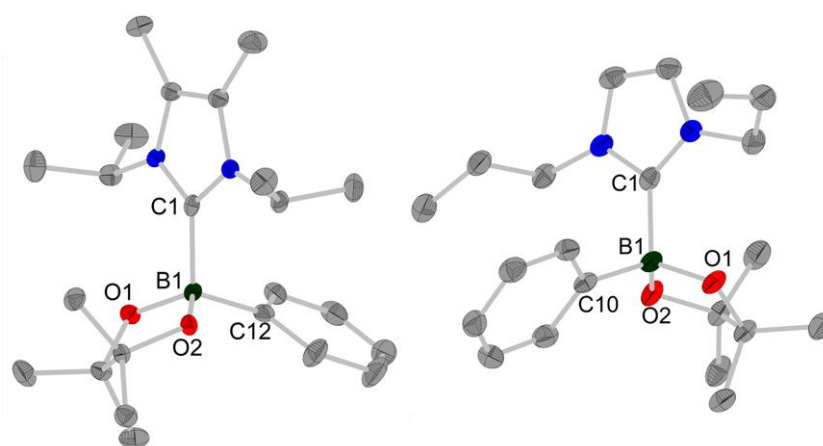


Figure 165: Element (color): carbon (grey), nitrogen (blue), boron (dark green), oxygen (red). Hydrogen atoms are omitted for clarity and the thermal ellipsoids are drawn at 50% probability. Left: Molecular structure of phenylBpin•Pr₂ImMe₂ ADD4. Selected bond lengths (Å) and angles (deg): C12-B1 1.632(2), C1-B1 1.689(2), C1-B1-C12 107.41(12), NC1N-C12B1 21.64(10), O1B1O2-C1B1C12 89.39(11) Right: Molecular structure of phenylBpin•Pr₂Im ADD3. Selected bond lengths (Å) and angles (deg): C10-B1 1.625(2), C1-B1 1.675(3), C1-B1-C10 103.46(11), NC1N-C10B1 20.67(8), O1B1O2-C1B1C10 87.67(10)

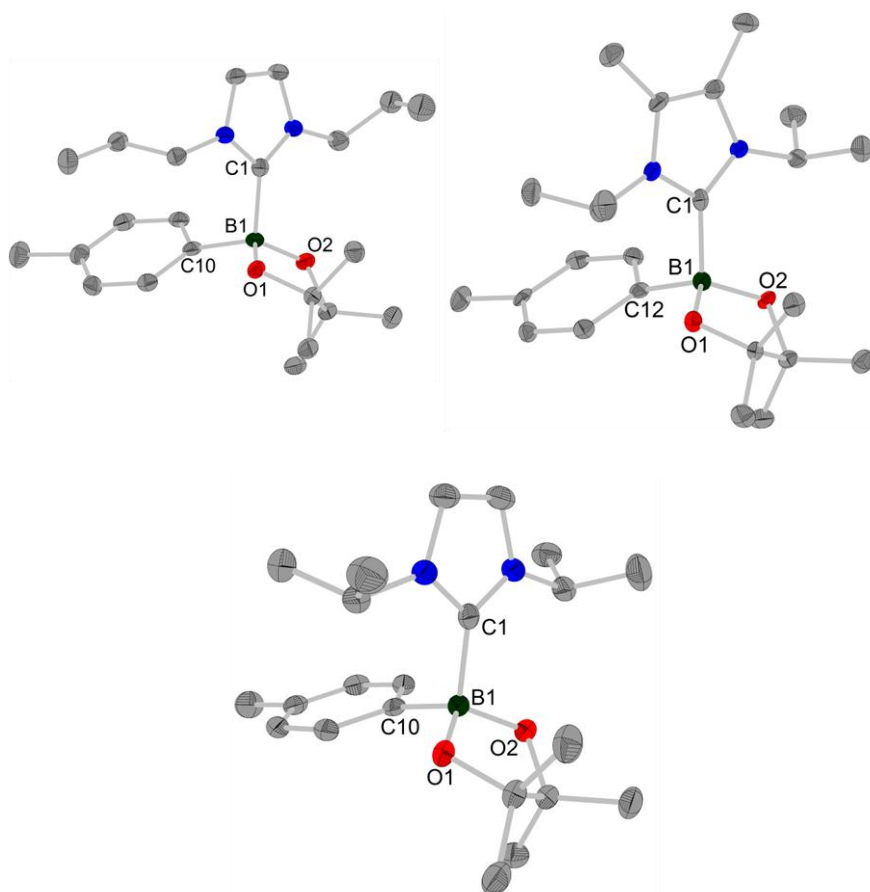


Figure 166: Element (color): carbon (grey), nitrogen (blue), boron (dark green), oxygen (red). Hydrogen atoms are omitted for clarity and the thermal ellipsoids are drawn at 50% probability. Top left: Molecular structure of *p*-tolylBpin·ⁿPr₂Im ADD6. Selected bond lengths (Å) and angles (deg): C10-B1 1.6325(17), C1-B1 1.6808(19), C1-B1-C10 103.51(10), NC1N-C10B1 22.45(6), O1B1O2-C1B1C10 87.83(7). Top right: Molecular structure of *p*-tolylBpin·ⁱPr₂ImMe₂ ADD7. Selected bond lengths (Å) and angles (deg): C12-B1 1.633(2), C1-B1 1.694(2), C1-B1-C12 103.46(11), NC1N-C12B1 20.67(8), O1B1O2-C1B1C12 87.67(10). Bottom: Molecular structure of *p*-tolylBpin·ⁱPr₂Im ADD5. Selected bond lengths (Å) and angles (deg): B1-C1 1.683(3), B1-C10 1.631(3), C10-B1-C1 104.64(14), NC1N-B1Cx 13.95(13), O1B1O2-C10B1C1 87.00(10)°.

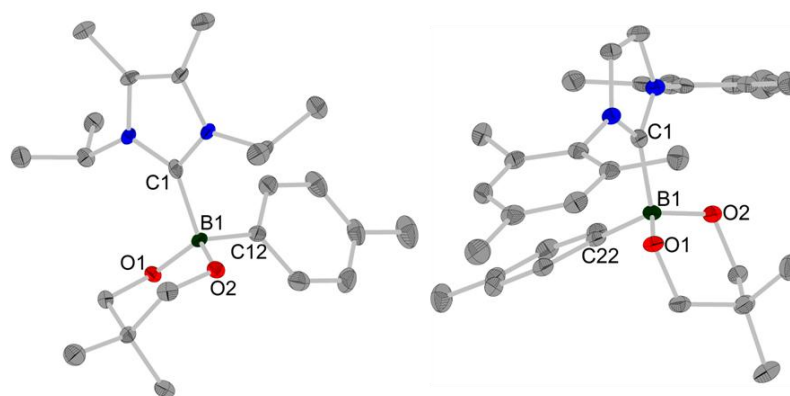


Figure 167: Element (color): carbon (grey), nitrogen (blue), boron (dark green), oxygen (red). Hydrogen atoms are omitted for clarity and the thermal ellipsoids are drawn at 50% probability. Left: Molecular structure of *p*-tolylBneop•Pr₂ImMe₂ ADD11. Selected bond lengths (Å) and angles (deg): C12-B1 1.620(2), C1-B1 1.697(2), C1-B1-C12 107.47(11), NC1N-C12B1 22.76(10), O1B1O2-C1B1C12 87.78(8). Right: Molecular structure of *p*-tolylBneop•Mes₂Im ADD10. Selected bond lengths (Å) and angles (deg): C22-B1 1.641(3) (1.640(3)), C1-B1 1.662(3) (1.665(3)), C1-B1-C22 109.15(16) (109.74(16)), NC1N-C22B1 19.41(17) (21.59(16)), O1B1O2-C1B1C22 88.32(15) (89.30(16))

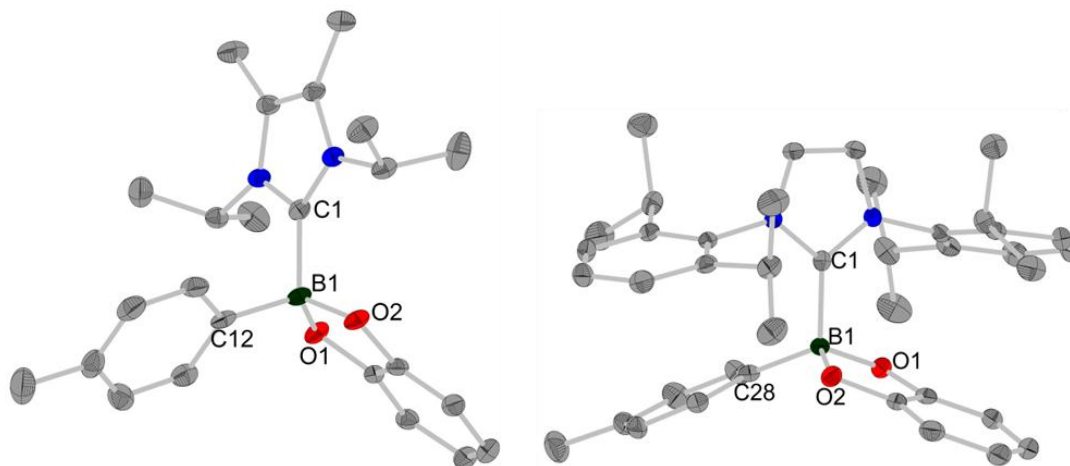


Figure 168: Element (color): carbon (grey), nitrogen (blue), boron (dark green), oxygen (red). Hydrogen atoms are omitted for clarity and the thermal ellipsoids are drawn at 50% probability. Left: Molecular structure of *p*-tolylBcat•Pr₂ImMe₂ ADD9. Selected bond lengths (Å) and angles (deg): C11-B1 1.616(2), C1-B1 1.666(3), C1-B1-C11 108.88(14), NC1N-C11B1 26.24(13), O1B1O2-C1B1C12 87.69(10). Right: Molecular structure of *p*-tolylBcat•Dipp₂Im ADD8. Selected bond lengths (Å) and angles (deg): C28-B1 1.6077(18), C1-B1 1.6742(17), C1-B1-C28 112.26(9), NC1N-C28B1 45.74(7), O1B1O2-C1B1C28 89.57(7).

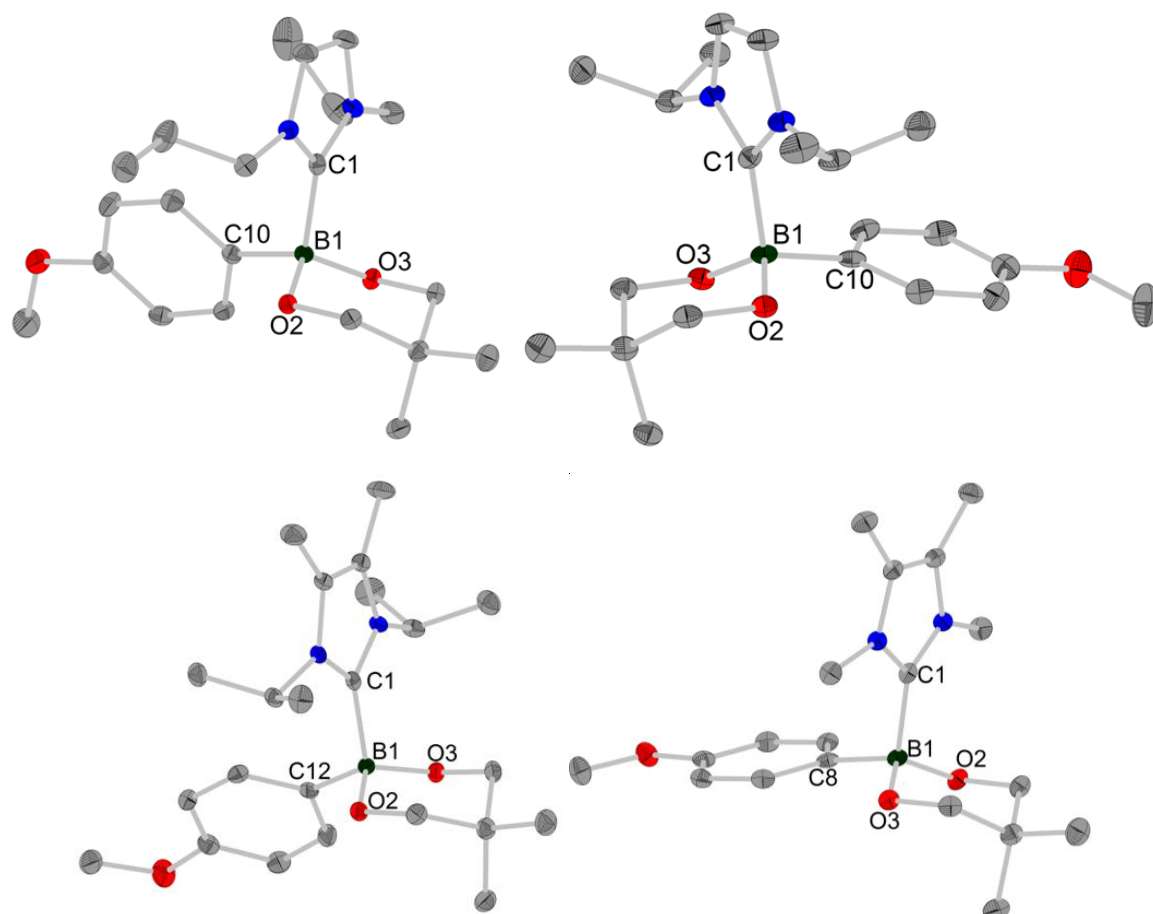


Figure 169: Element (color): carbon (grey), nitrogen (blue), boron (dark green), oxygen (red). Hydrogen atoms are omitted for clarity and the thermal ellipsoids are drawn at 50% probability. Top right: Molecular structure of 4-MeO-C₆H₄Bneop•ⁱPr₂Im ADD15. Selected bond lengths (Å) and angles (deg): C10-B1 1.613(3), C1-B1 1.694(3) C1-B1-C10 106.96(16), NC1N-C10B1 14.31(16), O1B1O2-C1B1C10 89.69(15). Top left: Molecular structure of 4-MeO-C₆H₄Bneop•ⁿPr₂Im ADD16. Selected bond lengths (Å) and angles (deg): C10-B1 1.6210(16), C1-B1 1.6860(16), C1-B1-C10 107.99(9), NC1N-C10B1 13.52(7), O1B1O2-C1B1C10 89.63(6). Bottom Left: Molecular structure of 4-MeO-C₆H₄Bneop•ⁱPr₂ImMe₂ ADD18. Selected bond lengths (Å) and angles (deg): C12-B1 1.6191(17), C1-B1 1.7194(19), C1-B1-C12 110.37(10), NC1N-C12B1 22.41(7), O1B1O2-C1B1C12 89.30(16). Bottom Right: 4-MeO-C₆H₄Bneop•Me₄Im ADD13. Selected bond lengths (Å) and angles (deg): C8-B1 1.615(2), C1-B1 1.706(2), C1-B1-C8 106.39(11), NC1N-C8B1 12.55, O1B1O2-C1B1C8 89.71.

Table 91: Comparison for important bond length and angles found in crystal structures of NHC organoboronic esters adducts.

	C _{Ar} -B1 [Å]	C1-B1 [Å]	C1-B1-C _{Ar} [°]	NC1N-B1C _{Ar} [°]	O1B1O2- C1B1C _{Ar} [°]
ADD3 phenylBpin• ⁿ Pr ₂ Im	1.625(2)	1.675(3)	103.46(11)	20.67(8)	87.67(10)
ADD4 phenylBpin• ⁱ Pr ₂ ImMe ₂	1.632(2)	1.689(2)	107.41(12)	21.64(10)	89.39(11)
ADD5 <i>p</i> -tolylBpin• ⁱ Pr ₂ Im	1.631(3)	1.683(3)	104.64(14)	13.95(13)	87.00(10)
ADD6 <i>p</i> -tolylBpin• ⁿ Pr ₂ Im	1.6325(17)	1.6808(19)	103.51(10)	22.45(6)	87.83(7)
ADD7 <i>p</i> -tolylBpin• ⁱ Pr ₂ ImMe ₂	1.633(2)	1.694(2)	103.46(11)	20.67(8)	87.67(10)
ADD8 <i>p</i> -tolylBcat•Dipp ₂ Im	1.6077(18)	1.6742(17)	112.26(9)	45.74(7)	89.57(7)
ADD9 <i>p</i> -tolylBcat• ⁱ Pr ₂ ImMe ₂	1.616(2)	1.666(3)	108.88(14)	26.24(13)	87.69(10)
ADD10 <i>p</i> -tolylBneop•Mes ₂ Im	1.641(3) (1.640(3))	1.662(3) (1.665(3))	109.15(16) (109.74(16))	19.41(17) (21.59(16))	88.32(15) (89.30(16))
ADD11 <i>p</i> -tolylBneop• ⁱ Pr ₂ ImMe ₂	1.620(2)	1.697(2)	107.47(11)	22.76(10)	87.78(8)
ADD13 4-MeO- C ₆ H ₄ Bneop•Me ₄ Im	1.615(2)	1.706(2)	106.39(11)	12.55(9)	89.71(7)
ADD14 4-MeO- C ₆ H ₄ Bpin• ⁱ Pr ₂ ImMe ₂	1.629(2)	1.691(3)	106.02(15)	18.12(15)	87.65(11)
ADD15 4-MeO- C ₆ H ₄ Benop• ⁱ Pr ₂ Im	1.613(3)	1.694(3)	106.96(16)	14.31(16)	89.69(15)
ADD16 4-MeO- C ₆ H ₄ Benop• ⁿ Pr ₂ Im	1.6210(16)	1.6860(16)	107.99(9)	13.52(7)	89.63(6)
ADD18 4-MeO- C ₆ H ₄ Bneop• ⁱ Pr ₂ ImMe ₂	1.6191(17)	1.7194(19)	110.37(10)	22.41(7)	89.30(16)

8.3.3 Aryl boronic esters

In the course of this study various aryl boronic esters were synthesized, of which some were studied by X-ray diffraction for the first time. In Figure 170 the corresponding crystal structures are displayed and Table 92 summarizes important bond length and angles for comparison.

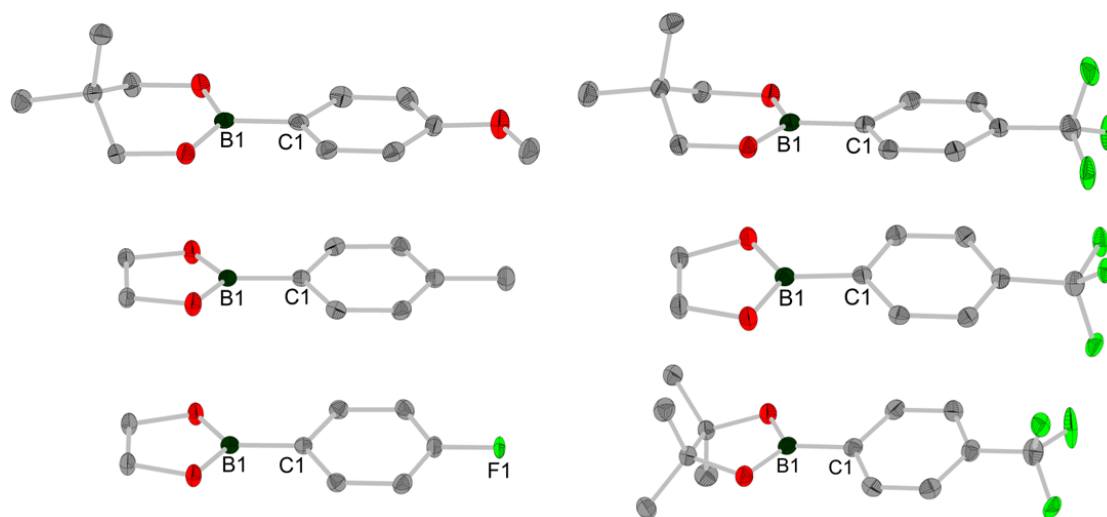


Figure 170: Element (color): carbon (grey), nitrogen (blue), boron (dark green), oxygen (red), fluorine (light green). Hydrogen atoms are omitted for clarity and the thermal ellipsoids are drawn at 50% probability. Left Top: Molecular structure of 4-MeO-C₆H₄Bneop. Selected bond lengths (Å) and angles (deg): C1-B1 1.555(3), B1-O2 1.369(2), B1-O3 1.363(3). Right Top: Molecular structure of 4-CF₃-C₆H₄Bneop. The minor part of the disorder is omitted for clarity. Selected bond lengths (Å) and angles (deg): C1-B1 1.576(2), B1-O1 1.3613(18), B1-O2 1.3560(19), O1B1O2-CC1C 1.78(12). Left Middle: Molecular structure of *p*-tolylBeg. Selected bond lengths (Å) and angles (deg): C1-B1 1.5586(19), B1-O1 1.3651(10), B1-O2 1.3651(10), O1B1O2-CC1C 5.21(3). Right Middle: Molecular structure of 4-CF₃-C₆H₄Beg. Selected bond lengths (Å) and angles (deg): C1-B1 1.562(2), B1-O1 1.3606(19), B1-O2 1.3660(19), O1B1O2-CC1C 6.18(16). Left Bottom: Molecular structure of 4-F-C₆H₄Beg. Selected bond lengths (Å) and angles (deg): C1-B1 1.551(2), B1-O1 1.3664(11), B1-O2 1.3664(12), O1B1O2-CC1C 5.58(4). Right Bottom: Molecular structure of 4-CF₃-C₆H₄Bpin. The minor part of the disorder is omitted for clarity. Selected bond lengths (Å) and angles (deg): C1-B1 1.5590(18), B1-O1 1.3613(18), B1-O2 1.3625(18), O1B1O2-CC1C 8.93(8).

Table 92: Comparison for important bond length and angles found in crystal structures of aryl boronic esters.

	Distance: B1-C1 [Å]	Distance: B1-O1 [Å]	Distance: B1-O2 [Å]	Angle: O1B1O2- CC1C [°]
4-MeO- C ₆ H ₄ Bneop	1.555(3)	1.369(2)	1.363(3)	8.27(9)
<i>p</i> -tolylBeg	1.5586(19)	1.3651(10)	1.3651(10)	5.21(3)
4-F- C ₆ H ₄ Beg	1.551(2)	1.3664(11)	1.3664(12)	5.58(4)
4-CF ₃ - C ₆ H ₄ Beg	1.562(2)	1.3606(19)	1.3660(19)	6.18(16)
4-CF ₃ - C ₆ H ₄ Bpin	1.5590(18)	1.3613(18)	1.3625(18)	8.93(8)
4-CF ₃ - C ₆ H ₄ Bneop	1.576(2)	1.3613(18)	1.3560(19)	1.78(12)

9 Bibliography

- [1] C. E. Tucker, J. Davidson, P. Knochel, *J. Org. Chem.* **1992**, *57*, 3482-3485.
- [2] A. Suzuki, *J. Organomet. Chem.* **1999**, *576*, 147-168.
- [3] M. A. Beenen, C. An, J. A. Ellman, *J. Am. Chem. Soc.* **2008**, *130*, 6910-6911.
- [4] C.-T. Yang, Z.-Q. Zhang, H. Tajuddin, C.-C. Wu, J. Liang, J.-H. Liu, Y. Fu, M. Czyzewska, P. G. Steel, T. B. Marder, L. Liu, *Angew. Chem. Int. Ed.* **2012**, *51*, 528-532.
- [5] L. Borissenko, M. Groll, *Chem. Rev.* **2007**, *107*, 687-717.
- [6] P. Pérez-Galán, G. Roué, N. Villamor, E. Montserrat, E. Campo, D. Colomer, *Blood* **2006**, *107*, 257-264.
- [7] N. Miyaura, A. Suzuki, *Chem. Rev.* **1995**, *95*, 2457-2483.
- [8] D. G. Hall, *Boronic Acids - Preparation, Applications in Organic Synthesis and Medicine (2nd Edition)* **2005**, Wiley-VCH, Weinheim, Germany.
- [9] I. Beletskaya, C. Moberg, *Chem. Rev.* **1999**, *99*, 3435-3462.
- [10] I. Beletskaya, C. Moberg, *Chem. Rev.* **2006**, *106*, 2320-2354.
- [11] D. M. T. Chan, K. L. Monaco, R. Li, D. Bonne, C. G. Clark, P. Y. S. Lam, *Tetrahedron Lett.* **2003**, *44*, 3863-3865.
- [12] P. Y. S. Lam, G. Vincent, D. Bonne, C. G. Clark, *Tetrahedron Lett.* **2003**, *44*, 4927-4931.
- [13] J. D. Sieber, S. Liu, J. P. Morken, *J. Am. Chem. Soc.* **2007**, *129*, 2214-2215.
- [14] R. Van Noorden, *Nature* **2010**, doi:10.1038/news.2010.1511
- [15] H. R. Snyder, J. A. Kuck, J. R. Johnson, *J. Am. Chem. Soc.* **1938**, *60*, 105-111.
- [16] P. A. McCusker, L. J. Glunz, *J. Am. Chem. Soc.* **1955**, *77*, 4253-4255.
- [17] P. B. Brindley, W. Gerrard, M. F. Lappert, *J. Chem. Soc.* **1955**, 2956-2958.
- [18] H. C. Mattraw, C. E. Erickson, A. W. Laubengayer, *J. Am. Chem. Soc.* **1956**, *78*, 4901-4904.
- [19] P. A. McCusker, E. C. Ashby, H. S. Makowski, *J. Am. Chem. Soc.* **1957**, *79*, 5179-5181.
- [20] R. M. Washburn, E. Levens, C. F. Albright, F. A. Billig, E. S. Cernak, *Metal-Organic Compounds* **1959**, *23*, 102-128.
- [21] H. C. Brown, T. E. Cole, *Organometallics* **1983**, *2*, 1316-1319.
- [22] H. C. Brown, M. Srebnik, T. E. Cole, *Organometallics* **1986**, *5*, 2300-2303.
- [23] K.-T. Wong, Y.-Y. Chien, Y.-L. Liao, C.-C. Lin, M.-Y. Chou, M.-k. Leung, *J. Org. Chem.* **2002**, *67*, 1041-1044.

- [24] K. Burgess, W. A. Van der Donk, S. A. Westcott, T. B. Marder, R. T. Baker, J. C. Calabrese, *J. Am. Chem. Soc.* **1992**, *114*, 9350-9359.
- [25] Y. Yang, *Angew. Chem. Int. Ed.* **2016**, *55*, 345-349.
- [26] R. Sakae, K. Hirano, T. Satoh, M. Miura, *Angew. Chem. Int. Ed.* **2015**, *54*, 613-617.
- [27] Y. Sasaki, C. Zhong, M. Sawamura, H. Ito, *J. Am. Chem. Soc.* **2010**, *132*, 1226-1227.
- [28] R. Sakae, N. Matsuda, K. Hirano, T. Satoh, M. Miura, *Org. Lett.* **2014**, *16*, 1228-1231.
- [29] H. Yoshida, I. Kageyuki, K. Takaki, *Synthesis* **2014**, *46*, 1924-1932.
- [30] S. Hong, M. Liu, W. Zhang, Q. Zeng, W. Deng, *Tetrahedron Lett.* **2015**, *56*, 2297-2302.
- [31] K. Kubota, Y. Watanabe, H. Ito, *Adv. Synth. Catal.* **2016**, *358*, 2379-2384.
- [32] Y. Sasaki, Y. Horita, C. Zhong, M. Sawamura, H. Ito, *Angew. Chem. Int. Ed.* **2011**, *50*, 2778-2782.
- [33] K. Kubota, E. Yamamoto, H. Ito, *Adv. Synth. Catal.* **2013**, *355*, 3527-3531.
- [34] X. Feng, H. Jeon, J. Yun, *Angew. Chem. Int. Ed.* **2013**, *52*, 3989-3992.
- [35] Y. Wen, J. Xie, C. Deng, C. Li, *J. Org. Chem.* **2015**, *80*, 4142-4147.
- [36] Y. Luo, I. D. Roy, A. G. Madec, H. W. Lam, *Angew. Chem. Int. Ed.* **2014**, *53*, 4186-4190.
- [37] T. Jia, P. Cao, D. Wang, Y. Lou, J. Liao, *Chem. Eur. J.* **2015**, *21*, 4918-4922.
- [38] N. Matsuda, K. Hirano, T. Satoh, M. Miura, *J. Am. Chem. Soc.* **2013**, *135*, 4934-4937.
- [39] K. M. Logan, K. B. Smith, M. K. Brown, *Angew. Chem. Int. Ed.* **2015**, *54*, 5228-5231.
- [40] H. C. Jiang, X. Y. Tang, M. Shi, *Chem. Commun.* **2016**, *52*, 5273-5276.
- [41] H. Ito, T. Toyoda, M. Sawamura, *J. Am. Chem. Soc.* **2010**, *132*, 5990-5992.
- [42] D. Noh, H. Chea, J. Ju, J. Yun, *Angew. Chem. Int. Ed.* **2009**, *48*, 6062-6064.
- [43] R. Sakae, K. Hirano, M. Miura, *J. Am. Chem. Soc.* **2015**, *137*, 6460-6463.
- [44] M. Guisan-Ceinos, A. Parra, V. Martin-Heras, M. Tortosa, *Angew. Chem. Int. Ed.* **2016**, *55*, 6969-6972.
- [45] H. Ito, Y. Kosaka, K. Nonoyama, Y. Sasaki, M. Sawamura, *Angew. Chem. Int. Ed.* **2008**, *47*, 7424-7427.
- [46] K. Semba, Y. Nakao, *J. Am. Chem. Soc.* **2014**, *136*, 7567-7570.
- [47] V. Hornillos, C. Vila, E. Otten, B. L. Feringa, *Angew. Chem. Int. Ed.* **2015**, *54*, 7867-7871.
- [48] K. Kubota, K. Hayama, H. Iwamoto, H. Ito, *Angew. Chem. Int. Ed.* **2015**, *54*, 8809-8813.
- [49] K. B. Smith, K. M. Logan, W. You, M. K. Brown, *Chem. Eur. J.* **2014**, *20*, 12032-12036.

- [50] W. Zhao, J. Montgomery, *Angew. Chem. Int. Ed.* **2015**, *54*, 12683-12686.
- [51] W. Su, T. J. Gong, X. Lu, M. Y. Xu, C. G. Yu, Z. Y. Xu, H. Z. Yu, B. Xiao, Y. Fu, *Angew. Chem. Int. Ed.* **2015**, *54*, 12957-12961.
- [52] K. Kato, K. Hirano, M. Miura, *Angew. Chem. Int. Ed.* **2016**, *55*, 14400-14404.
- [53] A. Parra, L. Amenos, M. Guisan-Ceinos, A. Lopez, J. L. Garcia Ruano, M. Tortosa, *J. Am. Chem. Soc.* **2014**, *136*, 15833-15836.
- [54] T. Itoh, T. Matsueda, Y. Shimizu, M. Kanai, *Chem. Eur. J.* **2015**, *21*, 15955-15959.
- [55] D. Männig, H. Nöth, *Angew. Chem. Int. Ed.* **1985**, *24*, 878-879.
- [56] K. Burgess, M. J. Ohlmeyer, *Chem. Rev.* **1991**, *91*, 1179-1191.
- [57] D. A. Evans, G. C. Fu, B. A. Anderson, *J. Am. Chem. Soc.* **1992**, *114*, 6679-6685.
- [58] I. Beletskaya, A. Pelter, *Tetrahedron* **1997**, *53*, 4957-5026.
- [59] R. T. Baker, P. Nguyen, T. B. Marder, S. A. Westcott, *Angew. Chem. Int. Ed.* **1995**, *34*, 1336-1338.
- [60] T. Ishiyama, M. Yamamoto, N. Miyaura, *Chem. Commun.* **1996**, 2073-2074.
- [61] C. N. Iverson, M. R. Smith, *Organometallics* **1997**, *16*, 2757-2759.
- [62] T. Ishiyama, M. Yamamoto, N. Miyaura, *Chem. Commun.* **1997**, 689-690.
- [63] T. Ishiyama, T. Kitano, N. Miyaura, *Tetrahedron Lett.* **1998**, *39*, 2357-2360.
- [64] C. Dai, T. B. Marder, E. G. Robins, D. S. Yufit, J. A. K. Howard, T. B. Marder, A. J. Scott, W. Clegg, *Chem. Commun.* **1998**, 1983-1984.
- [65] T. B. Marder, N. C. Norman, C. R. Rice, *Tetrahedron Lett.* **1998**, *39*, 155-158.
- [66] T. Ishiyama, S. Momota, N. Miyaura, *Synlett* **1999**, *1999*, 1790-1792.
- [67] G. Mann, K. D. John, R. T. Baker, *Org. Lett.* **2000**, *2*, 2105-2108.
- [68] F.-Y. Yang, C.-H. Cheng, *J. Am. Chem. Soc.* **2001**, *123*, 761-762.
- [69] P. Nguyen, R. B. Coapes, A. D. Woodward, N. J. Taylor, J. M. Burke, J. A. K. Howard, T. B. Marder, *J. Organomet. Chem.* **2002**, *652*, 77-85.
- [70] J. B. Morgan, S. P. Miller, J. P. Morken, *J. Am. Chem. Soc.* **2003**, *125*, 8702-8703.
- [71] N. F. Pelz, A. R. Woodward, H. E. Burks, J. D. Sieber, J. P. Morken, *J. Am. Chem. Soc.* **2004**, *126*, 16328-16329.
- [72] J. D. Sieber, J. P. Morken, *J. Am. Chem. Soc.* **2005**, *128*, 74-75.
- [73] J. Ramirez, R. Corberan, M. Sanau, E. Peris, E. Feràndez, *Chem. Commun.* **2005**, 3056-3058.
- [74] S. Trudeau, J. B. Morgan, M. Shrestha, J. P. Morken, *J. Org. Chem.* **2005**, *70*, 9538-9544.

- [75] R. Corberán, J. Ramírez, M. Poyatos, E. Peris, E. Fernández, *Tetrahedron: Asymmetry* **2006**, *17*, 1759-1762.
- [76] V. Lillo, M. R. Fructos, J. Ramírez, A. A. C. Braga, F. Maseras, M. M. Díaz-Requejo, P. J. Pérez, E. Fernández, *Chem. Eur. J.* **2007**, *13*, 2614-2621.
- [77] H. Y. Cho, J. P. Morken, *J. Am. Chem. Soc.* **2008**, *130*, 16140-16141.
- [78] G. Lesley, P. Nguyen, N. J. Taylor, T. B. Marder, A. J. Scott, W. Clegg, N. C. Norman, *Organometallics* **1996**, *15*, 5137-5154.
- [79] C. N. Iverson, M. R. Smith, *Organometallics* **1996**, *15*, 5155-5165.
- [80] T. Ishiyama, N. Miyaura, *J. Organomet. Chem.* **2000**, *611*, 392-402.
- [81] R. L. Thomas, F. E. S. Souza, T. B. Marder, *Dalton Trans.* **2001**, 1650-1656.
- [82] J. Yun, *Asian J Org Chem* **2013**, *2*, 1016-1025.
- [83] R. Barbeyron, E. Benedetti, J. Cossy, J.-J. Vasseur, S. Arseniyadis, M. Smietana, *Tetrahedron* **2014**, *70*, 8431-8452.
- [84] H. Yoshida, *ACS Catal.* **2016**, *6*, 1799-1811.
- [85] H. Yoshida, S. Kawashima, Y. Takemoto, K. Okada, J. Ohshita, K. Takaki, *Angew. Chem. Int. Ed.* **2012**, *51*, 235-238.
- [86] N. Nakagawa, T. Hatakeyama, M. Nakamura, *Chem. Eur. J.* **2015**, *21*, 4257-4261.
- [87] S. Krautwald, M. J. Bezdek, P. J. Chirik, *J. Am. Chem. Soc.* **2017**, *139*, 3868-3875.
- [88] T. Ishiyama, N. Matsuda, M. Murata, F. Ozawa, A. Suzuki, N. Miyaura, *Organometallics* **1996**, *15*, 713-720.
- [89] T. Ishiyama, N. Matsuda, N. Miyaura, A. Suzuki, *J. Am. Chem. Soc.* **1993**, *115*, 11018-11019.
- [90] T. Marder, N. Norman, *Top. Catal.* **1998**, *5*, 63-73.
- [91] T. Ishiyama, N. Miyaura, *Chem. Rec.* **2004**, *3*, 271-280.
- [92] T. Ishiyama, M. Murata, N. Miyaura, *J. Org. Chem.* **1995**, *60*, 7508-7510.
- [93] T. Ishiyama, Y. Itoh, T. Kitano, N. Miyaura, *Tetrahedron Lett.* **1997**, *38*, 3447-3450.
- [94] T. Ishiyama, K. Ishida, N. Miyaura, *Tetrahedron* **2001**, *57*, 9813-9816.
- [95] A. Fürstner, G. Seidel, *Org. Lett.* **2002**, *4*, 541-543.
- [96] C. Xu, J.-F. Gong, M.-P. Song, Y.-J. Wu, *Transit. Met. Chem.* **2009**, *34*, 175-179.
- [97] M. Murata, S. Watanabe, Y. Masuda, *J. Org. Chem.* **1997**, *62*, 6458-6459.
- [98] M. Murata, T. Oyama, S. Watanabe, Y. Masuda, *J. Org. Chem.* **1999**, *65*, 164-168.
- [99] O. Baudoin, D. Guénard, F. Guéritte, *J. Org. Chem.* **2000**, *65*, 9268-9271.

- [100] F. Labre, Y. Gimbert, P. Bannwarth, S. Olivero, E. Dunach, P. Y. Chavant, *Org. Lett.* **2014**, *16*, 2366-2369.
- [101] S. C. Schmid, R. Van Hoveln, J. W. Rigoli, J. M. Schomaker, *Organometallics* **2015**, *34*, 4164-4173.
- [102] R. J. Van Hoveln, S. C. Schmid, M. Tretbar, C. T. Buttke, J. M. Schomaker, *Chem. Sci.* **2014**, *5*, 4763-4767.
- [103] R. Van Hoveln, B. M. Hudson, H. B. Wedler, D. M. Bates, G. Le Gros, D. J. Tantillo, J. M. Schomaker, *J. Am. Chem. Soc.* **2015**, *137*, 5346-5354.
- [104] T. S. Zhao, Y. Yang, T. Lessing, K. J. Szabo, *J. Am. Chem. Soc.* **2014**, *136*, 7563-7566.
- [105] R. J. Van Hoveln, S. C. Schmid, J. M. Schomaker, *Org. Biomol. Chem.* **2014**, *12*, 7655-7658.
- [106] S. Ando, H. Matsunaga, T. Ishizuka, *J. Org. Chem.* **2015**, *80*, 9671-9681.
- [107] R. D. Grigg, R. Van Hoveln, J. M. Schomaker, *J. Am. Chem. Soc.* **2012**, *134*, 16131-16134.
- [108] A. B. Morgan, J. L. Jurs, J. M. Tour, *J. Appl. Polym. Sci.* **2000**, *76*, 1257-1268.
- [109] B. M. Rosen, C. Huang, V. Percec, *Org. Lett.* **2008**, *10*, 2597-2600.
- [110] D. A. Wilson, C. J. Wilson, B. M. Rosen, V. Percec, *Org. Lett.* **2008**, *10*, 4879-4882.
- [111] P. Nguyen, H. P. Blom, S. A. Westcott, N. J. Taylor, T. B. Marder, *J. Am. Chem. Soc.* **1993**, *115*, 9329-9330.
- [112] I. A. I. Mkhalid, J. H. Barnard, T. B. Marder, J. M. Murphy, J. F. Hartwig, *Chem. Rev.* **2009**, *110*, 890-931.
- [113] J. F. Hartwig, *Acc. Chem. Res.* **2011**, *45*, 864-873.
- [114] T. Ishiyama, J. Takagi, K. Ishida, N. Miyaoura, N. R. Anastasi, J. F. Hartwig, *J. Am. Chem. Soc.* **2001**, *124*, 390-391.
- [115] I. A. I. Mkhalid, D. N. Coventry, D. Albesa-Jove, A. S. Batsanov, J. A. K. Howard, R. N. Perutz, T. B. Marder, *Angew. Chem. Int. Ed.* **2006**, *45*, 489-491.
- [116] P. Harrisson, J. Morris, P. G. Steel, T. B. Marder, *Synlett* **2009**, *2009*, 147-150.
- [117] H. Tajuddin, L. Shukla, A. C. Maxwell, T. B. Marder, P. G. Steel, *Org. Lett.* **2010**, *12*, 5700-5703.
- [118] P. Harrisson, J. Morris, T. B. Marder, P. G. Steel, *Org. Lett.* **2009**, *11*, 3586-3589.
- [119] H. Chen, S. Schlecht, T. C. Semple, J. F. Hartwig, *Science* **2000**, *287*, 1995-1997.
- [120] J. D. Lawrence, M. Takahashi, C. Bae, J. F. Hartwig, *J. Am. Chem. Soc.* **2004**, *126*, 15334-15335.

- [121] C. S. Wei, C. A. Jiménez-Hoyos, M. F. Videa, J. F. Hartwig, M. B. Hall, *J. Am. Chem. Soc.* **2010**, *132*, 3078-3091.
- [122] Y. Kondo, D. García-Cuadrado, J. F. Hartwig, N. K. Boen, N. L. Wagner, M. A. Hillmyer, *J. Am. Chem. Soc.* **2002**, *124*, 1164-1165.
- [123] S. Shimada, A. S. Batsanov, J. A. K. Howard, T. B. Marder, *Angew. Chem. Int. Ed.* **2001**, *40*, 2168-2171.
- [124] T. Ishiyama, K. Ishida, J. Takagi, N. Miyaura, *Chem. Lett.* **2001**, *30*, 1082-1083.
- [125] S. H. Cho, J. F. Hartwig, *J. Am. Chem. Soc.* **2013**, *135*, 8157-8160.
- [126] M. A. Larsen, C. V. Wilson, J. F. Hartwig, *J. Am. Chem. Soc.* **2015**, *137*, 8633-8643.
- [127] W. N. Palmer, J. V. Obligacion, I. Pappas, P. J. Chirik, *J. Am. Chem. Soc.* **2016**, *138*, 766-769.
- [128] C. M. Kelly, J. T. Fuller, 3rd, C. M. Macaulay, R. McDonald, M. J. Ferguson, S. M. Bischof, O. L. Sydora, D. H. Ess, M. Stradiotto, L. Turculet, *Angew. Chem. Int. Ed.* **2017**, *56*, 6312-6316.
- [129] J. He, Q. Shao, Q. Wu, J. Q. Yu, *J. Am. Chem. Soc.* **2017**, *139*, 3344-3347.
- [130] T. J. Mazzacano, N. P. Mankad, *J. Am. Chem. Soc.* **2013**, *135*, 17258-17261.
- [131] S. R. Parmelee, T. J. Mazzacano, Y. Zhu, N. P. Mankad, J. A. Keith, *ACS Catal.* **2015**, *5*, 3689-3699.
- [132] V. W. Rosso, D. A. Lust, P. J. Bernot, J. A. Grosso, S. P. Modi, A. Rusowicz, T. C. Sedergran, J. H. Simpson, S. K. Srivastava, M. J. Humora, N. G. Anderson, *Org. Process Res. Dev.* **1997**, *1*, 311-314.
- [133] J. M. French, J. R. Griffiths, S. T. Diver, *Adv. Synth. Catal.* **2015**, *357*, 361-365.
- [134] C. E. Garrett, K. Prasad, *Adv. Synth. Catal.* **2004**, *346*, 889-900.
- [135] S. Enthaler, K. Junge, M. Beller, *Angew. Chem. Int. Ed.* **2008**, *47*, 3317-3321.
- [136] C. A. Flemming, J. T. Trevors, *Water Air and Soil Pollut* **1989**, *44*, 143-158.
- [137] B. E. Kim, T. Nevitt, D. J. Thiele, *Nat. Chem. Biol.* **2008**, *4*, 176-185.
- [138] V. Hong, N. F. Steinmetz, M. Manchester, M. G. Finn, *Bioconjug. Chem.* **2010**, *21*, 1912-1916.
- [139] S. Lutsenko, J. H. Kaplan, *Biochemistry* **1995**, *34*, 15607-15613.
- [140] M. Solioz, C. Vulpe, *Trends Biochem. Sci.* **1996**, *21*, 237-241.
- [141] J. Lee, M. J. Petris, D. J. Thiele, *J. Biol. Chem.* **2002**, *277*, 40253-40259.
- [142] Y. M. Kuo, B. Zhou, D. Cosco, J. Gitschier, *Proc. Natl. Acad. Sci. USA* **2001**, *98*, 6836-6841.

- [143] J. Lee, J. R. Prohaska, D. J. Thiele, *Proc. Natl. Acad. Sci. USA* **2001**, *98*, 6842-6847.
- [144] K. S. Egorova, V. P. Ananikov, *Angew. Chem. Int. Ed.* **2016**, *55*, 12150-12162.
- [145] G. Stavber, Z. Časar, *ChemCatChem* **2014**, *6*, 2162-2174.
- [146] S. R. Chemler, *Beilstein J. Org. Chem.* **2015**, *11*, 2252-2253.
- [147] A. Alexakis, N. Krause, S. Woodward, *Copper-Catalyzed Asymmetric Synthesis* **2014**, Wiley-VCH, Weinheim, Germany.
- [148] H. Ito, H. Yamanaka, J.-i. Tateiwa, A. Hosomi, *Tetrahedron Lett.* **2000**, *41*, 6821-6825.
- [149] K. Takahashi, T. Ishiyama, N. Miyaoura, *Chem. Lett.* **2000**, *29*, 982-983.
- [150] W. Zhu, D. Ma, *Org. Lett.* **2005**, *8*, 261-263.
- [151] C. Kleeberg, L. Dang, Z. Lin, T. B. Marder, *Angew. Chem. Int. Ed.* **2009**, *48*, 5350-5354.
- [152] G. H. Posner, *Organic Reactions* **1975**, *22*, 253.
- [153] B. H. Lipshutz, S. Sengupta, *Organic Reactions* **1992**, *40*, 641.
- [154] E. Erdik, *Tetrahedron* **1984**, *40*, 641-657.
- [155] G. Cahiez, C. Chaboche, M. Jézéquel, *Tetrahedron* **2000**, *56*, 2733-2737.
- [156] J. Terao, A. Ikumi, H. Kuniyasu, N. Kambe, *J. Am. Chem. Soc.* **2003**, *125*, 5646-5647.
- [157] J. Terao, H. Todo, S. A. Begum, H. Kuniyasu, N. Kambe, *Angew. Chem.* **2007**, *119*, 2132-2135.
- [158] G. Cahiez, O. Gager, J. Buendia, *Angew. Chem. Int. Ed.* **2010**, *49*, 1278-1281.
- [159] D. H. Burns, J. D. Miller, H.-K. Chan, M. O. Delaney, *J. Am. Chem. Soc.* **1997**, *119*, 2125-2133.
- [160] G. Cahiez, O. Gager, J. Buendia, *Synlett* **2010**, *2010*, 299-303.
- [161] R. Shen, T. Iwasaki, J. Terao, N. Kambe, *Chem. Commun.* **2012**, *48*, 9313-9315.
- [162] M. B. Thathagar, J. Beckers, G. Rothenberg, *J. Am. Chem. Soc.* **2002**, *124*, 11858-11859.
- [163] J. Mao, J. Guo, F. Fang, S.-J. Ji, *Tetrahedron* **2008**, *64*, 3905-3911.
- [164] S. Wang, M. Wang, L. Wang, B. Wang, P. Li, J. Yang, *Tetrahedron* **2011**, *67*, 4800-4806.
- [165] J. Liu, F. Dai, Z. Yang, S. Wang, K. Xie, A. Wang, X. Chen, Z. Tan, *Tetrahedron Lett.* **2012**, *53*, 5678-5683.
- [166] J.-H. Li, D.-P. Wang, *Eur. J. Org. Chem.* **2006**, *2006*, 2063-2066.
- [167] Y.-M. Ye, B.-B. Wang, D. Ma, L.-X. Shao, J.-M. Lu, *Catal. Lett.* **2010**, *139*, 141-144.
- [168] C.-T. Yang, Z.-Q. Zhang, Y.-C. Liu, L. Liu, *Angew. Chem. Int. Ed.* **2011**, *50*, 3904-3907.

- [169] S. K. Gurung, S. Thapa, A. Kafle, D. A. Dickie, R. Giri, *Org. Lett.* **2014**, *16*, 1264-1267.
- [170] Y. Zhou, W. You, K. B. Smith, M. K. Brown, *Angew. Chem. Int. Ed.* **2014**, *53*, 3475-3479.
- [171] S. Díez-González, N. Marion, S. P. Nolan, *Chem. Rev.* **2009**, *109*, 3612-3676.
- [172] M. Poyatos, J. A. Mata, E. Peris, *Chem. Rev.* **2009**, *109*, 3677-3707.
- [173] O. Schuster, L. Yang, H. G. Raubenheimer, M. Albrecht, *Chem. Rev.* **2009**, *109*, 3445-3478.
- [174] H. Braunschweig, R. D. Dewhurst, K. Hammond, J. Mies, K. Radacki, A. Vargas, *Science* **2012**, *336*, 1420-1422.
- [175] R. J. Baker, R. D. Farley, C. Jones, M. Kloth, D. M. Murphy, *Chem. Commun.* **2002**, 1196-1197.
- [176] M. Y. Abraham, Y. Wang, Y. Xie, P. Wei, H. F. Schaefer, P. v. R. Schleyer, G. H. Robinson, *Chem. Eur. J.* **2010**, *16*, 432-435.
- [177] N. Holzmann, A. Stasch, C. Jones, G. Frenking, *Chem. Eur. J.* **2011**, *17*, 13517-13525.
- [178] Y. Wang, Y. Xie, P. Wei, R. B. King, H. F. Schaefer, P. v. R. Schleyer, G. H. Robinson, *Science* **2008**, *321*, 1069-1071.
- [179] Y. Wang, Y. Xie, P. Wei, R. B. King, H. F. Schaefer, P. v. R. Schleyer, G. H. Robinson, *J. Am. Chem. Soc.* **2008**, *130*, 14970-14971.
- [180] A. Sidiropoulos, C. Jones, A. Stasch, S. Klein, G. Frenking, *Angew. Chem. Int. Ed.* **2009**, *48*, 9701-9704.
- [181] D. J. D. Wilson, S. A. Couchman, J. L. Dutton, *Inorg. Chem.* **2012**, *51*, 7657-7668.
- [182] F. Hering, J. Nitsch, U. Paul, A. Steffen, F. M. Bickelhaupt, U. Radius, *Chem. Sci.* **2015**, *6*, 1426-1432.
- [183] F. Hering, U. Radius, *Organometallics* **2015**, *34*, 3236-3245.
- [184] P. Hemberger, A. Bodi, T. Gerber, M. Wurtemberger, U. Radius, *Chem. Eur. J.* **2013**, *19*, 7090-7099.
- [185] P. Hemberger, A. Bodi, J. H. J. Berthel, U. Radius, *Chem. Eur. J.* **2015**, *21*, 1434-1438.
- [186] M. D. Su, *Inorg. Chem.* **2014**, *53*, 5080-5087.
- [187] R. Fang, L. Yang, Q. Wang, *Organometallics* **2014**, *33*, 53-60.
- [188] K. J. Iversen, D. J. Wilson, J. L. Dutton, *Dalton Trans.* **2013**, *42*, 11035-11038.
- [189] K. J. Iversen, D. J. D. Wilson, J. L. Dutton, *Organometallics* **2013**, *32*, 6209-6217.
- [190] K. J. Iversen, D. J. Wilson, J. L. Dutton, *Dalton Trans.* **2014**, *43*, 12820-12823.

- [191] D. Schmidt, J. H. Berthel, S. Pietsch, U. Radius, *Angew. Chem. Int. Ed.* **2012**, *51*, 8881-8885.
- [192] S. Pietsch, E. C. Neeve, D. C. Apperley, R. Bertermann, F. Mo, D. Qiu, M. S. Cheung, L. Dang, J. Wang, U. Radius, Z. Lin, C. Kleeberg, T. B. Marder *Chem. Eur. J.* **2015**, *21*, 7082-7098.
- [193] S. Wurtemberger-Pietsch, H. Schneider, T. B. Marder, U. Radius, *Chem. Eur. J.* **2016**, *22*, 13032-13036.
- [194] T. Wang, D. W. Stephan, *Chem. Eur. J.* **2014**, *20*, 3036-3039.
- [195] D. Franz, S. Inoue, *Chem. Asian J.* **2014**, *9*, 2083-2087.
- [196] M. Arrowsmith, M. S. Hill, G. Kociok-Kohn, D. J. MacDougall, M. F. Mahon, *Angew. Chem. Int. Ed.* **2012**, *51*, 2098-2100.
- [197] M. Arrowsmith, M. S. Hill, G. Kociok-Köhn, *Organometallics* **2015**, *34*, 653-662.
- [198] S. M. Al-Rafia, R. McDonald, M. J. Ferguson, E. Rivard, *Chem. Eur. J.* **2012**, *18*, 13810-13820.
- [199] S. Pietsch, U. Paul, I. A. Cade, M. J. Ingleson, U. Radius, T. B. Marder, *Chem. Eur. J.* **2015**, *21*, 9018-9021.
- [200] M. Eck, S. Wurtemberger-Pietsch, A. Eichhorn, J. H. Berthel, R. Bertermann, U. S. Paul, H. Schneider, A. Friedrich, C. Kleeberg, U. Radius, T. B. Marder, *Dalton Trans.* **2017**, *46*, 3661-3680.
- [201] D. M. Flanigan, F. Romanov-Michailidis, N. A. White, T. Rovis, *Chem. Rev.* **2015**, *115*, 9307-9387.
- [202] D. Enders, O. Niemeier, A. Henseler, *Chem. Rev.* **2007**, *107*, 5606-5655.
- [203] K.-S. Lee, A. R. Zhugralin, A. H. Hoveyda, *J. Am. Chem. Soc.* **2010**, *132*, 12766.
- [204] K.-S. Lee, A. R. Zhugralin, A. H. Hoveyda, *J. Am. Chem. Soc.* **2009**, *131*, 7253-7255.
- [205] X. Sanz, G. M. Lee, C. Pubill-Ulldemolins, A. Bonet, H. Gulyás, S. A. Westcott, C. Bo, E. Fernández, *Org. Biomol. Chem.* **2013**, *11*, 7004-7010.
- [206] A. Bonet, C. Sole, H. Gulyás, E. Fernández, *Org. Biomol. Chem.* **2012**, *10*, 6621-6623.
- [207] C. Pubill-Ulldemolins, A. Bonet, C. Bo, H. Gulyás, E. Fernández, *Chem. Eur. J.* **2012**, *18*, 1121-1126.
- [208] A. Bonet, C. Pubill-Ulldemolins, C. Bo, H. Gulyas, E. Fernandez, *Angew. Chem. Int. Ed.* **2011**, *50*, 7158-7161.
- [209] A. Bonet, H. Gulyas, E. Fernandez, *Angew. Chem. Int. Ed.* **2010**, *49*, 5130-5134.
- [210] V. Lillo, A. Bonet, E. Fernández, *Dalton Trans.* **2009**, 2899-2908.

- [211] C. Pubill-Ulldemolins, A. Bonet, H. Gulyás, C. Bo, E. Fernández, *Org. Biomol. Chem.* **2012**, *10*, 9677-9682.
- [212] J. Cid, J. J. Carbó, E. Fernández, *Chem. Eur. J.* **2012**, *18*, 12794-12802.
- [213] J. Cid, H. Gulyás, J. J. Carbo, E. Fernández, *Chem. Soc. Rev.* **2012**, *41*, 3558-3570.
- [214] C. Solé, H. Gulyás, E. Fernández, *Chem. Commun.* **2012**, *48*, 3769-3771.
- [215] H. Gulyás, A. Bonet, C. Pubill-Ulldemolins, C. Solé, J. Cid, E. Fernández, *Pure Appl. Chem.* **2012**, *84*, 2219-2231.
- [216] J. Cid, J. J. Carbó, E. Fernández, *Chem. Eur. J.* **2014**, *20*, 3616-3620.
- [217] N. Miralles, J. Cid, A. B. Cuenca, J. J. Carbo, E. Fernández, *Chem. Commun.* **2015**, *51*, 1693-1696.
- [218] B. Zhang, P. Feng, Y. Cui, N. Jiao, *Chem. Commun.* **2012**, *48*, 7280-7282.
- [219] J. M. O'Brien, A. H. Hoveyda, *J. Am. Chem. Soc.* **2011**, *133*, 7712-7715.
- [220] Y. Wang, D. Wei, Y. Wang, W. Zhang, M. Tang, *ACS Catal.* **2016**, *6*, 279-289.
- [221] B. S. Li, Y. Wang, Z. Jin, P. Zheng, R. Ganguly, Y. R. Chi, *Nat. Commun.* **2015**, *6*, 6207.
- [222] B. Han, C. Peng, Q. Zhao, L.-Y. Feng, W. Huang, X.-H. He, *Synlett* **2016**, *27*, 2034-2038.
- [223] I. R. Shaikh, *J. Catal.* **2014**, *2014*, 1-35.
- [224] P.T.Anastas, J.C.Warner, *Green Chemistry: Teory and Practice* **1998**, Oxford University Press, New York.
- [225] S. Díez-González, S. P. Nolan, *Synlett* **2007**, *2007*, 2158-2167.
- [226] A. Welle, S. Díez-González, B. Tinant, S. P. Nolan, O. Riant, *Org. Lett.* **2006**, *8*, 6059-6062.
- [227] M. R. Fructos, T. R. Belderrain, M. C. Nicasio, S. P. Nolan, H. Kaur, M. M. Díaz-Requejo, P. J. Pérez, *J. Am. Chem. Soc.* **2004**, *126*, 10846-10847.
- [228] C. Munro-Leighton, S. A. Delp, E. D. Blue, T. B. Gunnoe, *Organometallics* **2007**, *26*, 1483-1493.
- [229] S. Díez-González, E. D. Stevens, N. M. Scott, J. L. Petersen, S. P. Nolan, *Chem. Eur. J.* **2008**, *14*, 158-168.
- [230] G. G. Dubinina, H. Furutachi, D. A. Vicic, *J. Am. Chem. Soc.* **2008**, *130*, 8600-8601.
- [231] S. Díez-González, H. Kaur, F. K. Zinn, E. D. Stevens, S. P. Nolan, *J. Org. Chem.* **2005**, *70*, 4784-4796.
- [232] S. Díez-González, A. Correa, L. Cavallo, S. P. Nolan, *Chem. Eur. J.* **2006**, *12*, 7558-7564.

- [233] S. Díez-González, S. P. Nolan, *Angew. Chem. Int. Ed.* **2008**, *47*, 8881-8884.
- [234] S. Díez-González, E. D. Stevens, S. P. Nolan, *Chem. Commun.* **2008**, 4747-4749.
- [235] C. A. Citadelle, E. L. Nouy, F. Bisaro, A. M. Z. Slawin, C. S. J. Cazin, *Dalton Trans.* **2010**, *39*, 4489-4491.
- [236] S. Díez-González, E. C. Escudero-Adán, J. Benet-Buchholz, E. D. Stevens, A. M. Z. Slawin, S. P. Nolan, *Dalton Trans.* **2010**, *39*, 7595-7606.
- [237] W. J. Humenny, S. Mitzinger, C. B. Khadka, B. K. Najafabadi, I. Vieira, J. F. Corrigan, *Dalton Trans.* **2012**, *41*, 4413-4422.
- [238] K. Semba, M. Shinomiya, T. Fujihara, J. Terao, Y. Tsuji, *Chem. Eur. J.* **2013**, *19*, 7125-7132.
- [239] H. Kaur, F. K. Zinn, E. D. Stevens, S. P. Nolan, *Organometallics* **2004**, *23*, 1157-1160.
- [240] S. Díez-González, S. P. Nolan, *Angew. Chem. Int. Ed.* **2008**, *47*, 8881-8884.
- [241] C. Gibard, H. Ibrahim, A. Gautier, F. Cisnetti, *Organometallics* **2013**, *32*, 4279-4283.
- [242] B. Liu, X. Ma, F. Wu, W. Chen, *Dalton Trans.* **2015**, *44*, 1836-1844.
- [243] S. Díez-González, N. M. Scott, S. P. Nolan, *Organometallics* **2006**, *25*, 2355-2358.
- [244] J. R. Herron, Z. T. Ball, *J. Am. Chem. Soc.* **2008**, *130*, 16486-16487.
- [245] T. Fujihara, T. Xu, K. Semba, J. Terao, Y. Tsuji, *Angew. Chem. Int. Ed.* **2011**, *50*, 523-527.
- [246] S. Wu, W. Zeng, Q. Wang, F. X. Chen, *Org. Biomol. Chem.* **2012**, *10*, 9334-9337.
- [247] T. Vergote, F. Nagra, D. Peeters, O. Riant, T. Leyssens, *J. Organomet. Chem.* **2013**, *730*, 95-103.
- [248] T. Vergote, F. Nagra, A. Merschaert, O. Riant, D. Peeters, T. Leyssens, *Organometallics* **2014**, *33*, 1953-1963.
- [249] C. Janiak, E. Riedel, *Anorganische Chemie* **1999**, de Gruyter: Berlin.
- [250] O. Back, M. Henry-Ellinger, C. D. Martin, D. Martin, G. Bertrand, *Angew. Chem. Int. Ed.* **2013**, *52*, 2939-2943.
- [251] B. Rao, H. Tang, X. Zeng, L. Liu, M. Melaimi, G. Bertrand, *Angew. Chem. Int. Ed.* **2015**, *54*, 14915-14919.
- [252] N. P. Mankad, D. S. Laitar, J. P. Sadighi, *Organometallics* **2004**, *23*, 3369-3371.
- [253] J. Plotzitzka, C. Kleeberg, *Inorg. Chem.* **2016**, *55*, 4813-4823.
- [254] N. P. Mankad, T. G. Gray, D. S. Laitar, J. P. Sadighi, *Organometallics* **2004**, *23*, 1191-1193.

- [255] L. A. Goj, E. D. Blue, S. A. Delp, T. B. Gunnoe, T. R. Cundari, J. L. Petersen, *Organometallics* **2006**, *25*, 4097-4104.
- [256] L. Dang, Z. Lin, T. B. Marder, unpublished results.
- [257] H. Eriksson, M. Håkansson, *Organometallics* **1997**, *16*, 4243-4244.
- [258] E. M. Meyer, S. Gambarotta, C. Floriani, A. Chiesi-Villa, C. Guastini, *Organometallics* **1989**, *8*, 1067-1079.
- [259] M. Niemeyer, *Z. Anorg. Allg. Chem.* **2003**, *629*, 1535-1540.
- [260] T. Ohishi, M. Nishiura, Z. Hou, *Angew. Chem. Int. Ed.* **2008**, *47*, 5792-5795.
- [261] A. M. Whittaker, R. P. Rucker, G. Lalic, *Org. Lett.* **2010**, *12*, 3216-3218.
- [262] T. Braun, M. A. Salomon, K. Altenhoner, M. Teltewskoi, S. Hinze, *Angew. Chem. Int. Ed.* **2009**, *48*, 1818-1822.
- [263] R. Wada, K. Oisaki, M. Kanai, M. Shibasaki, *J. Am. Chem. Soc.* **2004**, *126*, 8910-8911.
- [264] M. C. Schwarzer, R. Konno, T. Hojo, A. Ohtsuki, K. Nakamura, A. Yasutome, H. Takahashi, T. Shimasaki, M. Tobisu, N. Chatani, S. Mori, *J. Am. Chem. Soc.* **2017**, *139*, 10347-10358.
- [265] D. S. Laitar, P. Müller, J. P. Sadighi, *J. Am. Chem. Soc.* **2005**, *127*, 17196-17197.
- [266] C. M. Wyss, J. Bitting, J. Bacsá, T. G. Gray, J. P. Sadighi, *Organometallics* **2016**, *35*, 71-74.
- [267] Y. Segawa, M. Yamashita, K. Nozaki, *Angew. Chem. Int. Ed.* **2007**, *46*, 6710-6713.
- [268] T. Kajiwara, T. Terabayashi, M. Yamashita, K. Nozaki, *Angew. Chem. Int. Ed.* **2008**, *47*, 6606-6610.
- [269] C. Borner, C. Kleeberg, *Eur. J. Inorg. Chem.* **2014**, *2014*, 2486-2489.
- [270] Y. Okuno, M. Yamashita, K. Nozaki, *Angew. Chem. Int. Ed.* **2011**, *50*, 920-923.
- [271] Kleeberg *et al.* manuscript in preparation.
- [272] Y. Okuno, M. Yamashita, K. Nozaki, *Eur. J. Org. Chem.* **2011**, *2011*, 3951-3958.
- [273] H. Saijo, M. Ohashi, S. Ogoshi, *J. Am. Chem. Soc.* **2014**, *136*, 15158-15161.
- [274] S. Chakraborty, J. Zhang, J. A. Krause, H. Guan, *J. Am. Chem. Soc.* **2010**, *132*, 8872-8873.
- [275] G. Povie, G. Villa, L. Ford, D. Pozzi, C. H. Schiesser, P. Renaud, *Chem. Commun.* **2010**, *46*, 803-805.
- [276] G. Heller, K. Seeger, *Z. Naturforsch. B* **1988**, *43*, 547 - 556.
- [277] L. Dang, H. Zhao, Z. Lin, T. B. Marder, *Organometallics* **2008**, *27*, 1178-1186.

- [278] B. L. Tran, D. Adhikari, H. Fan, M. Pink, D. J. Mindiola, *Dalton Trans.* **2010**, 39, 358-360.
- [279] O. Holloczki, P. Terleczky, D. Szieberth, G. Mourgas, D. Gudat, L. Nyulaszi, *J. Am. Chem. Soc.* **2011**, 133, 780-789.
- [280] S. Nave, R. P. Sonawane, T. G. Elford, V. K. Aggarwal, *J. Am. Chem. Soc.* **2010**, 132, 17096-17098.
- [281] R. W. Hoffmann, A. Endesfelder, H.-J. Zeiss, *Carbohydr. Res.* **1983**, 123, 320-325.
- [282] O. Baron, P. Knochel, *Angew. Chem. Int. Ed.* **2005**, 44, 3133-3135.
- [283] T. Umemoto, K. Adachi, *J. Org. Chem.* **1994**, 59, 5692-5699.
- [284] S. K. Bose, S. Brand, H. O. Omoregie, M. Haehnel, J. Maier, G. Bringmann, T. B. Marder, *ACS Catal.* **2016**, 6, 8332-8335.
- [285] E. A. Romero, J. L. Peltier, R. Jazzar, G. Bertrand, *Chem. Commun.* **2016**, 52, 10563-10565.
- [286] T. Ohishi, L. Zhang, M. Nishiura, Z. Hou, *Angew. Chem. Int. Ed.* **2011**, 50, 8114-8117.
- [287] L. A. Goj, E. D. Blue, C. Munro-Leighton, T. B. Gunnoe, J. L. Petersen, *Inorg. Chem.* **2005**, 44, 8647-8649.
- [288] M. Hill, G. Kehr, R. Fröhlich, G. Erker, *Eur. J. Inorg. Chem.* **2003**, 2003, 3583-3589.
- [289] L. A. Körte, S. Blomeyer, J.-H. Peters, A. Mix, B. Neumann, H.-G. Stammler, N. W. Mitzel, *Organometallics* **2017**, 36, 742-749.
- [290] J. Yuasa, M. Dan, T. Kawai, *Dalton Trans.* **2013**, 42, 16096-16101.
- [291] J. Huang, J. Chan, Y. Chen, C. J. Borths, K. D. Baucom, R. D. Larsen, M. M. Faul, *J. Am. Chem. Soc.* **2010**, 132, 3674-3675.
- [292] K. Semba, T. Fujihara, T. Xu, J. Terao, Y. Tsuji, *Adv. Synth. Catal.* **2012**, 354, 1542-1550.
- [293] P. J. Cox, A. Kaltzoglou, P. Aslanidis, *Inorg. Chim. Acta* **2006**, 359, 3183-3190.
- [294] E. Meyer, *J. Prakt. Chem.* **1888**, 37, 396-407.
- [295] C. R. Hauser, W. J. Humphlett, *J. Org. Chem.* **1950**, 15, 359-366.
- [296] A. R. Ronzio, W. B. Cook, *Organic Syntheses* **1944**, 24, 6.
- [297] R. Bossio, S. Marcaccini, V. Parrini, R. Pepino, *J. Heterocycl. Chem.* **1986**, 23, 889-891.
- [298] H. Takaya, T. Naota, S.-I. Murahashi, *J. Am. Chem. Soc.* **1998**, 120, 4244-4245.
- [299] X. Tao, T. Liu, H. Tao, R. Liu, Y. Qian, *J. Mol. Catal. A: Chem.* **2003**, 201, 155-160.

- [300] A. F. Eichhorn, S. Fuchs, M. Flock, T. B. Marder, U. Radius, *Angew. Chem. Int. Ed.* **2017**, *56*, 10209-10213.
- [301] A. F. Eichhorn, L. Kuehn, T. B. Marder, U. Radius, *Chem. Commun.* **2017**, *53*, 11694-11696.
- [302] R. D. Dewhurst, E. C. Neeve, H. Braunschweig, T. B. Marder, *Chem. Commun.* **2015**, *51*, 9594-9607.
- [303] E. C. Neeve, S. J. Geier, I. A. I. Mkhalid, S. A. Westcott, T. B. Marder, *Chem. Rev.* **2016**, *116*, 9091-9161.
- [304] C. Kleeberg, A. G. Crawford, A. S. Batsanov, P. Hodgkinson, D. C. Apperley, M. S. Cheung, Z. Lin, T. B. Marder, *J. Org. Chem.* **2012**, *77*, 785-789.
- [305] M. R. Momeni, E. Rivard, A. Brown, *Organometallics* **2013**, *32*, 6201-6208.
- [306] V. Lavallo, Y. Canac, B. Donnadieu, W. W. Schoeller, G. Bertrand, *Angew. Chem. Int. Ed.* **2006**, *45*, 3488-3491.
- [307] U. S. Paul, C. Sieck, M. Haehnel, K. Hammond, T. B. Marder, U. Radius, *Chem. Eur. J.* **2016**, *22*, 11005-11014.
- [308] G. D. Frey, V. Lavallo, B. Donnadieu, W. W. Schoeller, G. Bertrand, *Science* **2007**, *316*, 439-441.
- [309] O. Back, G. Kuchenbeiser, B. Donnadieu, G. Bertrand, *Angew. Chem. Int. Ed.* **2009**, *48*, 5530-5533.
- [310] C. D. Martin, C. M. Weinstein, C. E. Moore, A. L. Rheingold, G. Bertrand, *Chem. Commun.* **2013**, *49*, 4486-4488.
- [311] G. D. Frey, J. D. Masuda, B. Donnadieu, G. Bertrand, *Angew. Chem. Int. Ed. Engl.* **2010**, *49*, 9444-9447.
- [312] H. Li, X. Shangguan, Z. Zhang, S. Huang, Y. Zhang, J. Wang, *Org. Lett.* **2014**, *16*, 448-451.
- [313] H. Abu Ali, I. Goldberg, D. Kaufmann, C. Burmeister, M. Srebnik, *Organometallics* **2002**, *21*, 1870-1876.
- [314] P. Nguyen, G. Lesley, N. J. Taylor, T. B. Marder, N. L. Pickett, W. Clegg, M. R. J. Elsegood, N. C. Norman, *Inorg. Chem.* **1994**, *33*, 4623-4624.
- [315] A. J. Lennox, G. C. Lloyd-Jones, *Chem. Soc. Rev.* **2014**, *43*, 412-443.
- [316] W. Clegg, C. Dai, F. J. Lawlor, T. B. Marder, P. Nguyen, N. C. Norman, N. L. Pickett, W. P. Power, A. J. Scott, *Dalton Trans.* **1997**, 839-846.

- [317] G. Bramham, A. S. Batsanov, T. B. Marder, N. C. Norman, *Acta Crystallogr.* **2006**, *E62*, 972-973.
- [318] F. H. Allen, O. Kennard, D. G. Watson, L. Brammer, A. G. Orpen, R. Taylor, *J. Chem. Soc. Perkin Trans. 2* **1987**, S1.
- [319] D. R. Lide, *Tetrahedron* **1962**, *17*, 125-134.
- [320] T. Schaub, M. Backes, U. Radius, *Organometallics* **2006**, *25*, 4196-4206.
- [321] T. Schaub, U. Radius, A. Brucks, M. P. Choules, M. T. Olsen, T. B. Rauchfuss, *Inorg. Synth.* **2011**, *35*, 78-83.
- [322] N. M. Scott, R. Dorta, E. D. Stevens, A. Correa, L. Cavallo, S. P. Nolan, *J. Am. Chem. Soc.* **2005**, *127*, 3516-3526.
- [323] A. J. Arduengo III, R. Krafczyk, R. Schmutzler, H. A. Craig, J. R. Goerlich, W. J. Marshall, M. Unverzagt, *Tetrahedron* **1999**, *55*, 14523-14534.
- [324] X. Bantreil, S. P. Nolan, *Nat. Protoc.* **2011**, *6*, 69-77.
- [325] L. Hintermann, *Beilstein J. Org. Chem.* **2007**, *3*, 22.
- [326] S. Zhu, R. Liang, H. Jiang, *Tetrahedron* **2012**, *68*, 7949-7955.
- [327] N. Kuhn, T. Kratz, *Synthesis* **1993**, *1993*, 561-562.
- [328] R. Jazzar, R. D. Dewhurst, J. B. Bourg, B. Donnadieu, Y. Canac, G. Bertrand, *Angew. Chem. Int. Ed.* **2007**, *46*, 2899-2902.
- [329] P. Bissinger, H. Braunschweig, A. Damme, I. Krummenacher, A. K. Phukan, K. Radacki, S. Sugawara, *Angew. Chem. Int. Ed.* **2014**, *53*, 7360-7363.
- [330] G. J. Kubas, *Inorg. Synth.* **1990**, *28*, 68-70.
- [331] A. Jakob, Y. Shen, T. Wächtler, S. E. Schulz, T. Gessner, R. Riedel, C. Fasel, H. Lang, *Z. Anorg. Allg. Chem.* **2008**, *634*, 2226-2234.
- [332] L. A. Goj, E. D. Blue, S. A. Delp, T. B. Gunnoe, T. R. Cundari, A. W. Pierpont, J. L. Petersen, P. D. Boyle, *Inorg. Chem.* **2006**, *45*, 9032-9045.
- [333] D. A. Wilson, C. J. Wilson, C. Moldoveanu, A. M. Resmerita, P. Corcoran, L. M. Hoang, B. M. Rosen, V. Percec, *J. Am. Chem. Soc.* **2010**, *132*, 1800-1801.
- [334] D. C. Ebner, J. T. Bagdanoff, E. M. Ferreira, R. M. McFadden, D. D. Caspi, R. M. Trend, B. M. Stoltz, *Chem. Eur. J.* **2009**, *15*, 12978-12992.
- [335] B. P. Carrow, J. F. Hartwig, *J. Am. Chem. Soc.* **2011**, *133*, 2116-2119.
- [336] Y. Iwai, K. M. Gligorich, M. S. Sigman, *Angew. Chem. Int. Ed.* **2008**, *47*, 3219-3222.
- [337] K. Ukai, M. Aoki, J. Takaya, N. Iwasawa, *J. Am. Chem. Soc.* **2006**, *128*, 8706-8707.

- [338] J. J. Dunsford, I. A. Cade, K. L. Fillman, M. L. Neidig, M. J. Ingleson, *Organometallics* **2014**, *33*, 370-377.
- [339] H. Braunschweig, W. C. Ewing, T. Kramer, J. D. Mattock, A. Vargas, C. Werner, *Chem. Eur. J.* **2015**, *21*, 12347-12356.
- [340] R. Shintani, K. Takatsu, T. Hayashi, *Chem. Commun.* **2010**, *46*, 6822-6824.
- [341] W. R. Dolbier, *Guide to Fluorine NMR for Organic Chemists* John Wiley & Sons, Inc., Hoboken.
- [342] S. A. Westcott, H. P. Blom, T. B. Marder, R. T. Baker, J. C. Calabrese, *Inorg. Chem.* **1993**, *32*, 2175-2182.

10 Eidesstattliche Erklärung

Hiermit erkläre ich an Eides statt, die Dissertation "Copper(I) catalyzed borylation and cross-coupling reactions" eigenständig, d.h. insbesondere selbstständig und ohne Hilfe eines kommerziellen Promotionsberaters angefertigt und keinen anderen als die von mir angegebenen Quellen und Hilfsmittel verwendet zu haben.

Ich erkläre außerdem, dass die Dissertation weder in gleicher noch in ähnlicher Form bereits in einem anderen Prüfungsverfahren vorgelegen hat.

Würzburg, den

11 Affidavit

I hereby confirm that my thesis entitled "Copper(I) catalyzed borylation and cross-coupling reactions" is the result of my own work. I did not receive any help or support from commercial consultants. All sources and / or materials applied are listed and specified in the thesis.

Furthermore, I confirm that this thesis has not yet been submitted as part of another examination process neither in identical nor in similar form.

Würzburg,

12 List of publications

The publication listed below is partly reproduced in this dissertation with permission from Wiley-VCH and the Royal Society of Chemistry, respectively. The table itemizes to what extent the different sections of the paper have been reused at which position in this work.

Publication	Chapter
Antonius F. Eichhorn , S. Fuchs, M. Flock, T. B. Marder, U. Radius, <i>Angew. Chem. Int. Ed.</i> 2017 , <i>56</i> , 10209-10213.	4.4.1
	4.4.2
	4.4.3
	4.4.4
Antonius F. Eichhorn , L. Kuehn, T. B. Marder, U. Radius, <i>Chem. Comm.</i> 2017 , <i>53</i> , 11694-11696.	4.4.1

13 Acknowledgment/Danksagung

This project would not have been possible without the support of many people.

First of all I would like to express my special appreciation and thanks to Todd and Udo for their support, help and guidance throughout the whole thesis and the past years. It was a good time with ups and downs – Thank you.

I would like to thank my host family Elizabeth and Daniel for the comfort and their love – until the day we meet again.

Bei allen Mitarbeitern/innen im und um das Anorganische Institute möchte ich mich für Ihren Einsatz bedanken. Justin Wolf, Krzysztof Radacki, Rüdiger Bertermann, Marie-Luise Schäfer, Liselotte Michels, Sabine Timmroth, Christoph Mahler, Sabine Lorenz, Hildegard Holzinger, Alexandra Friedrich, Stephan Wagner, Conny Walter, Berthold Fertig, Michael Ramold, Manfred Reinhardt, Alfred Scherzer, Alois Ruf, Wolfgang Obert, Helga Diettrich, Stefanie Ziegler, Ellen Klaus, Patricia Schmidt, Bianca Putz, Maria Eckhardt und den 4x4 Jungs Danke für Rat und Tat und alles was ich lernen durfte!

Meinem Arbeitskreis Danke ich für die Unterstützung und die wunderbare Zeit (Laura, Jing, Peter, Bartosz, Heidi, Flo, Kuntze, Ertler, Rumpel, Katha, Max, Sabrina, Uli, David, Andi, Mirjam)! Ebenso den Stockkollegen für die gute Atmosphäre (Michel, Matti, Shorty, Jimbo, Drisch, Jan, Landmann, Raphael, Tatj, Maik). Den Marders danke ich für das tolle Zusammenarbeiten hier besonder: Martin, Shubankar, Lujia, Andreas, Martin, Emily und Jörn. Im zweiten Stock gilt mein Dank Marius, Dominic, Theresa, Jan, Bill, Valerie, Julie, Kai, Sundargopal, Thomas, Marco, Birgit und Holger. Ausserdem Danke ich Andreas, Johanna, Kim, Catherine, Tom sowie Sonja, Marco und Philip.

Für die Freundschaften die ich erfahren durfte bin ich von tiefstem Herzen Dankbar!

